Design, Synthesis and Biological Evaluation of Novel Histamine H_3 Receptor Ligands

Inaugural dissertation

for the attainment of the title of doctor
in the Faculty of Mathematics and Natural Sciences
at the Heinrich Heine University Düsseldorf

presented by

Mihajlo Gajić
from Niš

Düsseldorf, June 2025

from the Institute of Pharmaceutical and Medicinal Chemistry
at the Heinrich Heine University Düsseldorf

Published by permission of the
Faculty of Mathematics and Natural Sciences at
Heinrich Heine University Düsseldorf
This work was made possible with the support of a scholarship from the German Academic Exchange Service (DAAD)

Supervisor: Univ. Prof. Dr. Dr. h.c. Holger Stark
Co-supervisor: Univ. Prof. Dr. Thomas Kurz

Date of the oral examination:

To Nevena

Acknowledgements

This doctoral research was conducted at the Institute of Pharmaceutical and Medicinal Chemistry at Heinrich-Heine University Düsseldorf under the supervision of Prof. Dr. Dr. h.c. Holger Stark.

First and foremost, I am deeply grateful to Prof. Stark for his unwavering support, inspiring guidance, and constructive criticism throughout this challenging yet exciting project. His mentorship not only broadened my scientific horizons but also shaped me into a more confident researcher. I feel privileged to have been part of his dynamic working group.

I gratefully acknowledge the German Academic Exchange Service (DAAD) for funding my doctoral research.

I thank Prof. Dr. Thomas Kurz, my co-supervisor, for reading and evaluating this PhD thesis.

I am profoundly grateful to Dr. Aleksandra Živković, whose impact extended far beyond academic guidance. Whether discussing research, career choices, or life's uncertainties, her perspective was transformative. This work, and my growth as a scientist and individual, would not have been the same without her.

I sincerely thank Prof. Dr. Katarina Nikolić and her team for their expert collaboration in performing molecular docking studies, which advanced this research.

I extend my sincere gratitude to my colleague Tobias Werner for his meticulous execution of *in vitro* screening assays on *h*H_3R and G9a, as well as cytotoxicity assays, which were essential to this work.

To my labmates Martin Stark, Markus Schultes, and Tim Riemer - thank you for fostering a laboratory atmosphere that was both professionally stimulating and personally rewarding. I am grateful to Lars Seiffert and Elias Böttger for their insightful discussions and for the enriching interactions that extended beyond our research. I would also like to acknowledge Patrick Krolikowski, Jiteesh Joy, Mariam Dubiel, Luisa Leitzbach, and the rest of my colleagues for contributing to our working group's supportive environment. These friendships, along with the moments we shared both inside and outside the lab, made this journey truly memorable.

I thank my parents and sister for their unwavering support throughout my journey – their confidence motivated me through challenges, and their values shaped both my work and life.

Finally, my deepest gratitude goes to my fiancé, Nevena, who has walked beside me through every important chapter of our lives together. Your love, patience, and understanding have been my foundation through all of life's challenges and triumphs. Every success reflected in these pages belongs equally to both of us.

Affidavit

Ich versichere an Eides statt, dass die vorliegende Dissertation von mir selbstständig und ohne unzulässige fremde Hilfe unter Beachtung der Grundsätze zur Sicherung guter wissenschaftlicher Praxis an der Heinrich-Heine-Universität Düsseldorf erstellt worden ist.

Düsseldorf, June 2025

_____

Mihajlo Gajić

Table of Contents

Acknowledgements

Affidavit

Table of Contentsi

Abbreviations

1 Introduction 1

1.1 Histamine Metabolic Pathways 1

1.2 Histamine Receptors 3

1.3 Histamine H_1 Receptor 5

1.4 Histamine H_2 Receptor 8

1.5 Histamine H_3 Receptor 11

1.6 Histamine H_4 Receptor 23

1.7 Multi-target Directed Ligands 26

1.8 Epigenetic Regulation Through G9a Methyltransferase 29

1.9 Leucine-rich Repeat Kinase 2 35

2 Objectives 42

3 Chemistry 44

3.1 H_3R Pharmacophore-bearing Building Blocks 44

3.2 PINNER Pyrimidine Synthesis 48

3.3 Synthesis of Pyrimidin-4-amine Derivatives 50

3.4 Synthesis of Pyrimidin-2-amine Derivatives 54

3.5 Synthesis of Pyrimidine-2,4-diamine Derivatives 57

4 Pharmacology and Discussion 69

4.1 Pharmacological Assays 69

4.2 Principles of *h*H_3R Binding Affinity Determination 69

4.3 Principles of Enzyme Inhibition Determinations 73

4.4 Evaluation of Pyrimidin-4-amine Derivatives 76

4.5 Evaluation of Pyrimidin-2-amine Derivatives 79
4.6 Evaluation of Pyrimidine-2,4-diamine Derivatives 80
4.7 Lipophilicity Determination (logP and logD) 104
5 Summary 110
6 Experimental Section 113
6.1 General remarks 113
6.2 Chemical Experiments 116
6.3 Pharmacological Experiments 206
7 References 211
8 Supplementary Data 241
List of Publications 245
Curriculum Vitae 248

Abbreviations

5-HT_4R	5-hydroxytryptamine (serotonin) 4 receptor
α-Syn	α-synuclein
Aβ	amyloid-β protein
AC	adenylate cyclase
ACN	acetonitrile
AD	Alzheimer's disease
ADHD	attention deficit hyperactivity disorder
ADP	adenosine diphosphate
ALDH	aldehyde dehydrogenase
AlphaLISA	Amplified Luminescent Proximity Homogeneous Assay
AMP	adenosine monophosphate
ATP	adenosine triphosphate
BBB	blood-brain barrier
CaMKII	Ca^{2+}/calmodulin-dependant protein kinase II
cAMP	cyclic adenosine monophosphate
cGMP	cyclic guanosine monophosphate
CI	confidence interval
CNS	central nervous system
CREB	cAMP response element-binding protein
cS_NAr	concerted nucleophilic aromatic substitution
CYP450	cytochrome P450
DAG	1,2-diacylglycerol
DAO	diamine oxidase
DCE	1,2-dichloroethane
DCM	dichloromethane
DEMM	diethyl 2-(ethoxymethylene)malonate
DIPEA	*N,N*-diisopropylethylamine
DMF	dimethylformamide
DMSO	dimethyl sulfoxide

ECL	extracellular loop
EHMT2	euchromatic histone-lysine *N*-methyltransferase 2
ERK1/2	extracellular signal-regulated kinase 1/2
EtOAc	ethyl acetate
EtOH	ethanol
EWG	electron withdrawing group
GABA	γ-aminobutyric acid
GDI	GTP dissociation inhibitors
GDP	guanosine diphosphate
GLP	G9a-like protein
GMP	guanosine monophosphate
GTP	guanosine triphosphate
GPCR	G protein-coupled receptor
GSK-3β	glycogen synthase kinase-3β
$H_{1\text{-}4}R$	histamine $H_{1\text{-}4}$ receptor
HATs	histone acetyltransferases
HATU	*N*-[(dimethylamino)-1*H*-1,2,3-triazolo[4,5-b]pyridin-1-ylmethylene]-*N*-methylmethanaminium hexafluorophosphate *N*-oxide
HDACs	histone deacetylases
HDC	*L*-histidine decarboxylase
HMTs	histone methyltransferases
HNMT	histamine *N*-methyltransferase
HOAt	1-hydroxy-7-azabenzotriazole
HPLC	high-performance liquid chromatography
HVACC	high voltage activated Ca^{2+} channels
JAK	janus kinase
IC_{50}	half-maximal inhibitory concentration
ICL	intracellular loop
JNK	c-Jun N-terminal kinase
IP_3	inositol-1,4,5-triphosphate
IUPAC	International Union of Pure and Applied Chemistry

K_i	binding affinity
KMTs	histone lysin methyltransferase
KO	knockout
KO*t*Bu	potassium *tert*-butoxide
LC-MS	liquid chromatography – mass spectroscopy
LRRK2	leucin-rich repeat kinase 2
MAO-B	monoamine oxidase B
MeOH	methanol
MAP	microtubule-associated proteins
MAPK	mitogen-activated protein kinase
MARK1	microtubule affinity-regulating kinase 1
MTDL	multi-target directed ligands
$MT_{1\text{-}2}R$	melatonin 1 or melatonin 2 receptor
NET	norepinephrine transporter
NF-κB	nuclear factor κB
NHE	Na^+/H^+ exchanger
NO	nitric oxide
NREM	non-rapid eye movement sleep
NSF	*N*-ethylmaleimide-sensitive factor
OECD	Organisation for Economic Co-operation and Development
PD	Parkinson's disease
PI3K	phosphoinositide 3-kinase
PKA	protein kinase A
PKB	protein kinase B
PKC	protein kinase C
PKMTs	protein lysin methyltransferases
PLA_2	phospholipase A_2
PLC	phospholipase C
PRMTs	protein arginine methyl transferase
PROTACs	proteolysis targeting chimeras

PWS	Prader-Willi syndrome
REM	rapid-eye movement
RMSD	root mean square deviation
RPS15	ribosomal protein s15
SAH	*S*-adenosylhomocysteine
SAM	*S*-adenosylmethionine
SAR	structure-activity relationship
SCH	schizophrenia
SERT	serotonin reuptake transporter
S_EAr	electrophilic aromatic substitution
S_NAr	nucleophilic aromatic substitution
S_NV	nucleophilic vinylic substitution
STAT	signal transducer and activator of transcription
SWS	slow-wave sleep
TEA	triethylamine
TFA	trifluoroacetic acid
THF	tetrahydrofuran
TLC	thin-layer chromatography
TM	transmembrane domain
TMN	tuberomammillary nucleus
TNF-α	tumor necrosis factor-α
TR-FRET	time-resolved fluorescence resonance energy transfer

1 Introduction

Histamine, 2-(1*H*-imidazol-4-yl)ethan-1-amine (Figure 1), stands as one of the most extensively studied and physiologically significant biogenic amines, first isolated and characterized by Sir HENRY DALE and PATRICK LAIDLAW over a century ago.[1] Their seminal work unveiled histamine's profound influence on smooth muscle contraction and vascular dynamics, laying the foundation for its recognition as a critical signalling molecule. The ubiquitous distribution of this crucial signalling molecule across diverse tissues earned it the classification as a "tissue amine" a term derived from the Greek word *histos*, meaning tissue, reflecting its widespread presence in biological systems.[2] This discovery marked the beginning of a new era in biomedical research, establishing histamine as a fundamental mediator of numerous physiological and pathological processes.

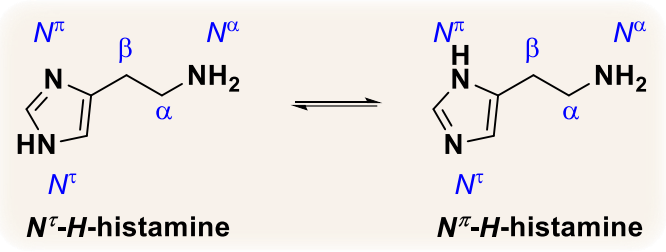

Figure 1. Tautomeric forms of histamine and their nomenclature by BLACK and GANELLIN.[3]

Histamine comprises two fundamental functional groups, an imidazole ring and an ethanamine side chain, with pK_a 6.04 and 9.75, respectively.[4] Under physiological conditions, only the primary amino function exists in the protonated form, while the amidine moiety within the imidazole heterocycle remains deprotonated. Beyond IUPAC nomenclature, the naming system proposed by BLACK and GANELLIN, which designates the nitrogen atoms and side chain carbon atoms using Greek letters, is widely used due to its practicality in referencing histamine's structure (Figure 1).[3]

1.1 Histamine Metabolic Pathways

Histamine is a versatile signalling molecule that functions as both a neurotransmitter in the nervous system and a local mediator in peripheral tissues. Its pleiotropic roles – including regulation of gastric acid secretion, vascular permeability, immune cell recruitment, and circadian rhythm – are tightly linked to its tissue-specific synthesis, storage, and degradation.[5]

The tissue distribution of histamine precisely aligns with its multifaceted functions. Large quantities are synthesized and stored within the granules of specialized immune cells – mast cells and basophils – where it forms complexes with heparin. Substantial concentrations are found in enterochromaffin-like cells of the stomach, lymphoid tissues (lymph nodes and thymus), with moderate levels detected in the liver, lungs, and histaminergic neuronal varicosities throughout the brain.[6, 7]

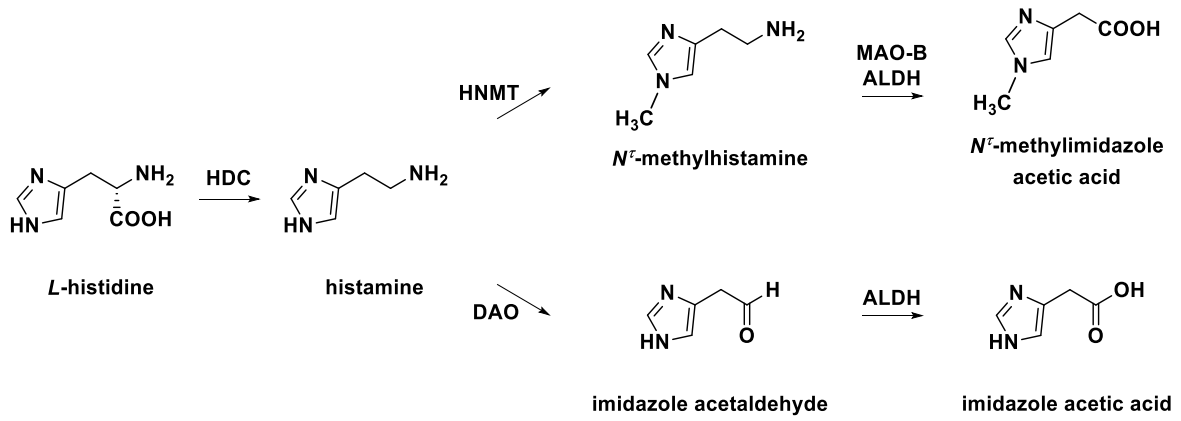

Figure 2. Biosynthesis and degradation of histamine. HDC – histidine decarboxylase; HNMT – histamine *N* methyltransferase; DAO – diamine oxidase; MAO-B – monoamine oxidase B; ALDH – aldehyde dehydrogenase.

This sophisticated tissue distribution is maintained through intricate metabolic pathways. The biosynthesis involves a single-step decarboxylation of *L*-histidine, catalysed by the pyridoxal phosphate-dependent enzyme *L*-histidine decarboxylase (HDC) (Figure 2).[8] Post-synthesis, histamine follows one of two distinct pathways: immediate release for rapid signalling, encountered in some haematopoietic cells, or storage in secretory granules via the vesicular monoamine transporter 2, found in histaminergic neurons, gastric enterochromaffin-like cells, mast cells and basophiles.[2, 9] Histamine metabolism exhibits marked tissue specificity, primarily through two distinct enzymatic pathways (Figure 2). In the central nervous system (CNS), histamine *N*-methyltransferase (HNMT) catalyses N^{τ}-methylation to produce N^{τ}-methylhistamine. This metabolite is than converted by monoamine oxidase B (MAO-B) into N^{τ}-methylimidazole acetaldehyde, which is subsequently oxidized to N^{τ}-methylimidazole acetic acid via aldehyde dehydrogenase (ALDH).[10, 11] In contrast, peripheral tissues such as the gastrointestinal tract rely predominantly on diamine oxidase (DAO) for histamine degradation. DAO mediates oxidative deamination of histamine, producing imidazole acetaldehyde, which is further oxidized by ALDH to yield imidazole acetic acid.[12] These pathways exhibit tissue specific dominance, with HNMT acting as the principal regulator

of histamine levels in the brain and DAO playing a critical role in peripheral tissues, particularly the gastrointestinal tract, where it ensures systemic histamine homeostasis.[13]

1.2 Histamine Receptors

Histamine mediates its multifaceted biological actions by binding to four evolutionarily conserved receptor subtypes (H_1R, H_2R, H_3R, and H_4R) (Table 1), all classified within the Class A (rhodopsin-like) G protein-coupled receptor (GPCR) superfamily.[5] These receptors share a canonical GPCR architecture, featuring an extracellular N-terminal domain, seven α helical transmembrane domains (TM1-TM7) that anchor the receptor within the plasma membrane, three extracellular loops (ECL1-3) that contribute to ligand recognition, three intracellular loops (ICL1-3) that interface with downstream signalling proteins, and a cytoplasmic C-terminal tail critical for receptor trafficking and regulatory interactions.[14] This shared architecture is a hallmark of GPCRs, enabling them to undergo conformational changes upon ligand binding, which in turn activates intracellular signalling pathways. Each histamine receptor subtype couples to distinctive G proteins, initiating specific intracellular signalling cascades that culminate in unique cellular responses and physiological outcomes. These receptor-specific pathways enable histamine to exert diverse and sometimes opposing effects across different tissues and cell types, thereby orchestrating complex physiological processes through a single mediator.[15]

Histamine receptors, like other GPCRs, exist in a dynamic equilibrium between active and inactive conformational states. In the absence of ligands, this equilibrium typically favours the inactive state. However, a subset of receptors spontaneously adopts the active conformation, resulting in constitutive activity (or basal activity), which enables these receptors to maintain baseline physiological tone even in an unbound state.[15, 16] Ligands interacting with histamine receptors are classified based on their modulation of this equilibrium. Agonists – whether endogenous or synthetic – stabilize the active receptor conformation, shifting the equilibrium to enhance signal transduction. In contrast, neutral antagonists bind to the receptor without preferentially stabilizing either the active or inactive state, leaving constitutive activity unaffected. By occupying the ligand-binding site, however, neutral antagonists competitively inhibit agonist-mediated receptor activation. Inverse agonists, formerly termed antagonists, stabilize the inactive conformation, shifting the equilibrium toward the inactive state and suppressing constitutive activity below basal levels.[17] While constitutive activity has been documented across all four histamine receptor subtypes, it is particularly pronounced in the

high-affinity receptors H_3R and H_4R, where basal signalling plays a significant role in their physiological and pathophysiological functions.[17, 18]

Table 1. Comparative overview of histamine receptor subtypes.

	H_1R	**H_2R**	**H_3R**	**H_4R**
Discovery	1919[19]	1972[20]	1983[21]	2000-2001[22-27]
Cloning	1991[28]	1991[29]	1999[30]	2000[22-27]
Structure determination	2011[31]	2023[32]	2022[33]	2024[32, 34]
G-Protein coupling[5]	$G\alpha_{q/11}$	$G\alpha_s$	$G\alpha_{i/o}$	$G\alpha_{i/o}$
Downstream signaling pathways[5]	PLC↑, Ca^{2+}↑	cAMP↑	cAMP↑, Ca^{2+}↓, MAPK↑	cAMP↑, Ca^{2+}↓, MAPK↑
Functional role[5]	Sleep-wake cycle regulation, vasoconstriction, bronchodilatation	Gastric acid secretion	Neurotransmitter release, sleep-wakefulness, cognition	Immune response
Receptor agonists[5, 35]	Histaprodifens	Dimaprit, ipromidine	Imetit, immepip, propoxyfan	VUF-8430, ST-1006
Receptor antagonists[5, 35]	Diphenhydramine, levocetirizine, desloratadine	Ranitidine, famotidine, zolantadine	Ciproxifan, thioperamide, pitolisant	JNJ-7777120, toreforant, adriforant

From an evolutionary perspective, histamine receptors show notable conservation across species, indicating their fundamental importance in biological systems. Phylogenetic analyses reveal that H_1R and H_2R emerged earlier in evolution, while H_3R and H_4R appeared later through gene duplication events. Unlike most aminergic receptor subtypes, histamine receptor subtypes exhibit relatively low sequence identities, reflecting considerable divergence. For instance, the overall sequence identity between human H_1R and H_2R is approximately 31%, whereas H_1R shares only 24-27% sequence identity with H_3R and H_4R. In contrast, H_3R and H_4R share a higher sequence identity of about 42%.[36, 37]

Histamine, serving as the endogenous ligand for all four receptor subtypes, demonstrates selectivity in its binding profile. The molecule exhibits substantially higher affinity for H_3R and H_4R receptors, with pK_i values of 8.0 and 7.8 respectively, compared to the significantly lower affinities observed at H_1R and H_2R receptors, where pK_i values reach only 4.2 and 4.3.[38] This differential binding pattern has profound implications for histamine's concentration-dependent effects across various tissues and physiological contexts, allowing for selective receptor activation based on local histamine concentrations.

1.3 Histamine H_1 Receptor

A major advancement in histamine research occurred during the 1960s and 1970s when studies utilizing existing antihistamines revealed that certain histamine-mediated responses were resistant to conventional antihistamine treatments. This pivotal observation led researchers to hypothesize the existence of multiple histamine receptor subtypes.[39] The definitive differentiation between H_1R and H_2R was achieved in 1972 with the discovery of burimamide, the first H_2R antagonist, marking a significant breakthrough in the field.[20] This pharmacological distinction preceded the molecular characterization of these receptors by almost two decades, as the successful cloning of both H_1R and H_2R cDNAs was achieved in 1991.[28, 29]

The human H_1R is a 56-kDa protein comprising 487 amino acids, encoded by a single-exon gene situated on the distal short arm of chromosome 3 at locus 25.[2, 40] The crystallographic structure of H_1R was resolved in 2011, providing critical insights into its binding pocket and conformational dynamics upon histamine or antagonist binding. This breakthrough was pivotal for structure-based drug design, enabling the development of more selective antihistamines with improved therapeutic profiles.[31] Histamine binds to TM3 and TM5 domains of H_1R, inducing a conformational change that activates the receptor and initiates its signalling cascade. H_1R activation primarily operates through the $G\alpha_{q/11}$ protein, which possesses GTPase activity and activates phospholipase C (PLC)[2, 41]. PLC subsequently hydrolyses phosphatidylinositol 4,5-bisphosphate to generate two secondary messengers: 1,2-diacylglycerol (DAG) and inositol-1,4,5-triphosphate (IP_3).[8, 42] DAG activates protein kinase C (PKC), which catalyses the phosphorylation of serine/threonine residues on downstream effectors, while IP_3 binds to receptors on the endoplasmic reticulum, triggering the release of Ca^{2+} ions from intracellular stores into the cytoplasm.[8, 43] Alternatively, H_1R signalling can also proceed via pertussis toxin-sensitive G_i/G_o proteins. Upon receptor activation, these G proteins stimulate phospholipase A_2 (PLA_2), resulting in the release of arachidonic acid. Concurrently, calcium-dependent nitric oxide synthase is activated, producing nitric oxide (NO), which subsequently activates guanylate cyclase in an NO-dependent manner. This leads to an elevation in cyclic GMP (cGMP) levels.[40]

H_1R exhibits widespread expression across diverse cell types, including neurons, endothelial cells, adrenal medulla, muscle cells, hepatocytes, chondrocytes, and various immune cells (monocytes, neutrophils, eosinophils, dendritic cells, T cells, and B cells).[44, 45] H_1R signalling cascades initiate multiple biological responses, triggering the synthesis of prostacyclins,

activation of platelet factor, production of NO, arachidonic acid and its metabolites, and thromboxane.[46, 47] These molecular pathways elicit distinct tissue-specific physiological responses. In vascular smooth muscle cells, H_1R activation produces dual effects: while inducing a direct contractile response through IP_3-mediated calcium elevation, it predominantly causes vasodilation through endothelial NO release.[48-50] Conversely, in bronchial smooth muscle, H_1R activation results in bronchoconstriction .[51-53] Within endothelial cells, H_1R stimulation induces cell contraction, enhancing vascular permeability[54, 55], while concurrently triggering NO release and prostacyclin production, which amplifies the vascular response.[5, 49, 50, 56] The actions of H_1R also regulate the synthesis and release of catecholamines from chromaffin cells in the adrenal medulla.[56]

In the mammalian brain, H_1R shows a distinctive distribution pattern, with notably high densities in regions controlling neuroendocrine function, behaviour, and nutritional state. These regions encompass the periventricular, suprachiasmatic, and ventromedial nuclei of the hypothalamus, along with aminergic and cholinergic brainstem nuclei, the thalamus, and the cortex.[11, 57] Through calcium-mediated signalling, H_1R activation excites neurons across multiple brain regions, including the brainstem[58, 59], hypothalamus[60], thalamus[61], amygdala, septum[62], hippocampus[63], olfactory bulb[64], and cortex.[65] This widespread neuronal activation enables H_1R to regulate crucial brain functions, including motor activity, mood, arousal, sleep, circadian rhythms, cognitive processes, and pain perception, while also contributing to thermoregulation, food intake, and energy expenditure.[60, 66]

1.3.1 Overview of H_1R Ligands

Early investigations into histamine receptors relied on ligand-based approaches, where chemical modifications of histamine and related molecules helped define receptor properties. This led to the discovery of a range of H_1R ligands, from agonists that mimic histamine's action to antagonists that block its effects.

The search for H_1R ligands began with modifications of histamine itself, focusing on its imidazole ring and aminoethyl side chain. Early efforts with non-imidazole derivatives, such as 2-(thiazol-2-yl)ethanamine (**L1**, Figure 3), yielded partial agonistic activity. However, full agonism was achieved most effectively by introducing a diphenylpropyl moiety at the C-2 position of the histamine scaffold. This modification not only amplified receptor activation but also exceeded histamine's maximal efficacy. The resulting compounds, termed histaprodifens – including histaprodifen (**L2**) and methylhistaprodifen (**L3**) among others – demonstrate a dual binding mechanism, engaging both the agonist and antagonist binding pockets of the H_1R.

The pharmacological behaviour of these ligands is highly sensitive to the length of the alkyl linker connecting the core structure to the diphenylpropyl group. Optimal agonistic activity occurs with three methylene units in the linker; shortening this chain reduces efficacy to partial agonism, while elongation shifts the profile toward antagonism.[5, 35] The H_1R agonists, however, have not found therapeutic utility, largely due to the receptor's role in mediating adverse inflammatory and allergic responses. Instead, they remain valuable as research tools for probing H_1R pharmacology and signalling pathways.

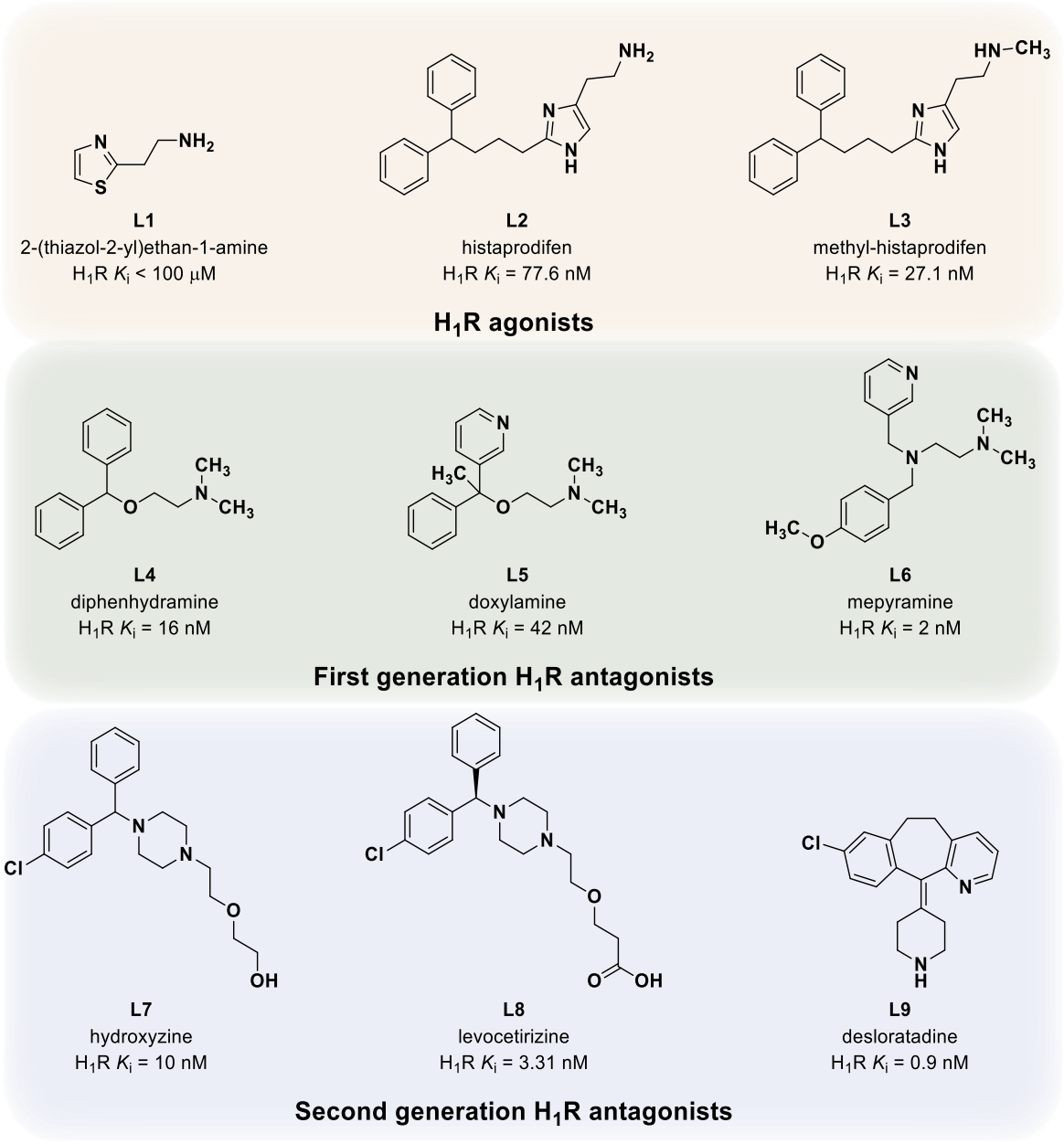

Figure 3. Selected representatives of H_1R agonists (**L1-L3**)[67, 68], along with first- (**L4-L6**)[67, 69] and second-generation antagonists (**L7-L9**)[70, 71].

In contrast to agonists, H_1R antagonists, commonly referred to as "antihistamines", have achieved remarkable clinical importance and represent one of the most extensively prescribed medication classes worldwide.[72] Their therapeutic applications span multiple conditions including allergic rhinitis, conjunctivitis, cutaneous allergic manifestations, and antiemetic therapy for nausea and vomiting.[5, 17] Antihistamines are traditionally classified into two generations based on their pharmacokinetic properties and side effect profiles.

First-generation H_1R antagonists typically feature a molecular architecture comprising two aromatic moieties linked to an aliphatic tertiary amino functionality, predominantly through three-carbon spacers (Figure 3). Representative members like diphenhydramine (**L4**), doxylamine (**L5**) and mepyramine (**L6**) are characterized by high lipophilicity, facilitating penetration of the blood-brain barrier (BBB). In addition to crossing the BBB, these compounds exhibit low receptor selectivity, interacting not only with H_1R but also with muscarinic, serotonergic, and adrenergic receptors. This CNS penetration, combined with off-target receptor binding, frequently results in sedation, weight gain, and, in many cases, anticholinergic effects that further limit their therapeutic utility.[57, 73]

To mitigate these central adverse effects, second-generation H_1R antagonists (Figure 3) were specifically designed to minimize central nervous system exposure. This was achieved either through increased polarity, thereby reducing BBB permeability, or by designing molecules with high affinity for ATP-dependent P-glycoprotein and organic anion transport polypeptide efflux pumps that actively transport the compounds out of the central nervous system.[74, 75] Consequently, second-generation antihistamines such as hydroxyzine (**L7**), levocetirizine (**L8**) or desloratadine (**L9**) incorporate polar functional groups that significantly reduce their propensity to cause sedation while maintaining or even enhancing their peripheral antihistaminic efficacy.

1.4 Histamine H_2 Receptor

Histamine H_2R is a 40 kDa protein consisting of 359 amino acids, encoded by a gene located on the long arm of chromosome 5, locus 35.[76] Structurally, H_2R shares similarities with the histamine H_1 receptor (H_1R), particularly in its histamine-binding mechanism, which involves transmembrane domains TM3 and TM5.[77] In 2023, the active-state conformation of H_2R was elucidated using cryo-electron microscopy at 2.56 Å resolution, revealing that both H_1R and H_2R possess an orthosteric imidazole recognition pocket and a secondary binding pocket.[32] H_2R signal transduction primarily operates through a $G\alpha_s$ protein-dependent pathway, initiating

with the stimulation of adenylate cyclase (AC) upon receptor activation.[78-80] This activation leads to elevated intracellular cAMP levels, which subsequently triggers protein kinase A (PKA) and activates the cAMP response element-binding protein (CREB) transcription factor.[40, 81] Additionally, H_2R employs an alternative signalling pathway through GTP-dependent PLC activation, resulting in the generation of secondary messengers DAG and IP_3.[77, 82]

H_2R demonstrates broad tissue distribution, being predominantly expressed in parietal cells of the gastric mucosa, with significant presence in smooth muscle cells, epithelial cells, endothelial cells, cardiomyocytes, neurons, hepatocytes, and various immune cells including neutrophils, eosinophils, monocytes, macrophages, dendritic cells, T and B cells.[2, 5] H_2R signalling mediates diverse physiological responses across these tissues. In the gastrointestinal system, H_2R primarily regulates acid secretion in parietal cells.[83] In the cardiovascular system, H_2R activation produces positive chronotropic and inotropic effects in atrial and ventricular tissues.[2] The receptor promotes smooth muscle relaxation in various tissues, including blood vessels, airways, uterus, and gastrointestinal tract.[48, 53, 56]

Within the immune system, H_2R exhibits predominantly inhibitory effects, including suppression of histamine release from basophils and mast cells, inhibition of antibody synthesis, reduction of T cell proliferation, and modulation of cytokine production.[84]

The H_2R is widely distributed throughout the central nervous system, with particularly high densities in the basal ganglia, hippocampus, amygdala, and cerebral cortex.[40, 85, 86] These receptors play crucial roles in various neurophysiological processes, including cognition, learning, and memory formation through their modulation of synaptic plasticity and neurotransmitter release.[6, 66]

1.4.1 Overview of H_2R Ligands

The diverse physiological roles of H_2R, particularly in gastric acid secretion, spurred the development of targeted ligands. Early efforts focused on modifying histamine's core structure to achieve receptor selectivity, balancing agonist/antagonist functionality with drug-like properties. This yielded two key classes of compounds: agonists as mechanistic probes and antagonists as therapeutic agents.

The search for potent and selective H_2R agonists has yielded several key compounds (Figure 4). Early studies produced 4(5)-methylhistamine (**L10**), which interestingly is now used as an H_4R agonist.[38, 87] Other notable H_2R agonists include amthamine (**L11**)[88], which replaces imidazole with thiazole, and dimaprit (**L12**)[89], an isothiourea compound with moderate

affinity and selectivity. Impromidine (**L13**) and (*R*)-(-)-sopromidine (**L14**) demonstrated increased affinity through their homohistamine-guanidine structure, with the guanidinium moiety essential for H_2R activation. Despite their potential as positive inotropic vasodilators for heart failure, these compounds were not suitable for oral administration due to their physicochemical properties.[90] To improve drug-like properties, researchers replaced the guanidine group with acylguanidine, reducing basicity while maintaining H_2R activity. However, many N^G-acylated imidazolylpropylguanidines, like UR-AK24 (**L15**), showed poor selectivity, with some compounds demonstrating partial agonist profiles for both H_1R and H_2R.[91] The selectivity issue was resolved by replacing imidazole with a 2-aminothiazole heterocycle, leading to the compounds like UR-BIT24 (**L16**)[92], which maintain potency at H_2R while eliminating significant activity at other histamine receptors. Despite significant advances in developing selective H_2R agonists, these compounds, like their H_1R agonist counterparts, remain primarily research tools without clinical applications.

The discovery that the thiourea derivative N^{α}-thioguanylhomohistamine acts as a partial H_2R agonist in gastric acid secretion tests led to the development of burimamide (**L17**), the first selective H_2R antagonist.[95] Paradoxically, burimamide was later identified as a potent H_3R antagonist and H_4R agonist.[35] The relationship between molecular structure and receptor selectivity is further exemplified by cimetidine (**L18**), the first clinically approved H_2R antagonist.[20, 96] Its polar cyanoguanidine moiety serves as a key pharmacophoric element that resembles the affinity-enhancing guanidine group found in impromidine, while modifications to other structural regions confer its antagonist properties rather than agonist activity. Subsequent H_2R antagonists like ranitidine (**L19**), famotidine (**L20**), and zolantidine (**L21**) feature reduced basicity, which – with the exception of zolantadine – decreased their BBB permeability.[5, 97] In these compounds, cimetidine's imidazole was replaced with bioisosteric heterocycles to minimize CYP3A4 enzyme interactions. Unlike cimetidine, later antagonists required lower doses and exhibited <10% of its CYP3A4 metabolic effects.[98] Improved safety profiles enabled some newer H_2R antagonists to become over-the-counter medication.

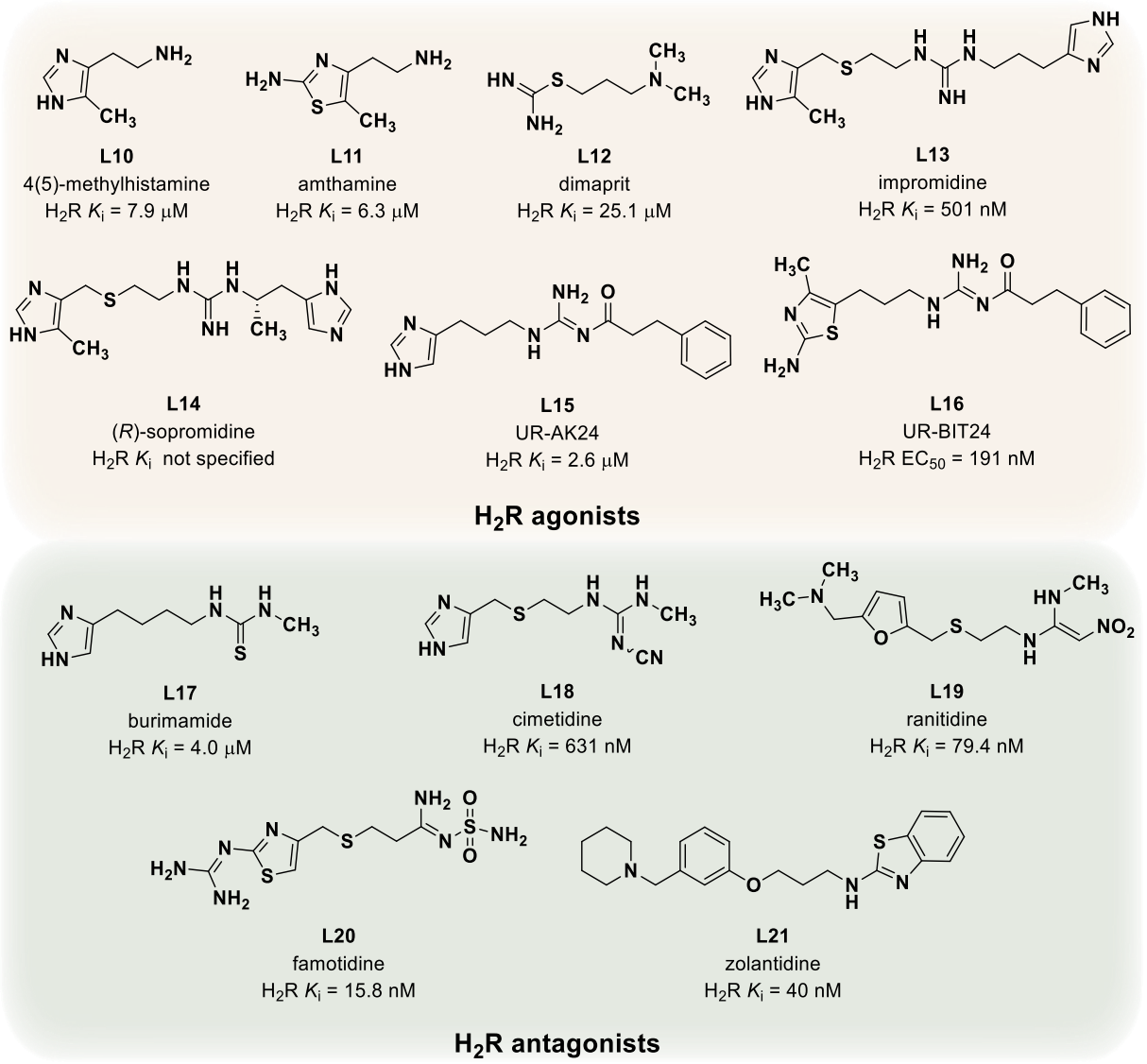

Figure 4. Selected representatives of H_2R agonists (**L10-L16**)[38, 92, 93] and antagonists (**L17-L21**).[38, 94]

1.5 Histamine H_3 Receptor

The histamine H_3 receptor was first identified and characterized by ARRANG et al. in 1983 as an auto-receptor controlling histamine synthesis and release in rat brain tissue.[21] Building on their initial discovery, in 1987 the same research group developed the first highly potent and selective H_3R ligands, (*R*)-α-methylhistamine as an agonist and thioperamide as an antagonist, which became essential tools for establishing the unique pharmacological profile and physiological functions of the H_3R.[99] A major breakthrough in H_3R research occurred in 1999 when LOVENBERG et al. successfully cloned and functionally expressed the human H_3R.[30] This milestone provided a molecular framework for understanding H_3R function and accelerated the development of novel therapeutic agents targeting this receptor. Structural understanding of H_3R progressed in 2022 with the first high-resolution cryo-EM structure

(2.60 Å), showing the receptor in an inactive state bound to the inverse agonist PF03654746 and coupled to a G_i protein. This provided key insights into ligand recognition and G protein interaction[33]

Histamine H_3R is a 70 kDa protein consisting of 445 amino acids, encoded by a gene located on the long arm of chromosome 20, locus 13.[100] Unlike H_1R and H_2R genes that are intronless[28, 29], H_3R consists of multiple exons and introns. Some reports indicate the existence of three exons and two introns[100, 101], while others suggest four exons and three introns.[102, 103] The complex genomic organization of the H_3R gene enables alternative splicing, resulting in at least 20 different isoforms identified to date. These splice variants differ in their distribution, signalling properties, and constitutive activity, contributing to the diverse functions of H_3R in different tissues.[15]

The activation of H_3R initiates a complex cascade of cellular events through their interaction with $G\alpha_{i/o}$ protein (Figure 5). The primary signalling pathway involves adenylyl cyclase-mediated cAMP production, which normally activates PKA, leading to CREB activation and subsequent gene transcription regulation. However, H_3R activation reduces cAMP levels, thereby diminishing CREB-dependent gene transcription and related cellular responses [104-106] Through PKA, the $G\alpha_{i/o}$ protein negatively modulates high voltage activated Ca^{2+} channels (HVACC), where decreased PKA activity results in reduced phosphorylation and activation of HVACC.[107-109] Changes in intracellular Ca^{2+} concentration influence exocytosis through both PKA-dependent and PKA-independent mechanisms [110] Additionally, both PKA and calcium/calmodulin-dependent protein kinase type II (CaMKII) can activate histidine decarboxylase (HDC) via distinct pathways, promoting histamine synthesis.[111] The H_3R-$G\alpha_{i/o}$ protein interaction triggers multiple parallel signalling cascades, including the mitogen-activated protein kinase (MAPK)[112] and PI3K pathways[113], while also inducing other cellular responses such as PLA_2 activation leading to arachidonic acid release[114] and Na^+/H^+ exchanger (NHE) inhibition.[115] Specifically, the $G\beta\gamma$ subunit of $G\alpha_{i/o}$ protein mediates the mobilization of both extracellular signal-related kinase 1/2 (ERK1/2) and c-Jun N-terminal kinase (JNK) from the MAPK family, thereby regulating synaptic plasticity.[112, 116] Furthermore, PI3K activation by $G\beta\gamma$ leads to protein kinase B (PKB) activation, which subsequently inhibits glycogen synthase kinase-3β (GSK-3β), an enzyme implicated in various neurological and neurodegenerative disorders.[113, 117, 118]

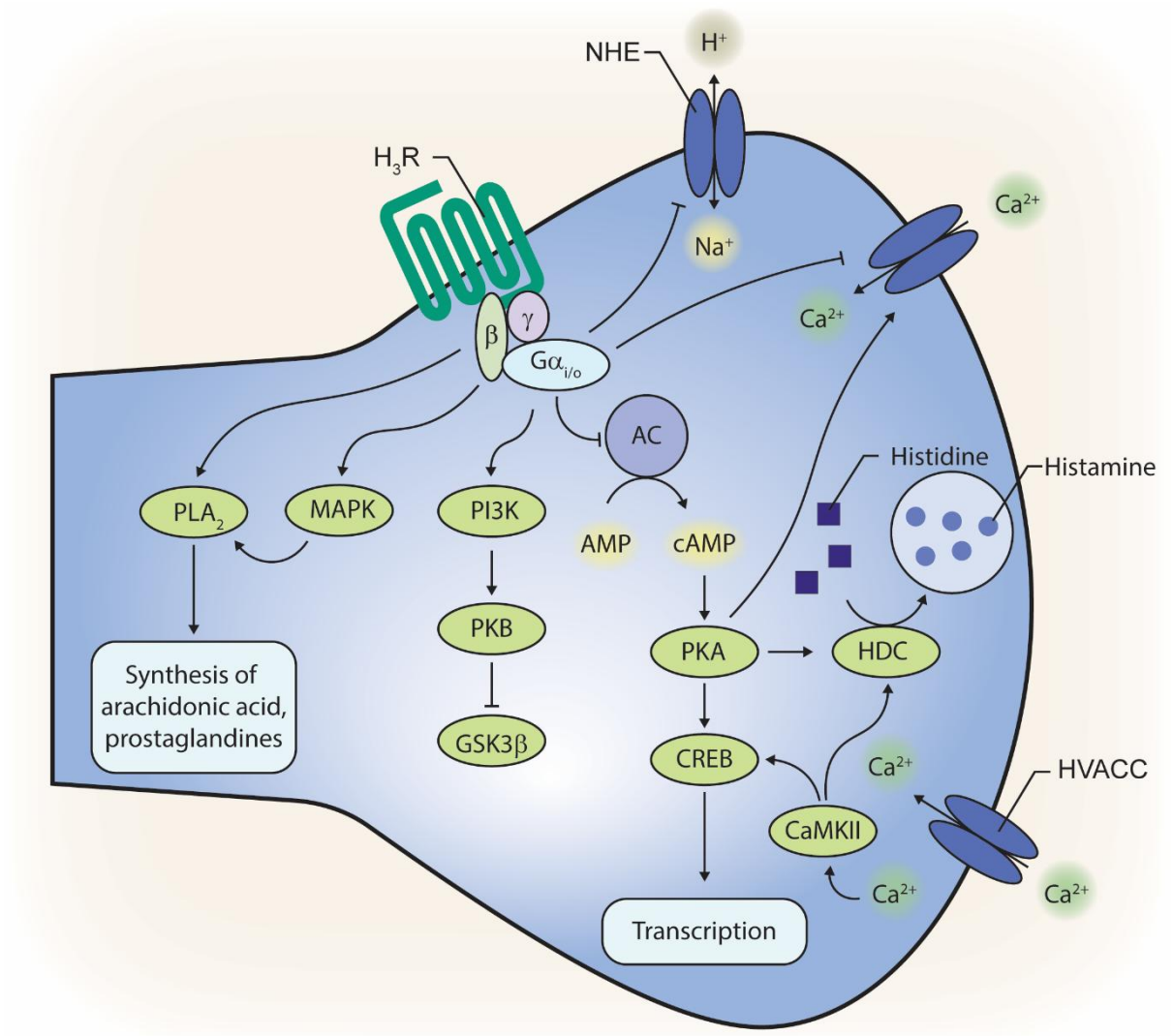

Figure 5. Molecular signalling pathways of H_3R. NHE – Na^+/H^+ exchanger; AC – adenylate cyclase; PLA_2 – phospholipase A2; MAPK – mitogen-activated protein kinase; PI3K – phosphoinositide 3-kinase; PKB – protein kinase B; PKA – protein kinase A, CREB – cAMP responsive element-binding protein; HDC – histidine deacetylase; CaMKII – Ca^{2+}/calmodulin-dependent protein kinase type II; HVACC – high voltage activated Ca^{2+} channels.

The H_3R exhibits predominant expression in the central nervous system and significantly lower levels in peripheral tissues. In the brain, H_3R is highly concentrated in regions crucial for cognitive functions, including the cerebral cortex, hippocampus, basal ganglia, and hypothalamus.[119] These receptors function as both presynaptic autoreceptors, regulating histamine synthesis and release, and heteroreceptors, controlling the release of various neurotransmitters such as GABA, acetylcholine (ACh), dopamine (DA), norepinephrine (NE), and serotonin (5-HT) (Figure 6).[5] This neuromodulatory role influences multiple physiological processes, including sleep-wake cycles, food intake, and cognitive functions.[120] Beyond the CNS, H_3R is present in the peripheral nervous system, particularly in sympathetic

nerve endings, where they modulate norepinephrine release and influence cardiovascular function.[121] The receptors are also found in gastrointestinal tract, modulating acid secretion and intestinal motility, and in airways, where they participate in bronchial tone regulation.[122]

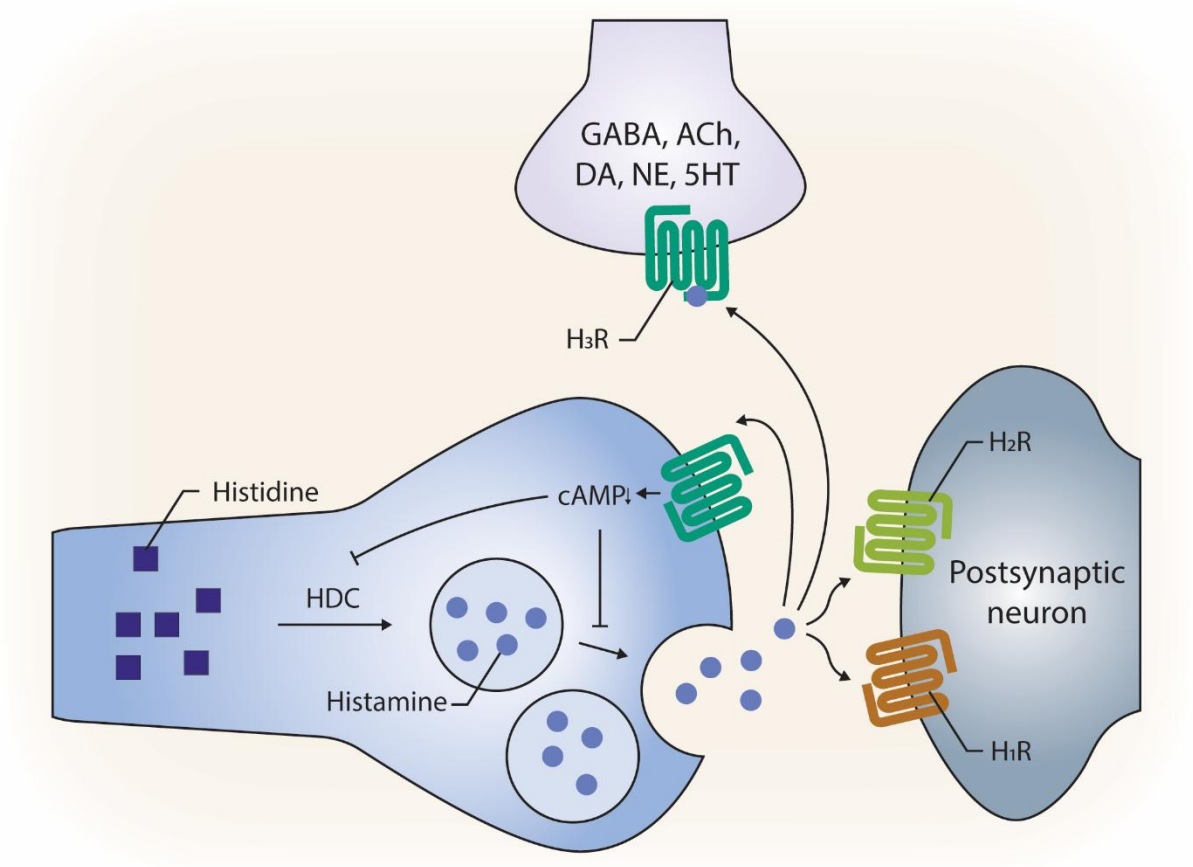

Figure 6. The H_3R functions as both an auto- and heteroreceptor. Activation of presynaptic H_3R autoreceptors inhibits histamine synthesis and release into the synaptic cleft, thereby suppressing histaminergic signalling to postsynaptic receptors. Conversely, activation of postsynaptic H_3Rs modulates the release of other neurotransmitters. HDC – histidine decarboxylase; GABA – γ-aminobutyric acid; ACh – acetylcholine; DA – dopamine; NE – norepinephrine; 5-HT – serotonin.

1.5.1 Overview of H_3R Ligands

Histamine is a potent H_3R agonist, thus its structural modifications have produced highly effective H_3R agonists (Figure 7). Among them, N^{α}-methylhistamine (**L22**)[99], though not H_3R-selective, is widely used in binding assays due to its high affinity and availability in tritiated form.[21, 56] *R*-(α)-methylhistamine (**L23**) is a potent *in vitro* tool[56] whose dipsogenic effect supports key *in vivo* models, though its H_4R activity remains a limitation.[5, 22, 27, 123, 124] Further advancements have yielded improved prodrugs such as BP2-94 (**L24**), which offers enhanced pharmacokinetics.[125, 126] More potent agonists followed, including imetit (**L25**), featuring an isothiourea moiety, and immepip (**L26**), distinguished by its elongated, cyclized

side chain.[5, 127] Both compounds exhibit activity at H_3R and H_4R.[5, 114, 128] Proxyfan (**L27**) was identified as the first protean agonist for H_3Rs, showing a spectrum from inverse agonist to agonist depending on the test system.[128, 129] Similar partial (ant)agonist properties were later observed in non-amine imidazole derivatives such as ciprilisant (**L28**), further expanding the range of H_3R modulators.[5, 128, 130-132]

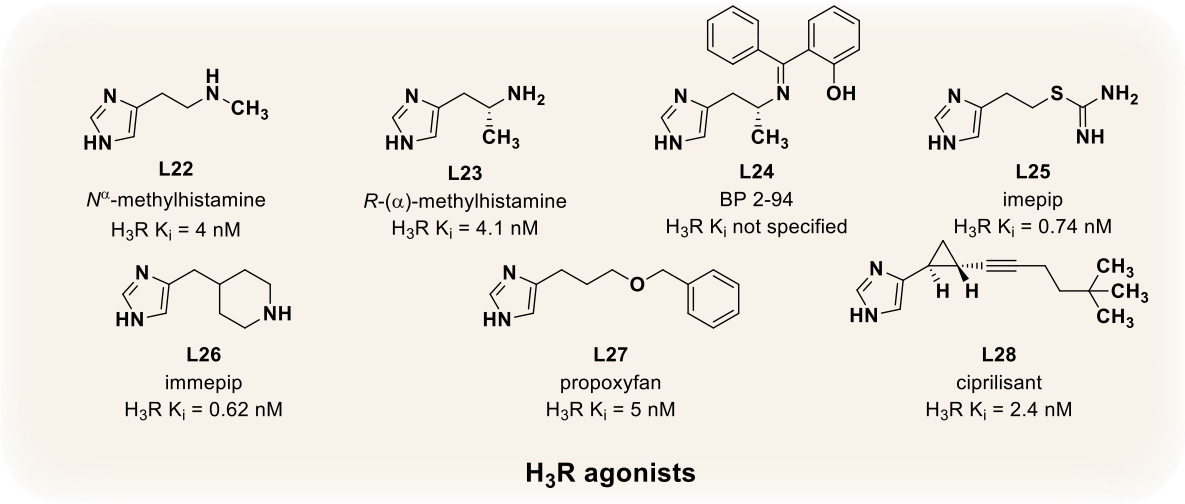

Figure 7. Selected representatives of H_3R agonists (**L22**-**L28**).[133]

Numerous H_3R antagonists (Figure 8) demonstrate preclinical efficacy in neurotransmitter release and animal models, driving research toward optimized agents with improved potency, selectivity, and drug-likeness. Antagonists have advanced to Phase I–III trials for conditions including sleep disorders, Alzheimer's disease (AD), Parkinson's disease (PD), Attention deficit hyperactivity disorder (ADHD), schizophrenia (SCH) epilepsy, neuropathic pain, and allergic rhinitis.[134]

The development of H_3R antagonists began with the repurposing of the H_2R antagonist burimamide (**L17**, Figure 4)[99], leading to imidazole-based ligands like thioperamide (**L29**), clobenpropit (**L30**), and ciproxifan (**L31**). Thioperamide showed efficacy in memory and behavioral models[135] and revealed H_3R's role in regulating food intake, highlighting therapeutic potential for obesity and diabetes.[136, 137] Clobenpropit improved working memory and Alzheimer's models [138, 139], though both compounds exhibit off-target H_4R activity.[140] Ciproxifan is selective and bioavailable, used in attentional models.[141, 142]

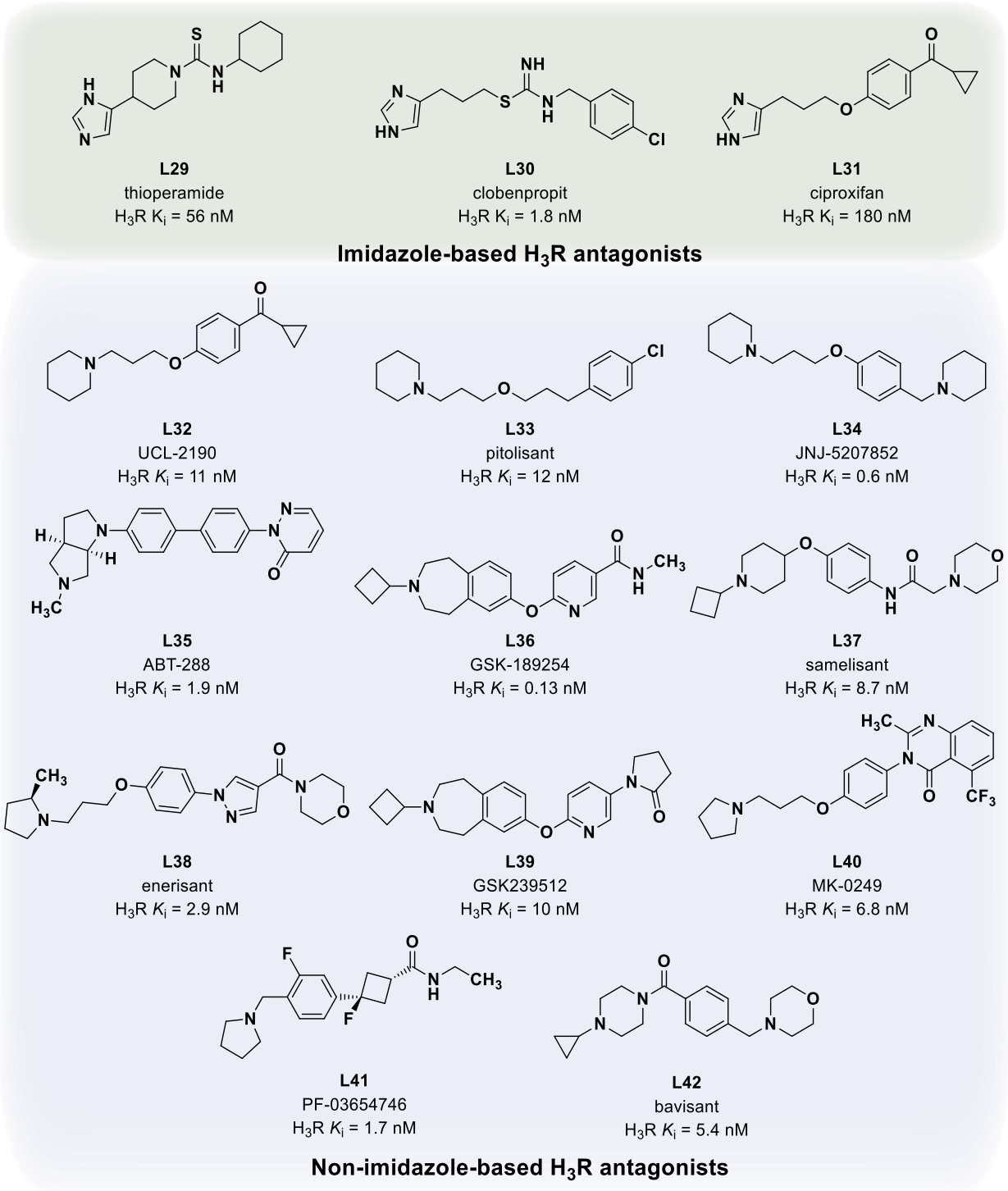

Figure 8. Selected representatives of imidazole- (**L29**-**L31**)[133] and non-imidazole-based H_3R antagonists H_3R (**L32**-**L42**).[143-151]

Imidazole-based ligands faced challenges like CYP450 inhibition and poor CNS penetration, prompting a shift to non-imidazoles.[5, 10] UCL-2190 (**L32**) was among the first compounds to replace the imidazole ring with a tertiary amine.[152] Pitolisant (**L33,** Wakix®)[152], the first FDA- and EMA-approved H_3R antagonist, is now used to treat narcolepsy and Parkinson's-

related excessive daytime sleepiness.[153, 154] Other diamine-based antagonists, such as JNJ-5207852 (**L34**), have also been explored for their wake-promoting effects.[155]

Several H_3R antagonists have progressed through clinical trials with mixed success. ABT-288 (**L35**) failed to demonstrate efficacy in mild-to-moderate AD[156] or cognitive impairment associated with SCH.[157] GSK-189254 (**L36**) showed promise in pain and narcolepsy models and as a PET tracer to directly assess H_3R occupancy by test compounds *in vivo* and in clinical settings[158-160], though results from a Phase I hyperalgesia study remain undisclosed.[161] Samelisant (**L37**) and enerisant (**L38**) recently completed Phase II trials for narcolepsy[162, 163], while GSK-239512 (**L39**) and MK-0249 (**L40**) failed to improve cognition in SCH.[164, 165] PF-03654746 (**L41**) was investigated in clinical trials for multiple therapeutic indications. This compound holds particular significance as it became the first H_3R ligand to have its bound complex with the receptor structurally characterized, with the H_3R-PF-03654746 complex being resolved by X-ray crystallography.[33, 134] Bavisant (**L42**) has been evaluated in ADHD trials across various age groups but has yet to demonstrate clear clinical efficacy.[33]

1.5.2 Pharmacophore Model of H_3R Ligands

The development of histamine H_3R ligands has led to a well-defined pharmacophore model through extensive structure-activity relationship (SAR) studies. Early efforts focused on imidazole-based scaffolds, which were initially considered essential for receptor binding affinity due to their structural resemblance to histamine.[166] However, these compounds exhibited significant limitations, including cross-species variability, lack of selectivity among histamine receptor subtypes, and undesirable inhibition of CYP450 enzymes, prompting the search for alternative chemotypes. A critical advance came with the replacement of the imidazole ring with cyclic amines such as piperidine or pyrrolidine, which retained high affinity while improving drug-like properties and selectivity.[144]

The modern H_3R pharmacophore model consists of three key regions (Figure 9).[144, 167] The first is an aminergic moiety, typically a protonatable tertiary cyclic amine (e.g., pyrrolidine, piperidine, or piperazine), which serves as the orthosteric anchor by forming an ionic interaction with the conserved Asp114 residue – a critical binding determinant.[168] This moiety effectively replaces the imidazole ring of early ligands while preserving essential interactions. The basic amine is linked via a flexible alkyl spacer, often incorporating polar functionalities, to a second region consisting of a central aromatic or heterocyclic core. This core engages in additional stabilizing interactions, particularly π-π stacking with aromatic residues in the binding pocket. The third region, referred to as the "arbitrary" or "eastern" region, tolerates

diverse structural modifications, including lipophilic groups, polar substituents, secondary basic moieties, or even acidic functionalities, which can enhance affinity or fine-tune functional activity. The flexibility of this region highlights the robustness of H_3R as a drug target and enables the design of multi-target directed ligands by incorporating structural motifs relevant to secondary targets.[167]

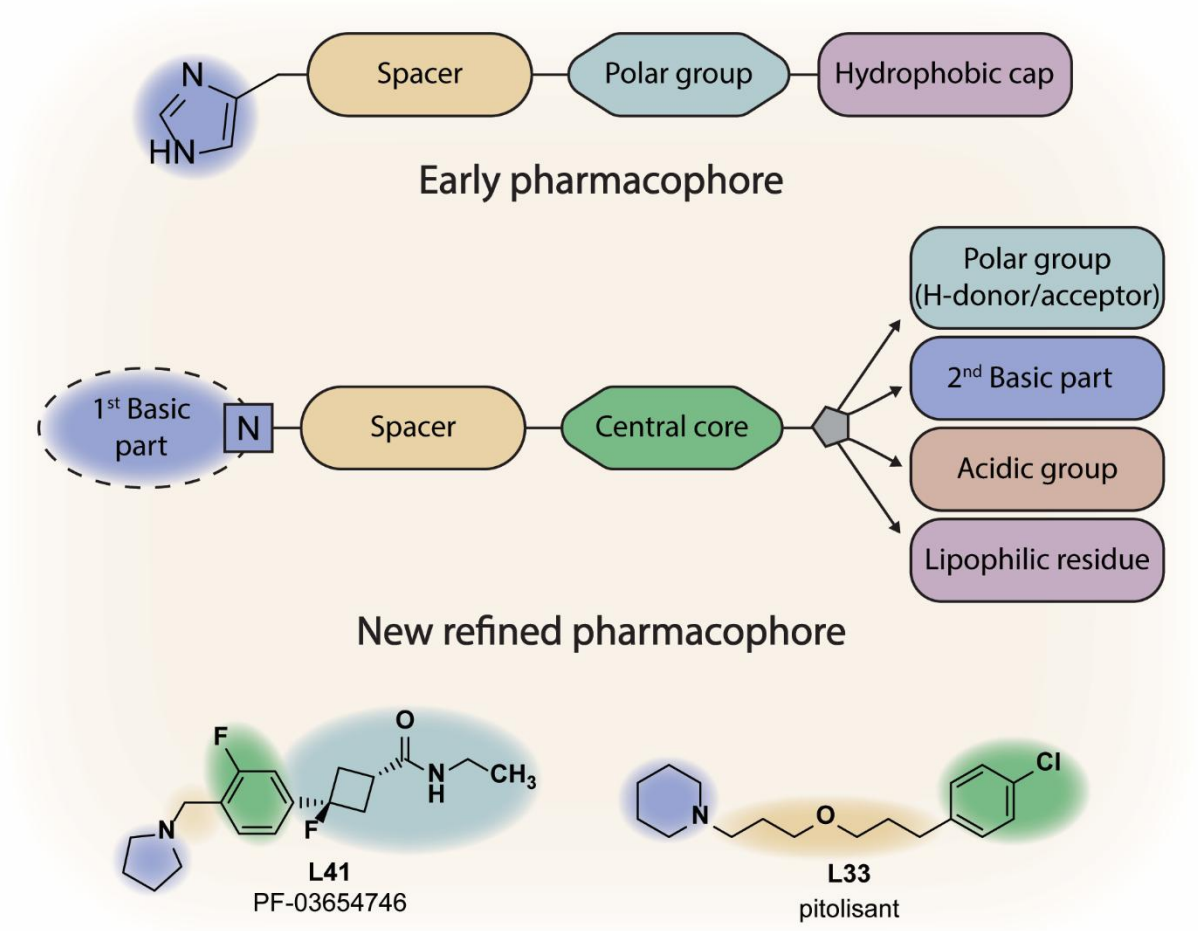

Figure 9. Histamine H_3R pharmacophore (Adopted from CELANIRE et al.[144]). The corresponding regions are highlighted on **L41**, the first ligand co-crystallized with H_3R, and **L33**, the first clinically approved H_3R ligand.

Historically, pharmacophore refinement relied on homology modelling based on related GPCR structures, mutational studies, and iterative SAR analysis.[169-171] However, the recent determination of the H_3R crystal structure bound to the non-imidazole antagonist PF-03654746 (**L41**) (2.6 Å resolution) has provided unprecedented insights into ligand-receptor interactions, validating earlier pharmacophore predictions while revealing new opportunities for rational design.[33] The ligand binds to a shallow extracellular orthosteric pocket formed by residues from TM helices 2, 3, 6, and 7, as well as ECL2, and extends into an extended binding pocket. Docking studies with nine additional H_3R ligands confirmed the critical role of the salt bridge

between the ligand's basic center and Asp114. Hydrophobic interactions between the heterocyclic core and residues Tyr115, Tyr374, Phe398, and Trp402 further stabilize binding, while the central region engages in hydrophobic contacts with Leu111, Trp110, and Phe193. Notably, the affinity of tested ligands correlated with the ability of the arbitrary region to form π-π stacking or OH/π hydrogen bonds with Tyr91, Tyr189, and other aromatic residues within the extended binding pocket.[33]

1.5.3 Role of H_3R Pathological Condition

The unique role of histamine H_3R as an auto- and heteroreceptor in CNS has attracted much research interest, especially as a pathophysiological component of neurodevelopmental and neuropsychiatric disorders. Brain histamine influence behaviour and play a role in neuropsychiatric disorders such as narcolepsy, AD, PD, SCH, ADHD, anxiety, autism spectrum disorder, Tourette syndrome and Prader-Willi syndrome (PWS), many of which share overlapping symptoms and pathophysiology.[172] Additionally, H_3R modulation shows promise in managing obesity through appetite regulation, epilepsy via seizure threshold modulation, and neuropathic pain by influencing nociceptive pathways.

Wakefulness

The clinical application of H_3R ligands has thus far been most successfully leveraged in the regulation of wakefulness. Histaminergic neurons project to key brain regions governing the sleep-wake cycle, including the cortex, thalamus, hypothalamus, and brainstem.[173] Wakefulness is directly mediated by the pacemaker-like firing activity of tuberomammillary nucleus (TMN) neurons, which exhibits a linear correlation with H_3R occupancy levels up to 80%.[174] Brain histaminergic neurons, alongside orexinergic neurons in the posterior hypothalamus, play complementary roles in maintaining the sleep-wake cycle. Histaminergic neurons within the TMN exhibit a distinctive "wake-selective" firing pattern, meaning they are predominantly active during wakefulness and virtually silent during sleep. These neurons demonstrate one of the most selective discharge patterns correlated with wakeful states among all neuronal populations in the CNS.[173]

Mechanistically, suppression of presynaptic H_3R constitutive activity enhances histamine release, activating postsynaptic H_1R to promote wakefulness and vigilance. Supporting this, chronic histamine depletion in mice caused by reduced HDC expression or conditional HDC knockout (KO) mice resulted in markedly decreased wakefulness and increased non-rapid eye movement (NREM) sleep.[175] Similarly, H_1R knockout mice and wild-type mice treated with

H_1R antagonists exhibited disrupted sleep architecture, including prolonged NREM sleep and reduced latency to NREM onset. In contrast, H_3R KO mice displayed heightened environmental and motivational arousal. Notably, H_1R antagonists exacerbated slow-wave sleep (SWS) in H_3R KO mice, further underscoring the interplay between histaminergic H_1R and H_3R signalling in sleep regulation.[176, 177]

These preclinical findings align with clinical observations, where H_3R antagonists and inverse agonists have demonstrated efficacy in improving excessive daytime sleepiness and cataplexy in narcolepsy patients.

Several H_3R antagonists and inverse agonists have shown promise in modulating sleep-wake disorders, with pitolisant (**L33**) standing out as the most clinically successful agent. Preclinical studies demonstrate the efficacy of these compounds in animal models of sleep disturbances. For instance, **L36** enhanced wakefulness and reduced both rapid-eye movement (REM) and slow-wave sleep (SWS) in orexin knockout mice, as measured by EEG and EMG recordings.[158] Similarly, **L37** decreased NREM sleep and episodes of direct REM sleep onset (DREM), exhibiting notable anti-cataplectic effects in the same model.[147] It also successfully completed Phase II clinical trial for the treatment of excessive daytime sleepiness in adult patients with narcolepsy and is on track to enter the Phase III study.[163] **L38** also promoted wakefulness by reducing SWS, though its effects were dose-dependent.[149] In spite of favourable pharmacokinetic profile, an optimal dose of **L38** could not be determined, as it showed large individual variabilities in terms of safety and efficacy in a Phase II study.[162]

Pitolisant (**L33**, Wakix®), a first-in-class clinically approved H_3R inverse agonist, represents a significant therapeutic advance. It enhances histaminergic neuronal activity, reduces abnormal transitions from wakefulness to REM sleep, and promotes sustained wakefulness in hypocretin-deficient mice. Approved in the EU in 2016 and the US in 2019 for narcolepsy with or without cataplexy, pitolisant has demonstrated comparable efficacy to modafinil in alleviating excessive daytime sleepiness. Clinical trials have confirmed its ability to improve wakefulness in narcolepsy patients, and ongoing studies continue to explore its potential in managing cataplexy and elucidating the broader role of histamine in sleep-wake regulation.[178, 179]

Cognitive impairments

Cognitive decline is a key feature of various neurological and psychiatric disorders, affecting memory, reasoning, attention, and executive function. Cognitive function relies not on single brain areas working in isolation, but on coordinated activity across interconnected cortical and subcortical networks working together as an integrated system.[180] While multiple

neurotransmitter systems contribute to cognitive processes, the histaminergic system has gained increasing attention for its role in modulating brain function. Among histamine receptors, H_3R plays a crucial role as both an autoreceptor and heteroreceptor, regulating the release of histamine and other neurotransmitters. Given its involvement in synaptic plasticity, wakefulness, and attention, dysregulation of H_3R has been implicated in cognitive impairments observed in neurodegenerative and neuropsychiatric diseases.

Alzheimer's disease is the most prevalent neurodegenerative disorder worldwide. Its hallmark features include the extracellular accumulation of insoluble amyloid-β protein (Aβ) that leads to progressive loss of neurons in CNS areas involved in memory and cognition. This neurodegeneration is accompanied by neurofibrillary tangles consisting primarily of hyperphosphorylated tau protein.[181] Among the brain regions affected by neurodegeneration is the TMN of the hypothalamus, resulting in lower histamine content in various brain regions including the hypothalamus, hippocampus, and temporal cortex, as evidenced by post-mortem analyses of AD patients' brains.[182-184] These alterations in the histaminergic system have been recognized to contribute significantly to cognitive impairments in AD patients.[180, 185] Preclinical investigations utilizing histamine receptor KO mouse models have consistently revealed that disruption of histaminergic signalling results in significant deficits in learning acquisition and memory consolidation.[186] The observed reduction in histamine concentrations within the brains of AD patients, coupled with diminished H_1R activity, has underscored the critical role of histaminergic neurotransmission in maintaining cognitive integrity. These findings have catalysed the development of histamine H_3R inverse agonists as promising therapeutic candidates for addressing cognitive dysfunction in AD.[187]

Parkinson's disease is the second most prevalent neurodegenerative disorder after AD. It is characterized by progressive dopaminergic neuronal loss in the substantia nigra and the intracellular accumulation of misfolded α-synuclein (α-Syn) protein aggregates, known as Lewy bodies.[188] The extensive histaminergic projections to the basal ganglia, coupled with abundant histamine receptor expression throughout the striatum, indicate histamine's involvement in motor control circuitry. This neuroanatomical relationship suggests that alterations in histaminergic neurotransmission may be implicated in the movement disorders characteristic of PD pathology.[189] Although histamine production in the TMN remains unchanged in PD patients compared to healthy controls, increased local release of histamine has been observed in the substantia nigra and putamen regions.[190] This altered histaminergic signalling may influence dopaminergic transmission and contribute to both motor and non-motor symptoms of PD. Excessive daytime sleepiness affects up to 20% of PD patients,

significantly impacting their quality of life.[191] Several case reports have documented successful treatment of narcolepsy comorbid with PD using pitolisant (**L33**), a selective histamine H_3R inverse agonist/antagonist. Importantly, these treatments did not exacerbate neurodegeneration, suggesting that modulating histaminergic transmission may represent a viable therapeutic approach for addressing sleep disturbances in PD without compromising neuronal integrity.[192]

Schizophrenia is a complex neuropsychiatric disorder traditionally associated with neurotransmitter imbalances, predominantly in the dopaminergic system. However, growing evidence suggests that dysregulation of the histaminergic system also contributes to several features of SCH. Notably, increased H_3R expression has been documented in the prefrontal cortex of SCH patients[193] Despite promising preclinical results with H_3R antagonists in ameliorating SCH-like symptoms in animal models[194, 195], these findings have not translated successfully to clinical applications. Several clinical trials with potent H_3R antagonists/inverse agonists have yielded disappointing outcomes. **L39** failed to demonstrate significant improvement in cognitive impairments in a Phase II clinical study.[164] **L35** not only lacked pro-cognitive effects but also increased the incidence of psychosis- and sleep-related adverse events.[157] **L40** similarly failed to demonstrate superiority over placebo in improving cognitive function in schizophrenia patients.[165]

Attention deficit hyperactivity disorder is a neurodevelopmental condition characterized by persistent patterns of inattention, hyperactivity, and impulsivity that interfere with functioning and development. The pathophysiology of ADHD involves dysregulation in dopaminergic and noradrenergic neurotransmission systems.[196] Given the modulatory role of H_3R on multiple neurotransmitter systems, H_3R antagonists emerged as potential therapeutic candidates. While preclinical studies demonstrated promising effects of H_3R antagonists on ADHD-like symptoms in animal models[197, 198], clinical translation has been disappointing. Notably, **L42**, a selective H_3R antagonist, failed to demonstrate efficacy in clinical trials involving adults with ADHD.[199]

Tourette's syndrome represents another neurodevelopmental disorder characterized by persistent motor and vocal tics – sudden, rapid, recurrent, nonrhythmic movements or vocalizations. The discovery of a rare mutation in the HDC gene in patients with Tourette's syndrome established a compelling link between histaminergic neurotransmission and this condition. This genetic evidence positioned H_3R antagonists as promising therapeutic candidates.[200, 201] However, a phase II study evaluating safety and efficacy of the H_3R antagonist **L41** in adults with Tourette's syndrome was terminated.[202]

Prader-Willi syndrome is a rare genetic disorder characterized by hypotonia, hyperphagia, obesity, excessive sleepiness and cognitive impairments. A recent case reports on the use of pitolisant (**L33**) in pediatric PWS patients that led not only to improvements in excessive daytime sleepiness, but also in cognition[203], inspired interest in epigenetic approaches that combine H_3R antagonism/inverse agonism with inhibitors of G9a methyltransferase with the aim of restoring expression of the candidate PWS genes on the maternally inherited chromosome[204]. This positive effects stimulated the initiation of Phase III clinical trial assessing efficacy and safety of **L33** in patients with PWS.[205]

1.6 Histamine H_4 Receptor

The histamine H_4R is the most recently identified member of the histamine receptor subfamily, discovered in the early 2000s through genomic database mining that leveraged its sequence homology with the previously cloned H_3R.[22, 24-27, 206] The gene encoding H_4R, consists of 3 exons and 2 large introns, is found on the long arm of chromosome 18 chromosome, locus 11.[23] The receptor protein exists in multiple molecular forms: the monomeric form has a molecular weight of 44-46 kDa, varying based on post-translational modifications, while the receptor also assembles into dimeric (85kDa) and oligomeric (>250 kDa) configurations.[25, 207] Structural understanding of H_4R advanced significantly in 2024 with the resolution of several high-resolution cryo-electron microscopy structures. These revealed key features of the receptor's ligand-binding pocket, activation mechanism, and G protein coupling interface, providing a crucial framework for rational ligand design and selective drug targeting.[32, 34]

The H_4R signal transduction cascade primarily operates through coupling with $G\alpha_{i/o}$ proteins, initiating multiple downstream signalling pathways. Upon receptor activation, the $G\alpha_{i/o}$ protein inhibits AC, resulting in decreased cAMP production and subsequent inhibition of downstream cellular events.[24, 26, 27, 206] The stimulation of H_4R also leads to the activation of MAPK pathways.[22] Additionally, the $G\beta\gamma$ subunit, released from the H_4R-$G\alpha_{i/o}$ complex following receptor engagement, triggers the PLC signalling cascade, culminating in IP_3-mediated elevation of intracellular calcium levels.[208, 209] The receptor's signalling repertoire extends to Janus kinase (JAK)/signal transducer and activator of transcription (STAT) pathway, which modulates tumour necrosis factor-α (TNF-α) and nuclear factor κB (NF-κB) activities.[210] Furthermore, H_4R activation induces the phosphorylation of ERK and PI3K, contributing to its diverse cellular effects.[211]

The H_4R exhibits a distinctive tissue distribution pattern that primarily encompasses cells of hematopoietic origin, with particularly high expression levels in mast cells, eosinophils, basophils, dendritic cells, T lymphocytes, and neutrophils.[207, 212-214] This distribution profile strongly indicates the receptor's crucial role in immune system regulation and inflammatory responses. Beyond immune cells, H_4R expression has been detected in various tissues including the spleen, thymus, small intestine, colon, heart, and skin.[24, 47, 215, 216] The activation of H_4R triggers multiple cellular responses, including chemotaxis of mast cells and eosinophils, modulation of cytokine and chemokine production, T cell differentiation, and dendritic cell activation.[217] These effects position the H_4R as a key mediator in various pathophysiological conditions, including allergic responses, pruritus, autoimmune disorders, and inflammatory diseases such as rheumatoid arthritis and asthma.[217, 218]

1.6.1 Overview of H_4R Ligands

Given the H_4R's significant role in immune regulation and inflammatory processes, considerable efforts have been devoted to developing selective ligands targeting this receptor. The structural and functional relationship between H_4R and H_3R has enabled the discovery of numerous dual-acting compounds, while also driving the development of highly selective H_4R modulators.

Numerous imidazole-containing ligands of the H_3R (Figure 8), such as (*R*)-α-methylhistamine (**L22**), imetit (**L25**), immepip (**L26**), and clobenpropit (**L30**), also exhibit H_4R agonists activity. Conversely, the H_3R neutral antagonist thioperamide (**L29**) acts as an inverse agonist at the H_4R.[26, 27, 38] Early H_4R agonists (Figure 10) included methylcyanoguanidine derivatives of tetrahydrofuranylimidazoles, such as OUP-16 (**L43**), though 4-methylhistamine (**L10**) remains the most selective agonist reported.[38, 219] Structural modifications of dimaprit led to VUF-8430 (**L44**), a full H_4R agonist with 30-fold H_3R selectivity.[220] The aminopyrimidine ST-1006 (**L45**) is among the most potent H_4R agonists (PEC50 = 8.95) identified to date.[221]

JNJ-7777120 (**L46**), a non-imidazole indole carboxamide, was the first selective H_4R antagonist and a key tool compound in preclinical studies.[222-227] However, its clinical advancement was hindered by suboptimal pharmacokinetic and pharmacodynamic properties.[228] Several other H_4R antagonists entered clinical trials for inflammatory and allergic conditions, including atopic dermatitis, pruritus, asthma, rheumatoid arthritis, and vestibular disorders. Toreforant (JNJ-38518168, **L47**), the first oral H_4R antagonist, progressed to Phase II trials for rheumatoid arthritis but was discontinued due to lack of efficacy.[229, 230] Similarly, Phase II trials in persistent eosinophilic asthma failed to demonstrate therapeutic

benefit[231, 232], while a trial for moderate-to-severe plaque psoriasis was completed without published results.[233] JNJ-39758979 (**L48**) reached Phase II trials for rheumatoid arthritis and uncontrolled asthma but was withdrawn due to safety concerns.[234, 235] In contrast, the oral H_4R antagonist adriforant (ZPL3893787, **L49**) showed promising efficacy in improving inflammatory skin lesions in atopic dermatitis with favourable safety in Phase II trials.[236] Selifornat (SENS-111, **L50**), tested for acute unilateral vestibulopathy, was safe and well-tolerated but did not meet its primary endpoint.[237] Another H_4R antagonist, izuforant (LEO 152020, **L51**), was evaluated in a Phase IIa trial for cholinergic urticaria but showed no significant improvement over placebo.[238] Despite extensive research, no H_4R ligands have yet achieved clinical approval.

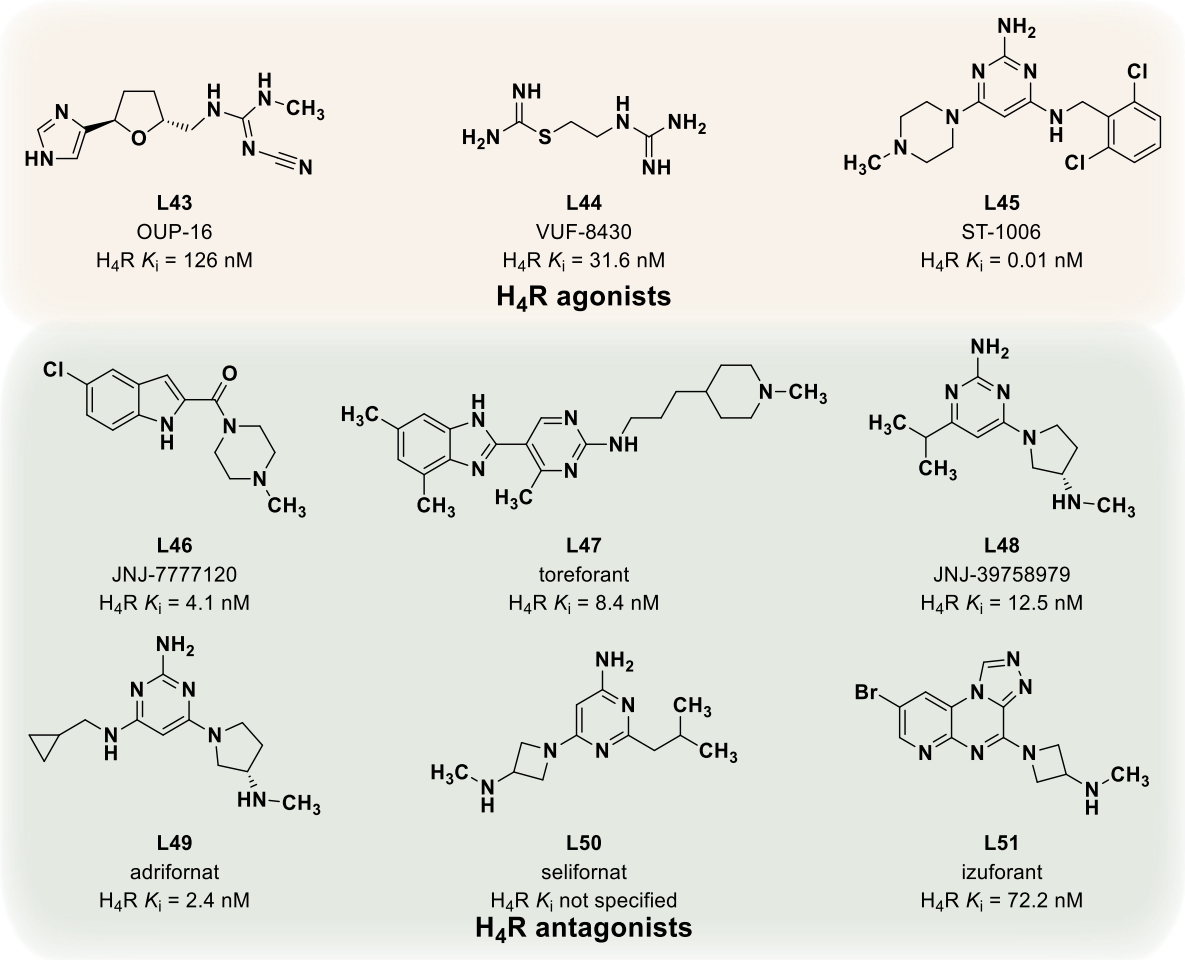

Figure 10. Selected representatives of H_4R agonists (**L43**-**L45**)[219, 239, 240] and antagonists (**L46**-**L51**).[222, 241-244]

1.7 Multi-target Directed Ligands

For over a century, drug development efforts have been dominated by highly selective drugs targeting single molecular pathways. This traditional "single-drug, single-target, single-disease" paradigm was reinforced by the correlation between adverse effects and unintended "off-target" interactions.[245] While this approach has yielded numerous successful therapeutics, the enhanced understanding of complex multifactorial diseases has challenged the efficacy of single-targeted interventions. Treatment protocols often require multiple single-targeted drugs affecting different mechanisms, whether combined in a single formulation or administered separately, which presents challenges in patient compliance and introduces complex pharmacokinetic and pharmacodynamic profiles.[246] The limitations of existing therapeutic options for multifactorial diseases, such as neurodegenerative[247-249] and psychiatric disorders[250-252], cancer[253-255], infectious diseases[256-258], metabolic and cardiovascular disease[259-261], have driven medicinal chemists to explore new strategies. This has led to the development of single-compound drugs capable of acting on multiple targets, introducing the concept of multi-target directed ligands (MTDLs) to the field.[246] MTDLs are specifically designed to address complex diseases by simultaneously modulating multiple targets involved in their pathogenesis.[262, 263]

The design of MTDLs encompasses two primary approaches: screening-based and knowledge-based methodologies.[262] Screening-based approaches involve the systematic evaluation of large compound libraries to identify candidates with potential activity on multiple targets. While effective, compounds identified through this method typically require optimization to achieve well-balanced affinity profiles across all targets of interest.[264] The knowledge-based approach leverages understanding of common pharmacophore elements to design multi-targeted compounds. Based on their molecular and pharmacophore architecture, MTDLs can be classified into three distinct categories: linked, fused, or merged structures (Figure 11).[262]

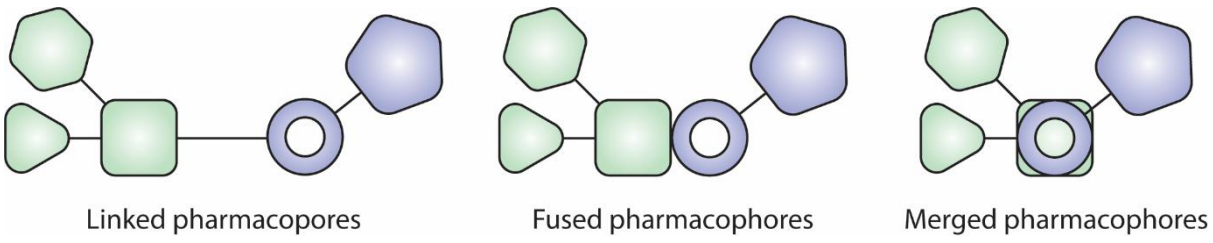

Figure 11. Design strategies of multi-target directed ligands.

The linking of pharmacophores through stable or biodegradable linkers represents the most straightforward strategy to combine multiple pharmacophores into a single molecular entity. While this approach allows minimal modifications to original pharmacophores, the resulting MTDLs are typically large molecules that often present challenging pharmacokinetic profiles.[265] The second class of MTDLs emerges from the direct fusion of two small bioactive molecules, eliminating the need for linkers.[262] Fused pharmacophores prove particularly advantageous when molecular targets share limited similarity, as this approach maintains the structural features responsible for activity on all targets while keeping the resulting molecule compact.[264] The most sophisticated MTDL design strategy involves merged pharmacophores.[262] In this approach, individual pharmacophore features are consolidated into a unified pharmacophore capable of acting on all targets of interest, with the prerequisite that the pharmacophores of molecular targets share structural commonalities.[265]

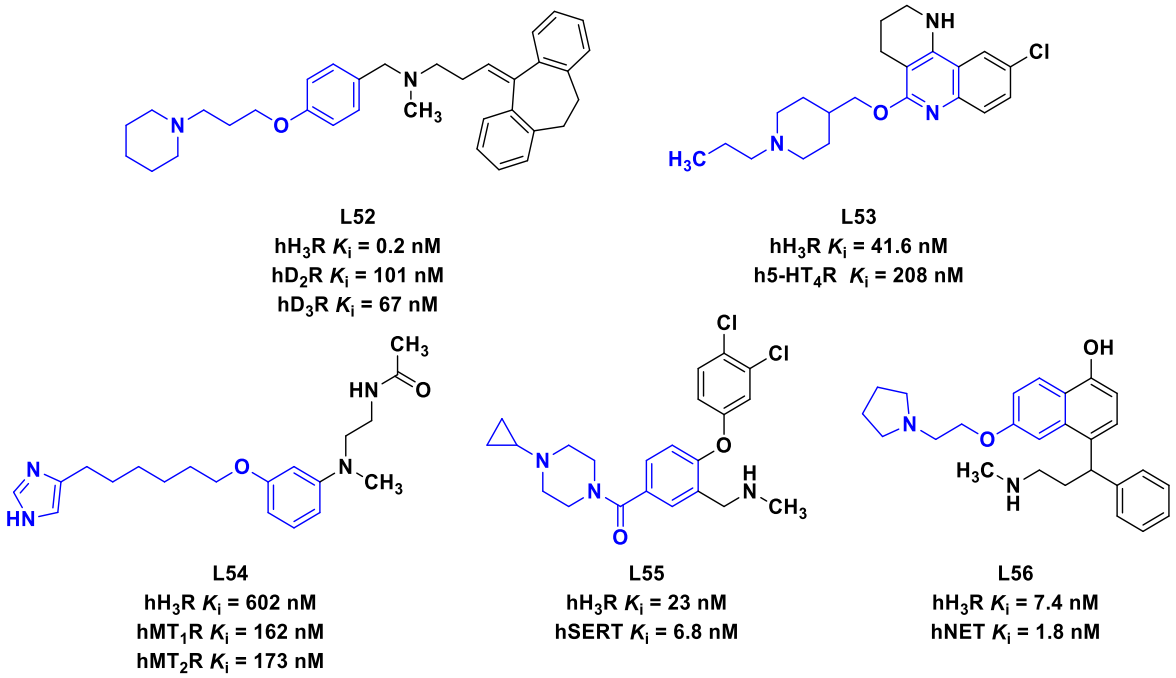

Figure 12. MTDLs designed by integrating the H_3R pharmacophore (highlighted in blue) with pharmacophore elements from other receptors (**L52**–**L54**) and transporters (**L55** and **L56**).

The regulatory role of H_3R on various neurotransmitters has driven numerous successful initiatives incorporating H_3R pharmacophore into MTDLs for treating neurodegenerative disorders. Research demonstrates successful integration of H_3R pharmacophore with pharmacophoric elements from diverse targets, including GPCRs, transporters, enzymes, and other disease-modifying components.[266] Notable examples include the fusion of H_3R ligand fragments with neuroleptics, creating multi-acting antipsychotic compounds that target H_3R,

D_2R, and D_3R simultaneously (**L52**, Figure 12).[267] Through screening-based approaches, researchers identified a ligand exhibiting high affinity for both H_3R and serotonin 4 receptor (5-HT_4R), showing promise in addressing AD symptoms (**L53**, Figure 12).[268] The combination of H_3R pharmacophore with melatonin structural elements has also yielded promising results, given the therapeutic potential of both compounds in cognitive and neurodegenerative disorders. This approach produced a ligand demonstrating submicromolar affinity for H_3R and melatonin receptors (MT_1R and MT_2R) (**L54**, Figure 12).[269] Beyond receptors, H_3R pharmacophore has been successfully combined in MTDLs targeting transporters such as serotonin reuptake transporter (SERT) (**L55**, Figure 12)[270] and norepinephrine transporter (NET) (**L56**, Figure 12).[271]

Prominent MTDL representatives incorporate neurotransmitter-catabolizing enzymes alongside H_3R as intended targets, strategically designed to increase neurotransmitter levels through both inverse agonism on H_3R and inhibition of neurotransmitter-inactivating enzymes. Consequentially, in addition to H_3R, some of the members act on HNMT (**L57**, Figure 13)[272], AChE and BChE (**L58**, Figure 13)[273], or even ChE and MAO (**L59**, Figure 13).[274]

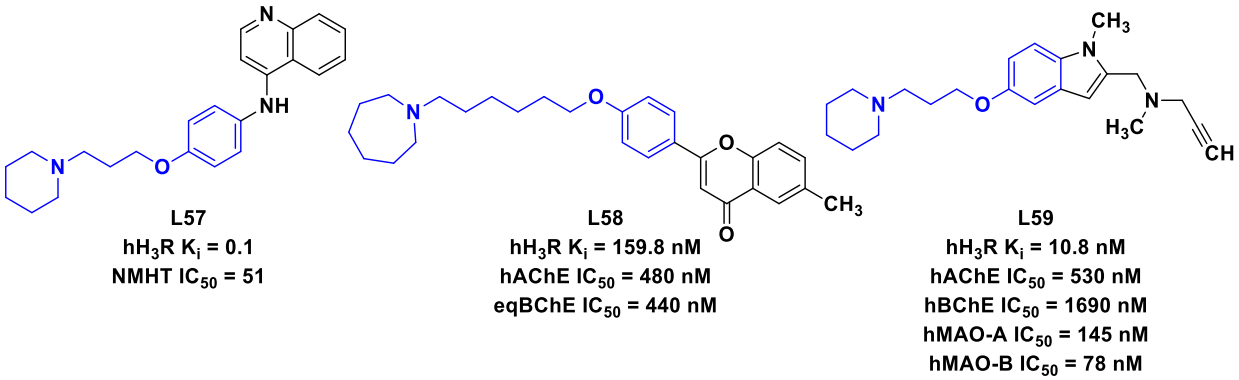

Figure 13. MTDLs designed by integrating the H_3R pharmacophore (highlighted in blue) with pharmacophore elements from enzymes (**L57**–**L59**).

Building on the promising outcomes of MTDLs incorporating H_3R pharmacophores – particularly in the treatment of neurodegenerative and psychiatric disorders – there is growing interest in expanding the multi-target approach to include epigenetic modulators. Given the complex interplay between neurotransmitter regulation and gene expression, integrating epigenetic targets such as the histone methyltransferase G9a offers a compelling strategy to further enhance therapeutic efficacy.

1.8 Epigenetic Regulation Through G9a Methyltransferase

Epigenetics is branch of genetics concerned with reversible environmental and heritable modifications in gene expression that occur without alterations to the underlying DNA nucleotide sequence.[275] Epigenetic mechanisms that regulate transcriptional activity include DNA methylation, which typically occurs at the 5-carbon of cytosine and is the only epigenetic modification that directly affects DNA, posttranslational modifications of nucleosomal histone proteins, and the activity of non-coding RNAs.[276]

The dynamic nature of epigenetic regulation relies on three main classes of proteins: writers, readers, and erasers. Writers catalyse the addition of chemical modifications, readers recognize and interpret these modifications, and erasers remove them, collectively enabling precise control of gene expression.[277]

Post-translational modifications transform histones into dynamic transcription regulators through a diverse repertoire of chemical alterations, including acetylation, methylation, phosphorylation, ubiquitination, SUMOylation, ADP-ribosylation, citrullination, glycosylation, hydroxylation, and isomerization.[278] The most prominent among them are acetylation and methylation. The acetylation status of histone proteins is dynamically controlled by two opposing enzyme families: the writer enzymes known as histone acetyltransferases (HATs), and the eraser enzymes called histone deacetylases (HDACs). Acetylation of lysine residues promotes transcriptionally active euchromatin, while deacetylation facilitates heterochromatin formation and gene silencing.[279] This reversible acetylation serves as a mechanism for regulating chromatin structure and gene expression.

Histone methylation represents an important class of epigenetic marks that can lead to either transcriptional activation or repression.[280] This process is catalysed by a class of writer enzymes known as histone methyltransferases (HMTs) and occurs on specific lysine (K) or arginine (R) residues. Accordingly, histone methyltransferases are categorized into two distinct groups: histone lysine methyltransferases (PKMTs) and protein arginine methyltransferases (PRMTs).[281] Lysine residues can be mono-, di- or trimethylated, while arginine residues can accommodate either one or two methyl groups.[282] PKMTs are further divided into two families: SET lysin methyltransferases[283], constituted of majority of PKMTs, and the 7 β-stranded methyltransferases, also known as class I family.[284]

The prominent SET-containing PKMT G9a (also designated as euchromatic histone-lysine *N*-methyltransferase 2 (EHMT2), lysine methyltransferase-1C (KMT1C), and HLA-B-associated transcript 8 (BAT8))[277], emerges as the strategic target for the MTDLs designed in this

doctoral thesis. G9a shares significant structural and functional homology with its paralog GLP (G9a-like protein, also known as EHMT1).[283] These enzymes form heterodimeric complexes *in vivo* and often work cooperatively in mediating H3K9 methylation, though they can also function independently.[285]

The G9a is encoded by a gene located on the short arm of chromosome 6 (6p21.33).[286] It exists in two isoforms: a full-length product comprising 1210 amino acids (isoform A) derived from 24 exons, and splice variant with 1176 amino acids (isoform B) emerging from excision of exon 10.[277] Seemingly, both isoforms share similar catalytic activity and ubiquitous tissue distribution, but vary in their relative ratio.[287, 288]

The functionality of G9a is determined by distinct structural domains (Figure 14). The SET domain (Su(var)3-9, Enhancer-of-zeste and Trithorax) represents the signature feature of both G9a and the entire PKMT family. This evolutionarily conserved domain, located at the C-terminal region, consists of β strands folded into three sheets forming a characteristic knot-like structure.[289] The SET domain executes methyltransferase activity and mediates protein-protein interactions.[286] Pre-SET and post-SET regions flank the catalytic core, providing structural stability and enabling substrate and cofactor binding.[290] Four zinc finger motifs, coordinated with cysteine residues from pre-SET and CRR domains, ensure proper protein folding and enzymatic activity.[281, 291] The ankyrin repeat domain functions as both a reader domain and binding module, specifically recognizing and binding mono- and dimethylated K9 residues.[292]

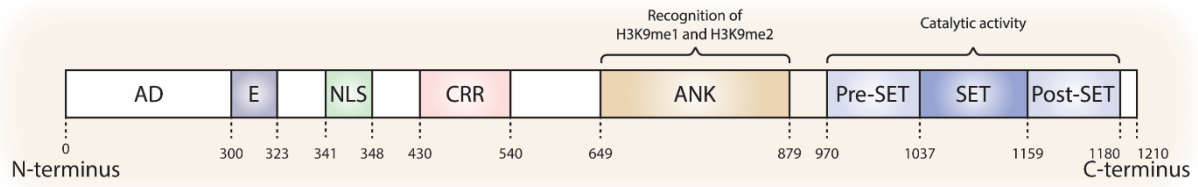

Figure 14. Schematic representation of G9a regions from N- to C-terminus: AD – activation domain, E – Glu-rich region, NLS – nuclear localization signal, CRR – Cys-rich region, ANK – ankyrin repeats region, and catalytic SET domain surrounded by Pre- and Post-SET regions.

G9a enzyme exhibits preferential methylation activity at the K9 residue on histone H3's N-terminal tail (Figure 15). The enzymatic reaction proceeds through the transfer of methyl groups from the cofactor S-adenosyl methionine (SAM) to the ε-amino group of the K9 residue. This results in either mono- or dimethylated products (H3K9me1 or H3K9me2), which are the predominant catalytic outcomes.[281, 292, 293] While trimethylation (H3K9me3) can occur, it is only detected after extended incubation periods and represents a minor product.[294]

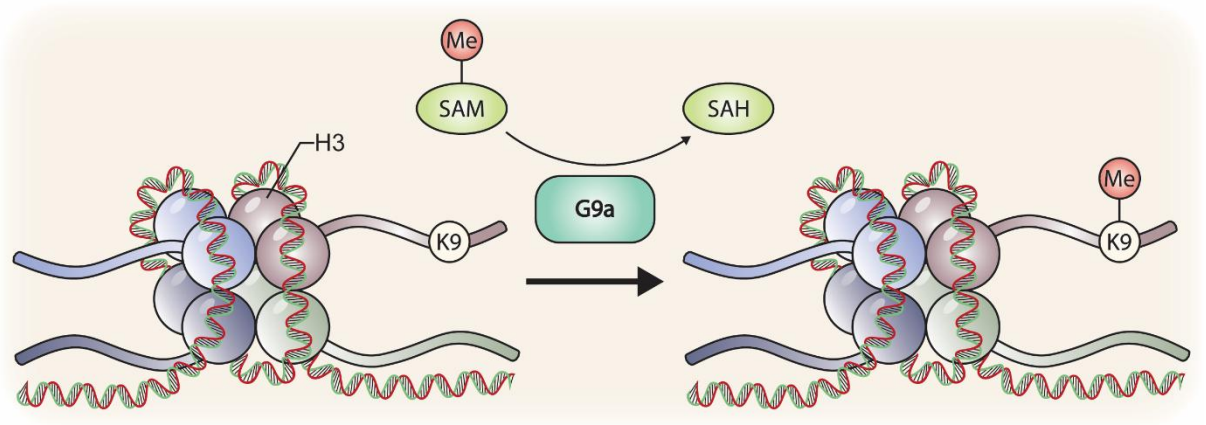

Figure 15. Schematic representation of G9a activity. The methyl group is transferred from S-adenosyl methionine (SAM) to K9 residue, producing S-adenosyl homocysteine (SAH) in the process.

Beyond its primary H3K9 methylation activity, G9a demonstrates broad substrate specificity across multiple targets. Within histones, G9a methylates additional lysine residues on H3 and other histone proteins, triggering distinct cellular responses (Table 2). The enzyme's versatility extends to non-histone substrates, where it methylates lysine residues in transcription factors, chromatin remodelling factors, and transcriptional coregulators.[277] This broad substrate recognition profile establishes G9a as a multifunctional methyltransferase in cellular regulation.

Table 2. Histone substrates of the G9a enzyme and the corresponding cellular effects of their methylation. Adopted from POULARD et al.[277]

Histone substrates	Sites	Cellular responses	References
Histone H3	H3K9	Transcriptional repression Heterochromatin formation	[295, 296]
Histone H3	H3K27	Transcriptional repression Heterochromatin formation	[296]
Histone H3	H3K56	DNA replication	[297]
Histone H1.2	H1.2K187	unknown	[298]
Histone H1.4	H1.4K26	Transcriptional repression Chromatin structure	[298, 299]

G9a's methylation imprint is primarily recognized by transcriptional repressors, establishing its key role in gene silencing.[300, 301] The ankyrin repeat domains specifically recognize H3K9 methylation marks and function as anchoring platforms for corepressor recruitment.[292] Interestingly, G9a exhibits dual functionality - while it primarily acts as a repressor, it can also serve as a coactivator when recruited to promoter or enhancer regions, thereby contributing to positive regulation of gene expression.[302-307]

1.8.1 Role of G9a in Selected Neurodegenerative Disorders

G9a methyltransferase has been extensively studied as a molecular target and disease modulator across diverse pathological conditions, demonstrating significant therapeutic potential in multiple cancers[285, 308, 309], autoimmune and inflammatory diseases[310, 311], as well as neuropsychiatric disorders.[281, 312] The convergence of G9a methyltransferase and histamine H_3R pathways in neuropsychiatric disorders represents a compelling area of investigation, as both molecular targets demonstrate significant involvement in cognitive function, arousal states, and memory formation. Their overlapping therapeutic indications, particularly in conditions such as AD, PD, SCH, and PWS, highlight the potential for innovative therapeutic approaches targeting both pathways simultaneously.

Elevated G9a levels in AD brain correlate with increased H3K9me2 methylation marks and higher Aβ concentration.[312, 313] Pharmacological inhibition of G9a demonstrates improvements in Aβ-induced deficits of long-term synaptic plasticity.[314] Studies on animal models of AD reveal a direct correlation between elevated G9a expression in the prefrontal cortex and reduced glutamate receptor transcription. Notably, G9a inhibition effectively reverses these methylation marks and restores glutamate receptor expression, leading to substantial improvements in recognition, working, and spatial memory.[313] Further studies using mouse models demonstrate that G9a inhibition results in significant reduction of Aβ plaques.[312, 315] Additionally, G9a inhibition shows effects in ameliorating neuroinflammation through modulation of glia maturation factor β and NF-κB signaling pathways.[312]

Studies demonstrate that α-Syn overexpression, a key molecular marker in PD, upregulates G9a mRNA expression, leading to elevated levels of the repressive histone modifications H3K9me1 and H3K9me2. Treatment with a G9a inhibitor effectively restored the expression of affected genes, including *SNAP25*, which facilitates synaptic vesicle trafficking.[316] In addition, G9a appears to contribute to PD pathophysiology through its effects on oxidative stress and neuroinflammation, known drivers of neurodegenerative disorders.[281]

Recent studies highlight the strong association between SCH and epigenetic modifications in genes essential for neurotransmission, neurodevelopment, and immune regulation.[317] Postmortem analysis of the parietal cortex from SCH patients revealed elevated G9a expression and corresponding increases in H3K9me2 repressive methylation marks.[318] Similar alterations were observed in peripheral blood mononuclear cells from SCH patients, which normalized following G9a inhibitor treatment.[319]

Prader-Willi syndrome is a neurodevelopmental disorder characterized by the absence of paternally expressed genes on chromosome 15, primarily due to deletion. While affected individuals carry functional genes on the maternally inherited chromosome, these genes remain epigenetically silenced.[320] G9a inhibitor treatment successfully reactivated PWS-associated genes on the maternal chromosome, both in patient-derived cells and PWS mouse models.[321] Recent investigations of the potent G9a inhibitor A-366 revealed its high affinity for H_3R, suggesting therapeutic potential through simultaneous G9a and H_3R targeting.[204] This dual-targeting approach is particularly promising given that the H_3R inverse agonist pitolisant (**L33**) improved cognitive function in PWS patients.[203]

1.8.2 Overview of G9a Inhibitors

In the nearly two decades since the discovery of the first G9a inhibitor, BIX-01294 (**L60**, Figure 16)[322], researchers have explored a diverse range of structural scaffolds in search of novel, efficacious, and safe G9a inhibitors. While quinazolines (**L60**-**L62**)[323, 324] and quinolines (**L63**)[325-327] dominate this space, the structural diversity extends to benzodiazepines (**L64**)[328], amino-indoles (**L65**)[329], and 2,4-diamino-6-methylpyrimidines (**L66** and **L67**)[293], among others. Based on their mechanism of action, G9a inhibitors can be classified into three distinct categories (Figure 16): substrate (protein) competitive (**L60**-**L67**), SAM cofactor competitive inhibitors (**L68** and **L69,** Figure 16), and Zn^{2+} ion ejectors (**L70**-**L72**).[330]

The first category comprises substrate (protein) competitive inhibitors (**L60**-**L67**), which directly bind to G9a's histone binding site, specifically targeting the substrate site while leaving the SAM binding pocket unaffected. The molecular structure of **L60** served as a crucial template for developing the highly selective and potent UNC series. While initial UNC compounds showed limited cellular potency due to pharmacokinetic constraints, subsequent optimization led to cell-active compounds like **L61** and **L62**. X-ray crystallography of the G9a-**L61** complex revealed that the (3-pyrrolidine-1-yl)propoxy side chain occupies a narrow lysine binding channel, significantly enhancing potency.[331, 332] This structural insight influenced subsequent designs (**L63**-**L67**), which retained this key fragment while exploring different core scaffolds.

The second category includes SAM cofactor competitive inhibitors (**L68** and **L69**), which bind to G9a's SAM-binding site, preventing SAM from providing methyl groups to G9a's substrates and thus blocking methyltransferase activity. However, they generally exhibit lower potency compared to substrate competitive inhibitors and face selectivity challenges due to high homology of SAM binding sites among methyltransferases.[328]

The third category consists of zinc ejectors including clinically used compounds such as disulfiram (**L70**), ebselen (**L71**), and cisplatin (**L72**), which inhibit G9a at low micromolar to submicromolar concentrations. While these compounds show lower potency and selectivity compared to the other two classes, they benefit from established clinical applications of some representatives.[291]

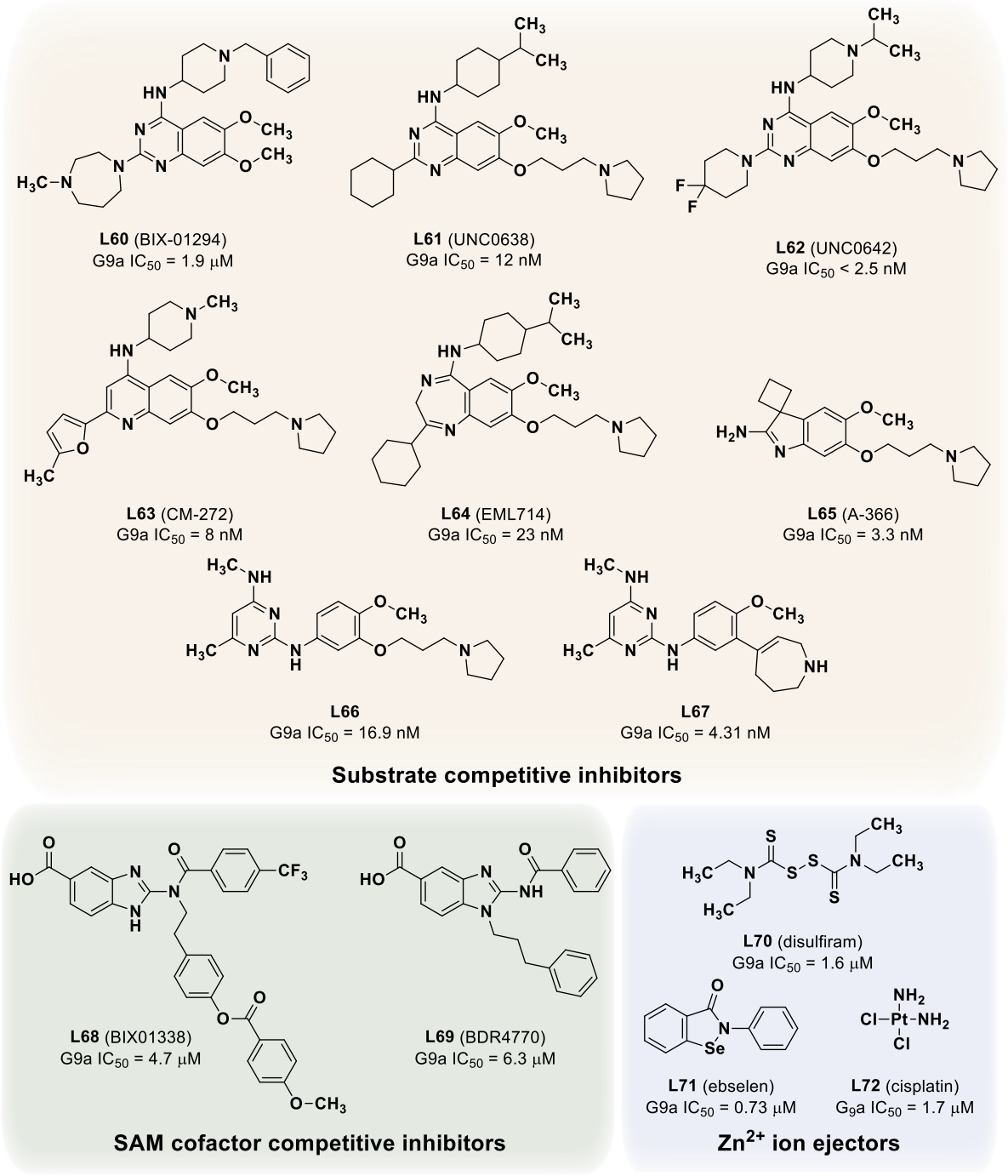

Figure 16. Selected representatives of G9a inhibitors (**L60**-**L72**) categorized by their mechanisms of action, along with their corresponding IC_{50} values.

Despite promising therapeutic potential, G9a inhibitors have faced challenges in pharmacokinetics and safety that have prevented their progression to clinical trials.[330, 333, 334] This situation presents both a challenge and an opportunity for continued drug development efforts to bring the first successful G9a inhibitor to market.

The exploration of G9a as a secondary target for H_3R-based MTDLs highlights the potential of addressing epigenetic mechanisms in neurodegeneration. However, the complex pathophysiology of neurodegenerative disorders extends beyond chromatin modifications to encompass multiple cellular pathways and regulatory mechanisms. Leucine-rich repeat kinase 2 (LRRK2) emerges as a particularly compelling target for integration with H_3R modulation, given its prominent role in neurodegeneration and its involvement in cellular processes that complement histaminergic neurotransmission.

1.9 Leucine-rich Repeat Kinase 2

Leucine-rich repeat kinase 2 (LRRK2) is a multifunctional member of the ROCO protein family that combines the defining ROCO family GTPase activity with serine-threonine kinase function.[335, 336] Identified in 2004, LRRK2 has since become the most frequently associated causative gene in both familial and sporadic cases of PD.[337, 338] This large protein consists of 2527 amino acids encoded by 51 exons of the *LRRK2* gene, located on chromosome 12.[337-339] The LRRK2 enzyme exhibits a complex architecture with seven distinct domains arranged sequentially (Figure 17): the N-terminal armadillo repeat region (ARM), ankyrin-like domain (ANK), leucin-rich repeat (LRR), Ras of complex (ROC) GTPase domain, C-terminal of ROC (COR) domain, kinase (KIN) domain and Trp-Asp-40 (WD40) domain at the C-terminus.[340, 341] The ROC-COR and kinase domains form the catalytic core responsible for enzymatic activities, while the ARM, ANK, LRR, and WD40 domains mediate protein-protein interactions.[342]

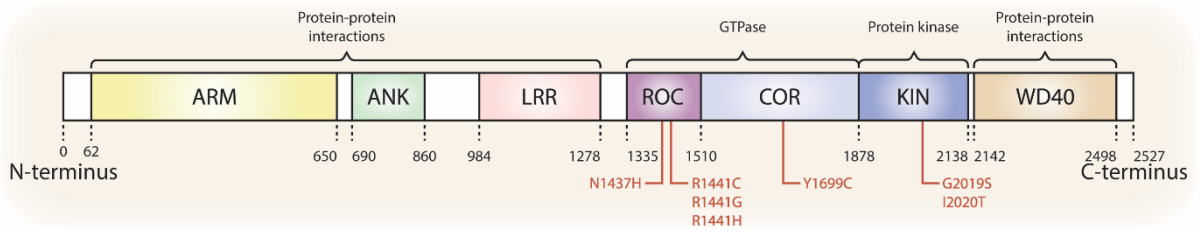

Figure 17. Domain architecture of LRRK2 protein showing the sequential arrangement from N- to C-terminus. Key functional domains are illustrated with their established roles, highlighting predominant pathogenic mutations within the catalytic core regions.

LRRK2, a key player in PD pathology, exhibits distinct expression patterns across neural tissues, with notable presence in the cerebral cortex, hippocampus, and substantia nigra pars compacta.[343-345] While neurons are its primary site of expression, LRRK2 also functions in glial cells, particularly astrocytes and microglia, where it modulates neuroinflammatory responses.[346] Beyond the nervous system, LRRK2's presence in liver, lungs, kidneys, heart, and immune cells points to its fundamental role in cellular homeostasis across multiple tissues.[346-348] At the molecular level, LRRK2 undergoes sophisticated regulation through dynamic cycling between monomeric and dimeric states (Figure 18, **A**-**F**). The protein predominantly exists as a GTP-bound inactive monomer, stabilized through direct interaction with the 14-3-3 adaptor protein (**A**). This crucial protein-protein interaction is precisely controlled by the phosphorylation status of two regulatory residues - Ser910 and Ser935 - positioned between the ANK and LRR domains of LRRK2. While phosphorylation promotes stable complex formation, dephosphorylation triggers complex dissociation.[349] The activation cycle of LRRK2 involves specific Rab GTPases, like Rab29, which guide monomeric LRRK2 to distinct membrane compartments (**B**).[350] Upon membrane recruitment, GTP hydrolysis drives the accumulation of GDP-bound LRRK2 monomers (**C**). The local concentration of these GDP-bound monomers facilitates dimerization, leading to enhanced kinase activity (**D**).[351] The activated kinase then phosphorylates a specific subset of 14 Rab proteins, with Rab8A, Rab10, and Rab29 being key targets in vesicular transport regulation (**E**).[352, 353] The dimeric LRRK2's low GDP affinity promotes GTP exchange, triggering monomerization and subsequent cytosolic redistribution, thus completing the regulatory cycle (**F**).[354]

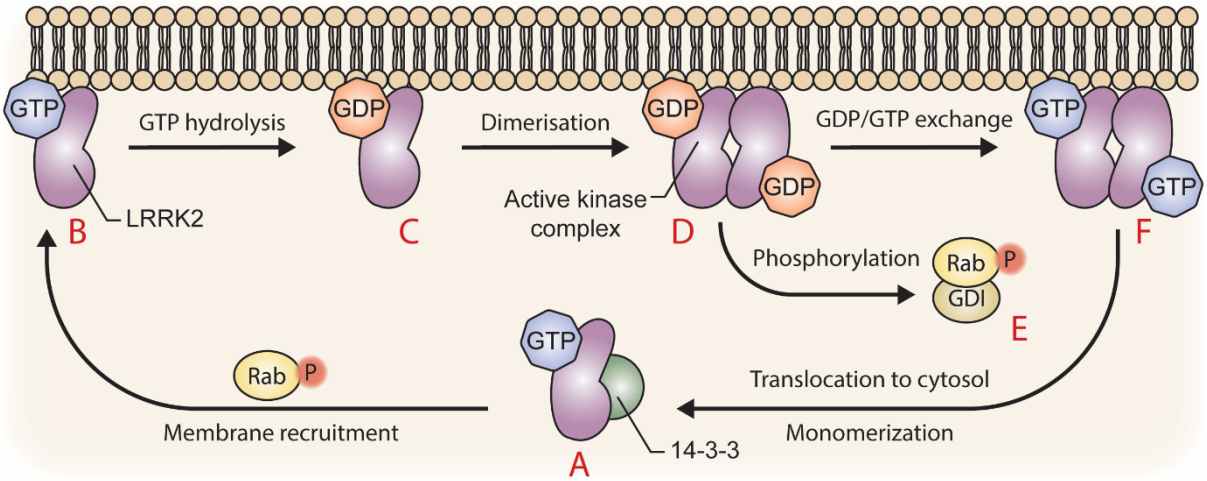

Figure 18. Dynamic regulation of LRRK2 through monomer-dimer cycling and membrane recruitment. GDI – GTP dissociation inhibitors.

LRRK2 kinase regulates multiple cellular processes through phosphorylation of diverse substrates, affecting cytoskeletal dynamics, protein expression, synaptic function, and membrane trafficking.[355]

1.9.1 Role of LRRK2 Enzyme in Parkinson's Disease

Point mutations in the LRRK2 gene represent the most common genetic cause of familial, autosomal-dominant PD and constitute a significant risk factor for sporadic PD.[356, 357] Of the numerous mutations identified, seven pathogenic variants are definitively associated with PD (Figure 17): N1437H and R1441C/G/H variants in the ROC domain, Y1699C in the COR domain, and G2019S and I2020T in the kinase domain.[358] These mutations cluster within the catalytic core (ROC-COR-kinase domains), disrupting enzymatic functions. The G2019S variant, found in 3 – 19% of familial and 1 – 6% of sporadic PD cases[359], increases kinase activity 2- to 3-fold via structural destabilization of the activation loop, promoting excessive substrate phosphorylation.[360, 361] In contrast, the I2020T mutation exhibits conflicting effects: *in vitro* studies report elevated autophosphorylation but reduced phosphorylation of substrates like Rab GTPases, suggesting mutation-specific substrate preferences or regulatory crosstalk between GTPase and kinase domains.[361, 362] R1441C/G/H and Y1699C mutations impair GTP hydrolysis, stabilizing LRRK2 in its active GTP-bound state and indirectly elevating kinase activity.[363] Collectively, pathogenic mutations drive LRRK2 kinase hyperactivation, resulting in aberrant phosphorylation of physiological substrates and downstream cellular dysfunction.[364]

In PD, pathological alterations stemming from LRRK2 activity manifest in vesicle trafficking, neurotransmitter release, cytoskeleton dynamics, autophagy, lysosomal/mitochondrial functions, and immune/microglial response.[341] LRRK2 exacerbates α-Syn neurotoxicity through kinase-dependent effects on α-Syn aggregation and clearance. While kinase inhibition reverses neurotoxicity in G2019S transgenic models, it fails in non-transgenic models, implying that LRRK2 hyperactivation may not be central to α-Syn toxicity in idiopathic PD.[365] Additionally, LRRK2 disrupts synaptic vesicle endocytosis by impairing interactions between synaptic proteins via hyperphosphorylation[366], leading to altered dopamine metabolism and accumulation of oxidized dopamine species with pathogenic effects.[367] LRRK2 also regulates neuroinflammation by modulating calcineurin pathways, activating AGE-RAGE/NF-κB signalling, and controlling microglial responses.[368] Beyond inflammation, LRRK2 affects mutations like G2019S impair α-Syn clearance in astrocytes and microglia[369, 370] and compromise cellular stress responses by disrupting autophagy and oxidative stress

management, contributing to neurodegeneration via glial dysfunction.[371] Mitochondrial and endoplasmic reticulum dysfunction in PD are further exacerbated by LRRK2's disruption of calcium homeostasis and mitochondrial lifecycle regulation. Mutations such as G2019S, Y1699C, and R1441C worsen mitochondrial/endoplasmic reticulum Ca^{2+} imbalance, while G2019S and R1441G inhibit mitophagy.[372-375] The enzymatic core of LRRK2 alone reduces mitochondrial biogenesis.[376] Rab GTPases are central to LRRK2-associated PD pathology: Rab5 and Rab35 contribute to α-Syn toxicity via defective endosomal formation[369, 377], Rab5/7/10 disrupt clathrin-mediated endocytosis[378], and Rab10/29 drive lysosomal stress and autolysosome defects.[379, 380]

1.9.2 Overview of LRRK2 Inhibitors

The understanding of LRRK2's role in PD pathology established LRRK2 enzyme as a valuable therapeutic target. Research efforts focused on developing small molecule inhibitors with optimal potency, selectivity, and pharmacokinetic profiles. The search for effective LRRK2 inhibitors began by screening kinase inhibitors from cancer research, leading to the identification of several non-selective kinase inhibitors (Figure 19), including staurosporine (**L73**)[381] and sunitinib (**L74**)[382]. These pan-kinase inhibitors demonstrated limited potency and insufficient BBB permeability.[383, 384]

Screening kinase inhibitor libraries led to the discovery of the first LRRK2 inhibitors with enhanced selectivity (Figure 19). These compounds featured a diaminopyrimidine scaffold, with LRRK2-IN-2 (**L75**) showing potency against both wild type and G2019S-LRRK2 while inhibiting only 12 out of 440 tested kinases.[385] Despite its improved selectivity, **L75** exhibited poor BBB permeability and was later associated with significant off-target effects in inflammatory pathways.[386] Similarly, CZC-25145 (**L76**) displayed comparable potency and selectivity but also suffered from inadequate BBB permeability.[387] The related compound TEA684 (**L77**) achieved BBB penetration but at the cost of reduced kinase selectivity.[388]

Optimization of this scaffold led to HG-10-102-01 (**L78**), which combined improved potency and selectivity. Molecular modelling studies revealed that small substituents on the phenyl ring, such as methoxy groups, were critical for enhancing kinase selectivity.[389] Notably, **L78** became the first LRRK2 inhibitor to demonstrate efficacy in the mouse brain following intraperitoneal administration.[390] Subsequent structural modifications of **L78** yielded GNE-7915 (**L79**), which incorporated a C-5 trifluoromethyl group to enhance potency and pharmacokinetic properties, a fluorine atom at the C-2 position of the phenyl ring to improve selectivity, and a C-4 aminoethyl substitution to prevent *N*-demethylation metabolism.[384, 391]

Further innovation through bioisosteric replacement of the aniline moiety with aminopyrazole led to a novel series of potent LRRK2 inhibitors.[392] Among these, GNE-0877 (**L80**) emerged as a standout candidate, maintaining high selectivity, potency, and favourable pharmacokinetic properties while addressing residual challenges such as undesirable CYP enzyme inhibition and induction.[393]

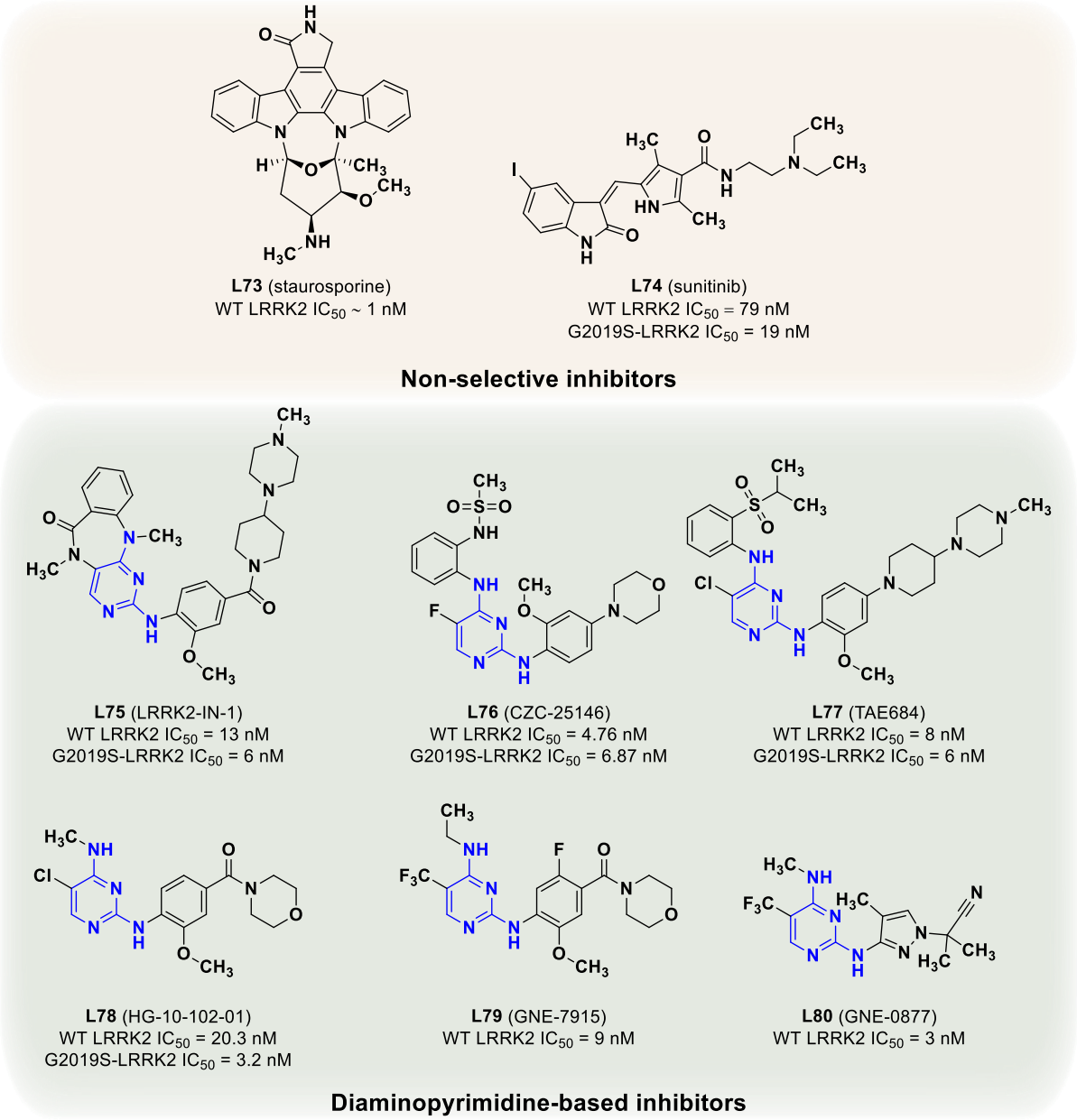

Figure 19. Chosen representatives of non-selective (**L73** and **L74**) and diaminopyrimidine based LRRK2 inhibitors (**L75-L80**).

The significant focus on diaminopyrimidine-based inhibitors reflects their historical importance in LRRK2 drug discovery. These compounds were among the first to demonstrate potent and selective LRRK2 inhibition, paving the way for extensive optimization efforts and

serving as foundational tools for understanding LRRK2 biology. While diaminopyrimidines remain valuable scaffold, the landscape of LRRK2-targeting therapies has expanded to include diverse modalities. Beyond diaminopyrimidines, researchers have successfully developed LRRK2 inhibitors incorporating diverse heterocyclic scaffolds (Figure 20). Notable examples include N-arylbenzamides (**L81**)[394], pyrrolopyrimidines (**L82**)[395], [1,2,4]triazolo[4,3-*b*]pyridazines (**L83**)[396], indolinones (**L84**)[397], quinolines (**L85**)[398], indazoles (**L86**)[399] and aminoquinazolines (**L87**)[400]. The representative compounds depicted in Figure 20 serve to highlight the diverse chemical space of LRRK2 inhibitors. These structures are the result of extensive optimization efforts, guided by advances in molecular modelling and enriched by SAR analyses. Key optimization criteria included improvements in potency, selectivity, and pharmacokinetic properties, as evidenced by studies detailed in references.[342, 348, 384, 401, 402]

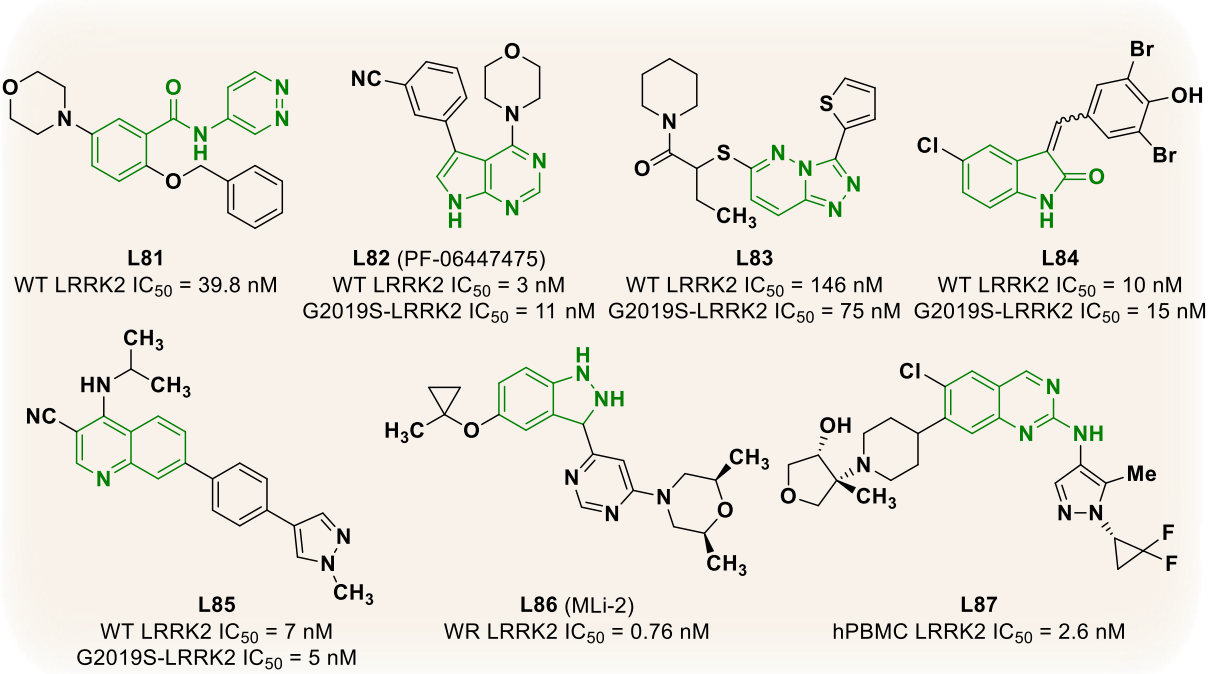

Figure 20. Selected representatives illustrating diverse chemical scaffolds utilized in LRRK2 inhibitors (**L81**-**L87**).

Compounds **L73**-**L87** belong to the type I class of ATP-competitive LRRK2 inhibitors, which bind to the kinase in its closed, active conformation. In contrast, type II inhibitors, which are less prevalent, stabilize the kinase in an open, inactive conformation.[403] Beyond ATP-competitive inhibition, alternative strategies to modulate LRRK2 function have been investigated.[401] These include GTP-binding inhibitors that prevent LRRK2 dimerization and subsequent kinase activation[404], proteolysis targeting chimeras (PROTACs) designed for

LRRK2 degradation[405], and antisense oligonucleotides that reduce LRRK2 protein expression.[406]

To date, five LRRK2-targeting compounds have advanced to clinical trials for the treatment of PD (Table 3). Among these, four are small-molecule kinase inhibitors, DNL201, DNL151, WXWH0226, and NEU-723, while BIIB-094 represents an antisense oligonucleotide approach. DNL201, also known as GNE-0877 (**L80**), is the only clinical candidate with a disclosed structure. It successfully completed Phase I trials, however, Denali Therapeutics Inc. (San Francisco, CA) strategically shifted its focus to DNL151. While DNL151's Phase III trial concluded due to a sponsor decision, two Phase II trials are currently recruiting participants. Among the remaining compounds, WXWH0226 is in the recruitment status of Phase I, while NEU-723 had its Phase I trial terminated as a business decision. BIIB-094 successfully completed Phase I, though the results have yet to be published.

Table 3. LRRK2-targeting compounds in clinical trials for Parkinson's disease treatment.

Substrate	Clinical trial	Status[a]
DNL201	Phase I	Completed[407, 408]
DNL151/BIIB22	Phase II Phase III	Recruiting[409, 410] Terminated[411]
WXWH0226	Phase I	Recruiting
NEU-723	Phase I	Terminated[412]
BIIB-094	Phase I	Completed[413]

[a] Sourced from https://clinicaltrials.gov and http://www.chinadrugtrials.org.cn (February 2025)

2 Objectives

The primary aim of this doctoral research is to advance the development of histamine H_3R ligands, encompassing both single-target and multi-functional profiles, through a systematic approach of rational design, synthesis, and biological evaluation. Building on the success of pitolisant (**L33**), the first clinically approved H_3R antagonist/inverse agonist for narcolepsy, this work explores H_3R-targeted drug discovery through two parallel approaches. The research encompasses the development of H_3R ligands as single-target compounds, alongside dual-targeting compounds that simultaneously modulate H_3R alongside either the epigenetic regulator G9a or the kinase LRRK2. These dual-targeting ligands aim to address the limitations of current mono-target therapies, particularly in complex neurological and neuropsychiatric disorders where synergies between neurotransmitter regulation via H_3R and complementary pathways may yield superior therapeutic outcomes.

The design strategy integrates structural insights from established H_3R pharmacophore models (Figure 9) with observed overlaps in scaffold similarity between H_3R ligands and inhibitors of G9a (Figure 16) or LRRK2 (Figure 19). All synthesized compounds incorporate an aminopyrimidine core – specifically pyrimidin-2-amine, pyrimidin-4-amine, or pyrimidine-2,4-diamine derivatives – as a unifying structural motif, enabling systematic exploration of substituent effects on target engagement. These experimental efforts are complemented by molecular docking simulations utilizing the recently resolved H_3R X-ray crystallographic structure to analyse ligand-receptor interactions and gain insight into structure-activity relationships.

The synthesis phase focuses on developing efficient and scalable routes to produce the target compounds. Subsequent biological evaluation involves *in vitro* assessment of H_3R binding affinities, as the primary target of interest. The multifunctional potential of selected ligands is explored through their ability to interact and inhibit their secondary intended target, either G9a or LRRK2 enzymes. The research includes preliminary pharmacokinetic assessment, focusing on lipophilicity and cytotoxicity, to evaluate lead compounds with high likelihood of BBB penetration and optimal safety profiles.

The H_3R represents a pivotal therapeutic target due to its regulatory role in neurotransmitter release and its involvement in diverse physiological processes, including wakefulness, cognition, and mood. While H_3R modulation primarily addresses symptomatic manifestations of neurological disorders through neurotransmitter regulation, the underlying disease pathology often requires intervention at causal molecular levels. Neurological disorders such

as PD, which involves LRRK2 dysregulation, or cognitive impairments like PWS, linked to G9a-mediated epigenetic silencing, exemplify conditions that require interventions beyond single-target modulation. G9a and LRRK2 represent causal targets that address fundamental disease mechanisms – epigenetic dysregulation and aberrant kinase signalling, respectively – rather than merely managing symptoms. This strategic combination leverages the immediate symptomatic benefits of H_3R antagonism while simultaneously addressing disease progression through modulation of causal pathways, potentially offering both short-term symptomatic improvement and long-term disease modification within a single therapeutic entity. By designing ligands that concurrently engage H_3R and either G9a or LRRK2, this research addresses the multifactorial nature of such diseases, potentially enhancing therapeutic efficacy while circumventing polypharmacy risks.

The clinical success of pitolisant has established H_3R ligands as a valuable therapeutic strategy, creating opportunities to expand their utility through targeted polypharmacology. Building on this foundation, this project explores the integration of complementary mechanisms by incorporating G9a and LRRK2 as secondary targets to address complex, multifactorial neuropsychiatric and neurodegenerative diseases. G9a inhibitors show promise in rescuing synaptic plasticity deficits, while LRRK2 inhibition demonstrates neuroprotective effects in PD models. By exploiting structural overlaps between these targets and H_3R, the project aims to develop first-in-class dual ligands with tailored polypharmacology. The outcomes of this work have the potential to inspire the development of next-generation therapies, offering improved efficacy, reduced side effects, and novel mechanisms to address multifaceted pathologies. Ultimately, this project aligns with the growing emphasis on precision medicine and multi-target approaches in neuropharmacology, positioning H_3R ligands as versatile tools in the evolving landscape of CNS drug discovery.

3 Chemistry

3.1 H_3R Pharmacophore-bearing Building Blocks

A well-researched H_3R pharmacophore typically comprises a basic center, often represented by cyclic aliphatic amines, connected to an aromatic center through an alkyl linker (Figure 9).[267, 274, 414-417] Following this pharmacophoric blueprint, the synthesis began with aliphatic fragments **P1**-**P3** that incorporated the essential pharmacophoric elements: a basic center connected by an alkyl linker (Scheme 1). The initial step involved a FINKELSTEIN S_N2 reaction between 3-chloropropan-1-ol and piperidine[418, 419], where *in situ* generation of the more reactive iodide intermediate facilitated nucleophilic substitution, yielding alcohol **P1**.[143, 152, 417, 420] Chlorination of **P1** with thionyl chloride produced **P2**.[417, 420] A second reaction converted **P2** to a carbamimidothioate intermediate, which underwent alkaline hydrolysis with aqueous sodium hydroxide to furnish thiol **P3**.[421] The complete H_3R pharmacophore was then constructed by coupling these aliphatic fragments to selected aromatic cores.

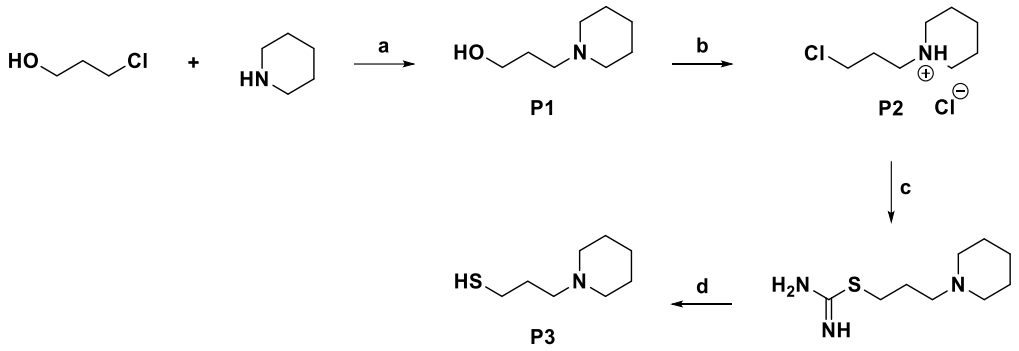

Scheme 1. Synthesis of precursors **P1-P3**. Reagents and conditions: a) K_2CO_3, KI, acetone, reflux 24 h; b) $SOCl_2$, THF, 65 °C for 3 h; c) thiourea, KI, ethanol, reflux 24 h; d) $NaOH_{(aq)}$, reflux 3 h.

A series of precursors (**P4**-**P11**) was synthesized following Scheme 2, based on the established pharmacophoric blueprint. The synthetic pathway was initiated with a WILLIAMSON ether synthesis[422] proceeding through an S_N2 mechanism, where an anion displaces a halide to form an ether (Scheme 2).[423] Precursor **P4** was synthesized following literature procedures[424, 425], where p-nitrophenol displaced bromide from 1-bromo-3-chloropropane to yield **P4**. While 1,3-dibromopropane could provide a superior leaving group for subsequent amine alkylation, 1-bromo-3-chloropropane was selected for its cost-effectiveness and favourable work-up characteristics due to its lower boiling point. Precursors **P5**-**P7**[425] were synthesized under FINKELSTEIN conditions[418, 419], enabling chloride-to-iodide transhalogenation before

reaction with the respective cyclic amines (1-methylpiperazine, 1-acetylpiperazine, and piperidine for **P5**, **P6**, and **P7**). While 2-methoxy-4-nitrophenol and 2-methoxy-5-nitrophenol were commercially sourced, 3-methoxy-4-nitrophenol (**P8**) was prepared from 4-fluoro-2-methoxy-1-nitrobenzene *via* nucleophilic aromatic substitution (S_NAr) (Scheme 2).[426] The methoxynitrophenol derivatives then underwent WILLIAMSON ether synthesis with 1-(3-chloropropyl)piperidine hydrochloride (**P2**), containing the H_3R pharmacophore fragment, yielding precursors **P9**-**P11**.[326, 427]

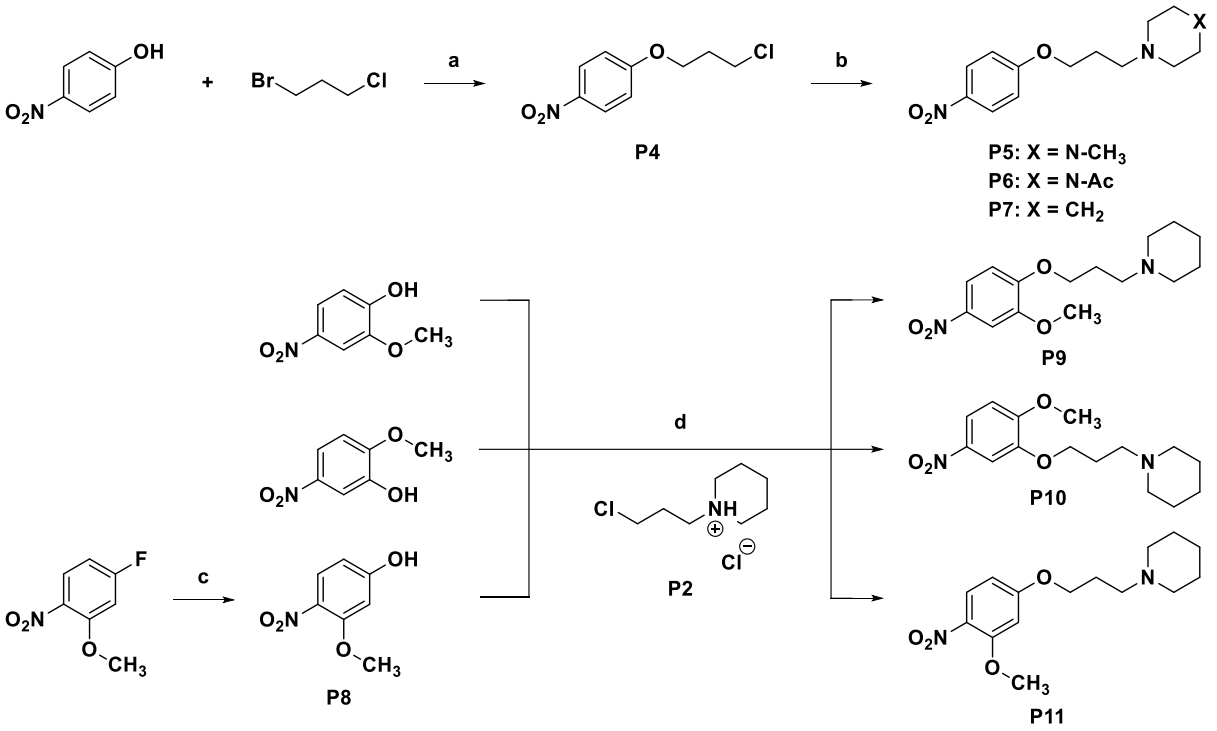

Scheme 2. Synthesis of precursors **P4**-**P11**. Reagents and conditions: a) K_2CO_3, ACN, reflux 10 h; b) corresponding cyclic amine, K_2CO_3, KI, acetone, reflux 48 h; c) $NaOH_{(aq)}$, DMSO, 80 °C for 20 h; d) K_2CO_3, DMF, rt 72 h.

The prepared precursors **P5**-**P7** and **P9**-**P11** underwent nitro group reduction to yield the corresponding functionalized anilines **P12**-**P17** (Scheme 3), which served as key nucleophilic building blocks for S_NAr reactions. The reduction proceeded efficiently through catalytic hydrogenation using palladium on activated carbon (Pd/C)[428], providing the desired products in high yields under mild conditions.

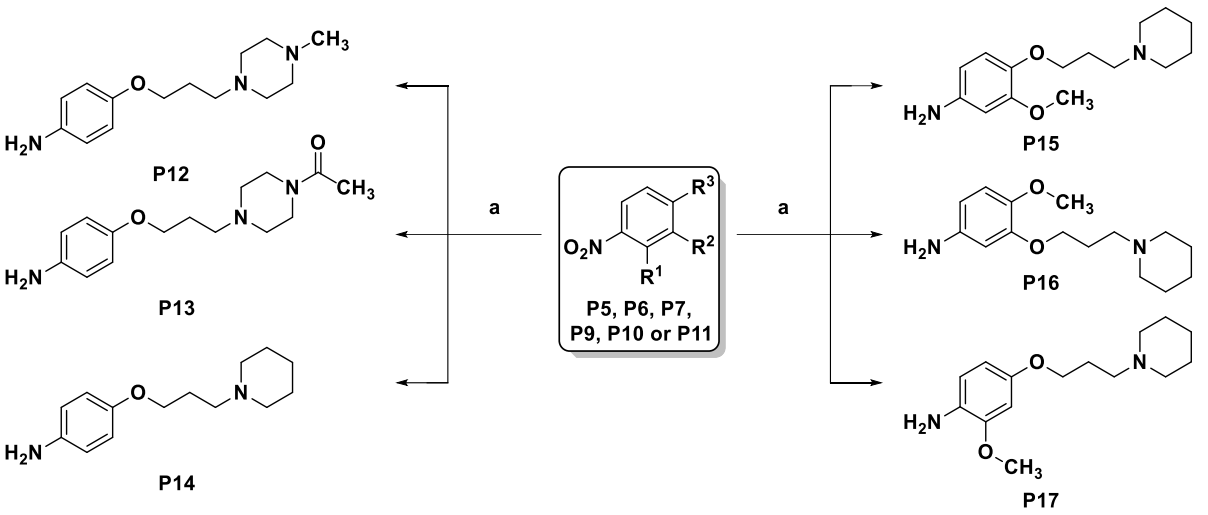

Scheme 3. Synthesis of precursors **P12-P17**. Reagents and conditions: a) H_2, 10% Pd/C, MeOH, rt 3 h.

The mechanism for nitrobenzene reduction was first proposed by Haber in the early 20th century.[429] The catalytic hydrogenation of the nitro group proceeds through multiple sequential reduction steps of key intermediates to yield amino derivatives (Scheme 4). This heterogeneous catalysis takes place on the Pd/C catalyst surface through an adsorption-reaction-desorption sequence.[430] The nitro group exhibits strong coordination with metal surfaces, enhancing hydrogenation efficiency, while the electron-deficient aromatic ring shows reduced coordination tendency.[431]

As illustrated in Scheme 4, the catalytic hydrogenation follows either a direct reduction pathway (**A**-**D**) or a condensation pathway (**E**-**G**). The direct pathway transforms nitrobenzene derivative **P5** (**A**) to a nitroso intermediate (**B**), then to hydroxylamine (**C**), and finally to aniline derivative **P12** (**D**). The concentrations of nitroso (**B**) and hydroxylamine (**C**) intermediates vary based on substrate structure, catalyst type, reaction temperature, hydrogen pressure, solvent, and pH.[430] Electron-deficient aromatic systems, low temperatures, and high hydrogen pressures promote hydroxylamine intermediate (**C**) accumulation.

The condensation pathway involves the reaction between nitroso (**B**) and hydroxylamine (**C**) intermediates to form azoxy derivative (**E**). Subsequent reductions generate azo (**F**) and hydrazo (**G**) compounds before converging with the direct pathway to yield the aniline derivative (**D**).[432] This alternative route predominates under strongly basic conditions or during slow reactions at low temperatures where hydroxylamine intermediate accumulation occurs.[430]

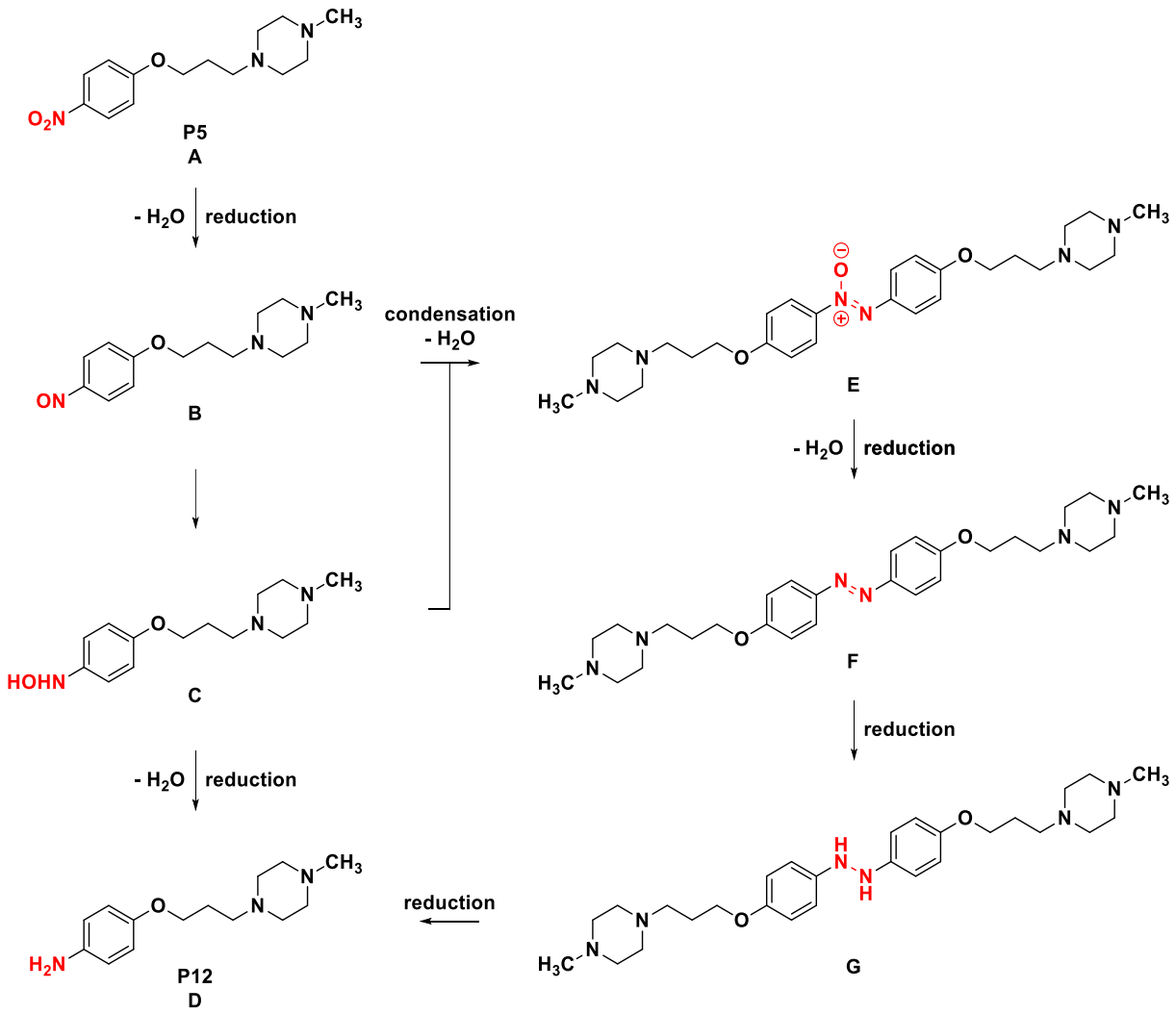

Scheme 4. Plausible mechanism of catalytic hydrogenation adopted from the literature and depicted using precursors **P5** and **P12**.[430, 433]

3.2 PINNER Pyrimidine Synthesis

The PINNER pyrimidine synthesis, also known as PINNER cyclocondensation or simply PINNER reaction, represents one of the classical approaches to pyrimidine preparation, first reported over a century ago.[434] This method involves a base-catalyzed cyclocondensation between α,β-dicarbonyl compounds (**A**) and non-*N*-substituted amidines (**B**) (Scheme 5). Since its discovery, various analogous building blocks have been employed to obtain differently substituted pyrimidine derivatives. The original 1,3-diketones have been successfully replaced in PINNER-like syntheses with β-keto esters[435, 436], α,β-unsaturated ketones[437-441], α,β-unsaturated acids[442], and masked β-dicarbonyl systems, such as (alkoxymethylene)malonates.[443] Furthermore, the N-C-N component has been diversified to include various amidines, ureas, thioureas, and guanidines as building blocks.[436, 443]

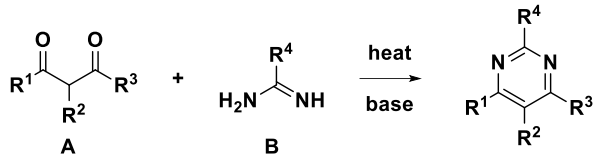

Scheme 5. Classical PINNER pyrimidine synthesis.

The reaction mechanism of both classical PINNER and PINNER-like reactions typically proceeds through two successive nucleophilic attacks. The first attack forms an intermediate, while the second leads to cyclization, forming the pyrimidine ring. The specific reaction pathway depends on the building blocks and reaction conditions used.

In this work, a PINNER-like reaction yields ethyl 4-hydroxy-2-(methylthio)pyrimidine-5-carboxylate (**P18**) (Scheme 6)[444] through a two-step reaction sequence.[445]

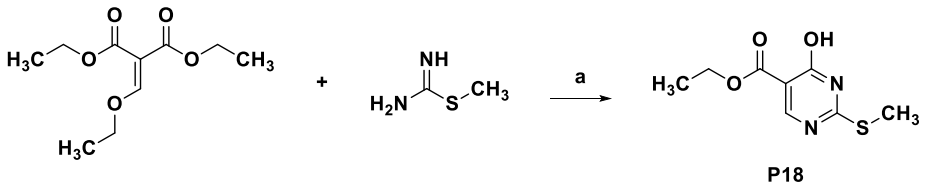

Scheme 6. Synthesis of precursor **P18**. Reagents and conditions: a) $NaOH_{(aq)}$, ethanol, rt for 10 h.

The starting material, diethyl 2-(ethoxymethylene)malonate (DEMM), represents a push-pull system with two electron-withdrawing ester functions.[445] This trifunctional electrophile enables negative charge delocalization, activating the double bond for nucleophilic attack. Consequently, nucleophilic vinylic substitution (S_NV) becomes the predominant reaction in the

presence of nucleophiles (first step)[446] even with a weak nucleofuge such as an alkoxy group.[447, 448]

The S_NV reaction follows an "addition-elimination" mechanism (Scheme 7, **A-C**).[446, 449] For **P18**, *S*-methylthiourea attacks the partially positive β-carbon atom of the polarized DEMM double bond (**A**), forming a zwitterionic intermediate (**B**). Deprotonation and ethoxy group elimination complete the reaction, yielding the thioureidomethylenemalonate intermediate (**C**). Due to the binucleophilic nature of *S*-methylthiourea[445], the second step of the PINNER-like reaction follows (Scheme 7, **D-F**).[438, 450] The unsubstituted amino group attacks the electron-deficient carbon of one ester function, forming a cyclic intermediate (**D**). Intramolecular proton transfer produces intermediate (**E**), which undergoes ethoxy group elimination and deprotonation to form the pyrimidine precursor **P18** (**F**).

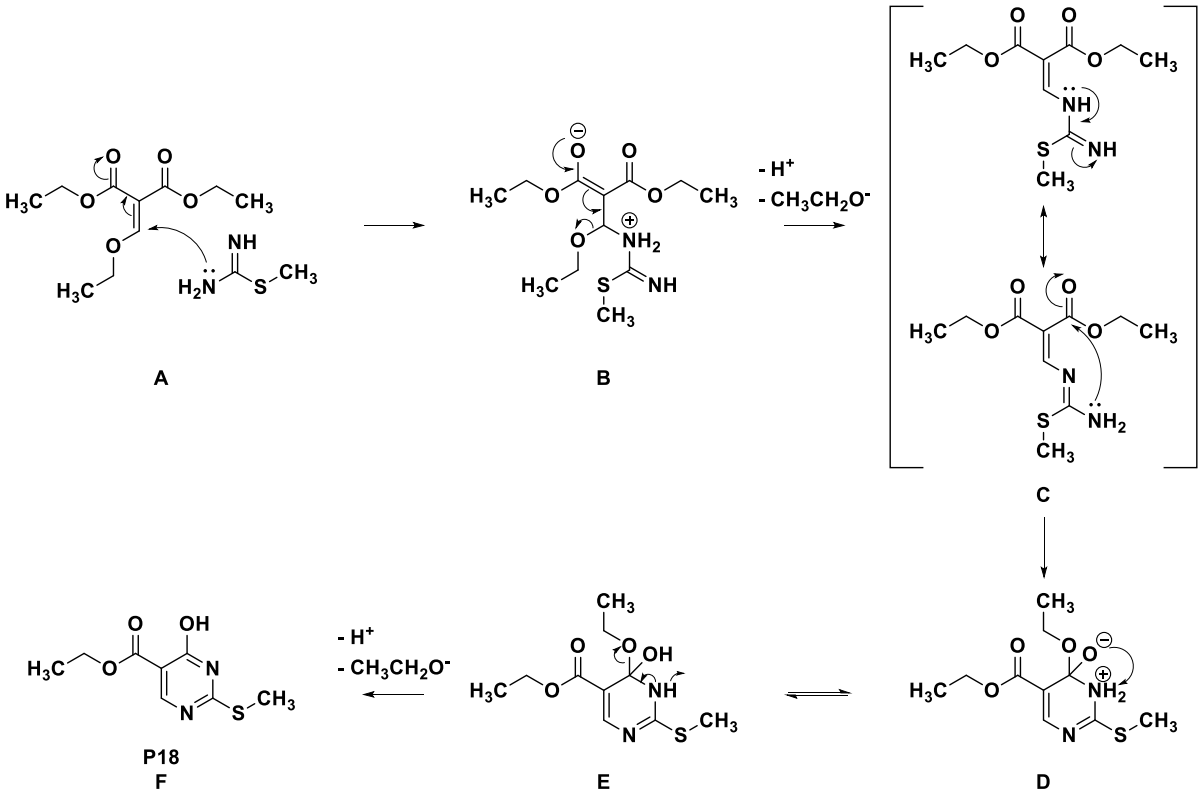

Scheme 7. A PINNER-like reaction mechanism consisting of nucleophilic vinylic substitution[446, 449] (**A-C**) and cyclization[438, 450] (**D-F**) steps.

3.3 Synthesis of Pyrimidin-4-amine Derivatives

A series of pyrimidin-4-amine scaffold-based compounds was synthesized by combining H_3R building blocks **P12**-**P14** with either ethyl pyrimidine-5-carboxylate product **P18** (obtained *via* PINNER-like reaction) or commercially available 4-chloro-2-(methylthio)pyrimidine-5-carbonitrile.

The precursor **P18** required activation for nucleophilic aromatic substitution through treatment with phosphorus(V)oxychloride, yielding the more reactive chlorinated precursor **P19** (Scheme 8). The subsequent S_NAr reaction occurred when the aniline moiety of nucleophile **P12** attacked the C4 position of **P19** electrophile, displacing the chloro substituent to yield compound **1**, featuring an ethyl carboxylate group at position 5 and H_3R pharmacophore at position 4 on the pyrimidine ring (Scheme 8).[444]

Alkaline hydrolysis of the ester function produced compound **2** containing a carboxylic acid function.[451] This intermediate was then transformed to amide **3** *via* coupling reaction[452]. Compound **4**, a nitrile derivative, was synthesized through S_NAr by directly attaching nucleophile **P12** to the pyrimidine core bearing a nitrile function at position **5**. Following the same methodology, analogous compounds **5**-**8** and **9**-**12** were prepared using nucleophiles **P13** and **P14**, respectively (Scheme 8).

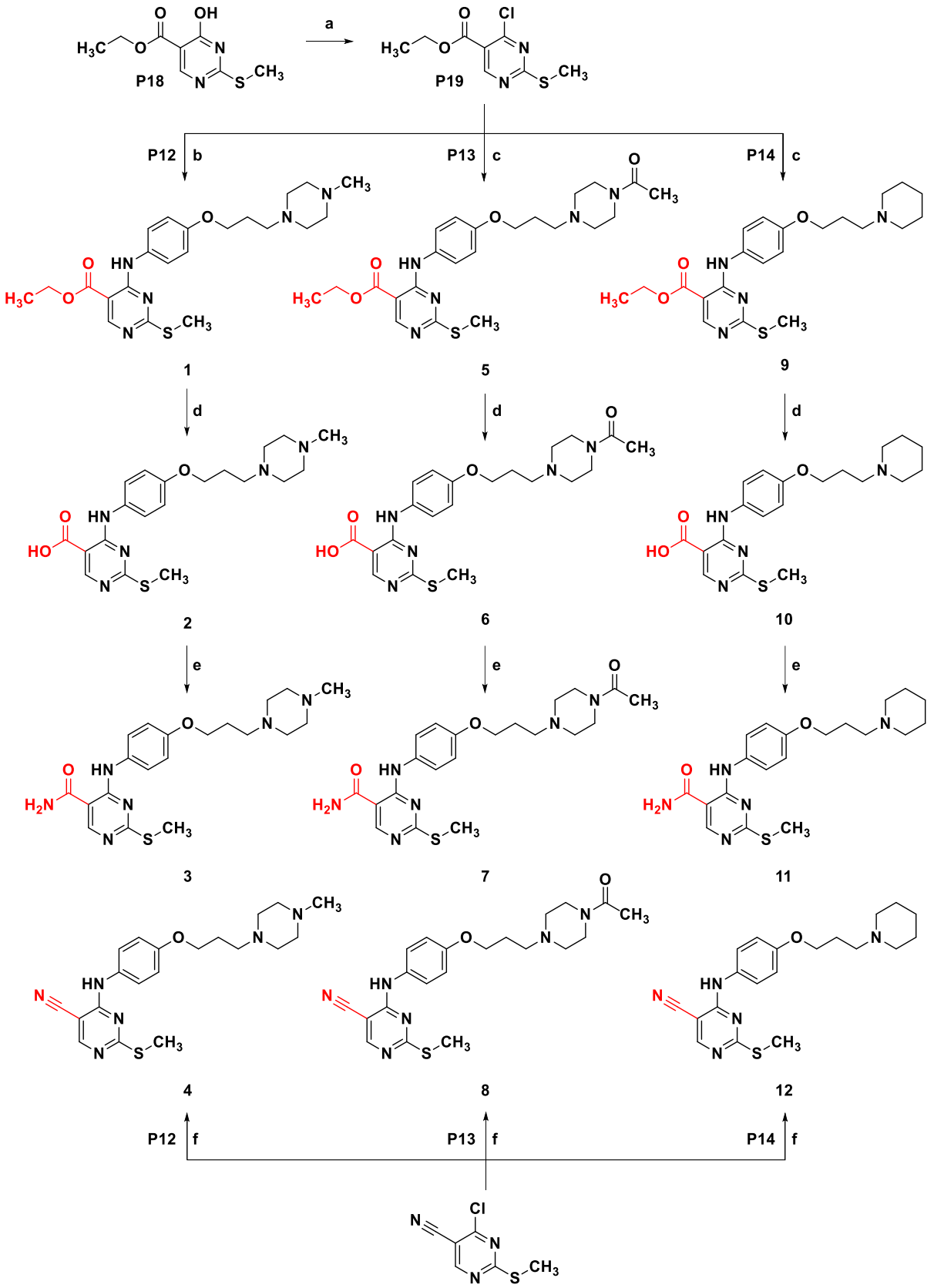

Scheme 8. Synthesis of precursor **P19** and final compounds **1-12**. Reagents and conditions: a) $POCl_3$, ACN, reflux 6 h; b) DIPEA, DMSO, 80 °C for 2 h; c) Isopropanol, 80 °C for 2 h, μW; d) LiOH, THF/H_2O, rt 3 h; e) NH_4Cl, HATU, DIPEA, DMF, rt 1 h; f) Isopropanol, 80 °C for 2 h, μW.

Compound **13**, featuring a 2-chloro substituent instead of the 2-methylthio group of **11**, was synthesized according to the route shown in Scheme 9. The starting 2,4-dihydroxypyrimidine-5-carboxylic acid was treated with chlorinating agents to obtain reactive acyl chloride derivative **P20**[453], which was then converted to amide **P21**.[454] The final compound **13** was obtained through a microwave-assisted S_NAr reaction using **P12** as the nucleophile.

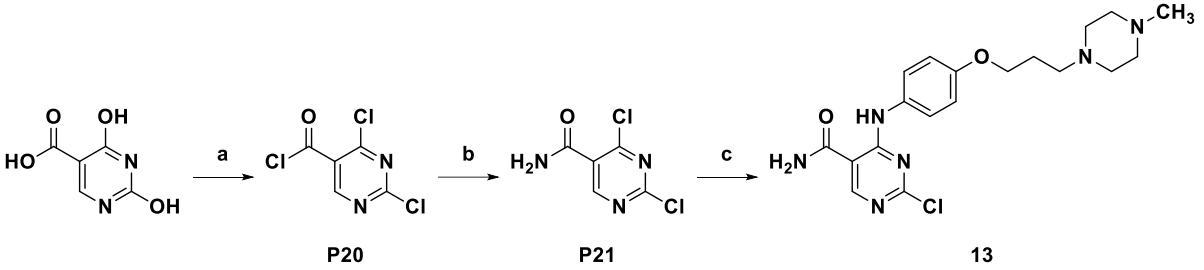

Scheme 9. Synthesis of precursors **P20** and **P21** and final compound **13**. Reagents and conditions: a) $POCl_3$, PCl_5, reflux 16 h[453]; b) $NH_4OH_{(aq)}$, DCM, 0 °C for 2 h[454]; c) **P12**, isopropanol, 50 °C for 1 h, µW.

3.3.1 HATU-mediated Amide Formation

Amide bonds serve as essential chemical linkages in biological systems, connecting amino acid building blocks to form proteins, and in the pharmaceutical industry as key components of active pharmaceutical ingredients.[455-457] A comprehensive survey of reaction types in drug development identified amide bond formation as one of the most frequently used chemical transformations.[458] This prevalence stems from the advantageous properties of amides, including their high polarity and stability.[455]

While direct condensation of carboxylic acids and amines would represent the most straightforward method for amide synthesis, this approach faces thermodynamic limitations, requiring elevated temperatures for water elimination. At room temperature, the reaction typically results in proton transfer between reactants, forming an ammonium carboxylate intermediate.[455, 457] To circumvent the high activation energy without employing harsh conditions that might compromise sensitive reactants, coupling reagents are utilized. These reagents activate the carboxylic acid by substituting its hydroxyl group (-OH) with a superior leaving group, enabling efficient amide formation. Depending on the coupling reagent, the reactive intermediates include acid chlorides, mixed carboxylic or carbonic acid anhydrides, or activated esters.[456, 457] The selection of coupling reagents considers factors such as reaction rate, conversion degree, by-products, and reaction scale.[457]

The synthesis of amide-containing final compounds **3**, **7**, and **11** from their corresponding carboxylic acids **2**, **6**, and **10** employed *N*-[(dimethylamino)-1*H*-1,2,3-triazolo[4,5-b]pyridin-

1-ylmethylene]-*N*-methylmethanaminium hexafluorophosphate *N*-oxide (HATU) as the coupling reagent (Scheme 8). HATU was chosen for its capacity to promote rapid amide bond formation with high yields under mild conditions.[456]

The HATU-mediated amide formation mechanism for compound **3** (Scheme 10) begins with proton transfer between carboxylic acid **2** and DIPEA, generating the required carboxylate anion (**A** and **B**). The carboxylate anion attacks HATU (**C**), proceeding through a transition state (**D**) to form an *O*-acyl(tetramethyl)isouronium intermediate. The 1-hydroxy-7-azabenzotriazole (HOAt) anion then attacks this intermediate (**E**), producing an activated HOAt ester and tetramethylurea as a by-product (**F**). Nucleophilic NH_3 attacks the activated HOAt ester, forming a transient intermediate (**G**), which yields the desired amide **3** with HOAt release (**H**).

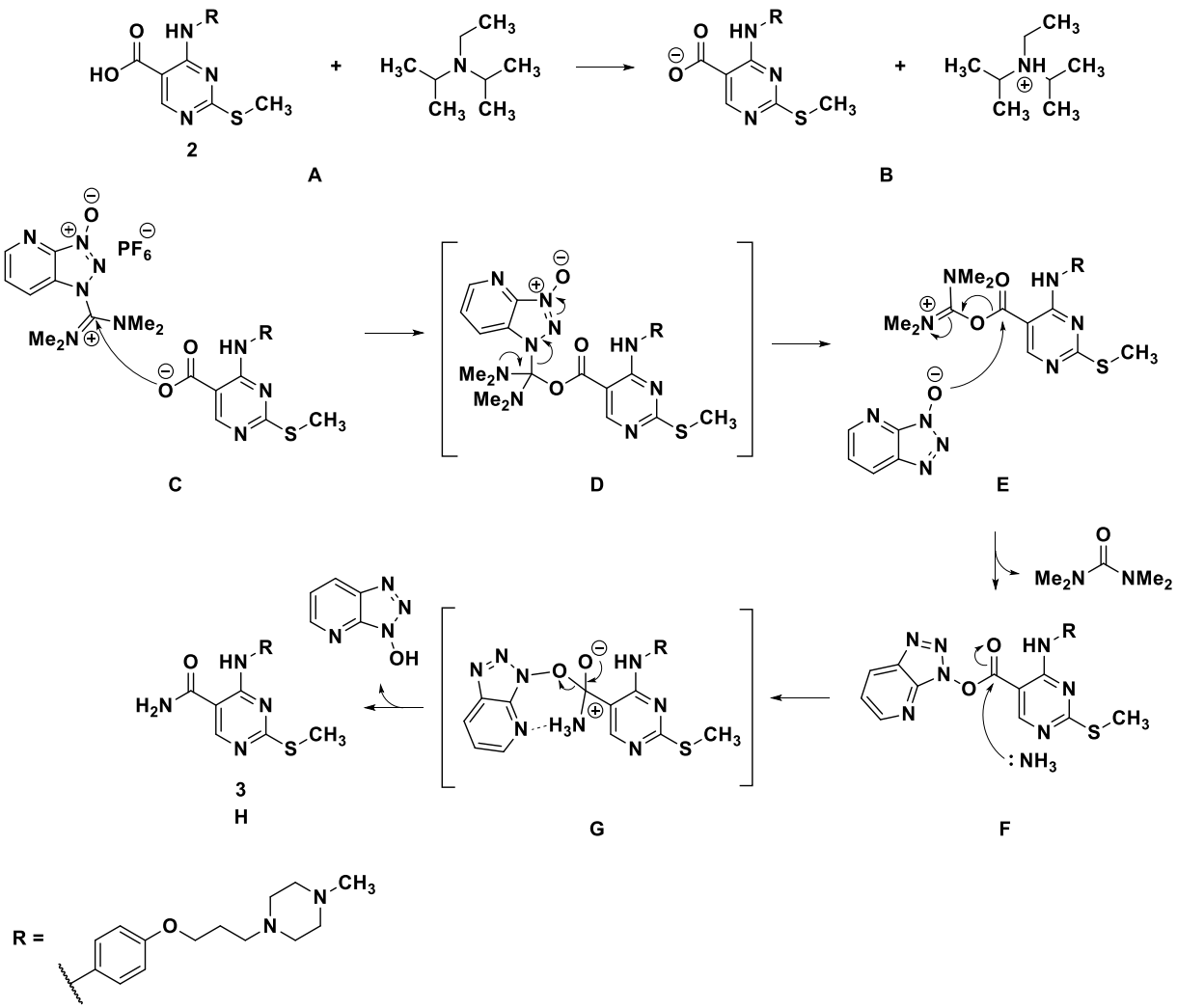

Scheme 10. Mechanism of HATU coupling depicted through the synthesis of compound **3** from its corresponding carboxylic acid precursor **2**.[456, 459]

3.4 Synthesis of Pyrimidin-2-amine Derivatives

A series of compounds was synthesized from pyrimidin-2-amines by incorporating a piperidine moiety at position 4 of the aromatic core via propyloxy or propylthio linkers, establishing the H_3R-pharmacophore. The series' structural diversity was achieved through various substituents at the pyrimidin-2-amine core's 6-position.

While unsubstituted, 6-methyl, 6-ethyl, and 6-isopropyl derivatives were commercially available, the 6-cyclopropyl building block required synthesis. Classical PINNER pyrimidine synthesis, involving the reaction of methyl 3-cyclopropyl-3-oxopropanoate with guanidine hydrochloride under strong basic conditions, yielded precursor **P22**. This intermediate was then converted to the 4-chloro substituted derivative **P23** (Scheme 11), providing a more suitable substrate for subsequent nucleophilic aromatic substitution.[460, 461]

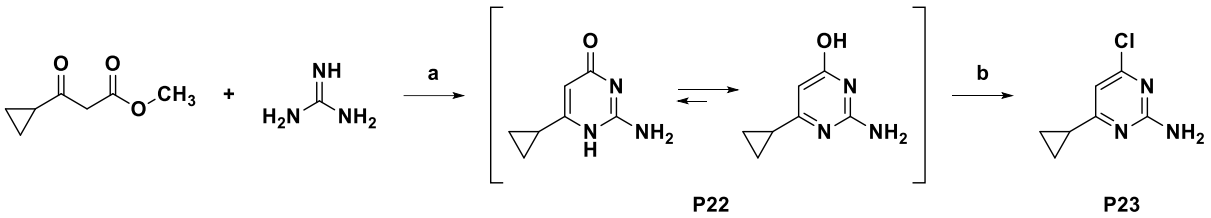

Scheme 11. Classical PINNER pyrimidine synthesis of precursor **P22** and its conversion to **P23**. Reagents and conditions: a) KO*t*Bu, MeOH, rt overnight; b) $POCl_3$, DCE, 75 °C overnight.

The H_3R pharmacophore assembly proceeded through an S_NAr reaction between 4-chloropyrimidin-2-amine derivatives and 3-(piperidin-1-yl)propan-1-ol (**P1**), yielding compounds **14-18** (Scheme 12) with a propyloxy linker connecting the aromatic ring to the basic aliphatic centers. The reaction was facilitated by deprotonating **P1**'s primary hydroxyl group under strong basic conditions, generating an alkoxide nucleophile that displaced the pyrimidine's chlorine substituent.[462]

Compounds **19-23**, featuring a propylthio linker, were synthesized analogously using 3-(piperidin-1-yl)propane-1-thiol (**P3**) (Scheme 12).[240] Thiols, being more effective nucleophiles than alcohols due to higher acidity, convert to thiolates under milder basic conditions.

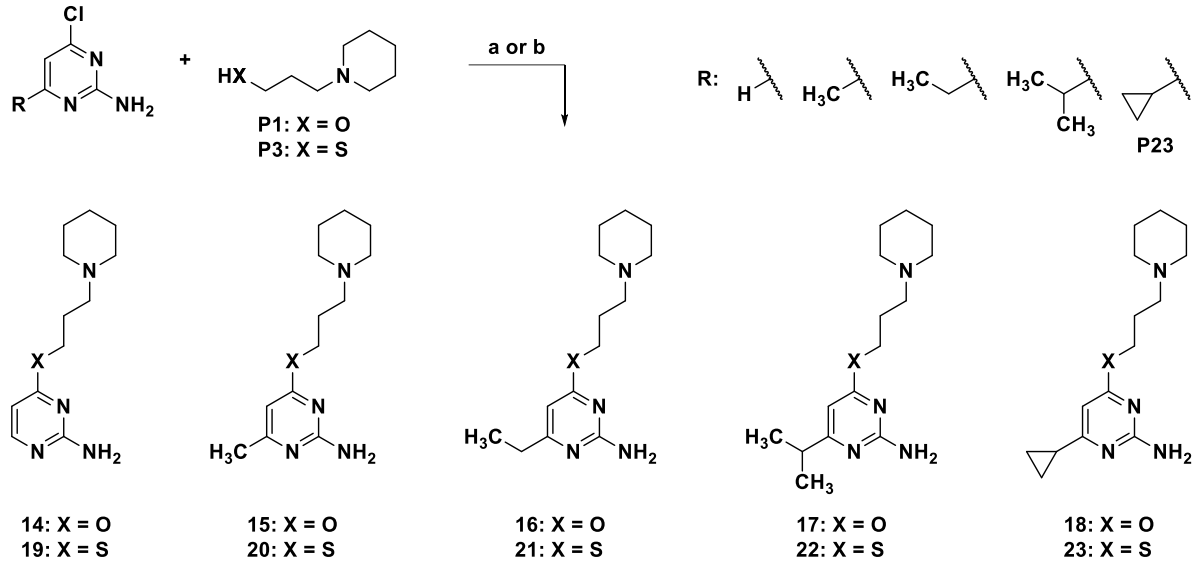

Scheme 12. Synthesis precursor **P23** and final compounds **14**-**23**. Reagents and conditions: a) NaH, THF, 75 °C overnight;[462] b) $NaOH_{(aq)}$, EtOH, reflux 4 h.[240]

To explore optimal conditions for an S_NAr reaction with a thiol nucleophile, five reaction conditions commonly reported in the literature were evaluated using compound **20**, with outcomes being monitored by LC-MS (Table 4, Scheme 13). Based on these results, condition **IV** was selected for the synthesis of compounds **19** and **21**-**23** (Scheme 12), as it provided the most favourable ratio between desired and side products.

Table 4. LC-MS monitoring of S_NAr reaction outcomes using a thiol nucleophile under various reaction conditions (cf. Scheme 13).

Entry	Conditions	Product (%)	Thiol (%)	Dimer (%)
I	NaH, THF, rt for 48 h[463]	0	0	21.5
II	THF, rt for 24 h	0	41.9	34.3
III	TEA, MeOH, 120 °C for 3.5 h, μW[464]	28.1	13.0	23.9
IV	$NaOH_{(aq)}$, EtOH, reflux for 4 h[240]	52.8	0	35.6
V	Cs_2CO_3, DMF, 60 °C for 2 h[465]	18.1	0	65.6

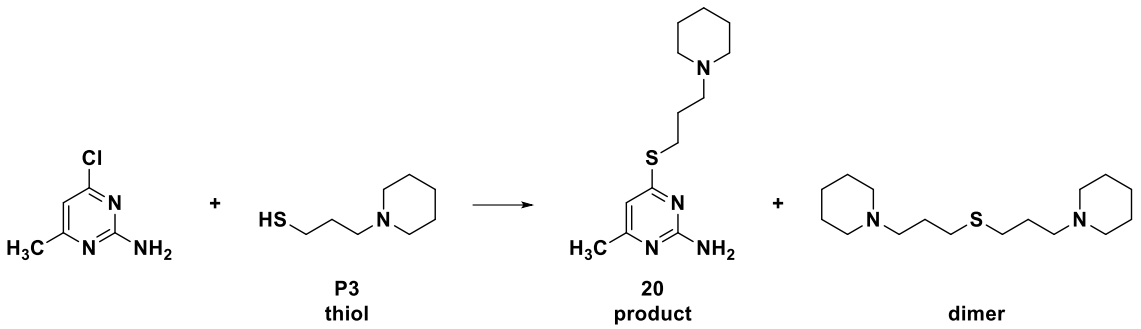

Scheme 13. Synthesis of target compound **20**. The reaction pathway is condition-dependent (Table 4), proceeding either via S_NAr to afford product **20** or through competing thiol-thiol S_N2 coupling of **P3**, yielding the thioether dimer as a side product via unexplored mechanism.

3.5 Synthesis of Pyrimidine-2,4-diamine Derivatives

The pyrimidine heterocycle represents a fundamental structural motif prevalent in both natural products and synthetic compounds[466], driving significant interest in developing efficient modification strategies. The electron-deficient nature of the pyrimidine ring makes it particularly suitable for S_NAr reactions, especially when its electrophilic character is enhanced by electron-withdrawing groups (EWGs), such as in halo- or nitro-substituted pyrimidines.[467, 468] The primary synthetic route to pyrimidine-2,4-diamines typically involves the functionalization of 2,4-dichloropyrimidines through S_NAr-mediated replacement of chlorine atoms with amines.[469]

Experimental studies reveal distinct reactivity patterns at different positions in halopyrimidines. The C-4 and C-6 positions exhibit the highest susceptibility to S_NAr, followed by C-2, while C-5 demonstrates notably lower reactivity.[466] In 2,4-dichloropyrimidine, while substitution occurs preferentially at C-4, concurrent reactivity at C-2 is observed.[470] The distribution of regioisomers varies considerably, primarily determined by stereoelectronic effects of pyrimidine ring substituents and the nature of the nucleophiles. For instance, 5-trifluoromethyl-2,4-dichloropyrimidine produces nearly equal amounts of C-2 and C-4 regioisomers, whereas its 5-chloro counterpart yields predominantly the C-4 isomer.[471] This limited regioselectivity impacts yields when a specific regioisomer is desired and necessitates complex separation procedures, reducing overall synthetic efficiency.

Researchers have developed numerous approaches to enhance regioselectivity toward either C-2 or C-4 substitution. The optimization of reaction conditions through base and solvent selection has shown promising results[468-473], while careful control of reaction parameters such as time and temperature has proven effective.[470-473] Additional advances include the strategic introduction of catalysts and additives[466, 469-471, 473], along with the implementation of microwave irradiation techniques.[474-476] with varying degrees of success. These methodological innovations have demonstrated varying degrees of success in controlling regioselectivity, offering synthetic chemists a diverse toolkit for achieving selective functionalization of pyrimidine rings

3.5.1 Synthesis of 6-Methylpyrimidine-2,4-diamine Derivatives

The synthesis of final compounds containing the 6-methylpyrimidin-2,4-diamine scaffold was accomplished through a two-step sequence of S_NAr reactions starting from 6-methyl-2,4-dichloropyrimidine. The initial nucleophilic substitution with aliphatic amines

yielded both C-2 and C-4 substitution products (**P24**-**P27**) (Scheme 14), reflecting the characteristic regioselectivity challenges in pyrimidine chemistry. This apparent limitation in regioselectivity was strategically leveraged as an advantage in synthesizing compounds with the 6-methylpyrimidine-2,4-diamine fragment. The approach efficiently generated two key intermediates in a single synthetic operation, enabling the preparation of final compounds with complementary substitution patterns, which proved valuable for comprehensive SAR analysis.

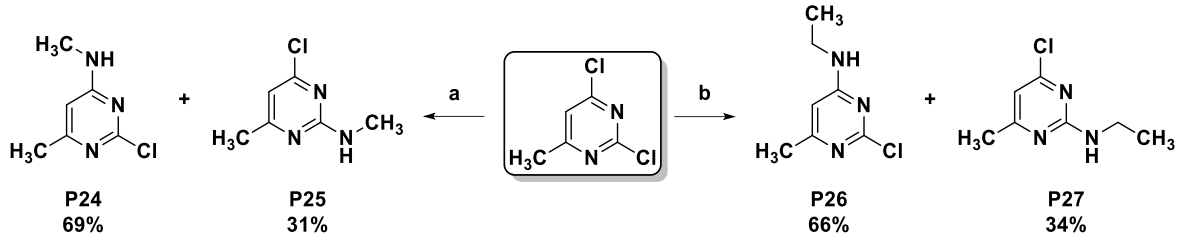

Scheme 14. Synthesis precursor **P24**-**P27**. Reagents and conditions: a) $CH_3NH_3^+Cl^-$, DIPEA, EtOH, 50 °C for 24 h[477]; b) $CH_3CH_2NH_3^+Cl^-$, K_2CO_3, DMF, rt for 5 h.[293, 478]

The synthetic sequence was completed through a second S_NAr reaction, where the monosubstituted pyrimidine intermediates **P24**-**P27** were coupled with previously synthesized aniline derivatives **P12**, **P14**-**P16**. This transformation successfully incorporated the H_3R pharmacophore into the target compounds **24**-**39** (Scheme 16), establishing a robust and versatile synthetic route to the desired molecular framework (Scheme 15).

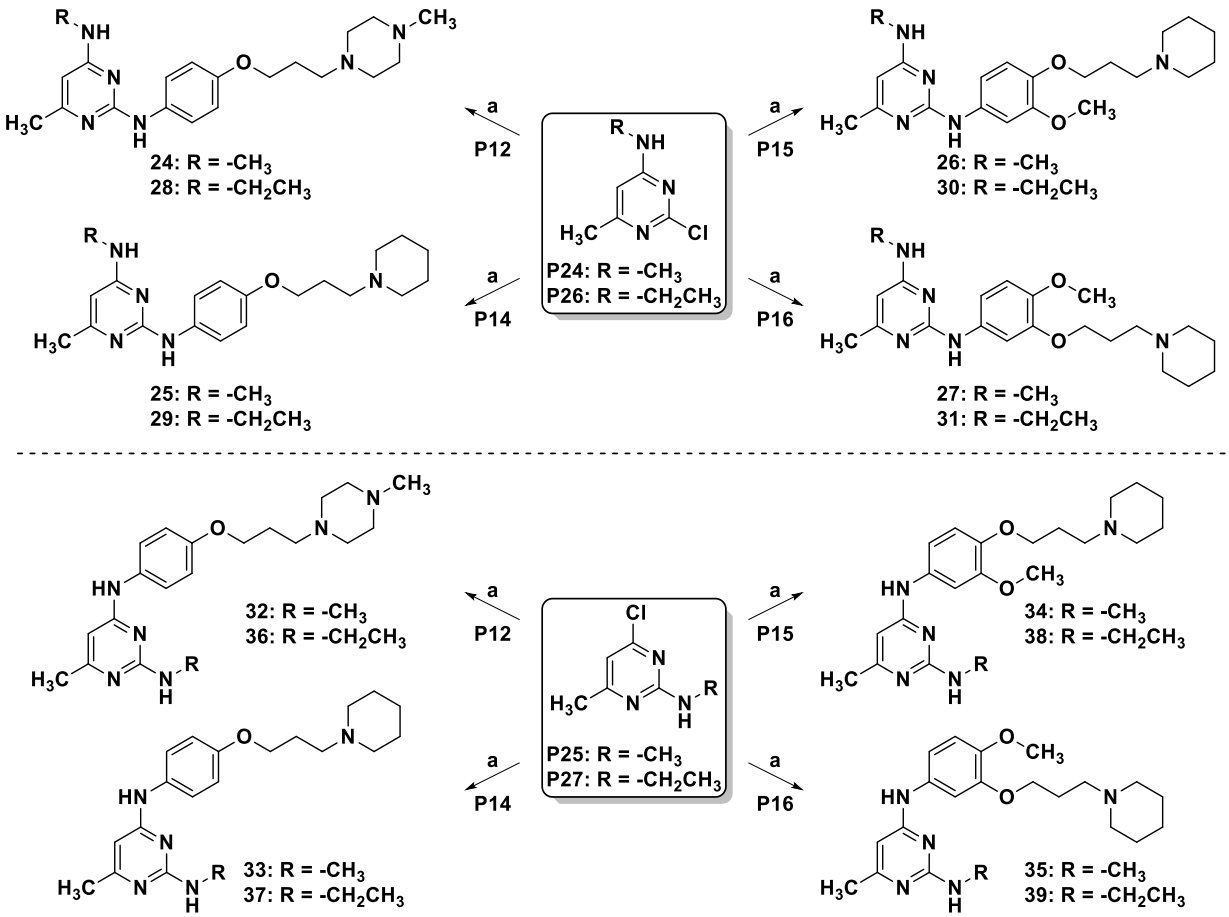

Scheme 15. Synthesis of final compounds **24-39**. Reagents and conditions: a) Corresponding nucleophile **P12**-**P16**, TFA, isopropanol, 140 °C for 1 h, μW[293].

3.5.2 Synthesis of 5-Chloropyrimidine-2,4-diamine Derivatives

Building upon the synthetic strategy developed for 6-methylpyrimidine-2,4-diamine derivatives, the synthesis of 5-chloropyrimidine-2,4-diamine derivatives proceeded through two sequential S_NAr reactions, beginning with aliphatic nucleophile substitutions (Scheme 16). The electron-withdrawing groups enhanced the electron-deficient nature of 2,4,5-trichloropyrimidine, resulting in predominant C-4 substitution products **P28** and **P29**. The reaction with methylamine hydrochloride yielded exclusively **P28** (97% yield), while ethylamine hydrochloride produced both regioisomers **P29** and **P30**, with strong preference for **P29** (96:4 ratio). This regioselectivity pattern aligns with documented literature findings.[471]

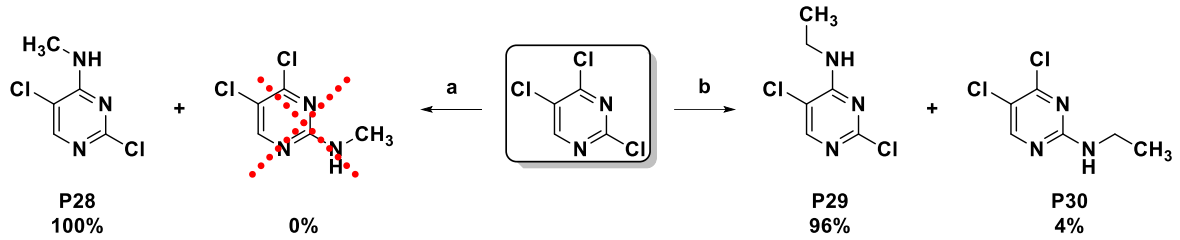

Scheme 16. Synthesis of precursors **P28**-**P30**. Reagents and conditions: a) $CH_3NH_3^+Cl^-$, K_2CO_3, DMF, rt for 5 h[293, 390]; b) $CH_3CH_2NH_3^+Cl^-$, DIPEA, EtOH, 50 °C for 24 h[477].

The subsequent S_NAr substitution of C-2 halogen in **P28** and **P29** with aromatic nucleophiles **P12**-**P17** was executed using TFA as an acid catalyst, generating compounds **40**-**51** (Scheme 17).[293] The application of acid catalysis proved particularly effective for facilitating the displacement of the C-2 halogen on the pyrimidine ring, especially when using weak nucleophiles derived from aniline. The reaction rate was significantly enhanced due to the protonation of the pyrimidine ring, which induced a partial positive charge on the C-2 carbon atom, thereby promoting the S_NAr mechanism.[479]

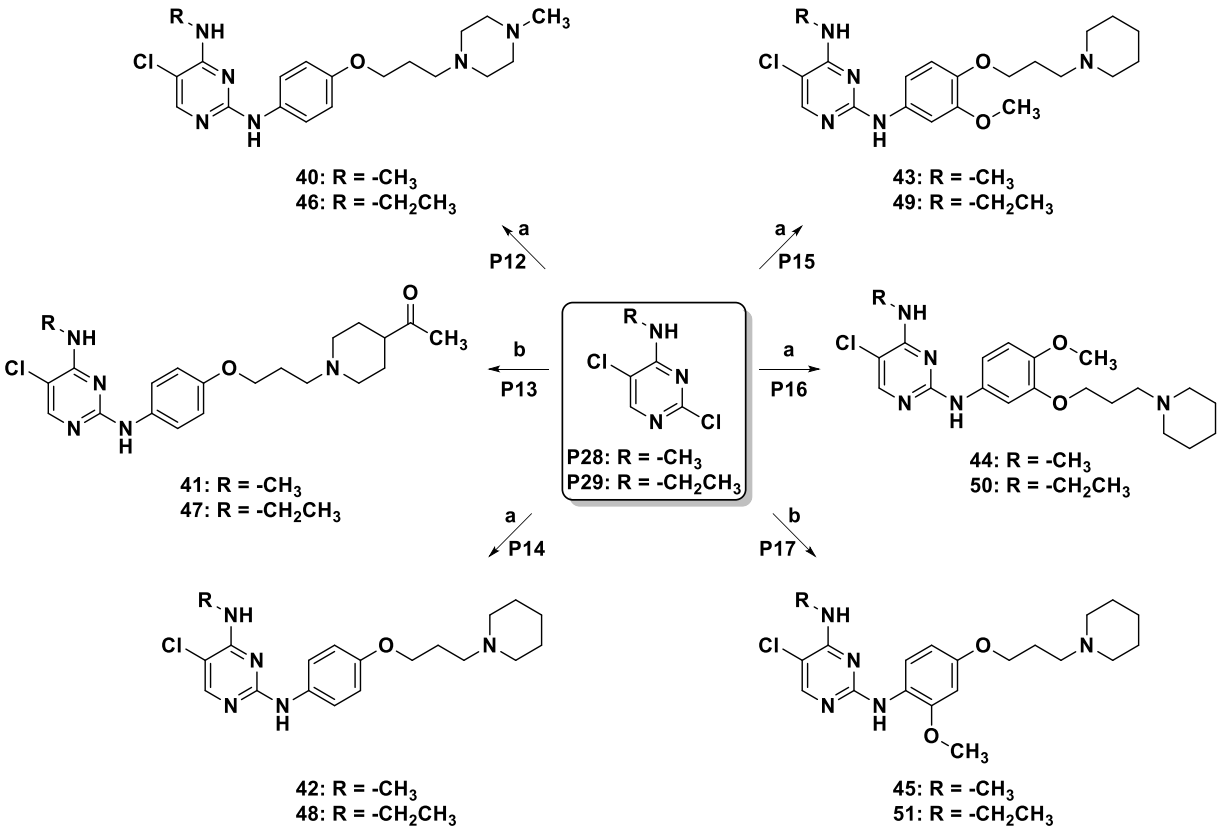

Scheme 17. Synthesis of final compounds **40**-**51**. Reagents and conditions: a) Corresponding nucleophile **P12**, **P14**, **P15** or **P16**, TFA, isopropanol, 140 °C for 1 h, μW[293]; b) Corresponding nucleophile **P13** or **P17**, TFA, isopropanol, rt for 24 h.[479]

The synthesis of structural analogues **40-51** with reversed substitution patterns required an alternative approach due to the regioselective nature of S_NAr reactions on 2,4,5-trichloropyrimidine. The solution involved initial introduction of H_3R-pharmacophore containing aromatic nucleophiles at the C-4 position, forming intermediates **P31-P36** (Scheme 18). These reactions proceeded efficiently under microwave irradiation, utilizing *in situ* generated HCl as an autocatalyst. Similar substitutions have been extensively studied for the C-6 position of purine heterocycles.[480]

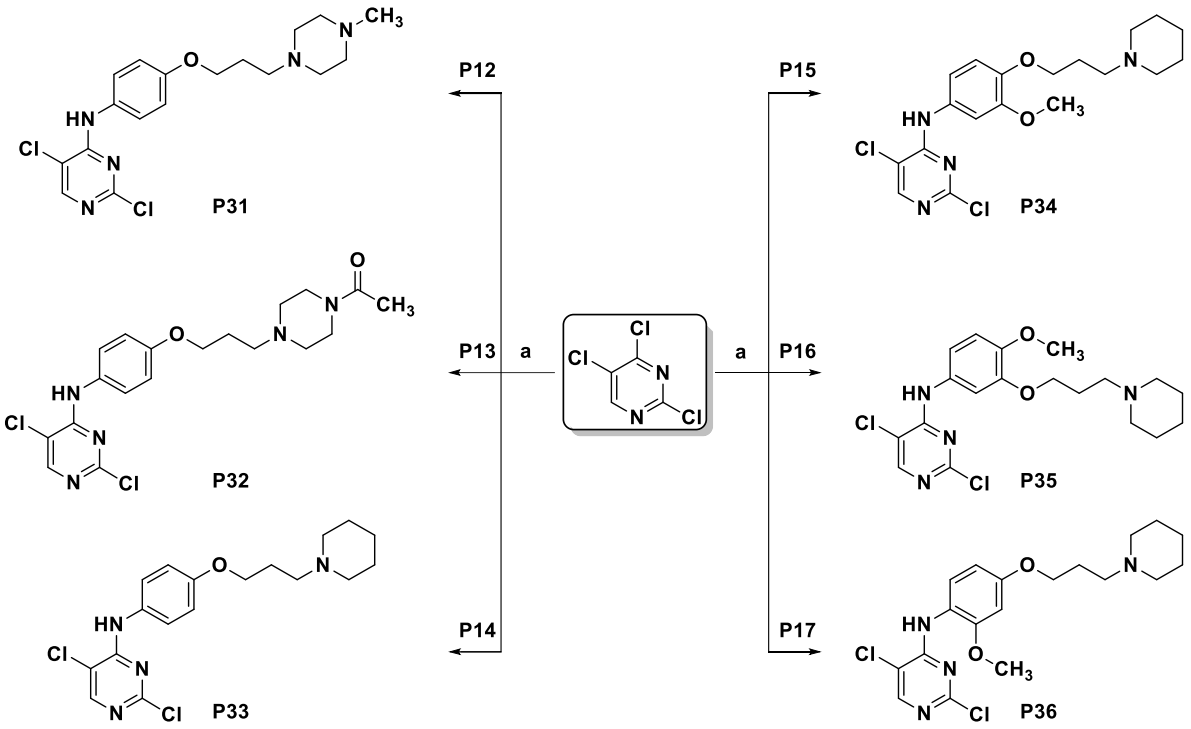

Scheme 18. Synthesis of precursors **P31-P36**. Reagents and conditions: a) Corresponding nucleophile **P12-P16**, Isopropanol, 50 °C for 1 h, μW.

The intermediates **P31-P36** underwent subsequent reactions with aliphatic alkylamines to produce compounds **52-57** and **59-63**, while compound **58** was synthesized separately from **P30** (Scheme 19).

The S_NAr reactions with aliphatic nucleophiles employed base catalysis to neutralize the generated HCl.[481-483] This approach was advantageous because alkylamines are stronger bases than pyrimidines.

Owing to the relatively small polarity difference between the parent precursors (**P31-P36**) and the resulting target compounds (**52-57**, **59-63**), unreacted precursors not only significantly hindered chromatographic purification, but also reduced the overall reaction yield. To address this issue, LC-MS monitoring of compound **60** synthesis was employed to optimize reaction

time, ensuring that precursor **P33** was fully utilized, while minimizing the formation of side products. LC-MS monitoring of compound **60** synthesis revealed almost complete consumption of precursor **P33** after 4 hours (Figure 21). These optimized conditions were subsequently extended to the synthesis of other analogues in the series, with the exception of compound **58** (Scheme 19).

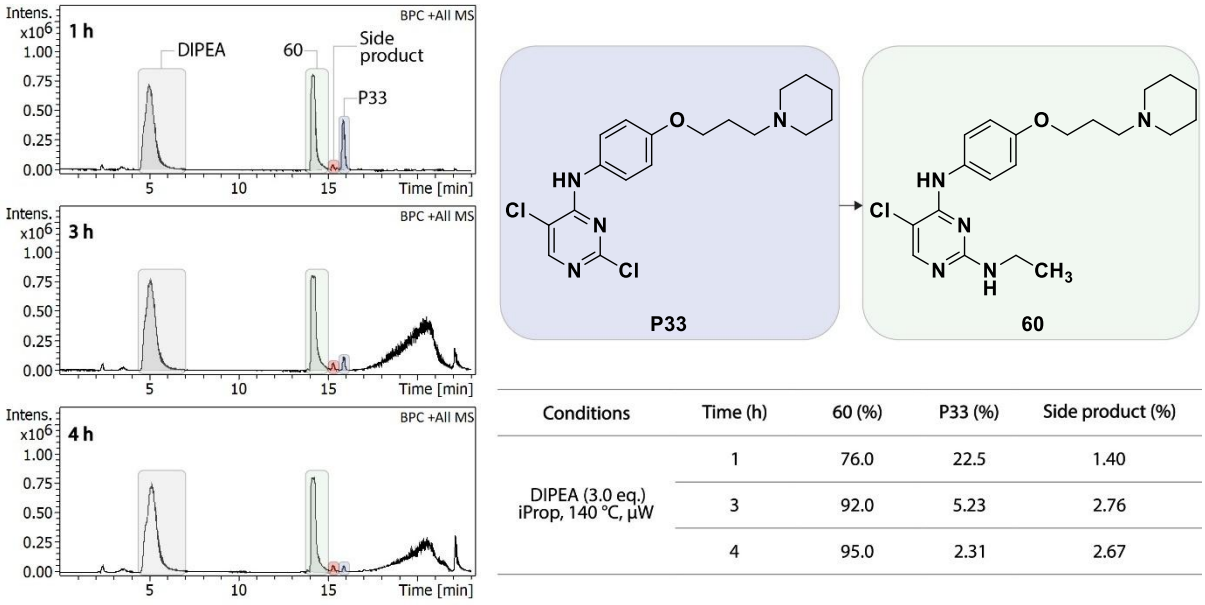

Conditions	Time (h)	60 (%)	P33 (%)	Side product (%)
DIPEA (3.0 eq.) iProp, 140 °C, µW	1	76.0	22.5	1.40
	3	92.0	5.23	2.76
	4	95.0	2.31	2.67

Figure 21. LC-MS-guided optimization of reaction time for compound **60** synthesis. Chromatograms track the consumption of **P33** (blue) concurrent with product **60** formation (green). An uncharacterized side product (red) emerges over time, presenting isolation challenges due to its similar retention time to **60**.

Unlike other compounds in this series (**52**-**57**, **59**-**63**), the synthesis of **58** presented unique challenges. While other analogues were successfully produced under LC-MS-optimized conditions, preparation of **58** from **P31** was unsuccessful due to predominant side product formation that prevented isolation. An alternative acid-catalysed S_NAr route employing **P12** and **P30,** successfully yielded **58** (Scheme 19). However, the practical utility of this approach was severely constrained by the inefficient preparation of **P30**, which was obtained as an extremely unfavourable regioisomer (3% yield, Scheme 16), precluding its application in large-scale synthesis.

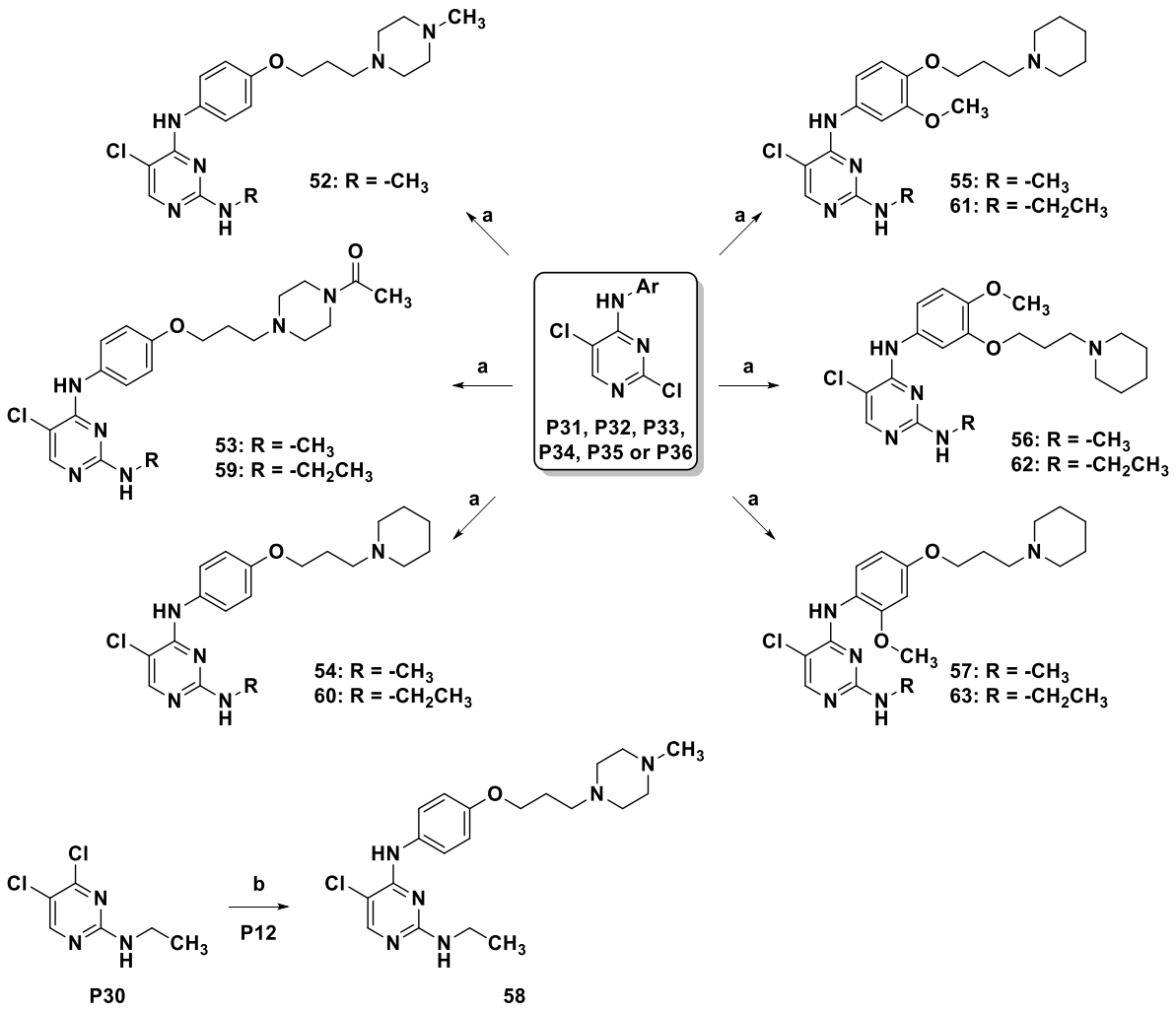

Scheme 19. Synthesis of final compounds **52**-**63**. Reagents and conditions: a) $CH_3NH_3^+Cl^-$ or $CH_3CH_2NH_3^+Cl^-$, DIPEA, isopropanol, 140 °C for 4 h, µW; b) Corresponding nucleophile **P12**, TFA, isopropanol, rt for 24 h.

3.5.3 Synthesis of 5-(Trifluoromethyl)pyrimidine-2,4-diamine Derivatives

Following the established synthetic strategy for pyrimidine-2,4-diamine derivatives, the synthesis of 5-(trifluoromethyl)pyrimidine-2,4-diamine compounds proceeded through two consecutive S_NAr reactions with 2,4-dichloro-5-(trifluoromethyl)pyrimidine. Unlike its 5-substituted analogs (H, F, Cl, Br, I, CH_3, CH_3O, or CN) which predominantly yield C-4 substitution products, 2,4-dichloro-5-(trifluoromethyl)pyrimidine displayed distinctive reactivity by generating nearly equal amounts of C-2 and C-4 substitution products.[471, 484] This uncommon behaviour stems from the steric effects of the CF_3 group at the C-4 position, enabling formation of both regioisomers. The steric hindrance created by the CF_3 group revealed a novel approach to control S_NAr regioselectivity, enabling selective C-2 substitution through Lewis acid catalysis.[471, 485-487] This selectivity arises from the CF_3 group preventing

Lewis acid coordination at C-4, directing it instead to N-1 and N-3 positions, thus activating the C-2 position[484]

The non-selective nature of 2,4-dichloro-5-(trifluoromethyl)pyrimidine proved advantageous in the synthesis of target compounds, enabling isolation of two valuable synthons from a single reaction. This dual-product outcome enhanced synthetic efficiency by reducing the required number of steps and simplifying the overall synthetic pathway.

The initial S_NAr substitution with methylamine hydrochloride or ethylamine hydrochloride generated precursors **P37**-**P40** (Scheme 20).[293, 405]

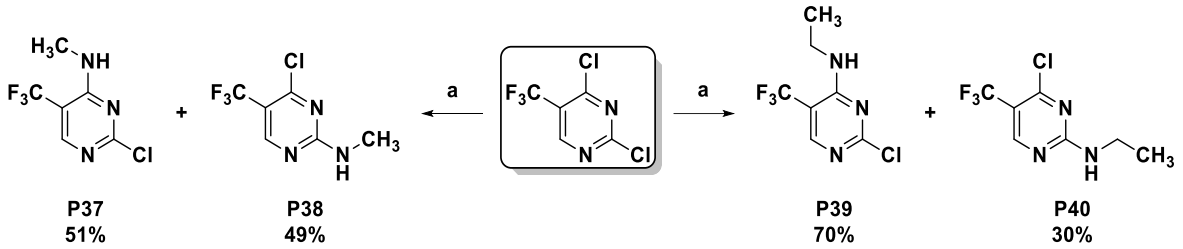

Scheme 20. Synthesis of precursors **P37**-**P40**. Reagents and conditions: a) $CH_3NH_3^+Cl^-$ or $CH_3CH_2NH_3^+Cl^-$, DIPEA, EtOH, rt for 1-5 h.[293, 405]

These intermediates underwent subsequent reaction with aromatic nucleophiles **P12**-**P17** under TFA catalysis to yield the target compounds **64**-**75** (Scheme 21) and **76**-**87** (Scheme 22).

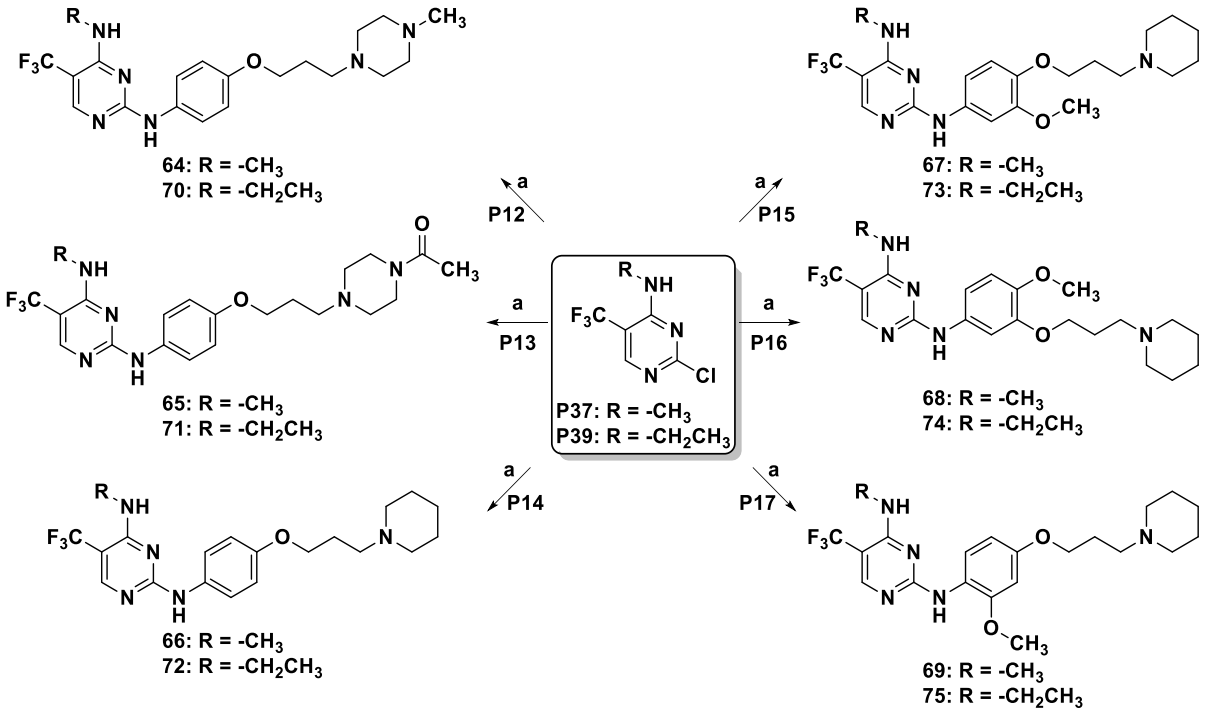

Scheme 21. Synthesis of target compounds **64**-**75**. Reagents and conditions: a) Corresponding nucleophile **P12**-**P17**, TFA, isopropanol, rt for 24 h.

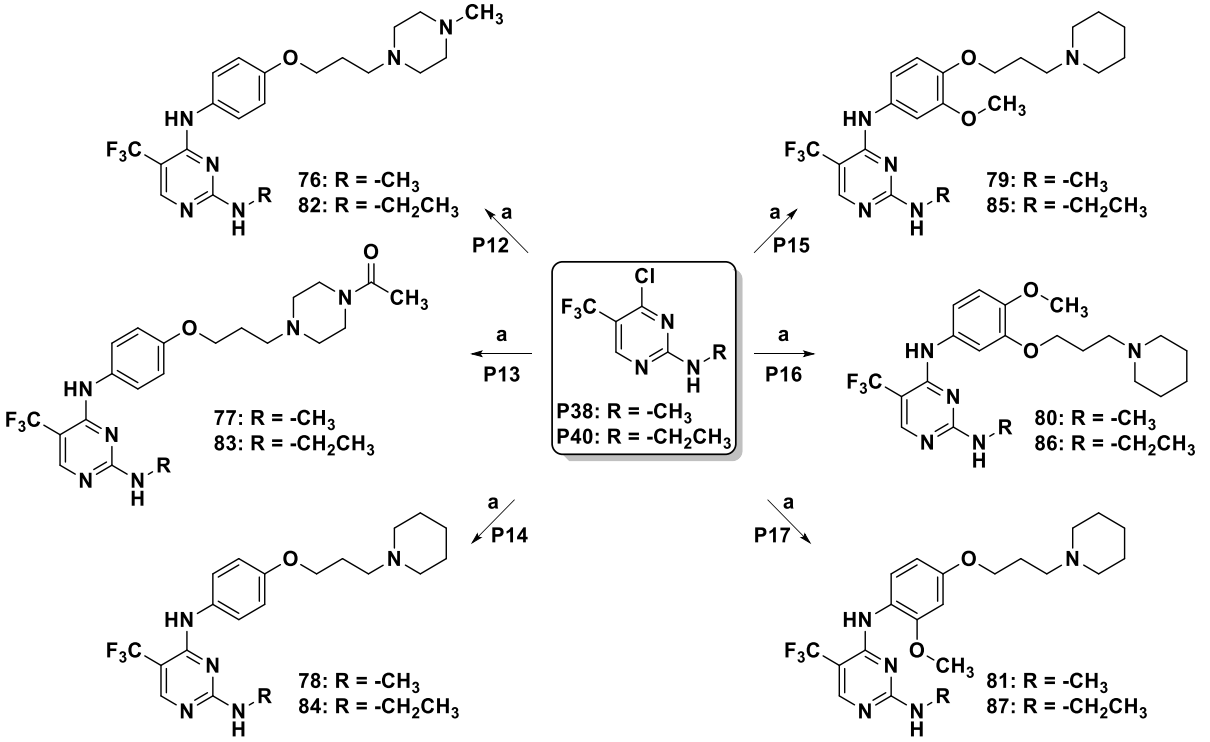

Scheme 22. Synthesis of target compounds **76**-**87**. Reagents and conditions: a) Corresponding nucleophile **P12**-**P17**, TFA, isopropanol, rt for 24 h.

3.5.4 Mechanism of Nucleophilic Aromatic Substitution

Nucleophilic aromatic substitution, discovered by FAUST and FITTIG in the 1870s[488, 489], involves nucleophiles displacing leaving groups on aromatic rings. This reaction typically occurs on electron-deficient aromatic systems activated by electron-withdrawing groups and is particularly valuable for the functionalization of halogenated aromatics.

Nitrogen-containing aromatic heterocycles, particularly pyrimidine, demonstrate enhanced reactivity toward S_NAr compared to simple arenes. The nitrogen atoms' higher electronegativity creates an electron distribution imbalance within the aromatic system, concentrating electron density on the nitrogen while depleting it from carbon atoms. This effect renders the α- (C-4) and γ-positions (C-6) highly susceptible to S_NAr substitution due to their increased electrophilicity.[490]

S_NAr proceeds through two distinct pathways: the stepwise addition-elimination mechanism or the concerted mechanism (cS_NAr) (Scheme 23).[490] The classical addition-elimination S_NAr mechanism, introduced by BUNNETT and ZAHLER[491], initiates with nucleophilic attack at the electron-deficient carbon (**A**), forming a dearomatized anionic intermediate (**B**) known as a Meisenheimer complex.[492] For neutral nucleophiles like alcohols or amines, this intermediate exists as a zwitterion containing an acidic proton, which undergoes removal by the nucleophile

or an external base (**C**). The subsequent rapid elimination of the leaving group (**D**) restores aromaticity, with the addition step typically determining the reaction rate.[493]

The S_NAr mechanisms exist on a continuum between stepwise and concerted processes, determined by substrate structure, nucleophile/leaving group nature, and reaction conditions.[494] Stepwise mechanisms predominate when strong electron-withdrawing groups (e.g., NO_2) pair with weak leaving groups in simple aryl systems. The concerted mechanism involves simultaneous nucleophilic attack and leaving group departure through a single transition state (Scheme 23, **E**) with partial bond formation/cleavage, without forming a stable intermediate.[494-496]

Mounting evidence from both experimental[495-499] and computational studies[500, 501] investigating the electronic factors governing S_NAr pathways suggests that the concerted mechanism dominates in most practical applications. A comprehensive study of 120 S_NAr reactions predicted 83% proceed via the concerted pathway [502], particularly in heterocyclic systems (pyridine, pyrazine, pyrimidine) with good leaving groups like chloride or bromide. This reveals the concerted mechanism is more prevalent in synthetically valuable S_NAr reactions than typically presented in educational contexts.[494, 502]

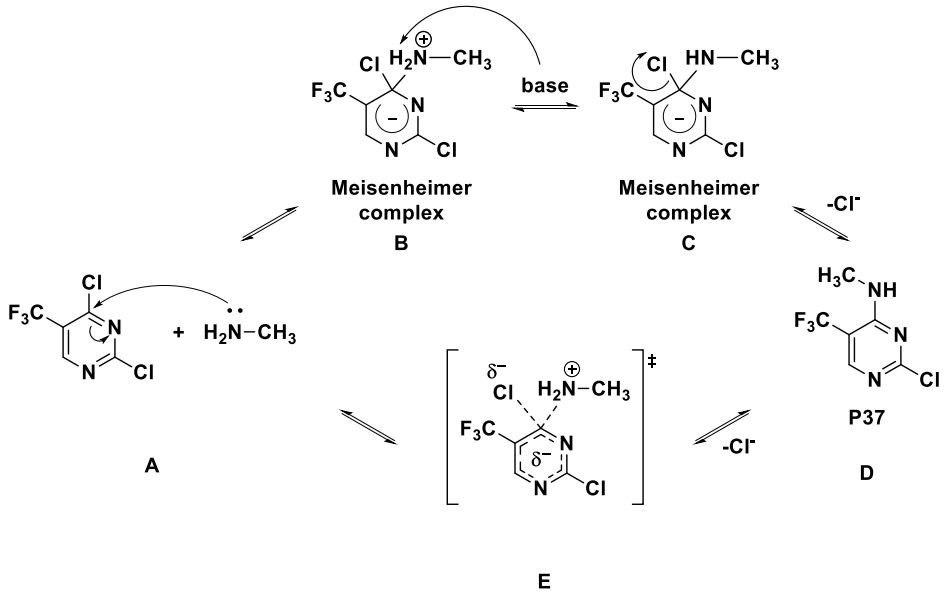

Scheme 23. Stepwise addition-elimination (**A**-**D**) and concerted (**E**) S_NAr mechanisms depicted on the formation of precursor **P37**.

While the classical S_NAr reactions typically proceed under basic or neutral conditions via stepwise or concerted mechanisms, a distinct and synthetically valuable acid-catalyzed variant expands their scope. By protonating the aromatic system, this approach enhances electrophilicity and enables nucleophilic substitution on less reactive substrates. Notably,

CARBAIN et al.[479] demonstrated an effective system using trifluoroacetic acid in 2,2,2-trifluoroethanol, facilitating S_NAr reactions between heterocycles and arylamines under mild conditions with high yields.

The mechanism proceeds through a classical addition-elimination pathway (Scheme 24, **A**-**D**), beginning with heterocycle protonation to enhance electrophilicity (**A**). The activated substrate undergoes nucleophilic attack (**B**), forming a Meisenheimer complex (**C**), followed by leaving group elimination and rearomatization (**D**). The acidic conditions serve a dual role: enhancing the substrate's electrophilicity while modulating the nucleophilicity of the incoming amine. Success of the reaction depends on maintaining optimal protonation states of both reaction partners, as excessive protonation of the amine nucleophile can inhibit the reaction, while insufficient substrate activation slows the process.

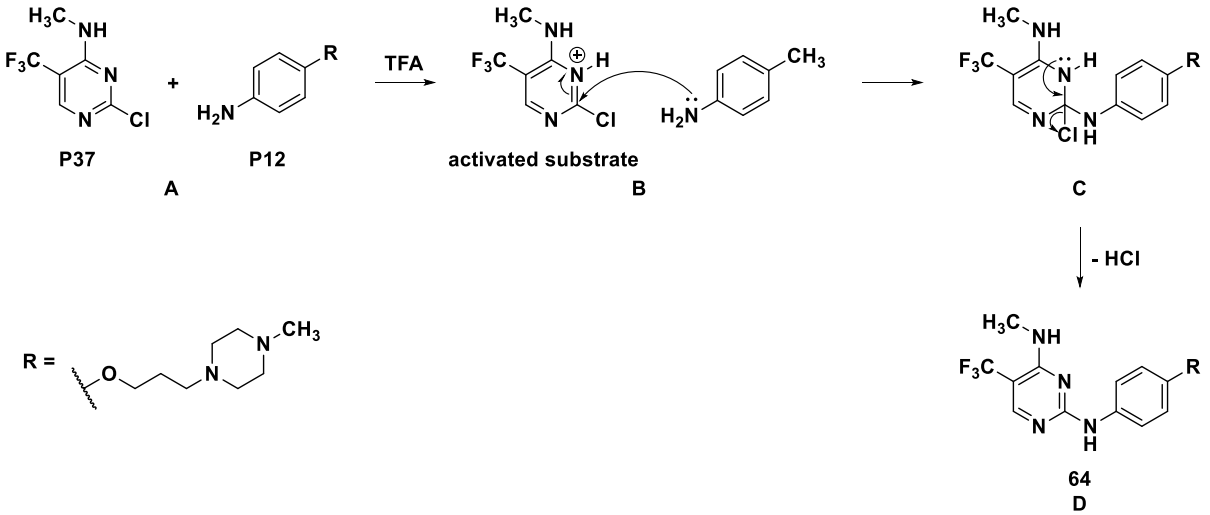

Scheme 24. The mechanism of acid-catalysed nucleophilic aromatic substitution depicted through the synthesis of target compound **64**.

3.5.5 Microwave-assisted S_NAr Reactions

Microwave-assisted organic synthesis has revolutionized S_NAr reactions through enhanced reaction rates, yields, and selectivity. Microwave heating functions via dipolar polarization and ionic conduction, where dipole molecules align with oscillating electric fields generating heat through friction[503], while ionic species produce heat via electromagnetic field interaction. This enables rapid, uniform energy transfer throughout the reaction medium.[504] Effectiveness depends on dielectric properties of reaction components, with polar solvents and ionic species (common in S_NAr reactions) coupling strongly with microwave radiation.[504] A key advantage is superheating – heating solvents beyond conventional boiling points under sealed conditions, allowing reactions at elevated temperatures.[505] Traditional S_NAr reactions requiring prolonged

heating under harsh conditions can complete in minutes with improved yields.[506] Microwave irradiation eliminates temperature gradients, ensuring uniform heating[503], while precise temperature control minimizes side reactions.[507] This approach transforms S_NAr reactions through efficient energy transfer mechanisms that overcome conventional heating limitations[504], enabling faster reactions, better yields, and enhanced selectivity.[506]

4 Pharmacology and Discussion

4.1 Pharmacological Assays

The initial characterization of the synthesized ligands involved determining their *in vitro* affinity for the *h*H_3R as their primary target. The dual-targeting compounds, designed to interact with both *h*H_3R and a secondary target, underwent additional evaluation for their inhibitory properties against G9a or LRRK2 enzymes. From these, the most promising candidates were selected for additional profiling, including cytotoxicity assessments, to evaluate their potential for further development. Meanwhile, the lipophilicity of all synthesized compounds was experimentally determined to assess their drug-like properties.

To gain deeper insights into the binding interactions between the ligands and their respective targets, a molecular docking study was conducted.

The *in vitro* pharmacological characterization was performed in the research group of Prof. Dr. Dr. h.c. HOLGER STARK. Contribution of Prof. Dr. KATARINA NIKOLIĆ and her co-workers, who conducted the *in silico* molecular docking studies, is gratefully acknowledged.

4.2 Principles of *h*H_3R Binding Affinity Determination

The binding of a ligand, whether endogenous or xenobiotic, to its target receptor initiates a complex signalling cascade that produces specific pharmacological effects. Receptors serve as crucial mediators in numerous physiological and pathological processes, establishing them as invaluable targets for therapeutic interventions. Small molecule drugs targeting receptors represent approximately 70% of all pharmaceuticals, with receptors comprising 45% of all drug targets, making them the most frequently utilized targets in drug development.[508, 509] This prevalence highlights the importance of quantitative assessment of ligand-receptor interactions in drug development campaigns.

The interaction between a ligand (L) and receptor (R) follows a reversible bimolecular reaction governed by the Law of Mass Action, resulting in the formation of a ligand-receptor complex (LR). At equilibrium, the forward and reverse reaction rates achieve balance, allowing the system to be characterized by the equilibrium dissociation constant K_d, defined as the ratio of dissociation (k_{-1}) to association rate constants (k_{+1}) (Equation 1).[510, 511]

$$L + R \underset{k_{-1}}{\overset{k_{+1}}{\rightleftharpoons}} LR \qquad K_d = \frac{k_{+1}}{k_{-1}} = \frac{[L] \bullet [R]}{[LR]}$$

Equation 1. L – ligand; R – Receptor, LR – ligand-receptor complex; k_{+1} – association rate constant; k_{-1} – dissociation rate constant; K_d – equilibrium binding constant.

The determination of binding affinity relies on labelled ligands, primarily those carrying radioactive isotopes or fluorophores, which produce quantifiable signals through liquid scintillation counting or fluorescence detection, respectively. Radioligand binding assays offer superior sensitivity, and the radioactive labels typically do not interfere with the ligand's receptor affinity. In contrast, fluorescent ligands provide a more cost-effective and safer alternative, eliminating the need for special handling of radioactive materials.[512] Both methods facilitate the determination of binding affinity for unlabelled ligands through competitive interaction at the same receptor binding site.[510]

Three distinct types of receptor binding experiments utilize radioactively labelled ligands, each providing valuable information about ligand-receptor interactions. 1) Saturation binding assays directly measure the binding of increasing concentrations of radioligand to the receptor, revealing both the maximum binding capacity (B_{max}) and the equilibrium dissociation constant (K_d), which together characterize the total number of binding sites and the ligand's affinity for the receptor. This generates a saturation curve, from which binding parameters are derived (Figure 22A and B). 2) Indirect binding, also known as competition or displacement assays, employs a fixed concentration of radioligand alongside increasing concentrations of unlabelled competitor compounds, enabling the determination of binding affinity (K_i) for unlabelled compounds. As the concentration of the unlabelled ligand increases, it displaces the radiolabelled ligand from the receptor, and the concentration required to displace 50% of the bound radioligand (IC_{50}) is used to calculate K_i (Figure 22C and D). 3) Lastly, kinetic binding assays provide insights into the rates of ligand association and dissociation. They measure the time course of radioligand binding, determining both association and dissociation rate constants, thereby providing insights into how quickly ligands bind to and dissociate from receptors, as well as revealing important mechanistic details about the binding process and drug-target residence time. These three complementary approaches form a comprehensive toolkit for understanding ligand-receptor interactions in drug discovery and development.[511, 513]

In receptor binding analyses, specific binding is defined when labelled ligands are bound to receptors. A binding maximum is approached due to the finite receptor population within tissue

samples. The maximum binding concentration (B_{max}) is determined when radioactive or fluorescent signals are displaced by saturating concentrations of unlabelled selective ligands. During these experimental procedures, labelled ligands are consistently entrapped within lipid membranes or experimental equipment, which is designated as nonspecific binding. Nonspecific binding refers to the signal not associated with the receptor and is measured in the presence of excessively high concentrations of an unlabelled ligand with high affinity. Ideally, nonspecific binding should not exceed 20% of the total signal. Unlike specific binding, nonspecific binding is not easily saturable. Total binding is established when specific and nonspecific binding values are combined.[514]

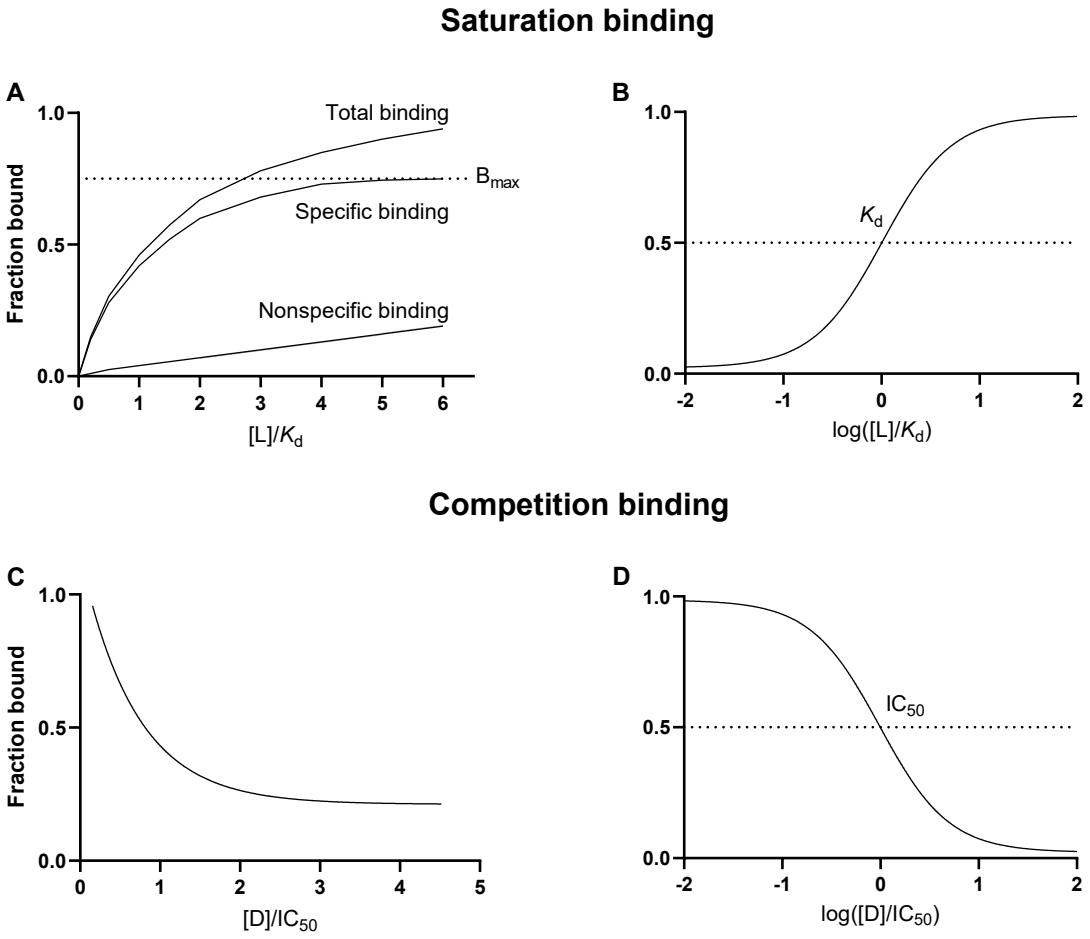

Figure 22 Saturation (A and B) and competition binding data (C and D), shown on arithmetic (A and C) and semilogarithmic plots (B and D). L – labelled ligand; K_d - equilibrium binding constant of labelled ligand; B_{max} – maximal specific binding; D – unlabelled ligand; IC_{50} – half-maximal inhibitory concentration. Modified from McKinney et al.[512]

In a saturation binding experiment, increasing concentrations of a labelled ligand are introduced to a receptor-containing tissue until all receptor sites are effectively occupied

(Figure 22A and B). In contrast, competition (displacement) assays involve fixed concentrations of a labelled ligand competing with increasing concentrations of an unlabelled ligand for receptor binding (Figure 22C and D). The competition assay is more commonly employed in screening and ligand characterization as it requires significantly lower amounts of radioligands and is, thus more economical. The IC_{50} value is defined as the concentration of the unlabelled competitor required to displace 50% of the specifically bound labelled ligand. If the ligand-receptor interaction reaches equilibrium and follows a bimolecular mechanism, the IC_{50} value is typically adjusted using the CHENG-PRUSOFF equation[515] to derive the equilibrium dissociation constant (K_i) for the unlabelled ligand (Equation 2)

$$K_i = \frac{IC_{50}}{1 + [L]/K_d}$$

Equation 2. CHENG-PRUSSOF equation. K_i – inhibition constant; IC_{50} – half-maximal inhibitory concentration; L – ligand; K_d - equilibrium binding constant.

Assessment of *in vitro* binding affinities of synthetized ligands **1**-**87** for *h*H_3R was performed utilizing radioligand displacement assay. The membrane fractions of HEK-293 cells stably expressing *h*H_3R were incubated with constant concentration of radiolabelled probe [^{3}H]*N*$^\alpha$-methylhistamine and different concentration of test ligands. Nonspecific binding was determined using high concentration of pitolisant (**L33**) as reference compound.[516] [^{3}H]*N*$^\alpha$-methylhistamine, a well-characterized H_3R agonist, was employed despite the expected antagonist-like behaviour of test compounds based on their structural similarity to established H_3R antagonists and inverse agonists. While agonist radioligands preferentially bind to the active receptor conformation, competitive displacement can still occur when antagonists have sufficient orthosteric site affinity. Although the measured K_i values may differ from those obtained with antagonist radioligands due to conformational selectivity, this approach provides valuable affinity rankings among structurally related compounds and suggests competitive interaction at the orthosteric binding site. The validity of this methodology is supported by numerous literature reports demonstrating effective displacement of agonist radioligands by known H_3R antagonists.[204, 420, 516]

4.3 Principles of Enzyme Inhibition Determinations

Enzymes are biological catalysts essential for life, accelerating biochemical reactions by lowering activation energy to sustain vital processes. While crucial for metabolic homeostasis, their dysregulation contributes to many diseases, making enzyme inhibition a key therapeutic strategy for conditions like hypertension, glaucoma, gout, infections, cancer, and PD, and many others.[517] The clinical importance of enzymes is highlighted by being the second most prevalent target of clinically approved small drug compounds, accounting for 29% of all drug targets, and only surpassed by receptors.[508]

Enzyme inhibition assays are vital in drug discovery, not only for identifying inhibitors but also for elucidating mechanisms of action, binding kinetics, potency (e.g., IC_{50}), and selectivity. This knowledge is essential for optimizing drug candidates to maximize efficacy and reduce side effects.

Enzyme activity is measured by tracking substrate depletion or product formation, detectable through changes in absorbance, fluorescence, luminescence, or other signals.[518, 519] Spectrophotometric methods can detect changes in absorption spectra as substrates are converted to products. Fluorescence-based techniques offer superior sensitivity by measuring either direct fluorescence changes or utilizing fluorescently labelled substrates. Advanced methods such as mass spectrometry provide detailed molecular-level information about reaction components, while calorimetric approaches measure the heat generated during enzymatic reactions, offering unique insights into reaction thermodynamics.[520]

To evaluate enzyme inhibition, the reaction is monitored both in the absence and presence of a potential inhibitor. The resulting data provide insights into the compound's potency, selectivity, and mechanism of action. Two primary approaches are used for enzyme reaction monitoring: continuous assays and discontinuous (sampling) assays. Continuous assays measure changes in real time, making them ideal for kinetic studies, while discontinuous assays involve stopping the reaction at a fixed time point and quantifying the signal, which is often more suitable for high-throughput screening.[521]

Of particular relevance to this research were two discontinuous enzyme inhibition assays aimed at G9a and LRRK2, as secondary targets aligned with the multitarget-directed ligand design strategy. Compound activity against these enzymes was evaluated using distinct screening platforms – an AlphaLISA assay for G9a and a TR-FRET-based assay for LRRK2. Both methods were selected based on their sensitivity, operational simplicity, and compatibility with synthesized library of compounds.

4.3.1 Principles of G9a screening assay

The G9a methyltransferase inhibition studies utilized AlphaLISA (Amplified Luminescent Proximity Homogeneous Assay), a bead-based homogeneous immunoassay that detects biomolecular interactions through a proximity-dependent energy transfer mechanism. This platform quantifies enzymatic activity by generating a luminescent signal when specific molecular events bring donor and acceptor beads into close proximity.[522]

The assay operates on a simple yet elegant principle (Figure 23). Donor beads containing a photosensitizer (phthalocyanine) are excited at 680 nm, converting ambient oxygen into reactive singlet oxygen molecules. These highly energetic but short-lived singlet oxygen species can diffuse approximately 200 nm in solution before returning to their ground state. When acceptor beads are positioned within this diffusion range, the singlet oxygen molecules transfer energy to thioxene derivatives within the acceptor beads, initiating a cascade of chemical reactions. This energy transfer triggers a chemiluminescent reaction within the acceptor beads, subsequently exciting nearby fluorophores that emit detectable light at 615 nm. The process creates significant signal amplification, as a single excitation event can generate multiple singlet oxygen molecules. Additionally, the time-resolved detection method leverages the fluorophore's long emission lifetime to minimize background interference, resulting in exceptional signal-to-noise ratios.[510]

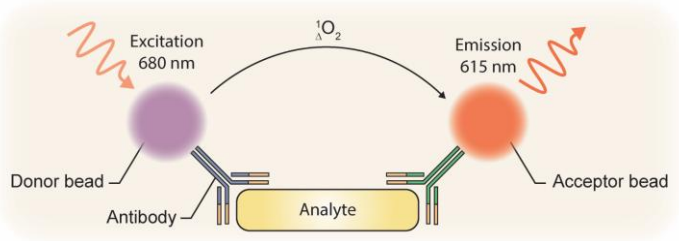

Figure 23. Schematic representation of AlphaLISA measuring principle.

For G9a methyltransferase inhibition studies, the assay system is designed to detect histone methylation. Streptavidin-conjugated donor beads specifically bind the biotinylated histone H3-derived peptide substrate, regardless of its methylation status. Acceptor beads, in turn, are coupled to antibodies targeting methylated histone H3 – specifically the H3K9me2 mark generated by G9a activity. This configuration ensures luminescent signal production only upon successful methylation of the substrate, which brings donor and acceptor beads into proximity for energy transfer.

The G9a inhibitory properties of 6-methylpyrimidine-2,4-diamine derivatives (**24**-**39**), designed as potential dual-targeting ligands for H_3R and G9a, were evaluated using the AlphaLISA screening assay.

4.3.2 Principles of LRRK2 screening assay

The LRRK2 kinase inhibition studies employed TR-FRET (Time-Resolved Fluorescence/Förster Resonance Energy Transfer), a homogeneous, proximity-based assay that quantifies enzymatic activity through a fluorescence resonance energy transfer mechanism.[510] This platform measures kinase activity by generating a FRET signal when phosphorylation-dependent molecular interactions bring donor and acceptor fluorophores into close proximity. The assay is widely used to screen kinase inhibitors, offering high sensitivity, versatility and compatibility with high-throughput screening workflows.[523]

The fundamental principle of TR-FRET involves a lanthanide complex donor fluorophore that, upon excitation, transfers energy non-radiatively to an acceptor molecule through dipole-dipole coupling. This energy transfer occurs exclusively when three critical conditions are met: appropriate spectral overlap between donor emission and acceptor absorption spectra, correct molecular orientation, and sufficient proximity (typically 1-10 nm) between the interacting fluorophores.[524] The acceptor subsequently emits detectable fluorescence at a characteristic wavelength, commonly 665 nm. A key advantage of the time-resolved measurement approach is the introduction of a temporal delay before detection, allowing transient background fluorescence from biological matrices and test compounds to decay, thereby enhancing signal specificity and assay robustness.

In the context of LRRK2 inhibition assessment, an ADP-quantification TR-FRET configuration that monitors reaction kinetics through direct measurement of reaction products has been implemented (Figure 24). This system employs europium-labelled anti-ADP antibodies as energy donors coupled with Alexa Fluor 647-conjugated ADP molecules serving as energy acceptors and competitive tracers. The assay operates on a competitive binding principle where both enzymatically-produced unlabelled ADP and fluorescently-tagged ADP tracer compete for limited antibody binding sites. Importantly, only tracer-antibody complexes generate the TR-FRET signal due to the proximity-induced energy transfer between the europium donor and Alexa Fluor 647 acceptor. The relationship between kinase activity and signal intensity follows an inverse correlation pattern. When LRRK2 kinase functions actively, substantial ATP consumption generates high concentrations of unlabelled ADP, which effectively outcompetes the fluorescent ADP tracer for antibody binding, resulting in

diminished TR-FRET signal intensity. Conversely, when potent inhibitors suppress LRRK2 activity, reduced ATP hydrolysis leads to lower unlabelled ADP production, allowing greater tracer-antibody complex formation and consequently producing enhanced TR-FRET signal. This elegant signal inversion mechanism provides a direct readout of inhibitor potency, enabling precise pharmacological characterization of candidate molecules targeting LRRK2 kinase activity.

The LRRK2 inhibitory properties of 5-chloro- and 5-(trifluoromethyl)pyrimidine-2,4-diamine derivatives (**40**-**87**), designed as potential dual-targeting ligands for H_3R and LRRK2, were evaluated using the TR-FRET-based screening assay.

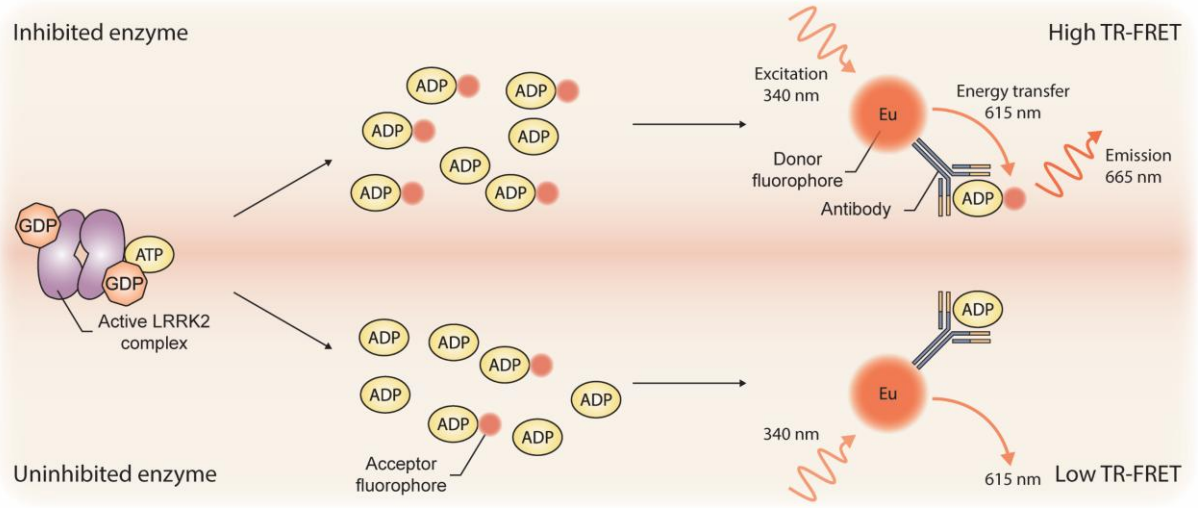

Figure 24. TR-FRET-based inhibition assessment of LRRK2 enzyme.

4.4 Evaluation of Pyrimidin-4-amine Derivatives

In the pursuit of novel histamine H_3R ligands, a small set of 13 pyrimidin-4-amine derivatives was designed and synthetized, adhering to a well-established H_3R pharmacophore blueprint (Figure 9).[267, 415, 416] Structural diversity within the set was introduced through systematic variations in the 1st basic moiety of the pharmacophore, incorporating methylpiperazine, acetylpiperazine, and piperidine. Additionally, pyrimidin-4-amine, employed as the 2nd basic moiety in the arbitrary region of the molecule, served as a secondary modification point. Structural diversity was introduced by modifying the C-5 position of the pyrimidine ring with various carboxylic acid derivatives, namely esters, acids, amides, and nitriles. This approach yielded **12** compounds (**1**-**12**), which were complemented by a structurally related analogue (**13**), as summarized in (Table 5).

The binding affinity data revealed a clear SAR, with the 1st basic moiety playing a crucial role in determining *h*H$_3$R binding affinity. The piperidine-containing compounds (**9**-**12**, K_i = 1.11 – 32.6 nM) demonstrated exceptional potency with low nanomolar affinities, significantly outperforming their methylpiperazine (**1**-**4**, K_i = 281 – 616 nM) and acetylpiperazine (**5**-**8**, K_i = 212 – 810 nM) counterparts, which showed moderate-to-high nanomolar or micromolar range activities. For example, replacing the 4-methylpiperazine in compound **1** (K_i = 281 nM) with piperidine in compound **9** (K_i = 1.97 nM) results in a 140-fold improvement in affinity, suggesting that the piperidine ring system is far more favourable for receptor binding than the substituted piperazine. The comparison between 4-methylpiperazine (**1**-**4**) and 4-acetylpiperazine (**5**-**8**) compounds reveals no consistent advantage for either substituent. Furthermore, replacing the methylthio group of compound **3** (K_i = 444 nM) with chloro substituent (**13**, K_i = 1620 nM) drastically diminishes binding, underscoring the importance of the thioether moiety.

Table 5. Binding affinities of compounds **1**-**13**.

Structure	R	Compd	*h*H$_3$R K_i [nM] [95% CI][a]
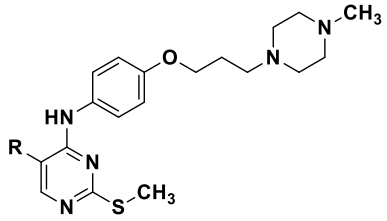	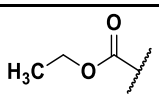	**1**	281 [98.6 – 801]
		**2**	444 [111 – 1771]
		**3**	444 [111 – 1771]
		**4**	616 [100 – 3805]
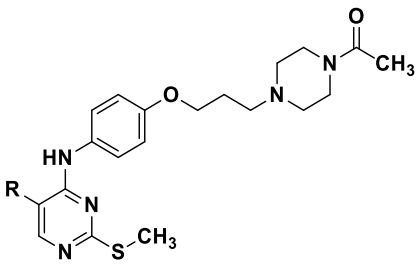	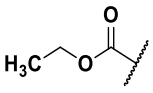	**5**	212 [89.1 – 504]
		**6**	810 [158 – 4155]
		**7**	717 [417 – 1232]
		**8**	241 [104 – 555]

[a] Affinity data are presented as mean K_i values with corresponding 95% confidence intervals, based on at least three independent experiments performed in duplicate.

Table 5. *Continued.*

Structure	R	Compd	*h*H$_3$R K_i [nM] [95% CI][a]
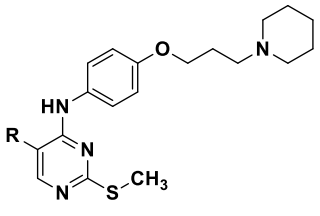	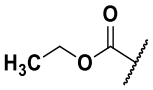	**9**	1.97 [0.44 – 8.76]
		**10**	1.11 [0.93 – 1.33]
		**11**	32.6 [22.6 – 47.0]
		**12**	1.63 [0.73 – 3.65]
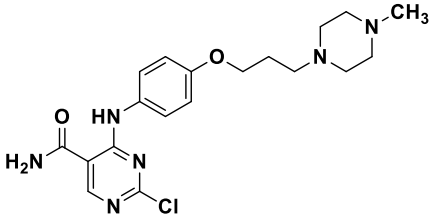		**13**	1620 [507 – 5180]
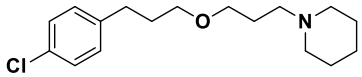		**Pitolisant (L33)**	13.2 [3.20 – 54.1]

[a] Affinity data are presented as mean K_i values with corresponding 95% confidence intervals, based on at least three independent experiments performed in duplicate.

Within the high-performing piperidine series, compounds featuring carboxylic acid (**10**), nitrile (**12**), and ester (**9**) functionalities achieved remarkable single-digit nanomolar affinities (K_i = 1.11 nM, 1.63 nM, and 1.97 nM, respectively), surpassing the binding affinity of the clinically validated reference compound pitolisant (**L33**) (K_i = 13.2 nM). While the amide variant maintained strong binding with a K_i of 32.6 nM, it showed somewhat reduced potency compared to its structural analogues.

The potent compounds from the piperidine series serve as promising leads for further development and expansion of pyrimidin-4-amine-based H$_3$R ligands. Further exploration of these scaffolds may enable mapping of ligand-receptor interactions, potentially offering insights into the contributions of specific functional groups. This understanding could guide the design of new H$_3$R ligands with refined pharmacological properties. The systematic structural variations implemented, together with the observed correlation between structural features and binding affinities, establish a reasonable basis for future efforts in this area.

4.5 Evaluation of Pyrimidin-2-amine Derivatives

A series of 10 novel pyrimidin-2-amine derivatives (**14**-**23**) was synthesized. The H_3R pharmacophore was assembled by attaching a propylpiperidine fragment to the C-4 position of pyrimidin-2-amine, which served as the central core. The compounds were designed with two distinct structural motifs: 3-(piperidin-1-yl)propyloxy (**14**-**18**) and 3-(piperidin-1-yl)propylthio (**19**-**23**). Structural diversity was introduced through systematic modification of the C-6 substituent on the pyrimidine core, including unsubstituted, methyl, ethyl, isopropyl, and cyclopropyl groups. This dual variation in both the linking group (O vs. S) and C-6 substituents enabled a comprehensive SAR analysis. Binding affinities (Table 6) for *h*H_3R were determined using a radioligand displacement assay, with pitolisant (**L33**) as a positive control.

The thio derivatives (**19-23**) consistently exhibited higher binding affinity (lower K_i values) compared to their alkoxy analogs (**14-18**) across all C-6 substituents, underscoring the advantage of sulfur-based linkers. In the alkoxy series, the size of the C-6 substituent showed a clear inverse correlation with affinity, with the trend being unsubstituted (K_i = 786 nM) > methyl (2103 nM) ≈ ethyl (2197 nM) ≈ isopropyl (2159 nM) > cyclopropyl (3572 nM). This suggests that bulkier substituents introduce steric hindrance, disrupting optimal interactions with the receptor. A similar trend was observed in the thio series, though it was less consistent due to wider confidence intervals. For example, the 6-ethyl derivative **21** (K_i = 720 nM), outperformed the 6-methyl analog **20** (K_i = 876 nM).

The data indicate that bulkier substituents generally reduce affinity, likely due to unfavourable steric interactions with the receptor binding pocket. However, the thio linker appears to mitigate this effect to some extent, as evidenced by the comparatively higher affinity of thio derivatives with larger substituents (e.g., cyclopropyl thio: 2338 nM vs. alkoxy: 3572 nM). The 6-unsubstituted thio derivative **19** emerged as the most potent compound in the series (K_i = 596 nM), highlighting the advantage of minimal steric demand at the C-6 position. These findings provide valuable insights for further optimization of pyrimidin-2-amine derivatives as *h*H_3R ligands, emphasizing the importance of both linker choice and substituent size in modulating receptor affinity.

Table 6. Binding affinities of compounds **14**-**23**.

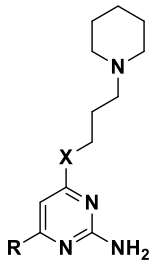

R	Compd X = O	*h*H$_3$R K_i [nM] [95% CI][a, b]	Compd X = S	*h*H$_3$R K_i [nM] [95% CI]
	**14**	786 [417 – 1479]	**19**	596 [316 – 986]
	**15**	2103 [1780 – 2485]	**20**	876 [311 – 2467]
	**16**	2197 [341 – 14144]	**21**	720 [346 – 1500]
	**17**	2159 [1959 – 2380]	**22**	1541 [491 – 4829]
	**18**	3572 [725 – 17595]	**23**	2338 [679 – 8059]

[a] Pitolisant (**L33**) was tested as a reference *h*H$_3$R ligand showing K_i = 13.2 nM

[b] Affinity data are presented as mean K_i values with corresponding 95% confidence intervals, based on at least three independent experiments performed in duplicate.

Based on the obtained K_i values, the prepared set of pyrimidin-2-amine derivatives showed moderate to low affinity for *h*H$_3$R especially when compared to pitolisant (**L33**) used as a reference *h*H$_3$R ligand.

4.6 Evaluation of Pyrimidine-2,4-diamine Derivatives

4.6.1 6-Methylpyrimidine-2,4-diamine Derivatives

The recent discovery of A-366 (**L65**, Figure 25) as the first dual-targeting H$_3$R/G9a ligand, coupled with the promising therapeutic potential of simultaneous H$_3$R/G9a targeting in PWS[204], led to the design of 16 novel 6-methylpyrimidine-2,4-diamine derivatives (**24**-**39**). The series aimed to explore the chemical space around the 6-methylpyrimidine-2,4-diamine scaffold and identify new dual-targeting H$_3$R/G9a ligands.

A key structural commonality exists between G9a inhibitors (i.e. **L65** and **L66**)[293, 329] and H$_3$R ligands (like **L32** and **L33**)[152] in the form of basic centrum attached to aromatic core via propyloxy linker that is important for the potency. X-ray crystallography confirmed that this

structural element occupies the lysine channel, enhancing G9a potency[329], while simultaneously serving as an established H_3R pharmacophore.[144] These structural insights enabled a knowledge-based approach[262] to design ligands with fused structural elements (Figure 25).

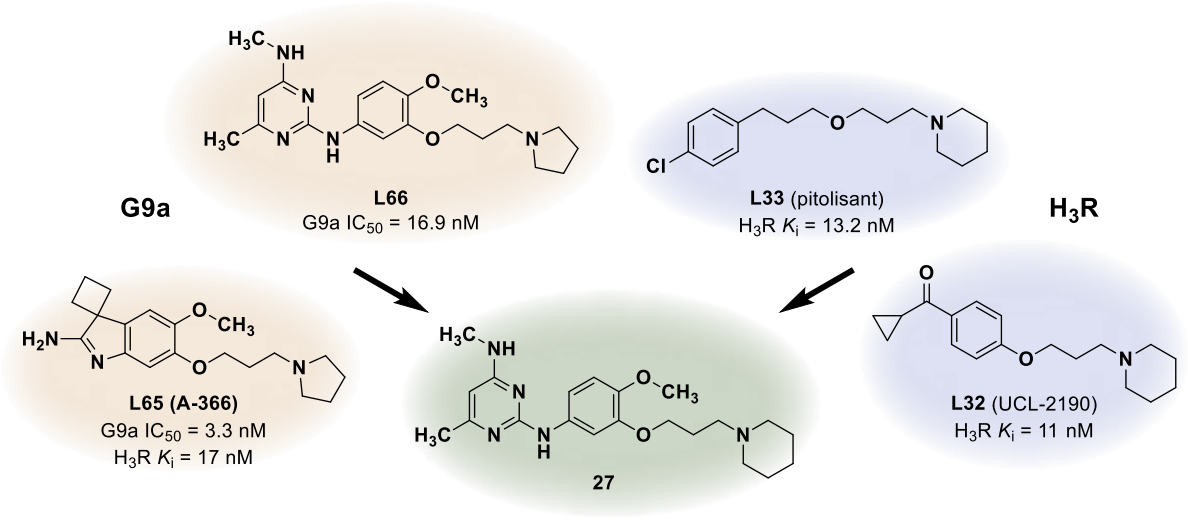

Figure 25. Design of compound **27** as dual targeting G9a/H_3R ligand by fusing structural fragments of known G9a and H_3R ligands. Excluding **L33** H_3R K_i value that was obtained in-house, all other IC_{50} and K_i values were compiled from published literature sources.[143, 293, 329]

The set of 6-methylpyrimidine-2,4-diamine derivatives exhibits systematic structural variation around target compound **27**. The diversity was generated through strategic placement of two alkylamino (methyl- or ethylamino) and four arylamino substituents (**P12, P14-P15**, Scheme 3) at the C-2 and C-4 positions.

The combinatorial arrangement of these substituents, alternating between the two positions, yielded a comprehensive series of 16 compounds (**24**-**39**) (Table 7). This design strategy enabled thorough exploration of SAR and positional effects of the substituents. The screening results reveal clear trends among the analysed compounds. In most cases compounds with 2-alkylamino substitution demonstrate higher affinity for *h*H_3R compared to their 4-substituted counterparts, indicating optimal interactions of 2-alkylamino substituents with the receptor. Derivatives containing the piperidine group in the arylamino substituent (**25**, **29**, **33** and **37**) emerge as the most potent compounds, consistently showing lower K_i values compared to their methylpiperazine counterparts (**24**, **29**, **32** and **36**). The superior affinity of compounds **25**, **29**, **33** and **37** aligns with their structural similarity with reference inhibitor pitolisant (**L33**).

Table 7. *h*H_3R binding affinities and single-point G9a inhibitory potencies of compounds **24**-**39**.

Ar	Compd	*h*H_3R K_i [nM] [95% CI][a, b, c]	G9a [%] ± SD at 10 µM[d]	Compd	*h*H_3R K_i [nM] [95% CI]	G9a [%] ± SD at 10 µM
		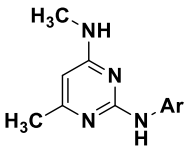			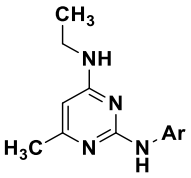	
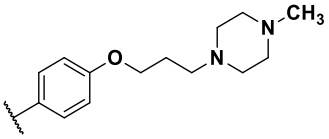	**24**	117 [42.8 – 729]	33.4 ± 18.5	**28**	244 [110 – 538]	52.3 ± 4.6
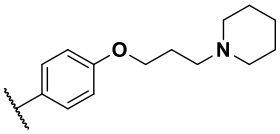	**25**	32.4 [11.4 – 92.1]	15.1 ± 12.2	**29**	25.0 [8.27 – 75.7]	21.0 ± 3.3
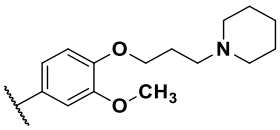	**26**	68.4 [44.7 – 105]	60.1 ± 14.7	**30**	45.4 [13.6 – 151]	70.4 ± 21.8
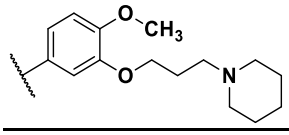	**27**	128 [61.1 – 272]	102.3 ± 2.1	**31**	25.2 [9.67 – 65.6]	108.4 ± 0.5
		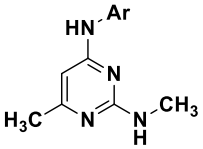			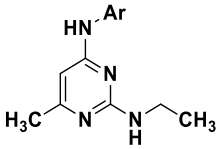	
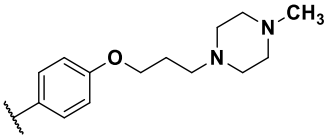	**32**	102 [49.9 – 209]	40.2 ± 4.2	**36**	20.9 [11.3 – 38.8]	25.2 ± 1.6
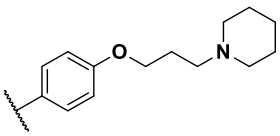	**33**	1.40 [0.23 – 8.37]	45.9 ± 1.5	**37**	18.0 [11.2 – 29.0]	51.7 ± 1.3
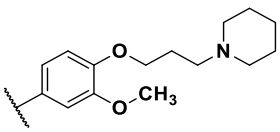	**34**	32.9 [15.4 – 70.2]	92.2 ± 0.7	**38**	65.3 [26.7 – 160]	70.0 ± 0.7
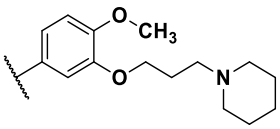	**35**	82.5 [30.8 – 221]	103.7 ± 1.1	**39**	138 [50.3 – 337]	103.0 ± 2.6

[a] Affinity data are presented as mean K_i values with corresponding 95% confidence intervals, based on at least three independent experiments performed in duplicate.

[b] Pitolisant (**L33**) was tested as a reference *h*H_3R ligand showing K_i = 13.2 [95% CI: 3.20 – 54.1].

[c] **L65** has reported values of *h*H_3R K_i = 17 nM and G9a IC_{50} = 2.5 nM.[204, 329]

[d] G9a inhibition was calculated as percentages related to control at a test concentration of 10 µM.

The introduction of methoxy substitution generally reduces *h*H_3R affinity, with compound **31** (K_i = 25.2 nM) being a notable exception, maintaining high affinity despite its 4-methoxy group. Compound **33** (K_i = 1.40 nM) stands out as the most potent in the series, displaying affinity comparable to the clinical H_3R inverse agonist pitolisant (**L33**).

The G9a inhibitory potential was evaluated at 10 µM, with results expressed as percentage of inhibited enzyme activity. Compounds showing both high *h*H_3R affinity and significant G9a inhibition at 10 µM underwent further G9a IC_{50} determination. The presented data (Table 7) revealed a distinct structure-activity relationship pattern, where the methoxy substitution plays a dual role - while reducing *h*H_3R affinity, it significantly enhances G9a inhibition. This finding provides valuable insights for the rational design of dual-acting compounds. Notably, methoxy-substituted derivatives consistently achieve high or complete enzyme inhibition.

Based on the combined *h*H_3R and G9a activity profiles, compounds **31**, **34**, and **35** were selected for G9a IC_{50} determination due to their complete enzyme inhibition and maintained receptor affinity. Additionally, compound **33** was included in this selection owing to its exceptional *h*H_3R potency, despite showing moderate G9a inhibition. Furthermore, the compounds cytotoxicity was assayed on SH-SY5Y cell line.

The compounds **33** and **34** exhibited weak G9a inhibition, with IC_{50} values in the micromolar range (Table 8). On the other hand, **31** (K_i = 25.2 nM, IC_{50} = 63.9 nM) and **35** (K_i = 82.5 nM, IC_{50} = 494 nM) demonstrate the feasibility of designing dual-action ligands, though **31** stands out for its notable potency and well-balance activity against both *h*H_3R and G9a. However, identified dual-targeting ligands are less potent on both targets compared to the reference **L65**, as first-in-class dual *h*H_3R/G9a ligand. The compound demonstrated minimal cytotoxic effects, as the cell viability remained consistently above 90%.

Table 8. *h*H_3R K_i and G9a IC_{50} values and of selected compounds and their effects on SH-SY5Y cell viability.[a]

Compound	***h*H$_3$R K$_i$ [nM] [95% CI]**	**G9a IC$_{50}$ [nM] [95% CI]**	**SH-SY5Y viability [%] ± SD at 10 µM**
31	25.2 [9.67 – 65.6]	63.9 [27.0 – 151]	92.7 ± 2.3
33	1.40 [0.23 – 8.37]	17765 [7159 – 43860]	103.7 ± 3.4
34	32.9 [15.4 – 70.2]	4298 [1276 – 14481]	95.0 ± 3.6
35	82.5 [30.8 – 221]	494 [269 – 906]	90.3 ± 4.3

[a] Data are presented as mean values with corresponding 95% confidence intervals or standard deviations, based on at least three independent experiments performed in duplicate.

To gain better insight into the interactions between ligands **24**-**39** with H_3R and G9a targets, the molecular docking study was performed. Initially, the docking protocol for both targets was first validated by re-docking the reference ligands, using the original co-crystalline ligands (**L41** for H_3R and **L66** for G9a) as reference. The conformations with the highest GoldScore and all key interactions with the amino acid residues in the binding sites (Figure 26 and Figure 27) were evaluated using the root mean square deviation (RMSD) values. The best predicted bioactive conformations for the H_3R antagonist **L41** and the G9a inhibitor **L66** showed all key interactions and comparable poses with the co-crystalline reference ligands with RMSD values of 0.552 and 0.637. Based on the validation criterion that the RMSD of the docked reference ligand has a value of 2 Å or less[525], it can be concluded that both the H_3R and G9a docking protocols are valid. The GoldScore values and key interactions of reference and synthesized compounds for both targets are listed in Table S1 (Supplementary Data).

To evaluate the docking results in terms of potency, some of the representative candidates (**28**, **31**, **34** and **35**) were selected.

In the case of G9a, **31** with the highest experimental potency (G9a IC_{50} = 63.9 nM) for the enzyme and **33** with the lowest experimental potency (G9a IC_{50} = 17765 nM) (Table S1) were selected to find relationships between potency, key interactions and the binding mode in the active site of the enzyme.

For H_3R, compounds **31** and **33** were selected based on their excellent potency (H_3R K_i = 25.2 nM and 1.4 nM, respectively) compared to the reference ligand (**L41**, H_3R K_i = 1.7 – 37.45 nM) (Table S1). To gain a better insight into the relationship between the behaviour of the ligands in the binding site of G9a and H_3R with the experimental IC_{50} and K_i values, compound **35** with middle experimental potency for G9a (G9a IC_{50} = 494 nM) and compound **28** with the lowest experimental potency for H_3R (H_3R K_i = 224 nM) were also discussed.

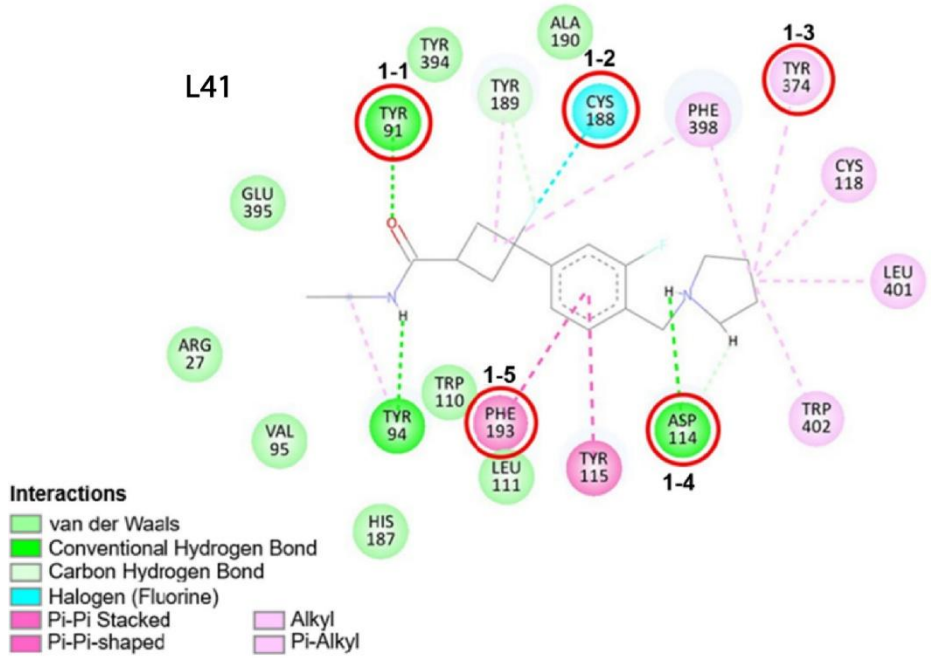

Figure 26. Interactions of the H_3R antagonist **L41** with the amino acid residues in active site of the PDB: 7f61 (H_3R). Highlighted with a red circle are hydrogen bonds (Asp114 and Tyr91), the halogen-O interaction of Cys188 and two hydrophobic interactions of Phe193 and Tyr374 that have been identified as important in the literature.[33]

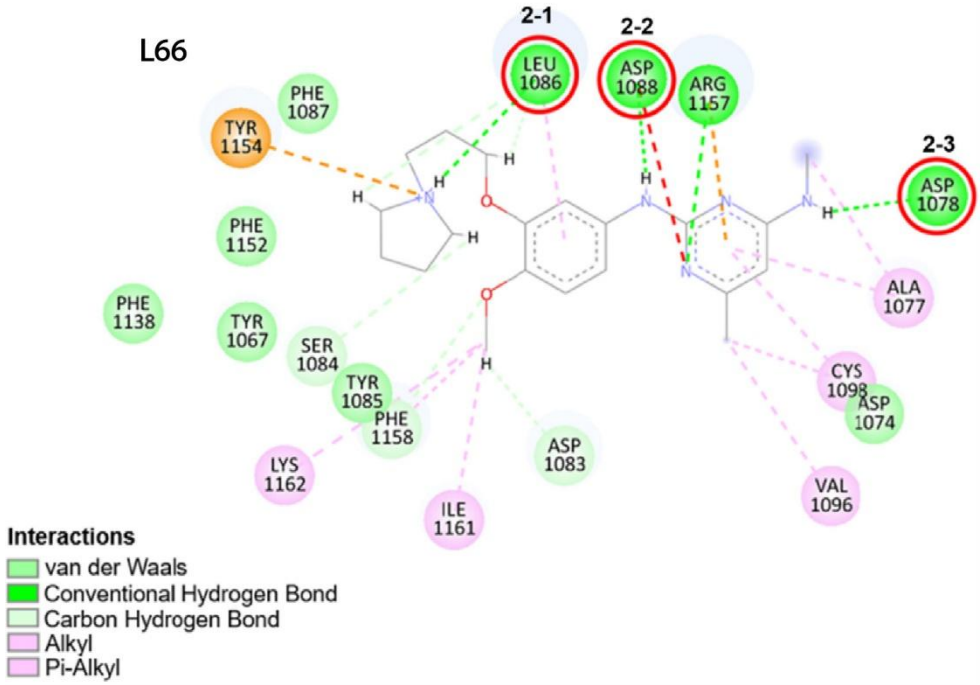

Figure 27. Interactions of the G9a inhibitor **L66** with the amino acid residues in active site of the PDB: 7btv (G9a). Hydrogen bonds that have been identified as important in literature are highlighted with a red circle.[293]

Compound **31**, a potent G9a inhibitor, forms two hydrogen bonds with Asp1088 and a hydrogen bond with Asp1078 in the active site of the G9a enzyme (Figure 28, left). Therefore, it forms two (Table S1, 2-2; 2-3) of three reference ligand interactions (Figure 27, PDB:7btv). In the case of H_3R compound **31**, a strong H_3R antagonist, forms hydrogen bond with the side chain of Asp114, hydrogen bond with Tyr91 and two hydrophobic interactions (Figure 28, right). Thus, it forms four (Table S1, 1-1; 1-3; 1-4; 1-5) of five reference ligand interactions in the H_3R binding pocket (Figure 26, PDB:7f61).

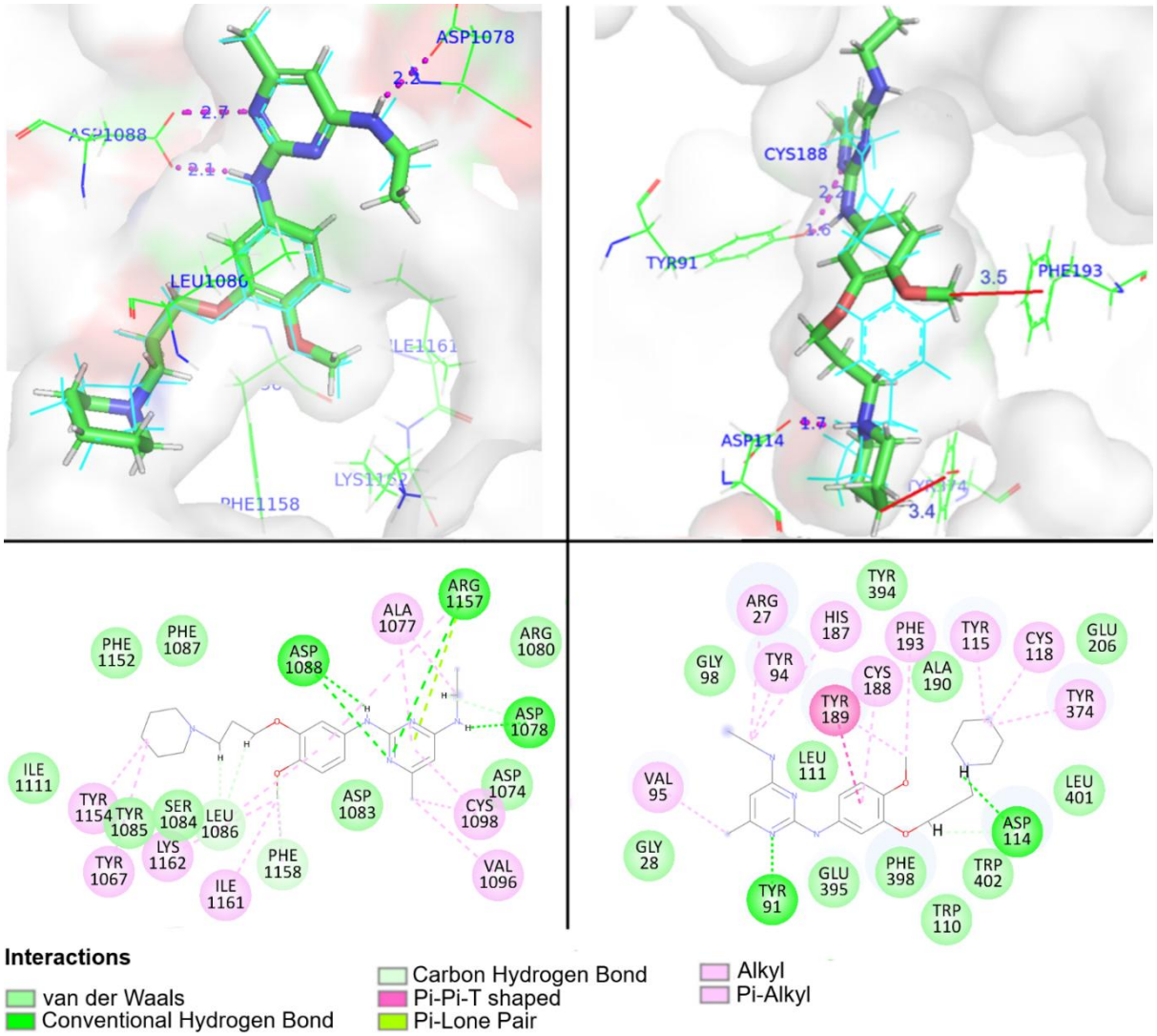

Figure 28. Pose of **31** with interactions in the active site of the G9a (PDB: 7btv) (left) and H_3R (PDB: 7f61) (right); the cyan lines represent the reference ligands of the PDBs, while the sticks represent the **31**.

Compound **33**, a weak G9a inhibitor, forms one hydrogen bond with the side chain of Asp1078 and one hydrogen bond with the side chain of Leu1086 (Figure 29, left), while it does not form hydrogen bonds with Asp1088. Therefore, it forms two (Table S1, 2-1; 2-2) of three reference ligand interactions (Figure 27, PDB:7btv). In the H_3R binding site compound **33**, a strong H_3R

antagonist, forms one hydrogen bond with the side chain of the Asp114 and hydrophobic bond with side chain of Tyr374 (Figure 29, right). Thus, it forms two (Table S1,1-3; 1-4) of five reference ligand interactions in the H_3R binding pocket (Figure 26, PDB:7f61).

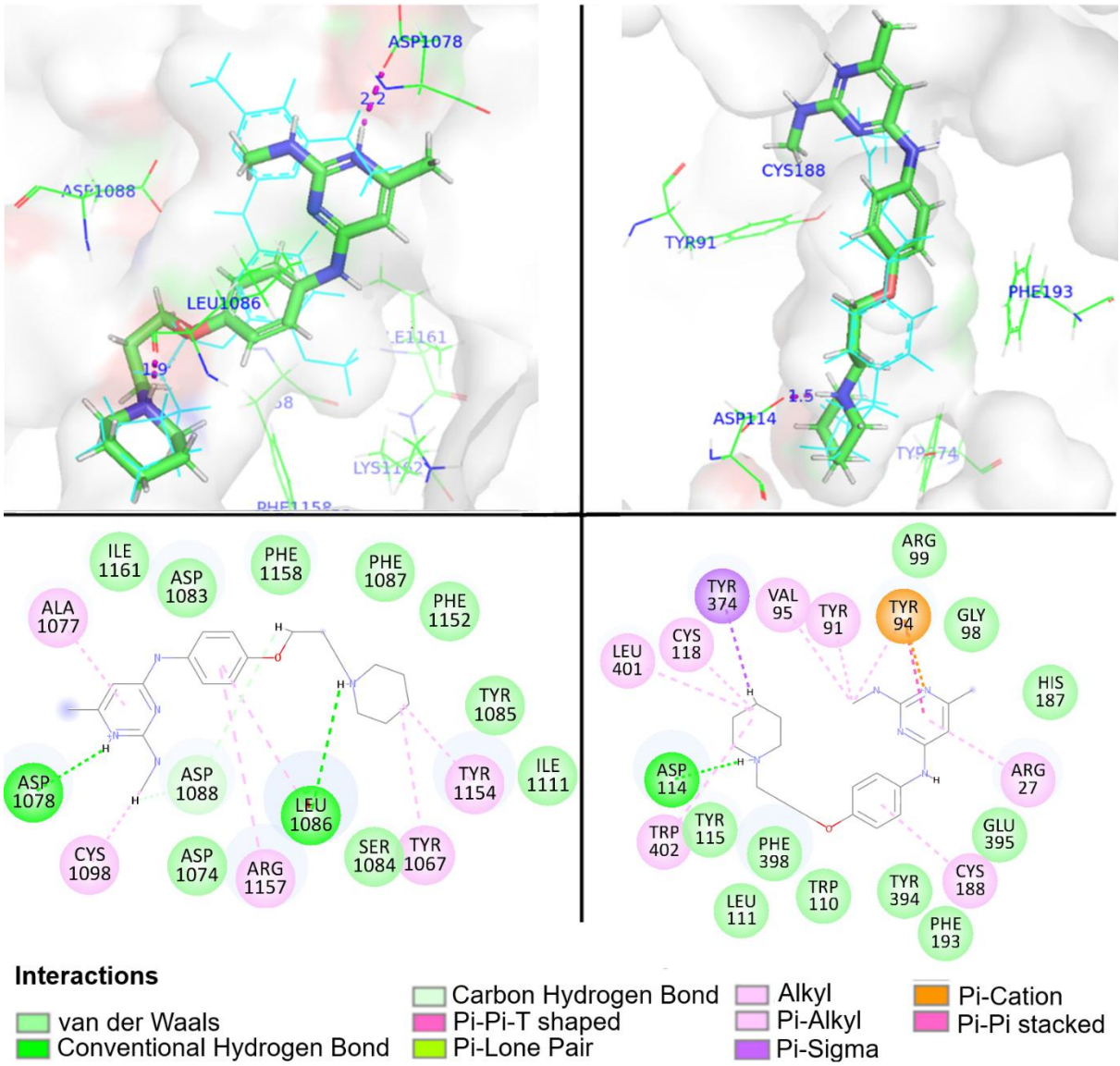

Figure 29. Pose of the 33 with interactions in the active site of G9a (PDB: 7btv) (left) and H_3R (PDB: 7f61) (right); the cyan lines represent the reference ligands of the PDBs, while the sticks represent **33**.

Compound **34**, a moderate G9a inhibitor, forms a hydrogen bond with the side chain of Asp1078 and a hydrogen bond with the side chain of Asp1088 (Figure 30, left). Therefore, it forms two (Table S1, 2-2; 2-3) of three reference ligand interactions (Figure 27, PDB:7btv).

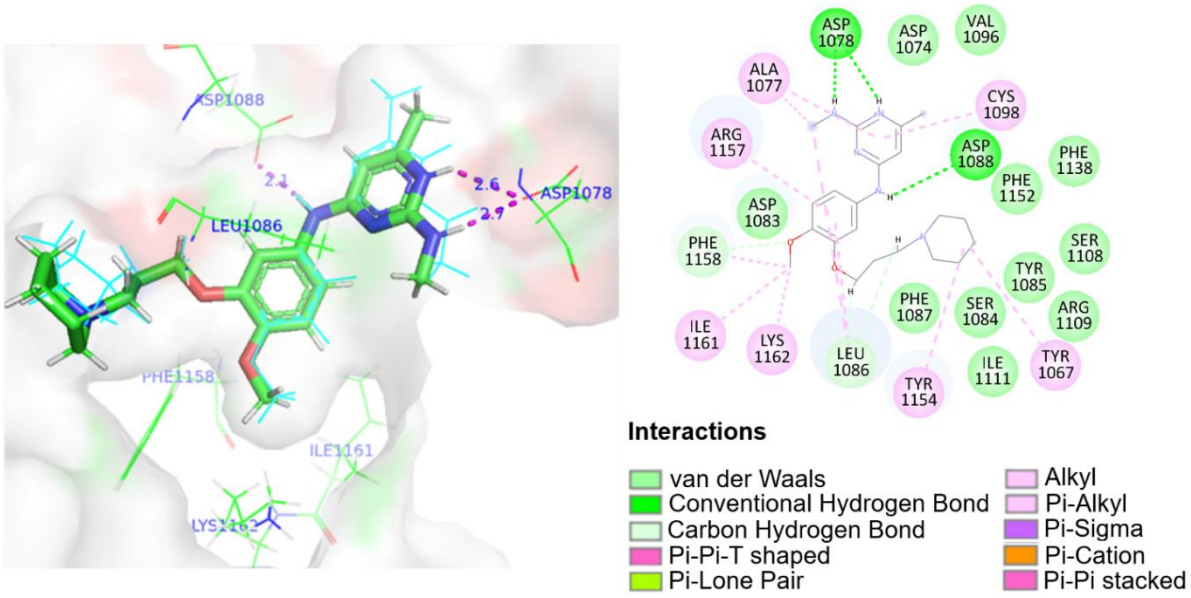

Figure 30. Pose of the **34** with interactions in the active site of G9a (PDB: 7btv) (left) and H3R (PDB: 7f61) (right); the cyan lines represent the reference ligands of the PDBs, while the sticks represent **34**.

Compound **28**, the least active compound on H_3R, forms two hydrogen bonds with the side chain of Asp114 and one hydrophobic bond with the side chain of Phe193 (Figure 31). Thus, it forms two (Table S1, 1-4; 1-5) of five reference ligand interactions in the H_3R binding pocket (Figure 26, PDB:7f61).

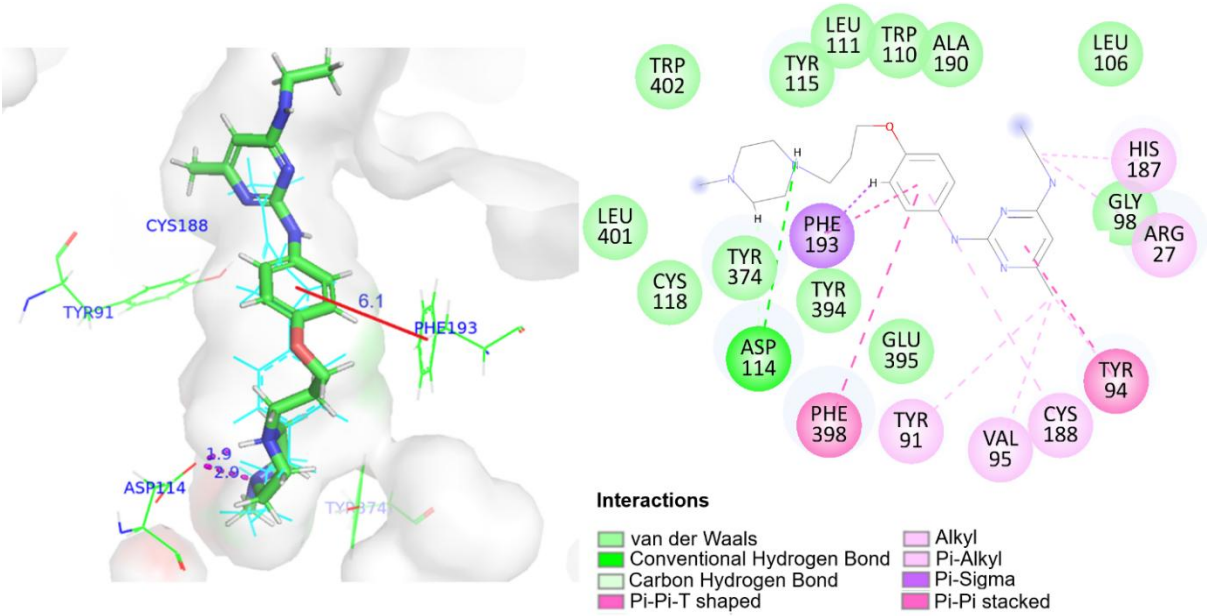

Figure 31. Pose of the **28** with interactions in the active site of the H_3R (PDB: 7f61); the cyan lines represent the reference ligands of the PDB, while the sticks represent the **28**.

In the case of G9a, it can be seen that the methoxy group of piperidine-propoxy-phenylamino moiety on pyrimidine of **31** and **34** fits into the hydrophobic pocket consisting of Ile1161,

Lys1162 and Phe1158 (Figure 28 and Figure 30), while unsubstituted piperidine-propoxy-phenylamino moiety on position-4 of pyrimidine of **33** does not fit into the hydrophobic G9a pocket (Figure 29). It can be concluded that a small lipophilic substituent, such as methoxy group, of phenyl moiety play an important role in filling the hydrophobic pocket of G9a, while a bigger lipophilic substitution at one of the amine groups of the pyrimidine plays an important role in the interactions with the lipophilic side chains of the amino acids that form the alpha-helix at the entrance of the active site of G9a. The piperidine-propoxy-phenylamino moiety on the position-2 of the pyrimidine ring of **31** forms two hydrogen bonds with Asp1088, the piperidine-propoxy-phenylamino moiety on the position-4 of the pyrimidine ring of **34** forms a hydrogen bond with Asp1088, while the piperidine-propoxy-phenylamino moiety on position-4 of the pyrimidine of **33** does not interact with Asp1088. It can be concluded that interactions with the hydrophobic G9a pocket together with two hydrogen bonds with Asp1088 are essential for a strong inhibition of G9a.

In the case of H_3R, **31** and **33** form a further hydrophobic interaction with Tyr374, whereas **28** does not form this bond. Almost all piperazine derivatives do not form this lipophilic interaction and have a lower potency than their piperidine analogues. Considering that **31** works best for G9a and at the same time has high potency for the H_3R, it could serve as a lead compound for further modifications to achieve even higher potency for both targets.

The starting point for the structural modifications should be given to replacing or attaching additional hydrogen donor groups to the methyl group at position-6 of the pyrimidine ring to test other hydrogen bonds with Asp1088 in G9a and their influence on potency. The hydrophobic interaction with the Tyr374 in H_3R should be retained as it was mentioned to be important for H_3R potency.

4.6.2 5-Chloro- and 5-(Trifluoromethyl)pyrimidine-2,4-diamine Derivatives

The design and synthesis of chloro- and 5-(trifluoromethyl)pyrimidine-2,4-diamine derivatives were inspired by the overlapping roles of the LRRK2 enzyme and the histamine H_3R in PD pathology. LRRK2 hyperactivity is a key driver of PD pathogenesis, impairing vesicle trafficking, neurotransmitter release, cytoskeleton dynamics, autophagy, lysosomal /mitochondrial functions, and immune/microglial response. Importantly, LRRK2 dysregulation promotes α-Syn aggregation and Lewy body formation, hallmark features of PD, positioning LRRK2 as a promising disease-modifying target.[341] On the other hand, H_3R modulation influences histaminergic neurotransmission, which is critical for cognitive function, alertness, and neuroprotection. Through its heteroreceptor functions in CNS, H_3R directly affects

dopaminergic transmission. Its antagonism has been shown to supress neuroinflammation and alleviate cognitive impairments. Notably, the H_3R antagonist pitolisant (**L33**) is clinically used to treat narcolepsy, a condition characterized by excessive daytime sleepiness, which is also a common non-motor symptom in PD patients. Recognizing these interconnected mechanisms, the knowledge-based MTDL approach[262] was employed to design compounds capable of simultaneously targeting LRRK2 and H_3R. For this purpose, the only LRRK2 inhibitor in clinical trials with disclosed structure **L80**, alongside its earlier iterations **L78** and **L79** was taken as a lead. Diaminopyrimidine scaffold responsible for LRRK2 inhibition was merged with H_3R pharmacophore from ligands **L32** and **L33** (Figure 32).

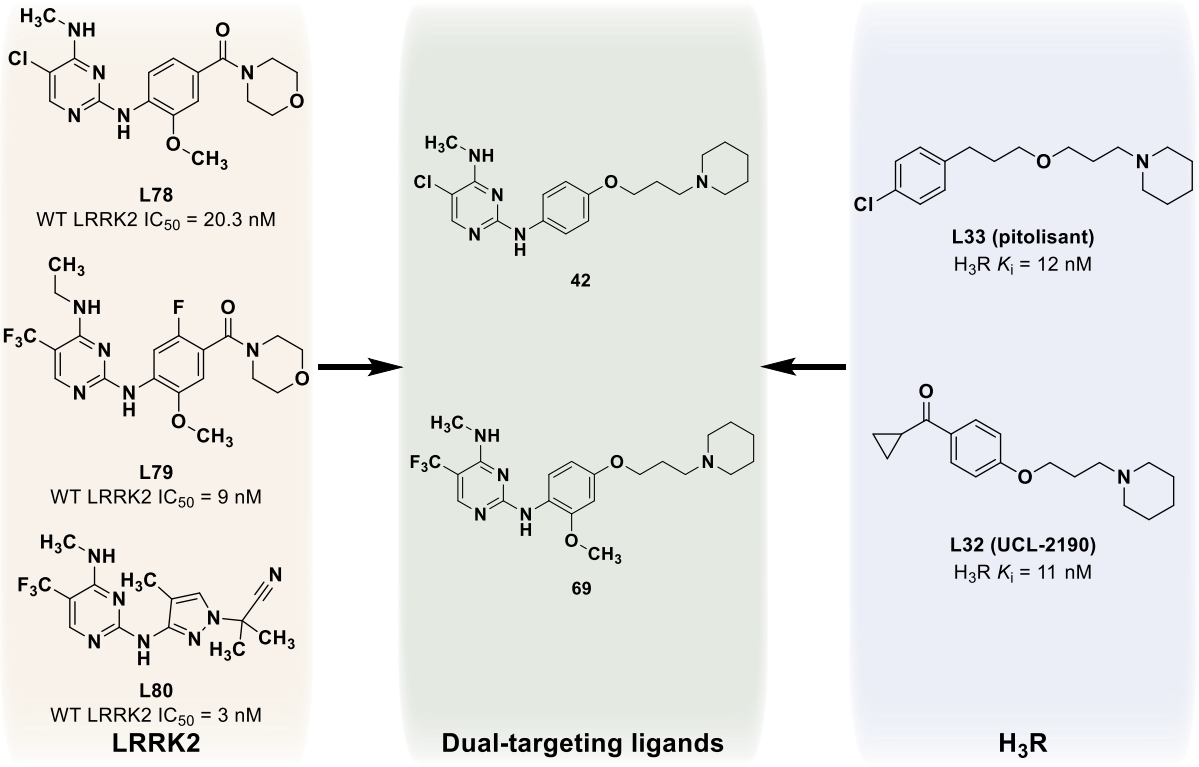

Figure 32. Design of dual targeting LRRK2/H_3R ligand by fusing structural fragments of known G9a and H_3R ligands. Excluding **L33** H_3R K_i value that was obtained in-house, all other IC_{50} and K_i values were compiled from published literature sources.[143, 390, 391, 393]

In addition to two target compounds, **42** and **69**, a set of 48 compounds (**40**-**87**, Table 9 and Table 10) was synthesized using 5-chloro- and 5-(trifluoromethyl)pyrimidine-2,4-diamine scaffolds. Structural diversity was introduced by pairing one of two alkylamino substituents (methyl- or ethylamino) with one of six arylamino substituents (**P12**-**P17**, Scheme 3), and systematically varying their substitution positions between the C-2 and C-4 sites of the pyrimidine ring. This strategy produced a focused compound library with controlled structural variations, enabling comprehensive SAR analysis for both H_3R and LRRK2 targets.

The complete set of compounds underwent evaluation for H_3R binding affinity, expressed as K_i values. The compounds were also tested for their LRRK2 inhibitory potential at a fixed concentration of 10 µM, with results presented as percentage of enzyme inhibition. The compounds demonstrating both potent hH$_3$R affinity and substantial LRRK2 inhibition were advanced to full LRRK2 IC_{50} determination to quantify their precise inhibitory potency.

Table 9. hH$_3$R binding affinities and single-point LRRK2 inhibitory potencies of compounds **40**-**63**.[a]

	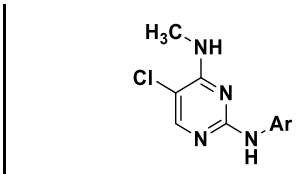			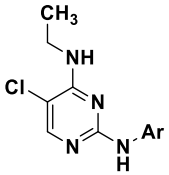		
Ar	**Compd**	**hH$_3$R K_i [nM] [95% CI][b]**	**LRRK2 [%] ± SD at 10 µM[c, d]**	**Compd**	**hH$_3$R K_i [nM] [95% CI]**	**LRRK2 [%] ± SD at 10 µM**
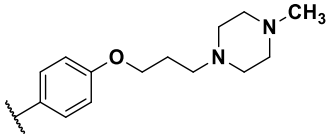	**40**	738 [470 – 1160]	102.8 ± 2.6	**46**	390 [114 – 1333]	99.2 ± 3.7
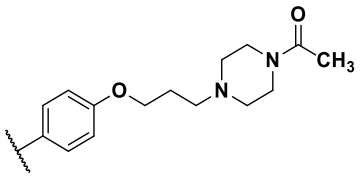	**41**	341 [119 – 980]	100.2 ± 5.0	**47**	916 [283 – 2964]	104.9 ± 1.2
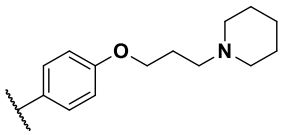	**42**	10.2 [7.18 – 14.4]	99.7 ± 2.8	**48**	4.4 [1.7 – 11.2]	86.3 ± 2.7
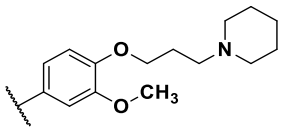	**43**	172 [24.2 – 1227]	88.4 ± 3.0	**49**	75.8 [33.0 – 174]	93.4 ± 1.2
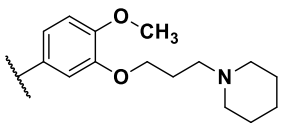	**44**	331 [124 – 883]	92.0 ± 8.8	**50**	46.3 [18.3 – 117]	84.5 ± 0.8
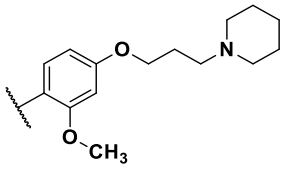	**45**	59.9 [21.9 – 164]	80.4 ± 1.9	**51**	33.1 [21.7 – 50.6]	94.7 ± 2.4

[a] Data are presented as mean values with corresponding 95% confidence intervals or standard deviations, based on at least two independent experiments performed in duplicate.

[b] Pitolisant (**L33**) was tested as a reference hH$_3$R ligand showing K_i = 13.2.

[c] LRRK2 inhibition was calculated as percentages related to control at a test concentration of 10 µM.

[d] Staurosporine (**L73**) was used as a reference LRRK2 ligand showing IC_{50} = 0.2 nM.

Table 9. *Continued.*[a]

Ar	Compd	*h*H$_3$R K_i [nM] [95% CI][b]	LRRK2 [%] ± SD at 10 µM[c, d]	Compd	*h*H$_3$R K_i [nM] [95% CI]	LRRK2 [%] ± SD at 10 µM
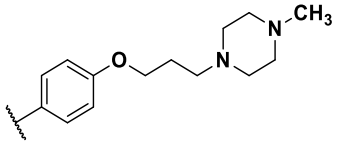	**52**	335 [106 – 1059]	54.6 ± 0.8	**58**	1034 [441 – 2598]	93.9 ± 13.1
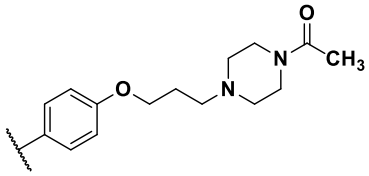	**53**	839 [296 – 2379]	45.1 ± 4.4	**59**	490 [164 – 1466]	78.6 ± 8.1
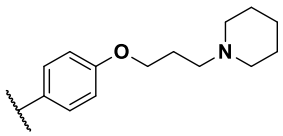	**54**	2.4 [1.1 – 5.3]	85.6 ± 9.0	**60**	4.8 [1.9 – 12.0]	80.8 ± 1.1
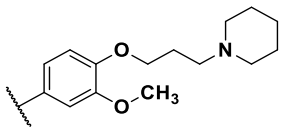	**55**	223 [83 – 603]	73.0 ± 2.5	**61**	185 [103 – 331]	54.1 ± 0.5
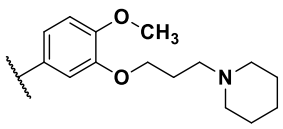	**56**	360 [124 – 1042]	64.0 ± 8.2	**62**	716 [554 – 926]	63.5 ± 4.5
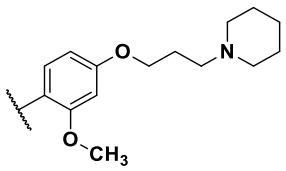	**57**	241 [74 – 781]	62.6 ± 3.9	**63**	106 [92 – 123]	71.2 ± 4.4

[a] Data are presented as mean values with corresponding 95% confidence intervals or standard deviations, based on at least two independent experiments performed in duplicate.

[b] Pitolisant (**L33**) was tested as a reference *h*H$_3$R ligand showing K_i = 13.2.

[c] LRRK2 inhibition was calculated as percentages related to control at a test concentration of 10 µM.

[d] Staurosporine (**L73**) was used as a reference LRRK2 ligand showing IC_{50} = 0.2 nM.

Table 10. *h*H_3R binding affinities and single-point LRRK2 inhibitory potencies of compounds **64-87**.[a]

Ar	Compd	*h*H_3R K_i [nM] [95% CI][b]	LRRK2 [%] ± SD at 10 µM[c, d]	Compd	*h*H_3R K_i [nM] [95% CI]	LRRK2 [%] ± SD at 10 µM
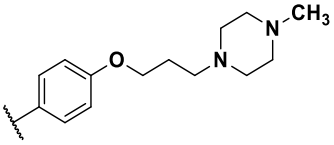	**64**	548 [346 – 869]	101.8 ± 7.5	**70**	862 [438 – 1697]	73.5 ± 11.2
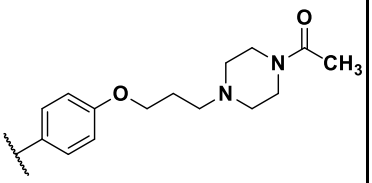	**65**	2096 [668 – 6581]	88.5 ± 1.4	**71**	6047 [5467 – 6689]	47.5 ± 14.0
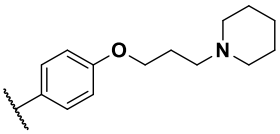	**66**	4.1 [1.9 – 8.4]	89.5 ± 3.5	**72**	8.1 [3.9 – 16.7]	78.5 ± 0.2
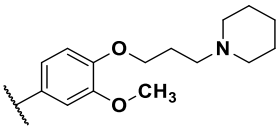	**67**	104 [44.5 – 244]	98.4 ± 8.0	**73**	159 [81.7 – 311]	62.3 ± 11.4
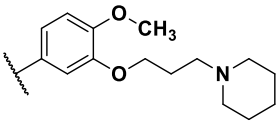	**68**	1645 [507 – 5333]	102.9 ± 1.2	**74**	53.6 [26.5 – 108]	37.7 ± 1.3
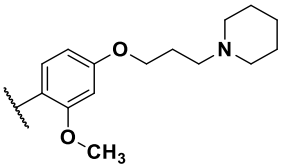	**69**	9.0 [5.2 – 15.7]	104.6 ± 5.5	**75**	82.1 [33.2 – 203]	54.5 ± 1.1

[a] Data are presented as mean values with corresponding 95% confidence intervals or standard deviations, based on at least two independent experiments performed in duplicate.

[b] Pitolisant (**L33**) was tested as a reference *h*H_3R ligand showing K_i = 13.2.

[c] LRRK2 inhibition was calculated as percentages related to control at a test concentration of 10 µM.

[d] Staurosporine (**L73**) was used as a reference LRRK2 ligand showing IC_{50} = 0.2 nM.

Table 10. *Continued.*[a]

Ar	Compd	*h*H$_3$R K_i [nM] [95% CI][b]	LRRK2 [%] ± SD at 10 µM[c, d]	Compd	*h*H$_3$R K_i [nM] [95% CI]	LRRK2 [%] ± SD at 10 µM
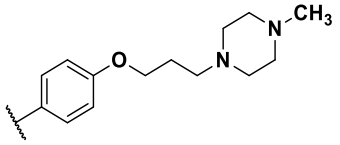	**76**	1026 [418 – 2519]	56.6 ± 8.5	**82**	141 [63 – 313]	99.7 ± 13.3
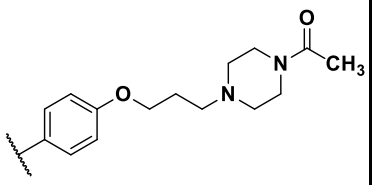	**77**	578 [172 – 1944]	42.9 ± 0.6	**83**	519 [195 – 1381]	90.3 ± 4.0
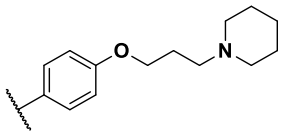	**78**	2.1 [0.8 – 5.6]	53.9 ± 1.4	**84**	11.1 [5.7 – 21.7]	95.1 ± 8.2
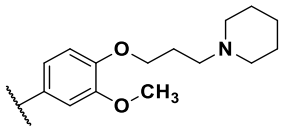	**79**	328 [114 – 1043]	38.2 ± 11.8	**85**	65.1 [29.9 – 142]	98.8 ± 2.1
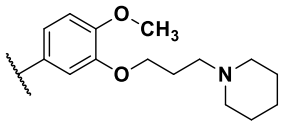	**80**	822 [647 – 1043]	47.0 ± 15.6	**86**	29.9 [10.9 – 82.5]	86.3 ± 3.5
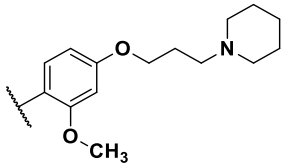	**81**	11.2 [4.8 – 26]	44.2 ± 0.1	**87**	41.6 [29.6 – 58.5]	94.2 ± 3.3

[a] Data are presented as mean values with corresponding 95% confidence intervals or standard deviations, based on at least two independent experiments performed in duplicate.

[b] Pitolisant (**L33**) was tested as a reference *h*H$_3$R ligand showing K_i = 13.2.

[c] LRRK2 inhibition was calculated as percentages related to control at a test concentration of 10 µM.

[d] Staurosporine (**L73**) was used as a reference LRRK2 ligand showing IC_{50} = 0.2 nM.

For H$_3$R receptor binding, compounds containing the 4-(3-(piperidin-1-yl)propoxy)anilino substituent consistently showed the highest affinity across all scaffold variations, with K_i values in the low nanomolar range (2.1-11.1 nM), rivalling the most potent H$_3$R ligands.[5, 35] This trend remained consistent regardless of the alkylamino group position (2- or 4-position) or the nature of the 5-substituent (chloro or trifluoromethyl). The introduction of methoxy groups to the anilino moiety typically reduced H$_3$R affinity, though compounds **69** and **81** maintained

strong potency (K_i = 9.0 and 11.2 nM respectively). Notably, the position of methoxy substitution influenced activity, with 2-methoxy derivatives generally performing better than their 3- or 4-methoxy counterparts. Compounds featuring 4-methylpiperazine or 4-acetylpiperazine exhibited substantially lower affinity, with K_i values often in the high nanomolar to micromolar range. While the alkylamino group position showed no consistent impact on H_3R affinity, the methylamino to ethylamino switch produced variable effects depending on other structural features.

LRRK2 inhibition demonstrates clear structure-activity relationships primarily governed by the alkylamino substitution nature and position on the pyrimidine ring. In the 5-chloro series, 4-alkylamino derivatives (**40**-**51**) consistently achieve higher LRRK2 inhibition (>80%) compared to their 2-alkylamino counterparts (**52**-**63**). This trend suggests that the 4-position of the alkylamino group is more favourable for LRRK2 inhibition in the 5-chloro series. Additionally, the type of alkylamino group does not show a significant difference in inhibition, as both methylamino and ethylamino substitutions at the 4-position yield high inhibition percentages.

The 5-trifluoromethyl series reveals more nuanced SAR. The 4-methylamino (**64**-**69**) and 2-ethylamino (**82**-**87**) derivatives achieve exceptional LRRK2 inhibition (>85%), while 4-ethylamino (**70**-**75**) and 2-methylamino (**76**-**81**) substitutions result in notably lower inhibition (<60%). This pattern suggests that specific combinations of position and alkyl chain length create optimal spatial arrangements for LRRK2 binding site interaction. The anilino substitution patterns, while important for H_3R activity, show less predictable effects on LRRK2 inhibition across both series.

Based on the H_3R affinity values, LRRK2 inhibition data, and key structural features identified through SAR analysis, 9 compounds were selected for detailed LRRK2 IC_{50} determination. All compounds demonstrated exceptional LRRK2 inhibitory potency with IC_{50} values in the low single-digit nanomolar range (1.1-9.3 nM) (Table 11). Notably, compounds **48**, **66**, **69**, and **84** achieved an optimal balance of activities, combining single-digit nanomolar H_3R binding affinities (3.3-11.1 nM) with potent LRRK2 inhibition.

The subsequent cytotoxicity evaluation at 10 μM in SH-SY5Y cells revealed distinct safety profiles correlating with structural features (Table 11). The 2-methoxy derivatives (**51**, **69**, and **87**) exhibited superior safety profiles with cell viability exceeding 97%. In contrast, the unsubstituted derivatives (**48**, **66**, and **84**) showed moderate effects on cell viability (58.8-76.7%), while the 3-methoxy compounds (**49**, **67**, and **85**) displayed variable impacts, with compound **85** showing significant cytotoxicity (16.5% viability). These results establish

2-methoxy substitution as optimal for maintaining cell viability while preserving target engagement.

Compound **69** emerged as the lead candidate, demonstrating excellent dual activity (*h*H_3R K_i = 9.0 nM, LRRK2 IC_{50} = 3.6 nM) while maintaining nearly complete cell viability (99.9%).

Table 11. *h*H_3R K_i and LRRK2 IC_{50} values of selected compounds alongside their effects on SH-SY5Y cell viability.[a]

Compd	Compound	*h*H_3R K_i [nM] [95% CI][b]	LRRK2 IC_{50} [nM] [95% CI][c]	SH-SY5Y viability [%] ± SD at 10 µM
48	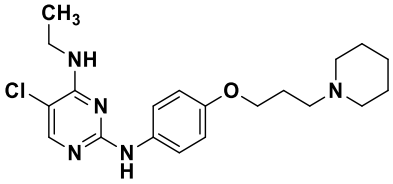	4.4 [1.7 – 11.2]	4.7 [2.7 – 6.8]	75.9 ± 1.7
49	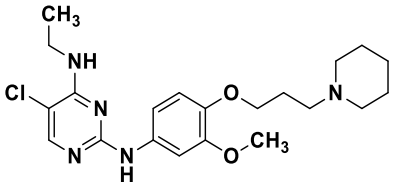	75.8 [33.0 – 174]	2.4 [1.1 – 3.6]	66.9 ± 1.0
51	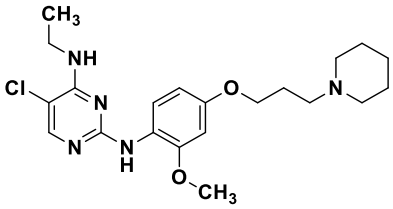	33.1 [21.7 – 50.6]	9.3 [1.0 – 18.0]	104.9 ± 6.6
66	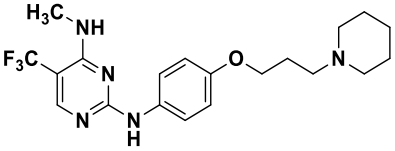	4.1 [1.9 – 8.4]	8.0 [5.1 – 11.0]	76.7 ± 2.4
67	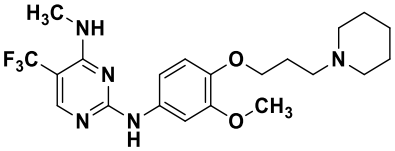	104 [44.5 – 244]	2.2 [0.8 – 3.6]	89.5 ± 1.9
69	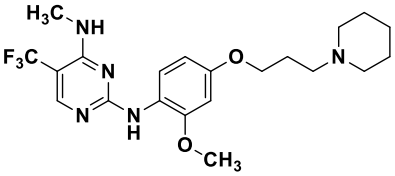	9.0 [5.2 – 15.7]	3.6 [1.6 – 5.6]	99.9 ± 4.6
84	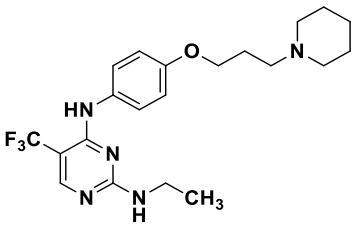	11.1 [5.7 – 21.7]	2.8 [0.9 – 4.7]	58.8 ± 2.6

Table 11. *Continued*

Compd	Compound	*h*H$_3$R K$_i$ [nM] [95% CI]	LRRK2 IC$_{50}$ [nM] [95% CI]	SH-SY5Y viability [%] ± SD at 10 µM
85	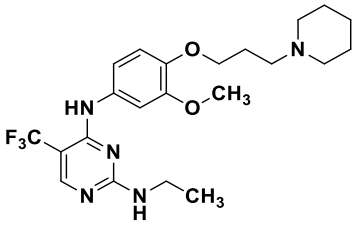	65.1 [29.9 – 142]	1.1 [0.8 – 1.3]	16.5 ± 12.3
87	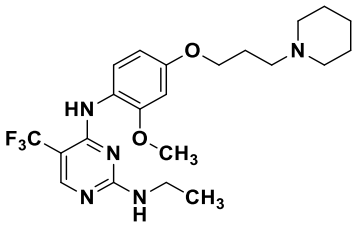	41.6 [29.6 – 58.5]	2.7 [1.1 – 4.3]	97.9 ± 2.5

[a] Data are presented as mean values with corresponding 95% confidence intervals or standard deviations, based on at least two independent experiments performed in duplicate.

[b] Pitolisant (**L33**) was tested as a reference *h*H$_3$R ligand showing K_i = 13.2.

[c] Staurosporine (**L73**) was used as a reference LRRK2 ligand showing IC$_{50}$ = 0.2 nM.

To gain better insight into the interactions between ligands **40**-**87** with H$_3$R and LRRK2, molecular docking study was performed. Initially, the original co-crystallized ligands (**L41** for H$_3$R and **L86** for LRRK2) were used as a reference to validate the docking protocols for the H$_3$R and LRRK2 enzyme by re-docking the reference ligands. The predicted poses with the highest ASP score for **L41** and PLP score for **L86** and the key interactions according to the literature binding mode (Figure 33 and Figure 34) were evaluated by root mean square deviation (RMSD). For the best predicted bioactive conformations for the H$_3$R antagonist **L41** and the LRRK2 inhibitor **L86**, the comparable poses with the reference ligands and all key interactions with the amino acid residues at the active site of both targets were confirmed with RMSD values of 0.8302 and 0.3396, respectively. In accordance with the validation criterion that the RMSD of the docked reference ligand has a value of 2 Å or less[525], it can be concluded that both the H$_3$R and LRRK2 docking protocols are valid.

The ASP and PLP score values, key interactions of the reference and synthesized compounds for both targets and their experimental activities are listed in Table S2 (Supplementary Data).

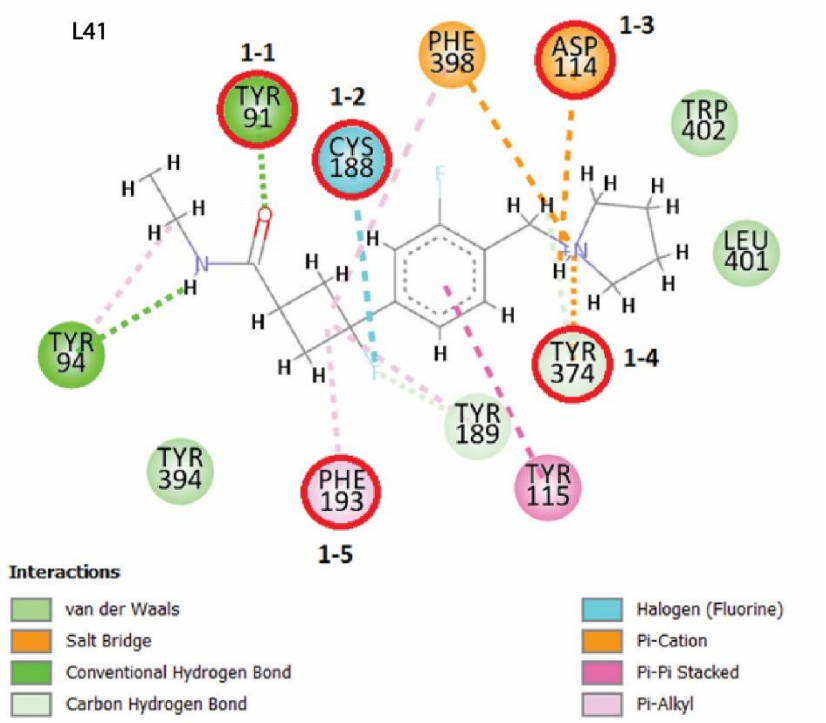

Figure 33. Interactions of the H_3R antagonist **L41** with the amino acid residues in active site of the PDB: 7F61 (H_3R). Important interactions according to literature, hydrogen bond with Tyr91, salt bridge with Asp114, the halogen-O interaction of Cys188, salt bridge and carbon hydrogen with Tyr374 and Pi-interactions with Phe193, are highlighted with a red circle.[33]

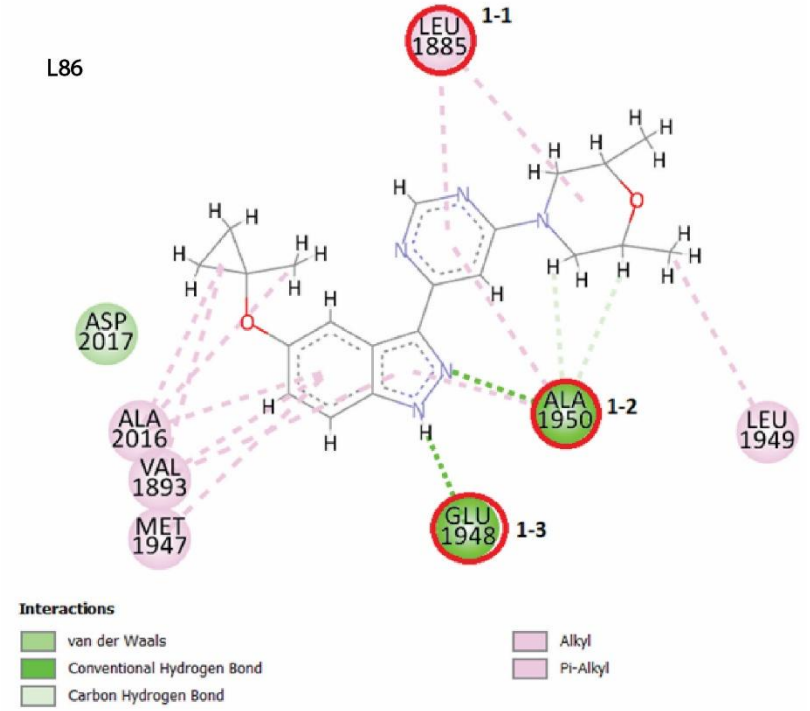

Figure 34. Interactions of the LRRK2 inhibitor **L86** with the amino acid residues in the active site of the PDB: 8TXZ (LRRK2). Important interactions according to literature (hydrophobic interactions of Leu1885 and hydrogen bonds of Ala1950 and Glu1948) are highlighted with a red circle.[526]

Some of the representative synthesized ligands (**49** ($K_i(H_3R)$ = 57.5 nM and IC_{50}(LRRK2) = 2.4 nM); **67** ($K_i(H_3R)$ = 104.0 nM and IC_{50}(LRRK2) = 2.2 nM); **69** ($K_i(H_3R)$ = 9.05 nM and IC_{50}(LRRK2) = 3.6 nM); **85** ($K_i(H_3R)$ = 65.1 nM and IC_{50}(LRRK2) = 1.1 nM)) were selected for interpretation of the docking results.

The most promising compound (**69**) with balanced single digit nanomolar $K_i(H_3R)$ and IC_{50}(LRRK2) values was selected for discussion. The compounds with the highest experimental potency (IC_{50}) for the LRRK2 enzyme as well as significant K_i activities for H_3R were discussed to gain a better insight into the relationships between potency of the ligands studied and the binding mode at the active site of H_3R and LRRK2.

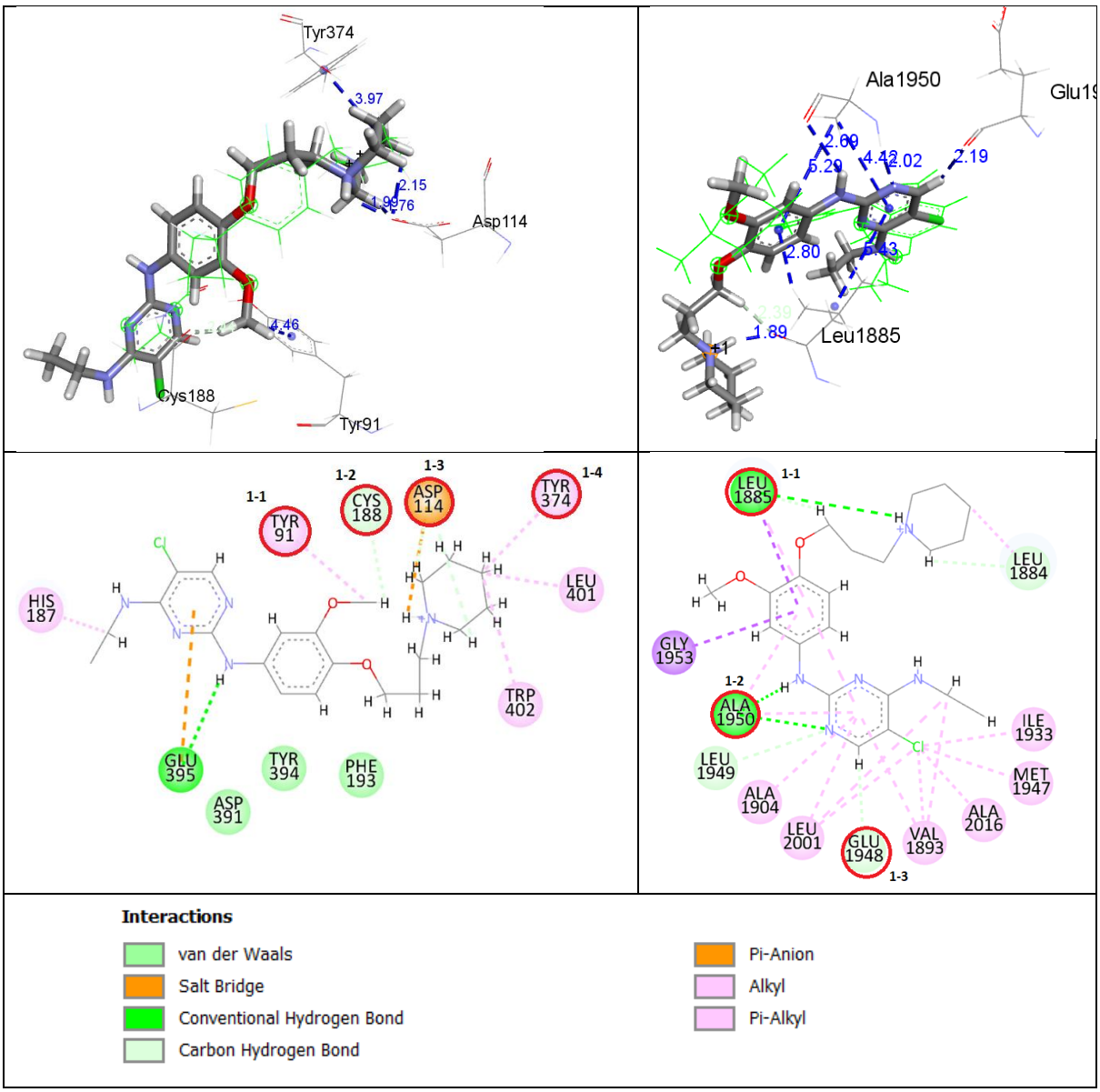

Figure 35. Pose of **49** with interactions in the active site of the H_3R (PDB: 7f61) (left) and LRRK2 (PDB: 8TXZ) (right). The reference ligands of the PDBs are presented with green lines, while the **49** is presented with sticks.

Compound **49** is a strong H_3R antagonist (K_i = 57.5 nM, Table S2), forming a salt bridge with Asp114, pi-interactions with Tyr91 and Tyr374 and van der Walls interactions with Cys188 in the H_3R binding pocket (Figure 35, left). This indicates that compound **49** forms four (Table S2, 1-1;1-2; 1-3; 1-4) out of five reference ligand interactions (Figure 33, PDB:7F61). In addition, compound **49** is a potent LRRK2 inhibitor (IC_{50} = 2.4 nM, Table S2) which forms two hydrogen bonds and pi-interactions with side chain of the Ala1950, hydrogen bond and pi-interactions with Leu1885 and van der Waals interactions with Glu1948 (Figure 35, right). This means that compound **49** forms three (Table S2, 1-1; 1-2; 1-3) of three reference ligand interactions in the active site of the LRRK2 enzyme (Figure 34, PDB:7TXZ).

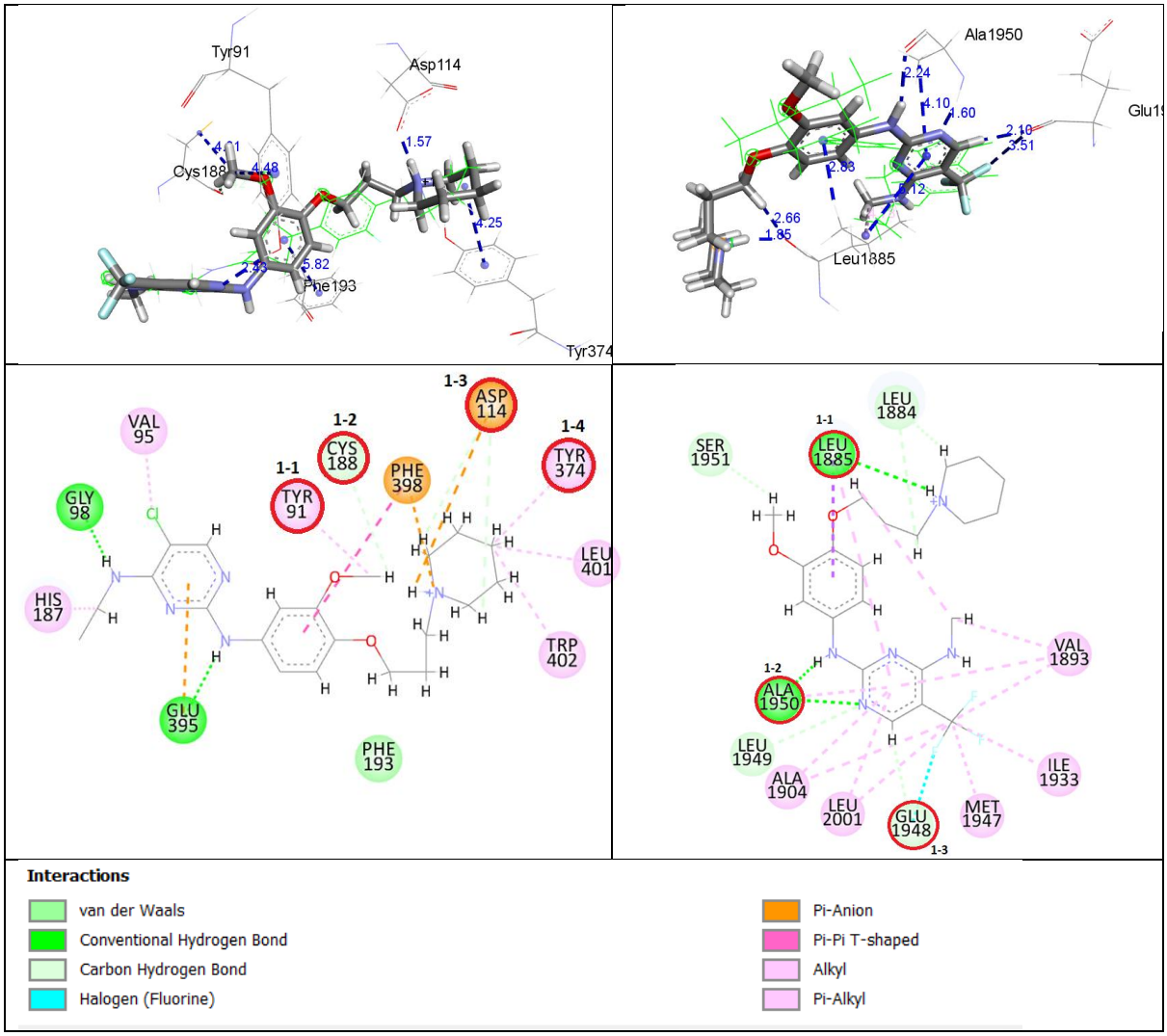

Figure 36. Pose of **67** with interactions in the active site of the H_3R (PDB: 7f61) (left) and LRRK2 (PDB: 8TXZ) (right). The reference ligands of the PDBs are presented with green lines, while the **67** is presented with sticks.

The compound **67** can be considered as a strong H_3R antagonist (K_i = 104.0 nM, Table S2), which forms pi-interactions with Tyr91, a salt bridge with Asp114, pi-interactions with Tyr374 and van der Walls interactions with Cys188 in the H_3R binding pocket (Figure 36, left). This

means that compound **67** forms four (Table S2, 1-1; 1-2; 1-3; 1-4) out of five reference ligand interactions (Figure 33, PDB:7F61). Compound **67** is a potent LRRK2 inhibitor (IC_{50} = 2.2 nM, Table S2), forming two hydrogen bonds and pi-interactions with the side chain of the Ala1950, hydrogen bonds and pi-interactions with Leu1885, and the halogen-O interactions with the side chain of Glu1948 (Figure 36, right). In total, compound **67** forms three (Table S2, 1-1; 1-2; 1-3) out of three reference ligand interactions in the active site of the LRRK2 enzyme (Figure 34, PDB:7TXZ).

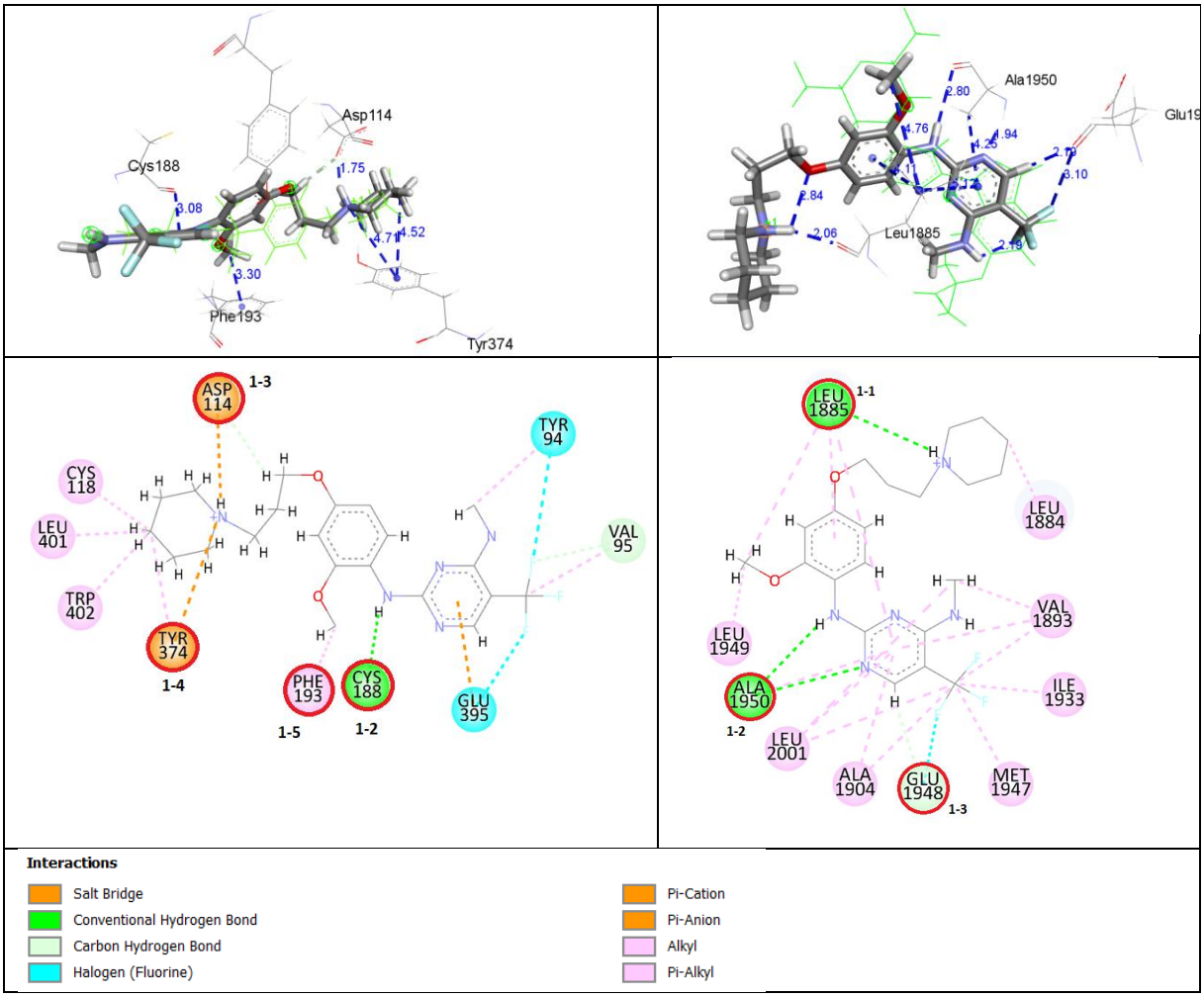

Figure 37. Pose of **69** with interactions in the active site of the H_3R (PDB: 7f61) (left) and LRRK2 (PDB: 8TXZ) (right). The reference ligands of the PDBs are presented with green lines, while the **69** is presented with sticks.

A ligand **69** is the most promising compound with balanced single-digit nanomolar K_i(H_3R) and IC_{50}(LRRK2) values. It is a potent H_3R ligand (K_i = 9.05 nM, Table S2) that forms a salt bridge with Asp114 side chain in the H_3R binding pocket, a hydrogen bond with Cys188, pi-interactions with Tyr374 and pi-interactions with Phe193 (Figure 37, left). Thus, compound **69** forms four (Table S2, 1-2; 1-3; 1-4; 1-5) out of five reference ligand interactions (Figure 33, PDB:7F61). In addition, compound **69** is a potent LRRK2 inhibitor (IC_{50} = 3.6 nM, Table S2),

forming two hydrogen bonds with Ala1950, hydrogen bonds and pi-interactions with Leu1885, and the halogen-O interactions with Glu1948 (Figure 37, right). This means that compound **69** forms three (Table S2, 1-1; 1-2; 1-3) of three reference ligand interactions in the active site of the LRRK2 enzyme (Figure 34, PDB:7TXZ).

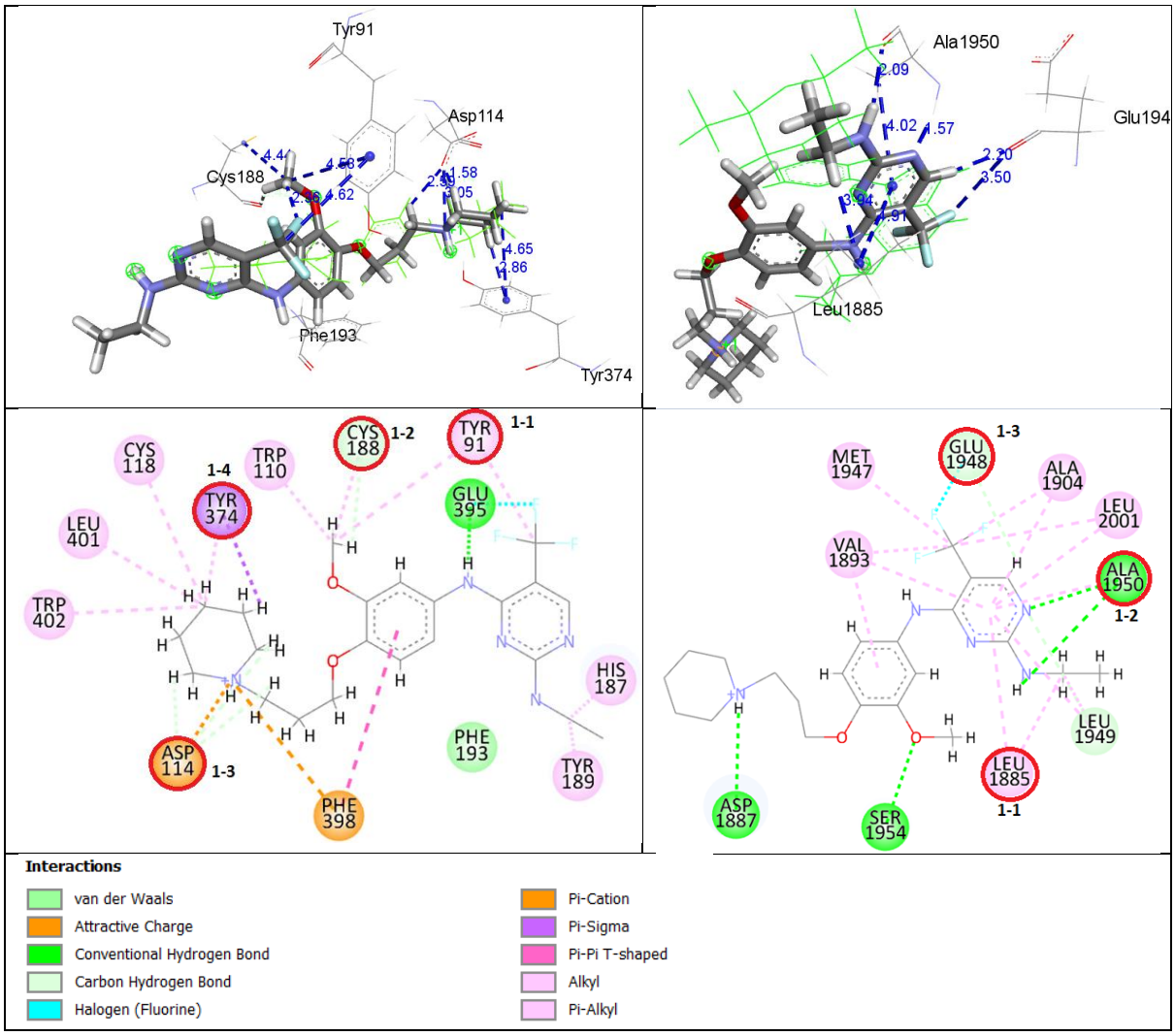

Figure 38. Pose of **85** with interactions in the active site of the H_3R (PDB: 7f61) (left) and LRRK2 (PDB: 8TXZ). The reference ligands of the PDBs are presented with green lines, while the **85** is presented with sticks.

Compound **85** is also a strong H_3R antagonist (K_i = 65.1 nM**,** Table S2) which forms pi-interactions with Tyr91 side chain, pi-interactions and carbon hydrogen bond with Cys188, pi-interactions with Tyr374 side chain and salt bridge with Asp114 side chain in the H_3R binding pocket (Figure 38, left). This means that compound **85** forms four (Table S2, 1-1;1-2; 1-3; 1-4) out of five reference ligand interactions (Figure 33, PDB:7F61). In terms of LRRK2 inhibitory activity, compound **85** is very potent LRRK2 inhibitor (IC_{50} = 1.1 nM, Table S2) forming two hydrogen bonds and pi-interactions with the side chain of the Ala1950, pi-interactions with Leu1885 side chain and the halogen-O interactions with the side chain of

Glu1948 (Figure 38, right). Overall, compound **85** forms three (Table S2, 1-1; 1-2; 1-3) of three reference ligand interactions in the active site of the LRRK2 enzyme (Figure 34, PDB:7TXZ). For all H_3R antagonists, interactions of the piperidine moiety with the binding pocket of H_3R were observed according to the binding mode described in the literature. The salt bridge with Asp114, which was identified as the most important interaction, was detected in almost all antagonists studied. On the other hand, pi-interaction of the piperidine moiety with Tyr374 is absent in the ligands with lower potency for the H_3R. The halogen-O interaction of Cys188 is observed with the small number of antagonists. The relationship between the interactions of the best docking poses and the experimentally determined activities of the H_3R antagonists indicates the importance of the piperidine moiety for the interactions in the binding pocket of H_3R.

The same type of interactions as in the reference ligand of LRRK2 can be seen in the hydrogen bonds with Ala1950 for almost all synthesized compounds. The pi-interactions between Leu1885 and the pyrimidine moieties are seen in the ligands with higher potency for LRRK2. In addition, compounds with trifluoromethyl group and higher potency for LRRK2 form the halogen-O interactions with Glu1948, in contrast to the chloropyrimidine derivatives. According to the experimentally determined LRRK2 inhibitory activity of the compounds, the observed binding modes point to the pyrimidine moiety and the trifluoromethyl group as structural features related to the higher potency for LRRK2.

4.7 Lipophilicity Determination (logP and logD)

Lipophilicity is a physicochemical property defined by the equilibrium distribution of solute molecules between aqueous and immiscible organic phases, demonstrating preferential partitioning into the organic phase.[527] This fundamental characteristic significantly influences both pharmacokinetic and pharmacodynamic properties of drugs, making it central to drug optimization efforts.[528] Drug absorption is governed by lipophilicity, as it determines a molecule's capacity to cross biological membranes and achieve sufficient bioavailability at target sites. Lipophilic compounds often display elevated volumes of distribution, driven by their propensity to accumulate in lipid-rich tissues. Furthermore, lipophilicity modulates plasma protein binding, directly impacts BBB permeability, and influences hepatic metabolism and toxicity profiles.[529] The pharmacodynamic behaviour of drugs is enhanced by lipophilicity through stronger ligand-target interactions, typically resulting in increased drug potency. However, this often leads to greater promiscuity and potential toxicity due to non-specific binding.[530]

Lipophilicity is commonly quantified via the 1-octanol/water partition coefficient (logP), determined through experimental or computational approaches.[531] The classical shake-flask method, a reference technique for experimental logP determination, involves direct measurement of solute concentrations in equilibrated 1-octanol and water phases.[532] However, this method is constrained to logP values between -2 and 4, requires substantial compound quantities, and is labor-intensive, limiting its practicality.[533]

Reverse-phase HPLC has emerged as the preferred standard procedure for logP determination, offering significant advantages over the shake-flask method.[534] These benefits include minimal sample requirements due to sensitive HPLC detection, broader applicability across logP values (0 to 6), resilience to sample impurities, automation capabilities, and facilitation of high-throughput screening with excellent accuracy.[533, 535] The method also enables the determination of lipophilicity under various physiologically relevant conditions, including different pH values and temperatures, providing valuable insights for drug development.

Chromatographic methods avoid direct quantification of sample concentrations in two immiscible solvents and instead indirectly assess lipophilicity by correlating it with a compound's retention behaviour on a lipophilic stationary phase. This approach involves constructing a linear regression model between experimentally determined logP values of reference compounds and their chromatographic retention parameters, typically expressed as the capacity factor k. The relationship is defined by the equation (Equation 3):

$$\log P = a + b \cdot \log k$$

Equation 3. logP - 1-octanol/water partition coefficient; a – regression coefficient; b – regression coefficient; logk – logarithm of capacity factor k.

where a and b are regression coefficients derived from the calibration curve. To determine the logP of an unknown compound, its retention time t_R is measured, and the capacity factor is calculated using (Equation 4):

$$k = \frac{t_R - t_0}{t_0}$$

Equation 4. k – capacity factor; t_R – retention time; t_0 – dead time.

where t_0 represents the column dead time. The calculated logk is then applied to the regression equation to determine logP.[534]

The partition coefficient describes the distribution of neutral, unionized molecules between two immiscible solvents. For ionizable compounds, however, the distribution coefficient (logD) at a specific pH is used. Unlike the partition coefficient, logD accounts for the partitioning of both ionized and neutral species in the 1-octanol/water system. In chromatographic models, logD correlates with the capacity factor (logk). This relationship allows for the indirect determination of logD by calibrating retention data against reference compounds with known distribution coefficients.

Most drug molecules contain functional groups that ionize at physiological pH. Consequently, logD measurements at specific pH values provide more relevant lipophilicity data by capturing the distribution of all molecular species present under those conditions.

Given the critical role of lipophilicity in influencing the pharmacokinetic and pharmacodynamic behaviour of drugs, the logP and logD values of 87 synthesized compounds (**1**-**87**) were determined using an indirect reverse-phase high-performance liquid chromatography (RP-HPLC) method. To account for the basic nature of the assessed compounds, logP values were determined at pH 11, a condition that suppresses ionization. In contrast, logD values were determined at pH 7.4 to reflect extracellular physiological conditions.

A set of reference compounds was selected to cover a broad range of lipophilicity (0 to 6 logP/logD units). The known logP and logD values of these reference compounds were plotted against their corresponding logk values to establish a calibration curve (Figure 39). The

parameters of the linear regression equation derived from this curve were then used to assess the lipophilicity.

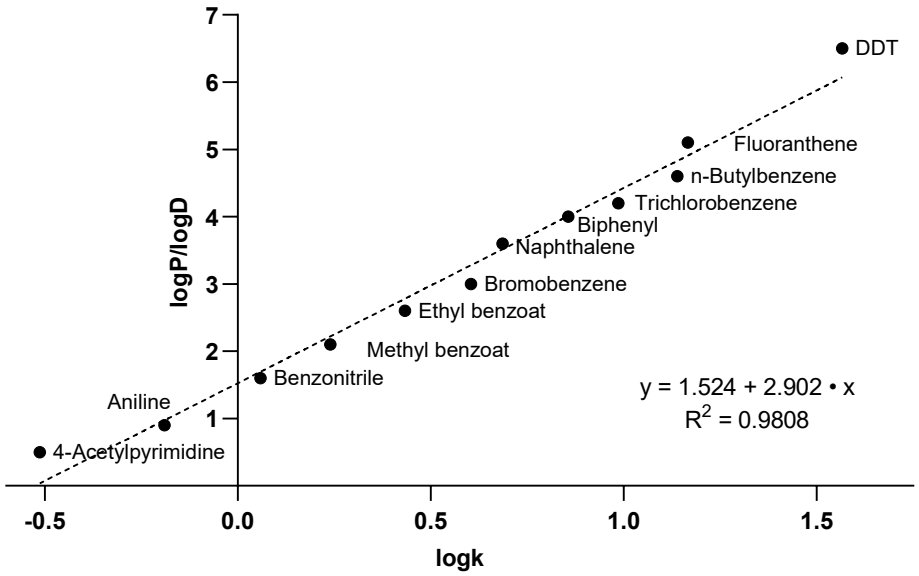

Figure 39. Calibration curves correlating capacity factors (logk) with literature logP and logD values for reference compounds.

To confirm the method's applicability, it was validated using substances from the reference list compiled by the OECD, which included literature-reported logP and logD values (Table 12).[534] In line with the literature[535], the absolute difference between the literature and experimental values higher than 0.6 was used to identify outliers. The only outlier in the validation set was 1-phenylpiperazine, which can be attributed to its high hydrophilicity, as its retention time is close to the dead time. Under these circumstances, even minor discrepancies in measurements can lead to significant errors in the calculation of logk values.

Table 12. Literature and experimental logP/logD values of the compounds used for validation.

Compound	Literature logP/logD	Experimental logP/logD	Difference
1-Phenylpiperazin	1.11	1.76	-0.65
4-Chloroaniline[a]	1.83	1.64	0.19
Atropine	1.83	2.01	-0.18
Propiophenone[a]	2.19	2.34	-0.15
Diphenhydramine	3.27	3.69	-0.42
Diphenylamine[a]	3.40	3.30	0.10
Acenaphthene[a]	3.92	4.20	-0.28
Amitriptyline	4.92	5.17	-0.25
Chlorpromazine	5.32	5.32	0.00

[a] Used for the validation of both logP and logD determination, while the remaining compounds were utilized solely for logP validation.

The validated method was used to determine the lipophilicity of compounds **1**-**87**. The logD values at pH 7.4 were particularly relevant since these compounds target H_3R and, in the case of pyrimidine-2,4-diamines derivatives, also target either G9a or LRRK2 - all proteins located in the central nervous system. These logD measurements provide valuable insights into the compounds' potential BBB permeability. BBB permeability is a major challenge in CNS drug design, and lipophilicity is widely regarded as one of the most influential physicochemical properties governing BBB penetration.[536] Optimal brain uptake is typically associated with compounds exhibiting logD values within the range of 1-4, as this balance supports passive diffusion while avoiding excessive hydrophobicity.[537]

Experimentally determined logP (pH 11) and logD (pH 7.4) data for the set of compounds **1**-**87** are presented in (Figure 40, Table S3), along with their calculated clogP and clogD (pH 7.4) values. Most compounds exhibited logD values within the 1-4 range, aligning with the lipophilicity window associated with BBB permeability. Notably, compound **31**, a promising dual H_3R/G9a ligand with balanced potency ($h$$H_3R$ K_i = 25.2 nM, G9a IC_{50} = 63.9 nM), displayed a logD of 2.06, while compound **69**, the most potent dual H_3R/LRRK2 ligand ($h$$H_3R$ K_i = 9.0 nM, LRRK2 IC_{50} = 3.6 nM), showed a higher logD of 3.57. These values suggest favourable CNS penetration potential for both candidates. Furthermore, both compounds comply with druglikeness criteria, as predicted by SwissADME tool.[538, 539]

Paradoxally, compounds bearing methylpiperazine or acetylpiperazine moieties exhibited anomalous behaviour, with logD values either matching or exceeding their logP values (logP < logD), a trend contradicting typical expectations for ionizable bases. This discrepancy may arise from the physicochemical properties of these derivatives, such as hydrogen bond capacity and acidity, which could influence retention times in the chromatographic method.[535]

The data presented in Figure 40 and Table S3 further underscore discrepancies between experimentally measured logP/logD values and their computationally derived counterparts (clogP/clogD). Notably, experimental values frequently exceeded calculated ones, suggesting that computational models systematically underestimate lipophilicity. This deviation becomes more prominent for compounds with high lipophilicity. While computational tools utilize sophisticated mathematical algorithms to predict partition and distribution coefficients[540], their primary value lies in screening large compound libraries during early-stage drug development. However, their predictive accuracy decreases for structurally complex molecules[528], highlighting the continued importance of experimentally determined results.

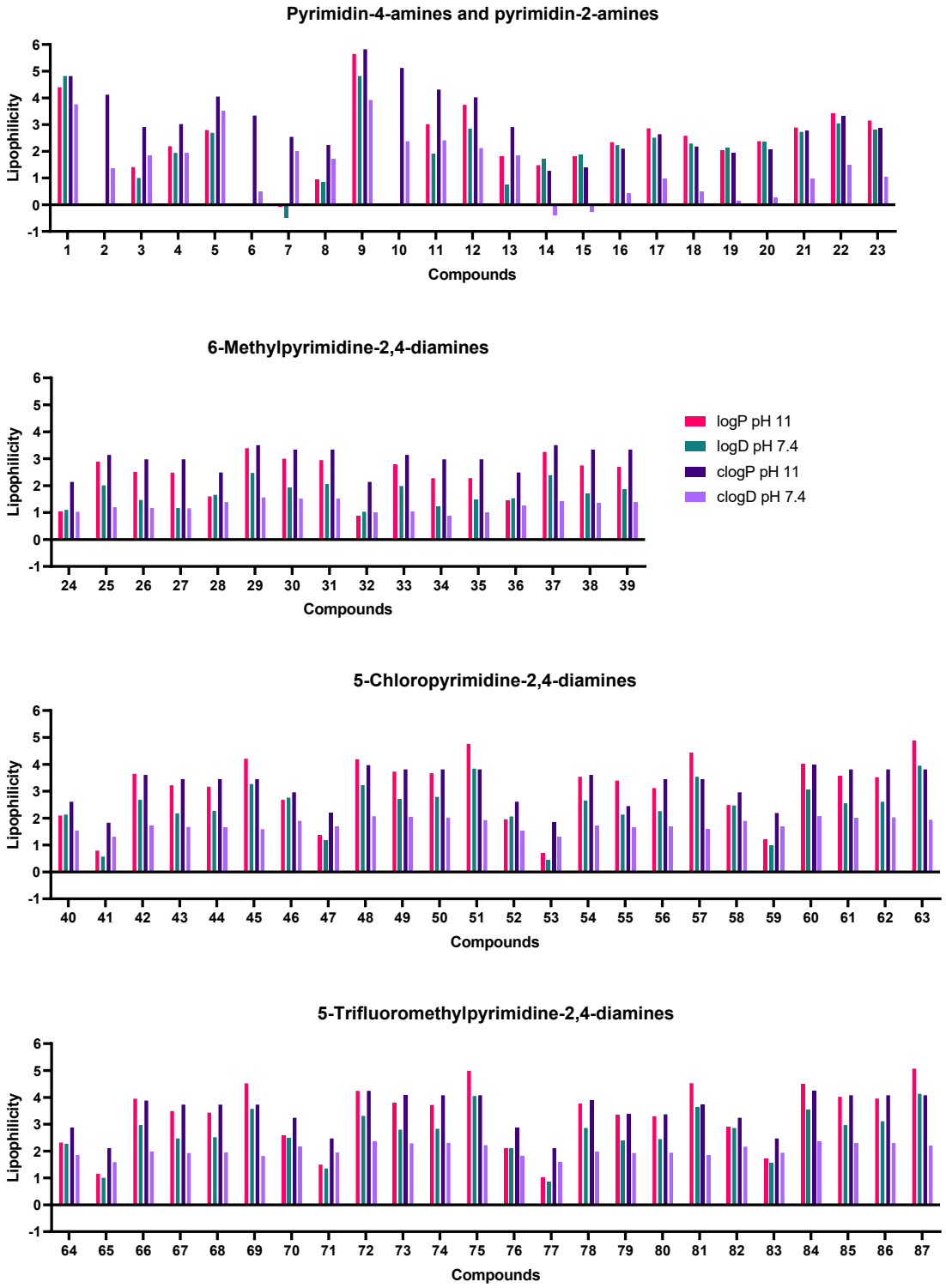

Figure 40. Experimentally determined and calculated logP and logD of compounds **1**-**87**.

To assess the potential correlation between histamine H_3R binding affinity and lipophilicity of the assayed compounds (**1**-**87**), a plot of H_3R K_i values versus logD at pH 7.4 was generated (Figure 41).

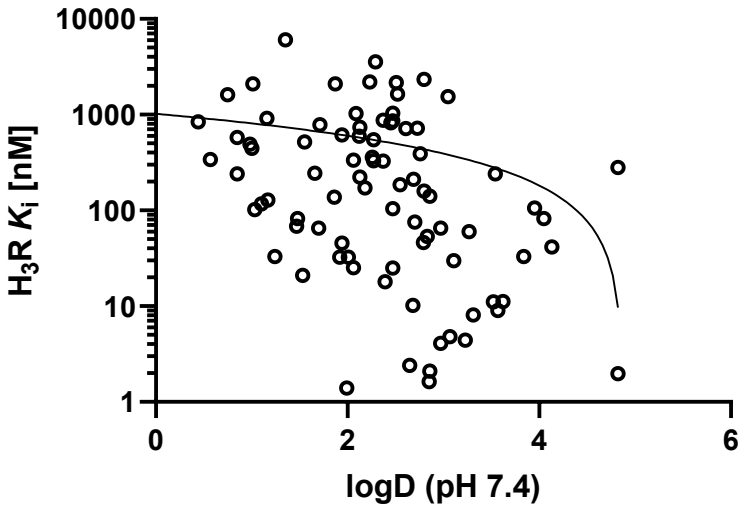

Figure 41. H_3R binding affinity (K_i) plotted against lipophilicity (logD (pH 7.4)) for compounds **1**-**87**, showing no direct correlation between these parameters.

Analysis of the correlation plot (Figure 41) reveals no significant correlation between lipophilicity (logD pH 7.4) and H_3R binding affinity for compounds **1**-**87**. The data demonstrate that potent H_3R ligands can be found across a wide range of lipophilicity values (logD -0.51 to 4.82), suggesting that factors other than lipophilicity are the primary determinants of H_3R binding affinity in this compound series. While lipophilicity stands as a pivotal physicochemical property in drug development, with increased lipophilicity commonly enhancing *in vitro* potency and representing an appealing optimization pathway, it also presents significant drawbacks, as higher lipophilicity correlates with decreased solubility, poor metabolic stability, and elevated risk of non-selective binding that can lead to undesirable toxicological profiles.[530, 536] The absence of lipophilicity-affinity correlation suggests that high H_3R potency in this series derives from specific structural features and selective receptor interactions rather than general lipophilic effects.

5 Summary

This doctoral research focused on the design, synthesis, and biological evaluation of novel H_3R ligands, emphasizing both single-target optimization and dual-target strategies to address complex neurological disorders. Leveraging the pyrimidinamine scaffold as a structural foundation, the study systematically explored three distinct ligand classes – pyrimidin-4-amines, pyrimidin-2-amines, and pyrimidine-2,4-diamines – to elucidate structure-activity relationships and advance therapeutic potential. The work builds on the clinical success of pitolisant (**L33**), the first approved H_3R antagonist for narcolepsy, while expanding into dual-target ligands to modulate complementary pathways implicated in neurodegenerative and neuropsychiatric diseases.

The study first focused on pyrimidin-4-amine derivatives, which underscored the critical role of the 1st basic moiety of H_3R pharmacophore in dictating affinity. Piperidine-containing compounds, such as **9**, **10**, and **12** (Figure 42), achieved exceptional potency with K_i values in the low nanomolar range (1.11-1.97 nM), surpassing pitolisant (K_i = 13.2 nM), and rivalling the most potent H_3R ligands. Methylpiperazine and acetylpiperazine analogs exhibited reduced affinity, underscoring the steric and electronic incompatibility of bulkier moieties with the H_3R binding pocket.

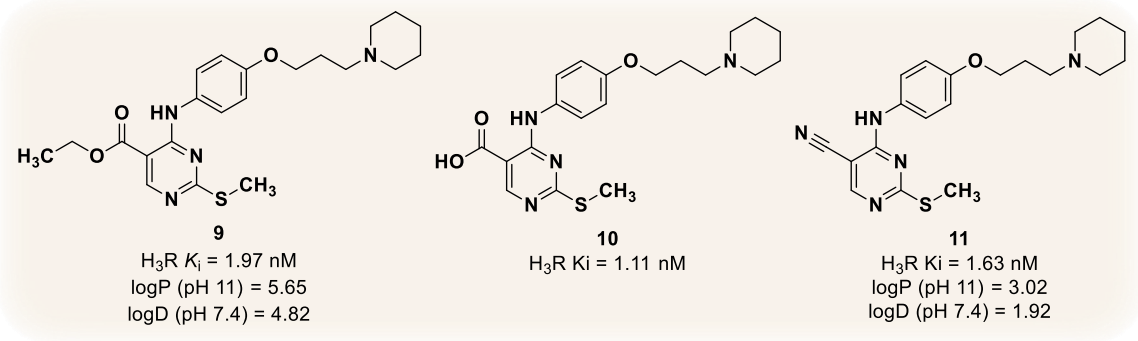

Figure 42. The most promising representatives of pyrimidin-4-amine derivatives and their corresponding pharmacological data.

The research expanded to pyrimidin-2-amine derivatives to probe the interplay between linker chemistry and steric effects. 3-(Piperidin-1-yl)propylthio derivatives (**19**-**23**) consistently outperformed their 3-(piperidin-1-yl)propyloxy counterparts (**14**-**18**), with the unsubstituted thio compound **19** (K_i = 596 nM) demonstrating the highest H_3R affinity. The sulfur atom's enhanced hydrophobic interactions and reduced steric demand likely facilitated receptor engagement. Bulkier C-6 substituents, such as cyclopropyl or isopropyl groups, diminished

binding due to steric clashes, while smaller groups (e.g., methyl) preserved moderate activity. Although this series exhibited lower potency compared to pyrimidin-4-amines, it provided insights into the role of linker flexibility and substituent size in optimizing receptor interactions.

The research then shifted to pyrimidine-2,4-diamine derivatives, designed to achieve dual-target engagement. Inspired by the first identified dual-target H_3R/G9a ligand A-366 (**L14**), 16 derivatives targeting H_3R and the epigenetic regulator G9a revealed structural synergies. Methoxy-substituted derivatives, such as **31** (H_3R K_i = 25.2 nM; G9a IC_{50} = 63.9 nM) (Figure 43), balanced dual activity by exploiting overlaps between the H_3R pharmacophore and G9a's lysine-binding channel. The methoxy group enhanced G9a inhibition by occupying a hydrophobic pocket (Ile1161/Lys1162), while the 3-(piperidin-1-yl)propyloxy moiety maintained H_3R engagement through salt bridges with Asp114. Comprehensive SAR analysis revealed that 2-alkylamino substitutions maximized H_3R affinity (e.g., **33**, K_i = 1.03 nM), whereas 4-methoxy groups favoured G9a inhibition. Although the members of the prepared series proved to be less potent than the reference compound **L14** on both targets, their significance lies not only in expanding the pool of known dual *h*H_3R/G9a-targeting ligands but also in providing valuable insights into SAR features. Specifically, the methoxy group's inverse effect on potency for both targets may guide future ligand development efforts.

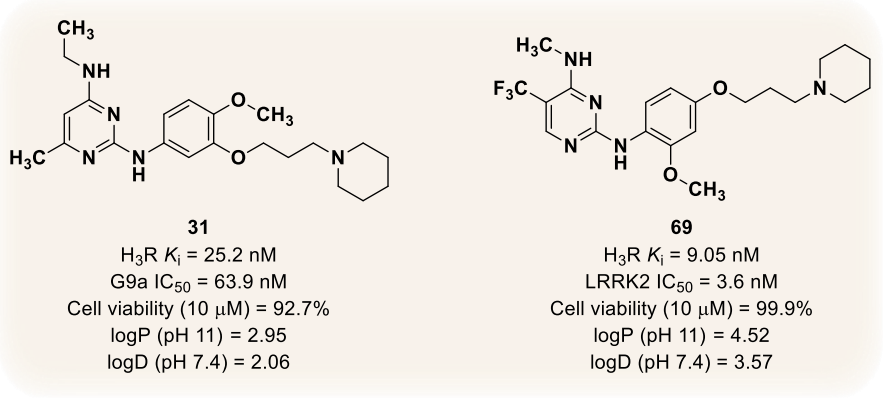

Figure 43. The most promising representatives of pyrimidine-2,4-diamine derivatives and their corresponding pharmacological data.

In parallel, 48 chloro- and trifluoromethylpyrimidine-2,4-diamines were synthesized to concurrently inhibit H_3R and LRRK2, a kinase implicated in PD. The 4-(3-piperidinopropoxy)anilino group proved essential for H_3R binding, with compound **69** (K_i = 9.05 nM) achieving single digit nanomolar potency. Trifluoromethyl substitution at C-5 enhanced LRRK2 inhibition (e.g., **69**, IC_{50} = 3.6 nM) via halogen interactions with

Glu1948, a key residue in LRRK2's catalytic domain. Methoxy derivatives, such as **69** and **87**, exhibited superior safety profiles (≥97% cell viability) compared to unsubstituted analogues, emphasizing the role of polarity in mitigating cytotoxicity. Compound **69** emerged as a lead candidate, combining single-digit nanomolar potency for both targets, favourable logD (3.57), and BBB permeability potential (Figure 43). Post-synthesis molecular docking validated key interactions – such as salt bridges with Asp114 (H_3R) and hydrogen bonds with Ala1950 (LRRK2) – providing retrospective insights into binding modes and guiding SAR refinement. The compounds from this series (**48**, **49**, **51**, **66**, **67**, **69**, **84**, **85**, **87**) exhibiting high potency at both targets (H_3R K_i = 4.1 – 104 nM; LRRK2 IC_{50} = 1.1 – 9.3 nM), represent the first reported dual-targeting H_3R/LRRK2 ligands to date.

Lipophilicity studies via RP-HPLC revealed that most compounds exhibited logD values (pH 7.4) within the optimal range for CNS penetration (1-4).

In conclusion, this research advances H_3R-targeted drug discovery by establishing aminopyrimidine derivatives as a versatile scaffold for both single- and dual-target ligands. Key achievements include:

- Identification of structural features critical for dual-target engagement,
- Expansion of the known H_3R/G9a ligand library, and
- Development of the first-in-class dual-target H_3R/LRRK2 ligands.

Notably, the most promising candidates – compound **31** (H_3R/G9a) and compound **69** (H_3R/LRRK2) – demonstrate balanced polypharmacology and CNS-compatible properties, underscoring their therapeutic potential.

By integrating medicinal chemistry, computational modelling, and experimental pharmacology, this work provides a strategic roadmap for designing next-generation multifunctional H_3R ligands. The findings highlight the promise of multi-target approaches in addressing unmet therapeutic needs in neurodegenerative and neuropsychiatric disorders, setting the stage for preclinical optimization and further therapeutic validation.

6 Experimental Section

6.1 General remarks

Reagents and solvents

All reagents and solvents were purchased from Acros Organics (Geel, Belgium), Alfa Aesar (Ward Hill, USA), Apollo Scientific, (Bredbury, UK), Fluka (Munich, Germany), Merck (Dramstadt, Germany), Sigma-Aldrich (Steinheim, Germany), TCI (Portland, USA), Macherey-Nagel (Düren, Germany) or VWR (Dramstadt, Germany) and used without further purification.

Thin-layer chromatography

Analytical TLC was performed on pre-coated sheets ALUGRAM® Xtra Sil G/UV_{254} (Macherey Nagel, Düren, Germany). Mobile phases for TLC separation were mixtures of dichloromethane, methanol, methanol saturated with ammonia, ethyl acetate and hexane in different ratios. Compounds were detected under 254 nm UV light, using TLC staining reagents – potassium permanganate solution (2.5 g $KMnO_4$, 17 g K_2CO_3, 4.2 mL NaOH (5%) in 250 mL water) and ninhydrin solution (2 g ninhydrin in 100 mL EtOH) – or by directly measuring compounds' mass spectrum from TLC plates utilizing Plate Express® plate reader coupled to expresse**ion**® CMS (Advion Interchim Scientific, Ithaca, USA).

Column chromatography

Column chromatography was performed using Silica gel 60 (0.04-0.063 mm) for column chromatography (Macherey-Nagel, Düren, Germany).

Flash chromatography

Flash column chromatography was performed on Biotage Isolera™ Spektra Systems with ACI™ and Assist (Biotage, Uppsala, Sweden). Prepacked normal-phase columns Biotage® Sfär Silica D and Biotage® Sfär Silica HC D (Biotage, Uppsala, Sweden) in sizes of 5 g, 10 g, 25 g, 50 g and 100 g were used with mobile phases consisting of varying ratio of DCM/MeOH, or EtOAc/*n*-hexane. Reverse-phase prepacked column Biotage® Sfär C18 Duo (Biotage, Uppsala, Sweden) in 6 g size was used with mobile phase consisting of ACN/H_2O + 0.1% CH_3COOH. Gradient and isocratic elution was used for both normal- and reverse-phase separation. Compounds were detected with UV/Vis-Detector in a wavelength range 200-800 nm.

High-performance liquid chromatography (HPLC)

Chromatographic lipophilicity assessment was performed using an Agilent 1260 II LC system comprising a flexible pump, temperature-controlled autosampler and column oven, along with fluorescence and UV-VIS detectors. Analyses were conducted on a Eurospher II 100-5 C18P column (50 × 4 mm, Knauer) using a mobile phase of 60% ACN and 40% pyrrolidine buffer (5 mM). Additional measurements employed a BETASIL C18 column (50 × 4.6 mm, ThermoFisher) with a mobile phase of 60% ACN and 40% PBS buffer (5 mM).

Microwave synthesis

Reactions under microwave irradiation were performed using Biotage Initiator+^{TM} Microwave system EU (Biotage, Uppsala, Sweden).

Melting point determination

The melting points of solid compounds were determined using Büchi Schmelzpunkt M-565 (Büchi, Flawil, Switzerland) with an open capillary tube and are uncorrected.

Liquid chromatography coupled with mass spectroscopy (LC-MS)

Determination of compounds' purity and monitoring of selected reactions was performed using LC-MS. All final compounds meet purity criteria of > 95%, as calculated using normalization method. Mass spectrometry data was acquired with an LC-MS system.

LC system: Elute SP LC System (Bruker Daltonics, Bremen, Germany) with vacuum degasser, binary pump, autosampler, column oven. Column: Intensity Solo 2 C18 (100 mm × 2.1 mm); Temperature: 50 °C; Mobile phase: A. water hypergrade with 0.1% formic acid (v/v) (Merck); B. Acetonitrile hypergrade (Merck); Flow Rate: 0.2 mL/min. Method 1 (bis 98%): 0-4 min 98% A, 4-5 min gradient 98 to 95% A, 5-9 min 95% A, 9-18 min gradient 95 to 5% A, 18-19 min 5 to 0.5% A, 19-20 min gradient 2 to 98% A; MS-System: Compact (Bruker Daltonics, Bremen, Germany) Ionisation: electronspray; Polarity: positive; Scan range: m/z: 50-1300; Nebulizer: Nitrogen, 1.8 Bar; Dry Gas: Nitrogen, 9 L/min, 220 °C; Massrange mode: UltraScan.

Mass spectroscopy

Mass spectra were determined using ex**pressei****on**® CMS equipped with Plate Express® automated TLC plate reader and ASAP® (Atmospheric Solids Analysis Probe) (Advion Interchim Scientific, Ithaca, USA). Ionisation: Atmospheric-pressure chemical ionization

(APCI); Polarity: positive and negative mode: Scan range: m/z 100-600; Nebulization gas: 0.5 L/min; Heated desolvation/APCI gas: 1 to 10 L/min. Data are shown as $[M+H^+]^+$ and $[M-H^+]^-$.

NMR spectroscopy

^1H and ^{13}C NMR spectra of compounds of interest were measured at Bruker Avance III - 300 and Bruker Avance III – 600 (Rheinstetten, Germany). As NMR solvents were used $CDCl_3$, DMSO-d_6 and D_2O with the addition of DCl. ^1H NMR data are reported in the following order: chemical shift (d) in ppm downfield from tetramethylsilane as internal reference; multiplicity (br, broad; s, singlet; d, doublet; dd, double doublet; t, triplet; m, multiplet; q, quintet); approximate coupling constants (*J*) in Hertz (Hz); number and assignment of protons. Depending on scanning time of ^{13}C NMR spectra, signal intensity of some quaternary carbons sometimes was too low to be detected.

Evaporation of solvents

Solvents were evaporated at Rotavapor R II (Büchi, Flawil, Switzerland) with PC 3001 VARIO Chemie-Vacuum pump (Vacuubrand, Wertheim, Germany) and CVC 3000 Vacuum controlling system. The compounds were dried at the high-vacuum pump (Vacuubrand Chemie- Hybrid-Pumpe RC 6 (Vacuubrand, Wertheim, Germany).

Freeze drying

Compounds were lyophilized with CHRIST ALPHA 1-4 LD Plus and ALPHA 2-4 D plus (Christ, Osterode am Harz, Germany). Freezing of the sample was achieved by swirling it in liquid nitrogen, with water being the main solvent component. The drying time varied depending on the solvent volume.

Microplate multimode reader

Tacan Infinite M100 Pro (Tecan, Maendorf, Switzerland).

Software

ChemDraw 23.1.1 was used for molecule drawing.[541] MarvinSketch 24.1.3 was used to estimate clogP and clogD values.[542] NMR spectrums were processed using MestReNova 14.1.2-25024.[543] *In vitro* assays were analyzed with GraphPad Prism 7.02.[544] AI language models were utilized to enhance text quality.[545, 546]

6.2 Chemical Experiments

3-(Piperidin-1-yl)propan-1-ol (P1)[417, 420]

Potassium carbonate (94.00 g, 0.680 mol, 4.4 eq.) and potassium iodide (1.00g, 6 mmol, 0.04 eq.) were suspended in 200 mL of acetone. To the stirred suspension, piperidine (23.2 mL, 0.235 mol, 1.5 eq.) and 3-chloropropan-1-ol (13.1 mL, 0.155 mol, 1.0 eq.) were added. The reaction mixture was then heated to reflux and stirred for 24 hours. After completion, the reaction mixture was cooled to room temperature, and the solids were removed by filtration. The filtrate was concentrated by evaporating the acetone under reduced pressure. The resulting crude liquid was then purified by fractional distillation to afford the desired product.

Yield:	26.7 g (60%)
Chemical formula:	$C_9H_{18}O$
Molecular mass:	142.24 g/mol
Appearance	Colorless oil
Internal code:	JH-03
^{1}H NMR (300 MHz, DMSO):	δ 4.48 (s, 1H), 3.42 (t, *J* = 6.3 Hz, 2H), 2.41 – 2.15 (m, 6H), 1.56 (dt, *J* = 7.8, 6.4 Hz, 2H), 1.51 – 1.42 (m, 4H), 1.41 – 1.31 (m, 2H)
MS (APCI-(+)):	m/z = 143.9 $[M+H^+]^+$

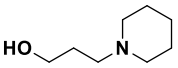

1-(3-Chloropropyl)piperidine hydrochloride (P2)[417, 420]

3-(Piperidin-1-yl)propan-1-ol (**P1**) (20.44 g, 142.7 mmol, 1.0 eq.) was dissolved in 320 mL of THF. Thionyl chloride (25.0 mL, 342.5 mmol, 2.4 eq.) was dissolved in 80 mL of THF and then added dropwise to the reaction mixture under stirring. The reaction mixture was then heated to 65°C and stirred for 3 hours. After completion, the mixture was cooled to room temperature and subsequently placed in an ice bath. Upon addition of 400 mL of diethyl ether under stirring, a precipitate formed. The solid was collected by filtration and dried to afford the desired product.

Yield:	24.8 g (87%)
Chemical formula:	$C_8H_{16}ClN \bullet HCl$
Molecular mass:	198.13 g/mol
Appearance	Beige solid
Internal code:	JH-04

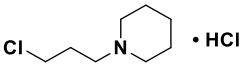

^{1}H NMR (300 MHz, DMSO):	δ 10.83 (s, 1H), 3.74 (t, *J* = 6.4 Hz, 2H), 3.38 (d, *J* = 12.7 Hz, 2H), 3.13 – 3.02 (m, 2H), 2.84 (tdd, *J* = 12.3, 9.0, 3.7 Hz, 2H), 2.29 – 2.15 (m, 2H), 1.87 – 1.62 (m, 5H), 1.36 (qt, *J* = 12.6, 4.7 Hz, 1H)
MS (APCI-(+)):	m/z = 162.0 $[M+H^+]^+$

3-(Piperidin-1-yl)propane-1-thiol (P3)[421]

A mixture of 1-(3-chloropropyl)piperidine (**P2**) (4.00 g, 20.19 mmol, 2.0 eq.), potassium iodide (1.67 g, 10.10 mmol, 1.0 eq.), and thiourea (2.30 g, 30.30 mmol, 3.0 eq.) was dissolved in 100 mL of ethanol and stirred under reflux for 24 hours. Afterward, an aqueous solution of NaOH (40.4 mmol, 8.1 mL, 4.0 eq.) was added, and the mixture was refluxed for an additional 3 hours. The reaction mixture was then cooled to room temperature, and the solvent was evaporated under reduced pressure. The resulting residue was dissolved in ethyl acetate, washed with brine, dried over anhydrous Na_2SO_4, and concentrated by evaporation. The obtained crude product was used in the next reaction step without further purification.

Yield:	2.8 g (87%)
Chemical formula:	$C_8H_{17}NS$
Molecular mass:	159.29 g/mol
Appearance	Yellow oil
Internal code:	MG-252
^{1}H NMR (300 MHz, $CDCl_3$):	δ 2.54 (t, *J* = 7.1 Hz, 2H), 2.44 – 2.25 (m, 6H), 1.78 (p, *J* = 7.2 Hz, 2H), 1.56 (p, *J* = 5.5 Hz, 4H), 1.42 (q, *J* = 5.8 Hz, 2H)
MS (APCI-(+)):	m/z = 157.9 $[M+H^+]^+$

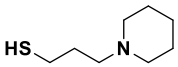

1-(3-Chloropropoxy)-4-nitrobenzene (P4)[424]

Potassium carbonate (14.90 g, 108 mmol, 3.0 eq.) was added to a solution of nitrophenol (5.00 g, 36 mmol, 1.0 eq.) in 150 mL of acetonitrile at room temperature. Subsequently, 1-bromo-3-chloropropane (3.52 mL, 36 mmol, 1 eq.) was added dropwise to the stirred suspension. The reaction mixture was then refluxed for 20 hours. After TLC control confirmed the consumption of the starting material, the reaction mixture was cooled to room temperature. The solid K_2CO_3 was removed by filtration, and the ACN was evaporated under reduced pressure. The residue was partitioned between DCM and water. The combined organic layers were washed with brine, dried over anhydrous $MgSO_4$, and filtered. Finally, DCM was evaporated under reduced pressure to afford the desired product.

Yield:	7.6 g (98%)
Chemical formula:	$C_8H_{17}ClN_2$
Molecular mass:	215.63 g/mol
Appearance	Brown oil
Internal code:	MG-239
^{1}H NMR (300 MHz, $CDCl_3$):	δ 8.19 (d, *J* = 9.3 Hz, 2H), 6.96 (d, *J* = 9.3 Hz, 2H), 4.22 (t, *J* = 5.9 Hz, 2H), 3.75 (t, *J* = 6.2 Hz, 2H), 2.28 (p, *J* = 6.0 Hz, 2H)
MS (APCI-(+)):	m/z = 215.8, 217.8 $[M+H^+]^+$

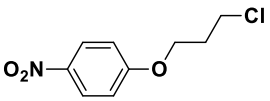

1-Methyl-4-(3-(4-nitrophenoxy)propyl)piperazine (P5)[425, 547]

1-(3-Chloropropoxy)-4-nitrobenzene (**P4**) (3.00g, 13.91 mmol, 1.0 eq.), 1-methylpiperazine (4.63 mL, 41.74 mmol, 3 eq.), potassium carbonate (5.77 g, 41.74 mmol, 3 eq.), and potassium iodide (4.62 g, 27.83 mmol, 2.0 eq.) were added to 100 mL of acetone. The reaction mixture was refluxed for 48 h. The reaction mixture was refluxed overnight under stirring. After completion, the reaction mixture was cooled to room temperature, and the solids were removed by filtration. The acetone was then evaporated under reduced pressure. The resulting residue was partitioned between ethyl acetate and water. The aqueous phase was washed twice with ethyl acetate. The combined organic layers were washed with brine, dried over anhydrous Na_2SO_4, and filtered. The solvent was evaporated under reduced pressure, and the crude product was purified by flash column chromatography (DCM:MeOH, 0-5% MeOH) to afford the desired product.

Yield:	2.8 g (73%)
Chemical formula:	$C_{14}H_{21}N_3O_3$
Molecular mass:	279.16 g/mol
Appearance	Yellow oil
Internal code:	MG-274
^{1}H NMR (300 MHz, $CDCl_3$):	δ 8.18 (d, *J* = 9.3 Hz, 2H), 6.94 (d, *J* = 9.3 Hz, 2H), 4.11 (t, *J* = 6.3 Hz, 2H), 2.63 – 2.36 (m, 9H), 2.28 (s, 3H), 2.07 – 1.92 (m, 3H)
MS (APCI-(+)):	m/z = 279.8 $[M+H^+]^+$

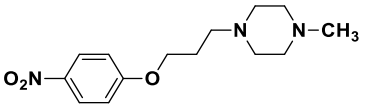

1-(4-(3-(4-Nitrophenoxy)propyl)piperazin-1-yl)ethan-1-one (P6)

1-(3-Chloropropoxy)-4-nitrobenzene (**P4**) (3.45 g, 16.0 mmol, 1.0 eq.), 1-acetylpiperazine (4.10 g, 32.0 mmol, 2.0 eq.), potassium carbonate (4.43 g, 32.0 mmol, 2.0 eq.), and potassium

iodide (5.32 g, 32.0 mmol, 2.0 eq.) were added to 50 mL of acetone. The reaction mixture was refluxed for 48 hours. After completion, the reaction mixture was cooled to room temperature, and the solids were removed by filtration. The acetone was then evaporated under reduced pressure. The resulting residue was partitioned between ethyl acetate and water. The aqueous phase was washed twice with ethyl acetate. The combined organic layers were washed with brine, dried over anhydrous Na_2SO_4, and filtered. The solvent was evaporated under reduced pressure, and the crude product was purified by flash column chromatography (DCM:MeOH, 0-5% MeOH) to afford the desired product.

Yield:	2.6 g (53%)
Chemical formula:	$C_{15}H_{21}N_3O_4$
Molecular mass:	307.35 g/mol
Appearance	Yellow solid
Internal code:	MG-324
^{1}H NMR (300 MHz, $CDCl_3$):	δ 8.19 (d, *J* = 9.3 Hz, 2H), 6.94 (d, *J* = 9.3 Hz, 2H), 4.12 (t, *J* = 6.3 Hz, 2H), 3.68 – 3.56 (m, 2H), 3.51 – 3.42 (m, 2H), 2.54 (t, *J* = 7.1 Hz, 2H), 2.50 – 2.37 (m, 4H), 2.08 (s, 3H), 2.01 (p, *J* = 6.5 Hz, 2H)
MS (APCI-(+)):	m/z = 308.0 $[M+H^+]^+$

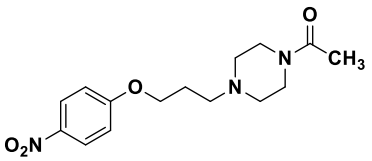

1-(3-(4-Nitrophenoxy)propyl)piperidine (P7)[547]

1-(3-Chloropropoxy)-4-nitrobenzene (**P4**) (3.60 g, 16.7 mmol, 1.0 eq.), piperidine (3.3 mL, 33.4 mmol, 2.0 eq.), potassium carbonate (6.90 g, 50.1 mmol, 3.0 eq.), potassium iodide (5.55 g, 33.4 mmol, 2.0 eq.) were added to 100 mL of acetone. The reaction mixture was refluxed for 48 h. After completion, the reaction mixture was cooled to room temperature, and the solids were removed by filtration. The acetone was then evaporated under reduced pressure. The resulting residue was partitioned between ethyl acetate and water. The aqueous phase was washed twice with ethyl acetate. The combined organic layers were washed with brine, dried over anhydrous Na_2SO_4, and filtered. The solvent was evaporated under reduced pressure, and the crude product was purified by flash column chromatography (DCM:MeOH, 0–5% MeOH) to afford the desired product.

Yield:	4.1 g (94%)
Chemical formula:	$C_{14}H_{20}N_2O_3$
Molecular mass:	264.32 g/mol
Appearance	Yellow oil

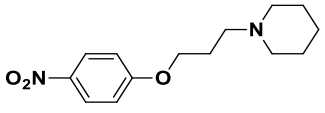

Internal code:	MG-242
^{1}H NMR (300 MHz, DMSO):	8.19 (d, *J* = 9.3 Hz, 2H), 7.13 (d, *J* = 9.3 Hz, 2H), 4.14 (t, *J* = 6.4 Hz, 2H), 2.41 – 2.23 (m, 6H), 1.88 (p, *J* = 6.7 Hz, 2H), 1.48 (p, *J* = 5.6 Hz, 4H), 1.43 – 1.29 (m, 2H)
MS (APCI-(+)):	m/z = 265.0 $[M+H^+]^+$

3-Methoxy-4-nitrophenol (P8)[426]

To a solution of 4-fluoro-2-methoxy-1-nitrobenzene (3.50 g, 20.45 mmol, 1.0 eq.) in 40 mL of DMSO, 40 mL of 1 M aqueous NaOH solution was added. The reaction mixture was stirred at 80 °C for 20 hours. After TLC indicated completion, the mixture was cooled to room temperature, and the pH was adjusted to 5 using 1 M HCl solution. The mixture was then extracted with ethyl acetate (3×). The combined organic layers were washed with brine, dried over anhydrous $MgSO_4$, and filtered. The solvent was evaporated under reduced pressure to afford the desired product.

Yield:	3.2 g (93%)
Chemical formula:	$C_{15}H_{24}N_2O_2$
Molecular mass:	169.14 g/mol
Appearance	Yellow solid
Internal code:	MG-304
^{1}H NMR (300 MHz, DMSO):	δ 10.90 (s, 1H), 7.88 (d, *J* = 9.0 Hz, 1H), 6.60 (d, *J* = 2.4 Hz, 1H), 6.46 (dd, *J* = 9.0, 2.4 Hz, 1H), 3.86 (s, 3H)
MS (APCI-(+)):	m/z = 170.0 $[M+H^+]^+$

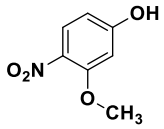

1-(3-(2-Methoxy-5-nitrophenoxy)propyl)piperidine (P9)[427]

1-(3-Chloropropyl)piperidin hydrochloride (**P2**) (2.57 g, 13.0 mmol, 1.1 eq.) and potassium carbonate (4.90 g, 35.5 mmol, 3.0 eq.) were added to a solution of 2-methoxy-4-nitrophenol (2.00 g, 11.8 mmol, 1.0 eq.) in 50 mL of DMF. The reaction mixture was stirred at room temperature for 72 hours. After TLC confirmed the consumption of the starting material, the reaction suspension was diluted with water and extracted twice with a 1:2 mixture of ethyl acetate and diethyl ether. The combined organic layers were washed with brine, dried over anhydrous $MgSO_4$, and filtered. The solvent was removed under reduced pressure to afford the desired product.

Yield:	3.5 g (quant.)
Chemical formula:	$C_{15}H_{22}N_2O_4$
Molecular mass:	294.35 g/mol
Appearance	Yellow oil
Internal code:	MG-220
^{1}H NMR (300 MHz, $CDCl_3$):	δ 7.88 (dd, *J* = 8.9, 2.6 Hz, 1H), 7.72 (d, *J* = 2.6 Hz, 1H), 6.94 (d, *J* = 9.0 Hz, 1H), 4.17 (t, *J* = 6.7 Hz, 2H), 3.93 (s, 3H), 2.46 (t, *J* = 7.2 Hz, 2H), 2.42 – 2.30 (m, 4H), 2.04 (p, *J* = 6.8 Hz, 2H), 1.57 (p, *J* = 5.5 Hz, 4H), 1.50 – 1.36 (m, 2H)
MS (APCI-(+)):	m/z = 295.2 $[M+H^+]^+$

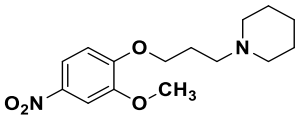

1-(3-(2-Methoxy-5-nitrophenoxy)propyl)piperidine (P10)[326]

1-(3-Chloropropyl)piperidin hydrochloride (**P2**) (16.26 mmol, 3.2 g, 1.1 eq.) and potassium carbonate (44.34 mmol, 6.1 g, 3.0 eq.) were added to a solution of 2-methoxy-5-nitrophenol (14.78 mmol, 2.5 g, 1 eq.) in 100 mL of DMF. The reaction mixture was stirred at room temperature for 72 hours. After TLC confirmed the consumption of the starting material, the reaction suspension was diluted with water and extracted twice with a 1:2 mixture of ethyl acetate and diethyl ether. The combined organic layers were washed with brine, dried over anhydrous $MgSO_4$, and filtered. The solvent was removed under reduced pressure to afford the desired product.

Yield:	3.5 g (81%)
Chemical formula:	$C_{15}H_{22}N_2O_4$
Molecular mass:	294.35 g/mol
Appearance	Yellow oil
Internal code:	MG-204
^{1}H NMR (300 MHz, DMSO):	δ 7.89 (dd, *J* = 9.0, 2.7 Hz, 1H), 7.71 (d, *J* = 2.7 Hz, 1H), 7.16 (d, *J* = 9.0 Hz, 1H), 4.09 (t, *J* = 6.5 Hz, 2H), 3.90 (s, 3H), 2.44 – 2.21 (m, 6H), 1.88 (p, *J* = 6.7 Hz, 2H), 1.48 (p, *J* = 5.4 Hz, 4H), 1.42 – 1.30 (m, 2H)
MS (APCI-(+)):	m/z = 295.4 $[M+H^+]^+$

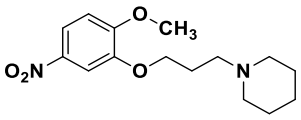

1-(3-(3-Methoxy-4-nitrophenoxy)propyl)piperidine (P11)

1-(3-Chloropropyl)piperidin hydrochloride (**P2**) (4.50g, 22.7 mmol, 1.2 eq.) and potassium carbonate (7.80 g, 56.8 mmol, 3.0 eq.) were added to a solution of 3-methoxy-4-nitrophenol (**P8**) (3.20 g, 18.9 mmol, 1.0 eq.) in 75 mL of DMF. The reaction mixture was stirred at room

temperature for 72 hours. After TLC confirmed the consumption of the starting material, the reaction suspension was diluted with water and extracted twice with a 1:2 mixture of ethyl acetate and diethyl ether. The combined organic layers were washed with brine, dried over anhydrous $MgSO_4$, and filtered. The solvent was removed under reduced pressure to afford the desired product.

Yield:	3.7 g (quant.)
Chemical formula:	$C_{15}H_{22}N_2O_4$
Molecular mass:	294.35 g/mol
Appearance	Orange oil
Internal code:	MG-313
^{1}H NMR (300 MHz, $CDCl_3$):	δ 7.99 (d, *J* = 9.4 Hz, 1H), 6.56 – 6.46 (m, 2H), 4.08 (t, *J* = 6.4 Hz, 2H), 3.94 (s, 3H), 2.50 – 2.31 (m, 6H), 2.05 – 1.93 (m, 2H), 1.58 (p, *J* = 5.4 Hz, 4H), 1.50 – 1.37 (m, 2H).
MS (APCI-(+)):	m/z = 295.2 $[M+H^+]^+$

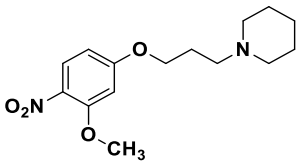

1-Methyl-4-(3-(4-nitrophenoxy)propyl)piperazine (P12)[547]

1-Methyl-4-(3-(4-nitrophenoxy)propyl)piperazine (**P5**) (2.80 g, 10.0 mmol, 1.0 eq.) was dissolved in 100 mL of methanol. A catalytic amount of 10% Pd/C was added, and the reaction mixture was stirred under a hydrogen atmosphere for 3 hours. After TLC confirmed the consumption of the starting material, the reaction mixture was filtered through a celite pad to remove the catalyst. The filtrate was concentrated under reduced pressure to afford the desired compound.

Yield:	2.3 g (92%)
Chemical formula:	$C_{14}H_{23}N_3O$
Molecular mass:	249.36 g/mol
Appearance	Red oil
Internal code:	MG-275
^{1}H NMR (300 MHz, DMSO):	δ 6.63 (d, *J* = 8.9 Hz, 2H), 6.49 (d, *J* = 8.9 Hz, 2H), 4.58 (s, 2H), 3.82 (t, *J* = 6.4 Hz, 2H), 2.48 – 2.18 (m, 10H), 2.14 (s, 3H), 1.85 – 1.70 (m, 2H)
MS (APCI-(+)):	m/z = 250.2 $[M+H^+]^+$

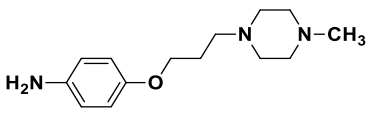

1-(4-(3-(4-Aminophenoxy)propyl)piperazin-1-yl)ethan-1-one (P13)

A 1-(4-(3-(4-nitrophenoxy)propyl)piperazin-1-yl)ethan-1-one (**P6**) (2.60 g, 12.0 mmol, 1.0 eq.) was dissolved in 100 mL of methanol. A catalytic amount of 10% Pd/C was added, and the reaction mixture was stirred under a hydrogen atmosphere for 3 hours. After TLC confirmed the consumption of the starting material, the reaction mixture was filtered through a celite pad to remove the catalyst. The filtrate was concentrated under reduced pressure to afford the desired compound.

Yield:	2.3 g (96%)
Chemical formula:	$C_{15}H_{23}N_3O_2$
Molecular mass:	277.37 g/mol
Appearance	Red solid
Internal code:	MG-326
^{1}H NMR (300 MHz, DMSO):	δ 6.74 (d, *J* = 8.9 Hz, 2H), 6.62 (d, *J* = 9.0 Hz, 2H), 3.93 (t, *J* = 6.3 Hz, 2H), 3.65 – 3.56 (m, 2H), 3.48 – 3.42 (m, 2H), 2.57 – 2.48 (m, 2H), 2.47 – 2.37 (m, 4H), 2.07 (s, 3H), 1.99 – 1.86 (m, 2H)
MS (APCI-(+)):	m/z = 278.2 $[M+H^+]^+$

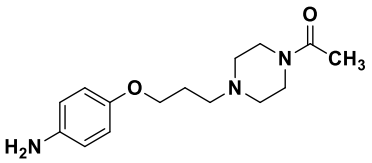

4-(3-(Piperidin-1-yl)propoxy)aniline (P14)[547]

1-(3-(4-nitrophenoxy)propyl)piperidine (**P7**) (4.10 g, 15.5 mmol, 1 eq.) was dissolved in 100 mL of methanol. A catalytic amount of 10% Pd/C was added, and the reaction mixture was stirred under a hydrogen atmosphere for 3 hours. After TLC confirmed the consumption of the starting material, the reaction mixture was filtered through a celite pad to remove the catalyst. The filtrate was concentrated under reduced pressure to afford the desired compound.

Yield:	3.7 g (quant.)
Chemical formula:	$C_{14}H_{22}N_2O$
Molecular mass:	234.34 g/mol
Appearance	Brown oil
Internal code:	MG-245
^{1}H NMR (300 MHz, DMSO):	δ 6.62 (d, *J* = 8.9 Hz, 2H), 6.49 (d, *J* = 8.9 Hz, 2H), 4.60 (s, 2H), 3.82 (t, *J* = 6.4 Hz, 2H), 2.42 – 2.21 (m, 6H), 1.85 – 1.70 (m, 2H), 1.54 – 1.43 (m, 4H), 1.42 – 1.32 (m, 2H)
MS (APCI-(+)):	m/z = 234.8 $[M+H^+]^+$

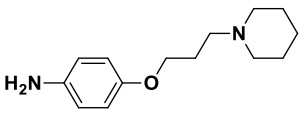

3-Methoxy-4-(3-(piperidin-1-yl)propoxy)aniline (P15)[427]

A 1-(3-(2-Methoxy-5-nitrophenoxy)propyl)piperidine **(P9)** (3.45 g, 11.72 mmol, 1.0 eq.) was dissolved in 100 mL of methanol. A catalytic amount of 10% Pd/C was added, and the reaction mixture was stirred under a hydrogen atmosphere for 3 hours. After TLC confirmed the consumption of the starting material, the reaction mixture was filtered through a celite pad to remove the catalyst. The filtrate was concentrated under reduced pressure to afford the desired compound.

Yield:	2.8 g (90%)
Chemical formula:	$C_{15}H_{24}N_2O_2$
Molecular mass:	264.37 g/mol
Appearance	Red oil
Internal code:	MG-221
^{1}H NMR (300 MHz, DMSO):	δ 6.62 (d, *J* = 8.4 Hz, 1H), 6.25 (d, *J* = 2.5 Hz, 1H), 6.04 (dd, *J* = 8.4, 2.5 Hz, 1H), 4.66 (s, 2H), 3.79 (t, *J* = 6.4 Hz, 2H), 3.66 (s, 3H), 2.40 – 2.25 (m, 6H), 1.82 – 1.67 (m, 2H), 1.48 (p, *J* = 5.4 Hz, 5H), 1.43 – 1.30 (m, 2H)
MS (APCI-(+)):	m/z = 265.2 $[M+H^+]^+$

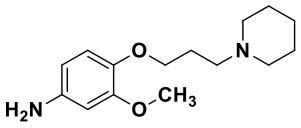

4-Methoxy-3-(3-(piperidin-1-yl)propoxy)aniline (P16)[326]

A 1-(3-(2-Methoxy-5-nitrophenoxy)propyl)piperidine (**P10**) (3.50 g, 11.92 mmol, 1.0 eq.) was dissolved in 100 mL of methanol. A catalytic amount of 10% Pd/C was added, and the reaction mixture was stirred under a hydrogen atmosphere for 3 hours. After TLC confirmed the consumption of the starting material, the reaction mixture was filtered through a celite pad to remove the catalyst. The filtrate was concentrated under reduced pressure to afford the desired compound.

Yield:	3.1 g (97%)
Chemical formula:	$C_{15}H_{24}N_2O_2$
Molecular mass:	264.37 g/mol
Appearance	Brown oil
Internal code:	MG-206
^{1}H NMR (300 MHz, DMSO):	δ 6.63 (d, *J* = 8.4 Hz, 1H), 6.25 (d, *J* = 2.5 Hz, 1H), 6.05 (dd, *J* = 8.4, 2.5 Hz, 1H), 4.63 (s, 2H), 3.86 (t, *J* = 6.5 Hz, 2H), 3.60 (s, 3H), 2.45 – 2.22 (m, 6H), 1.82 (p, *J* = 6.7 Hz, 2H), 1.48 (p, *J* = 5.5 Hz, 4H), 1.42 – 1.31 (m, 2H)
MS (APCI-(+)):	m/z = 265.3 $[M+H^+]^+$

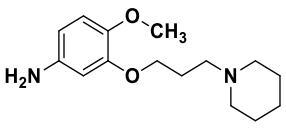

2-Methoxy-4-(3-(piperidin-1-yl)propoxy)aniline (P17)

A 1-(3-(3-Methoxy-4-nitrophenoxy)propyl)piperidine (**P11**) (5.70 g, 19.4 mmol, 1.0 eq.) was dissolved in 100 mL of methanol. A catalytic amount of 10% Pd/C was added, and the reaction mixture was stirred under a hydrogen atmosphere for 3 hours. After TLC confirmed the consumption of the starting material, the reaction mixture was filtered through a celite pad to remove the catalyst. The filtrate was concentrated under reduced pressure to afford the desired compound.

Yield:	4.4 g (88%)
Chemical formula:	$C_{15}H_{24}N_2O_2$
Molecular mass:	264.37 g/mol
Appearance	Dark red oil
Internal code:	MG-315
^{1}H NMR (300 MHz, $CDCl_3$):	δ 6.62 (d, *J* = 8.4 Hz, 1H), 6.44 (d, *J* = 2.6 Hz, 1H), 6.34 (dd, *J* = 8.4, 2.6 Hz, 1H), 3.93 (t, *J* = 6.4 Hz, 2H), 3.82 (s, 3H), 3.43 (s, 2H), 2.55 – 2.36 (m, 6H), 2.02 – 1.87 (m, 2H), 1.59 (p, *J* = 5.6 Hz, 4H), 1.49 – 1.37 (m, 2H)
MS (APCI-(+)):	m/z = 265.2 $[M+H^+]^+$

Ethyl 4-hydroxy-2-(methylthio)pyrimidine-5-carboxylate (P18)[444]

S-Methylthiourea hemisulfate (11.10 g, 80 mmol, 1.0 eq.) was added to a 50 mL of NaOH solution (4.42 mol/L) in a three-neck flask, while maintaining the mixture in an ice bath. The mixture was stirred for 30 minutes. Diethyl ethoxymethylenemalonate (19.4 mL, 96 mmol, 1.2 eq.) was dissolved in 32 mL of ethanol and added dropwise to the prepared mixture. After the dropwise addition was complete, the reaction mixture was stirred overnight at room temperature, resulting in the precipitation of the desired product as a white solid. The product was isolated by vacuum filtration, washed with water, and dried under high vacuum to afford the desired compound.

Yield:	11.9 g (69%)
Chemical formula:	$C_8H_{10}N_2O_3S$
Molecular mass:	214.24 g/mol
Appearance	White solid
Internal code:	MG-03
^{1}H NMR (300 MHz, DMSO):	δ 8.21 (s, 1H), 4.10 (q, *J* = 7.1 Hz, 2H), 2.29 (s, 3H), 1.22 (t, *J* = 7.1 Hz, 3H)
MS (APCI-(+)):	m/z = 214.8 $[M+H^+]^+$

Ethyl 4-chloro-2-(methylthio)pyrimidine-5-carboxylate (P19)[444]

Dried ethyl 4-hydroxy-2-(methylthio)pyrimidine-5-carboxylate **(P18)** (1.00 g, 4.67 mmol, 1.0 eq.) was added to 2.7 mL of acetonitrile and stirred for 25 minutes. Phosphoryl oxychloride (2.43 mL, 26.07 mmol, 5.6 eq.) was then slowly added to the mixture while maintaining the reaction temperature in an ice bath. After the addition was complete, the reaction mixture was refluxed for 6 hours. The solvents were then evaporated under reduced pressure, and the crude product was used directly in the next reaction without further purification.

Yield:	2.1 g (69%)
Chemical formula:	$C_8H_9ClN_2O_2S$
Molecular mass:	232.68 g/mol
Appearance	Yellow solid
Internal code:	MG-10
^{1}H NMR (300 MHz, DMSO):	δ 9.00 (s, 1H), 4.33 (q, *J* = 7.1 Hz, 2H), 2.58 (s, 3H), 1.32 (t, *J* = 7.1 Hz, 3H)

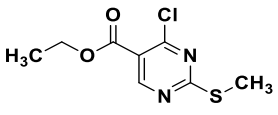

Ethyl 4-((4-(3-(4-methylpiperazin-1-yl)propoxy)phenyl)amino)-2-(methylthio) pyrimidine-5-carboxylate (1)

Ethyl 4-chloro-2-(methylthio)pyrimidine-5-carboxylate **(P19)** (771 mg, 3.31 mmol, 1.0 eq.) was dissolved together with 4-(3-(4-methylpiperazin-1-yl)propoxy)aniline **(P12)** (773 mg, 3.1 mmol, 1.0 eq.) in 5 mL of DMSO. The mixture was treated with DIPEA (1.62 mL, 9.3 mmol, 3.0 eq.) and stirred for 2 h at 80 °C. After TLC control indicated consumption of starting materials, the reaction was quenched with ice cold water (25 mL) and partitioned with ethyl acetate (3 × 25 mL). The combined organic layers were washed with brine (20 mL) and dried over $MgSO_4$. After filtration, solvent was evaporated under reduced pressure and the reaction crude was purified by column chromatography (DCM:MeOH = 95:5).

Yield:	280 mg (20%)
Chemical formula:	$C_{22}H_{31}N_5O_3S$
Molecular mass:	445.58 g/mol
Appearance	Light brown solid
Internal code:	MG-19, ST-2529
^{1}H NMR (300 MHz, $CDCl_3$)	δ 10.17 (s, 1H), 8.73 (s, 1H), 7.52 (d, *J* = 9.0 Hz, 2H), 6.88 (d, *J* = 9.0 Hz, 2H), 4.37 (q, *J* = 7.2 Hz, 2H), 4.01 (t, *J* = 6.3 Hz, 2H), 2.62 – 2.44 (m, 13H), 2.30 (s, 3H), 1.97 (p, *J* = 6.6 Hz, 2H), 1.39 (t, *J* = 7.1 Hz, 3H)

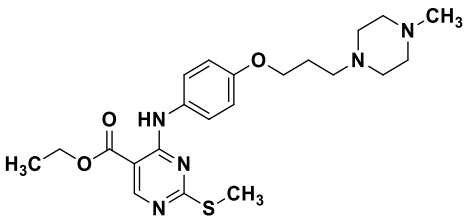

^{13}C NMR (75 MHz, $CDCl_3$)	δ 176.64, 167.25, 158.96, 158.42, 156.08, 130.83, 123.71, 114.65, 101.04, 66.63, 61.32, 55.23, 55.19, 53.21, 46.08, 26.90, 14.53, 14.37
Melting point	91.2 °C
MS (APCI-(+)):	m/z = 446.3 $[M+H^+]^+$
LC-MS-DAD purity:	98.98%
HRMS (ESI-(+)):	m/z = 446.2234 $[M+H^+]^+$ (calculated: 446.2220)

4-((4-(3-(4-Methylpiperazin-1-yl)propoxy)phenyl)amino)-2-(methylthio)pyrimidine-5-carboxylic acid (2)

Ethyl 4-((4-(3-(4-methylpiperazin-1-yl)propoxy)phenyl)amino)-2-(methylthio)pyrimidine-5-carboxylate **(1)** (100 mg, 0.22 mmol, 1.0 eq.) was dissolved 2.5 mL of THF. LiOH (22 mg, 0.90 mmol, 4.0 eq.) was dissolved in 2.5 mL of water and added to the stirred THF solution. The reaction mixture was stirred at room temperature for 3 h. Subsequently, solvent was evaporated, the residue was redissolved in water and pH value was adjusted with 1 M HCl solution until the precipitation occurred. The obtained suspension was left in the fridge overnight to allow the maturation of precipitate which was then filtered out and dried on a high vacuum pump to afford the desired compound.

Yield:	40 mg (40%)
Chemical formula:	$C_{20}H_{27}N_5O_3S$
Molecular mass:	417.53 g/mol
Appearance	White solid
Internal code:	MG-212, ST-2737

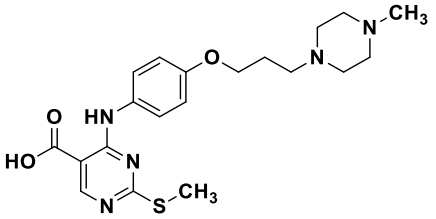

^{1}H NMR (300 MHz, DCl in D_2O)	δ 8.93 (s, 1H), 7.76 (d, *J* = 8.4 Hz, 2H), 7.25 (d, *J* = 8.6 Hz, 2H), 4.49 – 3.75 (m, 12H), 3.37 (s, 3H), 2.83 (s, 3H), 2.68 – 2.56 (m, 2H)
^{13}C NMR (75 MHz, DCl in D_2O)	δ 168.54, 166.20, 155.63, 147.77, 128.78, 124.40, 123.49, 115.27, 101.88, 55.37, 50.86, 50.43, 49.94, 49.60, 23.88, 15.20.
Melting point	224.1°C
MS (APCI-(+)):	m/z = 418.2 $[M+H^+]^+$
LC-MS-DAD purity:	100.000%
HRMS (ESI-(+)):	m/z = 418.1740 $[M+H^+]^+$ (calculated: 418.1749)

4-((4-(3-(4-Methylpiperazin-1-yl)propoxy)phenyl)amino)-2-(methylthio)pyrimidine-5-carboxamide (3)

4-((4-(3-(4-Methylpiperazin-1-yl)propoxy)phenyl)amino)-2-(methylthio)pyrimidine-5-carboxylic acid (**2**) (100 mg, 0.22 mmol, 1.0 eq.) and HATU (128 mg, 0.34 mmol, 1.5 eq.) were dissolved in 10 mL of DMF and allowed to stir for 5 min at room temperature. Subsequently, NH_4Cl (60 mg, 1.12 mmol, 5 eq.) and DIPEA (0.2 mL, 1.12 mmol, 5.0 eq.) were added, and the reaction mixture was stirred for 1 h at room temperature. After TLC control indicated consumption of starting material, the solvent was evaporated and the residue was purified using flash column chromatography (DCM:MeOH, 0-10% MeOH) to obtain the desired product.

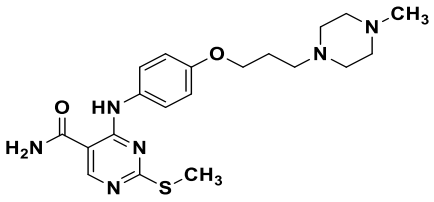

Yield:	90 mg (96%)
Chemical formula:	$C_{20}H_{28}N_6O_2S$
Molecular mass:	416.54 g/mol
Appearance	Off-white solid
Internal code:	MG-195, ST-2708
^{1}H NMR (300 MHz, $CDCl_3$):	δ 10.77 (s, 1H), 8.35 (s, 1H), 7.52 (d, *J* = 9.0 Hz, 2H), 6.87 (d, *J* = 9.0 Hz, 2H), 5.99 (s, 2H), 4.01 (t, *J* = 6.3 Hz, 2H), 2.58 – 2.42 (m, 11H), 2.28 (s, 3H), 1.97 (dt, *J* = 13.0, 6.5 Hz, 4H)
^{13}C NMR (75 MHz, $CDCl_3$):	δ 175.88, 169.30, 158.33, 156.03, 155.06, 130.95, 123.73, 114.63, 102.70, 77.36, 66.68, 55.28, 53.34, 46.19, 26.95, 14.51
Melting point	234.1 °C
MS (APCI-(+)):	m/z = 416.9 $[M+H^+]^+$
LC-MS-DAD purity:	100.00%
HRMS (ESI-(+)):	m/z = 417.2073 $[M+H^+]^+$ (calculated: 417.2067)

4-((4-(3-(4-Methylpiperazin-1-yl)propoxy)phenyl)amino)-2-(methylthio)pyrimidine-5-carbonitrile (4)

A solution of 4-chloro-2-(methylthio)pyrimidine-5-carbonitrile (100 mg, 0.54 mmol, 1.0 eq.) and 4-(3-(4-methylpiperazin-1-yl)propoxy)aniline **(P12)** (161 mg, 0.65 mmol, 1.2 eq.) in 5 mL of DCM was treated with DIPEA (0.54 mmol, 70 mg, 1.0 eq.). The reaction mixture was stirred at 40 °C overnight. Subsequently, DCM was washed with water and brine, dried over $MgSO_4$ and concentrated to dryness in vacuo. The obtained residue was purified using flash chromatography (DCM:MeOH, 0-10% MeOH) to afford the desired product.

Yield:	80 mg (37%)

Chemical formula:	$C_{20}H_{26}N_6OS$
Molecular mass:	398.53 g/mol
Appearance	Beige solid
Internal code:	MG-170, ST-2670

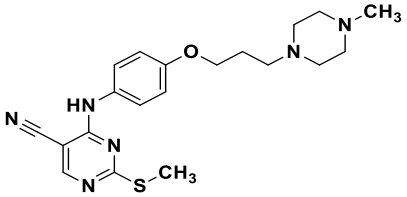

^{1}H NMR (300 MHz, DMSO):	δ 9.77 (s, 1H), 8.54 (s, 1H), 7.41 (d, *J* = 8.9 Hz, 2H), 6.91 (d, *J* = 9.0 Hz, 2H), 3.99 (t, *J* = 6.4 Hz, 2H), 2.49 – 2.24 (m, 13H), 2.19 (s, 3H), 1.92 – 1.79 (m, 2H)
^{13}C NMR (75 MHz, DMSO):	δ 174.72, 161.19, 158.16, 156.06, 129.96, 125.45, 115.50, 114.09, 86.68, 65.95, 54.50, 52.40, 45.41, 26.18, 13.65
Melting point	122.2 °C
MS (APCI-(+)):	m/z = 399.1 $[M+H^+]^+$
LC-MS-DAD purity:	97.37%
HRMS (ESI-(+)):	m/z = 399.1975 $[M+H^+]^+$ (calculated: 399.1962)

Ethyl 4-((4-(3-(4-acetylpiperazin-1-yl)propoxy)phenyl)amino)-2-(methylthio) pyrimidine-5-carboxylate (5)

A solution of ethyl 4-chloro-2-(methylthio)pyrimidine-5-carboxylate (300 mg, 1.29 mmol, 1.0 eq.) and 1-(4-(3-(4-aminophenoxy)propyl)piperazin-1-yl)ethan-1-one **(P13)** (393 mg, 1.42 mmol, 1.1 eq.) were dissolved in 11 mL of isopropanol in a microwave vial. The vial containing reaction mixture was transferred to the microwave reactor where the reaction mixture was stirred at 80 °C for 2 h under microwave irradiation. Subsequently, the solvent was evaporated, and the residue was partitioned between 2 M NaOH (30 mL) and DCM (3 × 30 mL). The organic layers were merged, washed with brine, dried over $MgSO_4$. After filtration solvent was evaporated, and the residue was purified using flash column chromatography (DCM:MeOH, 0-7% MeOH) in order to obtain desired product.

Yield:	546 mg (89%)
Chemical formula:	$C_{23}H_{31}N_5O_4S$
Molecular mass:	473.59 g/mol
Appearance	White solid
Internal code:	MG-343, ST-3043

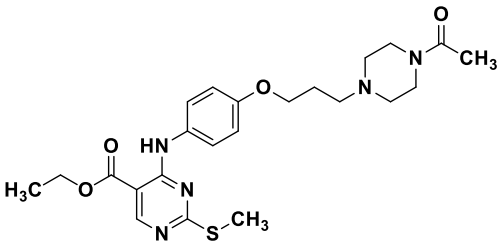

^{1}H NMR (300 MHz, $CDCl_3$)	δ 10.19 (s, 1H), 8.74 (s, 1H), 7.53 (d, *J* = 9.0 Hz, 2H), 6.88 (d, *J* = 9.0 Hz, 2H), 4.37 (q, *J* = 7.1 Hz, 2H), 4.03 (t, *J* = 6.3 Hz, 2H), 3.68 – 3.58 (m, 2H), 3.53 – 3.44 (m, 2H), 2.60 – 2.51 (m, 2H), 2.51 – 2.40 (m, 7H), 2.09 (s, 3H), 2.04 – 1.91 (m, 2H), 1.40 (t, *J* = 7.1 Hz, 3H)

^{13}C NMR (75 MHz, $CDCl_3$)	δ 187.09, 176.66, 169.03, 167.27, 158.44, 156.03, 130.92, 123.73, 114.64, 101.08, 66.62, 63.36, 61.35, 55.11, 53.32, 52.94, 46.46, 41.54, 26.83, 21.49, 14.38
Melting point	114.9 °C
MS (APCI-(+)):	m/z = 473.7 $[M+H^+]^+$
LC-MS-DAD purity:	100.00%
HRMS (ESI-(+)):	m/z = 474.2186 $[M+H^+]^+$ (calculated: 474.2170)

4-((4-(3-(4-Acetylpiperazin-1-yl)propoxy)phenyl)amino)-2-(methylthio)pyrimidine-5-carboxylic acid (6)

Ethyl 4-((4-(3-(4-acetylpiperazin-1-yl)propoxy)phenyl)amino)-2-(methylthio)pyrimidine-5-carboxylate (**5**) (380 mg, 0.80 mmol, 1.0 eq.) was dissolved 5 mL of THF. LiOH (135 mg, 3.21 mmol, 4.0 eq.) was dissolved in 5 mL of water and added to the stirred THF solution. The reaction mixture was stirred at room temperature for 3 h. Subsequently, solvent was evaporated, the residue was redissolved in water and pH value was adjusted with 1 M HCl solution until the precipitation occurred. The solid was filtered and purified using C18 RP-flash column chromatography (H_2O (1% CH_3COOH):MeOH, 0-100% MeOH) to obtain the desired product.

Yield:	190 mg (53%)
Chemical formula:	$C_{21}H_{27}N_5O_4S$
Molecular mass:	445.54 g/mol
Appearance	White solid
Internal code:	MG-350, ST-3044

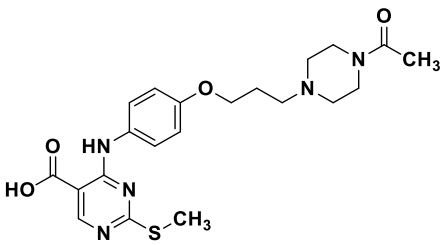

^{1}H NMR (300 MHz, DMSO)	δ 11.11 (s, 1H), 8.62 (s, 1H), 7.54 (d, *J* = 9.0 Hz, 2H), 6.91 (d, *J* = 9.0 Hz, 2H), 5.26 (s, 1H), 4.01 (t, *J* = 6.2 Hz, 2H), 3.52 (t, *J* = 4.9 Hz, 4H), 2.76 – 2.57 (m, 6H), 2.45 (s, 3H), 2.06 – 1.93 (m, 5H)
^{13}C NMR (75 MHz, DMSO)	δ 173.72, 168.57, 168.23, 158.28, 154.80, 135.14, 131.17, 122.67, 114.52, 65.62, 53.87, 44.68, 30.38, 25.27, 21.10, 13.72
Melting point	128.7 °C
MS (APCI-(-)):	m/z = 443.8 $[M-H^+]^-$
LC-MS-DAD purity:	97.75%
HRMS (ESI-(+)):	m/z = 446.1866 $[M+H^+]^+$ (calculated: 446.1857)

4-((4-(3-(4-acetylpiperazin-1-yl)propoxy)phenyl)amino)-2-(methylthio)pyrimidine-5-carboxamide (7)

4-((4-(3-(4-Acetylpiperazin-1-yl)propoxy)phenyl)amino)-2-(methylthio)pyrimidine-5-carboxylic acid (**6**) (110 mg, 0.25 mmol, 1 eq.) and HATU (141 mg, 0.37 mmol, 1.5 eq.) were dissolved in 10 mL of DMF and allowed to stir for 5 min at room temperature. Subsequently, NH_4Cl (66 mg, 1.23 mmol, 5 eq.) and DIPEA (0.22 mL, 1.23 mmol, 5 eq.) were added, and the reaction mixture was stirred for 2 h at room temperature. After consumption of the starting material, the reaction mixture was diluted with ethyl acetate and extracted with brine (3 × 50 mL). The organic layer was then extracted with 2 M NaOH (3 x 50 mL), and finally washed with brine, dried over MgSO4 and evaporated. The residue was then purified using flash column chromatography (DCM:MeOH, 0-7% MeOH) to obtain the desire product.

Yield:	71 mg (65%)
Chemical formula:	$C_{21}H_{28}N_6O_3S$
Molecular mass:	444.55 g/mol
Appearance	White solid
Internal code:	MG-351, ST-3045

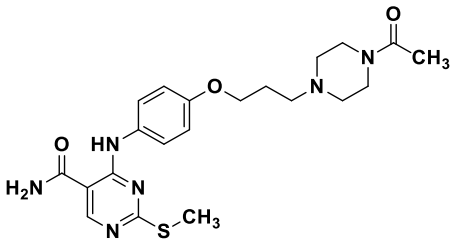

^{1}H NMR (300 MHz, $CDCl_3$)	δ 10.79 (s, 1H), 8.37 (s, 1H), 7.53 (d, *J* = 9.0 Hz, 2H), 6.87 (d, *J* = 9.0 Hz, 2H), 5.99 (s, 2H), 4.02 (t, *J* = 6.3 Hz, 2H), 3.62 (t, *J* = 5.1 Hz, 2H), 3.47 (t, *J* = 5.1 Hz, 2H), 2.60 – 2.37 (m, 9H), 2.09 (s, 3H), 1.97 (dt, *J* = 13.1, 6.6 Hz, 2H)
^{13}C NMR (151 MHz, $CDCl_3$)	δ 175.81, 169.36, 169.09, 158.33, 155.91, 131.08, 123.70, 114.59, 102.77, 66.37, 55.10, 53.51, 52.91, 46.45, 41.57, 26.85, 21.48, 14.48
Melting point	186.0 °C
MS (APCI-(+)):	m/z = 444.9 $[M+H^+]^+$
LC-MS-DAD purity:	100.00%
HRMS (ESI-(+)):	m/z = 445.2030 $[M+H^+]^+$ (calculated: 445.2016)

4-((4-(3-(4-Acetylpiperazin-1-yl)propoxy)phenyl)amino)-2-(methylthio)pyrimidine-5-carbonitrile (8)

A solution of 4-chloro-2-(methylthio)pyrimidine-5-carbonitrile (100 mg, 0.54 mmol, 1.0 eq.) and 1-(4-(3-(4-aminophenoxy)propyl)piperazin-1-yl)ethan-1-one (**P13**) (165 mg, 0.59 mmol, 1.1 eq.) were dissolved in 2.2 mL of isopropanol in a microwave vial. The vial containing reaction mixture was transferred to the microwave reactor where the reaction mixture was

stirred at 80 °C for 2 h under microwave irradiation. Subsequently, the solvent was evaporated, and the residue was partitioned between 2 M NaOH (30 mL) and DCM (3 × 30 mL). Combined organic layers were washed with brine (100 mL) and dried over $MgSO_4$. After filtration solvent was evaporated, and the residue was purified using flash column chromatography (DCM:MeOH, 0-7% MeOH) in order to obtain desired product.

Yield:	188 mg (82%)
Chemical formula:	$C_{21}H_{26}N_6O_2S$
Molecular mass:	426.54 g/mol
Appearance	White solid
Internal code:	MG-342, ST-3042

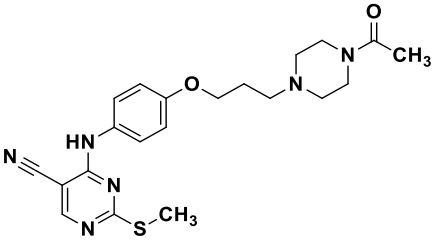

^{1}H NMR (300 MHz, $CDCl_3$)	δ 8.33 (s, 1H), 7.42 (d, *J* = 9.0 Hz, 2H), 7.18 (s, 1H), 6.90 (d, *J* = 9.0 Hz, 2H), 4.03 (t, *J* = 6.3 Hz, 2H), 3.62 (t, *J* = 5.0 Hz, 2H), 3.47 (t, 2H), 2.55 (t, *J* = 7.2 Hz, 2H), 2.49 – 2.40 (m, 7H), 2.08 (s, 3H), 2.04 – 1.93 (m, 2H)
^{13}C NMR (75 MHz, $CDCl_3$)	δ 176.83, 169.05, 159.64, 158.61, 156.98, 129.34, 124.45, 115.39, 114.80, 87.06, 66.39, 55.06, 53.53, 52.91, 46.42, 41.54, 26.79, 21.45, 14.47
Melting point	125.8 °C
MS (APCI-(+)):	m/z = 427.2 $[M+H^+]^+$
LC-MS-DAD purity:	97.46%
HRMS (ESI-(+)):	m/z = 427.1910 $[M+H^+]^+$ (calculated: 427.1911)

Ethyl 2-(methylthio)-4-((4-(3-(piperidin-1-yl)propoxy)phenyl)amino)pyrimidine-5-carboxylate (9)

Ethyl 4-chloro-2-(methylthio)pyrimidine-5-carboxylate (200 mg, 0.86 mmol, 1.0 eq.) and 4-(3-(piperidin-1-yl)propoxy)aniline (**P14**) (282 mg, 1.20 mmol, 1.4 eq.) were dissolved in 4 mL of isopropanol in a microwave vial. The vial containing reaction mixture was transferred to the microwave reactor where the reaction mixture was stirred at 80 °C for 2 h under microwave irradiation. The mixture was cooled to the room temperature which led to precipitate formation. The precipitate was collected through vacuum filtration and washed with isopropanol. The desired compound was obtained after purification using flash column chromatography (DCM:MeOH, 0-10% MeOH).

Yield:	205 mg (55%)
Chemical formula:	$C_{22}H_{30}N_4O_3S$
Molecular mass:	430.57 g/mol

Appearance	Off-white solid
Internal code:	MG-214, ST-2738

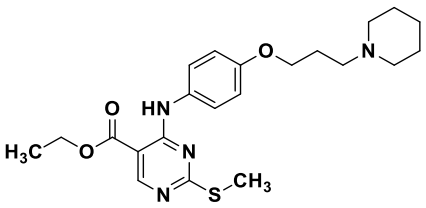

^{1}H NMR (300 MHz, $CDCl_3$):	δ 10.18 (s, 1H), 8.72 (s, 1H), 7.52 (d, *J* = 9.0 Hz, 2H), 6.84 (d, *J* = 9.0 Hz, 2H), 4.36 (q, *J* = 7.1 Hz, 2H), 4.06 (t, *J* = 5.6 Hz, 2H), 3.26 – 2.90 (m, 6H), 2.48 (s, 3H), 2.41 (dq, *J* = 11.5, 5.5 Hz, 5H), 2.04 (s, 4H), 1.65 (s, 2H), 1.39 (t, *J* = 7.1 Hz, 3H)
^{13}C NMR (75 MHz, $CDCl_3$):	δ 176.62, 167.20, 158.93, 158.38, 155.26, 131.40, 123.74, 114.53, 101.09, 65.43, 61.37, 55.51, 53.69, 24.22, 22.93, 22.42, 14.52, 14.33
Melting point	194.5 °C
MS (APCI-(+)):	m/z = 431.0 $[M+H^+]^+$
LC-MS-DAD purity:	100.00%
MS (ESI-(+)):	m/z = 431.2105 $[M+H^+]^+$ (calculated: 431.2111)

2-(Methylthio)-4-((4-(3-(piperidin-1-yl)propoxy)phenyl)amino)pyrimidine-5-carboxylic acid (10)

Ethyl 2-(methylthio)-4-((4-(3-(piperidin-1-yl)propoxy)phenyl)amino)pyrimidine-5-carboxylate (**9**) (310 mg, 0.72 mmol, 1.0 eq.) was dissolved 5 mL of THF. LiOH (104 mg, 4.32 mmol, 6.0 eq.) was dissolved in 5 mL of water and added to the stirred THF solution. The reaction mixture was stirred at room temperature for 3 h. Subsequently, solvent was evaporated, the residue was redissolved in water and pH value was adjusted with 1 M HCl solution until the precipitation occurred. The obtained suspension was left in the fridge overnight to allow the maturation of precipitate which was then filtered out and dried on a high vacuum pump to afford the desired compound.

Yield:	259 mg (90%)
Chemical formula:	$C_{20}H_{26}N_4O_3S$
Molecular mass:	402.51 g/mol
Appearance	Off-white solid
Internal code:	MG-218, ST-2735

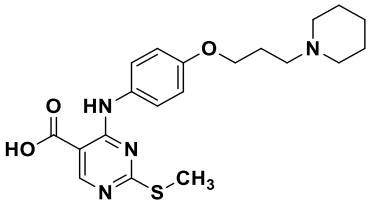

^{1}H NMR (300 MHz, DMSO)	δ 10.60 (s, 2H), 8.65 (s, 1H), 7.56 (d, *J* = 8.5 Hz, 2H), 6.95 (d, *J* = 8.5 Hz, 2H), 4.05 (t, *J* = 6.0 Hz, 2H), 3.16 (t, *J* = 8.0 Hz, 2H), 2.88 (s, 4H), 2.45 (s, 3H), 2.27 – 2.11 (m, 2H), 1.93 – 1.62 (m, 5H), 1.42 (s, 1H)
^{13}C NMR (75 MHz, DMSO)	174.64, 168.35, 158.57, 158.14, 154.88, 130.94, 123.22, 114.58, 102.37, 65.22, 53.38, 51.99, 23.34, 22.37, 21.41, 13.76.

Melting point	218.6 °C
MS (APCI-(+)):	m/z = 402.9 $[M+H^+]^+$
LC-MS-DAD purity:	100.00%
HRMS (ESI-(+)):	m/z = 403.1815 $[M+H^+]^+$ (calculated: 403.1798)

2-(Methylthio)-4-((4-(3-(piperidin-1-yl)propoxy)phenyl)amino)pyrimidine-5-carboxamide (11)

2-(Methylthio)-4-((4-(3-(piperidin-1-yl)propoxy)phenyl)amino)pyrimidine-5-carboxylic acid (**10**) (150 mg, 0.37 mmol, 1.0 eq.) and HATU (213 mg, 0.56 mmol, 1.5 eq.) were dissolved in 10 mL of DMF and allowed to stir for 5 min at room temperature. Subsequently, NH_4Cl (100 mg, 1.86 mmol, 5.0 eq.) and DIPEA (0.32 mL, 1.86 mmol, 5.0 eq.) were added, and the reaction mixture was stirred for 1 h at room temperature. After TLC control indicated consumption of starting material, the solvent was evaporated and the residue was purified using flash column chromatography (DCM:MeOH, 0-10% MeOH) to obtain the desired product.

Yield:	130 mg (87%)
Chemical formula:	$C_{20}H_{27}N_5O_2S$
Molecular mass:	401.53 g/mol
Appearance	Off-white solid
Internal code:	MG-227, ST-2736
^{1}H NMR (300 MHz, DMSO)	δ 11.29 (s, 1H), 8.67 (s, 1H), 8.24 (s, 1H), 7.68 (s, 1H), 7.53 (d, *J* = 8.9 Hz, 2H), 6.92 (d, *J* = 8.9 Hz, 2H), 3.97 (t, *J* = 6.4 Hz, 2H), 2.46 (s, 3H), 2.42 – 2.25 (m, 6H), 1.83 (p, *J* = 6.6 Hz, 2H), 1.48 (p, *J* = 5.4 Hz, 4H), 1.43 – 1.30 (m, 2H)
^{13}C NMR (75 MHz, DMSO)	δ 173.45, 168.81, 157.81, 155.80, 155.09, 130.86, 122.81, 114.54, 103.43, 66.11, 55.17, 54.12, 26.35, 25.62, 24.16, 13.69
Melting point	214.9 °C
MS (APCI-(+)):	m/z = 402.3 $[M+H^+]^+$
LC-MS-DAD purity:	100.00%
HRMS (ESI-(+)):	m/z = 402.1969 $[M+H^+]^+$ (calculated: 402.1958)

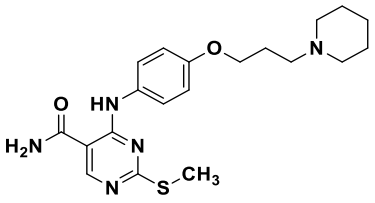

2-(Methylthio)-4-((4-(3-(piperidin-1-yl)propoxy)phenyl)amino)pyrimidine-5-carbonitrile (12)

A solution of 4-chloro-2-(methylthio)pyrimidine-5-carbonitrile (100 mg, 0.54 mmol, 1.0 eq.) and 4-(3-(piperidin-1-yl)propoxy)aniline (**P14**) (139 mg, 0.59 mmol, 1.1 eq.) were dissolved

in 2.2 mL of isopropanol in a microwave vial. The vial containing reaction mixture was transferred to the microwave reactor where the reaction mixture was stirred at 80 °C for 2 h under microwave irradiation. The mixture was cooled to the room temperature which led to precipitate formation. The precipitate was collected through vacuum filtration and washed with isopropanol. The desired compound was obtained after purification using flash column chromatography (DCM:MeOH, 0-10% MeOH).

Yield:	131 mg (63%)
Chemical formula:	$C_{20}H_{25}N_5OS$
Molecular mass:	383.51 g/mol
Appearance	Off-white solid
Internal code:	MG-215, ST-2734
^{1}H NMR (300 MHz, DMSO):	9.80 (s, 1H), 8.55 (s, 1H), 7.43 (d, *J* = 8.8 Hz, 2H), 6.94 (d, *J* = 8.9 Hz, 2H), 4.05 (t, *J* = 6.1 Hz, 2H), 3.27 – 2.65 (m, 6H), 2.38 (s, 3H), 2.26 – 2.10 (m, 2H), 1.89 – 1.71 (m, 4H), 1.70 – 1.32 (m, 2H)
^{13}C NMR (75 MHz, DMSO):	δ 174.70, 161.23, 158.15, 155.70, 130.26, 125.46, 115.48, 114.15, 86.71, 65.28, 53.50, 52.12, 23.48, 22.56, 21.61, 13.64
Melting point	198.5 °C
MS (APCI-(+)):	m/z = 384.0 $[M+H^+]^+$
LC-MS-DAD purity:	100.00%
HRMS (ESI-(+)):	m/z = 384.1874 $[M+H^+]^+$ (calculated: 384.1853)

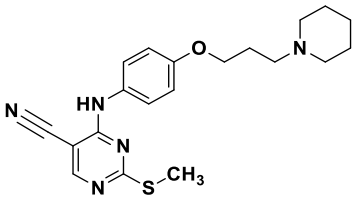

2,4-Dichloropyrimidine-5-carbonyl chloride (P20)[453]

2,4-Dihydroxypyrimidine-5-carboxylic acid (2.50 g, 16.0 mmol, 1.0 eq.) was dissolved in 10 mL of phosphorus(V) oxychloride in a 100 mL round bottom flask. The temperature of the mixture is reduced to 0 °C with an ice bath. Subsequently, phosphorus pentachloride (11.65 g, 55.95 mmol, 3.5 eq.) was portion wise added to the reaction mixture. The mixture was stirred under reflux for 16 h. The solvent was than evaporated under reduced pressure. The residue is taken up and triturated in 100 mL of toluene and then filtered. Trituration is repeated three times, and the filtrate is evaporated under reduced pressure yielding desired product that was directly used in the next reaction.

Yield:	3.4 g (quant.)
Chemical formula:	$C_5H_1Cl_3N_2O_2$
Molecular mass:	211.43g/mol
Appearance	Yellow oil

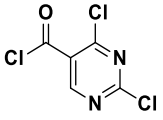

Internal code:	MG-182
^{1}H NMR (300 MHz, DMSO):	δ 9.12 (s, 1H)

2,4-Dichloropyrimidine-5-carboxamide (P21)[454]

To a solution of 2,4-dichloro-5-carbonyl chloride (**P20**) (3.40 g, 16.08 mmol, 1.0. eq.) in 20 mL of DCM ammonium hydroxide (25% aqueous solution) (2.5 mL, 32.16 mmol, 2.0 eq.) was added at 0 °C. The reaction mixture was stirred for 2 h at 0 °C and was subsequently poured into ice/water which led to precipitation. The solid was collected via vacuum filtration and lyophilized yielding desired product.

Yield:	2.17 g (70%)
Chemical formula:	$C_5H_3Cl_2N_3O$
Molecular mass:	192.0 g/mol
Appearance	White solid
Internal code:	MG-184
^{1}H NMR (300 MHz, DMSO):	δ 8.89 (s, 1H), 8.11 (d, *J* = 38.9 Hz, 2H)
MS (APCI-(+)):	m/z = 191.8, 193.8 $[M+H^+]^+$

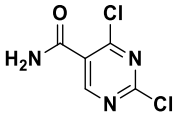

2-Chloro-4-((4-(3-(4-methylpiperazin-1-yl)propoxy)phenyl)amino)pyrimidine-5-carboxamide (13)

2,4-Dichloropyrimidine-5-carboxamide (**P21**) (100 mg, 0.52 mmol, 1.0 eq.) and 1-methyl-4-(3-(4-nitrophenoxy)propyl)piperazine (**P12**) (104 mg, 0.42 mmol, 0.8 eq.) were dissolved in 2.2 mL of isopropanol in a microwave vial. The vial containing reaction mixture was transferred to the microwave reactor where the reaction mixture was stirred at 50 °C for 1 h under microwave irradiation. The mixture was cooled to the room temperature which led to precipitate formation. The precipitate was collected through vacuum filtration and washed with isopropanol to afford the desired compound.

Yield:	181 mg (69%)
Chemical formula:	$C_{19}H_{25}ClN_6O_2$
Molecular mass:	404.90 g/mol
Appearance	Beige solid
Internal code:	MG-208, ST-2703

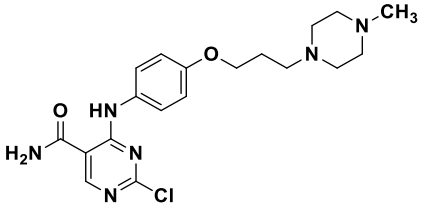

^{1}H NMR (300 MHz, DMSO):	δ 11.32 (s, 1H), 8.77 (s, 1H), 8.46 (s, 1H), 7.91 (s, 1H), 7.49 (d, *J* = 9.0 Hz, 2H), 6.96 (d, *J* = 9.0 Hz, 2H), 4.02 (t, *J* = 6.2 Hz, 2H), 3.32 – 2.52 (m, 13H), 1.97 (s, 2H)
^{13}C NMR (75 MHz, DMSO):	δ 167.86, 160.93, 159.66, 157.85, 155.49, 130.29, 123.37, 114.74, 106.84, 65.58, 53.28, 49.26, 25.49
Melting point	250.3 °C
MS (APCI-(+)):	m/z = 405.2, 407.2 $[M+H^+]^+$
LC-MS-DAD purity:	100.00%
HRMS (ESI-(+)):	m/z = 405.1805 $[M+H^+]^+$ (calculated: 405.1800)

2-Amino-6-cyclopropylpyrimidin-4(1*H*)-one (P22)[460]

To a solution of methyl 3-cyclopropyl-3-oxopropanoate (2.00 g, 14.07 mmol, 1.0 eq.) and guanidine hydrochloride (1.60 g, 16.88 mmol, 1.2 eq.) in 20 mL of methanol at a room temperature potassium *tert*-butoxide (7.90 g, 70.35 mmol, 5.0 eq.) was added portion wise over 15 mins with vigorous stirring. The reaction mixture was stirred at room temperature overnight. Afterwards, the mixture was concentrated, and the pH value was adjusted to 5 using 6 M HCl solution which led to precipitation. The mixture was matured overnight, the precipitate was isolated via filtration and dried on a high vacuum pump to afford the desired product.

Yield:	700 mg (43%)
Chemical formula:	$C_7H_9N_3O$
Molecular mass:	151.17 g/mol
Appearance	White crystal
Internal code:	MG-211
^{1}H NMR (300 MHz, DMSO):	δ 10.49 (s, 1H), 6.37 (s, 2H), 5.48 (s, 1H), 1.65 (tt, *J* = 7.9, 4.8 Hz, 1H), 0.88 – 0.80 (m, 2H), 0.80 – 0.72 (m, 2H)
MS (APCI-(+)):	m/z = 152.0 $[M+H^+]^+$

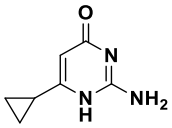

4-Chloro-6-cyclopropylpyrimidin-2-amine (P23)[461]

A solution of 2-Amino-6-cyclopropylpyrimidin-4(1*H*)-one (**P22**) (1.77 g, 11.71 mmol, 1 eq.) in 30 mL of DCE was treated with 20 mL of $POCl_3$. The reaction mixture was heated to 75 °C and stirred overnight. After TLC control indicated consumption of starting material, solvent was evaporated, the residue was quenched with 100 mL of cold $NaHCO_3$ solution and extracted with DCM (3 x 100 mL). The combined organic layers were washed with brine and dried over

Na_2SO_4. After filtration, solvent was evaporated under reduced pressure and the residue was purified using flash column chromatography (Hex:EE, 0-20% EE) to obtain the desired product.

Yield:	640 mg (32%)
Chemical formula:	$C_7H_8ClN_3$
Molecular mass:	169.61 g/mol
Appearance	White needles
Internal code:	MG-233
^{1}H NMR (300 MHz, DMSO):	δ 6.87 (s, 2H), 6.61 (s, 1H), 1.94 – 1.83 (m, 1H), 0.99 – 0.90 (m, 4H)
MS (APCI-(+)):	m/z = 169.7, 171.7 $[M+H^+]^+$

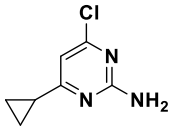

4-(3-(Piperidin-1-yl)propoxy)pyrimidin-2-amine (14)

To a stirred solution of 3-(piperidin-1-yl)propan-1-ol (**P1**) (663 mg, 4.63 mmol, 2.0 eq.) in 15 mL of THF, NaH (60% dispersion in mineral oil) (122 mg, 5.09 mmol, 2.2 eq.) was added in portions at 0 °C. The solution was allowed heat to room temperature and was stirred for 30 mins. Subsequently, 4-chloropyrimidin-2-amine (300 mg, 2.32 mmol, 1 eq.) was added to the solution, and the reaction mixture was refluxed overnight. After TLC control indicated consumption of starting material, the solvent was evaporated and the residue was purified using column chromatography, DCM:MeOH, up to 7% MeOH, to obtain the desired product.

Yield:	136 mg (25%)
Chemical formula:	$C_{12}H_{20}N_4O$
Molecular mass:	236.32 g/mol
Appearance	Off-white solid
Internal code:	MG-190, ST-2791
^{1}H NMR (300 MHz, DMSO):	δ 7.93 (d, *J* = 5.7 Hz, 1H), 6.48 (s, 2H), 5.97 (d, *J* = 5.6 Hz, 1H), 4.20 (t, *J* = 6.6 Hz, 2H), 2.48 – 2.30 (m, 6H), 1.84 (p, *J* = 6.8 Hz, 2H), 1.57 – 1.44 (m, 4H), 1.44 – 1.32 (m, 2H)
^{13}C NMR (75 MHz, DMSO):	δ 169.35, 163.51, 158.54, 96.19, 63.66, 54.95, 53.86, 25.58, 25.24, 23.84
Melting point	147.5°C
MS (APCI-(+)):	m/z = 236.9 $[M+H^+]^+$
LC-MS-DAD purity:	100.00%
HRMS (ESI-(+)):	m/z = 237.1748 $[M+H^+]^+$ (calculated: 237.1710)

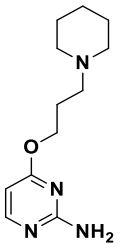

4-Methyl-6-(3-(piperidin-1-yl)propoxy)pyrimidin-2-amine (15)

To a stirred solution of 3-(piperidin-1-yl)propan-1-ol (**P1**) (599 mg, 4.18 mmol, 2.0 eq.) in 20 mL of THF, NaH (60% dispersion in mineral oil) (110 mg, 4.60 mmol, 2.0 eq.) was added in portions at 0 °C. The solution was allowed heat to room temperature and was stirred for 30 mins. Subsequently, 4-chloro-6-methylpyrimidin-2-amine (300 mg, 2.09 mmol, 1 eq.) was added to the solution, and the reaction mixture was refluxed overnight. After TLC control indicated consumption of starting material, the solvent was evaporated and the residue was purified using column chromatography, DCM:MeOH, up to 7% MeOH, to obtain the desired product.

Yield:	105 mg (20%)
Chemical formula:	$C_{13}H_{22}N_4O$
Molecular mass:	250.35 g/mol
Appearance	Yellow solid
Internal code:	MG-232, ST-2794

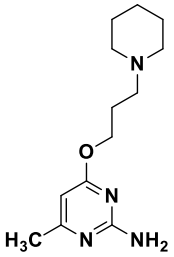

^{1}H NMR (300 MHz, DMSO):	δ 6.39 (s, 2H), 5.85 (s, 1H), 4.18 (t, *J* = 6.6 Hz, 2H), 2.38 – 2.24 (m, 6H), 2.11 (s, 3H), 1.79 (p, *J* = 6.8 Hz, 2H), 1.46 (q, *J* = 5.4 Hz, 4H), 1.42 – 1.30 (m, 2H)
^{13}C NMR (75 MHz, DMSO):	δ 170.01, 167.71, 163.16, 94.62, 63.69, 55.15, 54.07, 25.96, 25.57, 24.13, 23.28
Melting point	91.0 °C
MS (APCI-(+)):	m/z = 251.2 $[M+H^+]^+$
LC-MS-DAD purity:	97.34%
HRMS (ESI-(+)):	m/z = 251.1946 $[M+H^+]^+$ (calculated: 251.1866)

4-Ethyl-6-(3-(piperidin-1-yl)propoxy)pyrimidin-2-amine (16)

To a stirred solution of 3-(piperidin-1-yl)propan-1-ol (**P1**) (454 mg, 3.17 mmol, 2.0 eq.) in 15 mL of THF, NaH (60% dispersion in mineral oil) (114 mg, 4.76 mmol, 3.0 eq.) was added in portions at 0 °C. The solution was allowed heat to room temperature and was stirred for 30 mins. Subsequently, 4-chloro-6-ethylpyrimidin-2-amine (250 mg, 1.59 mmol, 1 eq.) was added to the solution, and the reaction mixture was refluxed overnight. After TLC control indicated consumption of starting material, the solvent was evaporated and the residue was purified using column chromatography, DCM:MeOH, up to 7% MeOH, to obtain the desired product.

Yield:	80 mg (20%)
Chemical formula:	$C_{14}H_{24}N_4O$
Molecular mass:	264.37 g/mol
Appearance	Off-white solid
Internal code:	MG-199, ST-2792

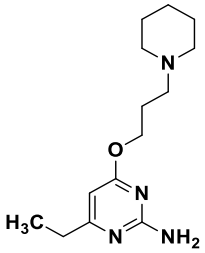

^{1}H NMR (300 MHz, DMSO):	δ 6.39 (s, 2H), 5.85 (s, 1H), 4.18 (t, *J* = 6.6 Hz, 2H), 2.48 – 2.24 (m, 8H), 1.80 (p, *J* = 6.8 Hz, 2H), 1.48 (p, *J* = 5.4 Hz, 4H), 1.37 (q, *J* = 5.7 Hz, 2H), 1.11 (t, *J* = 7.6 Hz, 3H)
^{13}C NMR (75 MHz, DMSO):	δ 172.73, 170.08, 163.23, 93.38, 63.68, 55.13, 54.03, 29.88, 25.91, 25.52, 24.08, 12.64
Melting point	73.4 °C
MS (APCI-(+)):	m/z = 236.9 $[M+H^+]^+$
LC-MS-DAD purity:	99.32%
HRMS (ESI-(+)):	m/z = 265.2026 $[M+H^+]^+$ (calculated: 265.2023)

4-Isopropyl-6-(3-(piperidin-1-yl)propoxy)pyrimidin-2-amine (17)

To a stirred solution of 3-(piperidin-1-yl)propan-1-ol (**P1**) (501 mg, 3.50 mmol,2.0 eq.) in 15 mL of THF, NaH (60% dispersion in mineral oil) (92 mg, 3.85 mmol, 2.2 eq.) was added in portions at 0 °C. The solution was allowed heat to room temperature and was stirred for 30 mins. Subsequently, 4-chloro-6-isopropylpyrimidin-2-amine (300 mg, 1.75 mmol, 1 eq.) was added to the solution, and the reaction mixture was refluxed overnight. After TLC control indicated consumption of starting material, the solvent was evaporated and the residue was purified using column chromatography, DCM:MeOH, up to 7% MeOH, to obtain the desired product.

Yield:	195 mg (40%)
Chemical formula:	$C_{15}H_{26}N_4O$
Molecular mass:	278.40 g/mol
Appearance	Off-white solid
Internal code:	MG-228, ST-2793

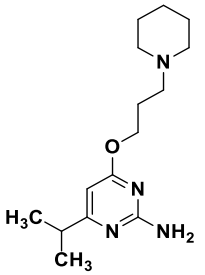

^{1}H NMR (300 MHz, DMSO):	δ 6.37 (s, 2H), 5.84 (s, 1H), 4.18 (t, *J* = 6.6 Hz, 2H), 2.62 (hept, *J* = 6.8 Hz, 1H), 2.38 – 2.26 (m, 6H), 1.80 (p, *J* = 6.8 Hz, 2H), 1.51 – 1.43 (m, 4H), 1.42 – 1.31 (m, 2H), 1.12 (d, *J* = 6.9 Hz, 6H)

^{13}C NMR (75 MHz, DMSO):	δ 176.62, 170.13, 163.23, 92.08, 63.70, 55.15, 54.04, 34.95, 25.92, 25.52, 24.09, 21.47
Melting point	86.8 °C
MS (APCI-(+)):	m/z = 279.2 $[M+H^+]^+$
LC-MS-DAD purity:	98.27%
HRMS (ESI-(+)):	m/z = 279.2269 $[M+H^+]^+$ (calculated: 279.2179)

4-Cyclopropyl-6-(3-(piperidin-1-yl)propoxy)pyrimidin-2-amine (18)

To a stirred solution of 3-(piperidin-1-yl)propan-1-ol (**P1**) (507 mg, 3.54 mmol, 2.0 eq.) in 20 mL of THF, NaH (60% dispersion in mineral oil) (93 mg, 3.89 mmol, 2.2 eq.) was added in portions at 0 °C. The solution was allowed heat to room temperature and was stirred for 30 mins. Subsequently, 4-chloro-6-cyclopropylpyrimidin-2-amine (**P23**) (300 mg, 1.77 mmol, 1 eq.) was added to the solution, and the reaction mixture was refluxed for 1 h. After TLC control indicated consumption of starting material, the solvent was evaporated and the residue was purified using column chromatography (DCM:MeOH(NH_3) = 95:5), to obtain the desired product.

Yield:	260 mg (59%)
Chemical formula:	$C_{15}H_{24}N_4O$
Molecular mass:	276.38 g/mol
Appearance	Off-white solid
Internal code:	MG-235, ST-2795

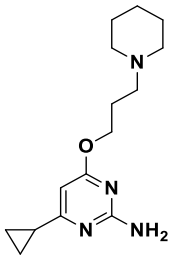

^{1}H NMR (300 MHz, DMSO):	δ 6.28 (s, 2H), 5.90 (s, 1H), 4.17 (t, *J* = 6.6 Hz, 2H), 2.42 – 2.22 (m, 6H), 1.87 – 1.70 (m, 3H), 1.48 (p, *J* = 5.5 Hz, 5H), 1.42 – 1.31 (m, 2H), 0.92 – 0.76 (m, 4H)
^{13}C NMR (75 MHz, DMSO):	δ 172.31, 169.57, 163.27, 92.89, 63.63, 55.11, 54.02, 25.91, 25.49, 24.06, 16.29, 8.81
Melting point	119.7 °C
MS (APCI-(+)):	m/z = 276.9 $[M+H^+]^+$
LC-MS-DAD purity:	98.63%
HRMS (ESI-(+)):	m/z = 277.2024 $[M+H^+]^+$ (calculated: 277.2023)

4-((3-(Piperidin-1-yl)propyl)thio)pyrimidin-2-amine (19)

4-Chloropyrimidin-2-amine (100 mg, 1.24 mmol, 1.0 eq.) was added to NaOH (35 mg, 0.89 mmol, 1.15 eq.) solution in 5 mL of water and 7.50 mL of ethanol. Subsequently, 3-(piperidin-1-yl)propane-1-thiol (**P3**) (197 mg, 1.24 mmol, 1.6 eq.) was added, and the reaction mixture was stirred under reflux for 4 h. After TLC control indicated consumption of starting material, the solvent was evaporated and the residue was purified using flash column chromatography (DCM:MeOH, 0-7% MeOH) to obtain the desired product.

Yield:	122 mg (63%)
Chemical formula:	$C_{12}H_{20}N_4S$
Molecular mass:	252.38 g/mol
Appearance	Off-white solid
Internal code:	MG-264, ST-2799

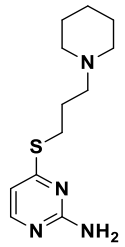

^{1}H NMR (300 MHz, DMSO):	δ 7.91 (d, *J* = 5.3 Hz, 1H), 6.58 (s, 2H), 6.46 (d, *J* = 5.3 Hz, 1H), 3.05 (t, *J* = 7.1 Hz, 2H), 2.46 – 2.24 (m, 6H), 1.78 (p, *J* = 7.2 Hz, 2H), 1.51 (p, *J* = 5.5 Hz, 4H), 1.38 (q, *J* = 5.9 Hz, 2H)
^{13}C NMR (75 MHz, DMSO):	δ 169.23, 162.73, 156.36, 106.95, 56.94, 53.83, 26.15, 25.91, 25.23, 23.82
Melting point	145.6 °C
MS (APCI-(+)):	m/z = 253.1 $[M+H^+]^+$
LC-MS-DAD purity:	100.00%
HRMS (ESI-(+)):	m/z = 253.1510 $[M+H^+]^+$ (calculated: 253.1481)

4-Methyl-6-((3-(piperidin-1-yl)propyl)thio)pyrimidin-2-amine (20)

4-Chloro-6-methylpyrimidin-2-amine (100 mg, 0.70 mmol, 1.0 eq.) was added to NaOH (32 mg, 0.80 mmol, 1.15 eq.) solution in 5 mL of water and 7.50 mL of ethanol. Subsequently, 3-(piperidin-1-yl)propane-1-thiol (**P3**) (178 mg, 1.11 mmol, 1.6 eq.) was added, and the reaction mixture was stirred under reflux for 4 h. After TLC control indicated consumption of starting material, the solvent was evaporated and the residue was purified using flash column chromatography (DCM:MeOH, 0-7% MeOH) to obtain the desired product.

Yield:	50 mg (27%)
Chemical formula:	$C_{13}H_{22}N_4S$
Molecular mass:	266.41 g/mol
Appearance	White solid

Internal code:	MG-260, ST-2796

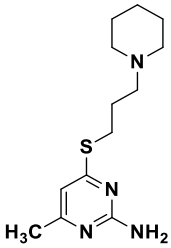

^{1}H NMR (300 MHz, DMSO):	δ 6.46 (s, 2H), 6.35 (s, 1H), 3.03 (t, *J* = 7.2 Hz, 2H), 2.37 – 2.24 (m, 6H), 2.13 (s, 3H), 1.73 (p, *J* = 7.1 Hz, 2H), 1.53 – 1.42 (m, 4H), 1.42 – 1.30 (m, 2H)
^{13}C NMR (75 MHz, DMSO):	169.16, 165.70, 162.55, 105.85, 57.29, 54.10, 26.31, 26.23, 25.62, 24.18, 23.27
Melting point	121.9 °C
MS (APCI-(+)):	m/z = 266.9 $[M+H^+]^+$
LC-MS-DAD purity:	100.00%
HRMS (ESI-(+)):	m/z = 267.1657 $[M+H^+]^+$ (calculated: 267.1638)

4-Ethyl-6-((3-(piperidin-1-yl)propyl)thio)pyrimidin-2-amine (21)

4-Chloro-6-ethylpyrimidin-2-amine (100 mg, 0.63 mmol, 1.0 eq.) was added to NaOH (29 mg, 0.73 mmol, 1.15 eq.) solution in 5 mL of water and 7.50 mL of ethanol. Subsequently, 3-(piperidin-1-yl)propane-1-thiol (**P3**) (162 mg, 1.02 mmol, 1.6 eq.) was added, and the reaction mixture was stirred under reflux for 4 h. After TLC control indicated consumption of starting material, the solvent was evaporated and the residue was purified using flash column chromatography (DCM:MeOH, 0-7% MeOH) to obtain the desired product.

Yield:	62 mg (35%)
Chemical formula:	$C_{14}H_{240}N_4S$
Molecular mass:	280.43 g/mol
Appearance	Off-white solid
Internal code:	MG-265, ST-2800

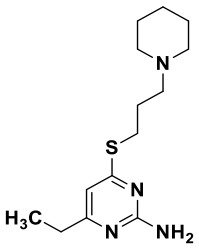

^{1}H NMR (300 MHz, DMSO):	δ 6.47 (s, 2H), 6.35 (s, 1H), 3.04 (t, *J* = 7.2 Hz, 2H), 2.41 (q, 2H), 2.36 – 2.20 (m, 6H), 1.74 (p, *J* = 7.1 Hz, 2H), 1.58 – 1.43 (m, 4H), 1.42 – 1.30 (m, 2H), 1.12 (t, *J* = 7.6 Hz, 3H)
^{13}C NMR (75 MHz, DMSO):	δ 170.49, 169.18, 162.64, 104.72, 57.28, 54.07, 29.86, 26.30, 26.21, 25.59, 24.15, 12.64
Melting point	94.0 °C
MS (APCI-(+)):	m/z = 281.1 $[M+H^+]^+$
LC-MS-DAD purity:	98.73%

HRMS (ESI-(+)):	m/z = 281.1841 $[M+H^+]^+$ (calculated: 291.1794)

4-Isopropyl-6-((3-(piperidin-1-yl)propyl)thio)pyrimidin-2-amine (22)

4-Chloro-6-isopropylpyrimidin-2-amine (150 mg, 0.87 mmol, 1.0 eq.) was added to NaOH (40 mg, 1.01 mmol, 1.15 eq.) solution in 5 mL of water and 7.5 mL of ethanol. Subsequently, 3-(piperidin-1-yl)propane-1-thiol (**P3**) (223 mg, 1.40 mmol, 1.6 eq.) was added, and the reaction mixture was stirred under reflux for 4 h. After TLC control indicated consumption of starting material, the solvent was evaporated and the residue was purified using flash column chromatography (DCM:MeOH, 0-7% MeOH) to obtain the desired product.

Yield:	124 mg (48%)
Chemical formula:	$C_{15}H_{26}N_4S$
Molecular mass:	294.46 g/mol
Appearance	Off-white solid
Internal code:	MG-263, ST-2798

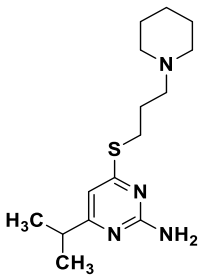

^{1}H NMR (300 MHz, DMSO):	δ 6.46 (s, 2H), 6.34 (s, 1H), 3.05 (t, *J* = 7.2 Hz, 2H), 2.64 (hept, *J* = 6.9 Hz, 1H), 2.37 – 2.23 (m, 6H), 1.74 (p, *J* = 7.1 Hz, 2H), 1.54 – 1.42 (m, 4H), 1.41 – 1.30 (m, 2H), 1.13 (d, *J* = 6.9 Hz, 6H)
^{13}C NMR (75 MHz, DMSO):	δ 174.25, 169.20, 162.67, 103.46, 57.30, 54.06, 34.99, 26.32, 26.23, 25.60, 24.16, 21.45
Melting point	84.9 °C
MS (APCI-(+)):	m/z = 295.3 $[M+H^+]^+$
LC-MS-DAD purity:	100.00%
HRMS (ESI-(+)):	m/z = 295.1996 $[M+H^+]^+$ (calculated: 295.1951)

4-Cyclopropyl-6-((3-(piperidin-1-yl)propyl)thio)pyrimidin-2-amine (23)

4-Chloro-6-cyclopropylpyrimidin-2-amine (**P23**) (250 mg, 1.47 mmol, 1.0 eq.) was added to NaOH (68 mg, 1.70 mmol, 1.15 eq.) solution in 10 mL of water and 12.5 mL of ethanol. Subsequently, 3-(piperidin-1-yl)propane-1-thiol (**P3**) (376 mg, 2.36 mmol, 1.6 eq.) was added, and the reaction mixture was stirred under reflux for 4 h. After TLC control indicated consumption of starting material, the solvent was evaporated and the residue was purified using flash column chromatography (DCM:MeOH, 0-7% MeOH) to obtain the desired product.

Yield:	94 mg (22%)
Chemical formula:	$C_{15}H_{24}N_4S$
Molecular mass:	292.17 g/mol
Appearance	Off-white resin
Internal code:	MG-262, ST-2797

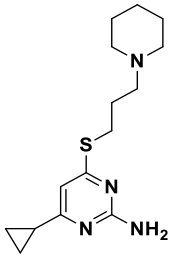

^{1}H NMR (300 MHz, DMSO):	δ 6.42 (s, 1H), 6.37 (s, 2H), 3.04 (t, *J* = 7.1 Hz, 2H), 2.50 – 2.34 (m, 6H), 1.85 – 1.72 (m, 3H), 1.59 – 1.45 (m, 4H), 1.44 – 1.33 (m, 2H), 0.96 – 0.78 (m, 4H)
^{13}C NMR (75 MHz, DMSO):	δ 170.36, 168.26, 162.67, 104.42, 56.87, 53.74, 26.07, 25.88, 25.06, 23.67, 16.18, 9.30
Melting point	n.a.
MS (APCI-(+)):	m/z = 292.9 $[M+H^+]^+$
LC-MS-DAD purity:	100.00%
HRMS (ESI-(+)):	m/z = 293.1835$[M+H^+]^+$ (calculated: 293.1794)

2-Chloro-*N*,6-dimethylpyrimidin-4-amine (P24)[477]

To a solution of 2,4-dichloro-6-methylpyrimidine (2.50 g, 15.3 mmol, 1.0 eq.) and DIPEA (6.30 g, 45.4 mmol, 3.0 eq.) in 50 mL of ethanol methylamine hydrochloride (1.00 g, 15.3 mmol, 1.0 eq.) was added, and the reaction mixture was stirred for 24 h at 50 °C. Afterwards, solvent was evaporated, and the residue was partitioned between water and EtOAc. The organic layers were merged, washed with brine and dried over anhydrous $MgSO_4$. After filtration, solvent was evaporated under reduced pressure to obtain crude consisting of 2-methylamino and 4-methylamino substituted structural isomers. The identity of structural isomers separated using flash column chromatography (Hex:EtOAc, 0-40% EtOAc) was confirmed with ^{1}H- and ROESY-NMR spectrums.

Yield:	1220 mg (51%)
Chemical formula:	$C_6H_8ClN_3$
Molecular mass:	157.60 g/mol
Appearance	White solid
Internal code:	MG-154F2
R_f-value	0.10 (Hex/EtOAc 4:1)

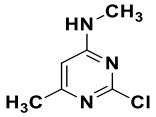

^{1}H NMR (300 MHz, DMSO):	δ 7.68 (s, 1H), 6.25 (s, 1H), 2.76 (d, *J* = 4.2 Hz, 3H), 2.16 (s, 3H)
MS (APCI-(+)):	m/z = 158.0, 160.0 $[M+H^+]^+$

4-Chloro-*N*,6-dimethylpyrimidin-2-amine (P25)[477]

The compound 4-chloro-*N*,6-dimethylpyrimidin-2-amine (**P25**) was obtained as a side product during the synthesis of compound **P24**.

Yield:	550 mg (23%)
Chemical formula:	$C_6H_8ClN_3$
Molecular mass:	157.60 g/mol
Appearance	White solid
Internal code:	MG-154F1
R_f-value	0.37 (Hex/EtOAc 4:1)
^{1}H NMR (300 MHz, DMSO):	δ 7.43 (s, 1H), 6.55 (s, 1H), 2.76 (d, J = 4.8 Hz, 3H), 2.23 (s, 3H)
MS (APCI-(+)):	m/z = 158.0, 160.0 $[M+H^+]^+$

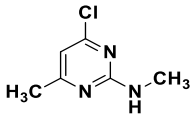

2-Chloro-*N*-ethyl-6-methylpyrimidin-4-amine (P26)[478]

To a suspension of 2,4-dichloro-6-methylpyrimidine (2.50 g, 15.3 mmol, 1.0 eq.) and K_2CO_3 (6.40 g, 46.0 mmol, 3.0 eq.) in 50 mL of DMF ethylamine hydrochloride (1.50 g, 18.4 mmol, 1.2 eq.) was added, and the reaction mixture was stirred for 5 h at room temperature. Afterwards, K_2CO_3 was filtered out, DMF was evaporated, and the residue was partitioned between water and EtOAc. The organic layers were merged, washed with brine and dried over anhydrous $MgSO_4$. After filtration, solvent was evaporated under reduced pressure to obtain crude consisting of 2-ethylamino and 4-ethylamino substituted structural isomers. The identity of structural isomers separated using flash column chromatography (Hex:EtOAc, 0-40% EtOAc) was confirmed with ^{1}H- and ROESY-NMR spectrums.

Yield:	1150 mg (44%)
Chemical formula:	$C_7H_{10}ClN_3$
Molecular mass:	171.63 g/mol
Appearance	White solid
Internal code:	MG-138F2
R_f-value	0.14 (Hex:EtOAC 4:1)
^{1}H NMR (300 MHz, DMSO):	δ 7.72 (t, J = 5.5 Hz, 1H), 6.23 (s, 1H), 3.25 (s, 2H), 2.16 (s, 3H), 1.10 (t, J = 7.2 Hz, 3H)
MS (APCI-(+)):	m/z = 172.1, 174.1 $[M+H^+]^+$

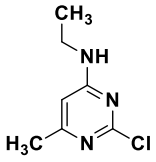

4-Chloro-*N*-ethyl-6-methylpyrimidin-2-amine (P27)[478]

The compound 4-chloro-*N*-ethyl-6-methylpyrimidin-2-amine (**P27**) was obtained as a side product during the synthesis of compound **P26**.

Yield:	600 mg (23%)
Chemical formula:	$C_7H_{10}ClN_3$
Molecular mass:	171.63
Appearance	White solid
Internal code:	MG-138F1
R_f-value	0.41 (Hex:EtOAC 4:1)
^{1}H NMR (300 MHz, DMSO):	δ 7.50 (t, *J* = 5.6 Hz, 1H), 6.53 (s, 1H), 3.25 (p, *J* = 6.8 Hz, 2H), 2.22 (s, 3H), 1.08 (t, *J* = 7.2 Hz, 3H)
MS (APCI-(+)):	m/z = 172.1, 174.1 $[M+H^+]^+$

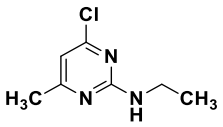

N^4,6-Dimethyl-N^2-(4-(3-(4-methylpiperazin-1-yl)propoxy)phenyl)pyrimidine-2,4-diamine (24)

To a solution of 2-chloro-*N*,6-dimethylpyrimidin-4-amine (**P24**) (200 mg, 1.27 mmol, 1.0 eq.) and 1-methyl-4-(3-(4-nitrophenoxy)propyl)piperazine (**P12**) (316 mg, 1.27 mmol, 1.0 eq.) in 4.5 mL of isopropanol in a microwave vial, TFA (0.39 mL, 5.08 mmol, 4.0 eq.) was added at room temperature. The vial containing reaction mixture was transferred to the microwave reactor where the reaction mixture was stirred at 140 °C for 1 h under microwave irradiation. The mixture was cooled to the room temperature which led to precipitate formation. The precipitate was collected through vacuum filtration, dissolved in 2 M NaOH (30 mL) and extracted with DCM (3 × 30 mL). The organic layers were merged, washed with brine, dried over Na_2SO_4 and evaporated to afford the desired compound.

Yield:	96 mg (33%)
Chemical formula:	$C_{20}H_{30}N_6O$
Molecular mass:	370.50 g/mol
Appearance	Beige resin
Internal code:	MG-139, ST-2656
^{1}H NMR (300 MHz, $CDCl_3$):	δ 7.47 (d, *J* = 9.0 Hz, 2H), 6.88 – 6.75 (m, 3H), 5.68 (s, 1H), 4.76 (s, 1H), 3.97 (t, *J* = 6.4 Hz, 2H), 2.90 (d, *J* = 5.1 Hz, 3H), 2.66 – 2.34 (m, 10H), 2.28 (s, 3H), 2.23 (s, 3H), 2.02 – 1.88 (m, 2H)

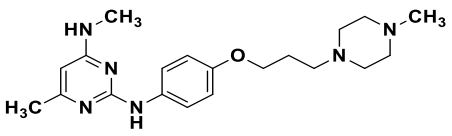

^{13}C NMR (75 MHz, $CDCl_3$):	δ 164.41, 159.99, 154.35, 133.64, 121.10, 114.86, 66.79, 66.09, 55.27, 53.34, 46.15, 28.36, 28.05, 26.99
Melting point	n.a.
MS (APCI-(+)):	m/z = 371.5 $[M+H^+]^+$
LC-MS-DAD purity:	100.00%
HRMS (ESI-(+)):	m/z = 371.2529 $[M+H^+]^+$ (calculated: 371.2554)

N^4,6-Dimethyl-*N*^{2}-(4-(3-(piperidin-1-yl)propoxy)phenyl)pyrimidine-2,4-diamine (25)

To a solution of 2-chloro-*N*,6-dimethylpyrimidin-4-amine (**P24**) (200 mg, 1.27 mmol, 1.0 eq.) and 4-(3-(piperidin-1-yl)propoxy)aniline (**P14**) (297 mg, 1.27 mmol, 1.0 eq.) in 4.5 mL of isopropanol in a microwave vial, TFA (0.39 mL, 5.08 mmol, 4.0 eq.) was added at room temperature. The vial containing reaction mixture was transferred to the microwave reactor where the reaction mixture was stirred at 140 °C for 1 h under microwave irradiation. The mixture was cooled to the room temperature which led to precipitate formation. The precipitate was collected through vacuum filtration, dissolved in 2 M NaOH (30 mL) and extracted with DCM (3 × 30 mL). The organic layers were merged, washed with brine, dried over Na_2SO_4 and evaporated to afford the desired compound.

Yield:	280 mg (62%)
Chemical formula:	$C_{20}H_{29}N_5O$
Molecular mass:	355.49 g/mol
Appearance	Brown resin
Internal code:	MG-137, ST-2655
^{1}H NMR (300 MHz, $CDCl_3$):	δ 7.52 – 7.43 (m, 2H), 6.88 – 6.75 (m, 3H), 5.68 (s, 1H), 4.77 (s, 1H), 3.97 (t, *J* = 6.4 Hz, 2H), 2.90 (d, *J* = 5.1 Hz, 3H), 2.52 – 2.43 (m, 2H), 2.40 (t, *J* = 5.3 Hz, 4H), 2.23 (s, 3H), 2.01 – 1.89 (m, 2H), 1.65 – 1.53 (m, 4H), 1.44 (q, *J* = 6.2 Hz, 2H)
^{13}C NMR (75 MHz, $CDCl_3$):	δ 164.42, 160.03, 154.39, 133.62, 121.07, 114.86, 67.06, 56.20, 54.77, 28.35, 27.04, 26.11, 24.75, 24.29
Melting point	n.a.
MS (APCI-(+)):	m/z = 356.6 $[M+H^+]^+$
LC-MS-DAD purity:	95.36%
HRMS (ESI-(+)):	m/z = 356.2430 $[M+H^+]^+$ (calculated: 356.2445)

N^2-(3-Methoxy-4-(3-(piperidin-1-yl)propoxy)phenyl)-N^4,6-dimethylpyrimidine-2,4-diamine (26)

To a solution of 2-chloro-*N*,6-dimethylpyrimidin-4-amine (**P24**) (100 mg, 0.63 mmol, 1.0 eq.) and 3-methoxy-4-(3-(piperidin-1-yl)propoxy)aniline (**P15**) (168 mg, 0.63 mmol, 1.0 eq.) in 2.2 mL of isopropanol in a microwave vial, 0.1 mL of TFA was added at room temperature. The vial containing reaction mixture was transferred to the microwave reactor where the reaction mixture was stirred at 140 °C for 1 h under microwave irradiation. The mixture was cooled to the room temperature which led to precipitate formation. The precipitate was collected through vacuum filtration, dissolved in 2 M NaOH (30 mL) and extracted with DCM (3 × 30 mL). The organic layers were merged, washed with brine, dried over Na_2SO_4 and evaporated to afford the desired compound.

Yield:	91 mg (37%)
Chemical formula:	$C_{21}H_{31}N_5O_2$
Molecular mass:	385.51 g/mol
Appearance	Brown resin
Internal code:	MG-156, ST-2663
^{1}H NMR (300 MHz, $CDCl_3$):	δ 7.49 (d, *J* = 2.4 Hz, 1H), 6.91 (dd, *J* = 8.6, 2.4 Hz, 1H), 6.87 – 6.79 (m, 2H), 5.70 (d, *J* = 0.7 Hz, 1H), 4.75 (s, 1H), 4.02 (t, *J* = 6.7 Hz, 2H), 3.85 (s, 3H), 2.93 (d, *J* = 5.1 Hz, 3H), 2.55 – 2.43 (m, 2H), 2.40 (t, *J* = 5.4 Hz, 4H), 2.23 (s, 3H), 2.05 – 1.91 (m, 2H), 1.58 (p, *J* = 5.5 Hz, 4H), 1.44 (t, *J* = 5.9 Hz, 2H)
^{13}C NMR (75 MHz, $CDCl_3$):	δ 164.37, 159.79, 149.74, 143.57, 134.58, 114.53, 111.16, 105.66, 105.04, 66.68, 56.09, 56.04, 54.70, 28.00, 26.92, 26.08, 24.25, 23.48.
Melting point	n.a.
MS (APCI-(+)):	m/z = 386.4 $[M+H^+]^+$
LC-MS-DAD purity:	100.00%
HRMS (ESI-(+)):	m/z = 386.2567 $[M+H^+]^+$ (calculated: 386.2551)

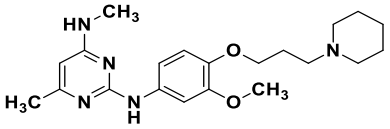

N^2-(4-Methoxy-3-(3-(piperidin-1-yl)propoxy)phenyl)-N^4,6-dimethylpyrimidine-2,4-diamine (27)

To a solution of 2-chloro-*N*,6-dimethylpyrimidin-4-amine (**P24**) (200 mg, 1.27 mmol, 1.0 eq.) and 4-methoxy-3-(3-(piperidin-1-yl)propoxy)aniline (**P16**) (335 mg, 1.27 mmol, 1.0 eq.) in 4.5 mL of isopropanol in a microwave vial, TFA (0.39 mL, 5.08 mmol, 4.0 eq.) was added at room temperature. The vial containing reaction mixture was transferred to the microwave reactor where the reaction mixture was stirred at 140 °C for 1 h under microwave irradiation.

The mixture was cooled to the room temperature which led to precipitate formation. The precipitate was collected through vacuum filtration, dissolved in 2 M NaOH (30 mL) and extracted with DCM (3 × 30 mL). The organic layers were merged, washed with brine, dried over Na_2SO_4 and evaporated to afford the desired compound.

Yield:	289 mg (59%)
Chemical formula:	$C_{21}H_{31}N_5O_2$
Molecular mass:	385.51 g/mol
Appearance	Beige solid
Internal code:	MG-134, ST-2654
^{1}H NMR (300 MHz, $CDCl_3$):	δ 7.49 (d, *J* = 2.5 Hz, 1H), 6.93 (dd, *J* = 8.6, 2.5 Hz, 1H), 6.84 (s, 1H), 6.78 (d, *J* = 8.7 Hz, 1H), 5.69 (s, 1H), 4.81 (s, 1H), 4.07 (t, *J* = 6.7 Hz, 2H), 3.82 (s, 3H), 2.92 (d, *J* = 5.0 Hz, 3H), 2.52 – 2.44 (m, 2H), 2.39 (t, *J* = 5.3 Hz, 4H), 2.23 (s, 3H), 2.04 (dq, *J* = 10.0, 6.8 Hz, 2H), 1.57 (p, *J* = 5.5 Hz, 4H), 1.43 (q, *J* = 5.8 Hz, 2H)
^{13}C NMR (75 MHz, $CDCl_3$):	δ 164.37, 159.96, 148.61, 144.66, 134.36, 112.66, 112.62, 111.11, 106.46, 67.72, 56.45, 56.09, 54.70, 28.37, 26.82, 26.08, 24.55, 24.10.
Melting point	56.5 °C
MS (APCI-(+)):	m/z = 386.5 $[M+H^+]^+$
LC-MS-DAD purity:	100.00%
HRMS (ESI-(+)):	m/z = 386.2574 $[M+H^+]^+$ (calculated: 386.2551)

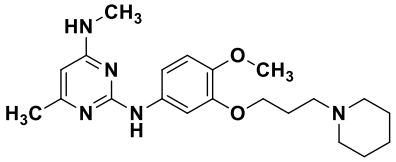

N^4-Ethyl-6-methyl-*N*^{2}-(4-(3-(4-methylpiperazin-1-yl)propoxy)phenyl)pyrimidine-2,4-diamine (28)

To a solution of 2-chloro-*N*-ethyl-6-methylpyrimidin-4-amine (**P26**) (150 mg, 0.87 mmol, 1.0 eq.) and 1-methyl-4-(3-(4-nitrophenoxy)propyl)piperazine (**P12**) (218 mg, 0.87 mmol, 1.0 eq.) in 3 mL of isopropanol in a microwave vial, TFA (0.27 mL, 3.5 mmol, 4 eq.) was added at room temperature. The vial containing reaction mixture was transferred to the microwave reactor where the reaction mixture was stirred at 140 °C for 1 h under microwave irradiation. The mixture was cooled to the room temperature which led to precipitate formation. The precipitate was collected through vacuum filtration, dissolved in 2 M NaOH (30 mL) and extracted with DCM (3 × 30 mL). The organic layers were merged, washed with brine, dried over Na_2SO_4 and evaporated to afford the desired compound.

Yield:	94 mg (27%)
Chemical formula:	$C_{21}H_{32}N_6O$

Molecular mass:	384.53 g/mol
Appearance	Beige resin
Internal code:	MG-145, ST-2659

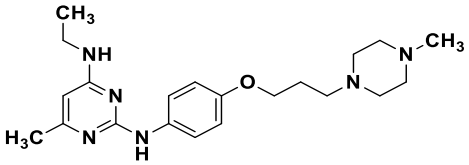

^{1}H NMR (300 MHz, $CDCl_3$):	δ 7.47 (d, *J* = 9.0 Hz, 2H), 6.87 – 6.79 (m, 2H), 6.77 (s, 1H), 5.66 (s, 1H), 4.66 (s, 1H), 3.97 (t, *J* = 6.4 Hz, 2H), 3.37 – 3.24 (m, 2H), 2.70 – 2.32 (m, 10H), 2.28 (s, 3H), 2.22 (s, 3H), 1.94 (dq, *J* = 8.3, 6.4 Hz, 2H), 1.22 (t, *J* = 7.2 Hz, 3H)
^{13}C NMR (75 MHz, $CDCl_3$):	δ 163.59, 160.06, 154.34, 133.67, 121.05, 114.86, 72.41, 66.80, 55.29, 53.36, 46.17, 36.29, 26.99, 24.08, 14.91
Melting point	n.a.
MS (APCI-(+)):	m/z = 385.3 $[M+H^+]^+$
LC-MS-DAD purity:	100.00%
HRMS (ESI-(+)):	m/z = 385.2714 $[M+H^+]^+$ (calculated: 385.2710)

N^4-Ethyl-6-methyl-*N*^{2}-(4-(3-(piperidin-1-yl)propoxy)phenyl)pyrimidine-2,4-diamine (29)

To a solution of 2-chloro-*N*-ethyl-6-methylpyrimidin-4-amine (**P26**) (150 mg, 0.87 mmol, 1.0 eq.) and 4-(3-(piperidin-1-yl)propoxy)aniline (**P14**) (205 mg, 0.87 mmol, 1.0 eq.) in 3 mL of isopropanol in a microwave vial, TFA (0.27 mL, 3.5 mmol, 4 eq.) was added at room temperature. The vial containing reaction mixture was transferred to the microwave reactor where the reaction mixture was stirred at 140 °C for 1 h under microwave irradiation. The mixture was cooled to the room temperature which led to precipitate formation. The precipitate was collected through vacuum filtration, dissolved in 2 M NaOH (30 mL) and extracted with DCM (3 × 30 mL). The organic layers were merged, washed with brine, dried over Na_2SO_4 and evaporated to afford the desired compound.

Yield:	190 mg (59%)
Chemical formula:	$C_{21}H_{31}N_5O$
Molecular mass:	369.51 g/mol
Appearance	Brown resin
Internal code:	MG-144, ST-2658

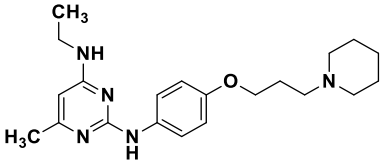

^{1}H NMR (300 MHz, $CDCl_3$):	δ 7.52 – 7.41 (m, 2H), 6.88 – 6.75 (m, 3H), 5.66 (s, 1H), 4.68 (s, 1H), 3.97 (t, *J* = 6.4 Hz, 2H), 3.40 – 3.23 (m, 2H), 2.51 – 2.43 (m, 2H), 2.40 (t, *J* = 5.4 Hz, 4H), 2.22 (s, 3H), 2.03 – 1.88 (m, 2H), 1.65 – 1.52 (m, 4H), 1.44 (td, *J* = 6.5, 3.3 Hz, 2H), 1.22 (t, *J* = 7.2 Hz, 3H)
^{13}C NMR (75 MHz, $CDCl_3$):	δ 163.58, 160.08, 154.37, 133.64, 121.04, 114.86, 67.05, 56.19, 54.77, 36.28, 27.05, 26.11, 24.57, 24.25, 14.89

Melting point	n.a.
MS (APCI-(+)):	m/z = 370.3 $[M+H^+]^+$
LC-MS-DAD purity:	97.86%
HRMS (ESI-(+)):	m/z = 370.2623 $[M+H^+]^+$ (calculated: 370.2601)

N^4-Ethyl-N^2-(3-methoxy-4-(3-(piperidin-1-yl)propoxy)phenyl)-6-methylpyrimidine-2,4-diamine (30)

To a solution of 2-chloro-*N*-ethyl-6-methylpyrimidin-4-amine (**P26**) (100 mg, 0.58 mmol, 1.0 eq.) and 3-methoxy-4-(3-(piperidin-1-yl)propoxy)aniline (**P15**) (154 mg, 0.58 mmol, 1.0 eq.) in 2.2 mL of isopropanol in a microwave vial, 0.1 mL of TFA was added at room temperature. The vial containing reaction mixture was transferred to the microwave reactor where the reaction mixture was stirred at 140 °C for 1 h under microwave irradiation. The mixture was cooled to the room temperature which led to precipitate formation. The precipitate was collected through vacuum filtration, dissolved in 2 M NaOH (30 mL) and extracted with DCM (3 × 30 mL). The organic layers were merged, washed with brine, dried over Na_2SO_4 and evaporated to afford the desired compound.

Yield:	187 mg (86%)
Chemical formula:	$C_{22}H_{33}N_5O_2$
Molecular mass:	385.51 g/mol
Appearance	Beige solid
Internal code:	MG-157, ST-2664
^{1}H NMR (300 MHz, $CDCl_3$):	δ 7.44 (d, *J* = 2.4 Hz, 1H), 6.92 (dd, *J* = 8.6, 2.5 Hz, 1H), 6.89 – 6.84 (m, 1H), 6.82 (d, *J* = 8.6 Hz, 1H), 5.68 (s, 1H), 4.68 (s, 1H), 4.02 (t, *J* = 6.7 Hz, 2H), 3.85 (s, 3H), 3.42 – 3.28 (m, 2H), 2.53 – 2.45 (m, 2H), 2.41 (q, *J* = 5.6, 4.4 Hz, 4H), 2.22 (s, 3H), 2.07 – 1.93 (m, 2H), 1.59 (p, *J* = 5.6 Hz, 4H), 1.43 (q, *J* = 6.1 Hz, 2H), 1.22 (t, *J* = 7.2 Hz, 3H)
^{13}C NMR (75 MHz, $CDCl_3$):	δ 163.54, 159.96, 149.74, 143.57, 134.58, 114.53, 111.25, 111.20, 105.06, 68.56, 56.07, 55.97, 54.68, 36.21, 26.88, 26.02, 24.43, 24.04, 14.96
Melting point	56.5 °C
MS (APCI-(+)):	m/z = 400.4 $[M+H^+]^+$
LC-MS-DAD purity:	96.33%
HRMS (ESI-(+)):	m/z = 400.2715 $[M+H^+]^+$ (calculated: 400.2707)

N^4-Ethyl-N^2-(4-methoxy-3-(3-(piperidin-1-yl)propoxy)phenyl)-6-methylpyrimidine-2,4-diamine (31)

To a solution of 2-chloro-*N*-ethyl-6-methylpyrimidin-4-amine (**P26**) (250 mg, 1.59 mmol, 1.0 eq.) and 4-methoxy-3-(3-(piperidin-1-yl)propoxy)aniline (**P16**) (461 mg, 1.74 mmol, 1.1 eq.) in 4.5 mL of isopropanol in a microwave vial, 0.2 mL of TFA was added at room temperature. The vial containing reaction mixture was transferred to the microwave reactor where the reaction mixture was stirred at 140 °C for 1 h under microwave irradiation. The mixture was cooled to the room temperature which led to precipitate formation. The precipitate was collected through vacuum filtration, dissolved in 2 M NaOH (30 mL) and extracted with DCM (3 × 30 mL). The organic layers were merged, washed with brine, dried over Na_2SO_4 and evaporated to afford the desired compound.

Yield:	460 mg (73%)
Chemical formula:	$C_{22}H_{33}N_5O_2$
Molecular mass:	399.54 g/mol
Appearance	Brown resin
Internal code:	MG-142, ST-2657
^{1}H NMR (300 MHz, $CDCl_3$):	δ 7.44 (d, *J* = 2.5 Hz, 1H), 6.95 (dd, *J* = 8.6, 2.5 Hz, 1H), 6.85 (s, 1H), 6.79 (d, *J* = 8.7 Hz, 1H), 5.68 (s, 1H), 4.74 (s, 1H), 4.07 (t, *J* = 6.6 Hz, 2H), 3.82 (s, 3H), 3.36 (q, *J* = 7.1 Hz, 2H), 2.57 – 2.51 (m, 2H), 2.50 – 2.40 (m, 4H), 2.23 (s, 3H), 2.14 – 2.00 (m, 2H), 1.61 (p, *J* = 5.6 Hz, 4H), 1.45 (q, *J* = 6.2 Hz, 2H), 1.23 (t, *J* = 7.2 Hz, 3H)
^{13}C NMR (75 MHz, $CDCl_3$):	δ 163.55, 159.87, 148.54, 144.73, 134.29, 112.65, 111.77, 110.87, 106.56, 67.59, 56.44, 56.05, 54.61, 46.37, 36.30, 26.60, 25.78, 24.37, 14.95
Melting point	n.a.
MS (APCI-(+)):	m/z = 400.4 $[M+H^+]^+$
LC-MS-DAD purity:	100.00%
HRMS (ESI-(+)):	m/z = 400.2735 $[M+H^+]^+$ (calculated: 400.2707)

N^2,6-Dimethyl-N^4-(4-(3-(4-methylpiperazin-1-yl)propoxy)phenyl)pyrimidine-2,4-diamine (32)

To a solution of 4-chloro-*N*,6-dimethylpyrimidin-2-amine (**P25**) (100 mg, 0.63 mmol, 1.0 eq.) and 1-methyl-4-(3-(4-nitrophenoxy)propyl)piperazine (**P12**) (158 mg, 0.63 mmol, 1.0 eq.) in 2.2 mL of isopropanol in a microwave vial, 0.1 mL of TFA was added at room temperature. The vial containing reaction mixture was transferred to the microwave reactor where the

reaction mixture was stirred at 140 °C for 1 h under microwave irradiation. The mixture was cooled to the room temperature which led to precipitate formation. The precipitate was collected through vacuum filtration, dissolved in 2 M NaOH (30 mL) and extracted with DCM (3 × 30 mL). The organic layers were merged, washed with brine, dried over Na_2SO_4 and evaporated to afford the desired compound.

Yield:	92 mg (39%)
Chemical formula:	$C_{20}H_{30}N_6O$
Molecular mass:	370.50 g/mol
Appearance	White solid
Internal code:	MG-165, ST-2669

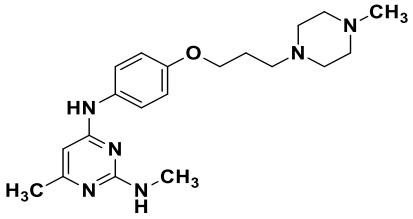

^{1}H NMR (300 MHz, $CDCl_3$):	δ 7.20 (d, 2H), 6.87 (d, 2H), 6.52 (s, 1H), 5.73 (s, 1H), 4.95 (d, *J* = 5.5 Hz, 1H), 4.00 (t, *J* = 6.3 Hz, 2H), 2.95 (d, *J* = 5.0 Hz, 3H), 2.69 – 2.34 (m, 10H), 2.28 (s, 3H), 2.15 (s, 3H), 2.02 – 1.91 (m, 2H)
^{13}C NMR (75 MHz, $CDCl_3$):	δ 166.82, 163.12, 162.88, 156.39, 131.67, 125.18, 115.20, 66.70, 57.22, 55.26, 53.35, 45.94, 28.48, 26.94, 24.14.
Melting point	166.9 °C
MS (APCI-(+)):	m/z = 371.8 $[M+H^+]^+$
LC-MS-DAD purity:	95.20%
HRMS (ESI-(+)):	m/z = 371.2561 $[M+H^+]^+$ (calculated: 371.2554)

N^2,6-Dimethyl-*N*^{4}-(4-(3-(piperidin-1-yl)propoxy)phenyl)pyrimidine-2,4-diamine (33)

To a solution of 4-chloro-*N*,6-dimethylpyrimidin-2-amine (**P25**) (45 mg, 0.29 mmol, 1.0 eq.) and 4-(3-(piperidin-1-yl)propoxy)aniline (**P14**) (67 mg, 0.29 mmol, 1.0 eq.) in 2.2 mL of isopropanol in a microwave vial, 0.1 mL of TFA was added at room temperature. The vial containing reaction mixture was transferred to the microwave reactor where the reaction mixture was stirred at 140 °C for 1 h under microwave irradiation. The mixture was cooled to the room temperature which led to precipitate formation. The precipitate was collected through vacuum filtration, dissolved in 2 M NaOH (30 mL) and extracted with DCM (3 × 30 mL). The organic layers were merged, washed with brine, dried over Na_2SO_4 and evaporated to afford the desired compound.

Yield:	33 mg (32%)
Chemical formula:	$C_{20}H_{29}N_5O$
Molecular mass:	583.53 g/mol
Appearance	Yellow solid

Internal code:	MG-164, ST-2668

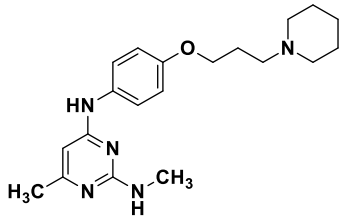

^{1}H NMR (600 MHz, $CDCl_3$):	δ 7.23 – 7.18 (m, 2H), 6.91 – 6.85 (m, 2H), 6.48 (s, 1H), 5.74 (s, 1H), 4.94 (s, 1H), 4.00 (t, *J* = 6.4 Hz, 2H), 2.96 (d, *J* = 5.0 Hz, 3H), 2.50 – 2.44 (m, 2H), 2.40 (s, 4H), 2.16 (s, 3H), 2.01 – 1.93 (m, 2H), 1.59 (p, *J* = 5.6 Hz, 4H), 1.44 (p, *J* = 5.7 Hz, 2H)
^{13}C NMR (151 MHz, $CDCl_3$):	δ 166.87, 163.15, 162.91, 156.47, 131.62, 125.20, 115.23, 92.62, 66.97, 56.13, 54.81, 28.50, 27.02, 26.14, 24.58, 24.19
Melting point	139.9 °C
MS (APCI-(+)):	m/z = 356.7 $[M+H^+]^+$
LC-MS-DAD purity:	100.00%
HRMS (ESI-(+)):	m/z = 356.2436 $[M+H^+]^+$ (calculated: 356.2445)

N^4-(3-Methoxy-4-(3-(piperidin-1-yl)propoxy)phenyl)-*N*^{2},6-dimethylpyrimidine-2,4-diamine (34)

To a solution of 4-chloro-*N*,6-dimethylpyrimidin-2-amine (**P25**) (100 mg, 0.63 mmol, 1.0 eq.) and 3-methoxy-4-(3-(piperidin-1-yl)propoxy)aniline (**P15**) (154 mg, 0.63 mmol, 1.0 eq.) in 2.2 mL of isopropanol in a microwave vial, 0.1 mL of TFA was added at room temperature. The vial containing reaction mixture was transferred to the microwave reactor where the reaction mixture was stirred at 140 °C for 1 h under microwave irradiation. The mixture was cooled to the room temperature which led to precipitate formation. The precipitate was collected through vacuum filtration, dissolved in 2 M NaOH (30 mL) and extracted with DCM (3 × 30 mL). The organic layers were merged, washed with brine, dried over Na_2SO_4 and evaporated to afford the desired compound.

Yield:	212 mg (87%)
Chemical formula:	$C_{21}H_{31}N_5O_2$
Molecular mass:	385.51 g/mol
Appearance	Beige solid
Internal code:	MG-162, ST-2667

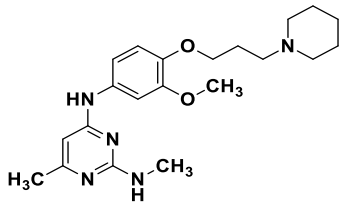

^{1}H NMR (300 MHz, $CDCl_3$):	δ 7.00 (d, *J* = 2.4 Hz, 1H), 6.86 (d, *J* = 8.5 Hz, 1H), 6.78 (dd, *J* = 8.5, 2.4 Hz, 1H), 6.56 (s, 1H), 5.77 (s, 1H), 4.97 (d, *J* = 5.8 Hz, 1H), 4.06 (t, *J* = 6.7 Hz, 2H), 3.83 (s, 3H), 2.96 (d, *J* = 5.0 Hz, 3H), 2.53 – 2.42

	(m, 2H), 2.39 (t, *J* = 5.4 Hz, 4H), 2.17 (s, 3H), 2.09 – 1.93 (m, 2H), 1.59 (q, *J* = 5.5 Hz, 4H), 1.43 (q, *J* = 6.2 Hz, 2H)
^{13}C NMR (75 MHz, $CDCl_3$):	δ 166.86, 163.16, 162.67, 149.93, 145.69, 132.45, 115.31, 113.92, 108.24, 68.24, 56.16, 56.01, 54.73, 28.53, 26.54, 26.13, 24.57, 24.22
Melting point	141.1 °C
MS (APCI-(+)):	m/z = 386.6 $[M+H^+]^+$
LC-MS-DAD purity:	100.00%
HRMS (ESI-(+)):	m/z = 386.2569 $[M+H^+]^+$ (calculated: 386.2551)

N^4-(4-Methoxy-3-(3-(piperidin-1-yl)propoxy)phenyl)-N^2,6-dimethylpyrimidine-2,4-diamine (35)

To a solution of 4-chloro-*N*,6-dimethylpyrimidin-2-amine (**P25**) (100 mg, 0.63 mmol, 1.0 eq.) and 4-methoxy-3-(3-(piperidin-1-yl)propoxy)aniline (**P16**) (154 mg, 0.63 mmol, 1.0 eq.) in 2.2 mL of isopropanol in a microwave vial, 0.1 mL of TFA was added at room temperature. The vial containing reaction mixture was transferred to the microwave reactor where the reaction mixture was stirred at 140 °C for 1 h under microwave irradiation. The mixture was cooled to the room temperature which led to precipitate formation. The precipitate was collected through vacuum filtration, dissolved in 2 M NaOH (30 mL) and extracted with DCM (3 × 30 mL). The organic layers were merged, washed with brine, dried over Na_2SO_4 and evaporated to afford the desired compound.

Yield:	207 mg (82%)
Chemical formula:	$C_{21}H_{31}N_5O_2$
Molecular mass:	385.51 g/mol
Appearance	Beige solid
Internal code:	MG-161, ST-2666
^{1}H NMR (300 MHz, $CDCl_3$):	δ 7.01 (s, 1H), 6.82 (s, 2H), 6.50 (s, 1H), 5.77 (s, 1H), 4.94 (d, *J* = 5.3 Hz, 1H), 4.04 (t, *J* = 6.7 Hz, 2H), 3.85 (s, 3H), 2.96 (d, *J* = 5.0 Hz, 3H), 2.46 (dd, *J* = 8.2, 6.5 Hz, 2H), 2.39 (d, *J* = 5.3 Hz, 4H), 2.17 (s, 3H), 2.02 (dq, *J* = 8.7, 6.8 Hz, 2H), 1.56 (p, *J* = 5.5 Hz, 4H), 1.42 (q, *J* = 6.0 Hz, 2H).
^{13}C NMR (75 MHz, $CDCl_3$):	δ 166.79, 163.15, 162.72, 148.95, 146.75, 132.30, 115.67, 112.34, 109.66, 92.99, 77.58, 77.16, 76.74, 55.93, 54.72, 28.54, 26.78, 26.10, 24.56
Melting point	50.9 °C
MS (APCI-(+)):	m/z = 386.6 $[M+H^+]^+$
LC-MS-DAD purity:	100.00%

HRMS (ESI-(+)):	m/z = 386.2578 $[M+H^+]^+$ (calculated: 386.2551)

N^2-Ethyl-6-methyl-N^4-(4-(3-(4-methylpiperazin-1-yl)propoxy)phenyl)pyrimidine-2,4-diamine (36)

To a solution of 4-chloro-*N*-ethyl-6-methylpyrimidin-2-amine (**P27**) (100 mg, 0.63 mmol, 1.0 eq.) and 1-methyl-4-(3-(4-nitrophenoxy)propyl)piperazine (**P12**) (158 mg, 0.63 mmol, 1.0 eq.) in 2.2 mL of isopropanol in a microwave vial, 0.1 mL of TFA was added at room temperature. The vial containing reaction mixture was transferred to the microwave reactor where the reaction mixture was stirred at 140 °C for 1 h under microwave irradiation. The mixture was cooled to the room temperature which led to precipitate formation. The precipitate was collected through vacuum filtration, dissolved in 2 M NaOH (30 mL) and extracted with DCM (3 × 30 mL). The organic layers were merged, washed with brine, dried over Na_2SO_4 and evaporated to afford the desired compound.

Yield:	33 mg (13%)
Chemical formula:	$C_{21}H_{33}N_6O$
Molecular mass:	384.53 g/mol
Appearance	Beige solid
Internal code:	MG-148, ST-2662

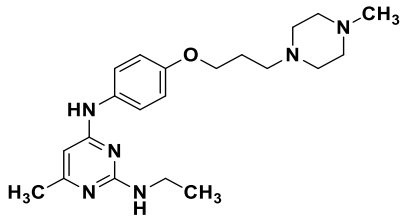

^{1}H NMR (300 MHz, $CDCl_3$):	δ 7.24 – 7.16 (m, 2H), 6.91 – 6.83 (m, 2H), 6.49 (s, 1H), 5.72 (s, 1H), 4.84 (d, *J* = 5.8 Hz, 1H), 4.00 (t, *J* = 6.4 Hz, 2H), 3.40 (qd, *J* = 7.2, 5.5 Hz, 2H), 2.52 (t, *J* = 7.4 Hz, 10H), 2.28 (s, 3H), 2.15 (s, 3H), 2.03 – 1.89 (m, 2H), 1.19 (t, *J* = 7.2 Hz, 3H)
^{13}C NMR (75 MHz, $CDCl_3$):	δ 166.83, 162.85, 162.42, 156.33, 131.73, 125.08, 115.18, 92.62, 70.27, 66.69, 55.26, 53.35, 46.20, 36.26, 26.92, 24.18, 15.23
Melting point	148.7 °C
MS (APCI-(+)):	m/z = 385.5 $[M+H^+]^+$
LC-MS-DAD purity:	95.70%
HRMS (ESI-(+)):	m/z = 385.2719 $[M+H^+]^+$ (calculated: 385.2710)

N^2-Ethyl-6-methyl-N^4-(4-(3-(piperidin-1-yl)propoxy)phenyl)pyrimidine-2,4-diamine (37)

To a solution of 4-chloro-*N*-ethyl-6-methylpyrimidin-2-amine (**P27**) (100 mg, 0.63 mmol, 1.0 eq.) and 4-(3-(piperidin-1-yl)propoxy)aniline (**P14**) (149 mg, 0.63 mmol, 1.0 eq.) in 2.2 mL of isopropanol in a microwave vial, 0.1 mL of TFA was added at room temperature. The vial

containing reaction mixture was transferred to the microwave reactor where the reaction mixture was stirred at 140 °C for 1 h under microwave irradiation. The mixture was cooled to the room temperature which led to precipitate formation. The precipitate was collected through vacuum filtration, dissolved in 2 M NaOH (30 mL) and extracted with DCM (3 × 30 mL). The organic layers were merged, washed with brine, dried over Na_2SO_4 and evaporated to afford the desired compound.

Yield:	86 mg (37%)
Chemical formula:	$C_{21}H_{31}N_5O$
Molecular mass:	369.51 g/mol
Appearance	Beige solid
Internal code:	MG-147, ST-2661
^{1}H NMR (300 MHz, $CDCl_3$):	δ 7.25 – 7.16 (m, 2H), 6.95 – 6.83 (m, 2H), 6.43 (s, 1H), 5.73 (s, 1H), 4.77 (s, 1H), 4.00 (t, *J* = 6.4 Hz, 2H), 3.41 (qd, *J* = 7.2, 5.6 Hz, 2H), 2.52 – 2.35 (m, 6H), 2.15 (s, 3H), 2.05 – 1.89 (m, 2H), 1.59 (p, *J* = 5.5 Hz, 4H), 1.44 (q, *J* = 6.1 Hz, 2H), 1.20 (t, *J* = 7.2 Hz, 3H)
^{13}C NMR (75 MHz, $CDCl_3$):	δ 166.83, 162.75, 162.67, 156.29, 131.55, 127.69, 124.99, 115.09, 66.85, 56.01, 54.69, 36.16, 26.90, 26.02, 24.46, 24.09, 15.15
Melting point	114.4 °C
MS (APCI-(+)):	m/z = 370.5 $[M+H^+]^+$
LC-MS-DAD purity:	97.15%
HRMS (ESI-(+)):	m/z = 370.2589 $[M+H^+]^+$ (calculated: 370.2601)

N^2-Ethyl-*N*^{4}-(3-methoxy-4-(3-(piperidin-1-yl)propoxy)phenyl)-6-methylpyrimidine-2,4-diamine (38)

To a solution of 4-chloro-*N*-ethyl-6-methylpyrimidin-2-amine (**P27**) (100 mg, 0.58 mmol, 1.0 eq.) and 3-methoxy-4-(3-(piperidin-1-yl)propoxy)aniline (**P15**) (154 mg, 0.58 mmol, 1.0 eq.) in 2.2 mL of isopropanol in a microwave vial, 0.1 mL of TFA was added at room temperature. The vial containing reaction mixture was transferred to the microwave reactor where the reaction mixture was stirred at 140 °C for 1 h under microwave irradiation. The mixture was cooled to the room temperature which led to precipitate formation. The precipitate was collected through vacuum filtration, dissolved in 2 M NaOH (30 mL) and extracted with DCM (3 × 30 mL). The organic layers were merged, washed with brine, dried over Na_2SO_4 and evaporated to afford the desired compound.

Yield:	173 mg (74%)

Chemical formula:	$C_{22}H_{33}N_5O_2$
Molecular mass:	399.54 g/mol
Appearance	Brown solid
Internal code:	MG-158, ST-2665

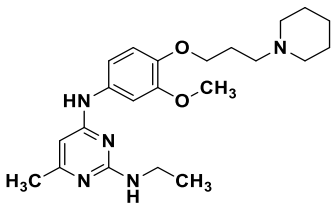

^{1}H NMR (300 MHz, $CDCl_3$):	δ 6.98 (d, *J* = 2.4 Hz, 1H), 6.86 (d, *J* = 8.6 Hz, 1H), 6.79 (dd, *J* = 8.5, 2.4 Hz, 1H), 6.50 (s, 1H), 5.76 (d, *J* = 0.6 Hz, 1H), 4.87 – 4.77 (m, 1H), 4.06 (t, *J* = 6.7 Hz, 2H), 3.83 (s, 3H), 3.41 (qd, *J* = 7.2, 5.6 Hz, 2H), 2.55 – 2.44 (m, 2H), 2.39 (t, *J* = 5.3 Hz, 4H), 2.21 – 2.12 (m, 3H), 2.08 – 1.96 (m, 2H), 1.58 (p, *J* = 5.5 Hz, 4H), 1.43 (q, *J* = 6.9, 6.3 Hz, 2H), 1.19 (t, *J* = 7.2 Hz, 3H)
^{13}C NMR (75 MHz, $CDCl_3$):	δ 166.73, 162.54, 162.31, 149.81, 145.56, 132.34, 115.15, 113.81, 108.10, 68.11, 62.39, 55.89, 54.61, 36.18, 26.76, 25.98, 24.39, 24.04, 15.18
Melting point	56.7 °C
MS (APCI-(+)):	m/z = 400.4 $[M+H^+]^+$
LC-MS-DAD purity:	100.00%
HRMS (ESI-(+)):	m/z = 400.2744 $[M+H^+]^+$ (calculated: 400.2707)

N^2-Ethyl-*N*^{4}-(4-methoxy-3-(3-(piperidin-1-yl)propoxy)phenyl)-6-methylpyrimidine-2,4-diamine (39)

To a solution of 4-chloro-*N*-ethyl-6-methylpyrimidin-2-amine (**P27**) (100 mg, 0.63 mmol, 1.0 eq.) and 4-methoxy-3-(3-(piperidin-1-yl)propoxy)aniline (**P16**) (168 mg, 0.63 mmol, 1.0 eq.) in 2.2 mL of isopropanol in a microwave vial, 0.1 mL of TFA was added at room temperature. The vial containing reaction mixture was transferred to the microwave reactor where the reaction mixture was stirred at 140 °C for 1 h under microwave irradiation. The mixture was cooled to the room temperature which led to precipitate formation. The precipitate was collected through vacuum filtration, dissolved in 2 M NaOH (30 mL) and extracted with DCM (3 × 30 mL). The organic layers were merged, washed with brine, dried over Na_2SO_4 and evaporated to afford the desired compound.

Yield:	170 mg (67%)
Chemical formula:	$C_{22}H_{33}N_5O_2$
Molecular mass:	399.54 g/mol
Appearance	Brown solid
Internal code:	MG-146, ST-2660

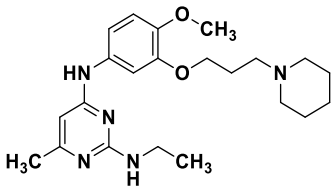

^{1}H NMR (300 MHz, $CDCl_3$):	δ 6.99 (s, 1H), 6.87 – 6.76 (m, 2H), 6.49 (s, 1H), 5.76 (s, 1H), 4.81 (s, 1H), 4.04 (t, *J* = 6.7 Hz, 2H), 3.85 (s, 3H), 3.41 (qd, *J* = 7.2, 5.6 Hz, 2H), 2.46 (dd, *J* = 8.2, 6.5 Hz, 2H), 2.38 (t, *J* = 5.3 Hz, 4H), 2.16 (s, 3H), 2.03

	(dt, *J* = 8.3, 6.8 Hz, 2H), 1.56 (p, *J* = 5.5 Hz, 4H), 1.42 (q, *J* = 6.1 Hz, 2H), 1.20 (t, *J* = 7.2 Hz, 3H)
^{13}C NMR (75 MHz, $CDCl_3$):	δ 166.87, 162.71, 162.45, 148.94, 146.73, 133.45, 132.33, 115.46, 112.35, 109.62, 67.82, 56.26, 55.94, 54.72, 36.30, 26.79, 26.10, 24.56, 24.19, 15.28
Melting point	117.6 °C
MS (APCI-(+)):	m/z = 400.3 $[M+H^+]^+$
LC-MS-DAD purity:	100.00%
HRMS (ESI-(+)):	m/z = 400.2719 $[M+H^+]^+$ (calculated: 400.2707)

2,5-Dichloro-*N*-methylpyrimidin-4-amine (P28)[390]

To a suspension of 2,4,5-trichloropyrimidine (1.00 g, 5.45 mmol, 1.0 eq.) and K_2CO_3 (2.26 g, 16.36 mmol, 3.0 eq.) in 50 mL of DMF methylamine hydrochloride (442 mg, 6.54 mmol, 2 eq.) was added, and the reaction mixture was stirred for 5 h at room temperature. Afterwards, K_2CO_3 was filtered out, DMF was evaporated, and the residue was partitioned between water and EtOAc. The organic layers were merged, washed with brine and dried over anhydrous $MgSO_4$. After filtration, solvent was evaporated under reduced pressure to obtain the desired compound. The identity of the compound was confirmed with ^{1}H-, ^{13}C- and HMBC-NMR spectrums.

Yield:	943 mg (97%)
Chemical formula:	$C_5H_5Cl_2N_3$
Molecular mass:	178.02 g/mol
Appearance	White crystal
Internal code:	MG-174
R_f-value	0.33 (Hex:EtOAC 4:1)
^{1}H NMR (300 MHz, DMSO):	δ 8.12 (s, 1H), 7.91 (s, 1H), 2.86 (s, 3H)
^{13}C NMR (75 MHz, DMSO):	δ 159.06, 157.50, 153.23, 112.99, 27.84
MS (APCI-(+)):	m/z = 177.8, 179.8, 181.8 $[M+H^+]^+$

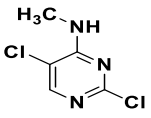

2,5-Dichloro-*N*-ethylpyrimidin-4-amine (P29)

A solution of 2,4,5-trichloropyrimidine (1025 mg, 5.63 mmol, 1.0 eq.) and ethylamine hydrochloride (551 mg, 6.76 mmol, 1.2 eq.) in 5 mL of ethanol was treated with DIPEA (2.94 mL, 16.90 mmol, 3.0 eq.) and the reaction mixture was stirred for 1 h at room temperature. Subsequently, ethanol was evaporated, and the residue was partitioned between water and EtOAc. The organic layers were merged, washed with brine and dried over anhydrous $MgSO_4$.

Structural isomers were separated using flash column chromatography (HEX:EE, 0-40% EE). The identity of the **P29** was confirmed with ^{1}H-, ^{13}C- and HMBC-NMR spectrums.

Yield:	924 mg (85%)
Chemical formula:	$C_6H_7Cl_2N_3$
Molecular mass:	192.04 g/mol
Appearance	Colorless liquid
Internal code:	MG-301F2
R_f-value	0.42 (Hex:EtOAC 4:1)
^{1}H NMR (300 MHz, DMSO):	δ 8.13 (s, 1H), 7.93 (s, 1H), 3.39 (qd, *J* = 7.1, 5.8 Hz, 2H), 1.13 (t, *J* = 7.2 Hz, 3H)
^{13}C NMR (75 MHz, DMSO):	δ 158.44, 157.47, 153.52, 112.80, 35.52, 14.05.
MS (APCI-(+)):	m/z = 191.7, 193.7 $[M+H^+]^+$

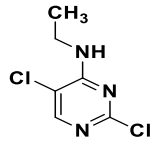

4,5-Dichloro-*N*-ethylpyrimidin-2-amine (P30)

The compound 4,5-dichloro-*N*-ethylpyrimidin-2-amine (**P30**) was obtained as a side product during the synthesis of compound **P29**.

Yield:	35 mg (3%)
Chemical formula:	$C_6H_7Cl_2N_3$
Molecular mass:	192.04 g/mol
Appearance	Colorless liquid
Internal code:	MG-301F1
R_f-value	0.55 (Hex:EtOAC 4:1)
MS (APCI-(+)):	m/z = 191.7, 193.7 $[M+H^+]^+$

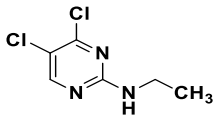

5-Chloro-N^4-methyl-N^2-(4-(3-(4-methylpiperazin-1-yl)propoxy)phenyl)pyrimidine-2,4-diamine (40)

To a solution of 2,5-dichloro-*N*-methylpyrimidin-4-amine (**P28**) (100 mg, 0.56 mmol, 1.0 eq.) and 1-methyl-4-(3-(4-nitrophenoxy)propyl)piperazine (**P12**) (154 mg, 0.62 mmol, 1.1 eq.) in 2.2 mL of isopropanol in a microwave vial, 0.1 mL of TFA was added at room temperature. The vial containing reaction mixture was transferred to the microwave reactor where the reaction mixture was stirred at 140°C for 1 h under microwave irradiation. The mixture was cooled to the room temperature which led to precipitate formation. The precipitate was collected through vacuum filtration, dissolved in 2 M NaOH (30 mL) and extracted with DCM

(3 × 30 mL). The organic layers were merged, washed with brine, dried over Na_2SO_4 and evaporated to afford the desired compound.

Yield:	80 mg (36%)
Chemical formula:	$C_{19}H_{27}ClN_6O$
Molecular mass:	390.92 g/mol
Appearance	Beige solid
Internal code:	MG-191, ST-2707
^{1}H NMR (600 MHz, $CDCl_3$):	δ 7.85 (s, 1H), 7.48 – 7.42 (m, 2H), 6.88 – 6.83 (m, 3H), 5.23 (q, *J* = 4.7 Hz, 1H), 3.99 (t, *J* = 6.4 Hz, 2H), 3.04 (d, *J* = 4.9 Hz, 3H), 2.81 – 2.32 (m, 10H), 2.29 (s, 3H), 1.99 – 1.93 (m, 2H)
^{13}C NMR (151 MHz, $CDCl_3$):	δδ 158.61, 158.59, 154.74, 152.88, 133.09, 121.40, 114.90, 104.70, 66.76, 55.33, 55.30, 53.38, 46.22, 28.01, 27.00
Melting point	151.9 °C
MS (APCI-(+)):	m/z = 391.0, 392.9 $[M+H^+]^+$
LC-MS-DAD purity:	100.00%
HRMS (ESI-(+)):	m/z = 391.2020 $[M+H^+]^+$ (calculated: 391.2008)

1-(4-(3-(4-((5-Chloro-4-(methylamino)pyrimidin-2-yl)amino)phenoxy)propyl)piperazin-1-yl)ethan-1-one (41)

To a solution of 2,5-dichloro-*N*-methylpyrimidin-4-amine (**P28**) (100 mg, 0.56 mmol, 1.0 eq.) and 1-(4-(3-(4-aminophenoxy)propyl)piperazin-1-yl)ethan-1-one (**P13**) (171 mg, 0.62 mmol, 1.1 eq.) in 2 mL of isopropanol in a microwave vial, 0.1 mL of TFA was added at room temperature. The reaction mixture was stirred at 60 °C for 24 h. After the TLC control indicated consumption of starting material, the solvent was evaporated, and the residue was partitioned between 2 M NaOH (30 mL) and ethyl acetate (3 × 30 mL). The organic layers were merged, washed with brine, dried over Na_2SO_4. After filtration solvent was evaporated, and the residue was purified using flash column chromatography (DCM:MeOH, 0-7% MeOH) in order to obtain desired product.

Yield:	108 mg (46%)
Chemical formula:	$C_{20}H_{27}ClN_6O_2$
Molecular mass:	418.93 g/mol
Appearance	White solid
Internal code:	MG-335, ST-2983

^{1}H NMR (300 MHz, $CDCl_3$):	δ 7.85 (s, 1H), 7.46 (d, *J* = 9.0 Hz, 2H), 6.86 (d, *J* = 9.0 Hz, 3H), 5.24 (d, *J* = 4.8 Hz, 1H), 4.00 (t, *J* = 6.3 Hz, 2H), 3.68 – 3.57 (m, 2H), 3.52 – 3.41 (m, 2H), 3.04 (d, *J* = 4.9 Hz, 3H), 2.59 – 2.48 (m, 2H), 2.44 (dt, *J* = 9.9, 5.1 Hz, 4H), 2.08 (s, 3H), 2.03 – 1.88 (m, 2H)
^{13}C NMR (151 MHz, $CDCl_3$):	δ 169.03, 158.62, 154.67, 152.89, 133.22, 121.41, 114.91, 104.78, 66.46, 55.13, 53.53, 52.94, 46.45, 41.56, 28.00, 26.89, 21.47
Melting point	137.8 °C
MS (APCI-(+)):	m/z = 418.5, 420.2 $[M+H^+]^+$
LC-MS-DAD purity:	100.00%
HRMS (ESI-(+)):	m/z = 419.1968 $[M+H^+]^+$ (calculated: 419.1957)

5-Chloro-*N*^{4}-methyl-*N*^{2}-(4-(3-(piperidin-1-yl)propoxy)phenyl)pyrimidine-2,4-diamine (42)

To a solution of 2,5-dichloro-*N*-methylpyrimidin-4-amine (**P28**) (50 mg, 0.28 mmol, 1.0 eq.) and 4-(3-(piperidin-1-yl)propoxy)aniline (**P14**) (72 mg, 0.31 mmol, 1.1 eq.) in 1 mL of isopropanol in a microwave vial, 0.1 mL of TFA was added at room temperature. The vial containing reaction mixture was transferred to the microwave reactor where the reaction mixture was stirred at 140 °C for 1 h under microwave irradiation. The mixture was cooled to the room temperature which led to precipitate formation. The precipitate was collected through vacuum filtration, dissolved in 2 M NaOH (30 mL) and extracted with DCM (3 × 30 mL). The organic layers were merged, washed with brine, dried over Na_2SO_4 and evaporated to afford the desired compound.

Yield:	68 mg (65%)
Chemical formula:	$C_{19}H_{26}ClN_5O$
Molecular mass:	375.90 g/mol
Appearance	Beige solid
Internal code:	MG-187, ST-2704

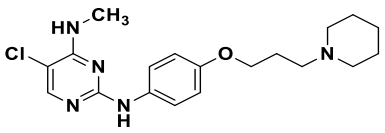

^{1}H NMR (600 MHz, $CDCl_3$):	δ 7.85 (s, 1H), 7.48 – 7.43 (m, 2H), 6.92 (s, 1H), 6.88 – 6.83 (m, 2H), 5.23 (q, *J* = 4.9 Hz, 1H), 3.98 (t, *J* = 6.4 Hz, 2H), 3.04 (d, *J* = 4.9 Hz, 3H), 2.50 – 2.46 (m, 2H), 2.46 – 2.34 (m, 4H), 2.00 – 1.93 (m, 2H), 1.59 (p, *J* = 5.7 Hz, 4H), 1.48 – 1.41 (m, 2H)
^{13}C NMR (151 MHz, $CDCl_3$):	158.62, 158.58, 154.76, 152.87, 133.06, 121.40, 114.89, 104.65, 66.99, 56.18, 54.76, 28.00, 27.00, 26.08, 24.54
Melting point	117.7 °C
MS (APCI-(+)):	m/z = 375.8, 377.8 $[M+H^+]^+$

LC-MS-DAD purity:	100.00%
HRMS (ESI-(+)):	m/z = 376.1889 $[M+H^+]^+$ (calculated: 376.1899)

5-Chloro-*N*^{2}-(3-methoxy-4-(3-(piperidin-1-yl)propoxy)phenyl)-*N*^{4}-methylpyrimidine-2,4-diamine (43)

To a solution of 2,5-dichloro-*N*-methylpyrimidin-4-amine (**P28**) (100 mg, 0.56 mmol, 1.0 eq.) and 3-methoxy-4-(3-(piperidin-1-yl)propoxy)aniline (**P16**) (163 mg, 0.62 mmol, 1.1 eq.) in 2.2 mL of isopropanol in a microwave vial, 0.1 mL of TFA was added at room temperature. The vial containing reaction mixture was transferred to the microwave reactor where the reaction mixture was stirred at 140 °C for 1 h under microwave irradiation. The mixture was cooled to the room temperature which led to precipitate formation. The precipitate was collected through vacuum filtration, dissolved in 2 M NaOH (30 mL) and extracted with DCM (3 × 30 mL). The organic layers were merged, washed with brine, dried over Na_2SO_4 and evaporated to afford the desired compound.

Yield:	147 mg (65%)
Chemical formula:	$C_{20}H_{28}ClN_5O_2$
Molecular mass:	405.93 g/mol
Appearance	Beige solid
Internal code:	MG-189, ST-2706
^{1}H NMR (600 MHz, $CDCl_3$):	δ 7.86 (s, 1H), 7.39 (d, *J* = 2.5 Hz, 1H), 7.08 (s, 1H), 6.92 (dd, *J* = 8.6, 2.5 Hz, 1H), 6.85 (d, *J* = 8.6 Hz, 1H), 5.27 (q, *J* = 4.9 Hz, 1H), 4.03 (t, *J* = 6.7 Hz, 2H), 3.86 (s, 3H), 3.06 (d, *J* = 4.9 Hz, 3H), 2.51 – 2.46 (m, 2H), 2.41 (s, 4H), 2.04 – 1.98 (m, 2H), 1.59 (p, *J* = 5.7 Hz, 4H), 1.43 (s, 2H)
^{13}C NMR (151 MHz, $CDCl_3$):	δ 158.58, 158.48, 152.87, 149.70, 143.93, 133.97, 114.27, 111.46, 105.03, 104.66, 68.42, 56.03, 56.01, 54.66, 28.08, 26.84, 26.02, 24.51
Melting point	90.2 °C
MS (APCI-(+)):	m/z = 406.0, 407.9 $[M+H^+]^+$
LC-MS-DAD purity:	100.00%
HRMS (ESI-(+)):	m/z = 406.2010 $[M+H^+]^+$ (calculated: 406.2004)

Chloro-N^2-(4-methoxy-3-(3-(piperidin-1-yl)propoxy)phenyl)-N^4-methylpyrimidine-2,4-diamine (44)

To a solution of 2,5-dichloro-*N*-methylpyrimidin-4-amine (**P28**) (50 mg, 0.28 mmol, 1.0 eq.) and 4-methoxy-3-(3-(piperidin-1-yl)propoxy)aniline (**P16**) (82 mg, 0.31 mmol, 1.1 eq.) in 1 mL of isopropanol in a microwave vial, 0.1 mL of TFA was added at room temperature. The vial containing reaction mixture was transferred to the microwave reactor where the reaction mixture was stirred at 140 °C for 1 h under microwave irradiation. The mixture was cooled to the room temperature which led to precipitate formation. The precipitate was collected through vacuum filtration, dissolved in 2 M NaOH (30 mL) and extracted with DCM (3 × 30 mL). The organic layers were merged, washed with brine, dried over Na_2SO_4 and evaporated to afford the desired compound.

Yield:	32 mg (28%)
Chemical formula:	$C_{20}H_{28}ClN_5O_2$
Molecular mass:	405.93 g/mol
Appearance	Brown solid
Internal code:	MG-188, ST-2705
^{1}H NMR (300 MHz, $CDCl_3$):	δ 7.86 (s, 1H), 7.39 (d, *J* = 2.5 Hz, 1H), 6.99 – 6.92 (m, 2H), 6.81 (d, *J* = 8.7 Hz, 1H), 5.26 (d, *J* = 4.9 Hz, 1H), 4.07 (t, *J* = 6.7 Hz, 2H), 3.83 (s, 3H), 3.06 (d, *J* = 4.9 Hz, 3H), 2.53 – 2.43 (m, 2H), 2.43 – 2.32 (m, 4H), 2.03 (dq, *J* = 8.6, 6.8 Hz, 2H), 1.57 (p, *J* = 5.4 Hz, 4H), 1.43 (q, *J* = 5.9 Hz, 2H)
^{13}C NMR (75 MHz, $CDCl_3$):	δ 158.60, 158.53, 152.93, 148.74, 145.08, 133.79, 112.58, 111.63, 106.48, 104.70, 67.78, 56.40, 56.05, 54.72, 28.09, 26.85, 26.12, 24.57
Melting point	104.6 °C
MS (APCI-(+)):	m/z = 406.0, 407.9 $[M+H^+]^+$
LC-MS-DAD purity:	100.00%
HRMS (ESI-(+)):	m/z = 406.1977 $[M+H^+]^+$ (calculated: 406.2004)

5-Chloro-N^2-(2-methoxy-4-(3-(piperidin-1-yl)propoxy)phenyl)-N^4-methylpyrimidine-2,4-diamine (45)

To a solution of 2,5-dichloro-*N*-methylpyrimidin-4-amine (**P28**) (100 mg, 0.56 mmol, 1.0 eq.) and 2-methoxy-4-(3-(piperidin-1-yl)propoxy)aniline **(P17)** (163 mg, 0.62 mmol, 1.1 eq.) in 3 mL of isopropanol in a microwave vial, 0.1 mL of TFA was added at room temperature. The reaction mixture was stirred at 60 °C for 24 h. After the TLC control indicated consumption of

starting material, the solvent was evaporated, and the residue was partitioned between 2 M NaOH (30 mL) and ethyl acetate (3 × 30 mL). The organic layers were merged, washed with brine, dried over Na_2SO_4. After filtration solvent was evaporated, and the residue was purified using flash column chromatography (DCM:MeOH, 0-7% MeOH) in order to obtain desired product.

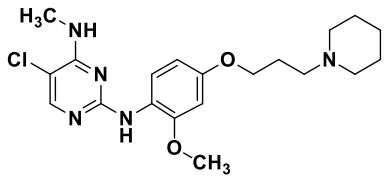

Yield:	46 mg (20%)
Chemical formula:	$C_{20}H_{28}ClN_5O_2$
Molecular mass:	405.93 g/mol
Appearance	Brown resin
Internal code:	MG-334, ST-2984
^{1}H NMR (600 MHz, $CDCl_3$):	δ 8.26 (d, *J* = 9.5 Hz, 1H), 7.86 (s, 1H), 7.24 (s, 1H), 6.52 – 6.47 (m, 2H), 5.22 (q, *J* = 5.2 Hz, 1H), 3.99 (t, *J* = 6.4 Hz, 2H), 3.85 (s, 3H), 3.07 (d, *J* = 4.9 Hz, 3H), 2.48 (t, *J* = 7.8 Hz, 2H), 2.41 (s, 4H), 2.00 – 1.94 (m, 2H), 1.59 (p, *J* = 5.6 Hz, 4H), 1.49 – 1.40 (m, 2H)
^{13}C NMR (151 MHz, $CDCl_3$):	δ 158.59, 158.44, 154.49, 152.89, 149.33, 123.21, 119.53, 104.60, 104.47, 99.36, 67.07, 56.21, 55.82, 54.79, 28.10, 27.07, 26.11, 24.57
Melting point	n.a.
MS (APCI-(+)):	m/z = 405.9, 407.7 $[M+H^+]^+$
LC-MS-DAD purity:	100.00%
HRMS (ESI-(+)):	m/z = 406.2007 $[M+H^+]^+$ (calculated: 406.2004)

5-Chloro-*N*^{4}-ethyl-*N*^{2}-(4-(3-(4-methylpiperazin-1-yl)propoxy)phenyl)pyrimidine-2,4-diamine (46)

To a solution of 2,5-dichloro-*N*-ethylpyrimidin-4-amine (**P29**) (100 mg, 0.52 mmol, 1.0 eq.) and 1-methyl-4-(3-(4-nitrophenoxy)propyl)piperazine (**P12**) (143 mg, 0.57 mmol, 1.1 eq.) in 2.2 mL of isopropanol in a microwave vial, 0.1 mL of TFA was added at room temperature. The vial containing reaction mixture was transferred to the microwave reactor where the reaction mixture was stirred at 140 °C for 1 h under microwave irradiation. The mixture was cooled to the room temperature which led to precipitate formation. The precipitate was collected through vacuum filtration, dissolved in 2 M NaOH (30 mL) and extracted with DCM (3 × 30 mL). The organic layers were merged, washed with brine, dried over Na_2SO_4 and evaporated to afford the desired compound.

Yield:	125 mg (60%)
Chemical formula:	$C_{20}H_{29}ClN_6O$

Molecular mass:	404.94 g/mol
Appearance	White solid
Internal code:	MG-201, ST-2701

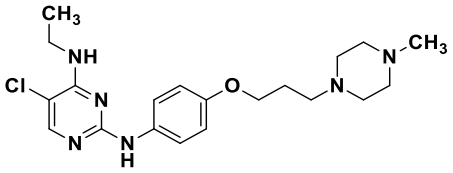

^{1}H NMR (600 MHz, $CDCl_3$):	δ 7.85 (s, 1H), 7.46 – 7.41 (m, 2H), 6.90 (s, 1H), 6.88 – 6.82 (m, 2H), 5.17 (t, *J* = 5.4 Hz, 1H), 3.99 (t, *J* = 6.4 Hz, 2H), 3.50 (qd, *J* = 7.2, 5.5 Hz, 2H), 2.87 – 2.30 (m, 10H), 2.28 (s, 3H), 1.99 – 1.92 (m, 2H), 1.27 (t, *J* = 7.2 Hz, 3H)
^{13}C NMR (151 MHz, $CDCl_3$):	δ 158.62, 157.91, 154.71, 153.00, 133.17, 121.34, 114.89, 104.47, 66.78, 55.32, 55.31, 53.38, 46.21, 36.01, 27.01, 14.89
Melting point	147.3 °C
MS (APCI-(+)):	m/z = 405.3 $[M+H^+]^+$
LC-MS-DAD purity:	100.00%
HRMS (ESI-(+)):	m/z = 405.2168 $[M+H^+]^+$ (calculated: 405.2164)

1-(4-(3-(4-((5-Chloro-4-(ethylamino)pyrimidin-2-yl)amino)phenoxy)propyl)piperazin-1-yl)ethan-1-one (47)

To a solution of 2,5-dichloro-*N*-ethylpyrimidin-4-amine (**P29**) (100 mg, 0.52 mmol, 1.0 eq.) and 1-(4-(3-(4-aminophenoxy)propyl)piperazin-1-yl)ethan-1-one (**P13**) (159 mg, 0.57 mmol, 1.1 eq.) in 2 mL of isopropanol in a microwave vial, 0.1 mL of TFA was added at room temperature. The reaction mixture was stirred at room temperature for 24 h. After the TLC control indicated consumption of starting material, the solvent was evaporated, and the residue was partitioned between 1 M NaOH (30 mL) and ethyl acetate (3 × 30 mL). The organic layers were merged, washed with brine, dried over Na_2SO_4. After filtration solvent was evaporated, and the residue was purified using flash column chromatography (DCM:MeOH, 0-7% MeOH) in order to obtain desired product.

Yield:	145 mg (64%)
Chemical formula:	$C_{21}H_{30}ClN_5O_2$
Molecular mass:	432.20 g/mol
Appearance	Beige solid
Internal code:	MG-328, ST-2980

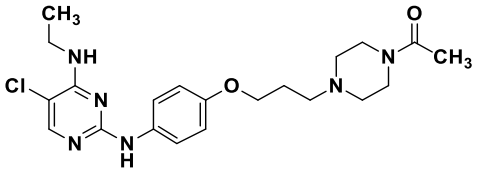

^{1}H NMR (300 MHz, $CDCl_3$):	δ 7.85 (s, 1H), 7.45 (d, *J* = 9.0 Hz, 1H), 6.93 – 6.81 (m, 2H), 5.19 (t, *J* = 5.4 Hz, 1H), 4.00 (t, *J* = 6.3 Hz, 2H), 3.62 (t, *J* = 5.0 Hz, 2H), 3.59 – 3.41 (m, 4H), 2.54 (t, *J* = 7.0 Hz, 2H), 2.50 – 2.36 (m, 4H), 2.08 (s, 3H), 1.95 (dq, *J* = 8.3, 6.3 Hz, 2H), 1.27 (t, *J* = 7.2 Hz, 3H)

^{13}C NMR (151 MHz, $CDCl_3$):	δ 169.05, 158.59, 157.92, 154.63, 152.98, 133.25, 121.35, 114.88, 104.56, 66.46, 55.13, 53.52, 52.93, 46.44, 41.56, 36.02, 26.89, 21.46, 14.89
Melting point	119.7 °C
MS (APCI-(+)):	m/z = 433.0, 434.8 $[M+H^+]^+$
LC-MS-DAD purity:	100.00%
HRMS (ESI-(+)):	m/z = 433.2122 $[M+H^+]^+$ (calculated: 433.2113)

5-Chloro-*N*^{4}-ethyl-*N*^{2}-(4-(3-(piperidin-1-yl)propoxy)phenyl)pyrimidine-2,4-diamine (48)

To a solution of 2,5-dichloro-*N*-ethylpyrimidin-4-amine (**P29**) (100 mg, 0.52 mmol, 1.0 eq.) and 4-(3-(piperidin-1-yl)propoxy)aniline (**P14**) (134 mg, 0.57 mmol, 1.1 eq.) in 2.2 mL of isopropanol in a microwave vial, 0.1 mL of TFA was added at room temperature. The vial containing reaction mixture was transferred to the microwave reactor where the reaction mixture was stirred at 140 °C for 1 h under microwave irradiation. The mixture was cooled to the room temperature which led to precipitate formation. The precipitate was collected through vacuum filtration, dissolved in 2 M NaOH (30 mL) and extracted with DCM (3 × 30 mL). The organic layers were merged, washed with brine, dried over Na_2SO_4 and evaporated to afford the desired compound.

Yield:	50 mg (25%)
Chemical formula:	$C_{20}H_{28}ClN_5O$
Molecular mass:	389.93 g/mol
Appearance	Beige solid
Internal code:	MG-202, ST-2702
^{1}H NMR (600 MHz, $CDCl_3$):	δ 7.85 (s, 1H), 7.46 – 7.42 (m, 2H), 6.89 – 6.84 (m, 2H), 6.83 (s, 1H), 5.17 (t, *J* = 5.5 Hz, 1H), 3.98 (t, *J* = 6.4 Hz, 2H), 3.51 (qd, *J* = 7.2, 5.5 Hz, 2H), 2.50 – 2.46 (m, 2H), 2.40 (s, 4H), 2.00 – 1.93 (m, 2H), 1.59 (p, *J* = 5.6 Hz, 4H), 1.44 (s, 2H), 1.27 (t, *J* = 7.2 Hz, 3H)
^{13}C NMR (151 MHz, $CDCl_3$):	δ 158.61, 157.90, 154.75, 153.00, 133.09, 121.33, 114.89, 104.47, 67.01, 56.20, 54.79, 36.02, 27.04, 26.12, 24.57, 14.89
Melting point	112.3 °C
MS (APCI-(+)):	m/z = 309.2 $[M+H^+]^+$
LC-MS-DAD purity:	96.39%
MS (ESI-(+)):	m/z = 390.2050 $[M+H^+]^+$ (calculated: 390.2055)

5-Chloro-N^4-ethyl-N^2-(3-methoxy-4-(3-(piperidin-1-yl)propoxy)phenyl)pyrimidine-2,4-diamine (49)

To a solution of 2,5-dichloro-*N*-ethylpyrimidin-4-amine **(P29)** (100 mg, 0.52 mmol, 1.0 eq.) and 3-methoxy-4-(3-(piperidin-1-yl)propoxy)aniline (**P15**) (151 mg, 0.57 mmol, 1.1 eq.) in 2.2 mL of isopropanol in a microwave vial, 0.1 mL of TFA was added at room temperature. The vial containing reaction mixture was transferred to the microwave reactor where the reaction mixture was stirred at 140 °C for 1 h under microwave irradiation. The mixture was cooled to the room temperature which led to precipitate formation. The precipitate was collected through vacuum filtration, dissolved in 2 M NaOH (30 mL) and extracted with DCM (3 × 30 mL). The organic layers were merged, washed with brine, dried over Na_2SO_4 and evaporated to afford the desired compound.

Yield:	120 mg (55%)
Chemical formula:	$C_{21}H_{30}ClN_5O_2$
Molecular mass:	419.95 g/mol
Appearance	Beige solid
Internal code:	MG-200, ST-2710
^{1}H NMR (600 MHz, $CDCl_3$):	δ 7.87 (s, 1H), 7.35 (d, *J* = 2.5 Hz, 1H), 7.04 (s, 1H), 6.92 (dd, *J* = 8.6, 2.5 Hz, 1H), 6.85 (d, *J* = 8.6 Hz, 1H), 5.20 (t, *J* = 5.4 Hz, 1H), 4.04 (t, *J* = 6.7 Hz, 2H), 3.85 (s, 3H), 3.54 (qd, *J* = 7.3, 5.5 Hz, 2H), 2.50 (t, *J* = 7.5 Hz, 2H), 2.41 (s, 4H), 2.01 (p, *J* = 6.9 Hz, 2H), 1.59 (p, *J* = 5.6 Hz, 4H), 1.44 (q, *J* = 5.9 Hz, 2H), 1.27 (t, *J* = 7.3 Hz, 3H).
^{13}C NMR (151 MHz, $CDCl_3$):	δ 158.50, 157.90, 153.02, 149.75, 143.97, 134.04, 114.35, 111.48, 105.08, 104.48, 68.46, 56.05, 56.00, 54.68, 36.03, 26.86, 26.02, 24.51, 14.94
Melting point	79.4 °C
MS (APCI-(+)):	m/z = 419.8, 421.8 $[M+H^+]^+$
LC-MS-DAD purity:	100.00%
HRMS (ESI-(+)):	m/z = 420.2155 $[M+H^+]^+$ (calculated: 420.2161)

5-Chloro-N^4-ethyl-N^2-(4-methoxy-3-(3-(piperidin-1-yl)propoxy)phenyl)pyrimidine-2,4-diamine (50)

To a solution of 2,5-dichloro-*N*-ethylpyrimidin-4-amine (**P29**) (100 mg, 0.52 mmol, 1.0 eq.) and 4-methoxy-3-(3-(piperidin-1-yl)propoxy)aniline (**P16**) (151 mg, 0.57 mmol, 1.1 eq.) in 1.0 mL of isopropanol in a microwave vial, 0.1 mL of TFA was added at room temperature. The vial containing reaction mixture was transferred to the microwave reactor where the

reaction mixture was stirred at 140 °C for 1 h under microwave irradiation. The mixture was cooled to the room temperature which led to precipitate formation. The precipitate was collected through vacuum filtration, dissolved in 2 M NaOH (30 mL) and extracted with DCM (3 × 30 mL). The organic layers were merged, washed with brine, dried over Na_2SO_4 and evaporated to afford the desired compound.

Yield:	73 mg (33%)
Chemical formula:	$C_{21}H_{30}ClN_5O_2$
Molecular mass:	419.95 g/mol
Appearance	Brown solid
Internal code:	MG-197, ST-2709
^{1}H NMR (300 MHz, $CDCl_3$):	δ 7.87 (s, 1H), 7.34 (d, *J* = 2.5 Hz, 1H), 6.96 (dd, *J* = 8.6, 2.4 Hz, 2H), 6.81 (d, *J* = 8.7 Hz, 1H), 5.19 (t, *J* = 5.5 Hz, 1H), 4.06 (t, *J* = 6.7 Hz, 2H), 3.83 (s, 3H), 3.53 (qd, *J* = 7.3, 5.5 Hz, 2H), 2.49 (dd, *J* = 8.4, 6.5 Hz, 2H), 2.40 (s, 4H), 2.04 (dq, *J* = 8.9, 6.8 Hz, 2H), 1.58 (p, *J* = 5.6 Hz, 4H), 1.51 – 1.38 (m, 2H), 1.28 (t, *J* = 7.2 Hz, 3H).
^{13}C NMR (75 MHz, $CDCl_3$):	δ 158.49, 157.90, 148.73, 145.09, 133.83, 112.60, 111.66, 106.50, 104.50, 101.56, 67.73, 56.07, 54.72, 53.55, 36.04, 26.85, 26.07, 24.55, 14.96.
Melting point	84.2 °C
MS (APCI-(+)):	m/z = 419.8, 421.8 $[M+H^+]^+$
LC-MS-DAD purity:	100.00%
HRMS (ESI-(+)):	m/z = 420.2155 $[M+H^+]^+$ (calculated: 420.2161)

5-Chloro-*N*^{4}-ethyl-*N*^{2}-(2-methoxy-4-(3-(piperidin-1-yl)propoxy)phenyl)pyrimidine-2,4-diamine (51)

To a solution of 2,5-dichloro-*N*-ethylpyrimidin-4-amine (**P29**) (80 mg, 0.42 mmol, 1.0 eq.) and 2-methoxy-4-(3-(piperidin-1-yl)propoxy)aniline (**P17**) (121 mg, 0.46 mmol, 1.1 eq.) in 2 mL of isopropanol in a microwave vial, 0.1 mL of TFA was added at room temperature. The reaction mixture was stirred at room temperature for 24 h. After the TLC control indicated consumption of starting material, the solvent was evaporated, and the residue was partitioned between 1 M NaOH (30 mL) and ethyl acetate (3 × 30 mL). The organic layers were merged, washed with brine, dried over Na_2SO_4. After filtration solvent was evaporated, and the residue was purified using flash column chromatography (DCM:MeOH, 0-7% MeOH) in order to obtain desired product.

Yield:	60 mg (34%)

Chemical formula:	$C_{21}H_{30}ClN_5O_2$
Molecular mass:	419.95 g/mol
Appearance	Beige solid
Internal code:	MG-322, ST-2979

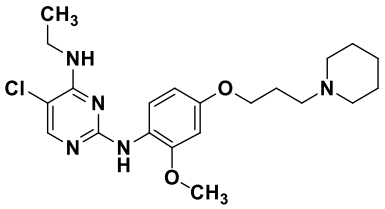

^{1}H NMR (300 MHz, DMSO):	δ 8.24 (d, *J* = 9.5 Hz, 1H), 7.87 (s, 1H), 7.23 (s, 1H), 6.54 – 6.44 (m, 2H), 5.16 (t, *J* = 5.4 Hz, 1H), 3.99 (t, *J* = 6.4 Hz, 2H), 3.85 (s, 3H), 3.55 (qd, *J* = 7.2, 5.3 Hz, 2H), 2.54 – 2.35 (m, 6H), 2.05 – 1.90 (m, 3H), 1.60 (p, *J* = 5.5 Hz, 4H), 1.45 (q, *J* = 6.2 Hz, 2H), 1.29 (t, *J* = 7.2 Hz, 4H)
^{13}C NMR (151 MHz, DMSO):	δ 158.43, 157.91, 154.45, 153.03, 149.30, 123.27, 119.41, 104.58, 104.26, 99.36, 67.07, 56.21, 55.83, 54.79, 36.11, 27.06, 26.10, 24.57, 14.91
Melting point	97.2 °C
MS (APCI-(+)):	m/z = 419.9, 421.7 $[M+H^+]^+$
LC-MS-DAD purity:	98.36%
HRMS (ESI-(+)):	m/z = 420.2174 $[M+H^+]^+$ (calculated: 420.2161)

2,5-Dichloro-*N*-(4-(3-(4-methylpiperazin-1-yl)propoxy)phenyl)pyrimidin-4-amine hydrochloride (P31)

2,4,5-Trichloropyrimidine (200 mg, 1.09 mmol, 1.0 eq.) and 1-methyl-4-(3-(4-nitrophenoxy)propyl)piperazine (**P12**) (304 mg, 1.2 mmol, 1.1 eq.) were dissolved in 2.2 mL of isopropanol in a microwave vial at room temperature. The vial containing reaction mixture was transferred to the microwave reactor where the reaction mixture was stirred at 50 °C for 1 h under microwave irradiation which led to precipitation. The precipitate was collected through vacuum filtration and washed with isopropanol to afford the desired compound that was used in the next reaction step without further purification.

Yield:	302 mg (73%)
Chemical formula:	$C_{18}H_{24}Cl_3N_5O$
Molecular mass:	432.77 g/mol
Appearance	White solid
Internal code:	MG-223

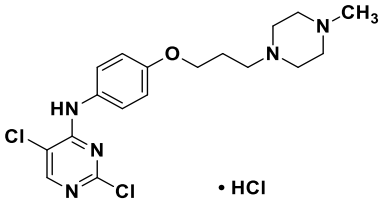

^{1}H NMR (300 MHz, DMSO):	δ 11.88 (s, 1H), 9.45 (s, 1H), 8.32 (s, 1H), 7.44 (d, *J* = 9.0 Hz, 2H), 6.99 (d, *J* = 9.0 Hz, 2H), 4.09 (t, *J* = 6.0 Hz, 2H), 3.95 – 3.40 (m, 10H), 2.82 (s, 3H), 2.31 – 2.08 (m, 2H)
MS (APCI-(+)):	m/z = 395.7, 397.7 $[M+H^+]^+$

1-(4-(3-(4-((2,5-Dichloropyrimidin-4-yl)amino)phenoxy)propyl)piperazin-1-yl)ethan-1-one (P32)

2,4,5-Trichloropyrimidine (150 mg, 0.82 mmol, 1.0 eq.) and 1-(4-(3-(4-aminophenoxy)propyl)piperazin-1-yl)ethan-1-one (**P13**) (250 mg, 0.90 mmol, 1.1 eq.) were dissolved in 3 mL of isopropanol in a microwave vial at room temperature. The vial containing reaction mixture was transferred to the microwave reactor where the reaction mixture was stirred at 50 °C for 1 h under microwave irradiation. After the TLC control indicated consumption of starting material, the solvent was evaporated, and the residue was partitioned between 2 M NaOH (30 mL) and DCM (3 × 30 mL). The organic layers were merged, washed with brine, dried over $MgSO_4$. After filtration solvent was evaporated to afford the desired compound.

Yield:	360 mg (quant.)
Chemical formula:	$C_{19}H_{23}Cl_2N_5O_2$
Molecular mass:	424.33
Appearance	Brown resin
Internal code:	MG-336

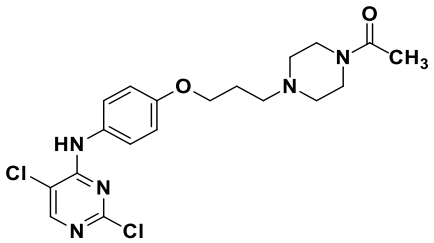

^{1}H NMR (300 MHz, $CDCl_3$):	δ 8.15 (s, 1H), 7.47 (d, *J* = 9.0 Hz, 2H), 7.16 (s, 1H), 6.92 (d, *J* = 9.0 Hz, 2H), 4.04 (t, *J* = 6.3 Hz, 2H), 3.62 (t, *J* = 5.2 Hz, 2H), 3.47 (t, *J* = 4.9 Hz, 2H), 2.60 – 2.51 (m, 2H), 2.50 – 2.39 (m, 4H), 2.09 (s, 3H), 2.05 – 1.90 (m, 2H)
MS (APCI-(+)):	m/z = 423.5, 425.4 $[M+H^+]^+$

2,5-Dichloro-*N*-(4-(3-(piperidin-1-yl)propoxy)phenyl)pyrimidin-4-amine hydrochloride (P33)

2,4,5-Trichloropyrimidine (314 mg, 1.71 mmol, 1.0 eq.) and 4-(3-(piperidin-1-yl)propoxy)aniline (**P14**) (441 mg, 1.88 mmol, 1.1 eq.) were dissolved in 3 mL of isopropanol in a microwave vial at room temperature. The vial containing reaction mixture was transferred to the microwave reactor where the reaction mixture was stirred at 50 °C for 1 h under microwave irradiation which led to precipitation. The mixture was cooled to the room temperature. The precipitate was collected through vacuum filtration and washed with EtOAc to afford the desired compound that was used in the next reaction step without further purification.

Yield:	709 mg (99%)
Chemical formula:	$C_{18}H_{23}Cl_3N_4O$
Molecular mass:	417.76 g/mol
Appearance	Beige solid
Internal code:	MG-238

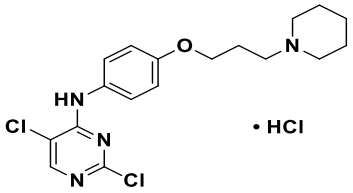

^{1}H NMR (300 MHz, DMSO):	δ 10.53 (s, 1H), 9.46 (s, 1H), 8.32 (s, 1H), 7.44 (d, *J* = 8.9 Hz, 2H), 6.97 (d, *J* = 9.0 Hz, 2H), 4.07 (t, *J* = 6.0 Hz, 2H), 3.57 – 3.39 (m, 2H), 3.15 (t, *J* = 8.2 Hz, 2H), 2.87 (s, 2H), 2.21 (dt, *J* = 10.6, 5.9 Hz, 2H), 2.00 – 1.63 (m, 5H), 1.39 (s, 1H)
MS (APCI-(+)):	m/z = 380.8, 382.8 $[M+H^+]^+$

2,5-Dichloro-*N*-(3-methoxy-4-(3-(piperidin-1-yl)propoxy)phenyl)pyrimidin-4-amine hydrochloride (P34)

2,4,5-Trichloropyrimidine (200 mg, 1.09 mmol, 1.0 eq.) and 3-methoxy-4-(3-(piperidin-1-yl)propoxy)aniline (**P15**) (317 mg, 1.20 mmol, 1.1 eq.) were dissolved in 2.2 mL of isopropanol in a microwave vial at room temperature. The vial containing reaction mixture was transferred to the microwave reactor where the reaction mixture was stirred at 50 °C for 1 h under microwave irradiation which led to precipitation. The precipitate was collected through vacuum filtration and washed with isopropanol to afford the desired compound that was used in the next reaction step without further purification.

Yield:	390 mg (80%)
Chemical formula:	$C_{19}H_{25}Cl_3N_4O_2$
Molecular mass:	447.79 g/mol
Appearance	Red solid
Internal code:	MG-224

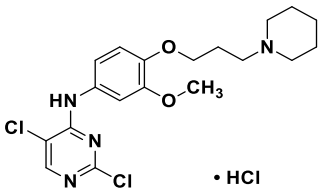

^{1}H NMR (300 MHz, DMSO):	δ 10.35 (s, 1H), 9.43 (s, 1H), 8.34 (s, 1H), 7.26 (d, *J* = 2.4 Hz, 1H), 7.14 (dd, *J* = 8.7, 2.4 Hz, 1H), 7.00 (d, *J* = 8.7 Hz, 1H), 4.05 (t, *J* = 6.0 Hz, 2H), 3.76 (s, 3H), 3.52 (s, 2H), 3.15 (t, *J* = 8.0 Hz, 2H), 2.88 (s, 2H), 2.19 (dq, *J* = 11.9, 6.0 Hz, 2H), 1.92 – 1.61 (m, 5H), 1.54 – 1.28 (m, 1H)
MS (APCI-(+)):	m/z = 411.0, 413.0 $[M+H^+]^+$

2,5-Dichloro-*N*-(4-methoxy-3-(3-(piperidin-1-yl)propoxy)phenyl)pyrimidin-4-amine hydrochloride (P35)

2,4,5-Trichloropyrimidine (200 mg, 1.09 mmol, 1.0 eq.) and 4-methoxy-3-(3-(piperidin-1-yl)propoxy)aniline (**P16**) (317 mg, 1.20 mmol, 1.1 eq.) were dissolved in 2.2 mL of isopropanol in a microwave vial at room temperature. The vial containing reaction mixture was transferred to the microwave reactor where the reaction mixture was stirred at 50 °C for 1 h under microwave irradiation. Subsequently, the solvent was evaporated and the residue was purified using flash column chromatography (DCM:MeOH, 0-10% MeOH) to obtain the desired product.

Yield:	425 mg (87%)
Chemical formula:	$C_{19}H_{25}Cl_3N_4O_2$
Molecular mass:	447.79 g/mol
Appearance	Red solid
Internal code:	MG-222
^{1}H NMR (300 MHz, DMSO):	δ 10.29 (s, 1H), 9.43 (s, 1H), 8.33 (s, 1H), 7.23 (d, *J* = 2.4 Hz, 1H), 7.14 (dd, *J* = 8.7, 2.4 Hz, 1H), 7.00 (d, *J* = 8.7 Hz, 1H), 4.02 (t, *J* = 6.0 Hz, 2H), 3.78 (s, 3H), 3.24 – 2.69 (m, 5H), 2.21 (q, *J* = 6.9 Hz, 2H), 1.90 – 1.72 (m, 4H), 1.41 (s, 1H), 1.19 (t, *J* = 7.3 Hz, 1H), 1.03 (d, *J* = 6.2 Hz, 1H)
MS (APCI-(+)):	m/z = 410.9, 412.9 $[M+H^+]^+$

2,5-Dichloro-*N*-(2-methoxy-4-(3-(piperidin-1-yl)propoxy)phenyl)pyrimidin-4-amine hydrochloride (P36)

2,4,5-Trichloropyrimidine (199 mg, 0.55 mmol, 1.0 eq.) and 2-methoxy-4-(3-(piperidin-1-yl)propoxy)aniline (**P17**) (159 mg, 0.60 mmol, 1.1 eq.) were dissolved in 2.2 mL of isopropanol in a microwave vial at room temperature. The vial containing reaction mixture was transferred to the microwave reactor where the reaction mixture was stirred at 50 °C for 1 h under microwave irradiation which led to precipitation. The precipitate was collected through vacuum filtration and washed with isopropanol to afford the desired compound that was used in the next reaction step without further purification.

Yield:	200 mg (82%)
Chemical formula:	$C_{19}H_{24}Cl_2N_4O_2$
Molecular mass:	447.79 g/mol
Appearance	White solid

Internal code:	MG-325

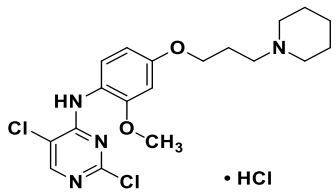

^{1}H NMR (300 MHz, DMSO):	δ 10.43 (s, 1H), 8.98 (s, 1H), 8.29 (s, 1H), 7.32 (d, *J* = 8.6 Hz, 1H), 6.69 (d, *J* = 2.6 Hz, 1H), 6.58 (dd, *J* = 8.7, 2.6 Hz, 1H), 4.10 (t, *J* = 6.0 Hz, 2H), 3.78 (s, 3H), 3.55 – 3.40 (m, 2H), 3.25 – 3.08 (m, 2H), 2.98 – 2.79 (m, 2H), 2.30 – 2.15 (m, 2H), 1.93 – 1.64 (m, 5H), 1.50 – 1.28 (m, 1H)
MS (APCI-(+)):	m/z = 410.8, 412.7 $[M+H^+]^+$

5-Chloro-N^2-methyl-N^4-(4-(3-(4-methylpiperazin-1-yl)propoxy)phenyl)pyrimidine-2,4-diamine (52)

A solution of 2,5-dichloro-*N*-(4-(3-(4-methylpiperazin-1-yl)propoxy)phenyl)pyrimidin-4-amine hydrochloride (**P31**) (167 mg, 0.42 mmol, 1.0 eq.) and methylamine hydrochloride (142 mg, 2.11 mmol, 5.0 eq.) in 3 mL of isopropanol was treated with DIPEA (0.22 mL, 1.26 mmol, 3.0 eq.). The vial containing reaction mixture was transferred to the microwave reactor where the reaction mixture was stirred at 140 °C for 4 h under microwave irradiation. After TLC control indicated consumption of starting material, solvent was evaporated, and the residue was partitioned between water and ethyl acetate. The combined organic layers were washed with brine and dried over Na_2SO_4. After filtration, solvent was evaporated under reduced pressure and the residue was purified using flash column chromatography (DCM:MeOH, 0-10% MeOH) to obtain the desired product.

Yield:	50 mg (30%)
Chemical formula:	$C_{19}H_{27}ClN_6O$
Molecular mass:	390.92 g/mol
Appearance	White solid
Internal code:	MG-267, ST-2883

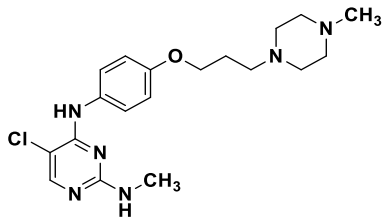

^{1}H NMR (300 MHz, DMSO):	δ 8.41 (s, 1H), 7.90 (s, 1H), 7.59 (d, *J* = 8.4 Hz, 2H), 6.86 (d, *J* = 9.1 Hz, 2H), 6.76 (s, 1H), 3.96 (t, *J* = 6.4 Hz, 2H), 2.70 (d, *J* = 4.8 Hz, 3H), 2.48 – 2.22 (m, 10H), 2.16 (s, 3H), 1.84 (p, *J* = 6.6 Hz, 2H)
^{13}C NMR (75 MHz, DMSO):	δ 161.06, 155.87, 155.00, 132.25, 129.00, 124.03, 114.29, 102.26, 66.20, 54.94, 54.67, 52.88, 45.88, 28.35, 26.54
Melting point	138.9 °C
MS (APCI-(+)):	m/z = 391.2 $[M+H^+]^+$

LC-MS-DAD purity:	99.24%
MS (ESI-(+)):	m/z = 391.2008 $[M+H^+]^+$ (calculated: 391.2008)

1-(4-(3-(4-((5-Chloro-2-(methylamino)pyrimidin-4-yl)amino)phenoxy)propyl)piperazin-1-yl)ethan-1-one (53)

A solution of 1-(4-(3-(4-((2,5-Dichloropyrimidin-4-yl)amino)phenoxy)propyl)piperazin-1-yl)ethan-1-one (**P32**) (150 mg, 0.35 mmol, 1.0 eq.) and methylamine hydrochloride (239 mg, 3.53 mmol, 10.0 eq.) in 3 mL of isopropanol was stirred at 140 °C for 14 h under microwave irradiation. After the TLC control indicated consumption of starting material, the solvent was evaporated, and the residue was partitioned between 1 M NaOH (30 mL) and DCM (3 × 30 mL). The organic layers were merged, washed with brine, dried over $MgSO_4$. After filtration solvent was evaporated, and the residue was purified using flash column chromatography (DCM:MeOH, 0-7% MeOH) in order to obtain desired product.

Yield:	77 mg (52%)
Chemical formula:	$C_{20}H_{27}ClN_6O_2$
Molecular mass:	418.93 g/mol
Appearance	White solid
Internal code:	MG-339, ST-2982

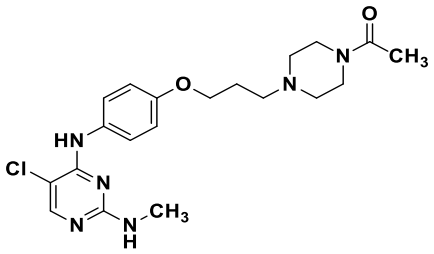

^{1}H NMR (300 MHz, $CDCl_3$):	δ 7.92 (s, 1H), 7.51 (d, *J* = 8.8 Hz, 2H), 6.87 (d, *J* = 8.9 Hz, 3H), 4.92 (d, *J* = 5.9 Hz, 1H), 4.02 (t, *J* = 6.3 Hz, 2H), 3.62 (t, *J* = 5.1 Hz, 2H), 3.46 (t, *J* = 4.8 Hz, 2H), 2.92 (d, *J* = 5.1 Hz, 3H), 2.54 (t, *J* = 7.2 Hz, 2H), 2.44 (dt, *J* = 10.1, 5.1 Hz, 4H), 2.08 (s, 3H), 2.04 – 1.91 (m, 2H)
^{13}C NMR (75 MHz, $CDCl_3$):	δ 169.03, 161.24, 155.81, 155.62, 154.13, 131.49, 122.88, 114.76, 66.29, 55.10, 53.52, 52.92, 46.43, 41.54, 28.78, 26.85, 21.45
Melting point	152.1 °C
MS (APCI-(+)):	m/z = 418.7, 420.5 $[M+H^+]^+$
LC-MS-DAD purity:	100.00%
HRMS (ESI-(+)):	m/z = 419.1961 $[M+H^+]^+$ (calculated: 419.1957)

5-Chloro-*N*^{2}-methyl-*N*^{4}-(4-(3-(piperidin-1-yl)propoxy)phenyl)pyrimidine-2,4-diamine (54)

A solution of 2,5-dichloro-*N*-(4-(3-(piperidin-1-yl)propoxy)phenyl)pyrimidin-4-amine hydrochloride (**P33**) (200 mg, 0.48 mmol, 1.0 eq.) and methylamine hydrochloride (65 mg,

0.96 mmol, 2.0 eq.) in 3 mL of isopropanol was treated with DIPEA (0.25 mL, 1.44 mmol, 3.0 eq.). The vial containing reaction mixture was transferred to the microwave reactor where the reaction mixture was stirred at 90 °C for 6 h under microwave irradiation. After TLC control indicated consumption of starting material, solvent was evaporated, and the residue was partitioned between water and ethyl acetate. The combined organic layers were washed with brine and dried over Na_2SO_4. After filtration, solvent was evaporated under reduced pressure and the residue was purified using flash column chromatography (DCM:MeOH, 0-10% MeOH) to obtain the desired product.

Yield:	40 mg (22%)
Chemical formula:	$C_{19}H_{26}ClN_5O$
Molecular mass:	375.90 g/mol
Appearance	Beige solid
Internal code:	MG-236, ST-2877

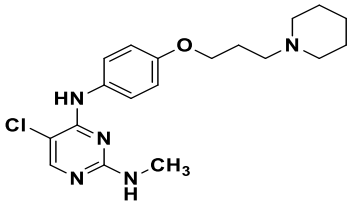

^{1}H NMR (300 MHz, DMSO):	δ 8.41 (s, 1H), 7.90 (s, 1H), 7.60 (d, *J* = 8.4 Hz, 2H), 6.87 (d, *J* = 8.9 Hz, 2H), 6.76 (s, 1H), 3.97 (t, *J* = 6.3 Hz, 2H), 2.70 (d, *J* = 4.7 Hz, 3H), 2.48 – 2.29 (m, 6H), 1.86 (p, *J* = 6.7, 6.1 Hz, 2H), 1.51 (p, *J* = 5.4 Hz, 4H), 1.45 – 1.33 (m, 2H)
^{13}C NMR (75 MHz, DMSO):	δ 160.80, 155.58, 154.69, 154.33, 138.08, 132.00, 123.73, 114.01, 65.95, 55.02, 53.93, 28.06, 26.07, 25.30, 23.87
Melting point	95.5 °C
MS (APCI-(+)):	m/z = 375.7, 377.7 $[M+H^+]^+$
LC-MS-DAD purity:	100.00%
HRMS (ESI-(+)):	m/z = 376.1897 $[M+H^+]^+$ (calculated: 376.1899)

5-Chloro-*N*^{4}-(3-methoxy-4-(3-(piperidin-1-yl)propoxy)phenyl)-*N*^{2}-methylpyrimidine-2,4-diamine (55)

A solution of 2,5-dichloro-*N*-(3-methoxy-4-(3-(piperidin-1-yl)propoxy)phenyl)pyrimidin-4-amine hydrochloride (**P34**) (200 mg, 0.45 mmol, 1.0 eq.) and methylamine hydrochloride (151 mg, 2.23 mmol, 5.0 eq.) in 3 mL of isopropanol was treated with DIPEA (0.23 mL, 1.34 mmol, 3.0 eq.). The vial containing reaction mixture was transferred to the microwave reactor where the reaction mixture was stirred at 140 °C for 4 under microwave irradiation. After TLC control indicated consumption of starting material, solvent was evaporated, and the residue was partitioned between water and ethyl acetate. The combined organic layers were washed with brine and dried over Na_2SO_4. After filtration, solvent was evaporated under reduced pressure

and the residue was purified using flash column chromatography (DCM:MeOH, 0-10% MeOH) to obtain the desired product.

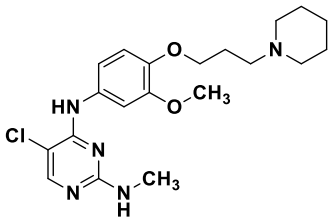

Yield:	100 mg (55%)
Chemical formula:	$C_{20}H_{28}ClN_5O_2$
Molecular mass:	405.93 g/mol
Appearance	White solid
Internal code:	MG-251, ST-2882
^{1}H NMR (300 MHz, DMSO):	δ 8.37 (s, 1H), 7.92 (s, 1H), 7.48 (s, 1H), 7.25 (dd, *J* = 8.6, 2.4 Hz, 1H), 6.95 – 6.73 (m, 2H), 3.94 (t, *J* = 6.4 Hz, 2H), 3.75 (s, 3H), 2.74 (d, *J* = 4.7 Hz, 3H), 2.37 (dd, *J* = 14.6, 7.3 Hz, 6H), 1.83 (p, *J* = 6.7 Hz, 2H), 1.49 (p, *J* = 5.5 Hz, 4H), 1.44 – 1.32 (m, 2H)
^{13}C NMR (75 MHz, DMSO):	δ 155.42, 148.59, 146.67, 144.26, 144.04, 141.97, 135.07, 132.72, 128.37, 113.26, 67.09, 55.18, 54.08, 28.15, 26.43, 25.55, 24.09, 20.01
Melting point	211.0 °C
MS (APCI-(+)):	m/z = 406.1, 408.1 $[M+H^+]^+$
LC-MS-DAD purity:	98.81%
HRMS (ESI-(+)):	m/z = 406.2019 $[M+H^+]^+$ (calculated: 406.2004)

5-Chloro-*N*^{4}-(4-methoxy-3-(3-(piperidin-1-yl)propoxy)phenyl)-*N*^{2}-methylpyrimidine-2,4-diamine (56)

A solution of 2,5-dichloro-*N*-(4-methoxy-3-(3-(piperidin-1-yl)propoxy)phenyl)pyrimidin-4-amine hydrochloride (**P35**) (150 mg, 0.36 mmol, 1.0 eq.) and methylamine hydrochloride (123 mg, 1.82 mmol, 5.0 eq.) in 3 mL of isopropanol was treated with DIPEA (0.19 mL, 1.09 mmol, 3 eq.). The vial containing reaction mixture was transferred to the microwave reactor where the reaction mixture was stirred at 140 °C for 4 under microwave irradiation. After TLC control indicated consumption of starting material, solvent was evaporated, and the residue was partitioned between water and ethyl acetate. The combined organic layers were washed with brine and dried over Na_2SO_4. After filtration, solvent was evaporated under reduced pressure and the residue was purified using flash column chromatography (DCM:MeOH, 0-10% MeOH) to obtain the desired product.

Yield:	138 mg (93%)
Chemical formula:	$C_{20}H_{28}ClN_5O_2$
Molecular mass:	405.93 g/mol
Appearance	White solid

Internal code:	MG-246, ST-2879

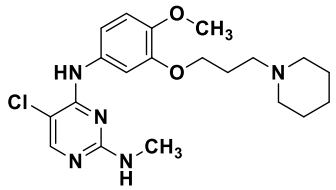

^{1}H NMR (300 MHz, DMSO):	δ 8.37 (s, 1H), 7.91 (s, 1H), 7.47 (s, 1H), 7.28 (dd, *J* = 8.8, 2.4 Hz, 1H), 6.98 – 6.68 (m, 2H), 3.96 (t, *J* = 6.6 Hz, 2H), 3.73 (s, 3H), 2.74 (d, *J* = 4.7 Hz, 3H), 2.43 – 2.23 (m, 6H), 1.86 (tt, *J* = 6.9, 6.8 Hz, 2H), 1.54 – 1.42 (m, 4H), 1.42 – 1.28 (m, 2H)
^{13}C NMR (75 MHz, DMSO):	δ 160.80, 155.45, 147.64, 139.21, 132.59, 124.98, 111.91, 55.92, 55.80, 55.15, 54.13, 26.37, 26.30, 25.58, 24.16
Melting point	117.4 °C
MS (APCI-(+)):	m/z = 405.6, 407.4 $[M+H^+]^+$
LC-MS-DAD purity:	98.14%
HRMS (ESI-(+)):	m/z = 406.2046 $[M+H^+]^+$ (calculated: 406.2004)

5-Chloro-*N*^{4}-(2-methoxy-4-(3-(piperidin-1-yl)propoxy)phenyl)-*N*^{2}-methylpyrimidine-2,4-diamine (57)

A solution of 2,5-dichloro-*N*-(2-methoxy-4-(3-(piperidin-1-yl)propoxy)phenyl)pyrimidin-4-amine hydrochloride (**P36**) (100 mg, 0.22 mmol, 1.0 eq.) and methylamine hydrochloride (151 mg, 2.23 mmol, 10.0 eq.) in 3 mL of isopropanol was stirred at 140 °C for 14 h under microwave irradiation. After the TLC control indicated consumption of starting material, the solvent was evaporated, and the residue was partitioned between 1 M NaOH (30 mL) and ethyl acetate (3 × 30 mL). The organic layers were merged, washed with brine, dried over Na_2SO_4. After filtration solvent was evaporated, and the residue was purified using flash column chromatography (DCM:MeOH, 0-7% MeOH) in order to obtain desired product.

Yield:	46 mg (51%)
Chemical formula:	$C_{20}H_{28}ClN_5O_2$
Molecular mass:	405.93 g/mol
Appearance	Beige solid
Internal code:	MG-330, ST-2985

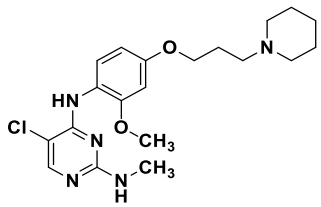

^{1}H NMR (300 MHz, $CDCl_3$):	δ 8.40 (d, *J* = 8.6 Hz, 1H), 7.91 (s, 1H), 7.56 (s, 1H), 6.57 – 6.39 (m, 2H), 4.90 (d, *J* = 5.2 Hz, 1H), 4.00 (t, *J* = 6.4 Hz, 2H), 3.90 (s, 3H), 2.98 (d, *J* = 5.1 Hz, 3H), 2.62 – 2.33 (m, 6H), 2.03 – 1.93 (m, 2H), 1.60 (p, *J* = 5.5 Hz, 4H), 1.45 (q, *J* = 5.9 Hz, 2H)

^{13}C NMR (151 MHz, $CDCl_3$):	δ 161.32, 155.47, 155.39, 153.79, 149.93, 121.94, 120.85, 104.51, 99.31, 67.05, 56.18, 56.07, 54.81, 28.92, 27.06, 26.13, 24.58
Melting point	126.5 °C
MS (APCI-(+)):	m/z = 406.0, 407.8 $[M+H^+]^+$
LC-MS-DAD purity:	100.00%
HRMS (ESI-(+)):	m/z = 406.2016 $[M+H^+]^+$ (calculated: 406.2004)

5-Chloro-*N*^{2}-ethyl-*N*^{4}-(4-(3-(4-methylpiperazin-1-yl)propoxy)phenyl)pyrimidine-2,4-diamine (58)

To a solution of 4,5-dichloro-*N*-ethylpyrimidin-2-amine (**P30**) (30 mg, 0.16 mmol, 1.0 eq.) and 1-methyl-4-(3-(4-nitrophenoxy)propyl)piperazine (**P12**) (43 mg, 0.17 mmol, 1.1 eq) in 3 mL of isopropanol in a microwave vial, 0.1 mL of TFA was added at room temperature. The reaction mixture was stirred at room temperature for 24 h. Subsequently, the solvent was evaporated, and the residue was partitioned between 1 M NaOH and DCM. The combined organic layers were washed with brine and dried over Na_2SO_4. After filtration, solvent was evaporated under reduced pressure and the residue was purified using through column chromatography (DCM:MeOH = 9:1) to obtain the desired product.

Yield:	29 mg (46%)
Chemical formula:	$C_{20}H_{29}ClN_6O$
Molecular mass:	404.94 g/mol
Appearance	Beige solid
Internal code:	MG-305, ST-2876

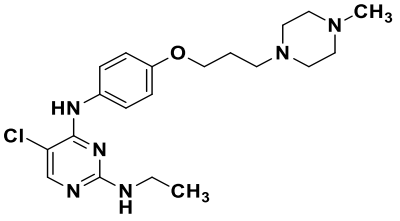

^{1}H NMR (300 MHz, $CDCl_3$):	δ 7.91 (s, 1H), 7.49 (d, *J* = 9.0 Hz, 2H), 6.93 – 6.80 (m, 3H), 4.87 (t, *J* = 5.2 Hz, 1H), 4.01 (t, *J* = 6.4 Hz, 2H), 3.36 (qd, *J* = 7.2, 5.6 Hz, 2H), 2.76 – 2.33 (m, 10H), 2.29 (s, 3H), 2.05 – 1.89 (m, 3H), 1.20 (t, *J* = 7.2 Hz, 3H)
^{13}C NMR (151 MHz, $CDCl_3$):	δ 160.57, 155.87, 155.73, 154.15, 131.41, 122.92, 114.81, 70.70, 66.72, 55.29, 53.37, 46.19, 36.71, 26.97, 15.06
Melting point	109.1 °C
MS (APCI-(+)):	m/z = 405.3, 407.3 $[M+H^+]^+$
LC-MS-DAD purity:	97.26%
HRMS (ESI-(+)):	m/z = 405.2172 $[M+H^+]^+$ (calculated: 405.2164)

1-(4-(3-(4-((5-Chloro-2-(ethylamino)pyrimidin-4-yl)amino)phenoxy)propyl)piperazin-1-yl)ethan-1-one (59)

A solution of 1-(4-(3-(4-((2,5-dichloropyrimidin-4-yl)amino)phenoxy)propyl)piperazin-1-yl)ethan-1-one **(P32)** (150 mg, 0.35 mmol, 1.0 eq.) and ethylamine hydrochloride (288 mg, 3.53 mmol, 10.0 eq.) in 3 mL of isopropanol was stirred at 140 °C for 14 h under microwave irradiation. After the TLC control indicated consumption of starting material, the solvent was evaporated, and the residue was partitioned between 1 M NaOH (30 mL) and ethyl acetate (3 × 30 mL). The organic layers were merged, washed with brine, dried over Na_2SO_4. After filtration solvent was evaporated, and the residue was purified using flash column chromatography (DCM:MeOH, 0-7% MeOH) in order to obtain desired product.

Yield:	61 mg (40%)
Chemical formula:	$C_{21}H_{29}ClN_6O_2$
Molecular mass:	432.95 g/mol
Appearance	White solid
Internal code:	MG-338, ST-2981

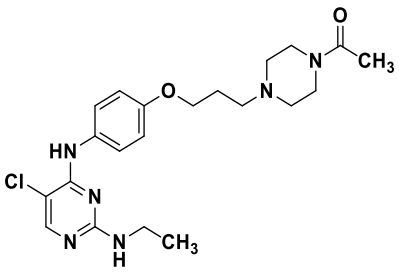

^{1}H NMR (300 MHz, $CDCl_3$):	δ 7.91 (s, 1H), 7.49 (d, *J* = 8.9 Hz, 2H), 6.95 – 6.83 (m, 3H), 4.90 (s, 1H), 4.02 (t, *J* = 6.3 Hz, 2H), 3.68 – 3.59 (m, 2H), 3.51 – 3.44 (m, 2H), 3.36 (qd, *J* = 7.2, 5.6 Hz, 2H), 2.60 – 2.51 (m, 2H), 2.45 (dt, *J* = 10.0, 5.1 Hz, 4H), 2.08 (s, 3H), 1.97 (dt, *J* = 13.1, 6.3 Hz, 2H), 1.19 (t, *J* = 7.2 Hz, 3H)
^{13}C NMR (75 MHz, $CDCl_3$):	δ 169.03, 160.52, 155.84, 155.63, 154.09, 131.50, 122.89, 114.76, 66.38, 55.11, 53.52, 52.92, 46.39, 41.51, 36.69, 26.82, 21.45, 15.05
Melting point	136.4 °C
MS (APCI-(+)):	m/z = 432.5, 434.2 $[M+H^+]^+$
LC-MS-DAD purity:	100.00%
HRMS (ESI-(+)):	m/z = 433.2119 $[M+H^+]^+$ (calculated: 433.2113)

5-Chloro-N^2-ethyl-N^4-(4-(3-(piperidin-1-yl)propoxy)phenyl)pyrimidine-2,4-diamine (60)

A solution of 2,5-dichloro-*N*-(4-(3-(piperidin-1-yl)propoxy)phenyl)pyrimidin-4-amine hydrochloride (**P33**) (200 mg, 0.48 mmol, 1.0 eq.) and ethylamine hydrochloride (195 mg, 2.39 mmol, 5.0 eq.) in 3 mL of isopropanol was treated with DIPEA (0.25 mL, 1.44 mmol, 3.0 eq.). The vial containing reaction mixture was transferred to the microwave reactor where the reaction mixture was stirred at 140 °C for 4 h under microwave irradiation. After TLC control indicated consumption of starting material, solvent was evaporated, and the residue was

partitioned between water and ethyl acetate. The combined organic layers were washed with brine and dried over Na_2SO_4. After filtration, solvent was evaporated under reduced pressure and the residue was purified using flash column chromatography (DCM:MeOH, 0-10% MeOH) to obtain the desired product.

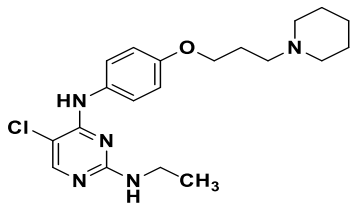

Yield:	169 mg (91%)
Chemical formula:	$C_{20}H_{28}ClN_5O$
Molecular mass:	389.93 g/mol
Appearance	White solid
Internal code:	MG-243, ST-2878
^{1}H NMR (300 MHz, DMSO):	δ 8.40 (s, 1H), 7.89 (s, 1H), 7.57 (d, *J* = 8.6 Hz, 2H), 6.99 – 6.71 (m, 3H), 3.96 (t, *J* = 6.4 Hz, 2H), 3.18 (p, *J* = 7.0 Hz, 2H), 2.43 – 2.23 (m, 6H), 1.92 – 1.77 (m, 2H), 1.59 – 1.44 (m, 4H), 1.44 – 1.31 (m, 2H), 1.06 (t, *J* = 7.1 Hz, 3H)
^{13}C NMR (75 MHz, DMSO):	δ 160.16, 155.62, 154.70, 154.36, 146.75, 131.93, 121.96, 113.97, 66.04, 55.18, 54.13, 35.62, 26.36, 25.62, 24.16, 14.73
Melting point	112.6 °C
MS (APCI-(+)):	m/z = 389.7, 391.6 $[M+H^+]^+$
LC-MS-DAD purity:	98.71%
HRMS (ESI-(+)):	m/z = 390.2081 $[M+H^+]^+$ (calculated: 390.2055)

5-Chloro-*N*^{2}-ethyl-*N*^{4}-(3-methoxy-4-(3-(piperidin-1-yl)propoxy)phenyl)pyrimidine-2,4-diamine (61)

A solution of 2,5-dichloro-*N*-(3-methoxy-4-(3-(piperidin-1-yl)propoxy)phenyl)pyrimidin-4-amine hydrochloride (**P34**) (232 mg, 0.52 mmol, 1.0 eq.) and ethylamine hydrochloride (211 mg, 2.59 mmol, 5.0 eq.) in 3 mL of isopropanol was treated with DIPEA (0.27 mL, 1.55 mmol, 3.0 eq.). The vial containing reaction mixture was transferred to the microwave reactor where the reaction mixture was stirred at 140 °C for 4 under microwave irradiation. After TLC control indicated consumption of starting material, solvent was evaporated, and the residue was partitioned between water and ethyl acetate. The combined organic layers were washed with brine and dried over Na_2SO_4. After filtration, solvent was evaporated under reduced pressure and the residue was purified using flash column chromatography (DCM:MeOH, 0-10% MeOH) to obtain the desired product.

Yield:	155 mg (71%)
Chemical formula:	$C_{21}H_{30}ClN_5O_2$

Molecular mass:	419.95 g/mol
Appearance	White solid
Internal code:	MG-249, ST-2881

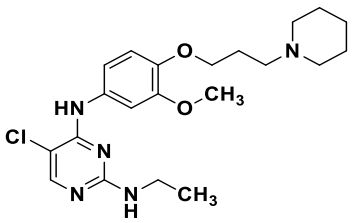

^{1}H NMR (300 MHz, DMSO):	δ 8.37 (s, 1H), 7.92 (s, 1H), 7.46 (s, 1H), 7.28 (dd, *J* = 8.7, 2.4 Hz, 1H), 6.90 (d, *J* = 8.8 Hz, 2H), 3.99 (t, *J* = 6.1 Hz, 2H), 3.76 (s, 3H), 3.27 – 3.18 (m, 2H), 3.18 – 2.52 (m, 6H), 2.16 – 1.94 (m, 2H), 1.78 – 1.61 (m, 4H), 1.58 – 1.35 (m, 2H), 1.08 (t, *J* = 7.1 Hz, 3H)
^{13}C NMR (75 MHz, DMSO):	δ 156.90, 152.72, 148.56, 145.59, 141.60, 135.92, 116.12, 113.08, 108.95, 66.33, 57.20, 53.61, 52.07, 36.02, 23.45, 22.42, 21.40, 14.17
Melting point	174.9 °C
MS (APCI-(+)):	m/z = 419.9, 421.8 $[M+H^+]^+$
LC-MS-DAD purity:	98.91%
HRMS (ESI-(+)):	m/z = 210.6165 $[M+2H^+]^{2+}$ (calculated: 210.6117)

5-Chloro-*N*^{2}-ethyl-*N*^{4}-(4-methoxy-3-(3-(piperidin-1-yl)propoxy)phenyl)pyrimidine-2,4-diamine (62)

A solution of 2,5-dichloro-*N*-(4-methoxy-3-(3-(piperidin-1-yl)propoxy)phenyl)pyrimidin-4-amine hydrochloride (**P35**) (130 mg, 0.32 mmol, 1.0 eq.) and ethylamine hydrochloride (129 mg, 1.58 mmol, 5.0 eq.) in 3 mL of isopropanol was treated with DIPEA (0.17 mL, 0.95 mmol, 3.0 eq.). The vial containing reaction mixture was transferred to the microwave reactor where the reaction mixture was stirred at 140 °C for 4 under microwave irradiation. After TLC control indicated consumption of starting material, solvent was evaporated, and the residue was partitioned between water and ethyl acetate. The combined organic layers were washed with brine and dried over Na_2SO_4. After filtration, solvent was evaporated under reduced pressure and the residue was purified using flash column chromatography (DCM:MeOH, 0-10% MeOH) to obtain the desired product.

Yield:	80 mg (60%)
Chemical formula:	$C_{21}H_{30}ClN_5O_2$
Molecular mass:	419.95 g/mol
Appearance	White solid
Internal code:	MG-247, ST-2880

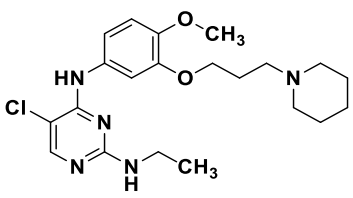

^{1}H NMR (300 MHz, DMSO):	δ 8.35 (s, 1H), 7.90 (s, 1H), 7.41 (s, 1H), 7.28 (dd, *J* = 8.7, 2.4 Hz, 1H), 6.87 (d, *J* = 8.8 Hz, 2H), 3.96 (t, *J* = 6.5 Hz, 2H), 3.73 (s, 3H), 3.29 – 3.16

	(m, 2H), 2.43 – 2.22 (m, 6H), 1.86 (tt, *J* = 6.7, 6.7 Hz, 2H), 1.54 – 1.43 (m, 4H), 1.43 – 1.30 (m, 2H), 1.08 (t, *J* = 7.1 Hz, 3H)
^{13}C NMR (75 MHz, MeOD):	δ 161.66, 157.75, 154.45, 149.59, 147.73, 133.70, 116.19, 113.46, 110.61, 68.77, 57.19, 56.87, 55.53, 37.33, 27.43, 26.49, 25.20, 15.19
Melting point	124.6 °C
MS (APCI-(+)):	m/z = 420.2 $[M+H^+]^+$
LC-MS-DAD purity:	98.73%
HRMS (ESI-(+)):	m/z = 420.2208 $[M+H^+]^+$ (calculated: 420.2161)

5-Chloro-*N*^{2}-ethyl-*N*^{4}-(2-methoxy-4-(3-(piperidin-1-yl)propoxy)phenyl)pyrimidine-2,4-diamine (63)

A solution of 2,5-dichloro-*N*-(2-methoxy-4-(3-(piperidin-1-yl)propoxy)phenyl)pyrimidin-4-amine hydrochloride **(P36)** (100 mg, 0.22 mmol, 1.0 eq.) and ethylamine hydrochloride (182 mg, 2.23 mmol, 10.0 eq.) in 3 mL of isopropanol was stirred at 140 °C for 14 h under microwave irradiation. After the TLC control indicated consumption of starting material, the solvent was evaporated, and the residue was partitioned between 1 M NaOH (30 mL) and ethyl acetate (3 × 30 mL). The organic layers were merged, washed with brine, dried over Na_2SO_4. After filtration solvent was evaporated, and the residue was purified using flash column chromatography (DCM:MeOH, 0-7% MeOH) in order to obtain desired product.

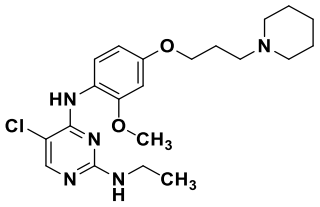

Yield:	46 mg (50%)
Chemical formula:	$C_{21}H_{30}ClN_5O_2$
Molecular mass:	419.95 g/mol
Appearance	Beige solid
Internal code:	MG-327, ST-2986
^{1}H NMR (300 MHz, $CDCl_3$):	δ 8.37 (d, *J* = 8.5 Hz, 1H), 7.90 (s, 1H), 7.55 (s, 1H), 6.50 (d, *J* = 8.4 Hz, 2H), 4.90 (s, 1H), 4.00 (t, *J* = 6.4 Hz, 2H), 3.89 (s, 3H), 3.41 (qd, *J* = 7.2, 5.5 Hz, 2H), 2.44 (dt, *J* = 19.7, 6.3 Hz, 6H), 2.03 – 1.92 (m, 3H), 1.59 (p, *J* = 5.5 Hz, 4H), 1.45 (q, *J* = 6.1 Hz, 2H), 1.24 (t, *J* = 7.2 Hz, 5H)
^{13}C NMR (151 MHz, $CDCl_3$):	δ 160.63, 155.48, 155.38, 153.81, 149.91, 121.95, 120.79, 104.49, 99.30, 67.05, 56.19, 56.06, 54.82, 36.81, 27.08, 26.16, 24.60, 15.09
Melting point	132.3 °C
MS (APCI-(+)):	m/z = 420.2 $[M+H^+]^+$
LC-MS-DAD purity:	99.70%
HRMS (ESI-(+)):	m/z = 420.2169 $[M+H^+]^+$ (calculated: 420.2161)

2-Chloro-*N*-methyl-5-(trifluoromethyl)pyrimidin-4-amine (P37)[405]

To a solution of 2,4-dichloro-5-(trifluoromethyl)pyrimidine (2.00 g, 9.22 mmol, 1.0 eq.) and DIPEA (4.8 mL, 27.65 mmol, 3.0 eq.) in 60 mL of ethanol methylamine hydrochloride (622 mg, 9.22 mmol, 1.0 eq.) was added, and the reaction mixture was stirred for 5 h at room temperature. Afterwards, solvent was evaporated, and the residue was partitioned between water and EtOAc. The organic layers were merged, washed with brine and dried over anhydrous Na_2SO_4. After filtration, solvent was evaporated under reduced pressure to obtain crude consisting of 2-methylamino and 4-methylamino substituted structural isomers. The identity of structural isomers separated using flash column chromatography (Hex:EtOAc, 0-40% EtOAc) was confirmed with ^{1}H-, ^{13}C-, ^{19}F-, HMBC- and NOESY-NMR spectrums.

Yield:	545 mg (28%)
Chemical formula:	$C_6H_5ClF_3N_3$
Molecular mass:	211.57 g/mol
Appearance	White solid
Internal code:	MG-244F1
R_f-value	0.13 (Hex:EtOAC 4:1)
^{1}H NMR (300 MHz, DMSO):	δ 8.36 (q, *J* = 1.0 Hz, 1H), 7.92 (s, 1H), 2.89 (d, *J* = 4.5 Hz, 3H)
MS (APCI-(+)):	m/z = 211.6, 213.6 $[M+H^+]^+$

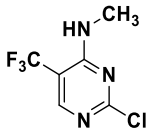

4-Chloro-*N*-methyl-5-(trifluoromethyl)pyrimidin-2-amine (P38)

The compound 4-chloro-*N*-methyl-5-(trifluoromethyl)pyrimidin-2-amine (**P38**) was obtained as a side product during the synthesis of compound **P37**.

Yield:	532 mg (27%)
Chemical formula:	$C_6H_5ClF_3N_3$
Molecular mass:	211.57 g/mol
Appearance	White solid
Internal code:	MG-244F2
R_f-value	0.38 (Hex:EtOAC 4:1)
^{1}H NMR (300 MHz, DMSO):	δ 8.58 (d, *J* = 25.7 Hz, 1H), 8.41 (s, 1H), 2.85 (dd, *J* = 7.0, 4.8 Hz, 3H)
MS (APCI-(+)):	m/z = 211.6, 213.6 $[M+H^+]^+$

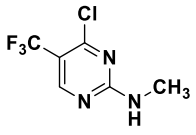

2-Chloro-*N*-ethyl-5-(trifluoromethyl)pyrimidin-4-amine (P39)

To a solution of 2,4-dichloro-5-(trifluoromethyl)pyrimidine (1.00 g, 4.61 mmol, 1.0 eq.) and DIPEA (2.41 mL, 13.83 mmol, 3.0 eq.) in 60 mL of ethanol ethylamine hydrochloride (413 mg, 5.07 mmol, 1.0 eq.) was added, and the reaction mixture was stirred for 1 h at room temperature. Afterwards, solvent was evaporated, and the residue was partitioned between water and EtOAc. The organic layers were merged, washed with brine and dried over anhydrous Na_2SO_4. After filtration, solvent was evaporated under reduced pressure to obtain crude consisting of 2-ethylamino and 4-ethylamino substituted structural isomers. The identity of structural isomers separated via column chromatography (Hex:EtOAc = 95:5) was confirmed with ^{1}H-, ^{13}C- and HMBC-NMR spectrums.

Yield:	470 mg (45%)
Chemical formula:	$C_7H_7ClF_3N_3$
Molecular mass:	225.60 g/mol
Appearance	White solid
Internal code:	MG-300F2
R_f-value	0.54 (Hex:EtOAC 4:1)
^{1}H NMR (300 MHz, DMSO):	δ 8.65 – 8.53 (m, 1H), 8.52 (s, 1H), 3.44 – 3.22 (m, 2H), 1.12 (td, *J* = 7.2, 2.0 Hz, 3H)
MS (APCI-(+)):	m/z = 225.8, 227.8 $[M+H^+]^+$

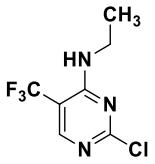

4-Chloro-*N*-ethyl-5-(trifluoromethyl)pyrimidin-2-amine (P40)

The compound 4-chloro-*N*-ethyl-5-(trifluoromethyl)pyrimidin-2-amine (**P40**) was obtained as a side product during the synthesis of compound **P39**.

Yield:	200 mg (19%)
Chemical formula:	$C_7H_7ClF_3N_3$
Molecular mass:	225.60 g/mol
Appearance	Colorless liquid
Internal code:	MG-300F1
R_f-value	0.62 (Hex:EtOAC 4:1)
^{1}H NMR (300 MHz, DMSO):	δ 8.44 – 8.29 (m, 1H), 7.97 (s, 1H), 3.44 (qd, *J* = 7.1, 5.6 Hz, 2H), 1.12 (t, *J* = 7.1 Hz, 3H)
MS (APCI-(+)):	m/z = 225.8, 227.8 $[M+H^+]^+$

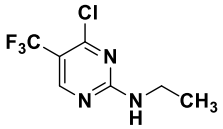

N^4-Methyl-N^2-(4-(3-(4-methylpiperazin-1-yl)propoxy)phenyl)-5-(trifluoromethyl) pyrimidine-2,4-diamine (64)

To a solution of 2-chloro-*N*-methyl-5-(trifluoromethyl)pyrimidin-4-amine **(P37)** (65 mg, 0.31 mmol, 1.0 eq.) and 1-methyl-4-(3-(4-nitrophenoxy)propyl)piperazine **(P12)** (84 mg, 0.34 mmol, 1.1 eq.) in 1 mL of isopropanol in a microwave vial, 0.1 mL of TFA was added. The reaction mixture was stirred at room temperature for 24 h. The precipitate was collected via vacuum filtration and washed with isopropanol. Subsequently, it was partitioned between 1 M NaOH (30 mL) and ethyl acetate (3 × 30 mL). The organic layers were merged, washed with brine, dried over Na_2SO_4. After filtration solvent was evaporated, and the residue was purified using column chromatography (DCM:MeOH(NH_3) = 9:1) in order to obtain desired product.

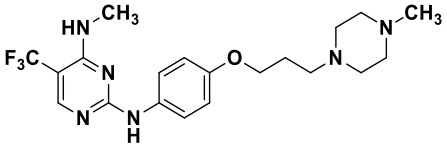

Yield:	80 mg (64%)
Chemical formula:	$C_{20}H_{27}F_3N_6O$
Molecular mass:	424.47 g/ mol
Appearance	Off-white solid
Internal code:	MG-284, ST-2887
^{1}H NMR (300 MHz, DMSO):	δ 9.42 (s, 1H), 8.12 (s, 1H), 7.64 (d, *J* = 8.7 Hz, 2H), 7.04 (d, *J* = 4.8 Hz, 1H), 6.85 (d, *J* = 9.0 Hz, 2H), 3.96 (t, *J* = 6.3 Hz, 2H), 2.91 (d, *J* = 4.3 Hz, 3H), 2.83 – 2.62 (m, 4H), 2.40 (s, 3H), 1.86 (p, *J* = 6.7 Hz, 2H)
^{13}C NMR (75 MHz, DMSO):	δ 160.94, 158.46, 154.18, 153.72, 133.27, 123.41, 121.08, 114.27, 101.59, 65.74, 53.95, 53.59, 51.27, 44.18, 28.01, 25.96.
Melting point	121.9 °C
MS (APCI-(+)):	m/z = 425.0 $[M+H^+]^+$
LC-MS-DAD purity:	100.00%
HRMS (ESI-(+)):	m/z = 425.2270 $[M+H^+]^+$ (calculated: 425.2271)

1-(4-(3-(4-((4-(Methylamino)-5-(trifluoromethyl)pyrimidin-2-yl)amino)phenoxy)propyl) piperazin-1-yl)ethan-1-one (65)

To a solution of 2-chloro-*N*-methyl-5-(trifluoromethyl)pyrimidin-4-amine **(P37)** (96 mg, 0.45 mmol, 1.0 eq.) and 1-(4-(3-(4-aminophenoxy)propyl)piperazin-1-yl)ethan-1-one **(P13)** (138 mg, 0.50 mmol, 1.1 eq.) in 3 mL of isopropanol in a microwave vial, 0.1 mL of TFA was added. The reaction mixture was stirred at room temperature for 24 h. Subsequently, the solvent was evaporated, and the residue was partitioned between 1 M NaOH (30 mL) and ethyl acetate (3 × 30 mL). The organic layers were merged, washed with brine, dried over Na_2SO_4. After

filtration solvent was evaporated, and the residue was purified using flash column chromatography (DCM:MeOH, 0-7% MeOH) in order to obtain desired product.

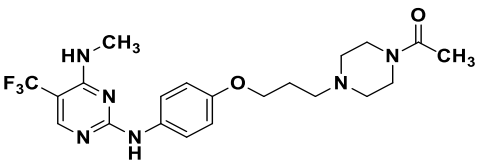

Yield:	120 mg (58%)
Chemical formula:	$C_{21}H_{27}F_3N_6O_2$
Molecular mass:	452.48 g/mol
Appearance	Off-white solid
Internal code:	MG-337, ST-3010
^{1}H NMR (300 MHz, $CDCl_3$):	δ 8.12 (q, *J* = 0.9 Hz, 1H), 7.48 (d, *J* = 9.0 Hz, 2H), 7.15 (s, 1H), 6.87 (d, *J* = 9.0 Hz, 2H), 5.16 (s, 1H), 4.01 (t, *J* = 6.3 Hz, 2H), 3.70 – 3.57 (m, 2H), 3.53 – 3.41 (m, 2H), 3.04 (d, *J* = 4.7 Hz, 3H), 2.60 – 2.50 (m, 2H), 2.49 – 2.38 (m, 4H), 2.09 (s, 3H), 1.96 (dt, *J* = 13.1, 6.4 Hz, 2H)
^{13}C NMR (151 MHz, DMSO):	δ 169.04, 161.35, 159.66, 155.22, 154.84, 154.81, 154.77, 154.74, 132.31, 127.92, 126.13, 124.34, 122.56, 122.10, 114.87, 66.43, 55.12, 53.54, 52.94, 46.45, 41.56, 28.21, 26.88, 21.48
Melting point	179.3 °C
MS (APCI-(+)):	m/z = 452.6 $[M+H^+]^+$
LC-MS-DAD purity:	100.00%
HRMS (ESI-(+)):	m/z = 453.2243 $[M+H^+]^+$ (calculated: 453.2220)

N^4-Methyl-*N*^{2}-(4-(3-(piperidin-1-yl)propoxy)phenyl)-5-(trifluoromethyl)pyrimidine-2,4-diamine (66)

To a solution of 2-chloro-*N*-methyl-5-(trifluoromethyl)pyrimidin-4-amine **(P37)** (60 mg, 0.28 mmol, 1.0 eq.) and 4-(3-(piperidin-1-yl)propoxy)aniline **(P14)** (73 mg, 0.31 mmol, 1.1 eq.) in 1 mL of isopropanol in a microwave vial, 0.1 mL of TFA was added. The reaction mixture was stirred at room temperature for 24 h. The precipitate was collected via vacuum filtration and washed with isopropanol. Subsequently, it was partitioned between 1 M NaOH (30 mL) and ethyl acetate (3 × 30 mL). The organic layers were merged, washed with brine, dried over Na_2SO_4. After filtration solvent was evaporated, and the residue was purified using flash column chromatography (DCM:MeOH, 0-7% MeOH) in order to obtain desired product.

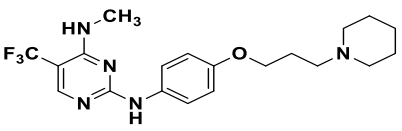

Yield:	65 mg (55%)
Chemical formula:	$C_{20}H_{26}F_3N_5O$
Molecular mass:	409.46 g/mol
Appearance	White solid
Internal code:	MG-278, ST-2884

^{1}H NMR (300 MHz, DMSO):	δ 9.42 (s, 1H), 8.12 (s, 1H), 7.64 (d, *J* = 9.0 Hz, 2H), 7.03 (d, *J* = 4.8 Hz, 1H), 6.92 – 6.80 (m, 2H), 3.96 (t, *J* = 6.3 Hz, 2H), 2.91 (d, *J* = 4.3 Hz, 3H), 1.97 – 1.82 (m, 2H), 1.63 – 1.49 (m, 4H), 1.47 – 1.34 (m, 2H)
^{13}C NMR (75 MHz, DMSO):	δ 160.92, 158.44, 154.22, 153.70, 133.26, 127.83, 121.05, 114.27, 106.74, 65.82, 54.83, 53.67, 28.00, 25.78, 25.58, 24.89.
Melting point	128.7 °C
MS (APCI-(+)):	m/z = 410.3 $[M+H^+]^+$
LC-MS-DAD purity:	100.00%
HRMS (ESI-(+)):	m/z = 410.2200 $[M+H^+]^+$ (calculated: 410.2162)

N^2-(3-Methoxy-4-(3-(piperidin-1-yl)propoxy)phenyl)-*N*^{4}-methyl-5-(trifluoromethyl) pyrimidine-2,4-diamine (67)

To a solution of 2-chloro-*N*-methyl-5-(trifluoromethyl)pyrimidin-4-amine **(P37)** (63 mg, 0.29 mmol, 1.0 eq.) and 3-methoxy-4-(3-(piperidin-1-yl)propoxy)aniline **(P15)** (85 mg, 0.32 mmol, 1.1 eq.) in 1 mL of isopropanol in a microwave vial, 0.1 mL of TFA was added. The reaction mixture was stirred at room temperature for 24 h. The precipitate was collected via vacuum filtration and washed with isopropanol. Subsequently, it was partitioned between 1 M NaOH (30 mL) and ethyl acetate (3 × 30 mL). The organic layers were merged, washed with brine, dried over Na_2SO_4. After filtration solvent was evaporated, and the residue was purified using column chromatography (DCM:MeOH(NH_3) = 9:1) in order to obtain desired product.

Yield:	80 mg (62%)
Chemical formula:	$C_{21}H_{28}F_3N_5O_2$
Molecular mass:	439.48g/mol
Appearance	Beige solid
Internal code:	MG-282, ST-2885

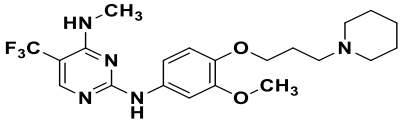

^{1}H NMR (300 MHz, DMSO):	δ 9.43 (s, 1H), 8.13 (s, 1H), 7.61 (s, 1H), 7.18 (dd, *J* = 8.7, 2.4 Hz, 1H), 7.08 (d, *J* = 4.7 Hz, 1H), 6.87 (d, *J* = 8.7 Hz, 1H), 3.94 (t, *J* = 6.3 Hz, 2H), 3.74 (s, 3H), 2.94 (d, *J* = 4.3 Hz, 3H), 1.98 – 1.80 (m, 2H), 1.64 – 1.50 (m, 4H), 1.49 – 1.35 (m, 2H)
^{13}C NMR (75 MHz, DMSO):	δ 160.84, 158.48, 154.15, 154.09, 148.90, 143.02, 134.17, 126.95, 114.09, 111.29, 104.97, 67.10, 55.44, 54.82, 53.58, 28.14, 25.91, 25.69, 24.78
Melting point	157.3 °C
MS (APCI-(+)):	m/z = 440.0 $[M+H^+]^+$
LC-MS-DAD purity:	100.00%

HRMS (ESI-(+)):	m/z = 440.2289 $[M+H^+]^+$ (calculated: 440.2268)

N^2-(4-Methoxy-3-(3-(piperidin-1-yl)propoxy)phenyl)-N^4-methyl-5-(trifluoromethyl) pyrimidine-2,4-diamine (68)

To a solution of 2-chloro-*N*-methyl-5-(trifluoromethyl)pyrimidin-4-amine **(P37)** (65 mg, 0.31 mmol, 1.0 eq.) and 4-methoxy-3-(3-(piperidin-1-yl)propoxy)aniline **(P16)** (86 mg, 0.34 mmol, 1.1 eq.) in 1 mL of isopropanol in a microwave vial, 0.1 mL of TFA was added. The reaction mixture was stirred at room temperature for 24 h. The precipitate was collected via vacuum filtration and washed with isopropanol. Subsequently, it was partitioned between 1 M NaOH (30 mL) and ethyl acetate (3 × 30 mL). The organic layers were merged, washed with brine, dried over Na_2SO_4. After filtration solvent was evaporated, and the residue was purified using column chromatography (DCM:MeOH(NH_3) = 9:1) in order to obtain desired product.

Yield:	80 mg (60%)
Chemical formula:	$C_{21}H_{28}F_3N_5O_2$
Molecular mass:	439.48 g/mol
Appearance	Beige solid
Internal code:	MG-283, ST-2886
^{1}H NMR (300 MHz, DMSO):	δ 9.42 (s, 1H), 8.13 (s, 1H), 7.61 (s, 1H), 7.19 (dd, *J* = 8.7, 2.4 Hz, 1H), 7.08 (d, *J* = 4.8 Hz, 1H), 6.87 (d, *J* = 8.8 Hz, 1H), 3.97 (t, *J* = 6.4 Hz, 2H), 3.72 (s, 3H), 2.94 (d, *J* = 4.4 Hz, 3H), 2.02 – 1.84 (m, 2H), 1.71 – 1.49 (m, 4H), 1.49 – 1.32 (m, 2H)
^{13}C NMR (75 MHz, DMSO):	δ 160.83, 158.46, 154.23, 154.16, 147.70, 144.18, 133.83, 126.95, 112.49, 111.51, 106.08, 66.53, 55.89, 54.77, 53.61, 53.56, 28.15, 24.85, 23.45
Melting point	146.7 °C
MS (APCI-(+)):	m/z = 439.9 $[M+H^+]^+$
LC-MS-DAD purity:	100.00%
HRMS (ESI-(+)):	m/z = 440.2286 $[M+H^+]^+$ (calculated: 440.2268)

N^2-(2-Methoxy-4-(3-(piperidin-1-yl)propoxy)phenyl)-N^4-methyl-5-(trifluoromethyl) pyrimidine-2,4-diamine (69)

To a solution of 2-chloro-*N*-methyl-5-(trifluoromethyl)pyrimidin-4-amine **(P37)** (80 mg, 0.38 mmol, 1.0 eq.) and 2-methoxy-4-(3-(piperidin-1-yl)propoxy)aniline **(P17)** (110 mg,

0.42 mmol, 1.1 eq.) in 2 mL of isopropanol in a microwave vial, 0.1 mL of TFA was added. The reaction mixture was stirred at room temperature for 24 h. The precipitate was collected via vacuum filtration and washed with isopropanol. Subsequently, it was partitioned between 1 M NaOH (30 mL) and ethyl acetate (3 × 30 mL). The organic layers were merged, washed with brine, dried over Na_2SO_4. After filtration solvent was evaporated, and the residue was purified using flash column chromatography (DCM:MeOH, 0-7% MeOH) in order to obtain desired product.

Yield:	97 mg (59%)
Chemical formula:	$C_{21}H_{28}F_3N_5O_2$
Molecular mass:	439.48 g/mol
Appearance	Brown resin
Internal code:	MG-320, ST-3007
^{1}H NMR (300 MHz, $CDCl_3$):	δ 8.27 (d, *J* = 9.5 Hz, 1H), 8.13 (d, *J* = 1.0 Hz, 1H), 7.47 (s, 1H), 6.57 – 6.43 (m, 2H), 5.15 (s, 1H), 4.00 (t, *J* = 6.4 Hz, 2H), 3.86 (s, 3H), 3.08 (d, *J* = 4.7 Hz, 3H), 2.52 – 2.35 (m, 6H), 2.03 – 1.95 (m, 2H), 1.60 (p, *J* = 5.6 Hz, 4H), 1.45 (q, *J* = 6.0 Hz, 2H)
^{13}C NMR (151 MHz, $CDCl_3$):	δ 161.08, 159.71, 155.13, 154.78, 154.75, 154.71, 154.68, 149.70, 126.23, 124.44, 122.33, 120.42, 104.59, 99.34, 67.03, 56.18, 55.86, 54.78, 28.34, 27.02, 26.08, 24.55
Melting point	n.a.
MS (APCI-(+)):	m/z = 440.1 $[M+H^+]^+$
LC-MS-DAD purity:	95.57%
HRMS (ESI-(+)):	m/z = 440.2269 $[M+H^+]^+$ (calculated: 440.2268)

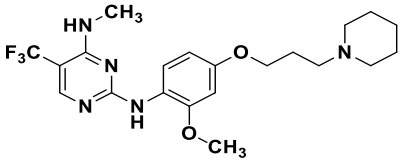

N^4-Ethyl-*N*^{2}-(4-(3-(4-methylpiperazin-1-yl)propoxy)phenyl)-5-(trifluoromethyl) pyrimidine-2,4-diamine (70)

To a solution of 2-chloro-*N*-ethyl-5-(trifluoromethyl)pyrimidin-4-amine **(P39)** (80 mg, 0.35 mmol, 1.0 eq.) and 1-methyl-4-(3-(4-nitrophenoxy)propyl)piperazine **(P12)** (97 mg, 0.39 mmol, 1.1 eq.) in 2 mL of isopropanol in a microwave vial, 0.1 mL of TFA was added. The reaction mixture was stirred at room temperature for 24 h. The reaction mixture was stirred at room temperature for 24 h. Subsequently, the solvent was evaporated, and the residue was partitioned between 1 M NaOH (30 mL) and ethyl acetate (3 × 30 mL). The organic layers were merged, washed with brine, dried over Na_2SO_4. After filtration solvent was evaporated,

and the residue was purified using flash column chromatography (DCM:MeOH, 0-7% MeOH) in order to obtain desired product.

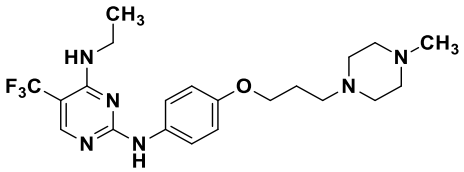

Yield:	123 mg (79%)
Chemical formula:	$C_{21}H_{29}F_3N_6O$
Molecular mass:	438.50 g/mol
Appearance	Beige solid
Internal code:	MG-309, ST-2997
^{1}H NMR (300 MHz, $CDCl_3$):	δ 8.16 (s, 1H), 7.40 (s, 2H), 6.88 (d, *J* = 9.0 Hz, 2H), 6.64 (s, 1H), 5.29 (s, 1H), 4.01 (t, *J* = 6.4 Hz, 2H), 3.50 – 3.28 (m, 2H), 2.75 – 2.35 (m, 10H), 2.29 (s, 3H), 1.97 (dq, *J* = 8.4, 6.4 Hz, 2H), 1.19 (t, *J* = 7.2 Hz, 3H)
^{13}C NMR (151 MHz, DMSO):	δ 163.05, 162.71, 157.51, 155.73, 130.79, 126.31, 124.33, 124.02, 114.67, 66.71, 55.30, 53.39, 46.21, 36.43, 26.96, 14.96
Melting point	111.5 °C
MS (APCI-(+)):	m/z = 439.2 $[M+H^+]^+$
LC-MS-DAD purity:	96.97%
HRMS (ESI-(+)):	m/z = 439.2446 $[M+H^+]^+$ (calculated: 439.2428)

1-(4-(3-(4-((4-(Ethylamino)-5-(trifluoromethyl)pyrimidin-2-yl)amino)phenoxy)propyl) piperazin-1-yl)ethan-1-one (71)

To a solution of 2-chloro-*N*-ethyl-5-(trifluoromethyl)pyrimidin-4-amine **(P39)** (100 mg, 0.44 mmol, 1.0 eq.) and 1-(4-(3-(4-aminophenoxy)propyl)piperazin-1-yl)ethan-1-one **(P13)** (136 mg, 0.49 mmol, 1.1 eq.) in 3 mL of isopropanol in a microwave vial, 0.1 mL of TFA was added. The reaction mixture was stirred at room temperature for 24 h. Subsequently, the solvent was evaporated, and the residue was partitioned between 2 M NaOH (30 mL) and ethyl acetate (3 × 30 mL). The organic layers were merged, washed with brine, dried over Na_2SO_4. After filtration solvent was evaporated, and the residue was purified using flash column chromatography (DCM:MeOH, 0-7% MeOH) in order to obtain desired product.

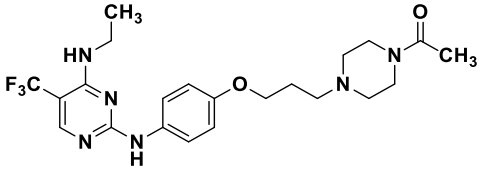

Yield:	128 mg (62%)
Chemical formula:	$C_{22}H_{29}F_3N_6O_2$
Molecular mass:	466.51 g/mol
Appearance	White solid
Internal code:	MG-341, ST-3012
^{1}H NMR (300 MHz, $CDCl_3$):	δ 8.16 (s, 1H), 7.41 (s, 2H), 6.88 (d, *J* = 9.0 Hz, 2H), 6.65 (s, 1H), 5.47 – 4.91 (m, 1H), 4.02 (t, *J* = 6.3 Hz, 2H), 3.68 – 3.58 (m, 2H), 3.51 – 3.43 (m, 2H),

	3.38 (s, 2H), 2.55 (t, *J* = 7.3 Hz, 2H), 2.45 (dt, *J* = 10.1, 5.1 Hz, 4H), 2.09 (s, 3H), 1.97 (dt, *J* = 13.2, 6.4 Hz, 2H), 1.19 (t, *J* = 7.2 Hz, 3H)
^{13}C NMR (151 MHz, $CDCl_3$):	δ 169.04, 163.06, 157.49, 155.78, 130.97, 128.07, 124.34, 123.99, 114.63, 66.39, 55.11, 53.54, 52.93, 46.43, 41.55, 36.43, 26.85, 21.47, 14.96
Melting point	136.3 °C
MS (APCI-(+)):	m/z = 466.6 $[M+H^+]^+$
LC-MS-DAD purity:	100.00%
HRMS (ESI-(+)):	m/z = 467.2376 $[M+H^+]^+$ (calculated: 467.2377)

N^4-Ethyl-N^2-(4-(3-(piperidin-1-yl)propoxy)phenyl)-5-(trifluoromethyl)pyrimidine-2,4-diamine (72)

To a solution of 2-chloro-*N*-ethyl-5-(trifluoromethyl)pyrimidin-4-amine **(P39)** (80 mg, 0.35 mmol, 1.0 eq.) and 4-(3-(piperidin-1-yl)propoxy)aniline **(P14)** (91 mg, 0.39 mmol, 1.1 eq.) in 2 mL of isopropanol in a microwave vial, 0.1 mL of TFA was added. The reaction mixture was stirred at room temperature for 24 h. Subsequently, the solvent was evaporated, and the residue was partitioned between 1 M NaOH (30 mL) and ethyl acetate (3 × 30 mL). The organic layers were merged, washed with brine, dried over Na_2SO_4. After filtration solvent was evaporated, and the residue was purified using flash column chromatography (DCM:MeOH, 0-7% MeOH) in order to obtain desired product.

Yield:	128 mg (85%)
Chemical formula:	$C_{21}H_{28}F_3N_5O$
Molecular mass:	423.48 g/mol
Appearance	Beige solid
Internal code:	MG-306,

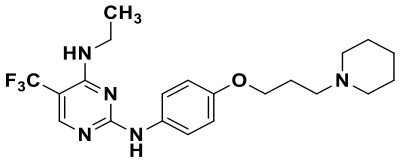

^{1}H NMR (300 MHz, $CDCl_3$):	δ 8.16 (s, 1H), 7.40 (s, 2H), 6.88 (d, *J* = 9.0 Hz, 2H), 6.64 (s, 1H), 5.24 (s, 1H), 4.01 (t, *J* = 6.4 Hz, 2H), 3.38 (s, 2H), 2.53 – 2.44 (m, 2H), 2.44 – 2.34 (m, 4H), 2.05 – 1.92 (m, 2H), 1.59 (p, *J* = 5.5 Hz, 4H), 1.45 (q, *J* = 6.0 Hz, 2H), 1.19 (t, *J* = 7.2 Hz, 3H)
^{13}C NMR (151 MHz, DMSO):	δ 163.06, 159.58, 157.43, 155.73, 124.74, 123.98, 114.69, 108.71, 105.65, 66.97, 56.15, 54.82, 36.42, 27.03, 26.16, 24.60, 14.96
Melting point	101.5 °C
MS (APCI-(+)):	m/z = 424.2 $[M+H^+]^+$
LC-MS-DAD purity:	98.33%
HRMS (ESI-(+)):	m/z = 424.2270 $[M+H^+]^+$ (calculated: 424.2319)

N^4-Ethyl-N^2-(3-methoxy-4-(3-(piperidin-1-yl)propoxy)phenyl)-5-(trifluoromethyl) pyrimidine-2,4-diamine (73)

To a solution of 2-chloro-*N*-ethyl-5-(trifluoromethyl)pyrimidin-4-amine **(P39)** (80 mg, 0.35 mmol, 1.0 eq.) and 3-methoxy-4-(3-(piperidin-1-yl)propoxy)aniline **(P15)** (103 mg, 0.39 mmol, 1.1 eq.) in 2 mL of isopropanol in a microwave vial, 0.1 mL of TFA was added. The reaction mixture was stirred at room temperature for 24 h. Subsequently, the solvent was evaporated, and the residue was partitioned between 1 M NaOH (30 mL) and ethyl acetate (3 × 30 mL). The organic layers were merged, washed with brine, dried over Na_2SO_4. After filtration solvent was evaporated, and the residue was purified using flash column chromatography (DCM:MeOH, 0-7% MeOH) in order to obtain desired product.

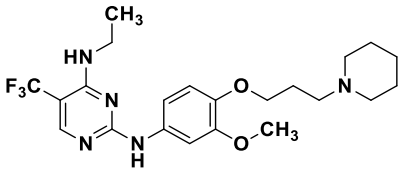

Yield:	126 mg (78%)
Chemical formula:	$C_{22}H_{30}F_3N_5O_2$
Molecular mass:	453.51 g/mol
Appearance	Off-white solid
Internal code:	MG-307, ST-2995
^{1}H NMR (300 MHz, $CDCl_3$):	δ 8.16 (s, 1H), 7.29 (s, 1H), 6.95 (dd, *J* = 8.6, 2.4 Hz, 1H), 6.87 (d, *J* = 8.6 Hz, 1H), 6.67 (s, 1H), 5.30 (s, 1H), 4.07 (t, *J* = 6.7 Hz, 2H), 3.87 (s, 3H), 3.41 (p, *J* = 6.5 Hz, 2H), 2.48 (t, *J* = 7.2 Hz, 2H), 2.45 – 2.33 (m, 4H), 2.11 – 1.95 (m, 2H), 1.59 (p, *J* = 5.5 Hz, 4H), 1.44 (q, *J* = 6.0 Hz, 2H), 1.19 (t, *J* = 7.2 Hz, 3H)
^{13}C NMR (151 MHz, DMSO):	δ 166.44, 163.06, 157.49, 155.78, 149.48, 131.56, 124.50, 115.65, 113.94, 113.47, 107.77, 68.22, 56.18, 56.02, 54.76, 36.46, 26.90, 26.16, 24.60, 15.01
Melting point	136.1 °C
MS (APCI-(+)):	m/z = 454.3 $[M+H^+]^+$
LC-MS-DAD purity:	100.00%
HRMS (ESI-(+)):	m/z = 454.2436 $[M+H^+]^+$ (calculated: 454.2424)

N^4-Ethyl-N^2-(4-methoxy-3-(3-(piperidin-1-yl)propoxy)phenyl)-5-(trifluoromethyl) pyrimidine-2,4-diamine (74)

To a solution of 2-chloro-*N*-ethyl-5-(trifluoromethyl)pyrimidin-4-amine **(P39)** (80 mg, 0.35 mmol, 1.0 eq.) and 4-methoxy-3-(3-(piperidin-1-yl)propoxy)aniline **(P16)** (103 mg, 0.39 mmol, 1.1 eq.) in 2 mL of isopropanol in a microwave vial, 0.1 mL of TFA was added. The reaction mixture was stirred at room temperature for 24 h. Subsequently, the solvent was evaporated, and the residue was partitioned between 1 M NaOH (30 mL) and ethyl acetate

(3 × 30 mL). The organic layers were merged, washed with brine, dried over Na_2SO_4. After filtration solvent was evaporated, and the residue was purified using flash column chromatography (DCM:MeOH, 0-7% MeOH) in order to obtain desired product.

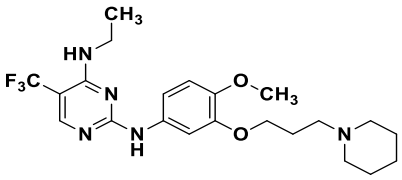

Yield:	137 mg (85%)
Chemical formula:	$C_{22}H_{30}F_3N_5O_2$
Molecular mass:	453.51 g/mol
Appearance	Beige solid
Internal code:	MG-308, ST-2996
^{1}H NMR (300 MHz, $CDCl_3$):	δ 8.16 (s, 1H), 7.28 (s, 1H), 6.97 (dd, *J* = 8.6, 2.5 Hz, 1H), 6.83 (d, *J* = 8.7 Hz, 1H), 6.66 (s, 1H), 5.29 (s, 1H), 4.07 (t, *J* = 6.7 Hz, 2H), 3.86 (s, 3H), 3.41 (p, *J* = 6.7 Hz, 2H), 2.53 – 2.44 (m, 2H), 2.44 – 2.31 (m, 4H), 2.04 (dq, *J* = 8.5, 6.8 Hz, 2H), 1.57 (p, *J* = 5.5 Hz, 4H), 1.43 (q, *J* = 6.0 Hz, 2H), 1.19 (t, *J* = 7.2 Hz, 3H)
^{13}C NMR (151 MHz, DMSO):	δ 163.05, 157.50, 155.75, 148.52, 146.61, 126.29, 124.50, 115.61, 114.49, 111.85, 109.07, 67.87, 56.43, 55.96, 54.75, 36.47, 26.84, 26.10, 24.56, 15.02
Melting point	113.2 °C
MS (APCI-(+)):	m/z = 454.3 $[M+H^+]^+$
LC-MS-DAD purity:	99.99%
HRMS (ESI-(+)):	m/z = 454.2431 $[M+H^+]^+$ (calculated: 454.2424)

N^4-Ethyl-*N*^{2}-(2-methoxy-4-(3-(piperidin-1-yl)propoxy)phenyl)-5-(trifluoromethyl) pyrimidine-2,4-diamine (75)

To a solution of 2-chloro-*N*-ethyl-5-(trifluoromethyl)pyrimidin-4-amine **(P39)** (102 mg, 0.53 mmol, 1.0 eq.) and 2-methoxy-4-(3-(piperidin-1-yl)propoxy)aniline **(P17)** (154 mg, 0.58 mmol, 1.1 eq.) in 2 mL of isopropanol in a microwave vial, 0.1 mL of TFA was added. The reaction mixture was stirred at 60 °C for 24 h. Subsequently, the solvent was evaporated, and the residue was partitioned between 2 M NaOH (30 mL) and ethyl acetate (3 × 30 mL). The organic layers were merged, washed with brine, dried over Na_2SO_4. After filtration solvent was evaporated, and the residue was purified using flash column chromatography (DCM:MeOH, 0-7% MeOH) in order to obtain desired product.

Yield:	135 mg (56%)
Chemical formula:	$C_{22}H_{30}F_3N_5O_2$
Molecular mass:	453.51 g/mol
Appearance	Beige solid

Internal code:	MG-331, ST-3009

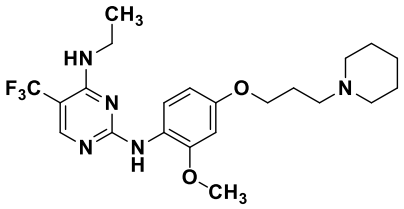

^{1}H NMR (300 MHz, $CDCl_3$):	δ 8.22 (d, *J* = 44.2 Hz, 2H), 7.46 (s, 1H), 6.57 – 6.39 (m, 2H), 5.30 (s, 1H), 4.01 (t, *J* = 6.4 Hz, 2H), 3.87 (s, 3H), 3.45 (qd, *J* = 7.2, 5.6 Hz, 2H), 2.54 – 2.34 (m, 6H), 2.03 – 1.91 (m, 2H), 1.60 (p, *J* = 5.5 Hz, 4H), 1.45 (q, *J* = 6.0 Hz, 2H), 1.24 (t, *J* = 7.2 Hz, 3H)
^{13}C NMR (151 MHz, $CDCl_3$):	δ 163.13, 156.66, 155.86, 155.47, 150.43, 126.26, 124.47, 121.94, 104.50, 99.29, 67.05, 56.18, 56.16, 54.83, 36.59, 27.07, 26.16, 24.60, 14.99
Melting point	133.7 °C
MS (APCI-(+)):	m/z = 454.0 $[M+H^+]^+$
LC-MS-DAD purity:	98.38%
HRMS (ESI-(+)):	m/z = 454.2429 $[M+H^+]^+$ (calculated: 454.2424)

N^2-Methyl-N^4-(4-(3-(4-methylpiperazin-1-yl)propoxy)phenyl)-5-(trifluoromethyl) pyrimidine-2,4-diamine (76)

To a solution of 4-chloro-*N*-methyl-5-(trifluoromethyl)pyrimidin-2-amine **(P38)** (62 mg, 0.29 mmol, 1.0 eq.) and 1-methyl-4-(3-(4-nitrophenoxy)propyl)piperazine **(P12)** (80 mg, 0.32 mmol, 1.1 eq.) in 1 mL of isopropanol in a microwave vial, 0.1 mL of TFA was added. The reaction mixture was stirred at room temperature for 24 h. The solvent was then evaporated, and the residue was partitioned between 1 M NaOH (30 mL) and ethyl acetate (3 × 30 mL). The organic layers were merged, washed with brine, dried over Na_2SO_4. After filtration solvent was evaporated, and the residue was purified using column chromatography (DCM:MeOH(NH_3) = 93:7) in order to obtain desired product

Yield:	100 mg (83%)
Chemical formula:	$C_{20}H_{27}F_3N_6O$
Molecular mass:	424.47 g/mol
Appearance	Off-white solid
Internal code:	MG-289, ST-2891

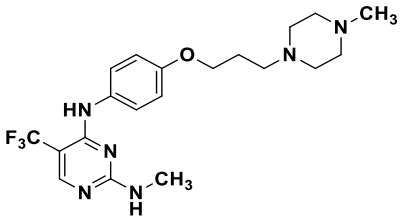

^{1}H NMR (300 MHz, DMSO):	δ 8.29 – 7.98 (m, 2H), 7.58 – 7.04 (m, 3H), 6.87 (d, *J* = 8.9 Hz, 2H), 3.97 (t, *J* = 6.4 Hz, 2H), 2.80 – 2.62 (m, 3H), 2.51 – 2.27 (m, 10H), 2.20 (s, 3H), 1.85 (p, *J* = 6.6 Hz, 2H)

^{13}C NMR (75 MHz, DMSO):	δ 163.27, 156.85, 155.39, 139.13, 131.18, 126.17, 125.50, 114.02, 113.71, 65.88, 54.45, 54.29, 52.35, 45.35, 27.65, 26.18
Melting point	125.7 °C
MS (APCI-(+)):	m/z = 425.2 $[M+H^+]^+$
LC-MS-DAD purity:	97.28%
HRMS (ESI-(+)):	m/z = 425.2290 $[M+H^+]^+$ (calculated: 425.2271)

1-(4-(3-(4-((2-(Methylamino)-5-(trifluoromethyl)pyrimidin-4-yl)amino)phenoxy)propyl) piperazin-1-yl)ethan-1-one (77)

To a solution of 4-chloro-*N*-methyl-5-(trifluoromethyl)pyrimidin-2-amine **(P38)** (100 mg, 0.47 mmol, 1.0 eq.) and 1-(4-(3-(4-aminophenoxy)propyl)piperazin-1-yl)ethan-1-one **(P13)** (144 mg, 0.52 mmol, 1.1 eq.) in 3 mL of isopropanol in a microwave vial, 0.1 mL of TFA was added. The reaction mixture was stirred at 60 °C temperature for 24 h. Subsequently, the solvent was evaporated, and the residue was partitioned between 2 M NaOH (30 mL) and ethyl acetate (3 × 30 mL). The organic layers were merged, washed with brine, dried over Na_2SO_4. After filtration solvent was evaporated, and the residue was purified using flash column chromatography (DCM:MeOH, 0-7% MeOH) in order to obtain desired product.

Yield:	147 mg (69%)
Chemical formula:	$C_{21}H_{27}F_3N_6O_2$
Molecular mass:	452.48 g/mol
Appearance	White solid
Internal code:	MG-340, ST-3011

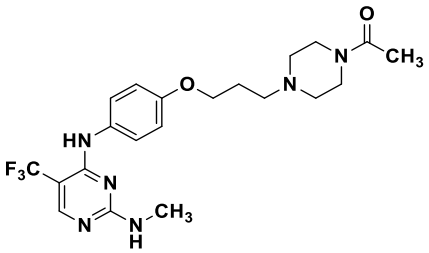

^{1}H NMR (300 MHz, $CDCl_3$):	δ 8.05 (s, 1H), 7.34 (s, 2H), 6.78 (d, *J* = 9.0 Hz, 2H), 6.58 (d, *J* = 2.3 Hz, 1H), 5.23 (s, 1H), 3.92 (t, *J* = 6.3 Hz, 2H), 3.59 – 3.46 (m, 2H), 3.43 – 3.32 (m, 2H), 2.84 (d, *J* = 5.0 Hz, 3H), 2.50 – 2.40 (m, 2H), 2.40 – 2.28 (m, 4H), 1.98 (s, 3H), 1.87 (dt, *J* = 13.1, 6.4 Hz, 2H)
^{13}C NMR (151 MHz, $CDCl_3$):	δ 169.04, 163.52, 157.47, 155.70, 131.01, 126.28, 124.57, 123.99, 114.64, 66.38, 55.09, 53.53, 52.92, 46.43, 41.55, 28.45, 26.84, 21.46
Melting point	150.3 °C
MS (APCI-(+)):	m/z = 452.5 $[M+H^+]^+$
LC-MS-DAD purity:	100.00%
HRMS (ESI-(+)):	m/z = 453.2230 $[M+H^+]^+$ (calculated: 453.2220)

N^2-Methyl-N^4-(4-(3-(piperidin-1-yl)propoxy)phenyl)-5-(trifluoromethyl)pyrimidine-2,4-diamine (78)

To a solution of 4-chloro-*N*-methyl-5-(trifluoromethyl)pyrimidin-2-amine **(P38)** (65 mg, 0.31 mmol, 1.0 eq.) and 4-(3-(piperidin-1-yl)propoxy)aniline **(P14)** (79 mg, 0.34 mmol, 1.1 eq.) in 1 mL of isopropanol in a microwave vial, 0.1 mL of TFA was added. The reaction mixture was stirred at room temperature for 24 h. Formed precipitate was collected via vacuum filtration and washed with isopropanol. Subsequently, then it was dissolved in methanol and treated with strong basic ion exchanger. The solvent was than evaporated to obtain the desired product.

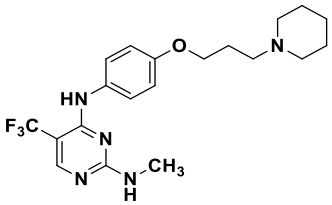

Yield:	40 mg (32%)
Chemical formula:	$C_{20}H_{26}F_3N_5O$
Molecular mass:	409.46 g/mol
Appearance	Beige solid
Internal code:	MG-286, ST-2888
^{1}H NMR (300 MHz, DMSO):	δ 8.22 (s, 1H), 8.12 (s, 1H), 7.60 – 7.03 (m, 3H), 6.88 (d, *J* = 8.9 Hz, 2H), 3.99 (t, *J* = 6.3 Hz, 2H), 2.88 – 2.50 (m, 9H), 1.91 (p, *J* = 6.5 Hz, 2H), 1.55 (p, *J* = 5.5 Hz, 4H), 1.42 (q, *J* = 5.3 Hz, 2H)
^{13}C NMR (75 MHz, DMSO):	δ 163.35, 156.85, 155.49, 148.13, 131.25, 126.16, 125.52, 114.03, 113.76, 65.81, 54.79, 53.66, 27.67, 25.66, 24.89, 23.53
Melting point	117.1 °C
MS (APCI-(+)):	m/z = 410.0 $[M+H^+]^+$
LC-MS-DAD purity:	100.00%
HRMS (ESI-(+)):	m/z = 410.2190 $[M+H^+]^+$ (calculated: 410.2162)

N^4-(3-Methoxy-4-(3-(piperidin-1-yl)propoxy)phenyl)-N^2-methyl-5-(trifluoromethyl)pyrimidine-2,4-diamine (79)

To a solution of 4-chloro-*N*-methyl-5-(trifluoromethyl)pyrimidin-2-amine **(P38)** (64 mg, 0.30 mmol, 1.0 eq.) and 3-methoxy-4-(3-(piperidin-1-yl)propoxy)aniline **(P15)** (88 mg, 0.33 mmol, 1.1 eq.) in 1 mL of isopropanol in a microwave vial, 0.1 mL of TFA was added. The reaction mixture was stirred at room temperature for 24 h. The solvent was then evaporated, and the residue was partitioned between 1 M NaOH (30 mL) and ethyl acetate (3 × 30 mL). The organic layers were merged, washed with brine, dried over Na_2SO_4. After filtration solvent was evaporated, and the residue was purified using column chromatography (DCM:MeOH(NH_3) = 93:7) in order to obtain desired product

Yield:	28 mg (21%)
Chemical formula:	$C_{21}H_{28}F_3N_5O_2$
Molecular mass:	439.48 g/mol
Appearance	White solid
Internal code:	MG-287, ST-2889
^{1}H NMR (300 MHz, DMSO):	δ 8.32 – 7.94 (m, 2H), 7.36 (d, *J* = 13.5 Hz, 1H), 7.28 – 6.98 (m, 2H), 6.89 (d, *J* = 8.2 Hz, 1H), 3.96 (t, *J* = 6.4 Hz, 2H), 3.75 (s, 3H), 2.81 – 2.68 (m, 3H), 2.43 (s, 6H), 1.86 (p, *J* = 6.4 Hz, 2H), 1.51 (q, *J* = 5.5 Hz, 4H), 1.39 (d, *J* = 7.1 Hz, 2H)
^{13}C NMR (75 MHz, DMSO):	δ 163.29, 156.67, 155.51, 152.09, 148.62, 148.32, 131.85, 115.49, 108.90, 107.58, 96.32, 66.93, 55.23, 55.04, 53.91, 27.77, 26.15, 25.28, 23.85
Melting point	147.1 °C
MS (APCI-(+)):	m/z = 440.0 $[M+H^+]^+$
LC-MS-DAD purity:	100.00%
HRMS (ESI-(+)):	m/z = 440.2283 $[M+H^+]^+$ (calculated: 440.2268)

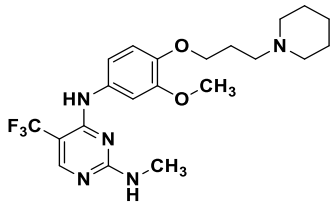

N^4-(4-Methoxy-3-(3-(piperidin-1-yl)propoxy)phenyl)-*N*^{2}-methyl-5-(trifluoromethyl) pyrimidine-2,4-diamine (80)

To a solution of 4-chloro-*N*-methyl-5-(trifluoromethyl)pyrimidin-2-amine **(P38)** (62 mg, 0.29 mmol, 1.0 eq.) and 4-methoxy-3-(3-(piperidin-1-yl)propoxy)aniline **(P16)** (85 mg, 0.32 mmol, 1.1 eq.) in 1 mL of isopropanol in a microwave vial, 0.1 mL of TFA was added. The reaction mixture was stirred at room temperature for 24 h. The solvent was then evaporated, and the residue was partitioned between 1 M NaOH (30 mL) and ethyl acetate (3 × 30 mL). The organic layers were merged, washed with brine, dried over Na_2SO_4. After filtration solvent was evaporated, and the residue was purified using column chromatography (DCM:MeOH(NH_3) = 93:7) in order to obtain desired product.

Yield:	60 mg (50%)
Chemical formula:	$C_{21}H_{28}F_3N_5O_2$
Molecular mass:	439.48 g/mol
Appearance	Beige solid
Internal code:	MG-288, ST-2890
^{1}H NMR (300 MHz, DMSO):	δ 8.29 – 8.01 (m, 2H), 7.48 – 7.03 (m, 3H), 6.91 (d, J = 8.4 Hz, 1H), 4.08 – 3.94 (m, 2H), 3.75 (s, 3H), 3.19 – 2.62 (m, 9H), 2.20 – 2.03 (m, 2H), 1.81 – 1.63 (m, 4H), 1.61 – 1.37 (m, 2H)

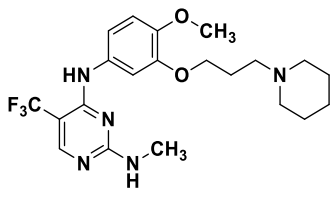

^{13}C NMR (75 MHz, DMSO):	δ 168.27, 163.32, 156.71, 155.53, 145.72, 142.12, 131.64, 130.66, 126.95, 116.54, 111.66, 103.67, 66.29, 55.72, 53.92, 52.50, 27.83, 27.71, 23.08, 22.09
Melting point	187.9 °C
MS (APCI-(+)):	m/z = 440.3 $[M+H^+]^+$
LC-MS-DAD purity:	100.00%
HRMS (ESI-(+)):	m/z = 440.2280 $[M+H^+]^+$ (calculated: 440.2268)

N^4-(2-Methoxy-4-(3-(piperidin-1-yl)propoxy)phenyl)-*N*^{2}-methyl-5-(trifluoromethyl) pyrimidine-2,4-diamine (81)

To a solution of 4-chloro-*N*-methyl-5-(trifluoromethyl)pyrimidin-2-amine **(P38)** (80 mg, 0.38 mmol, 1.0 eq.) and 2-methoxy-4-(3-(piperidin-1-yl)propoxy)aniline **(P17)** (110 mg, 0.42 mmol, 1.1 eq.) in 2 mL of isopropanol in a microwave vial, 0.1 mL of TFA was added. The reaction mixture was stirred at room temperature for 24 h. The solvent was then evaporated, and the residue was partitioned between 1 M NaOH (30 mL) and ethyl acetate (3 × 30 mL). The organic layers were merged, washed with brine, dried over Na_2SO_4. After filtration solvent was evaporated, and the residue was purified using flash column chromatography (DCM:MeOH, 0-7% MeOH) in order to obtain desired product.

Yield:	126 mg (79%)
Chemical formula:	$C_{21}H_{28}F_3N_5O_2$
Molecular mass:	439.48 g/mol
Appearance	Beige resin
Internal code:	MG-321, ST-3008
^{1}H NMR (300 MHz, $CDCl_3$):	δ 8.37 (s, 1H), 8.15 (s, 1H), 7.50 (s, 1H), 6.49 (d, *J* = 9.3 Hz, 2H), 5.32 (s, 1H), 4.00 (t, *J* = 6.4 Hz, 2H), 3.87 (s, 3H), 3.01 (d, *J* = 5.0 Hz, 3H), 2.55 – 2.28 (m, 6H), 2.05 – 1.92 (m, 2H), 1.59 (p, *J* = 5.5 Hz, 4H), 1.52 – 1.37 (m, 2H)
^{13}C NMR (151 MHz, DMSO):	δ 163.86, 156.88, 155.75, 155.41, 150.24, 126.26, 124.47, 122.04, 104.51, 99.29, 67.05, 56.17, 56.16, 54.83, 28.70, 27.07, 26.16, 24.60
Melting point	151.4 °C
MS (APCI-(+)):	m/z = 440.3 $[M+H^+]^+$
LC-MS-DAD purity:	97.64%
HRMS (ESI-(+)):	m/z = 440.2274 $[M+H^+]^+$ (calculated: 440.2268)

N^2-Ethyl-N^4-(4-(3-(4-methylpiperazin-1-yl)propoxy)phenyl)-5-(trifluoromethyl) pyrimidine-2,4-diamine (82)

To a solution of 4-chloro-*N*-ethyl-5-(trifluoromethyl)pyrimidin-2-amine **(P40)** (86 mg, 0.38 mmol, 1.0 eq.) and 1-methyl-4-(3-(4-nitrophenoxy)propyl)piperazine **(P12)** (105 mg, 0.42 mmol, 1.1 eq.) in 2 mL of isopropanol in a microwave vial, 0.1 mL of TFA was added. The reaction mixture was stirred at 60 °C for 24 h. The solvent was then evaporated, and the residue was partitioned between 1 M NaOH (30 mL) and ethyl acetate (3 × 30 mL). The organic layers were merged, washed with brine, dried over Na_2SO_4. After filtration solvent was evaporated, and the residue was purified using flash column chromatography (DCM:MeOH, 0-7% MeOH) in order to obtain desired product.

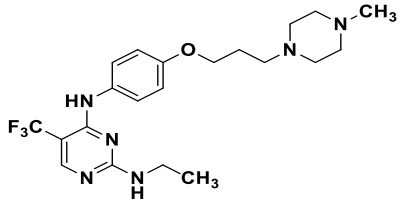

Yield:	97 mg (58%)
Chemical formula:	$C_{21}H_{29}F_3N_6O$
Molecular mass:	438.50 g/mol
Appearance	White solid
Internal code:	MG-318, ST-2999
^{1}H NMR (300 MHz, $CDCl_3$):	δ 8.11 (q, *J* = 0.9 Hz, 1H), 7.45 (d, *J* = 9.0 Hz, 2H), 7.23 (s, 1H), 6.87 (d, *J* = 9.0 Hz, 2H), 5.07 (s, 1H), 4.00 (t, *J* = 6.4 Hz, 2H), 3.52 (qd, *J* = 7.2, 5.3 Hz, 2H), 2.80 – 2.37 (m, 10H), 2.29 (s, 3H), 2.04 – 1.89 (m, 2H), 1.26 (t, *J* = 7.2 Hz, 3H)
^{13}C NMR (151 MHz, DMSO):	δ 161.35, 158.99, 155.27, 154.91, 154.88, 154.84, 154.81, 132.28, 127.99, 127.92, 126.14, 124.35, 122.49, 122.09, 121.95, 114.85, 66.72, 55.29, 55.26, 53.31, 46.15, 36.15, 26.97, 14.68.
Melting point	115.9 °C
MS (APCI-(+)):	m/z = 439.3 $[M+H^+]^+$
LC-MS-DAD purity:	100.00%
HRMS (ESI-(+)):	m/z = 439.2439 $[M+H^+]^+$ (calculated: 439.2428)

1-(4-(3-(4-((2-(Ethylamino)-5-(trifluoromethyl)pyrimidin-4-yl)amino)phenoxy)propyl) piperazin-1-yl)ethan-1-one (83)

To a solution of 4-chloro-*N*-ethyl-5-(trifluoromethyl)pyrimidin-2-amine **(P40)** (100 mg, 0.44 mmol, 100 mg, 1.0 eq.) and 1-(4-(3-(4-aminophenoxy)propyl)piperazin-1-yl)ethan-1-one **(P13)** (135 mg, 0.49 mmol, 1.1 eq.) in a mixture of hexane and isopropanol, 3 mL of TFA was added. The reaction mixture was stirred at 60 °C temperature for 24 h. Subsequently, the solvent was evaporated, and the residue was partitioned between 2 M NaOH (30 mL) and ethyl acetate

(3 × 30 mL). The organic layers were merged, washed with brine, dried over Na_2SO_4. After filtration solvent was evaporated, and the residue was purified using flash column chromatography (DCM:MeOH, 0-7% MeOH) in order to obtain desired product.

Yield:	128 mg (62%)
Chemical formula:	$C_{22}H_{29}F_3N_6O_2$
Molecular mass:	466.51 g/mol
Appearance	White solid
Internal code:	MG-349, ST-3014

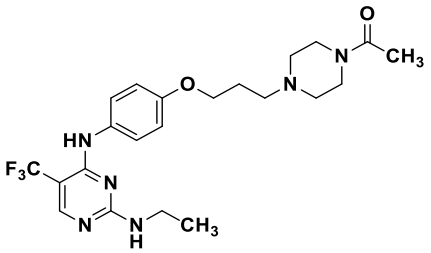

^{1}H NMR (300 MHz, $CDCl_3$):	δ 8.12 (d, *J* = 1.1 Hz, 1H), 7.46 (d, *J* = 9.0 Hz, 2H), 7.10 (s, 1H), 6.87 (d, *J* = 9.0 Hz, 2H), 5.08 (s, 1H), 4.01 (t, *J* = 6.2 Hz, 2H), 3.62 (t, *J* = 5.1 Hz, 2H), 3.54 (td, *J* = 7.2, 5.3 Hz, 2H), 3.49 – 3.44 (m, 2H), 2.60 – 2.49 (m, 2H), 2.44 (dt, *J* = 9.9, 5.1 Hz, 4H), 2.09 (s, 3H), 2.04 – 1.91 (m, 2H), 1.26 (t, *J* = 7.2 Hz, 3H)
^{13}C NMR (151 MHz, $CDCl_3$):	δ 169.05, 161.35, 159.00, 155.21, 154.94, 154.91, 154.88, 154.84, 132.34, 127.92, 126.13, 124.34, 122.06, 114.85, 66.43, 55.13, 53.54, 52.94, 46.45, 41.56, 36.15, 26.89, 21.48, 14.69
Melting point	147.0 °C
MS (APCI-(+)):	m/z = 466.9 $[M+H^+]^+$
LC-MS-DAD purity:	100.00%
HRMS (ESI-(+)):	m/z = 467.2385 $[M+H^+]^+$ (calculated: 467.2377)

N^2-Ethyl-*N*^{4}-(4-(3-(piperidin-1-yl)propoxy)phenyl)-5-(trifluoromethyl)pyrimidine-2,4-diamine (84)

To a solution of 4-chloro-*N*-ethyl-5-(trifluoromethyl)pyrimidin-2-amine **(P40)** (86 mg, 0.38 mmol, 1.0 eq.) and 4-(3-(piperidin-1-yl)propoxy)aniline **(P14)** (98 mg, 0.42 mmol, 1.1 eq.) in 2 mL of isopropanol in a microwave vial, 0.1 mL of TFA was added. The reaction mixture was stirred at room temperature for 24 h. Subsequently, the solvent was evaporated, and the residue was partitioned between 2 M NaOH (30 mL) and ethyl acetate (3 × 30 mL). The organic layers were merged, washed with brine, dried over Na_2SO_4. After filtration solvent was evaporated, and the residue was purified using flash column chromatography (DCM:MeOH, 0-7% MeOH) in order to obtain desired product.

Yield:	95 mg (59%)
Chemical formula:	$C_{21}H_{28}F_3N_5O$

Molecular mass:	423.48 g/mol
Appearance	Off-white solid
Internal code:	MG-317, ST-2998

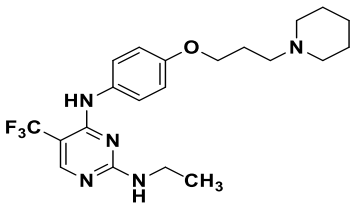

^{1}H NMR (300 MHz, $CDCl_3$):	δ 8.12 (d, *J* = 1.0 Hz, 1H), 7.45 (d, *J* = 9.0 Hz, 2H), 7.24 (s, 1H), 6.87 (d, *J* = 9.0 Hz, 2H), 5.08 (s, 1H), 4.00 (t, *J* = 6.4 Hz, 2H), 3.59 – 3.45 (m, 2H), 2.53 – 2.34 (m, 6H), 2.05 – 1.91 (m, 2H), 1.60 (p, *J* = 5.6 Hz, 4H), 1.45 (q, *J* = 6.2 Hz, 2H), 1.26 (t, *J* = 7.2 Hz, 3H)
^{13}C NMR (151 MHz, $CDCl_3$):	δ 161.36, 158.99, 155.31, 154.91, 154.87, 154.84, 154.81, 132.23, 127.93, 126.15, 124.36, 122.51, 122.08, 122.06, 114.86, 66.98, 56.16, 54.78, 36.16, 26.08, 24.55, 14.68
Melting point	115.4 °C
MS (APCI-(+)):	m/z = 424.3 $[M+H^+]^+$
LC-MS-DAD purity:	100.00%
HRMS (ESI-(+)):	m/z = 424.1997 $[M+H^+]^+$ (calculated: 424.2319)

N^2-Ethyl-*N*^{4}-(3-methoxy-4-(3-(piperidin-1-yl)propoxy)phenyl)-5-(trifluoromethyl) pyrimidine-2,4-diamine (85)

To a solution of 4-chloro-*N*-ethyl-5-(trifluoromethyl)pyrimidin-2-amine **(P40)** (100 mg, 0.44 mmol, 1.0 eq.) and 3-methoxy-4-(3-(piperidin-1-yl)propoxy)aniline **(P15)** (129 mg, 0.49 mmol, 1.1 eq.) in 3 mL of isopropanol in a microwave vial, 0.1 mL of TFA was added. The reaction mixture was stirred at 60 °C for 24 h. The solvent was then evaporated, and the residue was partitioned between 2 M NaOH (30 mL) and ethyl acetate (3 × 30 mL). The organic layers were merged, washed with brine, dried over Na_2SO_4. After filtration solvent was evaporated, and the residue was purified using flash column chromatography (DCM:MeOH, 0-7% MeOH) in order to obtain desired product.

Yield:	128 mg (63%)
Chemical formula:	$C_{22}H_{30}F_3N_5O_2$
Molecular mass:	453.51 g/mol
Appearance	Beige resin
Internal code:	MG-345, ST-3000

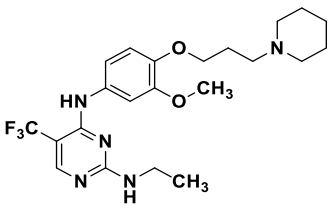

^{1}H NMR (300 MHz, $CDCl_3$):	δ 8.13 (s, 1H), 7.33 (d, *J* = 2.4 Hz, 1H), 7.21 (s, 1H), 6.96 (dd, *J* = 8.6, 2.5 Hz, 1H), 6.86 (d, *J* = 8.7 Hz, 1H), 5.09 (s, 1H), 4.06 (t, *J* = 6.7 Hz, 2H), 3.86 (s, 3H), 3.56 (qd, *J* = 7.2, 5.2 Hz, 2H), 2.55 – 2.47 (m, 2H), 2.46 – 2.36

	(m, 4H), 2.02 (p, *J* = 6.8 Hz, 2H), 1.60 (p, *J* = 5.5 Hz, 4H), 1.45 (q, *J* = 5.9 Hz, 2H), 1.26 (t, *J* = 7.3 Hz, 3H)
^{13}C NMR (151 MHz, $CDCl_3$):	δ 161.25, 159.02, 154.89, 149.72, 144.66, 133.02, 127.89, 126.11, 124.33, 122.54, 114.07, 112.32, 105.73, 68.37, 56.06, 56.04, 54.72, 36.18, 26.89, 26.09, 24.56, 14.74
Melting point	n.a.
MS (APCI-(+)):	m/z = 453.8 $[M+H^+]^+$
LC-MS-DAD purity:	100.00%
HRMS (ESI-(+)):	m/z = 454.2438 $[M+H^+]^+$ (calculated: 454.2424)

N^2-Ethyl-*N*^{4}-(4-methoxy-3-(3-(piperidin-1-yl)propoxy)phenyl)-5-(trifluoromethyl) pyrimidine-2,4-diamine (86)

To a solution of 4-chloro-*N*-ethyl-5-(trifluoromethyl)pyrimidin-2-amine **(P40)** (100 mg, 0.44 mmol, 1.0 eq.) and 4-methoxy-3-(3-(piperidin-1-yl)propoxy)aniline **(P16)** (129 mg, 0.49 mmol, 1.1 eq.) in 3 mL of isopropanol in a microwave vial, 0.1 mL of TFA was added. The reaction mixture was stirred at 60 °C for 24 h. The solvent was then evaporated, and the residue was partitioned between 2 M NaOH (30 mL) and ethyl acetate (3 × 30 mL). The organic layers were merged, washed with brine, dried over Na_2SO_4. After filtration solvent was evaporated, and the residue was purified using flash column chromatography (DCM:MeOH, 0-7% MeOH) in order to obtain desired product.

Yield:	96 mg (48%)
Chemical formula:	$C_{22}H30F_3N_5O_2$
Molecular mass:	453.51 g/mol
Appearance	Beige solid
Internal code:	MG-346, ST-3001
^{1}H NMR (300 MHz, $CDCl_3$):	δ 8.16 – 8.10 (m, 1H), 7.33 (d, *J* = 2.5 Hz, 1H), 7.20 (s, 1H), 6.99 (dd, *J* = 8.6, 2.5 Hz, 1H), 6.83 (d, *J* = 8.7 Hz, 1H), 5.09 (s, 1H), 4.06 (t, *J* = 6.6 Hz, 2H), 3.85 (s, 3H), 3.55 (qd, *J* = 7.3, 5.3 Hz, 2H), 2.55 – 2.48 (m, 2H), 2.47 – 2.37 (m, 4H), 2.06 (p, *J* = 6.8 Hz, 2H), 1.60 (p, *J* = 5.5 Hz, 4H), 1.44 (q, *J* = 6.0 Hz, 2H), 1.27 (t, *J* = 7.3 Hz, 3H)
^{13}C NMR (151 MHz, $CDCl_3$):	δ 161.27, 159.01, 154.91, 154.88, 154.85, 154.81, 148.68, 145.72, 132.86, 127.58, 126.12, 124.33, 122.55, 112.51, 112.38, 107.18, 67.75, 56.57, 56.02, 54.69, 36.18, 26.75, 25.97, 24.47, 14.76
Melting point	65.6 °C
MS (APCI-(+)):	m/z = 454.1 $[M+H^+]^+$
LC-MS-DAD purity:	95.81%

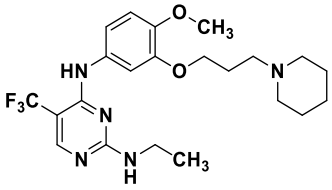

HRMS (ESI-(+)): m/z = 454.2431 $[M+H^+]^+$ (calculated: 454.2424)

N^2-Ethyl-N^4-(2-methoxy-4-(3-(piperidin-1-yl)propoxy)phenyl)-5-(trifluoromethyl) pyrimidine-2,4-diamine (87)

To a solution of 4-chloro-*N*-ethyl-5-(trifluoromethyl)pyrimidin-2-amine **(P40)** (100 mg, 0.44 mmol, 1.0 eq.) and 2-methoxy-4-(3-(piperidin-1-yl)propoxy)aniline **(P17)** (129 mg, 0.49 mmol, 1.1 eq.) in 50 mL of hexane and isopropanol, 3 mL of TFA was added. The reaction mixture was stirred at 60 °C for 24 h. The solvent was then evaporated, and the residue was partitioned between 2 M NaOH (30 mL) and DCM (3 × 30 mL). The organic layers were merged, washed with brine, dried over Na_2SO_4. After filtration solvent was evaporated, and the residue was purified using flash column chromatography (DCM:MeOH, 0-7% MeOH) in order to obtain desired product.

Yield:	38 mg (19%)
Chemical formula:	$C_{22}H_{30}F_3N_5O_2$
Molecular mass:	453.51 g/mol
Appearance	Brown resin
Internal code:	MG-348, ST-3013

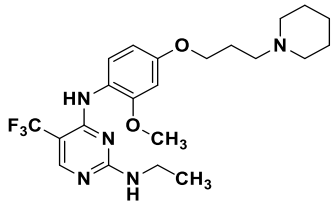

^{1}H NMR (300 MHz, $CDCl_3$):	δ 8.24 (d, *J* = 9.6 Hz, 1H), 8.13 (s, 1H), 7.44 (s, 1H), 6.55 – 6.46 (m, 2H), 5.07 (s, 1H), 4.00 (t, *J* = 6.4 Hz, 2H), 3.86 (s, 3H), 3.58 (td, *J* = 7.3, 5.3 Hz, 2H), 2.54 – 2.47 (m, 2H), 2.46 – 2.37 (m, 4H), 2.05 – 1.92 (m, 2H), 1.61 (p, *J* = 5.5 Hz, 4H), 1.45 (q, *J* = 6.3 Hz, 2H), 1.29 (t, *J* = 7.2 Hz, 3H)
^{13}C NMR (151 MHz, $CDCl_3$):	δ 161.08, 159.04, 155.10, 154.89, 154.86, 154.82, 154.79, 149.66, 126.23, 124.45, 122.37, 120.29, 104.56, 99.34, 67.03, 56.18, 55.85, 54.78, 36.27, 27.03, 26.08, 24.55, 14.70
Melting point	n.a.
MS (APCI-(+)):	m/z = 454.1 $[M+H^+]^+$
LC-MS-DAD purity:	97.59%
HRMS (ESI-(+)):	m/z = 454.2445 $[M+H^+]^+$ (calculated: 454.2424)

6.3 Pharmacological Experiments

6.3.1 *h*H_3R Radioligand Displacement Assay

Radioligand displacement assays were performed on the membrane fractions of HEK-293 cells stably expressing *h*H_3R, as described previously with slight modifications.[516] HEK-293-*h*H_3R cells were grown in Dulbecco's Modified Eagle Medium (DMEM) supplemented with 10% FBS, 100 µg/mL penicillin, 100 units/mL streptomycin and 10 mM HEPES solution at 37 °C in a humidified atmosphere of 5% CO_2. To prepare membrane fractions, cells were washed in phosphate-buffered saline (PBS) solution and harvested. The cells were centrifuged at 3000 × g for 10 min at 4 °C and homogenised with Ultraturrax® in ice-cold binding buffer (75 mM Tris-HCl, 10 mM $MgCl_2$, 100 mM NaCl, pH 7.4). The homogenate was centrifuged twice (20,000 × g, 20 min, 4 °C) and reconstituted in an ice-cold binding buffer. Test ligands, radiolabeled ligands, and membrane fractions (20 µg/well) were added to 96-well plates to a final assay volume of 200 µL. After 90 minutes of incubation with shaking at 25 °C, a cell harvester was used to separate bound from free ligands by filtration through GF/B filters pretreated with 0.3% (m/v) polyethylenimine. Radioactivity was determined by liquid scintillation counting. As the radiolabeled probe [^{3}H]N^{α}-methylhistamine was used at a final concentration of 2 nM (K*d* = 3.08 nM). The test ligands were evaluated at concentrations between 100 µM and 0.03 nM. To determine non-specific binding, 10 µM pitolisant was used. Specific binding was calculated by subtracting non-specific binding from the raw data. Data were obtained in duplicate from at least three independent experiments and analyzed using GraphPad Prism 7.02. using nonlinear regression. CHENG-PRUSOFF equation was used to calculate K_i values from the IC_{50} values.[515] Mean values and 95% confidence intervals were calculated using -log(K_i) and converted to nanomolar concentrations.

6.3.2 *In vitro* G9a Activity Assay

Inhibition of G9a was examined in an AlphaLISA based format with protocols provided by PerkinElmer.[204] Compounds were incubated for 30 min on white 384-well microplates at the indicated concentration and with 30 nM G9a, 100 nM histone H3 (1-21) fragment and 15 µM SAM in assay buffer (50 mM Tris-HCl (pH = 9.0); 50 mM NaCl, 1 mM dithiothreitol, 0.01% Tween-20). Incubation was terminated by addition of anti-H3K9me2 acceptor beads in provided detection buffer. After incubating the mixture for 60 min, streptavidin-coated donor beads were added to the mix for additional 30 min. Luminescence was then measured using the AlphaLISA luminescence filter of an Infinite M1000pro multiplate reader (Tecan,

Maennedorf, Switzerland) for 1,000 ms (integration time). Data were obtained in duplicate from at least two independent experiments.

6.3.3 *In vitro* LRRK2 Activity Assay

Screening of LRRK2 enzyme activity was performed as fluorescence-based immunoassay for the detection of ADP, utilizing the Adapta® Universal Kinase Assay Kit (Invitrogen) (Cat. PV5099). The activity of LRRK2 kinase (Cat. PV4873) was evaluated following incubation with different ligands, according to the protocol for Optimization of Adapta™ Kinase assay for LRRK2. Each assay was conducted in a total volume of 10 µL, consisting of LRRK2 kinase (6 nM), a LRRKtide substrate (200 µM) (Cat. PV5093), ATP cofactor (20 µM), kinase reaction buffer (50mM Tris-HCl pH 8.5, 10 mM $MgCl_2$, 1 mM EGTA, 0.01% Brij-35, and 2 mM DTT) (Cat. PV5213) and compound of interest in varying concentrations. Positive and negative control, as well as LRRK2 reference inhibitor Staurosporine, were incubated on the same plate along other assay mixtures. The positive control contained the same assay components as other assay mixtures, excluding the compound of interest (representing 0% enzyme inhibition), while the negative control lacked both the enzyme and the compound of interest (representing 100% enzyme inhibition). After 1 h of incubation at room temperature, 5 µL of the Adapta® Assay Detection Mix (Cat. PV5099) was added, consisting of 30 mM EDTA to stop the kinase reaction, 6 nM of the Adapta™ Eu-anti-ADP Antibody and 18.9 nM of the Alexa Fluor® 647 ADP Tracer. The plate was equilibrated at room temperature for at least 30 min before being read in a fluorescence microplate reader to establish the ratio of emissions at 665 nm (ADP Tracer) and at 615 nm (Eu-antibody) as a measure of ADP concentration by virtue of Fluorescence Resonance Energy Transfer (FRET).

Initially, a single-point measurement of ligands at 10 µM concentration were performed. Ligands with high affinity for H_3R (K_i < 100 nM) that inhibited more than 90% LRRK2 activity were further tested at an additional single-point measurement at 100 nM concentration. All ligands that inhibited more than 70% LRRK2 activity at 100 nM were subsequently assayed over a broader concentration range prepared as a 10-fold serial dilution (1000 nM, 100 nM, 10 nM, 1 nM, 0.1 nM and 0.01 nM). The results, obtained as TR-FRET emission ratios, were converted to % inhibition using following equation:

$$\%\ \text{inhibition} = \frac{\text{Ratio}_{\text{sample}} - \text{Ratio}_{0\%\ \text{inhibition}}}{\text{Ratio}_{100\%\ \text{inhibition}} - \text{Ratio}_{0\%\ \text{inhibition}}} \text{ x } 100$$

The % inhibition for ligand dilution series was plotted against the concentration, and the data was fit to a sigmoidal dose-response cure with a variable slope (GraphPad Prism 10). The IC_{50} was determined by the intersection of the fitted curve with the 50% activity measure. All measurements were obtained from two independent experiments performed in duplicate.

6.3.4 Cytotoxicity Assay on SH-SY5Y Cells

The cytotoxic effects of the tested ligands on neuroblastoma SH-SY5Y cells were determined using the alamar blue viability assay.[548] SH-SY5Y cells were grown in Minimum Essential Medium Eagle (MEME) supplemented with non-essential amino acids, 10% FBS, 100 µg/mL penicillin, 100 units/mL streptomycin, and 2 mM L-glutamine at 37 °C in a humidified atmosphere of 5% CO_2. SH-SY5Y cells were seeded in 96-well plates at a density of 8.0×10^3 cells per well and grown at 37 °C in a humidified atmosphere of 5% CO_2. 24 h after seeding, the test ligands were added at concentrations between 30 µM and 1 nM in a final assay volume of 100 µL per well and incubated for 24 h. Cells treated with 1-methyl-4-phenylpyridinium iodide (MPP+) served as a positive control for cytotoxic effects. The concentration of DMSO was limited to 1% for all the assay points. The medium supplemented with the test compounds was discarded, and 100 µL of resazurin solution in RP I-1640 medium (44 µM) was added. After two hours of incubation at 37 °C in a humidified atmosphere of 5% CO_2, fluorescence intensity (λ_{Em} = 535 nm, λ_{Ex} = 590 nm) was determined. Data were obtained in duplicate from at least three independent experiments. LC_{50} values were evaluated using GraphPad Prism 7.02. using a nonlinear regression.[544] Mean values and 95% confidence intervals were calculated using $-\log(K_i)$ and converted to nanomolar concentrations.

6.3.5 Molecular Docking Study

Molecular docking studies for compounds **24**-**39** were performed with G9a and H_3R targets in GOLD 2022.3.0 Software.[549] The Protein Data Bank website (https://www.rcsb.org) was the download source for the crystal structures of the target molecules. For G9a docking, the PDB structure 9btv[293] was used, while for H_3R docking the only available PDB structure 7f61[33] was used. PDB: 9btv was selected for G9a docking based on the most similar structure of the reference ligand with the synthesized and tested compounds. Both protein structures were protonated (at physiological pH = 7.4) and tautomerized in PDB2PQR 3.6.2[550] (https://server.poissonboltzmann.org/pdb2pqr) using the PARSE forcefield. Prior to the docking studies, the dominant species of the compounds and reference ligands were determined at pH = 7.4 in MarvinSketch 6.1.0 (http://www.chemaxon.com). The 3D structures were

aligned in the Flap software 2.2.2 using the graph alignment algorithm according to the maximum common subgraph.[551] Out of 50 conformers, the algorithm selected only one corresponding to the largest common graph defined by atom types and chemical bonds. Its geometry was additionally clarified in the Discovery Studio Visualizer.[552] GoldScore was used as the fitness function for docking. This function consists of four components: Protein-ligand hydrogen bond energy (external H-bond), protein-ligand van der Waals (vdW) energy (external vdW), ligand internal vdW energy (internal vdW) and ligand torsional strain energy (internal torsion). Discovery Studio Visualizer v21[552] and PyMol 3.0.5[553] were used for 2D and 3D visualization of the ligands in the binding sites of the targets. Literature interactions of the reference ligands, which were used as a reference for comparison with the docking results of the synthesized compounds.[33, 293]

Molecular docking studies for compounds **40**-**87** were performed with LRRK2 and H_3R targets. The chemical structures of synthesized compounds were built in *ChemDraw* software 7.0.1[554] and their ionization forms dominant at pH = 7.4 were estimated in *MarvinSketch* 6.1.0.[555] Geometry optimization of the synthesized 48 H_3R/LRRK2 inhibitors, as protonated piperidines and piperazines, was performed at the HF/3-21G (d,p) level in the gas phase using the *Gaussian 03* program.[556] The optimized 3D structures of the 48 H_3R/LRRK2 inhibitors were used for further molecular docking studies. *GOLD* 2022.3.0 software[549] was used to perform molecular docking studies of the 48 with H_3R/LRRK2 inhibitors. The crystal structures of the targets, H_3 receptor (PDB: 7F61) and LRRK2 enzyme (PDB: 8TXZ), were downloaded from the PDB website (*accessed in December 2024*). The target structures were protonated and the tautomeric forms of the residues under physiological conditions (pH = 7.4) were assigned using *PDB2PQR* 3.6.2 software (https://server.poissonboltzmann.org/pdb2pqr).[550] The docking procedure was performed using ChemASP and ChemPLP scoring functions for H_3R and LRRK2, respectively. The docking protocols were validated using the RMSD value (RMSD < 2 Å) of the docked co-crystallized ligand, while Discovery Studio software v24.1.0.23298[552] was used to visualize the docking poses of the ligands in the binding sites of H_3R and LRRK2.

6.3.6 Lipophilicity Determination (logP and logD)

The lipophilicity of compounds was determined following guidelines provided by the Organisation for Economic Co-operation and Development (OECD) for HPLC method.[534] Chromatographic analyses were performed using an Agilent 1260 II LC System equipped with a flexible pump, an autosampler featuring thermal control of the column oven, a fluorescence detector, and a UV-VIS detector. For the evaluation of logP values, a Eurospher II 100-5 C18P

column (50 × 4 mm, Knauer) with high pH stability (pH range 1–12) was employed. The mobile phase consisted of 60% acetonitrile and 40% pyrrolidine aqueous buffer (5 mM), adjusted to pH 11 to ensure the neutral form of the evaluated compounds during chromatographic analysis. For the determination of logD values, a BETASIL C18 column (50 × 4.6 mm, ThermoFisher) was used. The mobile phase comprised 60% ACN and 40% aqueous PBS buffer (5 mM), adjusted to pH 7.4 to mimic physiological conditions. Isocratic elution was applied at a flow rate of 1 mL/min. The column temperature was maintained at 30 °C, and detection was performed at 254 nm. The injection volume for each sample was 10 μL. Thiourea was used to determine the dead time. All reference and test compounds were initially prepared as 10 mM stock solutions in dimethyl sulfoxide (DMSO), except for thiourea, which was dissolved directly in the mobile phase. Samples were subsequently diluted with the mobile phase to a final concentration of 100 nM for analysis. Chromatograms were processed using the manufacturer-provided Agilent OpenLab CDS software.

7 References

[1] Dale, HH; Laidlaw, PP. The physiological action of β-iminazolylethylamine. *The Journal of Physiology* **1910**, *41* (5), 318-344. DOI: https://doi.org/10.1113/jphysiol.1910.sp001406.

[2] Jutel, M; Akdis, M; Akdis, CA. Histamine, histamine receptors and their role in immune pathology. *Clinical & Experimental Allergy* **2009**, *39* (12), 1786-1800. DOI: https://doi.org/10.1111/j.1365-2222.2009.03374.x.

[3] Black, JW; Ganellin, CR. Naming of substituted histamines. *Experientia* **1974**, *30* (1), 111-113. DOI: https://doi.org/10.1007/BF01921632.

[4] Paiva, T; Tominaga, M; Paiva, AC. Ionization of histamine, *N*-acetylhistamine, and their iodinated derivatives. *Journal of Medicinal Chemistry* **1970**, *13* (4), 689-692.

[5] Panula, P; Chazot, PL; Cowart, M; Gutzmer, R; Leurs, R; Liu, WLS; Stark, H; Thurmond, RL; Haas, HL. International Union of Basic and Clinical Pharmacology. XCVIII. Histamine Receptors. *Pharmacological Reviews* **2015**, *67* (3), 601-655. DOI: https://doi.org/10.1124/pr.114.010249.

[6] Panula, P; Nuutinen, S. The histaminergic network in the brain: basic organization and role in disease. *Nature Reviews Neuroscience* **2013**, *14* (7), 472-487. DOI: https://doi.org/10.1038/nrn3526.

[7] Zimmermann, AS; Burhenne, H; Kaever, V; Seifert, R; Neumann, D. Systematic analysis of histamine and N-methylhistamine concentrations in organs from two common laboratory mouse strains: C57Bl/6 and Balb/c. *Inflammation Research* **2011**, *60* (12), 1153-1159. DOI: https://doi.org/10.1007/s00011-011-0379-5.

[8] Brown, RE; Stevens, DR; Haas, HL. The physiology of brain histamine. *Progress in Neurobiology* **2001**, *63* (6), 637-672. DOI: https://doi.org/10.1016/S0301-0082(00)00039-3.

[9] Weihe, E; Eiden, LE. Chemical neuroanatomy of the vesicular amine transporters. *The FASEB Journal* **2000**, *14* (15), 2435-2449. DOI: https://doi.org/10.1096/fj.00-0202rev.

[10] Berlin, M; Boyce, CW; de Lera Ruiz, M. Histamine H_3 Receptor as a Drug Discovery Target. *Journal of Medicinal Chemistry* **2011**, *54* (1), 26-53. DOI: https://doi.org/10.1021/jm100064d.

[11] Schwartz, JC; Arrang, JM; Garbarg, M; Pollard, H; Ruat, M. Histaminergic transmission in the mammalian brain. *Physiological Reviews* **1991**, *71* (1), 1-51. DOI: https://doi.org/10.1152/physrev.1991.71.1.1.

[12] Maintz, L; Novak, N. Histamine and histamine intolerance. *The American Journal of Clinical Nutrition* **2007**, *85* (5), 1185-1196. DOI: https://doi.org/10.1093/ajcn/85.5.1185.

[13] Yoshikawa, T; Nakamura, T; Yanai, K. Histamine N-Methyltransferase in the Brain. *International Journal of Molecular Sciences* **2019**, *20* (3), 737. DOI: https://doi.org/10.3390/ijms20030737

[14] Leurs, R; Chazot, PL; Shenton, FC; Lim, HD; De Esch, IJ. Molecular and biochemical pharmacology of the histamine H_4 receptor. *British Journal of Pharmacology* **2009**, *157* (1), 14-23. DOI: https://doi.org/10.1111/j.1476-5381.2009.00250.x.

[15] Leurs, R; Bakker, RA; Timmerman, H; de Esch, IJP. The histamine H_3 receptor: from gene cloning to H_3 receptor drugs. *Nature Reviews Drug Discovery* **2005**, *4* (2), 107-120. DOI: https://doi.org/10.1038/nrd1631.

[16] Arrang, J-M; Morisset, S; Gbahou, F. Constitutive activity of the histamine H_3 receptor. *Trends in Pharmacological Sciences* **2007**, *28* (7), 350-357. DOI: https://doi.org/10.1016/j.tips.2007.05.002.

[17] Konttinen, YT; Henrik, H; Xia, H; Passani, MB; Ballerini, C; Vasily, S; Tarvo, S; Zygmunt, M. Non-professional histamine producing cells, immune responses and autoimmunity. In *Histamine H4 receptor: A novel drug target in immunoregulation and inflammation*, Holger Stark, 2013; pp 201-258.

[18] Bakker, RA. Histamine H_3-receptor isoforms. *Inflammation Research* **2004**, *53* (10), 509-516. DOI: https://doi.org/10.1007/s00011-004-1286-9.

[19] HH, D; PP, L. Histamine shock. *J Physiol* **1919**, *52*, 355-390.

[20] Black, JW; Duncan, WAM; Durant, CJ; Ganellin, CR; Parsons, EM. Definition and Antagonism of Histamine H_2-receptors. *Nature* **1972**, *236* (5347), 385-390. DOI: https://doi.org/10.1038/236385a0.

[21] Arrang, J-M; Garbarg, M; Schwartz, J-C. Auto-inhibition of brain histamine release mediated by a novel class (H_3) of histamine receptor. *Nature* **1983**, *302* (5911), 832-837. DOI: https://doi.org/10.1038/302832a0.

[22] Morse, KL; Behan, J; Laz, TM; West, RE, Jr.; Greenfeder, SA; Anthes, JC; Umland, S; Wan, Y; Hipkin, RW; Gonsiorek, W; et al. Cloning and characterization of a novel human histamine receptor. *J Pharmacol Exp Ther* **2001**, *296* (3), 1058-1066.

[23] Cogé, F; Guénin, S-P; Rique, H; Boutin, JA; Galizzi, J-P. Structure and Expression of the Human Histamine H_4-Receptor Gene. *Biochemical and Biophysical Research Communications* **2001**, *284* (2), 301-309. DOI: https://doi.org/10.1006/bbrc.2001.4976.

[24] Nakamura, T; Itadani, H; Hidaka, Y; Ohta, M; Tanaka, K. Molecular Cloning and Characterization of a New Human Histamine Receptor, *HH4R*. *Biochemical and Biophysical Research Communications* **2000**, *279* (2), 615-620. DOI: https://doi.org/10.1006/bbrc.2000.4008.

[25] Nguyen, T; Shapiro, DA; George, SR; Setola, V; Lee, DK; Cheng, R; Rauser, L; Lee, SP; Lynch, KR; Roth, BL; et al. Discovery of a Novel Member of the Histamine Receptor Family. *Molecular Pharmacology* **2001**, *59* (3), 427-433. DOI: https://doi.org/10.1016/S0026-895X(24)12231-6.

[26] Oda, T; Morikawa, N; Saito, Y; Masuho, Y; Matsumoto, S-i. Molecular Cloning and Characterization of a Novel Type of Histamine Receptor Preferentially Expressed in Leukocytes. *Journal of Biological Chemistry* **2000**, *275* (47), 36781-36786. DOI: https://doi.org/10.1074/jbc.M006480200.

[27] Liu, C; Ma, X; Jiang, X; Wilson, S; Hofstra, C; Blevitt, J; Pyati, J; Li, X; Chai, W; Carruthers, N. Cloning and pharmacological characterization of a fourth histamine receptor (H_4) expressed in bone marrow. *Molecular pharmacology* **2001**, *59* (3), 420-426.

[28] Yamashita, M; Fukui, H; Sugama, K; Horio, Y; Ito, S; Mizuguchi, H; Wada, H. Expression cloning of a cDNA encoding the bovine histamine H_1 receptor. *Proceedings of the National Academy of Sciences* **1991**, *88* (24), 11515-11519. DOI: https://doi.org/10.1073/pnas.88.24.11515.

[29] Gantz, I; Schäffer, M; DelValle, J; Logsdon, C; Campbell, V; Uhler, M; Yamada, T. Molecular cloning of a gene encoding the histamine H_2 receptor. *Proceedings of the National Academy of Sciences* **1991**, *88* (2), 429-433. DOI: https://doi.org/10.1073/pnas.88.2.429.

[30] Lovenberg, TW; Roland, BL; Wilson, SJ; Jiang, X; Pyati, J; Huvar, A; Jackson, MR; Erlander, MG. Cloning and Functional Expression of the Human Histamine H_3 Receptor. *Molecular Pharmacology* **1999**, *55* (6), 1101-1107. DOI: https://doi.org/10.1124/mol.55.6.1101.

[31] Shimamura, T; Shiroishi, M; Weyand, S; Tsujimoto, H; Winter, G; Katritch, V; Abagyan, R; Cherezov, V; Liu, W; Han, GW; et al. Structure of the human histamine H_1 receptor complex with doxepin. *Nature* **2011**, *475* (7354), 65-70. DOI: https://doi.org/10.1038/nature10236.

[32] Zhang, X; Liu, G; Zhong, Y-N; Zhang, R; Yang, C-C; Niu, C; Pu, X; Sun, J; Zhang, T; Yang, L; et al. Structural basis of ligand recognition and activation of the histamine receptor family. *Nature Communications* **2024**, *15* (1), 8296. DOI: https://doi.org/10.1038/s41467-024-52585-y.

[33] Peng, X; Yang, L; Liu, Z; Lou, S; Mei, S; Li, M; Chen, Z; Zhang, H. Structural basis for recognition of antihistamine drug by human histamine receptor. *Nature Communications* **2022**, *13* (1), 6105. DOI: https://doi.org/10.1038/s41467-022-33880-y.

[34] Xia, R; Shi, S; Xu, Z; Vischer, HF; Windhorst, AD; Qian, Y; Duan, Y; Liang, J; Chen, K; Zhang, A; et al. Structural basis of ligand recognition and design of antihistamines targeting histamine H_4 receptor. *Nature Communications* **2024**, *15* (1), 2493. DOI: https://doi.org/10.1038/s41467-024-46840-5.

[35] Sadek, B; Stark, H. Cherry-picked ligands at histamine receptor subtypes. *Neuropharmacology* **2016**, *106*, 56-73. DOI: https://doi.org/10.1016/j.neuropharm.2015.11.005.

[36] Ravhe, IS; Krishnan, A; Manoj, N. Evolutionary history of histamine receptors: Early vertebrate origin and expansion of the H3-H4 subtypes. *Molecular Phylogenetics and Evolution* **2021**, *154*, 106989. DOI: https://doi.org/10.1016/j.ympev.2020.106989.

[37] de Esch, IJP; Thurmond, RL; Jongejan, A; Leurs, R. The histamine H_4 receptor as a new therapeutic target for inflammation. *Trends in Pharmacological Sciences* **2005**, *26* (9), 462-469. DOI: https://doi.org/10.1016/j.tips.2005.07.002.

[38] Lim, HD; van Rijn, RM; Ling, P; Bakker, RA; Thurmond, RL; Leurs, R. Evaluation of Histamine H_1, H_2, and H_3 Receptor Ligands at the Human Histamine H_4 Receptor: Identification of 4-Methylhistamine as the First Potent and Selective H_4 Receptor Agonist. *Journal of Pharmacology and Experimental Therapeutics* **2005**, *314* (3), 1310-1321. DOI: https://doi.org/10.1124/jpet.105.087965.

[39] Ash, ASF; Schild, HO. RECEPTORS MEDIATING SOME ACTIONS OF HISTAMINE. *British Journal of Pharmacology and Chemotherapy* **1966**, *27* (2), 427-439. DOI: https://doi.org/10.1111/j.1476-5381.1966.tb01674.x.

[40] Haas, HL; Sergeeva, OA; Selbach, O. Histamine in the Nervous System. *Physiological Reviews* **2008**, *88* (3), 1183-1241. DOI: https://doi.org/10.1152/physrev.00043.2007.

[41] Leurs, R; Traiffort, E; Arrang, JM; Tardivel-Lacombe, J; Ruat, M; Schwartz, J-C. Guinea Pig Histamine H_1 Receptor. II. Stable Expression in Chinese Hamster Ovary Cells Reveals the Interaction with Three Major Signal Transduction Pathways. *Journal of Neurochemistry* **1994**, *62* (2), 519-527. DOI: https://doi.org/10.1046/j.1471-4159.1994.62020519.x.

[42] Bakker, RA; Schoonus, SBJ; Smit, MJ; Timmerman, H; Leurs, R. Histamine H_1-Receptor Activation of Nuclear Factor-κB: Roles for $G_{\beta\gamma}$- and $G_{\alpha q/11}$-Subunits in Constitutive and Agonist-Mediated Signaling. *Molecular Pharmacology* **2001**, *60* (5), 1133-1142. DOI: https://doi.org/10.1124/mol.60.5.1133.

[43] Zhou, Z; An, Q; Zhang, W; Li, Y; Zhang, Q; Yan, H. Histamine and receptors in neuroinflammation: Their roles on neurodegenerative diseases. *Behavioural Brain Research* **2024**, *465*, 114964. DOI: https://doi.org/10.1016/j.bbr.2024.114964.

[44] Togias, A. H_1-receptors: Localization and role in airway physiology and in immune functions. *Journal of Allergy and Clinical Immunology* **2003**, *112* (4), S60-S68. DOI: https://doi.org/10.1016/S0091-6749(03)01878-5.

[45] Leurs, R; Smit, MJ; Timmerman, H. Molecular pharmacological aspects of histamine receptors. *Pharmacology & Therapeutics* **1995**, *66* (3), 413-463. DOI: https://doi.org/10.1016/0163-7258(95)00006-3.

[46] Jutel, M; Blaser, K; Akdis, CA. The Role of Histamine in Regulation of Immune Responses. In *Allergy and Asthma in Modern Society: A Scientific Approach*, Crameri, R Ed.; Vol. 91; S.Karger AG, 2006; p 0.

[47] Branco, ACCC; Yoshikawa, FSY; Pietrobon, AJ; Sato, MN. Role of Histamine in Modulating the Immune Response and Inflammation. *Mediators of Inflammation* **2018**, *2018* (1), 9524075. DOI: https://doi.org/10.1155/2018/9524075.

[48] Toda, N. Mechanism of histamine actions in human coronary arteries. *Circulation Research* **1987**, *61* (2), 280-286. DOI: https://doi.org/10.1161/01.RES.61.2.280.

[49] Van De Voorde, J; Leusen, I. Role of the endothelium in the vasodilator response of rat thoracic aorta to histamine. *European Journal of Pharmacology* **1983**, *87* (1), 113-120. DOI: https://doi.org/10.1016/0014-2999(83)90056-0.

[50] Li, H; Burkhardt, C; Heinrich, U-R; Brausch, I; Xia, N; Förstermann, U. Histamine Upregulates Gene Expression of Endothelial Nitric Oxide Synthase in Human Vascular Endothelial Cells. *Circulation* **2003**, *107* (18), 2348-2354. DOI: https://doi.org/10.1161/01.CIR.0000066697.19571.AF.

[51] Kotlikoff, MI; Murray, RK; Reynolds, EE. Histamine-induced calcium release and phorbol antagonism in cultured airway smooth muscle cells. *American Journal of Physiology-Cell Physiology* **1987**, *253* (4), C561-C566. DOI: https://doi.org/10.1152/ajpcell.1987.253.4.C561.

[52] Hall, IP; Hill, SJ. β -Adrenoceptor stimulation inhibits histamine-stimulated inositol phospholipid hydrolysis in bovine tracheal smooth muscle. *British Journal of Pharmacology* **1988**, *95* (4), 1204-1212. DOI: https://doi.org/10.1111/j.1476-5381.1988.tb11757.x.

[53] Barnes, PJ. Histamine receptors in the lung. *Agents Actions Suppl* **1991**, *33*, 103-122. DOI: https://doi.org/10.1007/978-3-0348-7309-3_9 .

[54] Meyrick, B; Brigham, KL. Increased Permeability Associated with Dilatation of Endothelial Cell Junctions Caused by Histamine in Intimal Explants from Bovine Pulmonary Artery. *Experimental Lung Research* **1984**, *6* (1), 11-25. DOI: https://doi.org/10.3109/01902148409087892.

[55] Killackey, JJ; Johnston, MG; Movat, HZ. Increased permeability of microcarrier-cultured endothelial monolayers in response to histamine and thrombin. A model for the in vitro study of increased vasopermeability. *Am J Pathol* **1986**, *122* (1), 50-61.

[56] Hill, SJ; Ganellin, CR; Timmerman, H; Schwartz, JC; Shankley, NP; Young, JM; Schunack, W; Levi, R; Haas, HL. International Union of Pharmacology. XIII. Classification of Histamine Receptors. *Pharmacological Reviews* **1997**, *49* (3), 253-278.

[57] Hill, SJ. Distribution, properties, and functional characteristics of three classes of histamine receptor. *Pharmacological Reviews* **1990**, *42* (1), 45-83.

[58] Bárbara, A; Aceves, J; Arias-Montaño, J-A. Histamine H_1 receptors in rat dorsal raphe nucleus: pharmacological characterisation and linking to increased neuronal activity. *Brain Research* **2002**, *954* (2), 247-255. DOI: https://doi.org/10.1016/S0006-8993(02)03352-8.

[59] Korotkova, TM; Sergeeva, OA; Ponomarenko, AA; Haas, HL. Histamine excites noradrenergic neurons in locus coeruleus in rats. *Neuropharmacology* **2005**, *49* (1), 129-134. DOI: https://doi.org/10.1016/j.neuropharm.2005.03.001.

[60] Tabarean, IV. Functional pharmacology of H histamine receptors expressed in mouse preoptic/anterior hypothalamic neurons. *British Journal of Pharmacology* **2013**, *170* (2), 415-425. DOI: https://doi.org/10.1111/bph.12286.

[61] Zhou, F-W; Xu, J-J; Zhao, Y; LeDoux, MS; Zhou, F-M. Opposite Functions of Histamine H_1 and H_2 Receptors and H_3 Receptor in Substantia Nigra Pars Reticulata. *Journal of Neurophysiology* **2006**, *96* (3), 1581-1591. DOI: https://doi.org/10.1152/jn.00148.2006.

[62] Xu, C; Michelsen, KA; Wu, M; Morozova, E; Panula, P; Alreja, M. Histamine innervation and activation of septohippocampal GABAergic neurones: involvement of local ACh release. *The Journal of Physiology* **2004**, *561* (3), 657-670. DOI: https://doi.org/10.1113/jphysiol.2004.071712.

[63] Manahan-Vaughan, D; Reymann, KG; Brown, RE. In vivo electrophysiological investigations into the role of histamine in the dentate gyrus of the rat. *Neuroscience* **1998**, *84* (3), 783-790. DOI: https://doi.org/10.1016/S0306-4522(97)00540-X.

[64] Jahn, K; Haas, HL; Hatt, H. Patch clamp study of histamine activated potassium currents on rabbit olfactory bulb neurons. *Naunyn-Schmiedeberg's Archives of Pharmacology* **1995**, *352* (4), 386-393. DOI: https://doi.org/10.1007/BF00172775.

[65] Reiner, PB; Kamondi, A. Mechanisms of antihistamine-induced sedation in the human brain: H_1 receptor activation reduces a background leakage potassium current. *Neuroscience* **1994**, *59* (3), 579-588. DOI: https://doi.org/10.1016/0306-4522(94)90178-3.

[66] Schneider, EH; Neumann, D; Seifert, R. Modulation of behavior by the histaminergic system: Lessons from H_1R-and H_2R-deficient mice. *Neuroscience & Biobehavioral Reviews* **2014**, *42*, 252-266. DOI: https://doi.org/10.1016/j.neubiorev.2014.03.009.

[67] Venable, J; Thurmond, R. Development and chemistry of histamine H4 receptor ligands as potential modulators of inflammatory and allergic responses. *Anti-Inflammatory & Anti-Allergy Agents in Medicinal Chemistry (Formerly Current Medicinal Chemistry-Anti-Inflammatory and Anti-Allergy Agents)* **2006**, *5* (4), 307-322.

[68] Čarman-Kržan, M; Bavec, A; Zorko, M; Schunack, W. Molecular characterization of specific H1-receptor agonists histaprodifen and its Nα-substituted analogues on bovine aortic H1-receptors. *Naunyn-Schmiedeberg's Archives of Pharmacology* **2003**, *367* (5), 538-546. DOI: https://doi.org/10.1007/s00210-003-0702-y.

[69] Krystal, AD; Richelson, E; Roth, T. Review of the histamine system and the clinical effects of H1 antagonists: Basis for a new model for understanding the effects of insomnia medications. *Sleep Medicine Reviews* **2013**, *17* (4), 263-272. DOI: https://doi.org/10.1016/j.smrv.2012.08.001.

[70] Anthes, JC; Gilchrest, H; Richard, C; Eckel, S; Hesk, D; West, RE; Williams, SM; Greenfeder, S; Billah, M; Kreutner, W; et al. Biochemical characterization of desloratadine, a potent antagonist of the human histamine H_1 receptor. *European Journal of Pharmacology* **2002**, *449* (3), 229-237. DOI: https://doi.org/10.1016/S0014-2999(02)02049-6.

[71] Hishinuma, S; Tamura, Y; Kobayashi, C; Akatsu, C; Shoji, M. Differential Regulation of Thermodynamic Binding Forces of Levocetirizine and (S)-Cetirizine by Lys191 in Human Histamine H1 Receptors. *International Journal of Molecular Sciences* **2018**, *19* (12), 4067. DOI: https://doi.org/10.3390/ijms19124067.

[72] Bartho, L; Benko, R. Should antihistamines be re-considered as antiasthmatic drugs as adjuvants to anti-leukotrienes? *European Journal of Pharmacology* **2013**, *701* (1), 181-184. DOI: https://doi.org/10.1016/j.ejphar.2013.01.009.

[73] Nicholson, AN; Pascoe, PA; Turner, C; Ganellin, CR; Greengrass, PM; Casy, AF; Mercer, AD. Sedation and histamine H1-receptor antagonism: studies in man with the enantiomers of chlorpheniramine and dimethindene. *British Journal of Pharmacology* **1991**, *104* (1), 270-276. DOI: https://doi.org/10.1111/j.1476-5381.1991.tb12418.x.

[74] Devillier, P; Roche, N; Faisy, C. Clinical Pharmacokinetics and Pharmacodynamics of Desloratadine, Fexofenadine and Levocetirizine. *Clinical Pharmacokinetics* **2008**, *47* (4), 217-230. DOI: https://doi.org/10.2165/00003088-200847040-00001.

[75] Broccatelli, F; Carosati, E; Cruciani, G; Oprea, TI. Transporter-Mediated Efflux Influences CNS Side Effects: ABCB1, from Antitarget to Target. *Molecular Informatics* **2010**, *29* (1-2), 16-26. DOI: https://doi.org/10.1002/minf.200900075.

[76] Traiffort, E; Vizuete, ML; Tardivellacombe, J; Souil, E; Schwartz, JC; Ruat, M. The Guinea Pig Histamine H_2 Receptor: Gene Cloning, Tissue Expression and Chromosomal Localization of Its Human Counterpart. *Biochemical and Biophysical Research Communications* **1995**, *211* (2), 570-577. DOI: https://doi.org/10.1006/bbrc.1995.1851.

[77] Del Valle, J; Gantz, I. Novel insights into histamine H_2 receptor biology. *American Journal of Physiology-Gastrointestinal and Liver Physiology* **1997**, *273* (5), G987-G996. DOI: https://doi.org/10.1152/ajpgi.1997.273.5.G987.

[78] Baudry, M; Martres, M-P; Schwartz, J-C. H_1 and H_2 receptors in the histamine-induced accumulation of cyclic AMP in guinea pig brain slices. *Nature* **1975**, *253* (5490), 362-364. DOI: https://doi.org/10.1038/253362a0.

[79] Garbarg, M; Schwartz, JC. Synergism between histamine H_1- and H_2-receptors in the cAMP response in guinea pig brain slices: effects of phorbol esters and calcium. *Molecular Pharmacology* **1988**, *33* (1), 38-43.

[80] Traiffort, E; Ruat, M; Arrang, JM; Leurs, R; Piomelli, D; Schwartz, JC. Expression of a cloned rat histamine H_2 receptor mediating inhibition of arachidonate release and activation of cAMP accumulation. *Proceedings of the National Academy of Sciences* **1992**, *89* (7), 2649-2653. DOI: https://doi.org/doi:10.1073/pnas.89.7.2649.

[81] Sheng, M; Thompson, MA; Greenberg, ME. CREB: a Ca^{2+}-Regulated Transcription Factor Phosphorylated by Calmodulin-Dependent Kinases. *Science* **1991**, *252* (5011), 1427-1430. DOI: https://doi.org/10.1126/science.1646483.

[82] Wang, L; Gantz, I; DelValle, J. Histamine H_2 receptor activates adenylate cyclase and PLC via separate GTP-dependent pathways. *American Journal of Physiology-Gastrointestinal and Liver Physiology* **1996**, *271* (4), G613-G620. DOI: https://doi.org/10.1152/ajpgi.1996.271.4.G613.

[83] Keithley, JK. Histamine H_2-Receptor Antagonists. *Nursing Clinics of North America* **1991**, *26* (2), 361-373. DOI: https://doi.org/10.1016/S0029-6465(22)00252-3.

[84] Akdis, CA; Simons, FER. Histamine receptors are hot in immunopharmacology. *European Journal of Pharmacology* **2006**, *533* (1), 69-76. DOI: https://doi.org/10.1016/j.ejphar.2005.12.044.

[85] Jin, CY; Panula, P. The laminar histamine receptor system in human prefrontal cortex suggests multiple levels of histaminergic regulation. *Neuroscience* **2005**, *132* (1), 137-149. DOI: https://doi.org/10.1016/j.neuroscience.2004.12.017.

[86] Traiffort, E; Pollard, H; Moreau, J; Ruat, M; Schwartz, JC; Martinez-Mir, MI; Palacios, JM. Pharmacological Characterization and Autoradiographic Localization of Histamine H_2 Receptors in Human Brain Identified with [^{125}I]Iodoaminopotentidine. *Journal of Neurochemistry* **1992**, *59* (1), 290-299. DOI: https://doi.org/10.1111/j.1471-4159.1992.tb08903.x.

[87] Durant, GJ; Ganellin, CR; Parsons, ME. Chemical differentiation of histamine H1- and H2-receptor agonists. *Journal of Medicinal Chemistry* **1975**, *18* (9), 905-909. DOI: https://doi.org/10.1021/jm00243a009.

[88] Eriks, JC; van der Goot, H; Timmerman, H. New activation model for the histamine H2 receptor, explaining the activity of the different classes of histamine H2 receptor agonists. *Molecular Pharmacology* **1993**, *44* (4), 886-894. DOI: https://doi.org/10.1016/S0026-895X(25)13286-0.

[89] Garbarg, M; Arrang, JM; Rouleau, A; Ligneau, X; Tuong, MD; Schwartz, JC; Ganellin, CR. S-[2-(4-imidazolyl)ethyl]isothiourea, a highly specific and potent histamine H3 receptor agonist. *The Journal of Pharmacology and Experimental Therapeutics* **1992**, *263* (1), 304-310. DOI: https://doi.org/10.1016/S0022-3565(25)10340-6.

[90] Stefan, D; Sigurd, E; Roland, S; Armin, B. Structure-Activity Relationships of Histamine H_2 Receptor Ligands. *Mini-Reviews in Medicinal Chemistry* **2004**, *4* (9), 941-954. DOI: http://dx.doi.org/10.2174/1389557043403242.

[91] Ghorai, P; Kraus, A; Keller, M; Götte, C; Igel, P; Schneider, E; Schnell, D; Bernhardt, G; Dove, S; Zabel, M; et al. Acylguanidines as Bioisosteres of Guanidines: N^G-Acylated Imidazolylpropylguanidines, a New Class of Histamine H_2 Receptor Agonists. *Journal of Medicinal Chemistry* **2008**, *51* (22), 7193-7204. DOI: https://doi.org/10.1021/jm800841w.

[92] Kraus, A; Ghorai, P; Birnkammer, T; Schnell, D; Elz, S; Seifert, R; Dove, S; Bernhardt, G; Buschauer, A. NG-Acylated Aminothiazolylpropylguanidines as Potent and Selective Histamine H_2 Receptor Agonists. *ChemMedChem* **2009**, *4* (2), 232-240. DOI: https://doi.org/10.1002/cmdc.200800296.

[93] Xie, S-X; Kraus, A; Ghorai, P; Ye, Q-Z; Elz, S; Buschauer, A; Seifert, R. *N*1-(3-Cyclohexylbutanoyl)-*N*2-[3-(1*H*-imidazol-4-yl)propyl]guanidine (UR-AK57), a Potent Partial Agonist for the Human Histamine H1- and H2-Receptors. *The Journal of Pharmacology and Experimental Therapeutics* **2006**, *317* (3), 1262-1268. DOI: https://doi.org/10.1124/jpet.106.102897.

[94] Leurs, R; Smit, MJ; Menge, WMBP; Timmerman, H. Pharmacological characterization of the human histamine H_2 receptor stably expressed in Chinese hamster ovary cells. *British Journal of Pharmacology* **1994**, *112* (3), 847-854. DOI: https://doi.org/10.1111/j.1476-5381.1994.tb13157.x.

[95] Wyllie, JH; Hesselbo, T; Black, JW. EFFECTS IN MAN OF HISTAMINE H2-RECEPTOR BLOCKADE BY BURIMAMIDE. *The Lancet* **1972**, *300* (7787), 1117-1120. DOI: https://doi.org/10.1016/S0140-6736(72)92719-5.

[96] Ganellin, R. 1980 Award in medicinal chemistry. Medicinal chemistry and dynamic structure-activity analysis in the discovery of drugs acting at histamine H2 receptors. *Journal of Medicinal Chemistry* **1981**, *24* (8), 913-920. DOI: 10.1021/jm00140a001.

[97] Baker, JG. A study of antagonist affinities for the human histamine H2 receptor. *British Journal of Pharmacology* **2008**, *153* (5), 1011-1021. DOI: https://doi.org/10.1038/sj.bjp.0707644.

[98] Smit, MJ; Leurs, R; Alewijnse, AE; Blauw, J; Van Nieuw Amerongen, GP; Van De Vrede, Y; Roovers, E; Timmerman, H. Inverse agonism of histamine H_2 antagonist accounts for upregulation of spontaneously active histamine H_2 receptors. *Proceedings of the National Academy of Sciences* **1996**, *93* (13), 6802-6807. DOI: https://doi.org/10.1073/pnas.93.13.6802.

[99] Arrang, JM; Garbarg, M; Lancelo, JC; Lecomte, JM; Pollard, H; Robba, M; Schunack, W; Schwartz, JC. Highly potent and selective ligands for histamine H_3-receptors. *Nature* **1987**, *327* (6118), 117-123. DOI: https://doi.org/10.1038/327117a0.

[100] Tardivel-Lacombe, J; Morisset, S; Gbahou, F; Schwartz, J-C; Arrang, J-M. Chromosomal mapping and organization of the human histamine H_3 receptor gene. *NeuroReport* **2001**, *12* (2), 321-324.

[101] Wiedemann, P; Bönisch, H; Oerters, F; Brüss, M. Structure of the human histamine H_3 receptor gene (HRH3) and identification of naturally occurring variations. *Journal of Neural Transmission* **2002**, *109* (4), 443-453. DOI: https://doi.org/10.1007/s007020200036.

[102] Wellendorph, P; Goodman, MW; Burstein, ES; Nash, NR; Brann, MR; Weiner, DM. Molecular cloning and pharmacology of functionally distinct isoforms of the human histamine H_3 receptor. *Neuropharmacology* **2002**, *42* (7), 929-940. DOI: https://doi.org/10.1016/S0028-3908(02)00041-2.

[103] Cogé, F; Guénin, SP; Audinot, V; Renouard-Try, A; Beauverger, P; Macia, C; Ouvry, C; Nagel, N; Rique, H; Boutin, JA; et al. Genomic organization and characterization of splice variants of the human histamine H_3 receptor. *Biochem J* **2001**, *355* (Pt 2), 279-288. DOI: https://doi.org/10.1042/0264-6021:3550279 .

[104] Clark, EA; Hill, SJ. Sensitivity of histamine H_3 receptor agonist-stimulated [^{35}S]GTPγ[S]binding to pertussis toxin. *European Journal of Pharmacology* **1996**, *296* (2), 223-225. DOI: https://doi.org/10.1016/0014-2999(95)00800-4.

[105] Wieland, K; Bongers, G; Yamamoto, Y; Hashimoto, T; Yamatodani, A; Menge, WM; Timmerman, H; Lovenberg, TW; Leurs, R. Constitutive activity of histamine H_3 receptors stably expressed in SK-N-MC cells: display of agonism and inverse agonism by H_3 antagonists. *J Pharmacol Exp Ther* **2001**, *299* (3), 908-914.

[106] Johannessen, M; Moens, U. Transcription of genes in response to activated cAMP/protein kinase A signalling pathway: There is more to it than CREB. *Trends in Cellular Signalling* **2006**, 41-78.

[107] Haas, H; Panula, P. The role of histamine and the tuberomamillary nucleus in the nervous system. *Nature Reviews Neuroscience* **2003**, *4* (2), 121-130. DOI: https://doi.org/10.1038/nrn1034.

[108] Seyedi, N; Mackins, CJ; Machida, T; Reid, AC; Silver, RB; Levi, R. Histamine H_3-receptor-induced attenuation of norepinephrine exocytosis: a decreased protein kinase a activity mediates a reduction in intracellular calcium. *J Pharmacol Exp Ther* **2005**, *312* (1), 272-280. DOI: https://doi.org/10.1124/jpet.104.072504 .

[109] Silver, RB; Poonwasi, KS; Seyedi, N; Wilson, SJ; Lovenberg, TW; Levi, R. Decreased intracellular calcium mediates the histamine H_3-receptor-induced attenuation of norepinephrine exocytosis from cardiac sympathetic nerve endings. *Proceedings of the National Academy of Sciences* **2002**, *99* (1), 501-506. DOI: https://doi.org/10.1073/pnas.012506099.

[110] Seino, S; Shibasaki, T. PKA-Dependent and PKA-Independent Pathways for cAMP-Regulated Exocytosis. *Physiological Reviews* **2005**, *85* (4), 1303-1342. DOI: https://doi.org/10.1152/physrev.00001.2005.

[111] Torrent, A; Moreno-Delgado, D; Gómez-Ramírez, J; Rodríguez-Agudo, D; Rodríguez-Caso, C; Sánchez-Jiménez, F; Blanco, I; Ortiz, J. H_3 autoreceptors modulate histamine synthesis through calcium/calmodulin- and cAMP-dependent protein kinase pathways. *Mol Pharmacol* **2005**, *67* (1), 195-203. DOI: https://doi.org/10.1124/mol.104.005652.

[112] Goldsmith, ZG; Dhanasekaran, DN. G Protein regulation of MAPK networks. *Oncogene* **2007**, *26* (22), 3122-3142. DOI: https://doi.org/10.1038/sj.onc.1210407.

[113] Murga, C; Laguinge, L; Wetzker, R; Cuadrado, A; Gutkind, JS. Activation of Akt/Protein Kinase B by G Protein-coupled Receptors: A ROLE FOR α AND βγ SUBUNITS OF HETEROTRIMERIC G PROTEINS ACTING THROUGH PHOSPHATIDYLINOSITOL-3-OH KINASEγ*. *Journal of Biological Chemistry* **1998**, *273* (30), 19080-19085. DOI: https://doi.org/10.1074/jbc.273.30.19080.

[114] Morisset, S; Rouleau, A; Ligneau, X; Gbahou, F; Tardivel-Lacombe, J; Stark, H; Schunack, W; Ganellin, CR; Arrang, J-M. High constitutive activity of native H_3 receptors regulates histamine neurons in brain. *Nature* **2000**, *408* (6814), 860-864. DOI: https://doi.org/10.1038/35048583.

[115] Silver, RB; Mackins, CJ; Smith, NCE; Koritchneva, IL; Lefkowitz, K; Lovenberg, TW; Levi, R. Coupling of histamine H_3 receptors to neuronal Na^+/H^+ exchange: A novel protective mechanism in myocardial ischemia. *Proceedings of the National Academy of Sciences* **2001**, *98* (5), 2855-2859. DOI: https://doi.org/10.1073/pnas.051599198.

[116] Thomas, GM; Huganir, RL. MAPK cascade signalling and synaptic plasticity. *Nature Reviews Neuroscience* **2004**, *5* (3), 173-183. DOI: https://doi.org/10.1038/nrn1346.

[117] Bongers, G; Sallmen, T; Passani, MB; Mariottini, C; Wendelin, D; Lozada, A; Marle, Av; Navis, M; Blandina, P; Bakker, RA; et al. The Akt/GSK-3β axis as a new signaling pathway of the histamine H_3 receptor. *Journal of Neurochemistry* **2007**, *103* (1), 248-258. DOI: https://doi.org/10.1111/j.1471-4159.2007.04752.x.

[118] Rickle, A; Bogdanovic, N; Volkman, I; Winblad, B; Ravid, R; Cowburn, RF. Akt activity in Alzheimer's disease and other neurodegenerative disorders. *NeuroReport* **2004**, *15* (6), 955-959.

[119] Martinez-Mir, MI; Pollard, H; Moreau, J; Arrang, JM; Ruat, M; Traiffort, E; Schwartz, JC; Palacios, JM. Three histamine receptors (H1, H2 and H3) visualized in the brain of human and non-human primates. *Brain Research* **1990**, *526* (2), 322-327. DOI: https://doi.org/10.1016/0006-8993(90)91240-H.

[120] Schneider, EH; Neumann, D; Seifert, R. Modulation of behavior by the histaminergic system: Lessons from HDC-, H_3R- and H_4R-deficient mice. *Neuroscience & Biobehavioral Reviews* **2014**, *47*, 101-121. DOI: https://doi.org/10.1016/j.neubiorev.2014.07.020.

[121] Ishikawa, S; Sperelakis, N. A novel class (H_3) of histamine receptors on perivascular nerve terminals. *Nature* **1987**, *327* (6118), 158-160. DOI: https://doi.org/10.1038/327158a0.

[122] Bertaccimi, G; Corruzi, G; Poli, E. The histamine H_3-receptor: a novel prejunctional receptor regulating gastrointestinal function. *Alimentary Pharmacology & Therapeutics* **1991**, *5* (6), 585-591. DOI: https://doi.org/10.1111/j.1365-2036.1991.tb00526.x.

[123] Fox, GB; Pan, JB; Esbenshade, TA; Bitner, RS; Nikkel, AL; Miller, T; Kang, CH; Bennani, YL; Black, LA; Faghih, R; et al. Differential in vivo effects of H_3 receptor ligands in a new mouse dipsogenia model. *Pharmacology Biochemistry and Behavior* **2002**, *72* (3), 741-750. DOI: https://doi.org/10.1016/S0091-3057(02)00745-1.

[124] Clapham, J; Kilpatrick, GJ. Histamine H_3 receptor-mediated modulation of water consumption in the rat. *European Journal of Pharmacology* **1993**, *232* (1), 99-103. DOI: https://doi.org/10.1016/0014-2999(93)90733-X.

[125] Krause, M; Stark, H; Schunack, W. Azomethine Prodrugs of (*R*)-α-Methylhistamine, a Highly Potent and Selective Histamine H_3-Receptor Agonist. *Current Medicinal Chemistry* **2001**, *8* (11), 1329-1340. DOI: http://dx.doi.org/10.2174/0929867013372274.

[126] Stark, H; Krause, M; Rouleau, A; Garbarg, M; Schwartz, J-C; Schunack, W. Enzyme-catalyzed prodrug approaches for the histamine H_3-receptor agonist (*R*)-α-methylhistamine. *Bioorganic & Medicinal Chemistry* **2001**, *9* (1), 191-198. DOI: https://doi.org/10.1016/S0968-0896(00)00237-6.

[127] Coruzzi, G; Gambarelli, E; Bertaccini, G; Timmerman, H. Cardiovascular effects of selective agonists and antagonists of histamine H_3 receptors in the anaesthetized rat. *Naunyn-Schmiedeberg's Archives of Pharmacology* **1995**, *351* (6), 569-575. DOI: https://doi.org/10.1007/BF00170155.

[128] Tiligada, E; Evangelia, Z; Kerstin, S; and Stark, H. Histamine H_3 and H_4 receptors as novel drug targets. *Expert Opinion on Investigational Drugs* **2009**, *18* (10), 1519-1531. DOI: https://doi.org/10.1517/14728220903188438.

[129] Kenakin, T. Inverse, protean, and ligand-selective agonism: matters of receptor conformation. *The FASEB Journal* **2001**, *15* (3), 598-611. DOI: https://doi.org/10.1096/fj.00-0438rev.

[130] Tedford, CE; Phillips, JG; Gregory, R; Pawlowski, GP; Fadnis, L; Khan, MA; Ali, SM; Handley, MK; Yates, SL. Development of trans-2-[1 H-Imidazol-4-yl] Cyclopropane Derivatives as New High-Affinity Histamine H_3 Receptor Ligands. *The Journal of Pharmacology and Experimental Therapeutics* **1999**, *289* (2), 1160-1168. DOI: https://doi.org/10.1016/S0022-3565(24)38248-5.

[131] Liu, H; Kerdesky, FA; Black, LA; Fitzgerald, M; Henry, R; Esbenshade, TA; Hancock, AA; Bennani, YL. An Efficient Multigram Synthesis of the Potent Histamine H_3 Antagonist GT-2331 and the Reassessment of the Absolute Configuration. *The Journal of Organic Chemistry* **2004**, *69* (1), 192-194. DOI: https://doi.org/10.1021/jo035264t.

[132] Ito, S; Yoshimoto, R; Miyamoto, Y; Mitobe, Y; Nakamura, T; Ishihara, A; MacNeil, DJ; Kanatani, A; Tokita, S. Detailed pharmacological characterization of GT-2331 for the rat histamine H_3 receptor. *European Journal of Pharmacology* **2006**, *529* (1), 40-46. DOI: https://doi.org/10.1016/j.ejphar.2005.10.066.

[133] Wulff, BS; Hastrup, S; Rimvall, K. Characteristics of recombinantly expressed rat and human histamine H_3 receptors. *European Journal of Pharmacology* **2002**, *453* (1), 33-41. DOI: https://doi.org/10.1016/S0014-2999(02)02382-8.

[134] Ghamari, N; Zarei, O; Arias-Montaño, J-A; Reiner, D; Dastmalchi, S; Stark, H; Hamzeh-Mivehroud, M. Histamine H_3 receptor antagonists/inverse agonists: Where do they go? *Pharmacology & Therapeutics* **2019**, *200*, 69-84. DOI: https://doi.org/10.1016/j.pharmthera.2019.04.007.

[135] Komater, VA; Browman, KE; Curzon, P; Hancock, AA; Decker, MW; Fox, GB. H_3 receptor blockade by thioperamide enhances cognition in rats without inducing locomotor sensitization. *Psychopharmacology* **2003**, *167* (4), 363-372. DOI: https://doi.org/10.1007/s00213-003-1431-0.

[136] Masaki, T; Yoshimatsu, H; Chiba, S; Watanabe, T; Sakata, T. Targeted Disruption of Histamine H_1-Receptor Attenuates Regulatory Effects of Leptin on Feeding, Adiposity, and UCP Family in Mice. *Diabetes* **2001**, *50* (2), 385-391. DOI: https://doi.org/10.2337/diabetes.50.2.385.

[137] Yoshimoto, R; Miyamoto, Y; Shimamura, K; Ishihara, A; Takahashi, K; Kotani, H; Chen, AS; Chen, HY; MacNeil, DJ; Kanatani, A; et al. Therapeutic potential of histamine H_3 receptor agonist for the treatment of obesity and diabetes mellitus. *Proceedings of the National Academy of Sciences* **2006**, *103* (37), 13866-13871. DOI: https://doi.org/10.1073/pnas.0506104103.

[138] Harada, C; Hirai, T; Fujii, Y; Harusawa, S; Kurihara, T; Kamei, C. Intracerebroventricular administration of histamine H_3 receptor antagonists decreases seizures in rat models of epilepsia. *Methods and findings in experimental and clinical pharmacology* **2004**, *26* (4), 263-270.

[139] Fu, Q; Dai, H; He, P; Hu, W; Fan, Y; Zhang, W; Chen, Z. The H3 receptor antagonist clobenpropit protects against Aβ42-induced neurotoxicity in differentiated rat PC12 cells. *Die Pharmazie-An International Journal of Pharmaceutical Sciences* **2010**, *65* (4), 257-260.

[140] Lim, HD; Istyastono, EP; van de Stolpe, A; Romeo, G; Gobbi, S; Schepers, M; Lahaye, R; Menge, WMBP; Zuiderveld, OP; Jongejan, A; et al. Clobenpropit analogs as dual activity ligands for the histamine H_3 and H_4 receptors: Synthesis, pharmacological evaluation, and cross-target QSAR studies. *Bioorganic & Medicinal Chemistry* **2009**, *17* (11), 3987-3994. DOI: https://doi.org/10.1016/j.bmc.2009.04.007.

[141] Ligneau, X; Lin, JS; Vanni-Mercier, G; Jouvet, M; Muir, JL; Ganellin, CR; Stark, H; Elz, S; Schunack, W; Schwartz, JC. Neurochemical and Behavioral Effects of Ciproxifan, A Potent Histamine H_3-Receptor Antagonist. *The Journal of Pharmacology and Experimental Therapeutics* **1998**, *287* (2), 658-666. DOI: https://doi.org/10.1016/S0022-3565(24)37840-1.

[142] Stark, H; Sadek, B; Krause, M; Hüls, A; Ligneau, X; Ganellin, CR; Arrang, J-M; Schwartz, J-C; Schunack, W. Novel Histamine H_3-Receptor Antagonists with Carbonyl-Substituted 4-(3-(Phenoxy)propyl)-1H-imidazole Structures like Ciproxifan and Related Compounds. *Journal of Medicinal Chemistry* **2000**, *43* (21), 3987-3994. DOI: https://doi.org/10.1021/jm000966l.

[143] Affini, A; Hagenow, S; Zivkovic, A; Marco-Contelles, J; Stark, H. Novel indanone derivatives as MAO B/H_3R dual-targeting ligands for treatment of Parkinson's disease. *European Journal of Medicinal Chemistry* **2018**, *148*, 487-497. DOI: https://doi.org/10.1016/j.ejmech.2018.02.015.

[144] Celanire, S; Wijtmans, M; Talaga, P; Leurs, R; de Esch, IJP. Keynote review: Histamine H_3 receptor antagonists reach out for the clinic. *Drug Discovery Today* **2005**, *10* (23), 1613-1627. DOI: https://doi.org/10.1016/S1359-6446(05)03625-1.

[145] Esbenshade, TA; Browman, KE; Miller, TR; Krueger, KM; Komater-Roderwald, V; Zhang, M; Fox, GB; Rueter, L; Robb, HM; Radek, RJ; et al. Pharmacological Properties and Procognitive Effects of ABT-288, a Potent and Selective Histamine H_3 Receptor Antagonist. *The Journal of Pharmacology and Experimental Therapeutics* **2012**, *343* (1), 233-245. DOI: https://doi.org/10.1124/jpet.112.194126.

[146] Medhurst, AD; Atkins, AR; Beresford, IJ; Brackenborough, K; Briggs, MA; Calver, AR; Cilia, J; Cluderay, JE; Crook, B; Davis, JB; et al. GSK189254, a Novel H_3 Receptor Antagonist That Binds to Histamine H_3 Receptors in Alzheimer's Disease Brain and Improves Cognitive Performance in Preclinical Models. *The Journal of Pharmacology and Experimental Therapeutics* **2007**, *321* (3), 1032-1045. DOI: https://doi.org/10.1124/jpet.107.120311.

[147] Nirogi, R; Benade, V; Daripelli, S; Subramanian, R; Kamuju, V; Bhyrapuneni, G; Muddana, NR; Mekala, VR; Petlu, S; Jayarajan, P; et al. Samelisant (SUVN-G3031), a potent, selective and orally active histamine H_3 receptor inverse agonist for the potential treatment of narcolepsy: pharmacological and neurochemical characterisation. *Psychopharmacology* **2021**, *238* (6), 1495-1511. DOI: https://doi.org/10.1007/s00213-021-05779-x.

[148] Wager, TT; Pettersen, BA; Schmidt, AW; Spracklin, DK; Mente, S; Butler, TW; Howard, H, Jr.; Lettiere, DJ; Rubitski, DM; Wong, DF; et al. Discovery of Two Clinical Histamine H_3 Receptor Antagonists: trans-*N*-Ethyl-3-fluoro-3-[3-fluoro-4-(pyrrolidinylmethyl)phenyl]cyclobutanecarboxamide (PF-03654746) and trans-3-Fluoro-3-[3-fluoro-4-(pyrrolidin-1-ylmethyl)phenyl]-N-(2-methylpropyl)cyclobutanecarboxamide (PF-03654764). *Journal of Medicinal Chemistry* **2011**, *54* (21), 7602-7620. DOI: https://doi.org/10.1021/jm200939b.

[149] Hino, N; Marumo, T; Kotani, M; Shimazaki, T; Kaku-Fukumoto, A; Hikichi, H; Karasawa, J-i; Tomishima, Y; Komiyama, H; Tatsuda, E; et al. A Novel Potent and Selective Histamine H_3 Receptor Antagonist Enerisant: In Vitro Profiles, In Vivo Receptor Occupancy, and Wake-Promoting and Procognitive Effects in Rodents. *The Journal of Pharmacology and Experimental Therapeutics* **2020**, *375* (2), 276-285. DOI: https://doi.org/10.1124/jpet.120.000185.

[150] Nirogi, R; Shinde, A; Tiriveedhi, V; Kota, L; Saraf, SK; Badange, RK; Mohammed, AR; Subramanian, R; Muddana, N; Bhyrapuneni, G; et al. Benzamide derivatives and their constrained analogs as histamine H_3 receptor antagonists. *European Journal of Medicinal Chemistry* **2016**, *108*, 655-662. DOI: https://doi.org/10.1016/j.ejmech.2015.12.005.

[151] Letavic, MA; Aluisio, L; Apodaca, R; Bajpai, M; Barbier, AJ; Bonneville, A; Bonaventure, P; Carruthers, NI; Dugovic, C; Fraser, IC; et al. Novel Benzamide-Based Histamine H_3 Receptor Antagonists: The Identification of Two Candidates for Clinical Development. *ACS Medicinal Chemistry Letters* **2015**, *6* (4), 450-454. DOI: https://doi.org/10.1021/ml5005156.

[152] Meier, G; Apelt, J; Reichert, U; Graßmann, S; Ligneau, X; Elz, S; Leurquin, F; Ganellin, CR; Schwartz, J-C; Schunack, W; et al. Influence of imidazole replacement in different structural classes of histamine H3-receptor antagonists. *European Journal of Pharmaceutical Sciences* **2001**, *13* (3), 249-259. DOI: https://doi.org/10.1016/S0928-0987(01)00106-3.

[153] Ligneau, X; Perrin, D; Landais, L; Camelin, JC; Calmels, TPG; Berrebi-Bertrand, I; Lecomte, JM; Parmentier, R; Anaclet, C; Lin, JS; et al. BF2.649 [1-{3-[3-(4-Chlorophenyl)propoxy]propyl}piperidine, Hydrochloride], a Nonimidazole Inverse Agonist/Antagonist at the Human Histamine H_3 Receptor: Preclinical Pharmacology. *The Journal of Pharmacology and Experimental Therapeutics* **2007**, *320* (1), 365-375. DOI: https://doi.org/10.1124/jpet.106.111039.

[154] Schwartz, J-C. The histamine H_3 receptor: from discovery to clinical trials with pitolisant. *British Journal of Pharmacology* **2011**, *163* (4), 713-721. DOI: https://doi.org/10.1111/j.1476-5381.2011.01286.x.

[155] Barbier, AJ; Berridge, C; Dugovic, C; Laposky, AD; Wilson, SJ; Boggs, J; Aluisio, L; Lord, B; Mazur, C; Pudiak, CM; et al. Acute wake-promoting actions of JNJ-5207852, a novel, diamine-based H_3 antagonist. *British Journal of Pharmacology* **2004**, *143* (5), 649-661. DOI: https://doi.org/10.1038/sj.bjp.0705964.

[156] Haig, GM; Pritchett, Y; Meier, A; Othman, AA; Hall, C; Gault, LM; Lenz, RA. A Randomized Study of H_3 Antagonist ABT-288 in Mild-To-Moderate Alzheimer's Dementia1. *Journal of Alzheimer's Disease* **2014**, *42* (3), 959-971. DOI: https://doi.org/10.3233/jad-140291.

[157] Haig, GM; Bain, E; Robieson, W; Othman, AA; Baker, J; Lenz, RA. A Randomized Trial of the Efficacy and Safety of the H_3 Antagonist ABT-288 in Cognitive Impairment Associated With Schizophrenia. *Schizophrenia Bulletin* **2014**, *40* (6), 1433-1442. DOI: https://doi.org/10.1093/schbul/sbt240.

[158] Guo, R; Anaclet, C; Roberts, J; Parmentier, R; Zhang, M; Guidon, G; Buda, C; Sastre, J; Feng, J; Franco, P; et al. Differential effects of acute and repeat dosing with the H_3 antagonist GSK189254 on the sleep–wake cycle and narcoleptic episodes in Ox−/− mice. *British Journal of Pharmacology* **2009**, *157* (1), 104-117. DOI: https://doi.org/10.1111/j.1476-5381.2009.00205.x.

[159] McGaraughty, S; Chu, KL; Cowart, MD; Brioni, JD. Antagonism of Supraspinal Histamine H_3 Receptors Modulates Spinal Neuronal Activity in Neuropathic Rats. *The Journal of Pharmacology and Experimental Therapeutics* **2012**, *343* (1), 13-20. DOI: https://doi.org/10.1124/jpet.112.194761.

[160] Ashworth, S; Rabiner, EA; Gunn, RN; Plisson, C; Wilson, AA; Comley, RA; Lai, RYK; Gee, AD; Laruelle, M; Cunningham, VJ. Evaluation of ^{11}C-GSK189254 as a Novel Radioligand for the H_3 Receptor in Humans Using PET. *Journal of Nuclear Medicine* **2010**, *51* (7), 1021-1029. DOI: https://doi.org/10.2967/jnumed.109.071753.

[161] A Double-blind, Double-dummy, Placebo-controlled, Incomplete Block, Two Period Crossover Study of the Histamine H_3 Antagonist GSK189254 and Duloxetine in the Electrical Hyperalgesia Model of Central Sensitisation in Healthy Volunteers. https://clinicaltrials.gov/study/NCT00387413.

[162] Inoue, Y; Uchiyama, M; Umeuchi, H; Onishi, K; Ogo, H; Kitajima, I; Matsushita, I; Nishino, I; Uchimura, N. Optimal dose determination of enerisant (TS-091) for patients with narcolepsy: two randomized, double-blind, placebo-controlled trials. *BMC Psychiatry* **2022**, *22* (1), 141. DOI: https://doi.org/10.1186/s12888-022-03785-7.

[163] Nirogi, R; Shinde, A; Goyal, VK; Ravula, J; Benade, V; Jetta, S; Pandey, SK; Subramanian, R; Chowdary Palacharla, VR; Mohammed, AR; et al. Samelisant (SUVN-G3031), a histamine 3 receptor inverse agonist: Results from the phase 2 double-blind randomized placebo-controlled study for the treatment of excessive daytime sleepiness in adult patients with narcolepsy. *Sleep Medicine* **2024**, *124*, 618-626. DOI: https://doi.org/10.1016/j.sleep.2024.10.037.

[164] Jarskog, LF; Lowy, MT; Grove, RA; Keefe, RSE; Horrigan, JP; Ball, MP; Breier, A; Buchanan, RW; Carter, CS; Csernansky, JG; et al. A Phase II study of a histamine H_3 receptor antagonist GSK239512 for cognitive impairment in stable schizophrenia subjects on antipsychotic therapy. *Schizophrenia Research* **2015**, *164* (1), 136-142. DOI: https://doi.org/10.1016/j.schres.2015.01.041.

[165] Egan, MF; Zhao, X; Gottwald, R; Harper-Mozley, L; Zhang, Y; Snavely, D; Lines, C; Michelson, D. Randomized crossover study of the histamine H_3 inverse agonist MK-0249 for the treatment of cognitive impairment in patients with schizophrenia. *Schizophrenia Research* **2013**, *146* (1), 224-230. DOI: https://doi.org/10.1016/j.schres.2013.02.030.

[166] Stark, H. Recent advances in histamine H_3/H_4 receptor ligands. *Expert Opinion on Therapeutic Patents* **2003**, *13* (6), 851-865. DOI: https://doi.org/10.1517/13543776.13.6.851.

[167] Wingen, K; Stark, H. Scaffold variations in amine warhead of histamine H_3 receptor antagonists. *Drug Discovery Today: Technologies* **2013**, *10* (4), e483-e489. DOI: https://doi.org/10.1016/j.ddtec.2013.07.001.

[168] Schlegel, B; Laggner, C; Meier, R; Langer, T; Schnell, D; Seifert, R; Stark, H; Höltje, H-D; Sippl, W. Generation of a homology model of the human histamine H3 receptor for ligand docking and pharmacophore-based screening. *Journal of Computer-Aided Molecular Design* **2007**, *21* (8), 437-453. DOI: https://doi.org/10.1007/s10822-007-9127-x.

[169] Frandsen, IO; Boesgaard, MW; Fidom, K; Hauser, AS; Isberg, V; Bräuner-Osborne, H; Wellendorph, P; Gloriam, DE. Identification of Histamine H_3 Receptor Ligands Using a New Crystal Structure Fragment-based Method. *Scientific Reports* **2017**, *7* (1), 4829. DOI: https://doi.org/10.1038/s41598-017-05058-w.

[170] Jończyk, J; Malawska, B; Bajda, M. Hybrid approach to structure modeling of the histamine H_3 receptor: Multi-level assessment as a tool for model verification. *PLOS ONE* **2017**, *12* (10), e0186108. DOI: https://doi.org/10.1371/journal.pone.0186108.

[171] Mehta, P; Miszta, P; Filipek, S. Molecular Modeling of Histamine Receptors—Recent Advances in Drug Discovery. *Molecules* **2021**, *26* (6), 1778. DOI: https://doi.org/10.3390/molecules26061778

[172] Wright, C; Shin, JH; Rajpurohit, A; Deep-Soboslay, A; Collado-Torres, L; Brandon, NJ; Hyde, TM; Kleinman, JE; Jaffe, AE; Cross, AJ; et al. Altered expression of histamine signaling genes in autism spectrum disorder. *Translational Psychiatry* **2017**, *7* (5), e1126-e1126. DOI: https://doi.org/10.1038/tp.2017.87.

[173] Vanni-Mercier, G; Gigout, S; Debilly, G; Lin, JS. Waking selective neurons in the posterior hypothalamus and their response to histamine H_3-receptor ligands: an electrophysiological study in freely moving cats. *Behavioural Brain Research* **2003**, *144* (1), 227-241. DOI: https://doi.org/10.1016/S0166-4328(03)00091-3.

[174] Stevens, DR; Eriksson, KS; Brown, RE; Haas, HL. The mechanism of spontaneous firing in histamine neurons. *Behavioural Brain Research* **2001**, *124* (2), 105-112. DOI: https://doi.org/10.1016/S0166-4328(01)00219-4.

[175] Yamada, Y; Yoshikawa, T; Naganuma, F; Kikkawa, T; Osumi, N; Yanai, K. Chronic brain histamine depletion in adult mice induced depression-like behaviours and impaired sleep-wake cycle. *Neuropharmacology* **2020**, *175*, 108179. DOI: https://doi.org/10.1016/j.neuropharm.2020.108179.

[176] Scott Bitner, R. Cyclic AMP response element-binding protein (CREB) phosphorylation: A mechanistic marker in the development of memory enhancing Alzheimer's disease therapeutics. *Biochemical Pharmacology* **2012**, *83* (6), 705-714. DOI: https://doi.org/10.1016/j.bcp.2011.11.009.

[177] Alhusaini, M; Eissa, N; Saad, AK; Beiram, R; Sadek, B. Revisiting Preclinical Observations of Several Histamine H_3 Receptor Antagonists/Inverse Agonists in Cognitive Impairment, Anxiety, Depression, and Sleep–Wake Cycle Disorder. *Frontiers in Pharmacology* **2022**, *13*. DOI: https://doi.org/10.3389/fphar.2022.861094.

[178] Romigi, A; Vitrani, G; Lo Giudice, T; Centonze, D; Franco, V. Profile of pitolisant in the management of narcolepsy: design, development, and place in therapy. *Drug Design, Development and Therapy* **2018**, 2665-2675. DOI: https://doi.org/10.2147/DDDT.S101145.

[179] Davis, CW; Kallweit, U; Schwartz, J-C; Krahn, LE; Vaughn, B; Thorpy, MJ. Efficacy of pitolisant in patients with high burden of narcolepsy symptoms: pooled analysis of short-term, placebo-controlled studies. *Sleep Medicine* **2021**, *81*, 210-217. DOI: https://doi.org/10.1016/j.sleep.2021.02.037.

[180] Sadek, B; Saad, A; Sadeq, A; Jalal, F; Stark, H. Histamine H_3 receptor as a potential target for cognitive symptoms in neuropsychiatric diseases. *Behavioural Brain Research* **2016**, *312*, 415-430. DOI: https://doi.org/10.1016/j.bbr.2016.06.051.

[181] Masters, CL; Bateman, R; Blennow, K; Rowe, CC; Sperling, RA; Cummings, JL. Alzheimer's disease. *Nature Reviews Disease Primers* **2015**, *1* (1), 15056. DOI: https://doi.org/10.1038/nrdp.2015.56.

[182] Nakamura, S; Takemura, M; Ohnishi, K; Suenaga, T; Nishimura, M; Akiguchi, I; Kimura, J; Kimura, T. Loss of large neurons and occurrence of neurofibrillary tangles in the tuberomammillary nucleus of patients with Alzheimer's disease. *Neuroscience Letters* **1993**, *151* (2), 196-199. DOI: https://doi.org/10.1016/0304-3940(93)90019-H.

[183] Mazurkiewicz-Kwilecki, IM; Nsonwah, S. Changes in the regional brain histamine and histidine levels in postmortem brains of Alzheimer patients. *Canadian Journal of Physiology and Pharmacology* **1989**, *67* (1), 75-78. DOI: https://doi.org/10.1139/y89-013.

[184] Panula, P; Rinne, J; Kuokkanen, K; Eriksson, KS; Sallmen, T; Kalimo, H; Relja, M. Neuronal histamine deficit in Alzheimer's disease. *Neuroscience* **1997**, *82* (4), 993-997. DOI: https://doi.org/10.1016/S0306-4522(97)00353-9.

[185] Zlomuzica, A; Dere, D; Binder, S; De Souza Silva, MA; Huston, JP; Dere, E. Neuronal histamine and cognitive symptoms in Alzheimer's disease. *Neuropharmacology* **2016**, *106*, 135-145. DOI: https://doi.org/10.1016/j.neuropharm.2015.05.007.

[186] Dere, E; Zlomuzica, A; De Souza Silva, MA; Ruocco, LA; Sadile, AG; Huston, JP. Neuronal histamine and the interplay of memory, reinforcement and emotions. *Behavioural Brain Research* **2010**, *215* (2), 209-220. DOI: https://doi.org/10.1016/j.bbr.2009.12.045.

[187] Yoshikawa, T; Nakamura, T; Yanai, K. Histaminergic neurons in the tuberomammillary nucleus as a control centre for wakefulness. *British Journal of Pharmacology* **2021**, *178* (4), 750-769. DOI: https://doi.org/10.1111/bph.15220.

[188] Poewe, W; Seppi, K; Tanner, CM; Halliday, GM; Brundin, P; Volkmann, J; Schrag, A-E; Lang, AE. Parkinson disease. *Nature Reviews Disease Primers* **2017**, *3* (1), 17013. DOI: https://doi.org/10.1038/nrdp.2017.13.

[189] Bolam, JP; Ellender, TJ. Histamine and the striatum. *Neuropharmacology* **2016**, *106*, 74-84. DOI: https://doi.org/10.1016/j.neuropharm.2015.08.013.

[190] Shan, L; Bao, A-M; Swaab, DF. The human histaminergic system in neuropsychiatric disorders. *Trends in Neurosciences* **2015**, *38* (3), 167-177. DOI: https://doi.org/10.1016/j.tins.2014.12.008.

[191] Neikrug, AB; Maglione, JE; Liu, L; Natarajan, L; Avanzino, JA; Corey-Bloom, J; Palmer, BW; Loredo, JS; Ancoli-Israel, S. Effects of Sleep Disorders on the Non-Motor Symptoms of Parkinson Disease. *Journal of Clinical Sleep Medicine* **2013**, *09* (11), 1119-1129. DOI: https://doi.org/10.5664/jcsm.3148.

[192] Liguori, C; Placidi, F; Izzi, F; Mercuri, NB; Stefani, A; Pierantozzi, M. Pitolisant for treating narcolepsy comorbid with Parkinson's disease. *Sleep Medicine* **2020**, *69*, 86-87. DOI: https://doi.org/10.1016/j.sleep.2020.01.020.

[193] Jin, C; Anichtchik, O; Panula, P. Altered histamine H_3 receptor radioligand binding in post-mortem brain samples from subjects with psychiatric diseases. *British Journal of Pharmacology* **2009**, *157* (1), 118-129. DOI: https://doi.org/10.1111/j.1476-5381.2009.00149.x.

[194] Bardgett, ME; Points, M; Kleier, J; Blankenship, M; Griffith, MS. The H_3 antagonist, ciproxifan, alleviates the memory impairment but enhances the motor effects of MK-801 (dizocilpine) in rats. *Neuropharmacology* **2010**, *59* (6), 492-502. DOI: https://doi.org/10.1016/j.neuropharm.2010.07.004.

[195] Brown, JW; Whitehead, CA; Basso, AM; Rueter, LE; Zhang, M. Preclinical evaluation of non-imidazole histamine H_3 receptor antagonists in comparison to atypical antipsychotics for the treatment of cognitive deficits associated with schizophrenia. *International Journal of Neuropsychopharmacology* **2013**, *16* (4), 889-904. DOI: https://doi.org/10.1017/s1461145712000739.

[196] Carthy, E; Ellender, T. Histamine, Neuroinflammation and Neurodevelopment: A Review. *Frontiers in Neuroscience* **2021**, *Volume 15 - 2021*. DOI: https://doi.org/10.3389/fnins.2021.680214.

[197] Bardgett, ME; Davis, NN; Schultheis, PJ; Griffith, MS. Ciproxifan, an H_3 receptor antagonist, alleviates hyperactivity and cognitive deficits in the APPTg2576 mouse model of Alzheimer's disease. *Neurobiology of Learning and Memory* **2011**, *95* (1), 64-72. DOI: https://doi.org/10.1016/j.nlm.2010.10.008.

[198] Kim, Y-J; Goto, Y; Lee, Y-A. Histamine H_3 receptor antagonists ameliorate attention deficit/hyperactivity disorder-like behavioral changes caused by neonatal habenula lesion. *Behavioural Pharmacology* **2018**, *29* (1), 71-78. DOI: https://doi.org/10.1097/fbp.0000000000000343.

[199] Weisler, RH; Pandina, GJ; Daly, EJ; Cooper, K; Gassmann-Mayer, C. Randomized Clinical Study of a Histamine H_3 Receptor Antagonist for the Treatment of Adults with Attention-Deficit Hyperactivity Disorder. *CNS Drugs* **2012**, *26* (5), 421-434. DOI: https://doi.org/10.2165/11631990-000000000-00000.

[200] Ercan-Sencicek, AG; Stillman, AA; Ghosh, AK; Bilguvar, K; O'Roak, BJ; Mason, CE; Abbott, T; Gupta, A; King, RA; Pauls, DL; et al. L-Histidine Decarboxylase and Tourette's Syndrome. *New England Journal of Medicine* **2010**, *362* (20), 1901-1908. DOI: https://doi.org/10.1056/NEJMoa0907006.

[201] Rapanelli, M; Pittenger, C. Histamine and histamine receptors in Tourette syndrome and other neuropsychiatric conditions. *Neuropharmacology* **2016**, *106*, 85-90. DOI: https://doi.org/10.1016/j.neuropharm.2015.08.019.

[202] A Phase 2 Multicenter, Randomized, Double-Blind, Placebo-Controlled, Cross-Over Study Of The Safety And Efficacy Of PF-03654746 In Adults With Tourette's Syndrome. https://clinicaltrials.gov/study/NCT01475383.

[203] Pullen, LC; Picone, M; Tan, L; Johnston, C; Stark, H. Cognitive Improvements in Children with Prader-Willi Syndrome Following Pitolisant Treatment—Patient Reports. *The Journal of Pediatric Pharmacology and Therapeutics* **2019**, *24* (2), 166-171. DOI: https://doi.org/10.5863/1551-6776-24.2.166.

[204] Reiner, D; Seifert, L; Deck, C; Schüle, R; Jung, M; Stark, H. Epigenetics meets GPCR: inhibition of histone H3 methyltransferase (G9a) and histamine H_3 receptor for Prader–Willi Syndrome. *Scientific Reports* **2020**, *10* (1), 13558. DOI: https://doi.org/10.1038/s41598-020-70523-y.

[205] A Phase 3, Randomized, Double-Blind, Placebo-controlled, Efficacy and Safety Study of Pitolisant Followed by an Open-Label Extension in Patients with Prader-Willi Syndrome. https://clinicaltrials.gov/study/NCT06366464.

[206] Zhu, Y; Michalovich, D; Wu, H-L; Tan, KB; Dytko, GM; Mannan, IJ; Boyce, R; Alston, J; Tierney, LA; Li, X; et al. Cloning, Expression, and Pharmacological Characterization of a Novel Human Histamine Receptor. *Molecular Pharmacology* **2001**, *59* (3), 434-441. DOI: https://doi.org/10.1124/mol.59.3.434.

[207] van Rijn, R; Chazot, P; Shenton, F; Sansuk, K; Bakker, R; Leurs, R. Oligomerization of recombinant and endogenously expressed human histamine H_4 receptors. *Molecular Pharmacology* **2006**, *70* (2), 604-615. DOI: https://doi.org/10.1124/mol.105.020818.

[208] Hofstra, CL; Desai, PJ; Thurmond, RL; Fung-Leung, W-P. Histamine H4 Receptor Mediates Chemotaxis and Calcium Mobilization of Mast Cells. *The Journal of Pharmacology and Experimental Therapeutics* **2003**, *305* (3), 1212-1221. DOI: https://doi.org/10.1124/jpet.102.046581.

[209] Buckland, KF; Williams, TJ; Conroy, DM. Histamine induces cytoskeletal changes in human eosinophils via the H4 receptor. *British Journal of Pharmacology* **2003**, *140* (6), 1117-1127. DOI: https://doi.org/10.1038/sj.bjp.0705530.

[210] Ahmad, SF; Ansari, MA; Zoheir, KMA; Bakheet, SA; Korashy, HM; Nadeem, A; Ashour, AE; Attia, SM. Regulation of TNF-α and NF-κB activation through the JAK/STAT signaling pathway downstream of histamine 4 receptor in a rat model of LPS-induced joint inflammation. *Immunobiology* **2015**, *220* (7), 889-898. DOI: https://doi.org/10.1016/j.imbio.2015.01.008.

[211] Jemima, EA; Prema, A; Thangam, EB. Functional characterization of histamine H4 receptor on human mast cells. *Molecular Immunology* **2014**, *62* (1), 19-28. DOI: https://doi.org/10.1016/j.molimm.2014.05.007.

[212] Dijkstra, D; Leurs, R; Chazot, P; Shenton, FC; Stark, H; Werfel, T; Gutzmer, R. Histamine downregulates monocyte CCL2 production through the histamine H_4 receptor. *Journal of Allergy and Clinical Immunology* **2007**, *120* (2), 300-307. DOI: https://doi.org/10.1016/j.jaci.2007.03.024.

[213] Dijkstra, D; Stark, H; Chazot, PL; Shenton, FC; Leurs, R; Werfel, T; Gutzmer, R. Human Inflammatory Dendritic Epidermal Cells Express a Functional Histamine H_4 Receptor. *Journal of Investigative Dermatology* **2008**, *128* (7), 1696-1703. DOI: https://doi.org/10.1038/sj.jid.5701250.

[214] Bäumer, W; Wendorff, S; Gutzmer, R; Werfel, T; Dijkstra, D; Chazot, P; Stark, H; Kietzmann, M. Histamine H_4 receptors modulate dendritic cell migration through skin – immunomodulatory role of histamine. *Allergy* **2008**, *63* (10), 1387-1394. DOI: https://doi.org/10.1111/j.1398-9995.2008.01720.x.

[215] Morini, G; Becchi, G; Shenton, F; Chazot, P; Grandi, D. Histamine H_3 and H_4 receptors are expressed on distinct endocrine cell types in the rat fundic mucosa. *Inflammation research* **2008**, *57*, 57. DOI: https://doi.org/10.1007/s00011-007-0628-9.

[216] Ikawa, Y; Shiba, K; Ohki, E; Mutoh, N; Suzuki, M; Sato, H; Ueno, K. Comparative study of histamine H_4 receptor expression in human dermal fibroblasts. *The Journal of Toxicological Sciences* **2008**, *33* (4), 503-508. DOI: https://doi.org/10.2131/jts.33.503.

[217] Huang, J-F; Thurmond, RL. The new biology of histamine receptors. *Current Allergy and Asthma Reports* **2008**, *8* (1), 21-27. DOI: https://doi.org/10.1007/s11882-008-0005-y.

[218] Thurmond, RL; Gelfand, EW; Dunford, PJ. The role of histamine H_1 and H_4 receptors in allergic inflammation: the search for new antihistamines. *Nature Reviews Drug Discovery* **2008**, *7* (1), 41-53. DOI: https://doi.org/10.1038/nrd2465.

[219] Hashimoto, T; Harusawa, S; Araki, L; Zuiderveld, OP; Smit, MJ; Imazu, T; Takashima, S; Yamamoto, Y; Sakamoto, Y; Kurihara, T; et al. A Selective Human H_4-Receptor Agonist: (−)-2-Cyano-1-methyl-3-{(*2R*,*5R)*-5-[1*H*-imidazol-4(5)-yl]tetrahydrofuran-2-yl}methylguanidine. *Journal of Medicinal Chemistry* **2003**, *46* (14), 3162-3165. DOI: https://doi.org/10.1021/jm0300025.

[220] Lim, HD; Smits, RA; Bakker, RA; van Dam, CME; de Esch, IJP; Leurs, R. Discovery of S-(2-Guanidylethyl)-isothiourea (VUF 8430) as a Potent Nonimidazole Histamine H_4 Receptor Agonist. *Journal of Medicinal Chemistry* **2006**, *49* (23), 6650-6651. DOI: https://doi.org/10.1021/jm060880d.

[221] Gschwandtner, M; Koether, B; Werfel, T; Stark, H; Gutzmer, R. Profiling of histamine H_4 receptor agonists in native human monocytes. *British Journal of Pharmacology* **2013**, *170* (1), 136-143. DOI: https://doi.org/10.1111/bph.12237.

[222] Thurmond, RL; Desai, PJ; Dunford, PJ; Fung-Leung, W-P; Hofstra, CL; Jiang, W; Nguyen, S; Riley, JP; Sun, S; Williams, KN; et al. A Potent and Selective Histamine H_4 Receptor Antagonist with Anti-Inflammatory Properties. *The Journal of Pharmacology and Experimental Therapeutics* **2004**, *309* (1), 404-413. DOI: https://doi.org/10.1124/jpet.103.061754.

[223] Thurmond, RL. The histamine H_4 receptor: from orphan to the clinic. *Frontiers in Pharmacology* **2015**, *6*. DOI: https://doi.org/10.3389/fphar.2015.00065.

[224] Zhou, P; Homberg, JR; Fang, Q; Wang, J; Li, W; Meng, X; Shen, J; Luan, Y; Liao, P; Swaab, DF; et al. Histamine-4 receptor antagonist JNJ7777120 inhibits pro-inflammatory microglia and prevents the progression of Parkinson-like pathology and behaviour in a rat model. *Brain, Behavior, and Immunity* **2019**, *76*, 61-73. DOI: https://doi.org/10.1016/j.bbi.2018.11.006.

[225] Ahmad, SF; Nadeem, A; Ansari, MA; Bakheet, SA; Al-Mazroua, HA; Khan, MR; Alasmari, AF; Alanazi, WA; As Sobeai, HM; Attia, SM. The histamine-4 receptor antagonist JNJ7777120 prevents immune abnormalities by inhibiting RORγt/T-bet transcription factor signaling pathways in BTBR T^+ $Itpr3^{tf}$/J mice exposed to gamma rays. *Molecular Immunology* **2019**, *114*, 561-570. DOI: https://doi.org/10.1016/j.molimm.2019.09.007.

[226] Lee, C; Jones, TA. Effects of Several Therapeutic Agents on Mammalian Vestibular Function: Meclizine, Diazepam, and JNJ7777120. *Journal of the Association for Research in Otolaryngology* **2021**, *22* (5), 527-549. DOI: https://doi.org/10.1007/s10162-021-00803-5.

[227] Sağlam-Çifci, E; Güleç, İ; Şengelen, A; Karagöz-Güzey, F; Eren, B; Paşaoğlu, HE; Önay-Uçar, E. The H_4R antagonist, JNJ-7777120 treatments ameliorate mild traumatic brain injury by reducing oxidative

damage, inflammatory and apoptotic responses through blockage of the ERK1/2/NF-κB pathway in a rat model. *Experimental Neurology* **2025**, *385*, 115133. DOI: https://doi.org/10.1016/j.expneurol.2024.115133.

[228] Mehta, P; Miszta, P; Rzodkiewicz, P; Michalak, O; Krzeczyński, P; Filipek, S. Enigmatic Histamine Receptor H_4 for Potential Treatment of Multiple Inflammatory, Autoimmune, and Related Diseases. *Life* **2020**, *10* (4), 50. DOI: https://doi.org/10.3390/life10040050

[229] A Phase 2, Multicenter, Randomized, Double-Blind, Placebo-Controlled, Parallel Group Synovial Biopsy Study of JNJ-38518168 in Subjects With Active Rheumatoid Arthritis Despite Methotrexate Therapy. https://clinicaltrials.gov/study/NCT01862224.

[230] A Phase 2b Randomized, Double-blind, Multicenter, Placebo-controlled, Parallel Group, Dose Range Finding Study of JNJ-38518168 in Subjects With Active Rheumatoid Arthritis Despite Concomitant Methotrexate Therapy. https://clinicaltrials.gov/study/NCT01679951.

[231] Kollmeier, AP; Barnathan, ES; O'Brien, C; Chen, B; Xia, Y; Zhou, B; Loza, MJ; Silkoff, PE; Ge, M; Thurmond, RL. A phase 2a study of toreforant, a histamine H_4 receptor antagonist, in eosinophilic asthma. *Annals of Allergy, Asthma & Immunology* **2018**, *121* (5), 568-574. DOI: https://doi.org/10.1016/j.anai.2018.08.001.

[232] Kollmeier, AP; Greenspan, A; Xu, XL; Silkoff, PE; Barnathan, ES; Loza, MJ; Jiang, J; Zhou, B; Chen, B; Thurmond, RL. Phase 2a, randomized, double-blind, placebo-controlled, multicentre, parallel-group study of an H_4R-antagonist (JNJ-39758979) in adults with uncontrolled asthma. *Clinical & Experimental Allergy* **2018**, *48* (8), 957-969. DOI: https://doi.org/10.1111/cea.13154.

[233] A Phase 2 Multicenter, Randomized, Double-blind, Placebo-Controlled, Trial to Evaluate Toreforant (JNJ-38518168) for the Treatment of Subjects With Moderate to Severe Plaque-type Psoriasis. https://clinicaltrials.gov/study/NCT02295865.

[234] A Phase 2b Randomized, Double-blind, Multicenter, Placebo-controlled, Parallel-group, Dose Range Finding Study of JNJ-39758979 in Subjects With Active Rheumatoid Arthritis Despite Concomitant Methotrexate Therapy. https://clinicaltrials.gov/study/NCT01480388.

[235] A Phase 2, Randomized, Double-Blind, Placebo-Controlled, Multicenter, Parallel Group, 2-Part Study of JNJ-39758979 in Symptomatic Adult Subjects With Uncontrolled, Persistent Asthma. https://clinicaltrials.gov/study/NCT01493882.

[236] Werfel, T; Layton, G; Yeadon, M; Whitlock, L; Osterloh, I; Jimenez, P; Liu, W; Lynch, V; Asher, A; Tsianakas, A; et al. Efficacy and safety of the histamine H_4 receptor antagonist ZPL-3893787 in patients with atopic dermatitis. *Journal of Allergy and Clinical Immunology* **2019**, *143* (5), 1830-1837.e1834. DOI: https://doi.org/10.1016/j.jaci.2018.07.047.

[237] A Multicenter, Randomized, Double-blind, Placebo-controlled Study to Assess the Efficacy and Safety of 2 Dose Regimens of Orally Administered SENS-111 (100 mg and 200 mg) Given During 4 Days in Patients Suffering From Acute Unilateral Vestibulopathy. https://clinicaltrials.gov/study/NCT03110458.

[238] Grekowitz, E; Metz, M; Altrichter, S; Bauer, A; Brockow, K; Heine, G; Lionnet, L; Saday, KK; Hultsch, T; Søerensen, OE; et al. Targeting histamine receptor 4 in cholinergic urticaria with izuforant (LEO 152020): results from a phase IIa randomized double-blind placebo-controlled multicentre crossover trial. *British Journal of Dermatology* **2024**, *190* (6), 825-835. DOI: https://doi.org/10.1093/bjd/ljae038.

[239] Lim, HD; de Graaf, C; Jiang, W; Sadek, P; McGovern, PM; Istyastono, EP; Bakker, RA; de Esch, IJP; Thurmond, RL; Leurs, R. Molecular Determinants of Ligand Binding to H_4R Species Variants. *Molecular Pharmacology* **2010**, *77* (5), 734-743. DOI: https://doi.org/10.1124/mol.109.063040.

[240] Sander, K; Kottke, T; Tanrikulu, Y; Proschak, E; Weizel, L; Schneider, EH; Seifert, R; Schneider, G; Stark, H. 2,4-Diaminopyrimidines as histamine H4 receptor ligands—Scaffold optimization and pharmacological characterization. *Bioorganic & Medicinal Chemistry* **2009**, *17* (20), 7186-7196. DOI: https://doi.org/10.1016/j.bmc.2009.08.059.

[241] Thurmond, R; Chen, B; Dunford, P; Eckert, W; Karlsson, L; La D, WP; Xu, X; Greenspan, A. Pharmacology and clinical activity of toreforant, a histamine H_4 receptor antagonist. *J Ann Pharmacol Pharm* **2017**, 2(1): 1013.

[242] Thurmond, RL; Chen, B; Dunford, PJ; Greenspan, AJ; Karlsson, L; La, D; Ward, P; Xu, XL. Clinical and Preclinical Characterization of the Histamine H_4 Receptor Antagonist JNJ-39758979s. *The Journal of Pharmacology and Experimental Therapeutics* **2014**, *349* (2), 176-184. DOI: https://doi.org/10.1124/jpet.113.211714.

[243] Mowbray, CE; Bell, AS; Clarke, NP; Collins, M; Jones, RM; Lane, CAL; Liu, WL; Newman, SD; Paradowski, M; Schenck, EJ; et al. Challenges of drug discovery in novel target space. The discovery and evaluation of PF-3893787: A novel histamine H_4 receptor antagonist. *Bioorganic & Medicinal Chemistry Letters* **2011**, *21* (21), 6596-6602. DOI: https://doi.org/10.1016/j.bmcl.2011.07.125.

[244] Jin, BH; Hong, T; Yoo, BW; Kim, CO; Kim, D; Kim, YN; Park, MS. Pharmacokinetics, pharmacodynamics, and safety of izuforant, an H_4R inhibitor, in healthy subjects: A phase I single and

multiple ascending dose study. *Clinical and Translational Science* **2024**, *17* (10), e70032. DOI: https://doi.org/10.1111/cts.70032.

[245] Ramsay, RR; Popovic-Nikolic, MR; Nikolic, K; Uliassi, E; Bolognesi, ML. A perspective on multi-target drug discovery and design for complex diseases. *Clinical and Translational Medicine* **2018**, *7* (1), e3. DOI: https://doi.org/10.1186/s40169-017-0181-2.

[246] Cavalli, A; Bolognesi, ML; Minarini, A; Rosini, M; Tumiatti, V; Recanatini, M; Melchiorre, C. Multi-target-Directed Ligands To Combat Neurodegenerative Diseases. *Journal of Medicinal Chemistry* **2008**, *51* (3), 347-372. DOI: https://doi.org/10.1021/jm7009364.

[247] Wang, L; Esteban, G; Ojima, M; Bautista-Aguilera, OM; Inokuchi, T; Moraleda, I; Iriepa, I; Samadi, A; Youdim, MBH; Romero, A; et al. Donepezil + propargylamine + 8-hydroxyquinoline hybrids as new multifunctional metal-chelators, ChE and MAO inhibitors for the potential treatment of Alzheimer's disease. *European Journal of Medicinal Chemistry* **2014**, *80*, 543-561. DOI: https://doi.org/10.1016/j.ejmech.2014.04.078.

[248] Herrera-Arozamena, C; Estrada-Valencia, M; López-Caballero, P; Pérez, C; Morales-García, JA; Pérez-Castillo, A; Sastre, Ed; Fernández-Mendívil, C; Duarte, P; Michalska, P; et al. Resveratrol-Based MTDLs to Stimulate Defensive and Regenerative Pathways and Block Early Events in Neurodegenerative Cascades. *Journal of Medicinal Chemistry* **2022**, *65* (6), 4727-4751. DOI: https://doi.org/10.1021/acs.jmedchem.1c01883.

[249] Lamie, PF; Abdel-Fattah, MM; Philoppes, JN. Design and synthesis of new indole drug candidates to treat Alzheimer's disease and targeting neuro-inflammation using a multi-target-directed ligand (MTDL) strategy. *Journal of Enzyme Inhibition and Medicinal Chemistry* **2022**, *37* (1), 2660-2678. DOI: https://doi.org/10.1080/14756366.2022.2126464.

[250] Bawa, P; Pradeep, P; Kumar, P; Choonara, YE; Modi, G; Pillay, V. Multi-target therapeutics for neuropsychiatric and neurodegenerative disorders. *Drug Discovery Today* **2016**, *21* (12), 1886-1914. DOI: https://doi.org/10.1016/j.drudis.2016.08.001.

[251] Dekeyne, A; Brocco, M; Loiseau, F; Gobert, A; Rivet, J-M; Di Cara, B; Cremers, TI; Flik, G; Fone, KC; Watson, DJ. S32212, a novel serotonin type 2C receptor inverse agonist/α2-adrenoceptor antagonist and potential antidepressant: II. A behavioral, neurochemical, and electrophysiological characterization. *Journal of Pharmacology and Experimental Therapeutics* **2012**, *340* (3), 765-780. DOI: https://doi.org/10.1124/jpet.111.187534.

[252] Millan, MJ; la Cour, CM; Chanrion, B; Dupuis, DS; Di Cara, B; Audinot, V; Cussac, D; Newman-Tancredi, A; Kamal, M; Boutin, JA. S32212, a novel serotonin type 2C receptor inverse agonist/α_2-adrenoceptor antagonist and potential antidepressant: I. A mechanistic characterization. *Journal of Pharmacology and Experimental Therapeutics* **2012**, *340* (3), 750-764. DOI: https://doi.org/10.1124/jpet.111.187468.

[253] Mafi, S; Dehghani, M; Khalvati, B; Abidi, H; Ghorbani, M; Jalali, P; Whichelo, R; Salehi, Z; Markowska, A; Reyes, A; et al. Targeting PERK and GRP78 in colorectal cancer: Genetic insights and novel therapeutic approaches. *European Journal of Pharmacology* **2024**, *982*, 176899. DOI: https://doi.org/10.1016/j.ejphar.2024.176899.

[254] Brindisi, M; Kessler, SM; Kumar, V; Zwergel, C. Editorial: Multi-target directed ligands for the treatment of cancer. *Frontiers in Oncology* **2022**, *12*, Editorial. DOI: https://doi.org/10.3389/fonc.2022.980141.

[255] Raghavendra, NM; Pingili, D; Kadasi, S; Mettu, A; Prasad, SVUM. Dual or multi-targeting inhibitors: The next generation anticancer agents. *European Journal of Medicinal Chemistry* **2018**, *143*, 1277-1300. DOI: https://doi.org/10.1016/j.ejmech.2017.10.021.

[256] Roux, H; Touret, F; Rathelot, P; Vanelle, P; Roche, M. From the "One-Molecule, One-Target, One-Disease" Concept towards Looking for Multi-Target Therapeutics for Treating Non-Polio Enterovirus (NPEV) Infections. *Pharmaceuticals* **2024**, *17* (9), 1218. DOI: https://doi.org/10.3390/ph17091218.

[257] Joshi, RS; Jagdale, SS; Bansode, SB; Shankar, SS; Tellis, MB; Pandya, VK; Chugh, A; Giri, AP; Kulkarni, MJ. Discovery of potential multi-target-directed ligands by targeting host-specific SARS-CoV-2 structurally conserved main protease. *Journal of Biomolecular Structure and Dynamics* **2021**, *39* (9), 3099-3114. DOI: https://doi.org/10.1080/07391102.2020.1760137.

[258] East, SP; Silver, LL. Multitarget ligands in antibacterial research: progress and opportunities. *Expert Opinion on Drug Discovery* **2013**, *8* (2), 143-156. DOI: https://doi.org/10.1517/17460441.2013.743991.

[259] Tassopoulou, V-P; Tzara, A; Kourounakis, AP. Design of Improved Antidiabetic Drugs: A Journey from Single to Multitarget Agents. *ChemMedChem* **2022**, *17* (23), e202200320. DOI: https://doi.org/10.1002/cmdc.202200320.

[260] Lillich, FF; Imig, JD; Proschak, E. Multi-Target Approaches in Metabolic Syndrome. *Frontiers in Pharmacology* **2021**, *11*. DOI: https://doi.org/10.3389/fphar.2020.554961.

[261] Bisi, A; Gobbi, S; Belluti, F; Rampa, A. Design of Multifunctional Compounds for Cardiovascular Disease: From Natural Scaffolds to "Classical" Multitarget Approach. *Current Medicinal Chemistry* **2013**, *20* (13), 1759-1782. DOI: http://dx.doi.org/10.2174/0929867311320130012.

[262] Morphy, R; Rankovic, Z. Designed Multiple Ligands. An Emerging Drug Discovery Paradigm. *Journal of Medicinal Chemistry* **2005**, *48* (21), 6523-6543. DOI: https://doi.org/10.1021/jm058225d.

[263] Bolognesi, ML; Cavalli, A; Valgimigli, L; Bartolini, M; Rosini, M; Andrisano, V; Recanatini, M; Melchiorre, C. Multi-Target-Directed Drug Design Strategy: From a Dual Binding Site Acetylcholinesterase Inhibitor to a Trifunctional Compound against Alzheimer's Disease. *Journal of Medicinal Chemistry* **2007**, *50* (26), 6446-6449. DOI: https://doi.org/10.1021/jm701225u.

[264] Ma, H; Huang, B; Zhang, Y. Recent advances in multitarget-directed ligands targeting G-protein-coupled receptors. *Drug Discovery Today* **2020**, *25* (9), 1682-1692. DOI: https://doi.org/10.1016/j.drudis.2020.07.004.

[265] Proschak, E; Stark, H; Merk, D. Polypharmacology by Design: A Medicinal Chemist's Perspective on Multitargeting Compounds. *Journal of Medicinal Chemistry* **2019**, *62* (2), 420-444. DOI: https://doi.org/10.1021/acs.jmedchem.8b00760.

[266] Khanfar, MA; Affini, A; Lutsenko, K; Nikolic, K; Butini, S; Stark, H. Multiple Targeting Approaches on Histamine H_3 Receptor Antagonists. *Frontiers in Neuroscience* **2016**, *10*. DOI: https://doi.org/10.3389/fnins.2016.00201.

[267] von Coburg, Y; Kottke, T; Weizel, L; Ligneau, X; Stark, H. Potential utility of histamine H_3 receptor antagonist pharmacophore in antipsychotics. *Bioorganic & Medicinal Chemistry Letters* **2009**, *19* (2), 538-542. DOI: https://doi.org/10.1016/j.bmcl.2008.09.012.

[268] Lepailleur, A; Freret, T; Lemaître, S; Boulouard, M; Dauphin, F; Hinschberger, A; Dulin, F; Lesnard, A; Bureau, R; Rault, S. Dual Histamine H_3R/Serotonin 5-HT_4R Ligands with Antiamnesic Properties: Pharmacophore-Based Virtual Screening and Polypharmacology. *Journal of Chemical Information and Modeling* **2014**, *54* (6), 1773-1784. DOI: https://doi.org/10.1021/ci500157n.

[269] Pala, D; Scalvini, L; Lodola, A; Mor, M; Flammini, L; Barocelli, E; Lucini, V; Scaglione, F; Bartolucci, S; Bedini, A; et al. Synthesis and Characterization of New Bivalent Agents as Melatonin- and Histamine H_3-Ligands. *International Journal of Molecular Sciences* **2014**, *15* (9), 16114-16133. DOI: https://doi.org/10.3390/ijms150916114.

[270] Ly, KS; Letavic, MA; Keith, JM; Miller, JM; Stocking, EM; Barbier, AJ; Bonaventure, P; Lord, B; Jiang, X; Boggs, JD; et al. Synthesis and biological activity of piperazine and diazepane amides that are histamine H_3 antagonists and serotonin reuptake inhibitors. *Bioorganic & Medicinal Chemistry Letters* **2008**, *18* (1), 39-43. DOI: https://doi.org/10.1016/j.bmcl.2007.11.016.

[271] Altenbach, RJ; Black, LA; Strakhova, MI; Manelli, AM; Carr, TL; Marsh, KC; Wetter, JM; Wensink, EJ; Hsieh, GC; Honore, P; et al. Diaryldiamines with Dual Inhibition of the Histamine H_3 Receptor and the Norepinephrine Transporter and the Efficacy of 4-(3-(Methylamino)-1-phenylpropyl)-6-(2-(pyrrolidin-1-yl)ethoxy)naphthalen-1-ol in Pain. *Journal of Medicinal Chemistry* **2010**, *53* (21), 7869-7873. DOI: https://doi.org/10.1021/jm100666w.

[272] Apelt, J; Ligneau, X; Pertz, HH; Arrang, J-M; Ganellin, CR; Schwartz, J-C; Schunack, W; Stark, H. Development of a New Class of Nonimidazole Histamine H_3 Receptor Ligands with Combined Inhibitory Histamine N-Methyltransferase Activity. *Journal of Medicinal Chemistry* **2002**, *45* (5), 1128-1141. DOI: https://doi.org/10.1021/jm0110845.

[273] Bajda, M; Łażewska, D; Godyń, J; Zaręba, P; Kuder, K; Hagenow, S; Łątka, K; Stawarska, E; Stark, H; Kieć-Kononowicz, K; et al. Search for new multi-target compounds against Alzheimer's disease among histamine H_3 receptor ligands. *European Journal of Medicinal Chemistry* **2020**, *185*, 111785. DOI: https://doi.org/10.1016/j.ejmech.2019.111785.

[274] Bautista-Aguilera, ÓM; Hagenow, S; Palomino-Antolin, A; Farré-Alins, V; Ismaili, L; Joffrin, P-L; Jimeno, ML; Soukup, O; Janočková, J; Kalinowsky, L; et al. Multitarget-Directed Ligands Combining Cholinesterase and Monoamine Oxidase Inhibition with Histamine H_3R Antagonism for Neurodegenerative Diseases. *Angewandte Chemie International Edition* **2017**, *56* (41), 12765-12769. DOI: https://doi.org/10.1002/anie.201706072.

[275] Cavalli, G; Heard, E. Advances in epigenetics link genetics to the environment and disease. *Nature* **2019**, *571* (7766), 489-499. DOI: https://doi.org/10.1038/s41586-019-1411-0.

[276] Greer, EL; Shi, Y. Histone methylation: a dynamic mark in health, disease and inheritance. *Nature Reviews Genetics* **2012**, *13* (5), 343-357. DOI: https://doi.org/10.1038/nrg3173.

[277] Poulard, C; Noureddine, LM; Pruvost, L; Le Romancer, M. Structure, Activity, and Function of the Protein Lysine Methyltransferase G9a. *Life* **2021**, *11* (10), 1082. DOI: https://doi.org/10.3390/life11101082

[278] Strahl, BD; Allis, CD. The language of covalent histone modifications. *Nature* **2000**, *403* (6765), 41-45. DOI: https://doi.org/10.1038/47412.

[279] Liu, R; Wu, J; Guo, H; Yao, W; Li, S; Lu, Y; Jia, Y; Liang, X; Tang, J; Zhang, H. Post-translational modifications of histones: Mechanisms, biological functions, and therapeutic targets. *MedComm* **2023**, *4* (3), e292. DOI: https://doi.org/10.1002/mco2.292.

[280] Martin, C; Zhang, Y. The diverse functions of histone lysine methylation. *Nature Reviews Molecular Cell Biology* **2005**, *6* (11), 838-849. DOI: https://doi.org/10.1038/nrm1761.

[281] Bellver-Sanchis, A; Ribalta-Vilella, M; Irisarri, A; Gehlot, P; Choudhary, BS; Jana, A; Vyas, VK; Banerjee, DR; Pallàs, M; Guerrero, A; et al. G9a an Epigenetic Therapeutic Strategy for Neurodegenerative Conditions: From Target Discovery to Clinical Trials. *Medicinal Research Reviews* **2025**, *n/a* (n/a). DOI: https://doi.org/10.1002/med.22096.

[282] Millán-Zambrano, G; Burton, A; Bannister, AJ; Schneider, R. Histone post-translational modifications — cause and consequence of genome function. *Nature Reviews Genetics* **2022**, *23* (9), 563-580. DOI: https://doi.org/10.1038/s41576-022-00468-7.

[283] Dillon, SC; Zhang, X; Trievel, RC; Cheng, X. The SET-domain protein superfamily: protein lysine methyltransferases. *Genome Biology* **2005**, *6* (8), 227. DOI: https://doi.org/10.1186/gb-2005-6-8-227.

[284] Falnes, Pål Ø; Jakobsson, Magnus E; Davydova, E; Ho, A; Małecki, J. Protein lysine methylation by seven-β-strand methyltransferases. *Biochemical Journal* **2016**, *473* (14), 1995-2009. DOI: https://doi.org/10.1042/bcj20160117.

[285] Ni, Y; Shi, M; Liu, L; Lin, D; Zeng, H; Ong, C; Wang, Y. G9a in Cancer: Mechanisms, Therapeutic Advancements, and Clinical Implications. *Cancers* **2024**, *16* (12), 2175. DOI: https://doi.org/10.3390/cancers16122175

[286] Milner, CM; Campbell, RD. The G9a gene in the human major histocompatibility complex encodes a novel protein containing ankyrin-like repeats. *Biochemical Journal* **1993**, *290* (3), 811-818. DOI: https://doi.org/10.1042/bj2900811.

[287] Mauger, O; Klinck, R; Chabot, B; Muchardt, C; Allemand, E; Batsché, E. Alternative splicing regulates the expression of G9A and SUV39H2 methyltransferases, and dramatically changes SUV39H2 functions. *Nucleic Acids Research* **2015**, *43* (3), 1869-1882. DOI: https://doi.org/10.1093/nar/gkv013.

[288] Fiszbein, A; Giono, Luciana E; Quaglino, A; Berardino, Bruno G; Sigaut, L; von Bilderling, C; Schor, Ignacio E; Enriqué Steinberg, JH; Rossi, M; Pietrasanta, Lía I; et al. Alternative Splicing of G9a Regulates Neuronal Differentiation. *Cell Reports* **2016**, *14* (12), 2797-2808. DOI: https://doi.org/10.1016/j.celrep.2016.02.063.

[289] Taylor, WR; Xiao, B; Gamblin, SJ; Lin, K. A knot or not a knot? SETting the record 'straight' on proteins. *Computational Biology and Chemistry* **2003**, *27* (1), 11-15. DOI: https://doi.org/10.1016/S1476-9271(02)00099-3.

[290] Trievel, RC; Beach, BM; Dirk, LMA; Houtz, RL; Hurley, JH. Structure and Catalytic Mechanism of a SET Domain Protein Methyltransferase. *Cell* **2002**, *111* (1), 91-103. DOI: https://doi.org/10.1016/S0092-8674(02)01000-0.

[291] Lenstra, DC; Al Temimi, AHK; Mecinović, J. Inhibition of histone lysine methyltransferases G9a and GLP by ejection of structural Zn(II). *Bioorganic & Medicinal Chemistry Letters* **2018**, *28* (7), 1234-1238. DOI: https://doi.org/10.1016/j.bmcl.2018.02.043.

[292] Collins, RE; Northrop, JP; Horton, JR; Lee, DY; Zhang, X; Stallcup, MR; Cheng, X. The ankyrin repeats of G9a and GLP histone methyltransferases are mono- and dimethyllysine binding modules. *Nature Structural & Molecular Biology* **2008**, *15* (3), 245-250. DOI: https://doi.org/10.1038/nsmb.1384.

[293] Katayama, K; Ishii, K; Tsuda, E; Yotsumoto, K; Hiramoto, K; Suzuki, M; Yasumatsu, I; Igarashi, W; Torihata, M; Ishiyama, T; et al. Discovery of novel histone lysine methyltransferase G9a/GLP (EHMT2/1) inhibitors: Design, synthesis, and structure-activity relationships of 2,4-diamino-6-methylpyrimidines. *Bioorganic & Medicinal Chemistry Letters* **2020**, *30* (20), 127475. DOI: https://doi.org/10.1016/j.bmcl.2020.127475.

[294] Estève, P-O; Patnaik, D; Chin, HG; Benner, J; Teitell, MA; Pradhan, S. Functional analysis of the N- and C-terminus of mammalian G9a histone H3 methyltransferase. *Nucleic Acids Research* **2005**, *33* (10), 3211-3223. DOI: https://doi.org/10.1093/nar/gki635.

[295] Chang, Y; Zhang, X; Horton, JR; Upadhyay, AK; Spannhoff, A; Liu, J; Snyder, JP; Bedford, MT; Cheng, X. Structural basis for G9a-like protein lysine methyltransferase inhibition by BIX-01294. *Nature Structural & Molecular Biology* **2009**, *16* (3), 312-317. DOI: https://doi.org/10.1038/nsmb.1560.

[296] Tachibana, M; Sugimoto, K; Nozaki, M; Ueda, J; Ohta, T; Ohki, M; Fukuda, M; Takeda, N; Niida, H; Kato, H; et al. G9a histone methyltransferase plays a dominant role in euchromatic histone H3 lysine 9 methylation and is essential for early embryogenesis. *Genes Dev* **2002**, *16* (14), 1779-1791. DOI: https://doi.org/10.1101/gad.989402.

[297] Yu, Y; Song, C; Zhang, Q; DiMaggio, Peter A; Garcia, Benjamin A; York, A; Carey, Michael F; Grunstein, M. Histone H3 Lysine 56 Methylation Regulates DNA Replication through Its Interaction with PCNA. *Molecular Cell* **2012**, *46* (1), 7-17. DOI: https://doi.org/10.1016/j.molcel.2012.01.019.

[298] Weiss, T; Hergeth, S; Zeissler, U; Izzo, A; Tropberger, P; Zee, BM; Dundr, M; Garcia, BA; Daujat, S; Schneider, R. Histone H1 variant-specific lysine methylation by G9a/KMT1C and Glp1/KMT1D. *Epigenetics & Chromatin* **2010**, *3* (1), 7. DOI: https://doi.org/10.1186/1756-8935-3-7.

[299] Trojer, P; Zhang, J; Yonezawa, M; Schmidt, A; Zheng, H; Jenuwein, T; Reinberg, D. Dynamic Histone H1 Isotype 4 Methylation and Demethylation by Histone Lysine Methyltransferase G9a/KMT1C and the Jumonji Domain-containing JMJD2/KDM4 Proteins*. *Journal of Biological Chemistry* **2009**, *284* (13), 8395-8405. DOI: https://doi.org/10.1074/jbc.M807818200.

[300] Tachibana, M; Ueda, J; Fukuda, M; Takeda, N; Ohta, T; Iwanari, H; Sakihama, T; Kodama, T; Hamakubo, T; Shinkai, Y. Histone methyltransferases G9a and GLP form heteromeric complexes and are both crucial for methylation of euchromatin at H3-K9. *Genes & development* **2005**, *19* (7), 815-826. DOI: https://doi.org/10.1101/gad.1284005

[301] Tachibana, M; Matsumura, Y; Fukuda, M; Kimura, H; Shinkai, Y. G9a/GLP complexes independently mediate H3K9 and DNA methylation to silence transcription. *The EMBO Journal* **2008**, *27* (20), 2681-2690. DOI: https://doi.org/10.1038/emboj.2008.192.

[302] Bittencourt, D; Wu, D-Y; Jeong, KW; Gerke, DS; Herviou, L; Ianculescu, I; Chodankar, R; Siegmund, KD; Stallcup, MR. G9a functions as a molecular scaffold for assembly of transcriptional coactivators on a subset of Glucocorticoid Receptor target genes. *Proceedings of the National Academy of Sciences* **2012**, *109* (48), 19673-19678. DOI: https://doi.org/10.1073/pnas.1211803109.

[303] Lee, DY; Northrop, JP; Kuo, M-H; Stallcup, MR. Histone H3 Lysine 9 Methyltransferase G9a Is a Transcriptional Coactivator for Nuclear Receptors*. *Journal of Biological Chemistry* **2006**, *281* (13), 8476-8485. DOI: https://doi.org/10.1074/jbc.M511093200.

[304] Purcell, DJ; Jeong, KW; Bittencourt, D; Gerke, DS; Stallcup, MR. A Distinct Mechanism for Coactivator versus Corepressor Function by Histone Methyltransferase G9a in Transcriptional Regulation*. *Journal of Biological Chemistry* **2011**, *286* (49), 41963-41971. DOI: https://doi.org/10.1074/jbc.M111.298463.

[305] Purcell, DJ; Khalid, O; Ou, C-Y; Little, GH; Frenkel, B; Baniwal, SK; Stallcup, MR. Recruitment of coregulator G9a by Runx2 for selective enhancement or suppression of transcription. *Journal of Cellular Biochemistry* **2012**, *113* (7), 2406-2414. DOI: https://doi.org/10.1002/jcb.24114.

[306] Poulard, C; Bittencourt, D; Wu, DY; Hu, Y; Gerke, DS; Stallcup, MR. A post-translational modification switch controls coactivator function of histone methyltransferases G9a and GLP. *EMBO reports* **2017**, *18* (8), 1442-1459. DOI: https://doi.org/10.15252/embr.201744060.

[307] Oh, S-T; Kim, K-B; Chae, Y-C; Kang, J-Y; Hahn, Y; Seo, S-B. H3K9 histone methyltransferase G9a-mediated transcriptional activation of p21. *FEBS Letters* **2014**, *588* (5), 685-691. DOI: https://doi.org/10.1016/j.febslet.2014.01.039.

[308] Jan, S; Dar, MI; Wani, R; Sandey, J; Mushtaq, I; Lateef, S; Syed, SH. Targeting EHMT2/ G9a for cancer therapy: Progress and perspective. *European Journal of Pharmacology* **2021**, *893*, 173827. DOI: https://doi.org/10.1016/j.ejphar.2020.173827.

[309] Yang, X; Xu, L; Yang, L. Recent advances in EZH2-based dual inhibitors in the treatment of cancers. *European Journal of Medicinal Chemistry* **2023**, *256*, 115461. DOI: https://doi.org/10.1016/j.ejmech.2023.115461.

[310] Ren, X; Wang, R; Yu, X-t; Cai, B; Guo, F. Regulation of histone H3 lysine 9 methylation in inflammation. *All Life* **2021**, *14* (1), 492-508. DOI: https://doi.org/10.1080/26895293.2021.1931477.

[311] Fang, Z; Wang, Y; Huang, B; Chen, X; Jiang, R; Yin, M. Depletion of G9A attenuates imiquimod-induced psoriatic dermatitis via targeting EDAR-NF-κB signaling in keratinocyte. *Cell Death & Disease* **2023**, *14* (9), 627. DOI: https://doi.org/10.1038/s41419-023-06134-y.

[312] Bellver-Sanchis, A; Geng, Q; Navarro, G; Ávila-López, PA; Companys-Alemany, J; Marsal-García, L; Larramona-Arcas, R; Miró, L; Perez-Bosque, A; Ortuño-Sahagún, D; et al. G9a Inhibition Promotes Neuroprotection through GMFB Regulation in Alzheimer's Disease. *Aging and disease* **2024**, *15* (1), 311-337. DOI: https://doi.org/10.14336/ad.2023.0424-2.

[313] Zheng, Y; Liu, A; Wang, Z-J; Cao, Q; Wang, W; Lin, L; Ma, K; Zhang, F; Wei, J; Matas, E; et al. Inhibition of EHMT1/2 rescues synaptic and cognitive functions for Alzheimer's disease. *Brain* **2019**, *142* (3), 787-807. DOI: https://doi.org/10.1093/brain/awy354.

[314] Sharma, M; Dierkes, T; Sajikumar, S. Epigenetic regulation by G9a/GLP complex ameliorates amyloid-beta 1-42 induced deficits in long-term plasticity and synaptic tagging/capture in hippocampal pyramidal neurons. *Aging Cell* **2017**, *16* (5), 1062-1072. DOI: https://doi.org/10.1111/acel.12634.

[315] Griñán-Ferré, C; Marsal-García, L; Bellver-Sanchis, A; Kondengaden, SM; Turga, RC; Vázquez, S; Pallàs, M. Pharmacological inhibition of G9a/GLP restores cognition and reduces oxidative stress, neuroinflammation and β-Amyloid plaques in an early-onset Alzheimer's disease mouse model. *Aging (Albany NY)* **2019**, *11* (23), 11591-11608. DOI: https://doi.org/10.18632/aging.102558 .

[316] Sugeno, N; Jäckel, S; Voigt, A; Wassouf, Z; Schulze-Hentrich, J; Kahle, PJ. α-Synuclein enhances histone H3 lysine-9 dimethylation and H3K9me2-dependent transcriptional responses. *Scientific Reports* **2016**, *6* (1), 36328. DOI: https://doi.org/10.1038/srep36328.

[317] Smigielski, L; Jagannath, V; Rössler, W; Walitza, S; Grünblatt, E. Epigenetic mechanisms in schizophrenia and other psychotic disorders: a systematic review of empirical human findings. *Molecular Psychiatry* **2020**, *25* (8), 1718-1748. DOI: https://doi.org/10.1038/s41380-019-0601-3.

[318] Chase, KA; Gavin, DP; Guidotti, A; Sharma, RP. Histone methylation at H3K9: Evidence for a restrictive epigenome in schizophrenia. *Schizophrenia Research* **2013**, *149* (1), 15-20. DOI: https://doi.org/10.1016/j.schres.2013.06.021.

[319] Chase, KA; Feiner, B; Ramaker, MJ; Hu, E; Rosen, C; Sharma, RP. Examining the effects of the histone methyltransferase inhibitor BIX-01294 on histone modifications and gene expression in both a clinical population and mouse models. *PLOS ONE* **2019**, *14* (6), e0216463. DOI: https://doi.org/10.1371/journal.pone.0216463.

[320] Cassidy, SB; Schwartz, S; Miller, JL; Driscoll, DJ. Prader-Willi syndrome. *Genetics in Medicine* **2012**, *14* (1), 10-26. DOI: https://doi.org/10.1038/gim.0b013e31822bead0.

[321] Kim, Y; Lee, H-M; Xiong, Y; Sciaky, N; Hulbert, SW; Cao, X; Everitt, JI; Jin, J; Roth, BL; Jiang, Y-h. Targeting the histone methyltransferase G9a activates imprinted genes and improves survival of a mouse model of Prader–Willi syndrome. *Nature Medicine* **2017**, *23* (2), 213-222. DOI: https://doi.org/10.1038/nm.4257.

[322] Kubicek, S; O'Sullivan, RJ; August, EM; Hickey, ER; Zhang, Q; Teodoro, Miguel L; Rea, S; Mechtler, K; Kowalski, JA; Homon, CA; et al. Reversal of H3K9me2 by a Small-Molecule Inhibitor for the G9a Histone Methyltransferase. *Molecular Cell* **2007**, *25* (3), 473-481. DOI: https://doi.org/10.1016/j.molcel.2007.01.017.

[323] Charles, MRC; Dhayalan, A; Hsieh, H-P; Coumar, MS. Insights for the Design of Protein Lysine Methyltransferase G9a Inhibitors. *Future Medicinal Chemistry* **2019**, *11* (9), 993-1014. DOI: https://doi.org/10.4155/fmc-2018-0396.

[324] Cao, H; Li, L; Yang, D; Zeng, L; Yewei, X; Yu, B; Liao, G; Chen, J. Recent progress in histone methyltransferase (G9a) inhibitors as anticancer agents. *European Journal of Medicinal Chemistry* **2019**, *179*, 537-546. DOI: https://doi.org/10.1016/j.ejmech.2019.06.072.

[325] San José-Enériz, E; Agirre, X; Rabal, O; Vilas-Zornoza, A; Sanchez-Arias, JA; Miranda, E; Ugarte, A; Roa, S; Paiva, B; Estella-Hermoso de Mendoza, A; et al. Discovery of first-in-class reversible dual small molecule inhibitors against G9a and DNMTs in hematological malignancies. *Nature Communications* **2017**, *8* (1), 15424. DOI: https://doi.org/10.1038/ncomms15424.

[326] Rabal, O; Sánchez-Arias, JA; José-Enériz, ES; Agirre, X; De Miguel, I; Garate, L; Miranda, E; Sáez, E; Roa, S; Martínez-Climent, JA; et al. Detailed Exploration around 4-Aminoquinolines Chemical Space to Navigate the Lysine Methyltransferase G9a and DNA Methyltransferase Biological Spaces. *Journal of Medicinal Chemistry* **2018**, *61* (15), 6546 - 6573. DOI: https://doi.org/10.1021/acs.jmedchem.7b01925.

[327] Rabal, O; San José-Enériz, E; Agirre, X; Sánchez-Arias, JA; de Miguel, I; Ordoñez, R; Garate, L; Miranda, E; Sáez, E; Vilas-Zornoza, A; et al. Design and Synthesis of Novel Epigenetic Inhibitors Targeting Histone Deacetylases, DNA Methyltransferase 1, and Lysine Methyltransferase G9a with In Vivo Efficacy in Multiple Myeloma. *Journal of Medicinal Chemistry* **2021**, *64* (6), 3392-3426. DOI: https://doi.org/10.1021/acs.jmedchem.0c02255.

[328] Milite, C; Feoli, A; Horton, JR; Rescigno, D; Cipriano, A; Pisapia, V; Viviano, M; Pepe, G; Amendola, G; Novellino, E; et al. Discovery of a Novel Chemotype of Histone Lysine Methyltransferase EHMT1/2 (GLP/G9a) Inhibitors: Rational Design, Synthesis, Biological Evaluation, and Co-crystal Structure. *Journal of Medicinal Chemistry* **2019**, *62* (5), 2666-2689. DOI: https://doi.org/10.1021/acs.jmedchem.8b02008.

[329] Sweis, RF; Pliushchev, M; Brown, PJ; Guo, J; Li, F; Maag, D; Petros, AM; Soni, NB; Tse, C; Vedadi, M; et al. Discovery and Development of Potent and Selective Inhibitors of Histone Methyltransferase G9a. *ACS Medicinal Chemistry Letters* **2014**, *5* (2), 205-209. DOI: https://doi.org/10.1021/ml400496h.

[330] Cedillo-González, R; Medina-Franco, JL. Diversity and Chemical Space Characterization of Inhibitors of the Epigenetic Target G9a: A Chemoinformatics Approach. *ACS Omega* **2023**, *8* (33), 30694-30704. DOI: https://doi.org/10.1021/acsomega.3c04566.

[331] Vedadi, M; Barsyte-Lovejoy, D; Liu, F; Rival-Gervier, S; Allali-Hassani, A; Labrie, V; Wigle, TJ; DiMaggio, PA; Wasney, GA; Siarheyeva, A; et al. A chemical probe selectively inhibits G9a and GLP methyltransferase activity in cells. *Nature Chemical Biology* **2011**, *7* (8), 566-574. DOI: https://doi.org/10.1038/nchembio.599.

[332] Liu, F; Barsyte-Lovejoy, D; Li, F; Xiong, Y; Korboukh, V; Huang, X-P; Allali-Hassani, A; Janzen, WP; Roth, BL; Frye, SV; et al. Discovery of an in Vivo Chemical Probe of the Lysine Methyltransferases G9a

and GLP. *Journal of Medicinal Chemistry* **2013**, *56* (21), 8931-8942. DOI: https://doi.org/10.1021/jm401480r.

[333] Feng, Z; Yang, C; Zhang, Y; Li, H; Fang, W; Wang, J; Nie, Y; Wang, C-Y; Liu, Z; Jiang, Z; et al. Structure-Based Design and Characterization of the Highly Potent and Selective Covalent Inhibitors Targeting the Lysine Methyltransferases G9a/GLP. *Journal of Medicinal Chemistry* **2023**, *66* (12), 8086-8102. DOI: https://doi.org/10.1021/acs.jmedchem.3c00411.

[334] Li, D; Peng, X; Hu, Z; Li, S; Chen, J; Pan, W. Small molecules targeting selected histone methyltransferases (HMTs) for cancer treatment: Current progress and novel strategies. *European Journal of Medicinal Chemistry* **2024**, *264*, 115982. DOI: https://doi.org/10.1016/j.ejmech.2023.115982.

[335] Guo, L; Wang, W; Chen, SG. Leucine-rich repeat kinase 2: Relevance to Parkinson's disease. *The International Journal of Biochemistry & Cell Biology* **2006**, *38* (9), 1469-1475. DOI: https://doi.org/10.1016/j.biocel.2006.02.009.

[336] Wallings, R; Manzoni, C; Bandopadhyay, R. Cellular processes associated with LRRK2 function and dysfunction. *The FEBS Journal* **2015**, *282* (15), 2806-2826. DOI: https://doi.org/10.1111/febs.13305.

[337] Paisán-Ruíz, C; Jain, S; Evans, EW; Gilks, WP; Simón, J; van der Brug, M; de Munain, AL; Aparicio, S; Gil, AMn; Khan, N; et al. Cloning of the Gene Containing Mutations that Cause *PARK8*-Linked Parkinson's Disease. *Neuron* **2004**, *44* (4), 595-600. DOI: https://doi.org/10.1016/j.neuron.2004.10.023.

[338] Zimprich, A; Biskup, S; Leitner, P; Lichtner, P; Farrer, M; Lincoln, S; Kachergus, J; Hulihan, M; Uitti, RJ; Calne, DB; et al. Mutations in LRRK2 Cause Autosomal-Dominant Parkinsonism with Pleomorphic Pathology. *Neuron* **2004**, *44* (4), 601-607. DOI: https://doi.org/10.1016/j.neuron.2004.11.005.

[339] Santpere, G; Ferrer, I. LRRK2 and neurodegeneration. *Acta Neuropathologica* **2009**, *117* (3), 227-246. DOI: https://doi.org/10.1007/s00401-008-0478-8.

[340] Mata, IF; Wedemeyer, WJ; Farrer, MJ; Taylor, JP; Gallo, KA. LRRK2 in Parkinson's disease: protein domains and functional insights. *Trends in Neurosciences* **2006**, *29* (5), 286-293. DOI: https://doi.org/10.1016/j.tins.2006.03.006.

[341] Tolosa, E; Vila, M; Klein, C; Rascol, O. LRRK2 in Parkinson disease: challenges of clinical trials. *Nature Reviews Neurology* **2020**, *16* (2), 97-107. DOI: https://doi.org/10.1038/s41582-019-0301-2.

[342] Baidya, ATK; Deshwal, S; Das, B; Mathew, AT; Devi, B; Sandhir, R; Kumar, R. Catalyzing a Cure: Discovery and development of LRRK2 inhibitors for the treatment of Parkinson's disease. *Bioorganic Chemistry* **2024**, *143*, 106972. DOI: https://doi.org/10.1016/j.bioorg.2023.106972.

[343] Higashi, S; Biskup, S; West, AB; Trinkaus, D; Dawson, VL; Faull, RLM; Waldvogel, HJ; Arai, H; Dawson, TM; Moore, DJ; et al. Localization of Parkinson's disease-associated LRRK2 in normal and pathological human brain. *Brain Research* **2007**, *1155*, 208-219. DOI: https://doi.org/10.1016/j.brainres.2007.04.034.

[344] Han, B-S; Iacovitti, L; Katano, T; Hattori, N; Seol, W; Kim, K-S. Expression of the LRRK2 gene in the midbrain dopaminergic neurons of the substantia nigra. *Neuroscience Letters* **2008**, *442* (3), 190-194. DOI: https://doi.org/10.1016/j.neulet.2008.06.086.

[345] Westerlund, M; Belin, AC; Anvret, A; Bickford, P; Olson, L; Galter, D. Developmental regulation of leucine-rich repeat kinase 1 and 2 expression in the brain and other rodent and human organs: Implications for Parkinson's disease. *Neuroscience* **2008**, *152* (2), 429-436. DOI: https://doi.org/10.1016/j.neuroscience.2007.10.062.

[346] Miklossy, J; Arai, T; Guo, J-P; Klegeris, A; Yu, S; McGeer, EG; McGeer, PL. LRRK2 Expression in Normal and Pathologic Human Brain and in Human Cell Lines. *Journal of Neuropathology & Experimental Neurology* **2006**, *65* (10), 953-963. DOI: https://doi.org/10.1097/01.jnen.0000235121.98052.54.

[347] Thévenet, J; Pescini Gobert, R; Hooft van Huijsduijnen, R; Wiessner, C; Sagot, YJ. Regulation of LRRK2 Expression Points to a Functional Role in Human Monocyte Maturation. *PLOS ONE* **2011**, *6* (6), e21519. DOI: https://doi.org/10.1371/journal.pone.0021519.

[348] Estrada, AA; Sweeney, ZK. Chemical Biology of Leucine-Rich Repeat Kinase 2 (LRRK2) Inhibitors. *Journal of Medicinal Chemistry* **2015**, *58* (17), 6733-6746. DOI: https://doi.org/10.1021/acs.jmedchem.5b00261.

[349] Nichols, RJ; Dzamko, N; Morrice, Nicholas A; Campbell, David G; Deak, M; Ordureau, A; Macartney, T; Tong, Y; Shen, J; Prescott, Alan R; et al. 14-3-3 binding to LRRK2 is disrupted by multiple Parkinson's disease-associated mutations and regulates cytoplasmic localization. *Biochemical Journal* **2010**, *430* (3), 393-404. DOI: https://doi.org/10.1042/bj20100483.

[350] Deyaert, E; Wauters, L; Guaitoli, G; Konijnenberg, A; Leemans, M; Terheyden, S; Petrovic, A; Gallardo, R; Nederveen-Schippers, LM; Athanasopoulos, PS; et al. A homologue of the Parkinson's disease-associated protein LRRK2 undergoes a monomer-dimer transition during GTP turnover. *Nature Communications* **2017**, *8* (1), 1008. DOI: https://doi.org/10.1038/s41467-017-01103-4.

[351] Berwick, DC; Heaton, GR; Azeggagh, S; Harvey, K. LRRK2 Biology from structure to dysfunction: research progresses, but the themes remain the same. *Molecular Neurodegeneration* **2019**, *14* (1), 49. DOI: https://doi.org/10.1186/s13024-019-0344-2.

[352] Steger, M; Tonelli, F; Ito, G; Davies, P; Trost, M; Vetter, M; Wachter, S; Lorentzen, E; Duddy, G; Wilson, S; et al. Phosphoproteomics reveals that Parkinson's disease kinase LRRK2 regulates a subset of Rab GTPases. *eLife* **2016**, *5*, e12813. DOI: https://doi.org/10.7554/eLife.12813.

[353] Steger, M; Diez, F; Dhekne, HS; Lis, P; Nirujogi, RS; Karayel, O; Tonelli, F; Martinez, TN; Lorentzen, E; Pfeffer, SR; et al. Systematic proteomic analysis of LRRK2-mediated Rab GTPase phosphorylation establishes a connection to ciliogenesis. *eLife* **2017**, *6*, e31012. DOI: https://doi.org/10.7554/eLife.31012.

[354] Wauters, L; Versées, W; Kortholt, A. Roco Proteins: GTPases with a Baroque Structure and Mechanism. *International Journal of Molecular Sciences* **2019**, *20* (1), 147. DOI: https://doi.org/10.3390/ijms20010147.

[355] Jeong, GR; Lee, BD. Pathological Functions of LRRK2 in Parkinson's Disease. *Cells* **2020**, *9* (12), 2565. DOI: https://doi.org/10.3390/cells9122565.

[356] Rivero-Ríos, P; Romo-Lozano, M; Fasiczka, R; Naaldijk, Y; Hilfiker, S. LRRK2-Related Parkinson's Disease Due to Altered Endolysosomal Biology With Variable Lewy Body Pathology: A Hypothesis. *Frontiers in Neuroscience* **2020**, *14*. DOI: https://doi.org/10.3389/fnins.2020.00556.

[357] Rocha, EM; Keeney, MT; Di Maio, R; De Miranda, BR; Greenamyre, JT. LRRK2 and idiopathic Parkinson's disease. *Trends in Neurosciences* **2022**, *45* (3), 224-236. DOI: https://doi.org/10.1016/j.tins.2021.12.002.

[358] Cookson, MR. The role of leucine-rich repeat kinase 2 (LRRK2) in Parkinson's disease. *Nature Reviews Neuroscience* **2010**, *11* (12), 791-797. DOI: https://doi.org/10.1038/nrn2935.

[359] Artzi, M; Even-Sapir, E; Lerman Shacham, H; Thaler, A; Urterger, AO; Bressman, S; Marder, K; Hendler, T; Giladi, N; Ben Bashat, D; et al. DaT-SPECT assessment depicts dopamine depletion among asymptomatic G2019S LRRK2 mutation carriers. *PLOS ONE* **2017**, *12* (4), e0175424. DOI: https://doi.org/10.1371/journal.pone.0175424.

[360] Greggio, E; Cookson, MR. Leucine-Rich Repeat Kinase 2 Mutations and Parkinson's Disease: Three Questions. *ASN Neuro* **2009**, *1* (1), AN20090007. DOI: https://doi.org/10.1042/AN20090007.

[361] Ito, G; Utsunomiya-Tate, N. Overview of the Impact of Pathogenic LRRK2 Mutations in Parkinson's Disease. *Biomolecules* **2023**, *13* (5), 845. DOI: https://doi.org/10.3390/biom13050845.

[362] Ray, S; Bender, S; Kang, S; Lin, R; Glicksman, MA; Liu, M. The Parkinson Disease-linked LRRK2 Protein Mutation I2020T Stabilizes an Active State Conformation Leading to Increased Kinase Activity*. *Journal of Biological Chemistry* **2014**, *289* (19), 13042-13053. DOI: https://doi.org/10.1074/jbc.M113.537811.

[363] Cookson, MR. Mechanisms of Mutant LRRK2 Neurodegeneration. In *Leucine-Rich Repeat Kinase 2 (LRRK2)*, Rideout, HJ Ed.; Springer International Publishing, 2017; pp 227-239.

[364] Greggio, E; Jain, S; Kingsbury, A; Bandopadhyay, R; Lewis, P; Kaganovich, A; van der Brug, MP; Beilina, A; Blackinton, J; Thomas, KJ; et al. Kinase activity is required for the toxic effects of mutant LRRK2/dardarin. *Neurobiology of Disease* **2006**, *23* (2), 329-341. DOI: https://doi.org/10.1016/j.nbd.2006.04.001.

[365] Henderson, MX; Sengupta, M; McGeary, I; Zhang, B; Olufemi, MF; Brown, H; Trojanowski, JQ; Lee, VMY. LRRK2 inhibition does not impart protection from α-synuclein pathology and neuron death in non-transgenic mice. *Acta Neuropathologica Communications* **2019**, *7* (1), 28. DOI: https://doi.org/10.1186/s40478-019-0679-5.

[366] Pan, P-Y; Li, X; Wang, J; Powell, J; Wang, Q; Zhang, Y; Chen, Z; Wicinski, B; Hof, P; Ryan, TA; et al. Parkinson's Disease-Associated LRRK2 Hyperactive Kinase Mutant Disrupts Synaptic Vesicle Trafficking in Ventral Midbrain Neurons. *The Journal of Neuroscience* **2017**, *37* (47), 11366-11376. DOI: https://doi.org/10.1523/jneurosci.0964-17.2017.

[367] Nguyen, M; Krainc, D. LRRK2 phosphorylation of auxilin mediates synaptic defects in dopaminergic neurons from patients with Parkinson's disease. *Proceedings of the National Academy of Sciences* **2018**, *115* (21), 5576-5581. DOI: https://doi.org/10.1073/pnas.1717590115.

[368] Ravinther, AI; Dewadas, HD; Tong, SR; Foo, CN; Lin, Y-E; Chien, C-T; Lim, YM. Molecular Pathways Involved in LRRK2-Linked Parkinson's Disease: A Systematic Review. *International Journal of Molecular Sciences* **2022**, *23* (19), 11744. DOI: https://doi.org/10.3390/ijms231911744.

[369] Maekawa, T; Sasaoka, T; Azuma, S; Ichikawa, T; Melrose, HL; Farrer, MJ; Obata, F. Leucine-rich repeat kinase 2 (LRRK2) regulates α-synuclein clearance in microglia. *BMC Neuroscience* **2016**, *17* (1), 77. DOI: https://doi.org/10.1186/s12868-016-0315-2.

[370] Streubel-Gallasch, L; Giusti, V; Sandre, M; Tessari, I; Plotegher, N; Giusto, E; Masato, A; Iovino, L; Battisti, I; Arrigoni, G; et al. Parkinson's Disease–Associated LRRK2 Interferes with Astrocyte-

Mediated Alpha-Synuclein Clearance. *Molecular Neurobiology* **2021**, *58* (7), 3119-3140. DOI: https://doi.org/10.1007/s12035-021-02327-8.

[371] Russo, I; Kaganovich, A; Ding, J; Landeck, N; Mamais, A; Varanita, T; Biosa, A; Tessari, I; Bubacco, L; Greggio, E; et al. Transcriptome analysis of LRRK2 knock-out microglia cells reveals alterations of inflammatory- and oxidative stress-related pathways upon treatment with α-synuclein fibrils. *Neurobiology of Disease* **2019**, *129*, 67-78. DOI: https://doi.org/10.1016/j.nbd.2019.05.012.

[372] Verma, M; Callio, J; Otero, PA; Sekler, I; Wills, ZP; Chu, CT. Mitochondrial Calcium Dysregulation Contributes to Dendrite Degeneration Mediated by PD/LBD-Associated LRRK2 Mutants. *The Journal of Neuroscience* **2017**, *37* (46), 11151-11165. DOI: https://doi.org/10.1523/jneurosci.3791-16.2017.

[373] Kim, JW; Yin, X; Jhaldiyal, A; Khan, MR; Martin, I; Xie, Z; Perez-Rosello, T; Kumar, M; Abalde-Atristain, L; Xu, J; et al. Defects in mRNA Translation in LRRK2-Mutant hiPSC-Derived Dopaminergic Neurons Lead to Dysregulated Calcium Homeostasis. *Cell Stem Cell* **2020**, *27* (4), 633-645.e637. DOI: https://doi.org/10.1016/j.stem.2020.08.002.

[374] Liu, H; Ho, PW-L; Leung, C-T; Pang, SY-Y; Chang, EES; Choi, ZY-K; Kung, MH-W; Ramsden, DB; Ho, S-L. Aberrant mitochondrial morphology and function associated with impaired mitophagy and DNM1L-MAPK/ERK signaling are found in aged mutant Parkinsonian LRRK2R1441G mice. *Autophagy* **2021**, *17* (10), 3196-3220. DOI: https://doi.org/10.1080/15548627.2020.1850008.

[375] Bonello, F; Hassoun, S-M; Mouton-Liger, F; Shin, YS; Muscat, A; Tesson, C; Lesage, S; Beart, PM; Brice, A; Krupp, J; et al. LRRK2 impairs PINK1/Parkin-dependent mitophagy via its kinase activity: pathologic insights into Parkinson's disease. *Human Molecular Genetics* **2019**, *28* (10), 1645-1660. DOI: https://doi.org/10.1093/hmg/ddz004.

[376] Aufschnaiter, A; Kohler, V; Walter, C; Tosal-Castano, S; Habernig, L; Wolinski, H; Keller, W; Vögtle, F-N; Büttner, S. The Enzymatic Core of the Parkinson's Disease-Associated Protein LRRK2 Impairs Mitochondrial Biogenesis in Aging Yeast. *Frontiers in Molecular Neuroscience* **2018**, *11*, Original Research. DOI: https://doi.org/10.3389/fnmol.2018.00205.

[377] Bae, E-J; Kim, D-K; Kim, C; Mante, M; Adame, A; Rockenstein, E; Ulusoy, A; Klinkenberg, M; Jeong, GR; Bae, JR; et al. LRRK2 kinase regulates α-synuclein propagation via RAB35 phosphorylation. *Nature Communications* **2018**, *9* (1), 3465. DOI: https://doi.org/10.1038/s41467-018-05958-z.

[378] Connor-Robson, N; Booth, H; Martin, JG; Gao, B; Li, K; Doig, N; Vowles, J; Browne, C; Klinger, L; Juhasz, P; et al. An integrated transcriptomics and proteomics analysis reveals functional endocytic dysregulation caused by mutations in LRRK2. *Neurobiology of Disease* **2019**, *127*, 512-526. DOI: https://doi.org/10.1016/j.nbd.2019.04.005.

[379] Kuwahara, T; Funakawa, K; Komori, T; Sakurai, M; Yoshii, G; Eguchi, T; Fukuda, M; Iwatsubo, T. Roles of lysosomotropic agents on LRRK2 activation and Rab10 phosphorylation. *Neurobiology of Disease* **2020**, *145*, 105081. DOI: https://doi.org/10.1016/j.nbd.2020.105081.

[380] Boecker, CA; Goldsmith, J; Dou, D; Cajka, GG; Holzbaur, ELF. Increased LRRK2 kinase activity alters neuronal autophagy by disrupting the axonal transport of autophagosomes. *Current Biology* **2021**, *31* (10), 2140-2154.e2146. DOI: https://doi.org/10.1016/j.cub.2021.02.061.

[381] Covy, JP; Giasson, BI. Identification of compounds that inhibit the kinase activity of leucine-rich repeat kinase 2. *Biochemical and Biophysical Research Communications* **2009**, *378* (3), 473-477. DOI: https://doi.org/10.1016/j.bbrc.2008.11.048.

[382] Nichols, RJ; Dzamko, N; Hutti, Jessica E; Cantley, Lewis C; Deak, M; Moran, J; Bamborough, P; Reith, Alastair D; Alessi, Dario R. Substrate specificity and inhibitors of LRRK2, a protein kinase mutated in Parkinson's disease. *Biochemical Journal* **2009**, *424* (1), 47-60. DOI: https://doi.org/10.1042/bj20091035.

[383] Zhao, Y; Dzamko, N. Recent Developments in LRRK2-Targeted Therapy for Parkinson's Disease. *Drugs* **2019**, *79* (10), 1037-1051. DOI: https://doi.org/10.1007/s40265-019-01139-4.

[384] Domingos, S; Duarte, T; Saraiva, L; Guedes, RC; Moreira, R. Targeting Leucine-Rich Repeat Kinase 2 (LRRK2) for the Treatment of Parkinson's Disease. *Future Medicinal Chemistry* **2019**, *11* (15), 1953-1977. DOI: https://doi.org/10.4155/fmc-2018-0484.

[385] Deng, X; Dzamko, N; Prescott, A; Davies, P; Liu, Q; Yang, Q; Lee, J-D; Patricelli, MP; Nomanbhoy, TK; Alessi, DR; et al. Characterization of a selective inhibitor of the Parkinson's disease kinase LRRK2. *Nature Chemical Biology* **2011**, *7* (4), 203-205. DOI: https://doi.org/10.1038/nchembio.538.

[386] Luerman, GC; Nguyen, C; Samaroo, H; Loos, P; Xi, H; Hurtado-Lorenzo, A; Needle, E; Stephen Noell, G; Galatsis, P; Dunlop, J; et al. Phosphoproteomic evaluation of pharmacological inhibition of leucine-rich repeat kinase 2 reveals significant off-target effects of LRRK-2-IN-1. *Journal of Neurochemistry* **2014**, *128* (4), 561-576. DOI: https://doi.org/10.1111/jnc.12483.

[387] Ramsden, N; Perrin, J; Ren, Z; Lee, BD; Zinn, N; Dawson, VL; Tam, D; Bova, M; Lang, M; Drewes, G; et al. Chemoproteomics-Based Design of Potent LRRK2-Selective Lead Compounds That Attenuate

Parkinson's Disease-Related Toxicity in Human Neurons. *ACS Chemical Biology* **2011**, *6* (10), 1021-1028. DOI: https://doi.org/10.1021/cb2002413.

[388] Zhang, J; Deng, X; Choi, HG; Alessi, DR; Gray, NS. Characterization of TAE684 as a potent LRRK2 kinase inhibitor. *Bioorganic & Medicinal Chemistry Letters* **2012**, *22* (5), 1864-1869. DOI: https://doi.org/10.1016/j.bmcl.2012.01.084.

[389] Chen, H; Chan, BK; Drummond, J; Estrada, AA; Gunzner-Toste, J; Liu, X; Liu, Y; Moffat, J; Shore, D; Sweeney, ZK; et al. Discovery of Selective LRRK2 Inhibitors Guided by Computational Analysis and Molecular Modeling. *Journal of Medicinal Chemistry* **2012**, *55* (11), 5536-5545. DOI: https://doi.org/10.1021/jm300452p.

[390] Choi, HG; Zhang, J; Deng, X; Hatcher, JM; Patricelli, MP; Zhao, Z; Alessi, DR; Gray, NS. Brain Penetrant LRRK2 Inhibitor. *ACS Medicinal Chemistry Letters* **2012**, *3* (8), 658-662. DOI: https://doi.org/10.1021/ml300123a.

[391] Estrada, AA; Liu, X; Baker-Glenn, C; Beresford, A; Burdick, DJ; Chambers, M; Chan, BK; Chen, H; Ding, X; DiPasquale, AG; et al. Discovery of Highly Potent, Selective, and Brain-Penetrable Leucine-Rich Repeat Kinase 2 (LRRK2) Small Molecule Inhibitors. *Journal of Medicinal Chemistry* **2012**, *55* (22), 9416-9433. DOI: https://doi.org/10.1021/jm301020q.

[392] Chan, BK; Estrada, AA; Chen, H; Atherall, J; Baker-Glenn, C; Beresford, A; Burdick, DJ; Chambers, M; Dominguez, SL; Drummond, J; et al. Discovery of a Highly Selective, Brain-Penetrant Aminopyrazole LRRK2 Inhibitor. *ACS Medicinal Chemistry Letters* **2013**, *4* (1), 85-90. DOI: https://doi.org/10.1021/ml3003007.

[393] Estrada, AA; Chan, BK; Baker-Glenn, C; Beresford, A; Burdick, DJ; Chambers, M; Chen, H; Dominguez, SL; Dotson, J; Drummond, J; et al. Discovery of Highly Potent, Selective, and Brain-Penetrant Aminopyrazole Leucine-Rich Repeat Kinase 2 (LRRK2) Small Molecule Inhibitors. *Journal of Medicinal Chemistry* **2014**, *57* (3), 921-936. DOI: https://doi.org/10.1021/jm401654j.

[394] Ding, X; Stasi, LP; Dai, X; Long, K; Peng, C; Zhao, B; Wang, H; Sun, C; Hu, H; Wan, Z; et al. 5-Substituted-N-pyridazinylbenzamides as potent and selective LRRK2 inhibitors: Improved brain unbound fraction enables efficacy. *Bioorganic & Medicinal Chemistry Letters* **2019**, *29* (2), 212-215. DOI: https://doi.org/10.1016/j.bmcl.2018.11.054.

[395] Henderson, JL; Kormos, BL; Hayward, MM; Coffman, KJ; Jasti, J; Kurumbail, RG; Wager, TT; Verhoest, PR; Noell, GS; Chen, Y; et al. Discovery and Preclinical Profiling of 3-[4-(Morpholin-4-yl)-7H-pyrrolo[2,3-d]pyrimidin-5-yl]benzonitrile (PF-06447475), a Highly Potent, Selective, Brain Penetrant, and in Vivo Active LRRK2 Kinase Inhibitor. *Journal of Medicinal Chemistry* **2015**, *58* (1), 419-432. DOI: https://doi.org/10.1021/jm5014055.

[396] Liu, Z; Galemmo, RA; Fraser, KB; Moehle, MS; Sen, S; Volpicelli-Daley, LA; DeLucas, LJ; Ross, LJ; Valiyaveettil, J; Moukha-Chafiq, O; et al. Unique Functional and Structural Properties of the LRRK2 Protein ATP-binding Pocket*. *Journal of Biological Chemistry* **2014**, *289* (47), 32937-32951. DOI: https://doi.org/10.1074/jbc.M114.602318.

[397] Göring, S; Taymans, J-M; Baekelandt, V; Schmidt, B. Indolinone based LRRK2 kinase inhibitors with a key hydrogen bond. *Bioorganic & Medicinal Chemistry Letters* **2014**, *24* (19), 4630-4637. DOI: https://doi.org/10.1016/j.bmcl.2014.08.049.

[398] Garofalo, AW; Adler, M; Aubele, DL; Brigham, EF; Chian, D; Franzini, M; Goldbach, E; Kwong, GT; Motter, R; Probst, GD; et al. Discovery of 4-alkylamino-7-aryl-3-cyanoquinoline LRRK2 kinase inhibitors. *Bioorganic & Medicinal Chemistry Letters* **2013**, *23* (7), 1974-1977. DOI: https://doi.org/10.1016/j.bmcl.2013.02.041.

[399] Scott, JD; DeMong, DE; Greshock, TJ; Basu, K; Dai, X; Harris, J; Hruza, A; Li, SW; Lin, S-I; Liu, H; et al. Discovery of a 3-(4-Pyrimidinyl) Indazole (MLi-2), an Orally Available and Selective Leucine-Rich Repeat Kinase 2 (LRRK2) Inhibitor that Reduces Brain Kinase Activity. *Journal of Medicinal Chemistry* **2017**, *60* (7), 2983-2992. DOI: https://doi.org/10.1021/acs.jmedchem.7b00045.

[400] Keylor, MH; Gulati, A; Kattar, SD; Johnson, RE; Chau, RW; Margrey, KA; Ardolino, MJ; Zarate, C; Poremba, KE; Simov, V; et al. Structure-Guided Discovery of Aminoquinazolines as Brain-Penetrant and Selective LRRK2 Inhibitors. *Journal of Medicinal Chemistry* **2022**, *65* (1), 838-856. DOI: https://doi.org/10.1021/acs.jmedchem.1c01968.

[401] Cao, R; Chen, C; Wen, J; Zhao, W; Zhang, C; Sun, L; Yuan, L; Wu, C; Shan, L; Xi, M; et al. Recent advances in targeting leucine-rich repeat kinase 2 as a potential strategy for the treatment of Parkinson's disease. *Bioorganic Chemistry* **2023**, *141*, 106906. DOI: https://doi.org/10.1016/j.bioorg.2023.106906.

[402] Hu, J; Zhang, D; Tian, K; Ren, C; Li, H; Lin, C; Huang, X; Liu, J; Mao, W; Zhang, J. Small-molecule LRRK2 inhibitors for PD therapy: Current achievements and future perspectives. *European Journal of Medicinal Chemistry* **2023**, *256*, 115475. DOI: https://doi.org/10.1016/j.ejmech.2023.115475.

[403] Zhu, H; Hixson, P; Ma, W; Sun, J. Pharmacology of LRRK2 with type I and II kinase inhibitors revealed by cryo-EM. *Cell Discovery* **2024**, *10* (1), 10. DOI: https://doi.org/10.1038/s41421-023-00639-8.

[404] Li, T; Yang, D; Zhong, S; Thomas, JM; Xue, F; Liu, J; Kong, L; Voulalas, P; Hassan, HE; Park, J-S; et al. Novel LRRK2 GTP-binding inhibitors reduced degeneration in Parkinson's disease cell and mouse models. *Human Molecular Genetics* **2014**, *23* (23), 6212-6222. DOI: https://doi.org/10.1093/hmg/ddu341.

[405] Liu, X; Kalogeropulou, AF; Domingos, S; Makukhin, N; Nirujogi, RS; Singh, F; Shpiro, N; Saalfrank, A; Sammler, E; Ganley, IG; et al. Discovery of XL01126: A Potent, Fast, Cooperative, Selective, Orally Bioavailable, and Blood–Brain Barrier Penetrant PROTAC Degrader of Leucine-Rich Repeat Kinase 2. *Journal of the American Chemical Society* **2022**, *144* (37), 16930-16952. DOI: https://doi.org/10.1021/jacs.2c05499.

[406] Zhao, HT; John, N; Delic, V; Ikeda-Lee, K; Kim, A; Weihofen, A; Swayze, EE; Kordasiewicz, HB; West, AB; Volpicelli-Daley, LA. LRRK2 Antisense Oligonucleotides Ameliorate α-Synuclein Inclusion Formation in a Parkinson's Disease Mouse Model. *Molecular Therapy - Nucleic Acids* **2017**, *8*, 508-519. DOI: https://doi.org/10.1016/j.omtn.2017.08.002.

[407] A Phase 1b, Multicenter, Randomized, Placebo-Controlled, Double-Blind Study to Determine the Safety, Tolerability, Pharmacokinetics, and Pharmacodynamics of DNL201 in Subjects With Parkinson's Disease. https://clinicaltrials.gov/study/NCT03710707.

[408] A First-In-Human Study to Evaluate the Safety, Tolerability, Pharmacokinetics, and Pharmacodynamics of Single and Multiple Ascending Oral Doses of DNL201 in Healthy Subjects. https://clinicaltrials.gov/study/NCT04551534.

[409] A Phase 2b, Multicenter, Randomized, Double-Blind, Placebo-Controlled Study to Determine the Efficacy and Safety of BIIB122 in Participants With Parkinson's Disease. https://clinicaltrials.gov/study/NCT05348785.

[410] A Phase 2a, Multicenter, Randomized, Double-Blind, Placebo-Controlled Study to Evaluate the Safety and Pharmacodynamic Effects of BIIB122 in Participants With LRRK2-Associated Parkinson's Disease (LRRK2-PD). https://clinicaltrials.gov/study/NCT06602193.

[411] A Phase 3, Multicenter, Randomized, Double-Blind, Placebo-Controlled Study to Determine the Efficacy and Safety of BIIB122/DNL151 in Participants With Parkinson's Disease and Pathogenic LRRK2 Variants. https://clinicaltrials.gov/study/NCT05418673.

[412] A Phase 1, Single and Multiple Ascending Dose Study of NEU-723 Administered Orally to Evaluate Safety, Tolerability, Pharmacokinetics, and Pharmacodynamics in Healthy Subjects. https://clinicaltrials.gov/study/NCT05633745.

[413] A Phase 1 Single- and Multiple-Ascending-Dose Study to Assess the Safety, Tolerability, and Pharmacokinetics of BIIB094 Administered Intrathecally to Adults With Parkinson's Disease. https://clinicaltrials.gov/study/NCT03976349.

[414] Raga, MM; Sallares, J; Guerrero, M; Guglietta, A; Schwartz, J-C; Arrang, J-M; Lecomte, J-M; Ligneau, X; Schunack, W; Stark, H. Monohydrochloride salt of 1-[3-[3-(4-chlorophenyl) propoxy] propyl]-piperidine. Google Patents: 2006.

[415] Sander, K; von Coburg, Y; Camelin, J-C; Ligneau, X; Rau, O; Schubert-Zsilavecz, M; Schwartz, J-C; Stark, H. Acidic elements in histamine H3 receptor antagonists. *Bioorganic & Medicinal Chemistry Letters* **2010**, *20* (5), 1581-1584. DOI: https://doi.org/10.1016/j.bmcl.2010.01.089.

[416] Walter, M; Kottke, T; Weizel, L; Schwed, JS; Stark, H. Synthesis of 1,2,3-triazole elements in histamine H3 receptor ligands. *Synthesis* **2011**, (17), 2733-2736, Article. DOI: https://doi.org/10.1055/s-0030-1260103.

[417] Sadek, B; Schwed, JS; Subramanian, D; Weizel, L; Walter, M; Adem, A; Stark, H. Non-imidazole histamine H3 receptor ligands incorporating antiepileptic moieties. *European Journal of Medicinal Chemistry* **2014**, *77*, 269-279. DOI: https://doi.org/10.1016/j.ejmech.2014.03.014.

[418] Finkelstein, H. Darstellung organischer Jodide aus den entsprechenden Bromiden und Chloriden. *Berichte der deutschen chemischen Gesellschaft* **1910**, *43* (2), 1528-1532. DOI: https://doi.org/10.1002/cber.19100430257.

[419] Wang, Z. Finkelstein Reaction. In *Comprehensive Organic Name Reactions and Reagents*, Wang, Z Ed.; 2010; pp 1060-1063.

[420] Falkenstein, M; Reiner-Link, D; Zivkovic, A; Gering, I; Willbold, D; Stark, H. Histamine H3 receptor antagonists with peptidomimetic (keto)piperazine structures to inhibit Aβ oligomerisation. *Bioorganic & Medicinal Chemistry* **2021**, *50*, 116462. DOI: https://doi.org/10.1016/j.bmc.2021.116462.

[421] Zhu, S-J; Ying, H-Z; Wu, Y; Qiu, N; Liu, T; Yang, B; Dong, X-W; Hu, Y-Z. Design, synthesis and biological evaluation of novel podophyllotoxin derivatives bearing 4β-disulfide/trisulfide bond as cytotoxic agents. *RSC Advances* **2015**, *5* (125), 103172-103183. DOI: https://doi.org/10.1039/c5ra12837d.

[422] Williamson, A. Ueber die Theorie der Aetherbildung. *Justus Liebigs Annalen der Chemie* **1851**, *77* (1), 37-49. DOI: https://doi.org/10.1002/jlac.18510770104.

[423] Ouellette, RJ; Rawn, JD. 17 - Ethers and Epoxides. In *Organic Chemistry (Second Edition)*, Ouellette, RJ, Rawn, JD Eds.; Academic Press, 2018; pp 507-536.

[424] Song, Z; Huang, S; Yu, H; Jiang, Y; Wang, C; Meng, Q; Shu, X; Sun, H; Liu, K; Li, Y; et al. Synthesis and biological evaluation of morpholine-substituted diphenylpyrimidine derivatives (Mor-DPPYs) as potent EGFR T790M inhibitors with improved activity toward the gefitinib-resistant non-small cell lung cancers (NSCLC). *European Journal of Medicinal Chemistry* **2017**, *133*, 329-339. DOI: https://doi.org/10.1016/j.ejmech.2017.03.083.

[425] Ge, Y; Wang, C; Song, S; Huang, J; Liu, Z; Li, Y; Meng, Q; Zhang, J; Yao, J; Liu, K; et al. Identification of highly potent BTK and JAK3 dual inhibitors with improved activity for the treatment of B-cell lymphoma. *European Journal of Medicinal Chemistry* **2018**, *143*, 1847-1857. DOI: https://doi.org/10.1016/j.ejmech.2017.10.080.

[426] Bartkovitz, DJ; Chu, X-J; Ding, Q; Graves, BJ; Jiang, N; Zhang, J; Zhang, Z. SPIROINDOLINONE PYRROLIDINES. US2011/130398, **2011**.

[427] Hoang, V-H; Tran, P-T; Cui, M; Ngo, VTH; Ann, J; Park, J; Lee, J; Choi, K; Cho, H; Kim, H; et al. Discovery of Potent Human Glutaminyl Cyclase Inhibitors as Anti-Alzheimer's Agents Based on Rational Design. *Journal of Medicinal Chemistry* **2017**, *60* (6), 2573 - 2590. DOI: https://doi.org/10.1021/acs.jmedchem.7b00098.

[428] Buchanan, JL; Newcomb, JR; Carney, DP; Chaffee, SC; Chai, L; Cupples, R; Epstein, LF; Gallant, P; Gu, Y; Harmange, J-C; et al. Discovery of 2,4-bis-arylamino-1,3-pyrimidines as insulin-like growth factor-1 receptor (IGF-1R) inhibitors. *Bioorganic & Medicinal Chemistry Letters* **2011**, *21* (8), 2394-2399. DOI: https://doi.org/10.1016/j.bmcl.2011.02.075.

[429] Haber, F. Gradual electrolytic reduction of nitrobenzene with limited cathode potential. *Elektrochem. Angew. Phys. Chem* **1898**, *22*, 506-514.

[430] Blaser, H-U; Steiner, H; Studer, M. Selective Catalytic Hydrogenation of Functionalized Nitroarenes: An Update. *ChemCatChem* **2009**, *1* (2), 210-221. DOI: https://doi.org/10.1002/cctc.200900129.

[431] Leng, F; Gerber, IC; Lecante, P; Moldovan, S; Girleanu, M; Axet, MR; Serp, P. Controlled and Chemoselective Hydrogenation of Nitrobenzene over Ru@C60 Catalysts. *ACS Catalysis* **2016**, *6* (9), 6018-6024. DOI: https://doi.org/10.1021/acscatal.6b01429.

[432] Das, A; Mondal, S; Hansda, KM; Adak, MK; Dhak, D. A critical review on the role of carbon supports of metal catalysts for selective catalytic hydrogenation of chloronitrobenzenes. *Applied Catalysis A: General* **2023**, *649*, 118955. DOI: https://doi.org/10.1016/j.apcata.2022.118955.

[433] Campbell, CD; Stewart, MI. Reflections on the Teaching Practices for the Reduction of Nitroarenes: Updating Methodologies and Considerations of the Mechanism. *Journal of Chemical Education* **2023**, *100* (9), 3171-3178. DOI: https://doi.org/ 10.1021/acs.jchemed.3c00283.

[434] Pinner, A; Klein, F. Umwandlung der Nitrile in Imide. *Berichte der deutschen chemischen Gesellschaft* **1877**, *10* (2), 1889-1897. DOI: https://doi.org/10.1002/cber.187701002154.

[435] Vidal, M; García-Arriagada, M; Rezende, MC; Domínguez, M. Ultrasound-Promoted Synthesis of 4-Pyrimidinols and Their Tosyl Derivatives. *Synthesis* **2016**, *48* (23), 4246-4252. DOI: https://doi.org/10.1055/s-0035-1562788.

[436] Palanki, MSS; Erdman, PE; Gayo-Fung, LM; Shevlin, GI; Sullivan, RW; Goldman, ME; Ransone, LJ; Bennett, BL; Manning, AM; Suto, MJ. Inhibitors of NF-κB and AP-1 Gene Expression: SAR Studies on the Pyrimidine Portion of 2-Chloro-4-trifluoromethylpyrimidine-5-[N-(3‘,5‘-bis(trifluoromethyl)phenyl)carboxamide]. *Journal of Medicinal Chemistry* **2000**, *43* (21), 3995-4004. DOI: https://doi.org/10.1021/jm0001626.

[437] Jiao, Y; Ho, SL; Cho, CS. Copper-Powder-Catalyzed Synthesis of Pyrimidines from β-Bromo α,β-Unsaturated Ketones and Amidine Hydrochlorides. *Synlett* **2015**, *26* (08), 1081-1084. DOI: https://doi.org/10.1055/s-0034-1380410.

[438] Vadagaonkar, KS; Kalmode, HP; Prakash, S; Chaskar, AC. Greener [3+3] tandem annulation–oxidation approach towards the synthesis of substituted pyrimidines. *New Journal of Chemistry* **2015**, *39* (5), 3639-3645. DOI: https://doi.org/10.1039/C4NJ02345E.

[439] Guirado, A; Alarcón, E; Vicente, Y; Andreu, R. A new improved method for the synthesis of 2,4-diarylpyrimidines starting from 2,2,2-trichloroethylideneacetophenones. *Tetrahedron Letters* **2013**, *54* (37), 5115-5117. DOI: https://doi.org/10.1016/j.tetlet.2013.07.075.

[440] Guirado, A; Alarcón, E; Vicente, Y; Andreu, R; Bautista, D; Gálvez, J. A new convenient synthetic approach to diarylpyrimidines. *Tetrahedron* **2016**, *72* (27), 3922-3929. DOI: https://doi.org/10.1016/j.tet.2016.05.018.

[441] Gøgsig, TM; Nielsen, DU; Lindhardt, AT; Skrydstrup, T. Palladium Catalyzed Carbonylative Heck Reaction Affording Monoprotected 1,3-Ketoaldehydes. *Organic Letters* **2012**, *14* (10), 2536-2539. DOI: https://doi.org/10.1021/ol300837d.

[442] Ho, SL; Cho, CS. Microwave-Assisted Copper-Powder-Catalyzed Synthesis of Pyrimidinones from β-Bromo α,β-Unsaturated Carboxylic Acids and Amidines. *Synlett* **2013**, *24* (20), 2705-2708. DOI: https://doi.org/10.1055/s-0033-1340283.

[443] Theophil Eicher, SH, Andreas Speicher. Six-Membered Heterocycles: Sections 6. In *The Chemistry of Heterocycles*, 2012; pp 297-527.

[444] Yang, H; Huang, J; Luo, X. Preparation method of avanafil. CN108707141, **2018**.

[445] Sofia Botsi; Athanase Tsolomitis. ONE OR TWO STEP ACID MEDIATED CYCLOCONDENSATION PROCESS FOR THE PREPARATION OF 5-CARBETHOXY-2- THIOURACILS FROM DIETHYL ETHOXYMETHYLENEMALONATE AND THIOUREAS. *Heterocyclic Communications* **2007**, *13* (4), 229-234. DOI: https://doi.org/doi:10.1515/HC.2007.13.4.229.

[446] Rappoport, Z. Nucleophilic Vinylic Substitution. In *Advances in Physical Organic Chemistry*, Gold, V Ed.; Vol. 7; Academic Press, 1969; pp 1-114.

[447] Ilavsky, D; Krechl, J; Trska, P; Kuthan, J. ELECTRONIC-STRUCTURE AND PROPERTIES OF ALKOXYMETHYLENEMALONIC ACID-DERIVATIVES. *Collection of Czechoslovak Chemical Communications* **1979**, *44* (5), 1423-1433. DOI: https://doi.org/10.1135/cccc19791423.

[448] Bernasconi, CF; Rappoport, Z. Recent Advances in Our Mechanistic Understanding of SNV Reactions. *Accounts of Chemical Research* **2009**, *42* (8), 993-1003. DOI: https://doi.org/10.1021/ar900048q.

[449] Rappoport, Z; Topol, A. Nucleophilic attacks on carbon–carbon double bonds. Part XXII. Base catalysis, leaving group effects, and solvent effects in several nucleophilic vinylic substitutions by amines. *Journal of the Chemical Society, Perkin Transactions 2* **1975**, (8), 863-874. DOI: 10.1039/P29750000863.

[450] Wang, Z. Pinner Condensation. In *Comprehensive Organic Name Reactions and Reagents*, Wang, Z Ed.; 2010; pp 2233-2236.

[451] Wei, Y; Xu, X; Chu, H; He, L; Lei, F; Yan, J; He, Y; Wang, M; Su, G; Liu, B; et al. IMIDAZOLINONE DERIVATIVE AND USE THEREOF IN MEDICINE. EP4137491, **2023**.

[452] Nagy, MA; Hilgraf, R; Mortensen, DS; Elsner, J; Norris, S; Tikhe, J; Yoon, W; Paisner, D; Delgado, M; Erdman, P; et al. Discovery of the c-Jun N-Terminal Kinase Inhibitor CC-90001. *Journal of Medicinal Chemistry* **2021**, *64* (24), 18193-18208. DOI: https://doi.org/10.1021/acs.jmedchem.1c01716.

[453] Bernhart, C; McCort, G; Jegham, S; Herbert, JM; Casellas, P; Bouaboula, M; Duclos, O. Antineoplastic derivatives, preparation thereof and therapeutic use thereof. **2011**.

[454] Hao, Y; Lyu, J; Qu, R; Tong, Y; Sun, D; Feng, F; Tong, L; Yang, T; Zhao, Z; Zhu, L; et al. Design, Synthesis, and Biological Evaluation of Pyrimido[4,5-d]pyrimidine-2,4(1H,3H)-diones as Potent and Selective Epidermal Growth Factor Receptor (EGFR) Inhibitors against L858R/T790M Resistance Mutation. *Journal of Medicinal Chemistry* **2018**, *61* (13), 5609-5622. DOI: https://doi.org/10.1021/acs.jmedchem.8b00346.

[455] Pattabiraman, VR; Bode, JW. Rethinking amide bond synthesis. *Nature* **2011**, *480* (7378), 471-479. DOI: https://doi.org/10.1038/nature10702.

[456] Dunetz, JR; Magano, J; Weisenburger, GA. Large-Scale Applications of Amide Coupling Reagents for the Synthesis of Pharmaceuticals. *Organic Process Research & Development* **2016**, *20* (2), 140-177. DOI: https://doi.org/10.1021/op500305s.

[457] Valeur, E; Bradley, M. Amide bond formation: beyond the myth of coupling reagents. *Chem. Soc. Rev.* **2009**, *38* (2), 606-631. DOI: https://doi.org/10.1039/b701677h.

[458] Roughley, SD; Jordan, AM. The Medicinal Chemist's Toolbox: An Analysis of Reactions Used in the Pursuit of Drug Candidates. *Journal of Medicinal Chemistry* **2011**, *54* (10), 3451-3479. DOI: https://doi.org/10.1021/jm200187y.

[459] Shome, A; Jha, KT; Chawla, PA. Hexafluorophosphate Azabenzotriazole Tetramethyl Uronium (HATU): A Unique Cross-Coupling Reagent. *SynOpen* **2023**, *07* (04), 566-569. DOI: https://doi.org/10.1055/s-0042-1751499.

[460] Savall, BM; Chavez, F; Tays, K; Dunford, PJ; Cowden, JM; Hack, MD; Wolin, RL; Thurmond, RL; Edwards, JP. Discovery and SAR of 6-Alkyl-2,4-diaminopyrimidines as Histamine H4 Receptor Antagonists. *Journal of Medicinal Chemistry* **2014**, *57* (6), 2429-2439. DOI: https://doi.org/10.1021/jm401727m.

[461] Brenneman, JB; Krall, EB; Schlabach, M; Wylie, AA. Substituted pyrazolopyrimidines and substituted purines and their use as ubiquitin-specific-processing protease 1 (USP1) inhibitors. **2022**.

[462] Petrocchi, A; Leo, E; Reyna, NJ; Hamilton, MM; Shi, X; Parker, CA; Mseeh, F; Bardenhagen, JP; Leonard, P; Cross, JB; et al. Identification of potent and selective MTH1 inhibitors. *Bioorganic & Medicinal Chemistry Letters* **2016**, *26* (6), 1503-1507. DOI: https://doi.org/10.1016/j.bmcl.2016.02.026.

[463] Chen, X; Xu, W; Wang, K; Mo, M; Zhang, W; Du, L; Yuan, X; Xu, Y; Wang, Y; Shen, J. Discovery of a Novel Series of Imidazo[1,2-a]pyrimidine Derivatives as Potent and Orally Bioavailable Lipoprotein-Associated Phospholipase A2 Inhibitors. *Journal of Medicinal Chemistry* **2015**, *58* (21), 8529-8541. DOI: https://doi.org/10.1021/acs.jmedchem.5b01024.

[464] Brough, PA; Barril, X; Borgognoni, J; Chene, P; Davies, NGM; Davis, B; Drysdale, MJ; Dymock, B; Eccles, SA; Garcia-Echeverria, C; et al. Combining Hit Identification Strategies: Fragment-Based and in Silico Approaches to Orally Active 2-Aminothieno[2,3-d]pyrimidine Inhibitors of the Hsp90 Molecular Chaperone. *Journal of Medicinal Chemistry* **2009**, *52* (15), 4794-4809. DOI: https://doi.org/10.1021/jm900357y.

[465] Suda, A; Koyano, H; Hayase, T; Hada, K; Kawasaki, K-i; Komiyama, S; Hasegawa, K; Fukami, TA; Sato, S; Miura, T; et al. Design and synthesis of novel macrocyclic 2-amino-6-arylpyrimidine Hsp90 inhibitors. *Bioorganic & Medicinal Chemistry Letters* **2012**, *22* (2), 1136-1141. DOI: https://doi.org/10.1016/j.bmcl.2011.11.100.

[466] Palucki, M. Pyrimidines. In *Palladium in Heterocyclic Chemistry: A Guide for the Synthetic Chemist*, Li, JJ, Gribble, GW Eds.; Vol. 26; Elsevier, 2007; pp 475-509.

[467] Abdou, IM. Regioselective synthesis of new pyrimidine derivatives using organolithium reagents. *Journal of Chemical Research* **2006**, *2006* (12), 785-787. DOI: https://doi.org/10.3184/030823406780199686.

[468] Lee, M; Rucil, T; Hesek, D; Oliver, AG; Fisher, JF; Mobashery, S. Regioselective Control of the SNAr Amination of 5-Substituted-2,4-Dichloropyrimidines Using Tertiary Amine Nucleophiles. *The Journal of Organic Chemistry* **2015**, *80* (15), 7757-7763. DOI: https://doi.org/10.1021/acs.joc.5b01044.

[469] Averin, AD; Ulanovskaya, OA; Beletskaya, IP. Amination of 2-chloro-and 2,4-dichloropyrimidines by polyamines. *Chemistry of Heterocyclic Compounds* **2008**, *44* (9), 1146-1157. DOI: https://doi.org/10.1007/s10593-008-0165-7.

[470] Bruening, F; Lovelle, LE. Highly Regioselective Organocatalytic SNAr Amination of 2,4-Dichloropyrimidine and Related Heteroaryl Chlorides. *European Journal of Organic Chemistry* **2017**, *2017* (22), 3222-3228. DOI: https://doi.org/10.1002/ejoc.201700459.

[471] Richter, DT; Kath, JC; Luzzio, MJ; Keene, N; Berliner, MA; Wessel, MD. Selective addition of amines to 5-trifluoromethyl-2,4-dichloropyrimidine induced by Lewis acids. *Tetrahedron Letters* **2013**, *54* (35), 4610-4612. DOI: https://doi.org/10.1016/j.tetlet.2013.06.025.

[472] Montebugnoli, D; Bravo, P; Corradi, E; Dettori, G; Mioskowski, C; Volonterio, A; Wagner, A; Zanda, M. Regioselective 4-amino-de-chlorination of trichloro- and dichloro-pyrimidines with N-sodium carbamates. *Tetrahedron* **2002**, *58* (11), 2147-2153. DOI: https://doi.org/10.1016/S0040-4020(02)00084-4.

[473] Kuethe, JT; Journet, M; Peng, Z; Zhao, D; McKeown, A; Humphrey, GR. Development of a Multikilogram Scale Synthesis of a TRPV1 Antagonist. *Organic Process Research & Development* **2016**, *20* (2), 227-232. DOI: https://doi.org/10.1021/acs.oprd.5b00388.

[474] Luo, G; Chen, L; Poindexter, GS. Microwave-assisted synthesis of aminopyrimidines. *Tetrahedron Letters* **2002**, *43* (33), 5739-5742. DOI: https://doi.org/10.1016/S0040-4039(02)01190-5.

[475] Ceide, SC; Montalban, AG. Microwave-assisted, efficient and regioselective Pd-catalyzed C-phenylation of halopyrimidines. *Tetrahedron Letters* **2006**, *47* (26), 4415-4418. DOI: https://doi.org/10.1016/j.tetlet.2006.04.082.

[476] Campestre, C; Keglevich, G; Kóti, J; Scotti, L; Gasbarri, C; Angelini, G. Microwave-assisted simple synthesis of 2-anilinopyrimidines by the reaction of 2-chloro-4,6-dimethylpyrimidine with aniline derivatives. *RSC Advances* **2020**, *10* (21), 12249-12254. DOI: https://doi.org/10.1039/D0RA00833H.

[477] Hotra, A; Ragunathan, P; Ng, PS; Seankongsuk, P; Harikishore, A; Sarathy, JP; Saw, W-G; Lakshmanan, U; Sae-Lao, P; Kalia, NP; et al. Discovery of a Novel Mycobacterial F-ATP Synthase Inhibitor and its Potency in Combination with Diarylquinolines. *Angewandte Chemie International Edition* **2020**, *59* (32), 13295-13304. DOI: https://doi.org/10.1002/anie.202002546.

[478] Odell, LR; Abdel-Hamid, MK; Hill, TA; Chau, N; Young, KA; Deane, FM; Sakoff, JA; Andersson, S; Daniel, JA; Robinson, PJ; et al. Pyrimidine-Based Inhibitors of Dynamin I GTPase Activity: Competitive Inhibition at the Pleckstrin Homology Domain. *Journal of Medicinal Chemistry* **2017**, *60* (1), 349-361. DOI: https://doi.org/10.1021/acs.jmedchem.6b01422.

[479] Carbain, B; Coxon, CR; Lebraud, H; Elliott, KJ; Matheson, CJ; Meschini, E; Roberts, AR; Turner, DM; Wong, C; Cano, C; et al. Trifluoroacetic Acid in 2,2,2-Trifluoroethanol Facilitates SNAr Reactions of Heterocycles with Arylamines. *Chemistry – A European Journal* **2014**, *20* (8), 2311-2317. DOI: https://doi.org/10.1002/chem.201304336.

[480] Liu, J; Robins, MJ. SNAr Displacements with 6-(Fluoro, Chloro, Bromo, Iodo, and Alkylsulfonyl)purine Nucleosides: Synthesis, Kinetics, and Mechanism1. *Journal of the American Chemical Society* **2007**, *129* (18), 5962-5968. DOI: https://doi.org/10.1021/ja070021u.

[481] Liu, P; Yang, Y; Tang, Y; Yang, T; Sang, Z; Liu, Z; Zhang, T; Luo, Y. Design and synthesis of novel pyrimidine derivatives as potent antitubercular agents. *European Journal of Medicinal Chemistry* **2019**, *163*, 169-182. DOI: https://doi.org/10.1016/j.ejmech.2018.11.054.

[482] Qian, H; Ding, Y; Deng, X; Huang, W; Li, Z; Liu, F; Zhang, J; Wang, L; Liu, J; Yuan, Y; et al. Synthesis-accessibility-oriented design of c-Jun N-terminal kinase 1 inhibitor. *European Journal of Medicinal Chemistry* **2023**, *256*, 115442. DOI: https://doi.org/10.1016/j.ejmech.2023.115442.

[483] Ciszewski, L; Waykole, L; Prashad, M; Repić, O. A Practical Synthesis of 2-Arylamino-6-alkylaminopurines from 2,6-Dichloropurine. *Organic Process Research & Development* **2006**, *10* (4), 799-802. DOI: https://doi.org/10.1021/op060053m.

[484] Kagawa, T; Shigehiro, D; Kawada, K. Trifluoroethoxy group as a leaving group for regioselective sequential substitution reactions of 5-trifluoromethylpyrimidine derivative with heteroatom nucleophiles. *Journal of Fluorine Chemistry* **2015**, *179*, 150-158. DOI: https://doi.org/10.1016/j.jfluchem.2015.07.016.

[485] Konstantinidou, M; Oun, A; Pathak, P; Zhang, B; Wang, Z; ter Brake, F; Dolga, AM; Kortholt, A; Dömling, A. The tale of proteolysis targeting chimeras (PROTACs) for Leucine-Rich Repeat Kinase 2 (LRRK2). *ChemMedChem* **2021**, *16* (6), 959-965. DOI: https://doi.org/10.1002/cmdc.202000872.

[486] Walker, DP; Christopher Bi, F; Kalgutkar, AS; Bauman, JN; Zhao, SX; Soglia, JR; Aspnes, GE; Kung, DW; Klug-McLeod, J; Zawistoski, MP; et al. Trifluoromethylpyrimidine-based inhibitors of proline-rich tyrosine kinase 2 (PYK2): Structure–activity relationships and strategies for the elimination of reactive metabolite formation. *Bioorganic & Medicinal Chemistry Letters* **2008**, *18* (23), 6071-6077. DOI: https://doi.org/10.1016/j.bmcl.2008.10.030.

[487] Curtin, ML; Robin Heyman, H; Frey, RR; Marcotte, PA; Glaser, KB; Jankowski, JR; Magoc, TJ; Albert, DH; Olson, AM; Reuter, DR; et al. Pyrazole diaminopyrimidines as dual inhibitors of KDR and Aurora B kinases. *Bioorganic & Medicinal Chemistry Letters* **2012**, *22* (14), 4750-4755. DOI: https://doi.org/10.1016/j.bmcl.2012.05.067.

[488] Faust, A. Ueber das Verhalten des Monochlorphenols von 218° Siedepunkt in der Kalischmelze. *Berichte der deutschen chemischen Gesellschaft* **1873**, *6* (2), 1022-1023. DOI: https://doi.org/10.1002/cber.18730060246.

[489] Fittig, R; Mager, E. Beiträge zur Entscheidung der Stellungsfrage in der aromatischen Gruppe. *Berichte der deutschen chemischen Gesellschaft* **1874**, *7* (2), 1175-1180. DOI: https://doi.org/10.1002/cber.18740070277.

[490] Terrier, F. The SNAr Reactions: Mechanistic Aspects. In *Modern Nucleophilic Aromatic Substitution*, 2013; pp 1-94.

[491] Bunnett, JF; Zahler, RE. Aromatic Nucleophilic Substitution Reactions. *Chemical Reviews* **1951**, *49* (2), 273-412. DOI: https://doi.org/10.1021/cr60153a002.

[492] Meisenheimer, J. Ueber Reactionen aromatischer Nitrokörper. *Justus Liebigs Annalen der Chemie* **1902**, *323* (2), 205-246. DOI: https://doi.org/10.1002/jlac.19023230205.

[493] Błaziak, K; Danikiewicz, W; Mąkosza, M. How Does Nucleophilic Aromatic Substitution Really Proceed in Nitroarenes? Computational Prediction and Experimental Verification. *Journal of the American Chemical Society* **2016**, *138* (23), 7276-7281. DOI: https://doi.org/10.1021/jacs.5b13365.

[494] Rohrbach, S; Smith, AJ; Pang, JH; Poole, DL; Tuttle, T; Chiba, S; Murphy, JA. Concerted Nucleophilic Aromatic Substitution Reactions. *Angewandte Chemie International Edition* **2019**, *58* (46), 16368-16388. DOI: https://doi.org/10.1002/anie.201902216.

[495] Neumann, CN; Hooker, JM; Ritter, T. Concerted nucleophilic aromatic substitution with 19F− and 18F−. *Nature* **2016**, *534* (7607), 369-373. DOI: https://doi.org/10.1038/nature17667.

[496] Neumann, CN; Ritter, T. Facile C–F Bond Formation through a Concerted Nucleophilic Aromatic Substitution Mediated by the PhenoFluor Reagent. *Accounts of Chemical Research* **2017**, *50* (11), 2822-2833. DOI: https://doi.org/10.1021/acs.accounts.7b00413.

[497] Hunter, A; Renfrew, M; Taylor, JA; Whitmore, JMJ; Williams, A. A single transition state in nucleophilic aromatic substitution: reaction of phenolate ions with 2-(4-nitrophenoxy)-4,6-dimethoxy-1,3,5-triazine in aqueous solution. *Journal of the Chemical Society, Perkin Transactions 2* **1993**, (10), 1703-1704. DOI: https://doi.org/10.1039/P29930001703.

[498] Hunter, A; Renfrew, M; Rettura, D; Taylor, JA; Whitmore, JMJ; Williams, A. Stepwise versus Concerted Mechanisms at Trigonal Carbon: Transfer of the 1,3,5-Triazinyl Group between Aryl Oxide Ions in Aqueous Solution. *Journal of the American Chemical Society* **1995**, *117* (20), 5484-5491. DOI: https://doi.org/10.1021/ja00125a008.

[499] Shakes, J; Raymond, C; Rettura, D; Williams, A. Concerted displacement mechanisms at trigonal carbon: the aminolysis of 4-aryloxy-2,6-dimethoxy-1,3,5-triazines. *Journal of the Chemical Society, Perkin Transactions 2* **1996**, (8), 1553-1557. DOI: https://doi.org/10.1039/P29960001553.

[500] Glukhovtsev, MN; Bach, RD; Laiter, S. Single-Step and Multistep Mechanisms of Aromatic Nucleophilic Substitution of Halobenzenes and Halonitrobenzenes with Halide Anions: Ab Initio Computational Study. *The Journal of Organic Chemistry* **1997**, *62* (12), 4036-4046. DOI: https://doi.org/10.1021/jo962096e.

[501] Fernández, I; Frenking, G; Uggerud, E. Rate-Determining Factors in Nucleophilic Aromatic Substitution Reactions. *The Journal of Organic Chemistry* **2010**, *75* (9), 2971-2980. DOI: https://doi.org/10.1021/jo100195w.

[502] Kwan, EE; Zeng, Y; Besser, HA; Jacobsen, EN. Concerted nucleophilic aromatic substitutions. *Nature Chemistry* **2018**, *10* (9), 917-923. DOI: https://doi.org/10.1038/s41557-018-0079-7.

[503] de la Hoz, A; Díaz-Ortiz, Á; Moreno, A. Microwaves in organic synthesis. Thermal and non-thermal microwave effects. *Chemical Society Reviews* **2005**, *34* (2), 164-178. DOI: https://doi.org/10.1039/B411438H.

[504] Kappe, CO. Controlled Microwave Heating in Modern Organic Synthesis. *Angewandte Chemie International Edition* **2004**, *43* (46), 6250-6284. DOI: https://doi.org/10.1002/anie.200400655.

[505] Lidström, P; Tierney, J; Wathey, B; Westman, J. Microwave assisted organic synthesis—a review. *Tetrahedron* **2001**, *57* (45), 9225-9283. DOI: https://doi.org/10.1016/S0040-4020(01)00906-1.

[506] Larhed, M; Hallberg, A. Microwave-assisted high-speed chemistry: a new technique in drug discovery. *Drug Discovery Today* **2001**, *6* (8), 406-416. DOI: https://doi.org/10.1016/S1359-6446(01)01735-4.

[507] Caddick, S; Fitzmaurice, R. Microwave enhanced synthesis. *Tetrahedron* **2009**, *65* (17), 3325-3355. DOI: https://doi.org/10.1016/j.tet.2009.01.105.

[508] Rask-Andersen, M; Almén, MS; Schiöth, HB. Trends in the exploitation of novel drug targets. *Nature Reviews Drug Discovery* **2011**, *10* (8), 579-590. DOI: https://doi.org/10.1038/nrd3478.

[509] Santos, R; Ursu, O; Gaulton, A; Bento, AP; Donadi, RS; Bologa, CG; Karlsson, A; Al-Lazikani, B; Hersey, A; Oprea, TI; et al. A comprehensive map of molecular drug targets. *Nature Reviews Drug Discovery* **2017**, *16* (1), 19-34. DOI: https://doi.org/10.1038/nrd.2016.230.

[510] de Jong, LAA; Uges, DRA; Franke, JP; Bischoff, R. Receptor–ligand binding assays: Technologies and Applications. *Journal of Chromatography B* **2005**, *829* (1), 1-25. DOI: https://doi.org/10.1016/j.jchromb.2005.10.002.

[511] Flanagan, CA. Chapter 10 - GPCR-radioligand binding assays. In *Methods in Cell Biology*, K. Shukla, A Ed.; Vol. 132; Academic Press, 2016; pp 191-215.

[512] McKinney, M; Raddatz, R. Practical Aspects of Radioligand Binding. *Current Protocols in Pharmacology* **2006**, *33* (1), 1.3.1-1.3.42. DOI: https://doi.org/10.1002/0471141755.ph0103s33.

[513] Hulme, EC; Trevethick, MA. Ligand binding assays at equilibrium: validation and interpretation. *British Journal of Pharmacology* **2010**, *161* (6), 1219-1237. DOI: https://doi.org/10.1111/j.1476-5381.2009.00604.x.

[514] Mendel, CM; Mendel, DB. 'Non-specific' binding. The problem, and a solution. *Biochemical Journal* **1985**, *228* (1), 269-272. DOI: https://doi.org/10.1042/bj2280269.

[515] Yung-Chi, C; Prusoff, WH. Relationship between the inhibition constant (K_I) and the concentration of inhibitor which causes 50 per cent inhibition (I_{50}) of an enzymatic reaction. *Biochemical Pharmacology* **1973**, *22* (23), 3099-3108. DOI: https://doi.org/10.1016/0006-2952(73)90196-2.

[516] Kottke, T; Sander, K; Weizel, L; Schneider, EH; Seifert, R; Stark, H. Receptor-specific functional efficacies of alkyl imidazoles as dual histamine H3/H4 receptor ligands. *European Journal of Pharmacology* **2011**, *654* (3), 200-208. DOI: https://doi.org/10.1016/j.ejphar.2010.12.033.

[517] Copeland, RA. Why Enzymes as Drug Targets? In *Evaluation of Enzyme Inhibitors in Drug Discovery*, Copeland, RA Ed.; 2013; pp 1-23.

[518] Bisswanger, H. Enzyme assays. *Perspectives in Science* **2014**, *1* (1), 41-55. DOI: https://doi.org/10.1016/j.pisc.2014.02.005.

[519] Smirnovienė, J; Baranauskienė, L; Zubrienė, A; Matulis, D. A standard operating procedure for an enzymatic activity inhibition assay. *European Biophysics Journal* **2021**, *50* (3), 345-352. DOI: https://doi.org/10.1007/s00249-021-01530-8.

[520] Likhtenshtein, GI. Methods of Analysis in Enzyme Processes. In *Enzyme Catalysis Today and the Chemistry of the 21st Century*, Likhtenshtein, GI Ed.; Springer Nature Switzerland, 2025; pp 43-97.

[521] Ramsay, RR; Tipton, KF. Assessment of Enzyme Inhibition: A Review with Examples from the Development of Monoamine Oxidase and Cholinesterase Inhibitory Drugs. *Molecules* **2017**, *22* (7), 1192.

[522] Beaudet, L; Rodriguez-Suarez, R; Venne, M-H; Caron, M; Bédard, J; Brechler, V; Parent, S; Bielefeld-Sévigny, M. AlphaLISA immunoassays: the no-wash alternative to ELISAs for research and drug discovery. *Nature Methods* **2008**, *5* (12), an8-an9. DOI: https://doi.org/10.1038/nmeth.f.230.

[523] Li, Y; Xie, W; Fang, G. Fluorescence detection techniques for protein kinase assay. *Analytical and Bioanalytical Chemistry* **2008**, *390* (8), 2049-2057. DOI: https://doi.org/10.1007/s00216-008-1986-z.

[524] Algar, WR; Hildebrandt, N; Vogel, SS; Medintz, IL. FRET as a biomolecular research tool — understanding its potential while avoiding pitfalls. *Nature Methods* **2019**, *16* (9), 815-829. DOI: https://doi.org/10.1038/s41592-019-0530-8.

[525] Ramírez, D; Caballero, J. Is It Reliable to Take the Molecular Docking Top Scoring Position as the Best Solution without Considering Available Structural Data? *Molecules* **2018**, *23* (5), 1038. DOI: https://doi.org/10.3390/molecules23051038.
[526] Weng, J-H; Ma, W; Wu, J; Sharma, PK; Silletti, S; McCammon, JA; Taylor, S. Capturing Differences in the Regulation of LRRK2 Dynamics and Conformational States by Small Molecule Kinase Inhibitors. *ACS Chemical Biology* **2023**, *18* (4), 810-821. DOI: https://doi.org/10.1021/acschembio.2c00868.
[527] Duffus, JH; Nordberg, M; Templeton, DM. Glossary of terms used in toxicology, 2nd edition (IUPAC Recommendations 2007). *Pure and Applied Chemistry* **2007**, *79* (7), 1153-1344. DOI: https://doi.org/10.1351/pac200779071153.
[528] Soares, JX; Santos, Á; Fernandes, C; Pinto, MMM. Liquid Chromatography on the Different Methods for the Determination of Lipophilicity: An Essential Analytical Tool in Medicinal Chemistry. *Chemosensors* **2022**, *10* (8), 340. DOI: https://doi.org/10.3390/chemosensors10080340.
[529] Arnott, JA; Planey, SL. The influence of lipophilicity in drug discovery and design. *Expert Opinion on Drug Discovery* **2012**, *7* (10), 863-875. DOI: https://doi.org/10.1517/17460441.2012.714363.
[530] Leeson, PD; Springthorpe, B. The influence of drug-like concepts on decision-making in medicinal chemistry. *Nature Reviews Drug Discovery* **2007**, *6* (11), 881-890. DOI: https://doi.org/10.1038/nrd2445.
[531] Coutinho, AL; Cristofoletti, R; Wu, F; Shoyaib, AA; Dressman, J; Polli, JE. A robust, viable, and resource sparing HPLC-based logP method applied to common drugs. *International Journal of Pharmaceutics* **2023**, *644*, 123325. DOI: https://doi.org/10.1016/j.ijpharm.2023.123325.
[532] OECD. *Test No. 107: Partition Coefficient (n-octanol/water): Shake Flask Method*; OECD Publishing, 1995. DOI: https://doi.org/10.1787/9789264069626-en.
[533] Pallicer, JM; Calvet, C; Port, A; Rosés, M; Ràfols, C; Bosch, E. Extension of the liquid chromatography/quantitative structure–property relationship method to assess the lipophilicity of neutral, acidic, basic and amphotheric drugs. *Journal of Chromatography A* **2012**, *1240*, 113-122. DOI: https://doi.org/10.1016/j.chroma.2012.03.089.
[534] OECD. *Test No. 117: Partition Coefficient (n-octanol/water), HPLC Method*; OECD Publishing, 2022. DOI: doi:https://doi.org/10.1787/9789264069824-en.
[535] Pallicer, JM; Sales, J; Rosés, M; Ràfols, C; Bosch, E. Lipophilicity assessment of basic drugs (logPo/w determination) by a chromatographic method. *Journal of Chromatography A* **2011**, *1218* (37), 6356-6368. DOI: https://doi.org/10.1016/j.chroma.2011.07.002.
[536] Rankovic, Z. CNS Drug Design: Balancing Physicochemical Properties for Optimal Brain Exposure. *Journal of Medicinal Chemistry* **2015**, *58* (6), 2584-2608. DOI: https://doi.org/10.1021/jm501535r.
[537] van de Waterbeemd, H; Camenisch, G; Folkers, G; Chretien, JR; Raevsky, OA. Estimation of Blood-Brain Barrier Crossing of Drugs Using Molecular Size and Shape, and H-Bonding Descriptors. *Journal of Drug Targeting* **1998**, *6* (2), 151-165. DOI: https://doi.org/10.3109/10611869808997889.
[538] Daina, A; Michielin, O; Zoete, V. SwissADME: a free web tool to evaluate pharmacokinetics, drug-likeness and medicinal chemistry friendliness of small molecules. *Scientific Reports* **2017**, *7* (1), 42717. DOI: https://doi.org/10.1038/srep42717.
[539] *SwissADME*. http://www.swissadme.ch/index.php# (accessed 2025 May).
[540] Mannhold, R; Poda, GI; Ostermann, C; Tetko, IV. Calculation of Molecular Lipophilicity: State-of-the-Art and Comparison of LogP Methods on more than 96,000 Compounds. *Journal of Pharmaceutical Sciences* **2009**, *98* (3), 861-893. DOI: https://doi.org/10.1002/jps.21494.
[541] *ChemDraw v23.1.1*; Revvity Signals Software, Inc.: Waltham, MA, USA, 2024.
[542] *MarvinSketch 24.1.3*; ChemAxon Ltd.: Budapest, Hungary, 2024.
[543] *MestReNova 14.1.2-25024*; Mestrelab Research: Santiago de Compostela, Spain, 2020.
[544] *GraphPad Prism 7.02*; GraphPad Software, Inc.: Boston, MA, USA, 2016.
[545] *ChatGPT*. https://chatgpt.com/ (accessed 2025).
[546] *Cody*. https://sourcegraph.com/cody/chat (accessed 2025).
[547] Song, H; Lee, YS; Roh, EJ; Seo, JH; Oh, K-S; Lee, BH; Han, H; Shin, KJ. Discovery of potent and selective rhodanine type IKKβ inhibitors by hit-to-lead strategy. *Bioorganic & Medicinal Chemistry Letters* **2012**, *22* (17), 5668-5674. DOI: https://doi.org/10.1016/j.bmcl.2012.06.088.
[548] Werner, T; Añazco, T; Osses-Mendoza, P; Castro-Álvarez, A; Salas, CO; Bridi, R; Stark, H; Espinosa-Bustos, C. First Report on Cationic Triphenylphosphonium Compounds as Mitochondriotropic H3R Ligands with Antioxidant Properties. *Antioxidants* **2024**, *13* (11), 1345. DOI: https://doi.org/10.3390/antiox13111345.
[549] Jones, G; Willett, P; Glen, RC; Leach, AR; Taylor, R. Development and validation of a genetic algorithm for flexible docking. *Journal of Molecular Biology* **1997**, *267* (3), 727-748. DOI: https://doi.org/10.1006/jmbi.1996.0897.

[550] Jurrus, E; Engel, D; Star, K; Monson, K; Brandi, J; Felberg, LE; Brookes, DH; Wilson, L; Chen, J; Liles, K; et al. Improvements to the APBS biomolecular solvation software suite. *Protein Science* **2018**, *27* (1), 112-128. DOI: https://doi.org/10.1002/pro.3280.
[551] Baroni, M; Cruciani, G; Sciabola, S; Perruccio, F; Mason, JS. A Common Reference Framework for Analyzing/Comparing Proteins and Ligands. Fingerprints for Ligands And Proteins (FLAP): Theory and Application. *Journal of Chemical Information and Modeling* **2007**, *47* (2), 279-294. DOI: https://doi.org/10.1021/ci600253e.
[552] *Discovery Studio Visualizer v21.1.0.20298*; Dassault Systèmes Biovia Corp.
[553] *PyMOL Molecular Graphics System*; Version 3.0 Schrödinger, LLC.
[554] *ChemDraw*. https://chemdraw-ultra.software.informer.com/7.0 (accessed 2024 November).
[555] *MarvinSketch*. https://marvinsketch.software.informer.com/6.1/ (accessed 2024 November).
[556] *Gaussian 03 Rev. C.02*; Wallingford, CT, 2004.

8 Supplementary Data

Table S1. Experimental activities and docking score values of synthesized (**24**-**39**) and reference (**L41** and **L66**) compounds.

	H$_3$R			G9a			
	Gold Score	**H$_3$R K_i [nM] [95% CI]**	**Interactions[a]**	**Gold Score**	**Inhibition [%] ± SD at 10 µM**	**IC$_{50}$ [nM] [95% CI]**	**Interactions[b]**
24	86.6428	117 [42.8 – 729]	1-4	72.8441	33.4 ± 18.5	/	2-1
25	84.0869	32.4 [11.4 – 92.1]	1-3; 1-4	71.6834	15.1 ± 12.2	/	2-1
26	85.1639	68.4 [44.7 – 105]	1-3; 1-4; 1-5	77.1961	60.1 ± 14.7	/	2-1; 2-3
27	82.9205	128 [61.1 – 272]	1-3; 1-4; 1-5	82.2618	102.3 ± 2.1	/	2-2; 2-3
28	91.7351	244 [110 – 538]	1-4; 1-5	81.6797	52.3 ± 4.6	/	2-1; 2-2
29	91.0553	25.0 [8.27 – 75.7]	1-3; 1-4; 1-5	71.7428	21.0 ± 3.3	/	2-1; 2-2; 2-3
30	80.8695	45.5 [13.6 – 151]	1-3; 1-4; 1-5	75.1751	70.4 ± 21.8	/	2-2
31	83.7709	25.2 [9.67 – 65.6]	1-1; 1-3; 1-4; 1-5	84.8478	108.4 ± 0.5	63.9 [27.0 – 151]	2-2; 2-3
32	93.1081	102 [49.9 – 209]	1-4	81.3374	40.2 ± 4.3	/	2-1; 2-2; 2-3
33	90.045	1.40 [0.23 – 8.37]	1-3; 1-4	71.219	45.9 ± 1.5	17765 [7159 – 43860]	2-1; 2-2
34	85.109	32.9 [15.4 – 70.2]	1-3; 1-4; 1-5	73.2977	92.2 ± 0.7	4298 [1276 – 14481]	2-1; 2-3
35	52.3931	82.5 [30.8 – 221]	1-3; 1-4; 1-5	81.4385	103.7 ± 1.1	494 [269 – 906]	2-2; 2-3
36	93.8079	20.9 [11.3 – 38.8]	1-4; 1-5	78.1088	25.2 ± 1.6	/	2-1; 2-2; 2-3
37	87.0864	18.0 [11.2 – 29.0]	1-3; 1-4; 1-5	72.9594	51.7 ± 1.3	/	2-2; 2-3
38	79.8414	65.3 [26.7 – 160]	1-3; 1-4	76.3941	70.0 ± 0.7	/	2-2
39	78.4993	138 [50.3 – 337]	1-3; 1-4; 1-5	77.5181	103.0 ± 2.6	/	2-2; 2-3
L41	82.4323	1.7- 37.15 nM in 7 assays (pdb: 7f61)	/	/	/	/	2-1; 2-2; 2-3
L66	/	/	1-1; 1-2; 1-3; 1-4; 1-5	88.9434	/	IC$_{50}$: 17 nM (PDB: 7btv)	2-1; 2-2; 2-3

[a] Key interactions from Figure 26.

[b] Key interactions from Figure 27.

Table S2. Experimental activities and docking score values of synthesized (**40**-**87**) and reference (**L41** and **L86**) compounds.

	H_3R			LRRK2			
	ASP Score	**H_3R K_i [nM] [95% CI]**	**Interactions[a]**	**PLP Score**	**LRRK2 inhibition [%] ± SD at 10 µM**	**LRRK2 IC_{50} [nM] [95% CI]**	**Interactions[b]**
40	76.4973	738 [470 – 1160]	1-1; 1-3; 1-5	74.4423	102.8 ± 2.6		1-1; 1-2; 1-3
41	72.5102	341 [119 – 980]	1-1, 1-3, 1-4	69.9946	100.2 ± 5.0 (3)		1-1; 1-2; 1-3
42	73.1656	10.2 [7.2 – 14.4]	1-1; 1-3; 1-4; 1-5	63.4466	99.7 ± 2.8		1-1; 1-2
43	76.9280	172 [24.2 –1227]	1-1; 1-2; 1-3; 1-4	75.2654	88.4 ± 3.0		1-1: 1-2; 1-3
44	66.8896	331 [124 – 883]	1-3; 1-4; 1-5	76.7828	92.0 ± 8.8 (3)		1-1; 1-2; 1-3
45	74.1114	59.9 [21.9 – 164]	1-3; 1-4; 1-5	66.2026	80.4 ± 1.9		1-1; 1-2
46	77.1895	390 [114 – 1333]	1-1; 1-3;	77.8194	84.5 ± 0.8		1-1; 1-2; 1-3
47	75.0935	916 [283 – 2964]	1-1, 1-3	79.1477	94.7 ± 2.4	2.2 [0.8 – 3.6]	1-1; 1-2; 1-3
48	76.2658	4.4 [1.7 – 11.2]	1-2; 1-3; 1-4	75.1411	99.2 ± 3.7	4.7 [2.7 – 6.8]	1-1; 1-2; 1-3
49	78.9027	75.8 [33.0 – 174]	1-1; 1-2; 1-3; 1-4;	79.2089	104.9 ± 1.2	2.4 [1.1 – 3.6]	1-1; 1-2; 1-3
50	51.8651	46.3 [18.3 – 117]	1-1; 1-3; 1-4; 1-5	75.821	86.3 ± 2.7		1-1; 1-2
51	74.1146	33.1 [21.7 – 50.6]	1-1; 1-3; 1-4; 1-5	78.9644	93.4 ± 1.2	9.3 [1.0 – 18.0]	1-1; 1-2; 1-3
52	75.9429	335 [106 – 1059]	1-3; 1-4	64.4554	54.6 ± 0.8		1-1; 1-2; 1-3
53	78.0760	839 [296 – 2379]	1-3; 1-4	70.6495	45.1 ± 4.4		1-1; 1-2; 1-3
54	72.7720	2.38 [1.07 – 5.29]	1-3; 1-4	78.7227	85.6 ± 9.0 (3)		1-1; 1-2; 1-3
55	76.2792	223 [83 – 603]	1-1; 1-3; 1-4; 1-5	76.6696	73.0 ± 2.5		1-1; 1-2; 1-3
56	67.3688	360 [124 – 1042]	1-1; 1-3; 1-4; 1-5	76.8317	64.0 ± 8.2		1-1; 1-2; 1-3
57	73.1135	241 [74.4 – 781]	1-1; 1-2; 1-3; 1-4	78.6856	62.6 ± 3.9		1-1; 1-2; 1-3
58	76.7371	1034 [411 – 2598]	1-3	74.9001	93.9 ± 13.1 (3)		1-1; 1-2; 1-3
59	76.7348	490 [164 – 1466]	1-3; 1-4	80.4597	78.6 ± 8.1		1-1; 1-2; 1-3
60	74.6044	4.77 [1.89 – 12.0]	1-3; 1-4;	82.1214	80.8 ± 1.1		1-1; 1-2; 1-3
61	80.4097	185 [103 – 331]	1-1; 1-2; 1-3; 1-4	70.6602	54.1 ± 0.5		1-1; 1-2; 1-3
62	65.0334	716 [554 – 926]	1-1; 1-3; 1-4; 1-5	73.6186	63.5 ± 4.5		1-1
63	74.0470	106 [91.6 – 123]	1-3; 1-4; 1-5	84.0723	71.2 ± 4.4		1-1; 1-2; 1-3
64	79.5061	548.0 [346 – 869]	1-1; 1-3; 1-5	81.3935	101.8 ± 7.5 (3)		1-1; 1-2; 1-3
65	70.0179	2096 [668 – 6581]	1-1, 1-3; 1-4	80.2906	88.5 ± 1.4		1-1; 1-2; 1-3
66	77.9691	4.1 [1.95 – 8.40]	1-3; 1-4; 1-5	77.0421	89.5 ± 3.5	8.0 [5.1 – 11.0]	1-1; 1-2; 1-3
67	77.5780	104.0 [44.5 –244.0]	1-1; 1-2; 1-3; 1-4	81.7570	98.4 ± 8.0 (3)	2.2 [0.8 – 3.6]	1-1; 1-2; 1-3

[a] Key interactions from Figure 33
[b] Key interactions from Figure 34

Table S2. *Continued.*

	H_3R			LRRK2			
	ASP Score	**H_3R K_i [nM] [95% CI]**	**Interactions[a]**	**PLP Score**	**LRRK2 inhibition [%] ± SD at 10 µM**	**LRRK2 IC_{50} [nM] [95% CI]**	**Interactions[b]**
68	66.6784	1645.0 [507 – 5333]	1-1; 1-3; 1-4; 1-5	79.0218	102.9 ± 1.2		1-1; 1-2; 1-3
69	72.2074	9.05 [5.21 – 15.7]	1-2; 1-3; 1-4; 1-5	81.7353	104.6 ± 5.5 (3)	3.6 [1.6 – 5.6]	1-1; 1-2; 1-3
70	79.1601	862.0 [438 – 1697]	1-3; 1-5	84.5559	73.5 ± 11.2		1-1; 1-2; 1-3
71	74.9518	6047 [5467 – 6689]	1-1; 1-3; 1-4; 1-5	79.3302	47.5 ± 14.0		1-1; 1-2; 1-3
72	78.3994	8.08 [3.92 – 16.7]	1-1; 1-3; 1-4; 1-5	83.5612	78.5 ± 0.2		1-1; 1-2; 1-3
73	78.7081	159 [81.7 – 311]	1-1; 1-2; 1-3; 1-4	82.9732	62.3 ± 11.4		1-1; 1-2; 1-3
74	66.1362	53.6 [26.5 – 108]	1-1; 1-3; 1-4, 1-5	80.0503	37.7 ± 1.3		1-1; 1-2; 1-3
75	73.1797	82.1 [33.2 – 203]	1-3; 1-4, 1-5	84.1765	54.5 ± 1.1		1-1; 1-2; 1-3
76	81.6597	1026 [418 – 2519]	1-1; 1-3	68.7502	56.6 ± 8.5		1-1; 1-2; 1-3
77	82.9593	578 [172 – 1944]	1-1; 1-2; 1-3; 1-4	78.1911	42.9 ± 0.6		1-1; 1-2; 1-3
78	78.5925	2.08 [0.77 – 5.61]	1-1; 1-3; 1-4	67.0680	53.9 ± 1.4		1-1; 1-2
79	78.6328	328.0 [114 – 945]	1-1; 1-2; 1-3; 1-4; 1-5	74.0994	38.2 ± 11.8		1-1; 1-2; 1-3
80	63.3973	822.0 [647 – 1043]	1-1; 1-3; 1-4; 1-5	80.403	47.0 ± 15.6		1-1; 1-2; 1-3
81	72.8132	11.2 [4.85 – 26.0]	1-1; 1-3; 1-4; 1-5	79.8385	44.2 ± 0.1		1-1; 1-2; 1-3
82	83.1997	141 [63.4 – 313]	1-1; 1-3	78.9944	99.7 ± 13.3 (3)		1-1; 1-2; 1-3
83	84.6474	519 [195 – 1381]	1-1; 1-3; 1-4	89.6963	90.3 ± 4.0		1-1; 1-2; 1-3
84	78.5748	11.1 [5.68 – 21.7]	1-1; 1-3; 1-4	75.7759	95.1 ± 8.2 (3)	2.8 [0.9 – 4.7]	1-1; 1-2; 1-3
85	76.3403	65.1 [29.9 – 142]	1-1, 1-2, 1-3; 1-4	87.3991	98.8 ± 2.1	1.1 [0.8 – 1.3]	1-1; 1-2; 1-3
86	56.9563	29.9 [10.9 – 82.5]	1-1; 1-3; 1-4; 1-5	79.8450	86.3 ± 3.5		1-1; 1-2; 1-3
87	75.5936	41.6 [29.6 – 58.5]	1-1; 1-3; 1-4; 1-5	91.4438	94.2 ± 3.3	2.7 [1.1 – 4.3]	1-1; 1-2; 1-3
L41	62.7293						
L86				80.0281			

[a] Key interactions from Figure 33
[b] Key interactions from Figure 34

Table S3. Experimentally determined and calculated LogP and LogD values of compounds **1**-**87**.

Compd	LogP (pH 11)	LogD (pH 7.4)	cLogP[a]	cLogD (pH 7.4)[b]
	Pyrimidin-4-amines			
1	4.40	4.82	4.82	3.76
2	n.d.**	n.d.	4.12	1.35
3	1.41	1.00	2.91	1.85
4	2.19	1.94	3.02	1.95
5	2.80	2.69	4.05	3.52
6	n.d.	n.d.	3.34	0.49
7	-0.08	-0.51	2.54	2.01
8	0.96	0.85	2.24	1.72
9	5.65	4.82	5.82	3.92
10	n.d.	n.d.	5.12	2.38
11	3.02	1.92	4.31	2.41
12	3.74	2.85	4.02	2.12
13	1.81	0.75	2.91	1.85
	Pyrimidin-2-amines			
14	1.48	1.71	1.27	-0.40
15	1.82	1.87	1.40	-0.28
16	2.34	2.23	2.10	0.42
17	2.86	2.51	2.64	0.97
18	2.58	2.29	2.18	0.51
19	2.05	2.12	1.95	0.14
20	2.38	2.37	2.08	0.26
21	2.89	2.73	2.78	0.97
22	3.41	3.05	3.32	1.51
23	3.15	2.80	2.86	1.05
	6-Methylpyrimidine-2,4-diamines			
24	1.03	1.10	2.14	1.03
25	2.89	2.01	3.14	1.20
26	2.51	1.47	2.98	1.17
27	2.48	1.17	2.98	1.16
28	1.60	1.66	2.49	1.39
29	3.39	2.47	3.50	1.56
30	3.00	1.94	3.34	1.52
31	2.95	2.06	3.34	1.52
32	0.87	1.03	2.14	0.99
33	2.78	1.99	3.14	1.04
34	2.28	1.24	2.98	0.88
35	2.28	1.48	2.98	1.01
36	1.45	1.53	2.49	1.25
37	3.25	2.39	3.50	1.41
38	2.75	1.70	3.34	1.36
39	2.70	1.86	3.34	1.37

Compd	LogP (pH 11)	LogD (pH 7.4)	cLogP	cLogD (pH 7.4)
	5-Chloropyrimidine-2,4-diamines			
40	2.10	2.13	2.61	1.54
41	0.79	0.57	1.83	1.31
42	3.65	2.68	3.61	1.71
43	3.22	2.18	3.45	1.67
44	3.17	2.27	3.45	1.66
45	4.21	3.27	3.45	1.59
46	2.68	2.76	2.96	1.90
47	1.36	1.16	2.19	1.67
48	4.19	3.23	3.97	2.07
49	3.73	2.70	3.81	2.03
50	3.67	2.79	3.81	2.02
51	4.76	3.84	3.81	1.93
52	1.96	2.06	2.61	1.54
53	0.69	0.44	1.83	1.31
54	3.54	2.65	3.61	1.71
55	3.40	2.13	2.45	1.66
56	3.12	2.26	3.45	1.67
57	4.44	3.54	3.45	1.58
58	2.49	2.47	2.96	1.90
59	1.21	0.98	2.19	1.67
60	4.01	3.07	3.97	2.07
61	3.58	2.55	3.81	2.01
62	3.52	2.61	3.81	2.03
63	4.89	3.95	3.81	1.94
	5-Trifluoromethylpyrimidine-2,4-diamines			
64	2.32	2.27	2.88	1.86
65	1.16	1.01	2.11	1.59
66	3.95	2.97	3.88	1.99
67	3.49	2.47	3.73	1.93
68	3.43	2.52	3.73	1.95
69	4.52	3.57	3.73	1.82
70	2.59	2.47	3.24	2.17
71	1.50	1.35	2.47	1.95
72	4.24	3.31	4.24	2.34
73	3.79	2.80	4.08	2.29
74	3.72	2.83	4.08	2.31
75	4.99	4.05	4.08	2.22
76	2.11	2.09	2.88	1.82
77	1.01	0.85	2.11	1.58
78	3.77	2.86	3.88	1.98
79	3.34	2.37	3.37	1.93
80	3.30	2.45	3.37	1.94
81	4.53	3.62	3.73	1.85
82	2.91	2.86	3.24	2.17
83	1.70	1.55	2.47	1.94
84	4.49	3.52	4.24	2.34
85	4.02	2.97	4.08	2.28
86	3.96	3.11	4.08	2.30
87	5.07	4.13	4.08	2.21

[a] clogP and clogD values were calculated using MarvinSketch

[b] n.d – Not determined. Highly hydrophilic compounds that could not be assessed under used chromatographic conditions.

List of Publications

Dissertation-related Articles

Hajar, M; Werner, T; **Gajic, M**; Stark, H; Sadek, B. Targeting Histone H3K9 Methyltransferase G9a as a Potential Therapeutic Strategy for Neuropsychiatric Disorders. *Medicinal Research Reviews* **2025**, Early View, DOI: https://doi.org/10.1002/med.22119. IF_{2025} = 11.6

The review article focuses on the (patho)physiological role of the epigenetic G9a enzyme in neuropsychiatric disorders and provides an overview of known G9a inhibitors along with their respective mechanisms of action and therapeutic potential. The work on the manuscript contributed to the development of dual-targeting G9a/H_3R ligands and examined the underlying rationale for concurrently modulating these two targets as a therapeutic strategy for neuropsychiatric disorders, both of which are of direct relevance to the present thesis. Intensive recherché on publications and patents on new compound developments and writing of the respective parts of the manuscript in addition to a thorough revision of all parts was done by Gajić M in collaboration with co-authors.

Gajic, M; Knez, D; Sosič, I: Mravljak, J; Meden, A; Košak, U; Leitzbach, L; George, S; Hofmann, B; Zivkovic, A; Steinhilber, D; Stark, H; Gobec, S; Smelcerovic, A; Anderluh, M. Repurposing of 8-hydroxyquinoline-based butyrylcholinesterase and cathepsin B ligands as potent nonpeptidic deoxyribonuclease I inhibitors. *ChemMedChem* **2022**, 17(5), e202100694. DOI: https://doi.org/10.1002/cmdc.202100694. IF_{2022} = 3.4

The article investigated a library of 8-hydroxyquinoline-based butyrylcholinesterase and cathepsin B ligands on additional targets relevant to neurodegenerative disorders, including dopamine D_2/D_3, histamine H_3/H_4 receptors, 5-lipoxygenase, and deoxyribonuclease I (DNase I). This research aligns with the broader objectives of the thesis by employing a multi-target-directed ligand strategy, particularly through the inclusion of histamine H_3R, to explore heterocyclic scaffolds for development of multifunctional ligands relevant to neurodegenerative disorders. Gajić M. contributed by performing compound screening on the DNase I enzyme, preparing the initial manuscript draft, and revising the final version in collaboration with co-authors.

Other Articles

Kocic, G; **Gajic, M**; Tomovic, K; Hadzi-Djokic, J; Anderluh, M; Smelcerovic, A. Purine adducts as presumable missing link for aristolochic acid nephropathy-related cellular energy crisis, potential anti-fibrotic prevention and treatment. *British Journal of Pharmacology* **2021**, 178(22), 4411-4427. DOI: https://doi.org/10.1111/bph.15618. IF_{2021} = 9.473

Gajić, M; Džambaski, Z; Ilić, BS; Kocić, G; Bondžić, BP; Šmelcerović, A. Synthesis and analysis of 4-oxothiazolidines as potential dual inhibitors of deoxyribonuclease I and xanthine oxidase. *Chemico-Biological Interactions* **2021**, 345, 109536. DOI: https://doi.org/10.1016/j.cbi.2021.109536. IF_{2021} = 5.168

Gajić, M; Ilić, BS; Bondžić, BP; Džambaski, J; Kojić, VV; Jakimov, DS; Kocić, G; Šmelcerović, A. 1,2,3,4-Tetrahyodroisoquinoline Derivatives as Novel Deoxyribonuclease I Inhibitors. *Chemistry and Biodiversity* **2021**, 18(8), e2100261. DOI: https://doi.org/10.1002/cbdv.202100261. IF_{2021} = 2.745

Ilić, BS; **Gajić, M**; Bondžić, BP; Džambaski, Z; Kocić, G; Šmelcerovic, A. Deoxyribonuclease I Inhibitory Properties, Molecular Docking and Molecular Dynamics Simulations of 1-(Pyrrolidin-2-yl)propan-2-one Derivatives. *Chemistry and Biodiversity* **2021**, 18(3), e2000996. DOI: https://doi.org/10.1002/cbdv.202000996. IF_{2021} = 2.745

Gajić, M; Ilić, BS; Bondžić, B; Džambaski, Z; Filipović, A; Kocić, G; Šmelcerović, A. Xanthine oxidase inhibitory properties of 1,2,3,4-tetrahydroisoquinoline derivatives. *Acta Medicae Medianae* **2021**, 60, 48-55. DOI: https://doi.org/10.5633/amm.2021.0106

Kocic, G; Hadzi-Djokic, J; Cukuranovic-Kokoris, J; **Gajic, M**; Veljkovic, A; Cukuranovic, R; Basic, D; Jovanovic, I; Smelcerovic, A. Predictive Markers for Malignant Urothelial Transformation in Balkan Endemic Nephropathy: A Case-Control Study. *Cancers* **2020**, 12, 2945. DOI: https://doi.org/10.3390/cancers12102945. IF_{2020} = 6.639

Smelcerovic, A; Kocic, G; **Gajic, M**; Tomovic, K; Djordjevic, V; Stankovic-Djordjevic, D; Anderluh, M. DPP-4 Inhibitors in the Prevention/Treatment of Pulmonary Fibrosis, Hearth and Kidney Injury Caused by COVID-19 – A Therapeutic Approach of Choice in Type 2 Diabetic Patients. *Frontiers in Pharmacology* **2020**, 11, 1185. DOI: https://doi.org/10.3389/fphar.2020.01185. IF_{2020} = 5.811

Articles in Preparation

Gajic, M; Werner, T; Hajar, M; Cebzan, A; Djokovic, N; Nikolic, K; Sadek, B; Zivkovic, A; Stark, H. Design, Synthesis, and Biological Evaluation of Pyrimidine-2,4-diamine-Based Dual H_3R/G9a Ligands. *In Preparation*

Gajic, M; Werner, M; Popovic Nikolic, M; Djokovic, N; Nikolic, K; Zivkovic, A; Stark, H. First-in-Class Pyrimidine-2,4-diamines Targeting H_3R and LRRK2 for Parkinson's Disease Treatment. *In Preparation*

Bekljas, M; Zukic, S; Mirjacic Martinovic, K; Djuric, A; Vuletic, A; Jallet, C; Hölzel, J; Böttger, E; **Gajić, M**; Santibanez, JF; Stark, H; Živković, A; Srdic-Rajic, T; Arimondo, PB; Marak, U; Nikolic, K; Petkovic, M; Oljacic, S. Molecular Docking, Machine Learning-Guided Design, Synthesis, and Biological Evaluation of Novel Multitarget HDAC/ROCK Inhibitors. ChemRxiv **2025**; DOI: https://doi.org/10.26434/chemrxiv-2025-xhmlv

Gajic, M; Werner, T; Zivkovic, A; Stark, H. Design, Synthesis, and Biological Evaluation of Novel Histamine H_3 Receptor Ligands. *In Preparation*

Presentations at International Conferences

Gajić, M; Knez, D; Sosič, I; Mravljak, J; Meden, A; Košak, U; Leitzbach, L; George, S; Hofmann, B; Zivkovic, A; Steinhilber, D; Stark, H; Gobec, S; Smelcerovic, A; Anderluh, M. Potent Nonpeptidic Multi-Target Directed Deoxyribonuclease I Inhibitors Based on the 8-Hydroxyquinoline Motif. Proceeding of the XXVII EFMC International Symposium on Medicinal Chemistry, Nice, France, September **2022**. Abstract book, P524.

Curriculum Vitae

Mihajlo Gajić

Addreess:	Hüttenstraße 48, 40215 Düsseldorf, Germany
Phone	+49 176 31561534
E-mail:	mihajlo.gajic@hhu.de mihajlo.gajic94@gmail.com
Date of birth:	08. June 1994

Education

PhD studies 2021 – present	**Institute for Pharmaceutical and Medicinal Chemistry, Heinrich Heine University, Düsseldorf, Germany** Pharmaceutical and Medicinal Chemistry
PhD studies 2018 – present	**Faculty of Medicine, University of Niš, Niš, Serbia** Pharmaceutical sciences
Master degree 2013 – 2018	**Department of Pharmacy, Faculty of Medicine, University of Niš, Niš, Serbia** Integrated Master's Studies (Overall grade: 10.00 / 10.00) **Master thesis:** *In silico* study of phisico-chemical, pharmacokinetic and toxicological properties of tyrosine kinase inhibitors
2009 – 2013	**Gymnasium "Bora Stanković", Niš, Serbia** (Overall grade: 5.00 / 5.00) Awarded multiple certificates and prizes for competing in chemistry, mathematics and physics as a primary and high school student

Awards and Scholarships

Oct 2021 – present	**DAAD Scholarship –** Research Grants - Doctoral Programmes in Germany, 2021/22
2020	**Charter by the City of Niš**, awarded to the students who graduated with the highest possible overall grade in 2018

Work Experience

Apr 2024 – Sept 2024	**University Teaching Assistant** in the lab course "Quality Control"
2022 – present	**University Teaching Assistant** in the lab course "Instrumentelle Analytik" with particular focus on chromatographic and spectroscopic techniques (HPLC, GC, LC-MS, TLC-MS, NMR, IR, UV-Vis, AAS)

Nov 2020	**Pharmacy Practice Resident** (pre-requested for The State Exam) at the Clinical Center Niš, Niš, Serbia
Jun – Oct 2020	**Pharmacy Practice Resident** (pre-requested for The State Exam) at the Public Pharmacy Viva, Niš, Serbia
2020 – 2021	**Researcher** on the project "Synthesis and biological evaluation of novel inhibitors of medicinally significant oxidoreductases and hydrolases" of Faculty of Medicine, University of Niš, Niš, Serbia
Mar 2019 – Oct 2021	**Researcher** on the project "Synthesis, physico-chemical characterization, analytics and biological activity of pharmacologically active compounds" funded by Ministry of Education, Science and Technological Development of the Republic of Serbia (Grant No. OI 172044)
2016 – 2017	**Undergraduate teaching assistant/ Laboratory demonstrator** Organic Chemistry, Department of Chemistry

Memberships and Activities

2022 – present	Member of Deutsche Pharmazeutische Gesellschaft (DPhG)
2018	Public Health volunteer for actions organized by Nis Pharmacy Students' Association (NiPSA)
2017 – 2018	Member of Center for students' scientific research (CSSR)
2013 – 2018	Member of National Association of Pharmacy Students – Serbia (NAPSer)

Languages

Serbian (Native)
English (CAE certificate)
German (Goethe-Zertifikat B2)

Computer Skills

MS Office, ChemDraw, MestreNova, Adobe Illustrator, Adobe InDesign,

Other Interests

Cooking, sport, video games, traveling, reading books